

---

Characterization of programmed death ligand 1 expression  
and  
analyses of its immune-regulatory role  
in pancreatic ductal adenocarcinoma

---

Dissertation

zur Erlangung des akademischen Grades  
Doktor der Naturwissenschaften (Dr. rer. nat.)  
der Mathematisch-Naturwissenschaftlichen Fakultät  
der Christian-Albrechts Universität zu Kiel

**Sascha Rahn**

Kiel, 2019

First Reviewer: Prof. Dr. rer. nat. Susanne Sebens  
Second Reviewer: Prof. Dr. rer. nat. Regina Scherließ  
Disputation: 04.12.2019

Parts of this dissertation have been already published in:

**Rahn, S.**, Krüger, S., Röcken, C., Helm, O., & Sebens, S. (2019). Response to: 'Patterns of PD-L1 expression and CD8 T cell infiltration in gastric adenocarcinomas and associated immune stroma'. *Gut*, 68(1), 179-180.

**Rahn, S.**, Krüger, S., Mennrich, R., Goebel, L., Wesch, D., Oberg, H. H., ... & Sebens, S. (2019). POLE Score: a comprehensive profiling of programmed death 1 ligand 1 expression in pancreatic ductal adenocarcinoma. *Oncotarget*, 10(16), 1572.

## Zusammenfassung

Das duktales Pankreasadenokarzinom (engl.: *pancreatic ductal adenocarcinoma*; PDAC) stellt eine der tödlichsten Tumorentitäten dar, denn die Erkrankung wird meist erst im lokal fortgeschrittenen oder metastasierten Stadium diagnostiziert und die Mehrheit der Patienten mit örtlich begrenzten Tumoren entwickelt nach Resektion entweder lokale Rezidive oder Metastasen. Aufgrund des eingeschränkten Behandlungsspektrums, welches sich für über 80% der PDAC Patienten auf palliative Chemotherapie beschränkt, wird intensiv nach effizienten Alternativen gesucht. Antagonistische Antikörper gegen die co-inhibitorischen Immun-Checkpoint-Moleküle *programmed death protein 1* (PD-1) und *programmed death ligand 1* (PD-L1) haben die Therapiekonzepte für etliche Krebserkrankungen revolutioniert, aber zeigten bisher noch keine Wirkung in der Behandlung von PDAC Patienten. Daher war das Ziel der vorliegenden Studie die tumor-biologische Rolle von PD-L1 im PDAC näher zu untersuchen. Immunohistochemische Analysen in pankreatischen Gewebeschnitten von 59 PDAC Patienten wiesen eine deutliche inter- und intratumorale Heterogenität der PD-L1 Expression nach, welche mit pathohistologischen Veränderungen sowie einem kürzeren postoperativen Überleben der Patienten korrelierte. Daraufhin wurde das POLE Score System entwickelt, welches die PD-L1 Expression im gesamten Tumor, in Tumor-/Stromazellen und Tumor-assoziierten Lymphfollikeln klassifiziert sowie die räumliche Verteilung PD-L1<sup>+</sup> Zellen beschreibt. Nachfolgende Auswertungen zeigten, dass PD-L1 nur in einem Drittel der PDAC Gewebe nachweisbar und vorwiegend in Leukozytenpopulationen wie Tumor-assoziierten Makrophagen (TAMs) vorzufinden ist. Des Weiteren wiesen Untersuchungen in seriellen Gewebeschnitten darauf hin, dass eine starke PD-L1 Expression vorwiegend im Bereich der Tumorfront sowie der Grenze zwischen Tumor und lymphatischem Gewebe lokalisiert ist sowie mit hoher Infiltration von TAMs und CD8<sup>+</sup> T Lymphozyten (CD8T) einhergeht. Basierend auf diesen Befunden wurde ein *in vitro* System etabliert, welches die PDAC Zelllinie PancTu-I, M1-polarisierte primäre humane Makrophagen (M1 MΦ) und autologe voraktivierte CD8T beinhaltet, um die Interaktion zwischen diesen Zellpopulationen sowie die Rolle von PD-L1 darin näher zu untersuchen. Kokultur-Experimente zeigten, dass PD-L1<sup>+</sup> M1 MΦ sowohl den Effektorphänotyp von CD8T als auch die Wachstums-inhibierende Wirkung von CD8T auf PancTu-I Zellen verstärkten. Gleichzeitig förderten CD8T eine stärker ausgeprägte M1-Polarisierung in M1 MΦ. Im Gegensatz dazu wiesen CD8T unter Kokultur mit PD-L1<sup>+</sup> PancTu-I Zellen eine verminderte Proliferation sowie einen abgeschwächten Effektorphänotyp auf und förderten die Ausbildung einer mesenchymaleren Differenzierung von PancTu-I Zellen. Die Auswirkungen der PD-L1 Blockade mittels Durvalumab auf die jeweiligen Zellpopulation hingen stark von der Zellzusammensetzung innerhalb der Kulturbedingungen ab. So wiesen Durvalumab behandelte M1 MΦ eine stärker ausgeprägte M1-Polarisierung auf. Während CD8T nach Durvalumab Behandlung in Monokultur eine niedrigere Sekretion von Effektormolekülen aufwies, führte selbige Behandlung in Kokultur mit M1 MΦ zu einer erhöhten PD-1 Expression sowie in Kokultur mit PancTu-I Zellen zu einer gesteigerten Proliferation und einem stärker ausgeprägten Effektorphänotyp von CD8T.

---

## Summary

Pancreatic ductal adenocarcinoma (PDAC) represents one of the most fatal malignancies. The dismal prognosis is attributed to the late detection of PDAC in already locally advanced or metastatic stages and high recurrence rates in patients that have undergone curative surgical resection. Since, palliative chemotherapeutic regimens constitute the only therapeutic option for most of PDAC patients, efficient alternatives are urgently needed. Targeting of the immune checkpoint co-inhibitory molecules programmed death protein 1 and programmed death ligand 1 (PD-L1) revolutionized therapy concepts for several malignancies but has not been proven effective in the treatment of PDAC patients. Hence, the present study aimed to gain a deeper insight into the tumor biological role of PD-L1 in PDAC.

Immunohistochemical PD-L1 staining in pancreatic tissue sections of 59 PDAC patients revealed a pronounced inter- and intra-tumoral heterogeneity, which correlated with malignancy-associated alterations in pancreatic tissues and reduced post-surgical patient survival. Considering staining heterogeneity, the POLE Score system has been developed to classify differences in overall PD-L1 staining, tumoral/stromal origin, tumor-associated lymph follicles and the spatial distribution of PD-L1<sup>+</sup> cells. Analyses indicated that PD-L1 is expressed in only a third of the PDAC tissues and staining is predominantly located in leukocyte populations like tumor-associated macrophages (TAMs). Moreover, lineage marker analyses in serial tissue section revealed that strong PD-L1 staining is mainly located at the tumor-lymphatics interface as well as the tumor margin accompanied by pronounced TAM and CD8<sup>+</sup> T lymphocyte (CD8T) infiltration. In order to study the interaction between PDAC cells, TAMs and T cells as well as the role of PD-L1 in more detail, an *in vitro* setting has been established composed of the cell line PancTu-I, M1-like polarized primary human macrophages (M1 MΦ) and autologous pre-activated CD8T. Co-culture experiments showed that PD-L1<sup>+</sup> M1 MΦ promoted the effector phenotype of CD8T as well as the CD8T-mediated growth inhibition of PancTu-I cells. In turn, CD8T augmented M1-polarization of M1 MΦ. In contrast, PD-L1<sup>+</sup> PancTu-I cells attenuated the proliferation and effector phenotype of CD8T, while *vice versa* CD8T fostered epithelial-to-mesenchymal transition-associated alterations in PancTu-I cells. The effects of PD-L1 blockade via application of Durvalumab on each cell population markedly differed in dependence the cellular composition within the cultures. Thus, Durvalumab treated M1 MΦ exhibited a more pronounced M1-like phenotype. Considering CD8T, Durvalumab treatment was associated with significantly reduced secretion of effector molecules in mono-culture, elevated PD-1 cell surface levels in co-culture with M1 MΦ as well as enhanced proliferation and improved effector phenotype in co-culture with PancTu-I cells.

## List of Abbreviations

|                    |  |
|--------------------|--|
| ·g                 | Force of gravity (9.81 m/s <sup>2</sup> )  |
| °C                 | Degree Celsius   |
| μ                  | Micro (1 · 10 <sup>-6</sup> )  |
| μg                 | <b>M</b> ikrogram (1 · 10 <sup>-6</sup> g)   |
| μl                 | <b>M</b> ikroliter (1 · 10 <sup>-6</sup> l)  |
| A                  | <b>A</b> mpere   |
| AP-1               | <b>A</b> ctivator <b>p</b> rotein <b>1</b>   |
| APC                | <b>A</b> llophycocyanin  |
| APCs               | <b>A</b> ntigen- <b>p</b> resenting <b>c</b> ells  |
| APS                | <b>A</b> mmonium <b>p</b> ersulfate  |
| AT                 | <b>A</b> ustria  |
| ATCC               | <b>A</b> merican <b>T</b> ype <b>C</b> ulture <b>C</b> ollection                           |
| BRCA2              | <b>B</b> reast <b>c</b> ancer <b>2</b>   |
| BSA                | <b>B</b> ovine <b>s</b> erum <b>a</b> lbumin   |
| CAF                | <b>C</b> ancer- <b>a</b> ssociated <b>f</b> ibroblast                                      |
| CAR T cell         | <b>C</b> himeric <b>a</b> ntigen <b>r</b> eceptor <b>T</b> <b>c</b> ell                    |
| CC                 | <b>C</b> ell <b>c</b> ulture   |
| CD                 | <b>C</b> luster of <b>D</b> ifferentiation   |
| CDKN2A             | <b>C</b> yclin- <b>d</b> epending <b>k</b> inase <b>i</b> nhibitor <b>2A</b>               |
| cDNA               | <b>C</b> omplementary <b>d</b> esoxyribonucleic <b>a</b> cid                               |
| cm                 | <b>C</b> entimeter (1 · 10 <sup>-2</sup> meter)  |
| CP                 | <b>C</b> hronic <b>p</b> ancreatitis   |
| Ct                 | <b>C</b> ycle <b>t</b> hreshold  |
| CTL                | <b>C</b> ytotoxic <b>T</b> <b>l</b> ymphocyte  |
| CTLA-4             | <b>C</b> ytotoxic <b>T</b> <b>l</b> ymphocyte- <b>a</b> ssociated <b>p</b> rotein <b>4</b> |
| Ctrl               | <b>C</b> ontrol  |
| d                  | <b>D</b> ay(s)   |
| ddH <sub>2</sub> O | <b>D</b> ouble <b>d</b> istilled <b>w</b> ater   |
| DE                 | <b>G</b> ermany  |
| DMEM               | <b>D</b> ulbecco's <b>M</b> odified <b>E</b> agle <b>M</b> edium                           |
| DNA                | <b>D</b> esoxyribonucleic <b>a</b> cid   |
| DPC4               | <b>D</b> eleted in <b>p</b> ancreatic <b>c</b> ancer- <b>4</b>                             |

|              |   |
|--------------|---|
| ECM          | <b>Extracellular matrix</b>                               |
| EDTA         | <b>Ethylenediaminetetraacetic acid</b>                    |
| EGF          | <b>Epidermal Growth Factor</b>                            |
| EM           | <b>Emission</b> (wavelength range of a bandpass filter)   |
| EMA          | <b>European Medicines Agency</b>                          |
| EMT          | <b>Epithelial to Mesenchymal Transition</b>               |
| ERK1/2       | <b>Extracellular-signal Regulated Kinase 1 and 2</b>      |
| EX           | <b>Excitation</b> (wavelength range of a bandpass filter) |
| Fc           | <b>Fragment crystallisable</b>                            |
| FC           | <b>Flow cytometry</b>                                     |
| FCS          | <b>Fetal calf serum</b>                                   |
| FDA          | <b>Food and Drug Administration</b>                       |
| FITC         | <b>Fluorescein isothiocyanate</b>                         |
| FoV          | <b>Field of view</b>                                      |
| FoxP3        | <b>Forkhead box P3</b>                                    |
| FSC          | <b>Forward scatter</b>                                    |
| fw           | <b>Forward</b>  |
| g            | <b>Gram</b>   |
| GAPDH        | <b>Glycerinaldehyd-3-phosphate Dehydrogenase</b>          |
| GM-CSF       | <b>Granulocyte-Macrophage Colony-Stimulating Factor</b>   |
| GTP          | <b>Guanosine triphosphate</b>                             |
| h            | <b>Hour(s)</b>  |
| HCC          | <b>Hepatocellular carcinoma</b>                           |
| HPDE         | <b>Human pancreatic ductal epithelium</b>                 |
| HRP          | <b>Horseradish peroxidase</b>                             |
| IF           | <b>Immunofluorescence</b>                                 |
| IFN $\gamma$ | <b>Interferon gamma</b>                                   |
| Ig           | <b>Immunoglobulin</b>                                     |
| IHC          | <b>Immunohistochemistry</b>                               |
| IL           | <b>Interleukin</b>  |
| IPMN         | <b>Intraductal papillary mucinous neoplasm</b>            |
| IrAE         | <b>Immune-related adverse events</b>                      |
| IRS          | <b>Immunoreactivity scoring system</b>                    |
| ITAM         | <b>Immunoreceptor tyrosine-based activation motif</b>     |

|               |   |
|---------------|---|
| ITIM          | <b>I</b> mmunoreceptor <b>t</b> yrosine-based <b>i</b> nhibitory <b>m</b> otif                |
| ITSM          | <b>I</b> mmunoreceptor <b>t</b> yrosine-based <b>s</b> witch <b>m</b> otif                    |
| JNK           | <b>C</b> -Jun <b>N</b> -terminal <b>k</b> inase   |
| kDa           | <b>K</b> ilo <b>D</b> alton ( $1 \cdot 10^3$ Da)  |
| k-ras         | <b>V</b> - <b>K</b> i-ras2 <b>K</b> irsten <b>r</b> at sarcoma viral oncogene homolog         |
| l             | <b>L</b> iter   |
| LAT           | <b>L</b> inker of <b>a</b> ctivated <b>T</b> cells  |
| LCK           | <b>L</b> ymphocyte-specific protein tyrosine <b>k</b> inase                                   |
| LED           | <b>L</b> ight-emitting <b>d</b> iode  |
| L-Gln         | <b>L</b> - <b>G</b> lutamine  |
| LPS           | <b>L</b> ipopolysaccharide  |
| mA            | <b>M</b> illi <b>A</b> mpere ( $1 \cdot 10^{-3}$ A)   |
| MAPK          | <b>M</b> itogen- <b>a</b> ctivated <b>p</b> rotein <b>k</b> inase                             |
| MCN           | <b>M</b> ucinous <b>c</b> ystic <b>n</b> eoplasm  |
| M-CSF         | <b>M</b> acrophage <b>C</b> olony- <b>S</b> timulating <b>F</b> actor                         |
| MDSC          | <b>M</b> yeloid- <b>d</b> erived <b>s</b> uppressor <b>c</b> ell                              |
| MHC           | <b>M</b> ajor <b>h</b> istocompatibility <b>c</b> omplex                                      |
| min           | <b>M</b> inute(s)   |
| miRNA         | <b>M</b> icro <b>R</b> NA   |
| ml            | <b>M</b> illiliter ( $1 \cdot 10^{-3}$ l)   |
| mM            | <b>M</b> illimolar ( $1 \cdot 10^{-3}$ M)   |
| MMP           | <b>M</b> atrix <b>m</b> etalloproteinase  |
| mTOR          | <b>M</b> ammalian <b>t</b> arget of <b>r</b> apamycin   |
| NFAT          | <b>N</b> uclear <b>f</b> actor of <b>a</b> ctivated <b>T</b> cells                            |
| NF $\kappa$ B | <b>N</b> uclear <b>f</b> actor <b>k</b> appa-light-chain-enhancer of activated <b>B</b> cells |
| ng            | <b>N</b> anogram ( $1 \cdot 10^{-9}$ g)   |
| NK cell       | <b>N</b> atural <b>k</b> iller <b>c</b> ell   |
| nm            | <b>N</b> anometer ( $1 \cdot 10^{-9}$ m)  |
| NSCLC         | <b>N</b> on-small <b>c</b> ellular <b>l</b> ung <b>c</b> ancer                                |
| PanCK         | <b>P</b> an- <b>C</b> ytokeratin  |
| PanIN         | <b>P</b> ancreatic <b>i</b> ntraepithelial <b>n</b> eoplasia                                  |
| PBMCs         | <b>P</b> eripheral <b>b</b> lood <b>m</b> ononuclear <b>c</b> ells                            |
| PBS           | <b>P</b> hosphate- <b>b</b> uffered <b>s</b> aline  |
| PD-1          | <b>P</b> rogrammed <b>d</b> eath protein <b>1</b>   |

|              |   |
|--------------|---|
| PDAC         | <b>P</b> ancreatic <b>d</b> uctal <b>a</b> deno <b>c</b> arcinoma                           |
| PDECs        | <b>P</b> ancreatic <b>d</b> uctal epithelial cells  |
| PD-L1/2      | <b>P</b> rogrammed <b>d</b> eath <b>l</b> igand <b>1/2</b>                                  |
| PE           | <b>P</b> hycoerythrin   |
| Pen/Strep    | <b>P</b> enicillin and <b>s</b> treptomycin   |
| PerCP        | <b>P</b> eridinin chlorophyll   |
| PFA          | <b>P</b> araformaldehyde  |
| pH           | Decimal logarithm of reciprocal <b>h</b> ydrogen ion activity                               |
| PI3K         | <b>P</b> hosphoinositide <b>3</b> -kinases  |
| PKB/AKT      | <b>P</b> rotein kinase <b>B</b>   |
| PKC $\theta$ | <b>P</b> rotein kinase <b>C</b> <b>theta</b>  |
| pMHC         | <b>P</b> eptide-loaded <b>M</b> H <b>C</b> complex  |
| pmol         | <b>P</b> ikomole ( $1 \cdot 10^{-12}$ mole)   |
| PSC          | <b>P</b> ancreatic stellate cell  |
| PVDF         | <b>P</b> olyvinylidene fluoride   |
| qPCR         | <b>Q</b> uantitative real-time <b>p</b> olymerase chain reaction                            |
| RNA          | <b>R</b> ibonucleic acid  |
| RNI          | <b>R</b> eactive <b>n</b> itrogen intermediates   |
| ROS          | <b>R</b> eactive <b>o</b> xygen species   |
| rpm          | <b>R</b> ounds <b>p</b> er <b>m</b> inute   |
| RPMI         | <b>R</b> oswell <b>P</b> ark <b>M</b> emorial <b>I</b> nstitute                             |
| RT           | <b>R</b> oom temperature  |
| rv           | <b>R</b> everse   |
| RvT          | <b>R</b> everse transcriptase   |
| s            | <b>S</b> econd(s)   |
| SCCHN        | <b>S</b> quamous cell carcinoma of the <b>h</b> ead and <b>n</b> eck                        |
| SDS-PAGE     | <b>S</b> odium dodecyl sulfate <b>p</b> olyacrylamide <b>g</b> el electrophoresis           |
| SEM          | <b>S</b> tandard <b>e</b> rror of the <b>m</b> ean  |
| SHP1/2       | <b>S</b> rc <b>h</b> omology region 2 domain-containing <b>p</b> hosphatase- <b>1/2</b>     |
| SMAD4        | <b>M</b> others <b>a</b> gainst <b>d</b> ecapentaplegic homolog <b>4</b>                    |
| SSC          | <b>S</b> ide <b>s</b> catter  |
| Stat         | <b>S</b> ignal <b>t</b> ransducer and <b>a</b> ctivator of <b>t</b> ranscription            |
| Stat1/3      | <b>S</b> ignal <b>t</b> ransducer and <b>a</b> ctivator of <b>t</b> ranscription <b>1/3</b> |
| TAMs         | <b>T</b> umor-associated <b>m</b> acrophages  |



---

|                |  |
|----------------|--|
| TBS-T          | <b>T</b> ris- <b>b</b> uffered saline supplemented with <b>T</b> ween 20 |
| Tc             | <b>T</b> cell  |
| TCR            | <b>T</b> cell <b>R</b> eceptor   |
| TGF- $\beta$ 1 | <b>T</b> ransforming <b>G</b> rowth <b>F</b> actor <b>B</b> eta <b>1</b> |
| TIL            | <b>T</b> umor- <b>i</b> nfiltrating lymphocyte(s)                        |
| TLO            | <b>T</b> ertiary lymphoid <b>o</b> rgan                                  |
| TMB            | <b>T</b> umor <b>m</b> utational <b>b</b> urden                          |
| TNF $\alpha$   | <b>T</b> umor <b>N</b> ecrosis <b>F</b> actor <b>A</b> lpha              |
| Treg           | <b>R</b> egulatory <b>T</b> lymphocyte                                   |
| U              | <b>U</b> nits  |
| UC             | <b>U</b> rothelial carcinoma   |
| UK             | <b>U</b> nited <b>K</b> ingdom   |
| US             | <b>U</b> nited <b>S</b> tates  |
| UV             | <b>U</b> ltraviolet  |
| V              | <b>V</b> olt   |
| v/v            | <b>V</b> olume per volume  |
| VEGF           | <b>V</b> ascular <b>E</b> ndothelial <b>G</b> rowth <b>F</b> actor       |
| w/v            | <b>W</b> eight per volume  |
| WB             | <b>W</b> estern <b>B</b> lot   |
| Zap70          | <b>Z</b> eta-chain-associated protein kinase <b>70</b>                   |
| Zeb-1          | <b>Z</b> inc finger <b>E</b> -box-binding homeobox <b>1</b>              |

---

## Table of Contents

|   |             |
|---|-------------|
| <b>Zusammenfassung</b> .....  | <b>I</b>    |
| <b>Summary</b> .....  | <b>II</b>   |
| <b>List of Abbreviations</b> .....                                  | <b>III</b>  |
| <b>Table of Contents</b> .....                                      | <b>VIII</b> |
| <b>1. Introduction</b> .....  | <b>1</b>    |
| 1.1 Pancreatic ductal adenocarcinoma.....                           | 1           |
| 1.1.1 Epidemiology .....  | 1           |
| 1.1.2 Etiology .....  | 2           |
| 1.1.3 Pathogenesis.....   | 2           |
| 1.1.4 Epithelial to mesenchymal transition in PDAC progression..... | 4           |
| 1.2 Tumor stroma in PDAC.....                                       | 6           |
| 1.2.1 (Tumor-associated) macrophages .....                          | 7           |
| 1.2.2 Tumor-infiltrating T lymphocytes.....                         | 10          |
| 1.3 T lymphocyte maturation and priming .....                       | 12          |
| 1.3.1 T cell receptor and CD28 co-stimulatory signaling .....       | 16          |
| 1.3.2 Programmed death protein 1 signaling.....                     | 18          |
| 1.4 Cancer Immunity and Immunotherapy.....                          | 19          |
| 1.4.1 PD-1 and PD-L1 as targets in cancer therapy .....             | 22          |
| 1.4.2 Durvalumab (Imfinzi) .....                                    | 24          |
| 1.5 Aim of the study .....  | 26          |
| <b>2. Materials</b> .....   | <b>27</b>   |
| 2.1 Chemicals and Reagents.....                                     | 27          |
| 2.2 Buffers .....   | 29          |
| 2.3 Cell culture material .....                                     | 30          |
| 2.3.1 Cell lines.....   | 30          |
| 2.3.2 Culture media .....   | 32          |
| 2.3.3 Growth factors and cytokines.....                             | 33          |
| 2.4 Patient derived material .....                                  | 33          |
| 2.4.1 Ethics statement.....   | 33          |
| 2.4.2 Histopathology and study cohort.....                          | 34          |
| 2.5 Molecular biological material.....                              | 34          |
| 2.5.1 Primer .....  | 34          |
| 2.5.2 Antibodies .....  | 35          |

---

|           |   |           |
|-----------|---|-----------|
| 2.6       | Consumables.....  | 38        |
| 2.7       | Kit systems .....   | 39        |
| 2.8       | Software.....   | 40        |
| 2.9       | Laboratory Devices.....   | 40        |
| <b>3.</b> | <b>Methods.....</b>   | <b>44</b> |
| 3.1       | Cell biological methods .....   | 44        |
| 3.1.1     | Cultivation of human pancreatic ductal epithelial cells .....                         | 44        |
| 3.1.2     | Cell counting .....   | 44        |
| 3.1.3     | Isolation of peripheral mononuclear blood cells .....                                 | 44        |
| 3.1.4     | Counterflow centrifugation .....  | 45        |
| 3.1.5     | Long-term storage of PDEC lines and primary human lymphocytes in liquid nitrogen..... | 47        |
| 3.1.6     | Isolation of primary human naive CD8 <sup>+</sup> T cells.....                        | 47        |
| 3.1.7     | Carboxyfluorescein succinimidyl ester staining .....                                  | 48        |
| 3.1.8     | Activation and cultivation of primary human naïve (CD8 <sup>+</sup> ) T cells .....   | 49        |
| 3.1.9     | Differentiation and cultivation of primary human polarized macrophages .....          | 49        |
| 3.1.10    | <i>In vitro</i> mono- and co-culture settings .....                                   | 50        |
| 3.1.11    | Single-cell dissociation from human PDAC tissues .....                                | 51        |
| 3.2       | Immunobiological methods .....  | 52        |
| 3.2.1     | Immunofluorescence staining .....   | 52        |
| 3.2.2     | Immunohistochemistry.....   | 55        |
| 3.2.3     | Multiplex analysis of culture supernatants.....                                       | 55        |
| 3.3       | Molecular biological methods .....  | 57        |
| 3.3.1     | RNA Isolation and quantification .....  | 57        |
| 3.3.2     | Complementary DNA synthesis <i>via</i> reverse transcription .....                    | 57        |
| 3.3.3     | Quantitative real-time polymerase chain reaction.....                                 | 58        |
| 3.4       | Biochemical methods .....   | 60        |
| 3.4.1     | Isolation and quantification of proteins.....   | 60        |
| 3.4.2     | Sodium dodecyl sulfate polyacrylamide gel electrophoresis .....                       | 60        |
| 3.4.3     | Western blotting .....  | 61        |
| 3.5       | Microscopical analysis .....  | 62        |
| 3.5.1     | Evaluation of PD-L1 staining in pancreatic tissue sections from PDAC patients.....    | 62        |
| 3.5.2     | Cellular confluency analysis .....  | 63        |
| 3.6       | Statistical analysis.....   | 64        |

---

|   |           |
|---|-----------|
| <b>4. Results</b> .....   | <b>65</b> |
| 4.1 <i>In situ</i> characterization of PD-L1 expression in PDAC tissue .....  | 65        |
| 4.1.1 Pancreatic tumor tissues from PDAC patients displays high heterogeneity in terms of PD-L1 staining in various tumor compartments.....                                   | 66        |
| 4.1.2 PD-L1 staining is characteristic for malignancy-associated desmoplastic but not healthy pancreatic tissue .....   | 68        |
| 4.1.3 PD-L1 staining correlates with patient survival and tumor differentiation grade.....  | 69        |
| 4.1.4 PD-L1 staining is predominantly located to stromal but not neoplastic cells in PDAC .....   | 71        |
| 4.1.5 Comprehensive IHC-based determination of PD-L1 status in PDAC by POLE Score .....   | 72        |
| 4.1.6 POLE Score correlates with a pattern of immunological markers that characterizes a distinct cellular tumor stroma composition .....                                     | 74        |
| 4.1.7 PD-L1 staining in PDAC tissues is predominantly found within distinct tumor regions and associated with a local accumulation of specific immune cell populations .....  | 77        |
| 4.1.8 Tumor-associated macrophages represent one of the major PD-L1 expressing stromal cell populations in PDAC .....   | 80        |
| 4.2 <i>In vitro</i> analyses on the immune-regulatory role of PD-L1 in co-culture settings that resemble cellular compositions in PDAC tissues .....                          | 82        |
| 4.2.1 Premalignant pancreatic ductal epithelial cell lines and most PDAC cell lines exhibit basal surface expression of PD-L1 but not PD-1.....                               | 82        |
| 4.2.2 IFN $\gamma$ is the strongest inducer of PD-L1 expression in pre-malignant PDEC and most PDAC cell lines .....  | 83        |
| 4.2.3 GM-CSF differentiated M1-like polarized primary human macrophages exhibit remarkable PD-L1 surface expression levels.....   | 86        |
| 4.2.4 GM-CSF, M-CSF and IFN $\gamma$ are potent inducers of PD-L1 expression in human macrophages .....   | 88        |
| 4.2.5 Characterization of T lymphocyte activation status after stimulation with CD3- and CD28-targeting antibodies .....  | 90        |
| 4.2.6 Isolation and activation of CD8 <sup>+</sup> T lymphocytes from whole lymphocyte population for subsequent co-culture experiments .....                                 | 99        |
| 4.2.7 M1 M $\Phi$ and activated autologous CD8 <sup>+</sup> T lymphocytes exhibit a more distinct phenotype after direct co-culture compared to mono-culture conditions ..... | 104       |
| 4.2.8 PD-L1 cell surface levels of PDAC cells might affect activation the status of pre-activated CD8 <sup>+</sup> T lymphocytes.....   | 110       |
| 4.2.9 Co-culture of activated CD8 <sup>+</sup> T lymphocytes with PancTu-I cells and M1 M $\Phi$ .....  | 113       |

---

|           |  |             |
|-----------|--|-------------|
| 4.2.10    | Application of Durvalumab does not affect the phenotype and proliferation but PD-L1 cell surface levels and cytokine secretion profile of mono-cultured activated CD8 <sup>+</sup> T lymphocytes ..... | 124         |
| 4.2.11    | Durvalumab application in direct co-cultures markedly alters PD-1 cell surface levels of CD8 <sup>+</sup> T lymphocytes and PD-L1 cell surface levels in both M1 MΦ and T lymphocytes .....            | 127         |
| 4.2.12    | Durvalumab treatment has only minor effects on CD8 <sup>+</sup> T lymphocytes and PancTu-I cells in direct co-culture settings .....   | 136         |
| <b>5.</b> | <b>Discussion.....</b>   | <b>145</b>  |
| 5.1       | Classification of the PD-L1 status by immunohistochemistry in general and as a prognostic biomarker in PDAC .....  | 145         |
| 5.2       | The clinical potential PD-1 and PD-L1 antagonists for the treatment of PDAC patients .....   | 153         |
| 5.3       | Intrinsic regulation and cell-specific role of PD-L1 .....   | 157         |
| 5.4       | Correlation between tumor infiltration by CTLs, PD-L1 expression and efficiency of PD-1/PD-L1 targeted therapies as well as tumor progression .....  | 164         |
| 5.5       | Qualitative assessment of the established <i>in vitro</i> setting's capacity to resemble <i>in vivo</i> relevant cellular phenotypes and cellular interactions .....                                   | 170         |
| <b>6.</b> | <b>Conclusion .....</b>  | <b>181</b>  |
|           | <b>References .....</b>  | <b>182</b>  |
|           | <b>List of Figures .....</b>   | <b>220</b>  |
|           | <b>List of Tables.....</b>   | <b>237</b>  |
|           | <b>Supplementary Data .....</b>  | <b>i</b>    |
|           | Supplementary Tables .....   | i           |
|           | Supplementary Figures .....  | iv          |
|           | <b>Declaration on oath .....</b>   | <b>vii</b>  |
|           | <b>Acknowledgements.....</b>   | <b>viii</b> |
|           | <b>Curriculum Vitae .....</b>  | <b>x</b>    |
|           | <b>Original Publications .....</b>   | <b>xii</b>  |
|           | <b>Conference Paper .....</b>  | <b>xiii</b> |

# 1. Introduction

## 1.1 Pancreatic ductal adenocarcinoma

### 1.1.1 Epidemiology

Pancreatic ductal adenocarcinoma (PDAC) represents the 14<sup>th</sup> most common cancer entity worldwide. In 2018, 458,918 new PDAC have been estimated, accounting for 2.5 % of all cancer diagnoses [1]. Despite its low incidence rate, PDAC ranks at the 7<sup>th</sup> place of cancer associated deaths worldwide by accounting for 432,242 estimated deaths in 2018 (4.5 % of all cancer-related deaths worldwide) [1]. With a poor 5-year survival rate of 5 %, PDAC is one of the most fatal malignancies [2]. The high mortality associated with PDAC is mainly attributed to the lack of reliable tests or markers for early detection of the disease as well its unspecific symptoms. Thus, over 80 % of patients suffering from PDAC are diagnosed at an advanced stage of the disease when primary tumors are either unresectable or have formed metastases in other organs, which are preferentially localized to nearby lymph nodes (stage II B) or the liver and the lung (stage III + IV) [3]. Therefore, surgical resection of locally restricted tumors is currently the only curative treatment for PDAC. However, even patients who undergo curative pancreatectomy with tumor-free surgical margin (R0 resection) only show a median survival of 12.6 months [4].

In Germany, PDAC is even the 4<sup>th</sup> most common cause of cancer-related deaths among both men (6.8 % of cancer deaths) and women (8.2 % of cancer deaths) with incidence rates of 21.6 (men) and 20.8 (women) per 100,000 persons. With a median age at diagnosis of 72 in men and 75 in women, PDAC onset is clearly associated with an advanced age (Robert Koch-Institut; Zentrum für Krebsregisterdaten, Stand 2013/2014).

Nevertheless, due to the lack of clinical progress in early detection and treatment of advanced PDAC stages in comparison to other cancer entities as well as the demographic shifts, PDAC is estimated to become the 2<sup>nd</sup> most common cause of cancer deaths by 2030 [5].

### 1.1.2 Etiology

Only about 10 % of PDAC cases can be referred to a hereditary component. For example, hereditary pancreatitis is associated with a cumulative lifetime risk for PDAC development of 40 % to 70 %. [3,6]. Notably, since a chronically inflamed microenvironment represents a general driver of malignant transformation, also sporadic chronic pancreatitis is a major risk factor for PDAC. Hence, Raimondi and colleagues demonstrated that chronic pancreatitis is associated with a relative risk of 13.3 for PDAC [7].

In contrast to hereditary factors, 90 % of PDAC cases originate from sporadic disease onset, which is assumed to be mainly attributed to life style factors [3,6]. Major life style-associated risk factors include tobacco abuse and excessive alcohol consumption [8–12]. Moreover, the onset of chronic metabolic disorders like diabetes mellitus and severe obesity are associated with an increased risk for developing PDAC [13,14].

### 1.1.3 Pathogenesis

PDAC arises from the ductal epithelium in the exocrine compartment of the pancreas and represent with 95 % the major type of pancreatic malignances [3]. Histological and molecular biological studies have identified three types of precursor lesions for PDAC, namely mucinous cystic neoplasia (MCNs), intraductal mucinous cystic neoplasia (IPMNs) and pancreatic intraepithelial neoplasia (PanINs) [15]. Among these, PanINs are the best characterized premalignant lesion in the pancreas. Mouse models indicate that PanINs emerge due to genomic alteration-induced ductal reprogramming from different pancreatic cell types, preferentially centro-acinar or ductal epithelial cells [16]. In 2000, Hruban and colleagues proposed a multi-step model for the development of PDAC from PanIN precursor lesions, which classifies based on histological abnormalities three distinct progressive grades, namely PanIN-1A/B, -2 and -3 (**Figure 1**) [16]. According to this model, a higher grade is correlated with increasing morphologic dysplasia. Therefore, PanIN-1A lesions are characterized by tall columnar cells, which form a papillary epithelial architecture in the progression to PanIN-1B stage. In the further progress to PanIN-2 lesion, nuclear abnormalities like crowding and enlargement as well as atypical hyperplasia are observed. PanIN-3 stage exhibits loss of polarity, luminal necroses as well as the formation of a multilayered epithelium. The last step from PanIN-3 stage, also termed as *carcinoma in situ*, to PDAC is the invasive growth beyond the basement membrane [16]

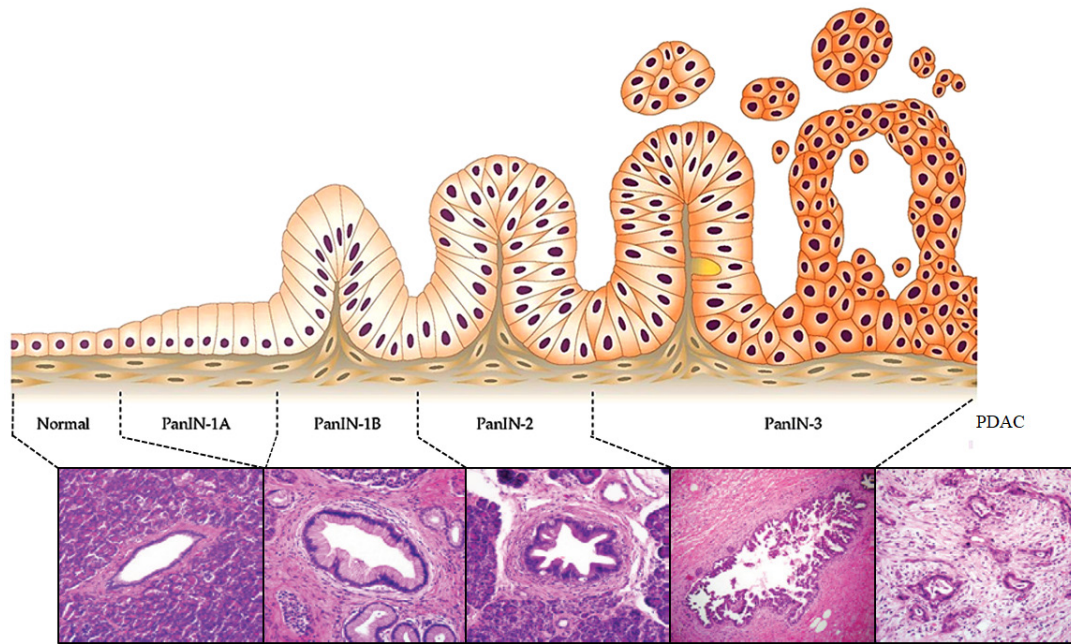


**Figure 1: Pancreatic ductal adenocarcinoma (PDAC) arises from pancreatic intraepithelial neoplasia (PanINs) in a multi-step progress.** Schematic illustration of increasing cellular dysplasia associated with progressive PanIN grade (above) as well as representative hematoxylin and eosin staining images of respective PanIN stages (below) and fully developed PDAC. Adapted from [16,17].

Molecular analyses fostered the assumption that PDAC arises from these three types of precursor lesions [18,19]. Hence, it has been shown that some driver mutations identified in PDAC are already present in distinct PanIN stages. Notably, the number of mutations correlates with increased degree of dysplasia. One of the first and best investigated type of mutations in pancreatic carcinogenesis leads to the constitutive activation of Kirsten rat sarcoma viral oncogene homolog (k-Ras), a 21 kDa guanosine triphosphatase that is essentially involved in the regulation of cell proliferation, differentiation and survival by forwarding mitogen-induced signaling cascades [20,21]. Studies have identified point mutations at codons 12, 13 and 61 of *k-ras* as cause for structural changes, which lead to an impaired inactivation of its GTP-bound active state due to compromised intrinsic GTPase activity [22]. Since preferentially G12V and G12D mutations are already present in more than 90 % of PanIN-1 lesions, constitutive activation of K-Ras is supposed to play a pivotal role in pancreatic carcinogenesis [21]. Further early genomic alterations include the overexpression of HER-2/neu gene and telomere shortening [23,24]. More advanced PanIN stages frequently exhibit inactivating mutations, epigenetic silencing or homozygous deletion of tumor suppressors such as cyclin-dependent kinase inhibitor 2A (p16<sup>INK4A</sup>/CDKN2A), tumor protein p53 (TP53) and breast cancer 2 early onset gene (BRCA2) [25]. Next to TP53, p16<sup>INK4A</sup> and BRCA2, a large proportion of PanIN-3 lesions and PDACs exhibit resistance towards Transforming Growth Factor-beta (TGF- $\beta$ )-induced cell cycle arrest due to either homozygous deletion or mutations in mothers against



decapentaplegic homolog 4 (SMAD4/DPC4) gene, a downstream mediator of TGF- $\beta$  signaling, or TGF- $\beta$  receptor II [26]. Nevertheless, these well-known mutations represent just a small proportion of genomic alterations acquired during the development of PDAC. In 2012, a large exome sequencing project identified 2016 non-silent mutations and 1628 copy-number variations in a cohort of 142 PDAC patients [27]. Highlighting the clinical relevance of individual genomic alteration patterns, correlational studies on transcriptional profiles identified three distinct PDAC subtypes, which differently responded to current chemotherapeutic regimens [28]. However, in comparison to other cancer entities, PDAC displays a very low median tumor mutational burden [29].

#### **1.1.4 Epithelial to mesenchymal transition in PDAC progression**

Epithelial to mesenchymal transition (EMT) is a central process in embryogenesis, wound healing and tissue regeneration [30–32]. Besides these physiological relevant processes, EMT has been shown to play a pivotal role in the progression and metastasis of solid tumors such as PDAC [33–35]. Basically, EMT is characterized by the loss of apical-basal polarity, decomposition of cell-cell contacts and reorganization of the cytoskeleton in epithelial cells. Morphologically, this process goes along with the acquisition of an elongated spindle-shaped morphology and front-rear polarization [36,37]. On a functional level, EMT enables former epithelial cells to acquire a motile phenotype. This phenotype allows them to exit their epithelial network without the induction of anoikis, a form of programmed cell death in epithelial cells that lose their contact to the basement membrane, and invade into the surrounding tissue [30]. On the molecular level EMT is associated with the downregulation/loss of epithelial proteins, e.g. E-cadherin, claudins and cytokeratins, and the upregulation/gain of mesenchymal proteins, e.g. vimentin, L1CAM, N-cadherin and fibronectin [32,38]. This commonly reversible switch in gene expression is most frequently mediated by transcription factors of the Snail, ZEB and basic helix-loop-helix family as well as micro RNAs (miRNA), but rarely by mutations or gene deletions [38–41]. In PDAC, an EMT phenotype in neoplastic cells has been correlated with poor patient prognosis [34,42]. As key drivers of EMT induction oncogenic K-Ras signaling as well as tumor-associated inflammation and hypoxia have been identified, which all represent characteristics of PDAC [43–46]. In terms of tumor-associated inflammation, especially cytokines secreted by tumor-associated macrophages (TAMs) and tumor-infiltrating lymphocytes (TILs) like TGF- $\beta$ , Tumor Necrosis Factor alpha (TNF $\alpha$ ), Interleukin-1-beta (IL-

1 $\beta$ ), Interleukin-6 (IL-6) and Interferon gamma (IFN $\gamma$ ) have been shown to exhibit great EMT-inducing potential (**Figure 2**) [47–52].

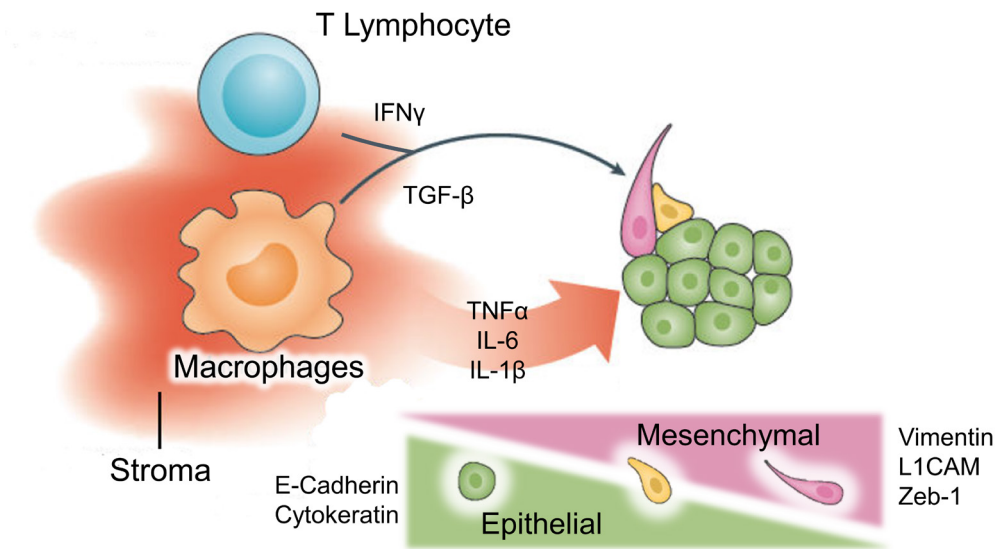


**Figure 2: Epithelial to Mesenchymal Transition is induced by an inflammatory microenvironment.** Schematic illustration of EMT induction in epithelial tumor cells due to T lymphocyte secreted IFN $\gamma$  as well as TGF- $\beta$ , TNF $\alpha$ , IL-6 and IL-1 $\beta$  produced by tumor-associated macrophages. EMT progression goes along with the loss/downregulation of epithelial protein expression (E-cadherin and cytokeratin) and simultaneous induction of mesenchymal proteins' expression (vimentin and L1CAM) as well as activation of transcription factors like Zeb-1. Adapted from [45].

In the last decades, the regulation of various EMT markers have been studied in PDAC and some of these proteins have been verified to play a functional role in promoting the motility of PDECs *in vitro* as well as the dissemination and metastasis formation of PDAC cells *in vivo* [53]. In order to name a few, the loss or downregulation of E-cadherin expression, the acquisition of vimentin and L1CAM expression as well as the transcriptional activity of Zeb-1 have been shown to be associated with EMT induction, increased motility and dissemination in PDAC [41,54–59]. Interestingly, Rhim and colleagues showed that EMT induction followed by dissemination of PDECs is not exclusively a late stage phenomenon in PDAC, but occurs already in precursor lesions – a finding that has revolutionized the general understanding of EMT in the time course of PDAC progression [56,60].

## 1.2 Tumor stroma in PDAC

PDAC is characterized by a dense stromal reaction, termed desmoplasia, which constitutes up to 90 % of the tumor volume [61]. This stromal compartment comprises both cellular and non-cellular components. Prominent cell populations in the tumor stroma of PDAC are pancreatic stellate cells (PSCs) and cancer-associated fibroblasts (CAFs) as well as various leukocyte populations like TAMs, myeloid-derived suppressor cells (MDSCs), neutrophil granulocytes and TILs, e.g. regulatory T lymphocytes (Tregs), T helper lymphocytes and cytotoxic T lymphocytes (CTLs) [62].

The non-cellular compartment consists of tightly packed extracellular matrix (ECM) molecules like collagens I and III, fibronectin, laminins, glycosaminoglycans and thrombospondin, but also cytokines, chemokines and growth factors, e.g.  $\text{IFN}\gamma$ ,  $\text{TNF}\alpha$ ,  $\text{TGF-}\beta$ , Interleukin-8 (IL-8), Vascular Endothelial Growth Factor (VEGF) and Epidermal Growth Factor (EGF) (**Figure 3**) [62,63].

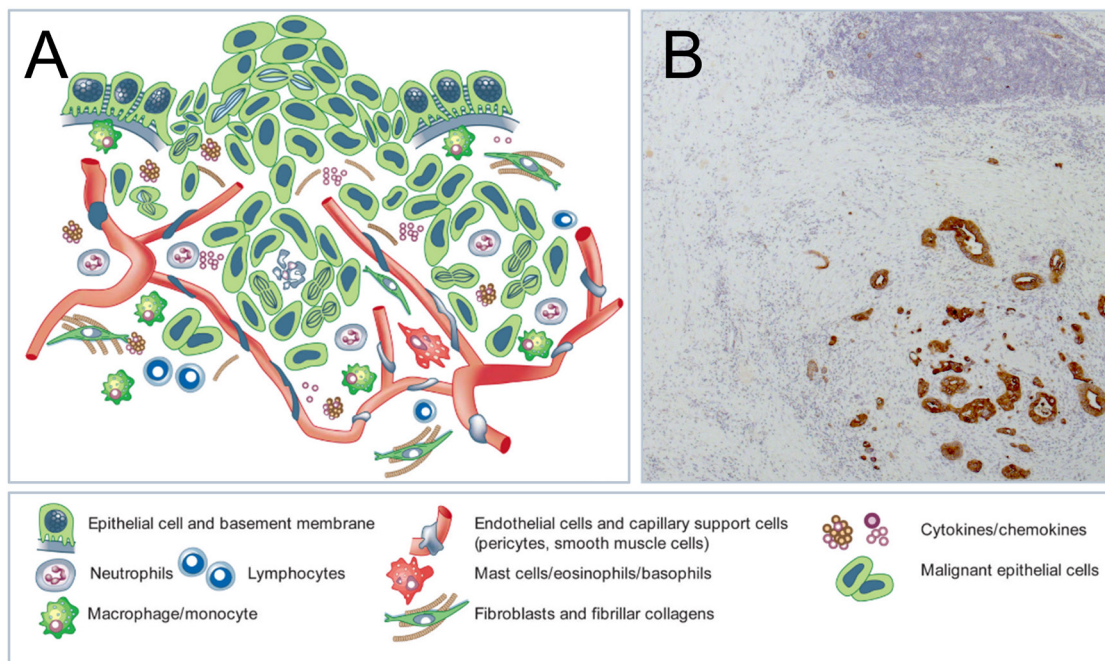


**Figure 3: Tumor- and stromal compartment in pancreatic ductal adenocarcinoma.** (A) Schematic illustration of the cellular and non-cellular compartments in PDAC. Adapted from [64]. (B) Representative image of a formalin-fixed paraffin-embedded PDAC tissue section stained for pan-cytokeratin (brownish). Nuclei were stained with hematoxylin (violet).

Based on the enhanced deposition of ECM components as well as the high infiltration by various cell populations, both tumor stiffness and interstitial fluid pressure are increased, which in turn causes poor vascularization and formation of hypoxic areas. As a consequence, PDAC tumors often display large necrotic areas [65].

Several studies indicate that the complex tumor stroma and its microenvironment play a central

role in promoting tumor aggressiveness and therapy resistance of PDAC [62,63,66]. In contrast, Rhim and colleagues showed in a PDAC mouse model that stroma depletion was associated with an even more aggressive tumor progression [67]. Taken together, the role and prognostic relevance of the tumor stromal compartment in PDAC are controversially discussed.

In the following sections, TAMs and CTLs will be introduced in more detail, since both leukocyte populations play a central role in the present study.

## **1.2.1 (Tumor-associated) macrophages**

### **1.2.1.1 Origin and functional polarization of macrophages**

Macrophages are specialized phagocytotic cells with antigen-presenting properties that link innate and adaptive immunity. Tissue resident macrophages are present in almost every tissue of the human body, while infiltrated macrophages differentiate from monocytes that originate from bone marrow-derived myeloid progenitor cells [68,69]. Macrophages display a leukocyte population of high functional diversity and cellular plasticity. The functional differentiation status of macrophages is mainly attributed to the stimuli provided by the respective microenvironment they infiltrate into. In the process of wound healing, macrophages orchestrate every step from initiation of an immune response via tissue repair to reestablishment of tissue homeostasis [70]. In order to adapt their function to the needs of the respective microenvironment, macrophages exhibit a broad spectrum of both cell surface- and intracellular-located receptors for DNA, RNA, lipids and polysaccharides as well as cytokines, chemokines and growth factors. These include for example lipopolysaccharide (LPS)-binding receptor CD14 [71], the scavenger receptor CD163 [72] and the mannose receptor CD206 [68,73]. Macrophages play an essential role in the activation of T lymphocytes. For this purpose, phagocytosed molecules are intracellularly degraded, loaded onto either major histocompatibility complex (MHC) class II or via cross-presentation onto MHC class I molecules and presented at nearby lymph nodes to naïve T lymphocytes to induce clonal expansion of antigen-specific effector T lymphocytes [68]. According to the T lymphocyte nomenclature, macrophages exhibiting a pro-inflammatory polarization are termed M1-macrophages [74]. Molecules inducing this classical activated phenotype include among others various bacterial products like glycoproteins or LPS as well as IFN $\gamma$  and Granulocyte Macrophage-Colony Stimulating Factor (GM-CSF) [70]. M1-like polarized macrophages are characterized by the secretion of pro-inflammatory cytokines (e.g. IL-1 $\beta$ , TNF $\alpha$ , Interleukin-12 (IL-12) and Interleukin-23 (IL-23)) and chemokines (e.g. CXCL9, CXCL10, CXCL11 and

CCL2), which promote an inflammatory immune response by recruitment and activation of monocytes, dendritic cells, neutrophil granulocytes, T lymphocytes, B cells and NK cells (**Figure 4**) [70,75].

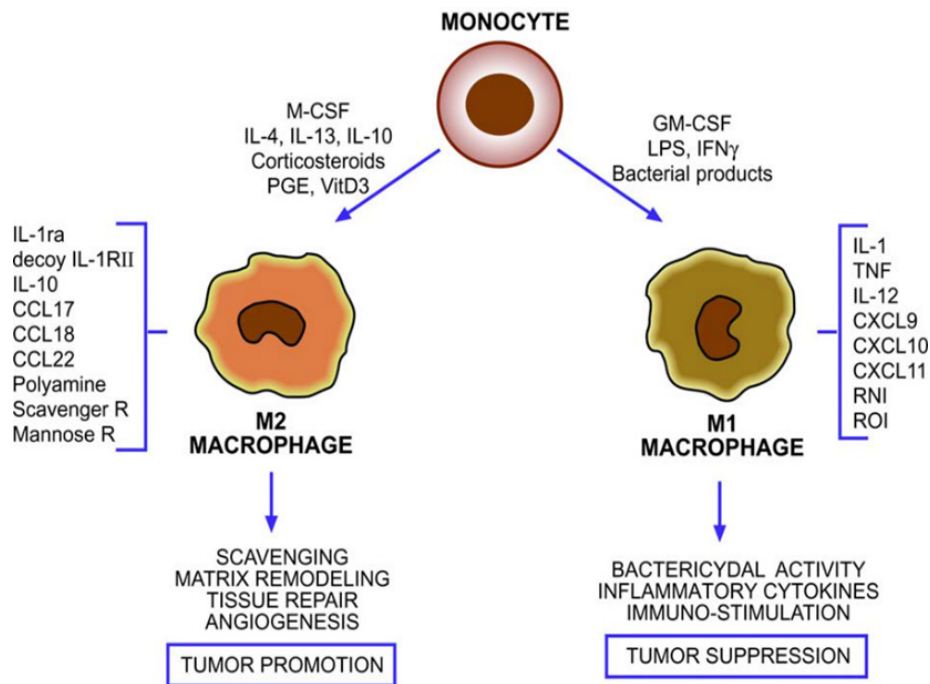


**Figure 4: Monocytes differentiate into various subsets of macrophages in dependence of the respective microenvironment.** Monocytes differentiate by stimulation with M-CSF, anti-inflammatory cytokines (e.g. IL-4, IL-13 and IL-10) as well as corticosteroids, prostaglandins and vitamin D3 into an anti-inflammatory M2-macrophage type. GM-CSF, IFN $\gamma$  as well as LPS or other bacterial products lead to the differentiation of a pro-inflammatory M1-phenotype. Both phenotypes differ regarding their gene expression profile and resulting functions. Adapted from [76].

Besides their pro-inflammatory qualities, macrophages also contribute to damping and termination of acute inflammation by a process termed phenotype switch. This process, which represents a critical turning point between acute and chronic inflammation, is induced by phagocytosis of cellular debris and apoptotic neutrophils and characterized by the upregulation of anti-inflammatory cytokine expression [70]. Hence, this gradually switch in macrophages' gene expression profile leads to a positive feedback loop that causes the acquisition of an alternatively activated phenotype, termed M2 polarization. Soluble factors that promote M2-like macrophage polarization are Macrophage Colony-Stimulating Factor (M-CSF), Interleukin-4, -10 and -13 as well as corticosteroids, prostaglandins and vitamin D3 [74,77]. M2-polarized macrophages are characterized by the secretion of anti-inflammatory cytokines like IL-1 receptor antagonist (IL-1ra), TGF- $\beta$ 1 and IL-10, Th2 response-promoting chemokines CCL17, CCL18 and CCL22 as well as high cell surface levels of CD163 and CD206 [73,78]. Moreover, M2-polarized macrophages promote cell proliferation, tissue vascularization and remodeling by the secretion of growth factors like EGF and VEGF as well as the synthesis of

polyamines and various matrix-metalloproteases (MMPs) (**Figure 4**). Not at least because of this secretome profile, M2- rather than M1-polarized TAMs are considered to promote tumor progression [74,76,79,80].

### 1.2.1.2 Tumor-associated macrophages in PDAC

Tumor-associated macrophages represent one of the dominant stromal cell populations in PDAC [81]. In general, PDAC cells have been shown to produce a great variety of chemokines and growth factors that attract monocytes from the vascular system. These factors include amongst others CCL2, -3, -4, -5 and -12 as well as M-CSF and VEGF [82,83]. For example, Monti and colleagues showed that serum CCL2 levels from PDAC patients significantly correlated with macrophage tumor infiltration. They also demonstrated that pancreatic ductal epithelial cells (PDECs) in PDACs secreted higher amounts of CCL2 in a synergistic manner by IFN $\gamma$ , TNF $\alpha$  and IL-1 $\beta$  stimulation than those PDECs from healthy tissues [84]. Monocytes recruited into the tumor are assumed to be driven into an M2-polarization due to the tumor-associated microenvironment [79]. As outlined in **section 1.2.1.1**, M2-polarized TAMs secrete various cytokines, chemokines and other molecules that potentially promote malignant progression. Indeed, several studies indicate that high numbers of infiltrated TAMs correlate with a worse prognosis in PDAC. Hence, Kurahara and colleagues showed that an increased presence of CD163<sup>+</sup> and CD204<sup>+</sup> macrophages correlates with high incidence of lymph node metastases and poor prognosis [80]. Moreover, a study by Zhu and colleagues indicated that blockade of CSF1R, the receptor for M-CSF, results in decreased metastases formation in a PDAC mouse model [85]. Other studies revealed that targeting both CSF1R and CCR2 results in a decrease of TAMs and simultaneously increase of CD8<sup>+</sup> T cells in PDAC stroma correlating with an improved response towards chemotherapy [86,87]. However, in contrast to the general assumption that TAMs commonly display an M2-polarized phenotype, a study by Helm and colleagues indicated that TAMs in PDAC rather exhibit a mixed phenotype comprising both M1- and M2-properties. Additionally, they provided evidence that isolated TAMs from PDAC tissues possess the ability to induce EMT in PDAC cells *in vitro* [58,88].

In summary, these and other studies indicate that TAMs play an important role in progression and therapy resistance of PDAC. Therefore, interfering with monocyte recruitment, repolarization of TAMs as well as blocking of TAM-associated cytokines is the aim of newly designed treatment strategies for PDAC in several current clinical trials (NCT03767582, NCT02550327, NCT02583477).

### 1.2.2 Tumor-infiltrating T lymphocytes

T lymphocytes are a highly abundant leukocyte population in the stroma of PDAC that shows increased infiltration along with disease progression from early precursor lesions to invasive carcinoma [89,90]. However, T lymphocyte populations also display high phenotypic and functional diversity that is defined by the maturation process from naïve CD8<sup>+</sup> or CD4<sup>+</sup> T lymphocytes into respective subsets [68]. In the concept of cancer immunoediting, CD8<sup>+</sup> CTLs, CD4<sup>+</sup> T helper lymphocytes and Tregs are regarded as the key T cell subsets that essentially contribute to tumor elimination and escape, respectively. Therefore, the overall presence as well as the proportion of each subset in tumor tissues are associated with better or worse patient prognosis in several tumor entities [91].

CD8<sup>+</sup> T lymphocytes represent the primary cytotoxic T lymphocyte subset that mediates lysis of virus infected, damaged and neoplastic cells. Upon T cell receptor (TCR)-specific activation in secondary lymphoid organs and clonal expansion (introduced in **section 1.3**), CD8<sup>+</sup> CTLs intravasate into the circulation and extravasate through activated endothelium into the target tissue. Within infiltrated tissues CD8<sup>+</sup> CTLs search for cells that present the respective TCR-specific antigens via major histocompatibility complex (MHC) class I molecules. Binding to target cells results in the formation of an immunological synapse, in which CD8<sup>+</sup> CTLs release cytotoxic effector molecules like Perforin, Granzyme A, Granzyme B, soluble Fas ligand and Granulysin that either cause direct target cell lysis or induction of apoptosis via activation of effector caspases [68]. Moreover, activated CTLs secrete IFN $\gamma$ , which has been shown to induce antigen presentation via MHC class I/II molecules as well as cell cycle arrest in target cells [92,93].

CD4<sup>+</sup> T helper lymphocytes represent a way more diverse T lymphocyte subset than CD8<sup>+</sup> CTLs. Like monocyte differentiation and macrophage polarization, their functional differentiation is essentially conducted by the cytokine composition provided by the respective microenvironment. For the acquisition of a TH1, TH2, TH17 or Treg phenotype, especially IL-2, IL-4, IL-6, IL-12, IFN $\gamma$  and TGF- $\beta$  levels, respectively, are important (**Figure 5**) [94]. In general, all CD4<sup>+</sup> T helper lymphocyte subsets play a critical role in the regulation of immune responses and, therefore, hold both pro- and anti-inflammatory potential [95]. Notably, TH1 CD4<sup>+</sup> T helper lymphocytes are a major source of IL-2, which is crucial for proliferation and survival of CD8<sup>+</sup> CTLs [68].

Regulatory T lymphocytes originate either from naïve FoxP3 Tregs (natural Tregs) or differentiate from naïve CD4<sup>+</sup> T lymphocytes (induced Tregs). Generally, Tregs display an immunosuppressive phenotype. In contrast to CD8<sup>+</sup> CTLs, Tregs recognize self-antigens in

order to maintain self-tolerance, regulate inflammatory responses and restore tissue homeostasis [68]. On the molecular level, Tregs are characterized by the phenotypic markers  $CD4^+$ ,  $CD25^+$ ,  $FoxP3^+$ ,  $CTLA-4^+$  and  $GITR^+$  as well as the secretion of IL-10 and TGF- $\beta$  [96].

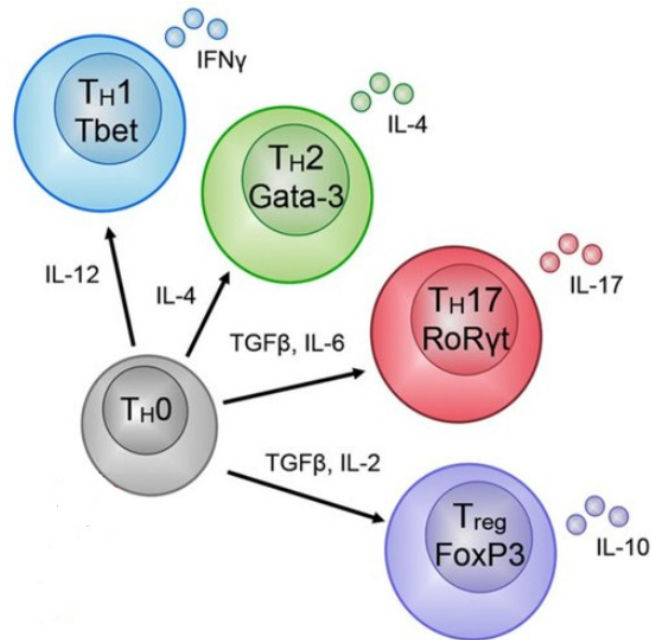


**Figure 5: Schematic illustration of T helper cell maturation into functionally different subsets by various cytokines.**  $T_{H0}$  helper cells differentiate upon activation in dependence on cytokines present in the respective microenvironment into  $T_{H1}$ ,  $T_{H2}$ ,  $T_{H17}$  or Treg cells. Key transcription factors that render these functional phenotypes are Tbet, Gata-3, RoRyt and FoxP3, respectively. Adapted from [97]

PDAC is regarded as a poorly immunogenic tumor, also termed cold tumor, based on its low median tumor mutational burden that results in scarce overall amount of neoantigens as well as its immunosuppressive tumor microenvironment [98]. Therefore, several studies indicated that high infiltration by  $CD8^+$  T lymphocytes significantly correlates with better patient prognosis in terms of post-surgical survival and overall survival as well as slower tumor progression in endogenous PDAC mouse models [89,99–102]. However, overall  $CD8^+$  T lymphocyte infiltration in PDAC is commonly low. Hence, a study by Fukunaga and colleagues showed that only 13 of 80 PDAC specimens (16.3 %) exhibited a pronounced tumor infiltration by  $CD8^+$  T lymphocytes [89]. Furthermore, they and others found that not  $CD8^+$  T lymphocytes' abundance alone but concurrently high infiltration by  $CD4^+$  T lymphocytes is associated with a better prognosis [89,99,102]. The synergic effect of  $CD4^+$  and  $CD8^+$  T lymphocytes' interaction in promoting an improved anti-tumor response has been also described by Marzo and colleagues as well as Huang and colleagues [103,104]. However, it is still controversially discussed which factors contribute to T lymphocyte exclusion in PDAC. Besides the non-



cellular compartment within desmoplastic reaction, which provides a physical barrier for T lymphocyte infiltration into the tumor, a number of stromal cell populations have been shown to participate in the establishment of an immunosuppressive microenvironment that leads to both exclusion and inactivation of tumor-reactive T lymphocytes. These stromal cell populations include pancreatic stellate cells, CAFs, MDSCs, TAMs and Tregs [90,100,105–108]. In this context, a study in an endogenous PDAC mouse model indicated that at the stage of invasive carcinoma MDSCs and Tregs cause the inactivation of tumor-infiltrating CTLs [90].

### 1.3 T lymphocyte maturation and priming

T lymphocytes originate from lymphoid progenitor cells that derive in the bone marrow and migrate to the thymus, the central organ for T lymphocyte maturation [109]. Only in the thymus, these lymphoid progenitor cells are primed for the development into T lymphocytes by stromal signals that induce the activation of genes essential for TCR expression [110]. The expression and activation of enzymes associated with this T lymphocyte specific genetic program leads to the induction of a process termed V(D)J recombination, a clone-specific somatic rearrangement of variable (V), diversity (D) and joining (J) gene segments that causes the diversity in the TCR repertoire of estimated up to  $10^{15}$  different variants [111]. Besides the genetic arrangement of TCR variants, this process goes along with differentiation into two T lymphocyte subsets, those that exhibit a TCR composed of an alpha and a beta subunit ( $\alpha\beta$  T lymphocytes) and those exhibiting a TCR composed of a gamma and a delta subunit ( $\gamma\delta$  T lymphocytes) [112]. Moreover, during this process so called “double-negative”  $\alpha\beta$  T lymphocytes ( $\text{TCR}^- \text{CD3}^- \text{CD4}^- \text{CD8}^-$ ) develop into “double-positive”  $\alpha\beta$  T lymphocytes ( $\alpha\beta\text{TCR}^+ \text{CD3}^+ \text{CD4}^+ \text{CD8}^+$ ) that express both CD4 and CD8 co-receptor [113]. Afterwards, “double-positive”  $\alpha\beta$  T lymphocytes undergo a maturation step termed positive selection. At this step, T lymphocytes are confronted with MHC presented self-antigens by the thymus stromal cells. Only T lymphocytes that recognize these self-antigens presented by self-MHC complexes pass this selection step, while T lymphocytes that do not undergo apoptosis [114,115]. This step is important to eliminate T lymphocytes with a TCR variant that potentially recognizes antigens presented by non-self MHC complexes. Moreover, during this step the  $\text{CD4}^+ \text{CD8}^-$  and  $\text{CD4}^- \text{CD8}^+$  T lymphocyte lineages emerge, because TCR variants that bind to antigens presented by MHC class I molecules only need the CD8 co-receptor for stabilization of the interaction while TCR variants that recognize antigens in a MHC class II dependent manner only need the co-receptor CD4 [116]. In the final maturation step within the thymus, T lymphocytes are confronted with self-

antigens presented by dendritic cells and macrophages. In this step, termed negative selection, T lymphocytes expressing autoreactive TCR variants are eliminated and only self-tolerant T lymphocytes pass without induction of apoptosis [117]. Mature naïve CD8<sup>+</sup> or CD4<sup>+</sup> T lymphocytes that have passed both positive and negative selection leave the thymus and migrate through the vascular and lymphatic system.

Lymphocyte activation takes place in secondary lymphoid organs, especially the spleen and lymph nodes. Here, naïve T lymphocytes that have migrated into the T cell zone of the respective peripheral secondary lymphoid organ encounter antigen-presenting cells (APCs) (dendritic cells and macrophages), which present pre-processed antigens with a size of either 8-10 amino acids or 13-25 amino acids in an MHC-I and MHC-II dependent manner, respectively [118]. Notably, the cellular origin of antigens presented via MHC-I and MHC-II complexes differs from each other. Hence, intracellular antigens are predominantly presented via MHC-I and extracellular phagocytosed antigens are mainly associated with MHC-II molecules. However, extracellular antigens can also be presented in an MHC-I dependent context and intracellular antigens also via MHC-II by a process termed cross presentation [119,120]. Overall, there are three types of signals that are needed to be delivered by the APC in order to prime a T lymphocyte (**Figure 6**). The first signal, also termed activation signal, is conducted via TCR specificity for the respective peptide-MHC complex presented by the APC. Binding of the TCR-CD3 complex to the peptide-MHC complex leads to additional linkage via CD4 and CD8 binding to the conserved region of the peptide-MHC complex, respectively [121].

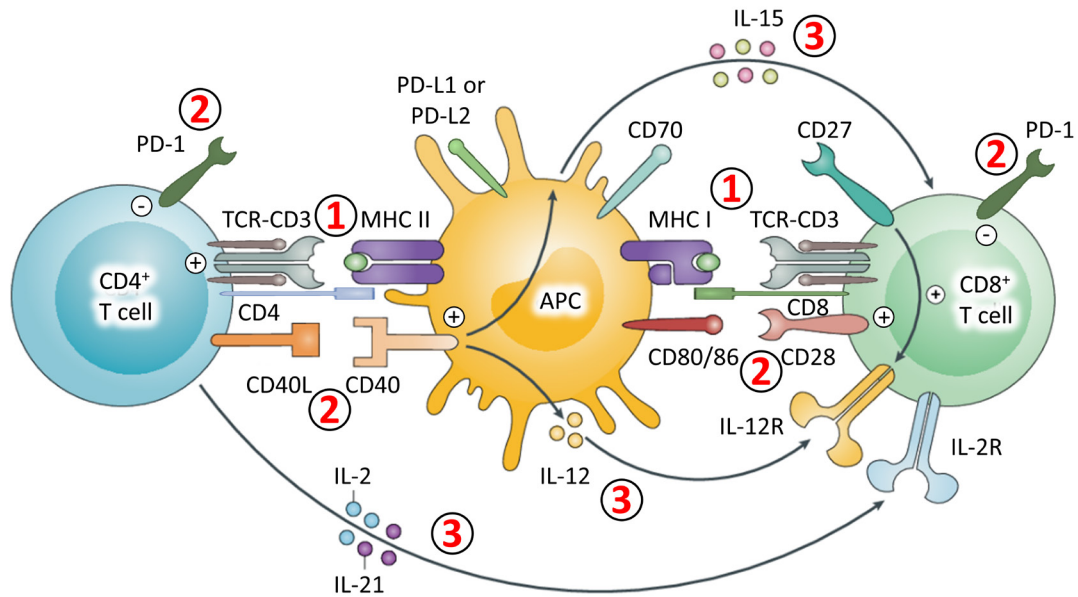


**Figure 6: Three types of signals are necessary for the priming of CD4<sup>+</sup> T helper lymphocytes and CD8<sup>+</sup> cytotoxic T lymphocytes by antigen-presenting cells in the secondary lymphoid organ.** Schematic illustration of the interaction between antigen-presenting cells (APC) and CD4<sup>+</sup>/CD8<sup>+</sup> T cells in the process of T lymphocyte priming. The first signal (1) provided by APCs is the pre-processed MHC-loaded antigen, which is presented via MHC-II or MHC-I to CD4<sup>+</sup> and CD8<sup>+</sup> T cells, respectively. Binding of peptide-MHC complex to antigen-specific TCR variants is accompanied by CD4 and CD8 co-receptor crosslinking, respectively. The second signal (2) is provided by either co-stimulatory (+) or co-inhibitory (-) receptor-ligand binding. Co-stimulatory signals between APCs and T cells are provided by CD40-CD40L, CD28-CD80/CD86 and CD27/CD70 interaction. In contrast, binding of PD-L1 or PD-L2 to its receptor PD-1 impedes T lymphocyte activation. The third signal (3) is mediated via cytokines like IL-2, IL-12, IL-15 and IL-21 that affect T lymphocyte differentiation, proliferation, survival and functional activity. Adapted from [122].

The second signal, also termed survival signal, is provided by co-stimulatory and co-inhibitory receptors and their ligands expressed by both APCs and T lymphocytes. In the recent decades, a wide variety of both co-stimulatory and co-inhibitory molecules have been identified, of which many belong the family of B7 molecules. One of the best characterized co-stimulatory signals for T lymphocyte priming represents the signaling via CD28-CD80/C86 interaction [123,124]. A selection of known co-inhibitory/-stimulatory receptors expressed by T lymphocytes and their respective ligands is listed in **Table 1**. Noteworthy, these molecules play a central role in the regulation of peripheral tolerance since some autoreactive TCR variants cannot be eliminated during negative selection in the thymus due the fact that some antigens are expressed only in distinct organs, e.g. the thyroid gland or the pancreas [125]. Moreover, it has been suggested that some regulators of peripheral tolerance mainly play a role in the priming phase of T lymphocytes within secondary lymphoid organs (e.g. cytotoxic T lymphocyte-associated protein 4 (CTLA-4)) while others rather mediate peripheral tolerance in the effector phase within target tissues (e.g. programmed death protein 1 (PD-1)) [126].

**Table 1: Selection of T lymphocyte expressed receptors and their respective ligands involved in T lymphocyte co-stimulation.** In the column termed “Effect” co-stimulatory interactions are denoted with a “+” and molecules involved in the mediation of co-inhibitory signals are marked with a “-”.

| Receptor       | Ligand(s)                      | Effect | Reference |
|----------------|--------------------------------|--------|-----------|
| CD137 (4-1BB)  | CD137L                         | +      | [127,128] |
| CD152 (CTLA-4) | CD80, CD86                     | -      | [126,129] |
| CD226          | CD112                          | +      | [130]     |
| CD27           | CD70                           | +      | [131]     |
| CD278 (ICOS)   | ICOSL                          | +      | [132]     |
| CD279 (PD-1)   | PD-L1 (CD274)<br>PD-L2 (CD273) | -      | [133]     |
| CD28           | CD80, CD86                     | +      | [123,124] |
| CD96           | CD155                          | +      | [134]     |
| GITR (CD357)   | GITRL                          | +      | [135]     |
| LAG-3 (CD223)  | MHC-II                         | -      | [136]     |
| OX40 (CD134)   | OX40L                          | +      | [137]     |
| TIGIT          | CD155, CD112                   | -      | [134,138] |
| TIM-3          | Galectin-9, CEACAM1            | -      | [139]     |
| VISTA          | unknown                        | -      | [140,141] |

The third signal for T lymphocyte priming, also termed as differentiation signal, is mediated via cytokines that are secreted by both APCs and T lymphocytes. As depicted in **Figure 5**, these cytokines play an essential role in regulating the functional differentiation of CD4<sup>+</sup> T lymphocytes [97]. Moreover, cytokines secreted by activated APCs and T helper cells, e.g. IL-2, IL-12, IL-15 and IL-21, are indispensable for CD8<sup>+</sup> CTLs to develop their full cytotoxic potential as well as to activate downstream signaling pathways, which maintain proliferation and survival of primed CD8<sup>+</sup> CTLs (**Figure 6**) [142–146].

T lymphocyte clones having successfully undergone priming phase in secondary lymphoid organs start to differentiate and proliferate, a process termed clonal expansion, before they enter the blood circulation and infiltrate into activated target tissues [68,147]. However, all three types of signals needed for T lymphocyte priming are by no means only “yes/no decisions” in terms of signal availability but their efficacy is rather determined by signal duration and composition, both factors that are poorly understood [148,149]. Hence, there is a fine line in T lymphocyte priming between over- and under-stimulation that both end in induction of anergy or apoptosis [125,150].

### 1.3.1 T cell receptor and CD28 co-stimulatory signaling

T lymphocyte activation is a tightly regulated process, in which antigen-specific T lymphocyte clones are primed to either generate an active immune response against foreign or neoantigens or attenuate initiated immune reactions. When these control mechanisms fail, severe autoimmune reactions or harmful chronic inflammatory diseases may occur [151]. On the molecular level, the TCR and its downstream signaling pathways are essential control points for both the priming and effector phase of all T lymphocyte subsets **Figure 7**. In detail, when an APC encounters a T lymphocyte the formation of an immunological synapse is initiated by interaction of various cell-cell adhesion molecules [152–154]. Upon engagement of the TCR with a matching peptide-MHC (pMHC) complex within the center of the immunological synapse, CD4 on CD4<sup>+</sup> and CD8 on CD8<sup>+</sup> T lymphocytes are recruited to the TCR-CD3 complex [155]. These co-receptors foster the interaction between TCR and pMHC complex by binding the conserved region of the respective pMHC complex [156]. Subsequently, actin reorganization around the TCR cluster leads to the recruitment of the protein-tyrosine kinase LCK to the CD4/CD8 co-receptors [157]. LCK catalyzes the phosphorylation of so called immunoreceptor tyrosine-based activation motifs (ITAMs) in the TCR-associated CD3 $\delta$ , CD3 $\epsilon$  and CD3 $\zeta$  chains [158]. In turn, phosphorylation of CD3 ITAMs enables the binding of adaptor protein-tyrosine kinases Fyn and Zap70, which bind to ITAMs in CD3 $\delta/\epsilon$  and CD3 $\gamma$  chains, respectively [159,160]. Hereafter, Fyn and LCK phosphorylate Zap70, which stabilizes Zap70 ITAM binding and causes a conformational switch that leads to Zap70 activation [161–163]. The main target of Zap70 is the transmembrane protein linker for activation of T cells (LAT). In cooperation with LCK, Zap70 catalyzes multiple phosphorylation of LAT, which in turn generates binding sites for docking molecules. Therefore, LAT represents a multimolecular signalosome that provides the basis for distribution and regulation of TCR downstream signaling into various pathways that control cell proliferation, cytoskeleton reorganization as well as the expression of genes associated with respective T lymphocyte functions like cytokines and effector molecules [164]. In summary, essential TCR downstream events include the activation mitogen-activated protein kinase (MAPK) pathway via ERK1/2 phosphorylation as well as the activation of protein kinase C theta (PKC $\theta$ ) and calcineurin (**Figure 7**) [164].

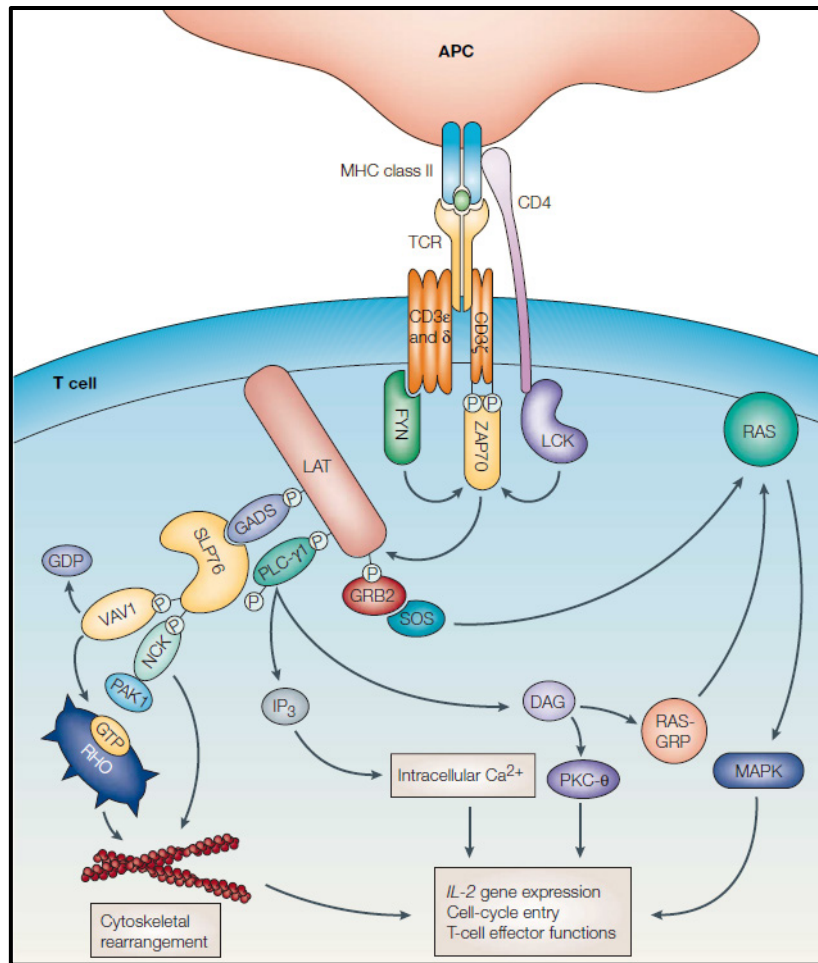


**Figure 7: Signal transduction downstream of the T cell receptor.** In CD4<sup>+</sup> T lymphocytes, T cell receptor (TCR) binding to a complementary peptide-MHC II complex on the surface of an antigen-presenting cell (APC) leads to the recruitment of CD4 co-receptor, which binds to the conserved region of the MHC complex. Subsequently, the protein kinase Lck is recruited to CD4 and phosphorylates CD3 $\epsilon$ , - $\delta$  and - $\zeta$  chains associated with the TCR. This phosphorylation enables binding of adaptor protein kinases Fyn and Zap70 to CD3 chains. Then, Zap70 is activated by Fyn- and Lck-mediated phosphorylation and in turn phosphorylates the linker for activation of T cells (LAT) at multiple sites. These modifications generate binding sites for several other adaptor molecules like GADS, PLC- $\gamma$ 1 and Grb-2, which in turn recruit other adaptor molecules and protein kinases leading to the activation of downstream signaling pathways that initiate cytoskeletal rearrangements, cell proliferation as well as the expression of genes associated with respective T lymphocyte function. Adapted from [165].

As outlined in the previous section, TCR signaling has to be accompanied by a second, co-stimulatory signal in order to accomplish T cell priming. Within this group, co-stimulatory signaling via CD28 represents one of best characterized pathways as well as a prominent target for co-inhibitory signaling pathways that impede T lymphocyte activation, e.g. PD-1 signaling. CD28 supports and amplifies TCR signaling in multiple ways. On the biophysical level, CD28 binding to CD80/CD86 within the immunological synapse fosters T lymphocyte adhesion to the respective APC and, thereby, prolongs TCR-pMHC complex interaction [166]. On the molecular level, the intracellular domain of CD28 provides binding sites for adaptor proteins that contain SH2 and SH3 domains. When phosphorylated by protein-tyrosine kinases like LCK, the membrane proximal YNMN motif enables the binding of phosphoinositide 3-kinases

(PI3K) that catalyze the conversion of PIP<sub>2</sub> into phosphatidylinositol 3,4,5-phosphate (PIP<sub>3</sub>) [167]. PIP<sub>3</sub> functions as an adaptor molecule for protein kinase B (PKB/AKT) and phosphoinositide-dependent kinase 1 (PDK1) that are recruited to the cell membrane. Activating phosphorylation of AKT and PDK1 results in the initiation of downstream signaling pathways relevant in cell survival (Bcl-X<sub>L</sub> and IL-2 expression), acquisition of a glycolytic metabolism due to the activation of PKC $\theta$  and the mammalian target of rapamycin (mTOR) as well as inhibition of the glycogen synthase kinase 3 (GSK3) [168–170]. Moreover, CD28-recruited adaptor kinases initiate the downstream activation and translocation of central transcription factors like Jun, Fos, NF- $\kappa$ B and AP-1 [171] as well as cytoskeletal rearrangements [172–174].

### 1.3.2 Programmed death protein 1 signaling

Programmed death protein 1 (PD-1/CD279) is a type I transmembrane receptor predominantly expressed in activated T lymphocytes and B cells that belongs to the B7 family. There are two known ligands for PD-1, namely programmed death ligand 1 (PD-L1/CD274) and -2 (PD-L2/CD273), which have been shown to be expressed by wide variety of cell populations including dendritic cells and macrophages as well as activated T- and B cells [175]. In contrast to the co-stimulatory effects of CD28-CD80/CD86 interaction, signaling via PD-1 strongly hampers TCR signal transduction and, therefore, PD-1 and its ligands belong to the class of co-inhibitory immune checkpoint regulators [176]. In the last decade, PD-1 signaling attracted particular attention due the fact that aberrant PD-L1 expression by neoplastic cells in several tumor entities has been shown to play a major role in the suppression of T cell mediated anti-tumor responses [177,178]. Although the signal transduction via PD-1 has not been solved in detail yet, recent studies indicate that PD-1 interferes with TCR and CD28 signaling at different levels. Like CD28, PD-1 exhibits an intracellular domain that contains two tyrosine-based adaptor sites, namely a membrane proximal immunoreceptor tyrosine-based inhibitory motif (ITIM) and a C-terminal immunoreceptor tyrosine-based switch motif (ITSM). Phosphorylation of both ITIM and ITSM enables the binding of Src homology 2 domain-containing phosphatases 1 and -2 (SHP1/2), respectively [179,180]. Hence, it has been shown that SHP1 binds to both the ITIM and ITSM, while SHP2 only binds to the ITSM. However, the role of SHP1 and -2 in mediating the direct inhibitory effects of PD-1 signaling is controversially discussed, since SHP2 but not SHP1 has been detected PD-1/TCR signalosome-associated microclusters, but a recent study published by Rota and colleagues indicated that

SHP2 is dispensable for PD-1 signaling in murine CD8<sup>+</sup> T cells [181,182]. Nevertheless, PD-1 has to be ligated and in close proximity to the TCR signalosome within the immunological synapse to deploy its full inhibitory potential. Therefore, it is suggested that PD-1 recruited SHP1/2 preferentially target central downstream mediators of TCR and CD28 signaling like Zap70 and PI3K for dephosphorylation [180]. Besides this direct effect mechanism, PD-1 downstream signaling has been implicated in the downregulation of protein kinase CK2, which in turn is a negative regulator of phosphatase and tensin homolog (PTEN) protein that catalyzes the dephosphorylation of PIP<sub>3</sub> and, therefore, shuts down AKT and PDK1 signaling pathways [183]. Additionally, PD-1 signaling might indirectly contribute to TCR internalization [184], blockade of Zap70 binding to CD3 $\zeta$  [133,185] and PI3K inactivation by upregulation of E3-ubiquitin ligase expression [186]. Finally, PD-1 signaling associated inactivation of MAPK and mTOR signaling has been shown to cause a shift from glycolytic metabolism to elevated  $\beta$ -oxidation, a metabolic state that is commonly associated with an inactive memory T cell phenotype [187].

Nevertheless, there are currently many open questions concerning the molecular mechanisms and the physiological role of PD-1 signaling. In contrast to CD28, PD-1 is constantly expressed only in activated T lymphocytes and clinical trials on PD-1 and PD-L1 antagonists showed less severe immune-related adverse events (IrAE) in comparison to the application of CTLA-4 targeting blocking antibodies [188]. Hence, these data indicate that physiological PD-1 signaling predominantly mediates peripheral tolerance in the effector phase [189]. However, the results from a recent study by Mizuno and colleagues also indicate a role of PD-1 signaling in the priming phase of T lymphocyte activation [190].

## 1.4 Cancer Immunity and Immunotherapy

The immune system is our vitally important shield against both exogenous pathogens, e.g. bacteria, viruses and parasites, and endogenous harms like cancer [68]. Hence, even minor deficits in the maturation or function of innate and adaptive immune cell populations can cause immune compromised phenotypes that face life-threatening conditions when confronted with exogenous and endogenous harms, respectively. In terms of malignant diseases, the concept of cancer immune surveillance and immunoediting summarizes how the immune system on the one hand contributes to the elimination of neoplastic cells but on the other hand also puts pressure on tumor cell evolution, which finally leads to immune escape followed disease manifestation and progression [191]. Therefore, the concept behind cancer immunotherapy is mainly based on the reactivation and boosting of the innate and adaptive anti-tumor responses.



However, in order to achieve these goals, it is necessary to understand at which point the anti-tumor response machinery lacks efficiency or is hampered. Empowered by the enormous progress made in the fields of cell and molecular biology within the last century, we have just started to get an overview of the key steps in the complex regulation of anti-tumor immunity in the last decade. Chen and Mellman summed up our current knowledge in the concept of the Cancer-Immunity Cycle, which classifies seven distinct steps for the induction of an effective anti-tumor response [192]. The first step depicts the release of cancer-associated neoantigens. In the second step, these neoantigens are engulfed, processed and presented via MHC class I/II molecules by APCs like dendritic cells and macrophages. The third step describes the priming and activation phase of antigen-specific T lymphocytes by APCs in nearby lymph nodes. The fourth and fifth step summarize the intravasation of activated T lymphocytes into the blood circulation and their extravasation at the target tissue site. The last and very critical phases include the recognition and subsequent killing of cancer cells by tumor-infiltrating CTLs, which in turn causes the release of more tumor-associated antigens (**Figure 8**) [192].

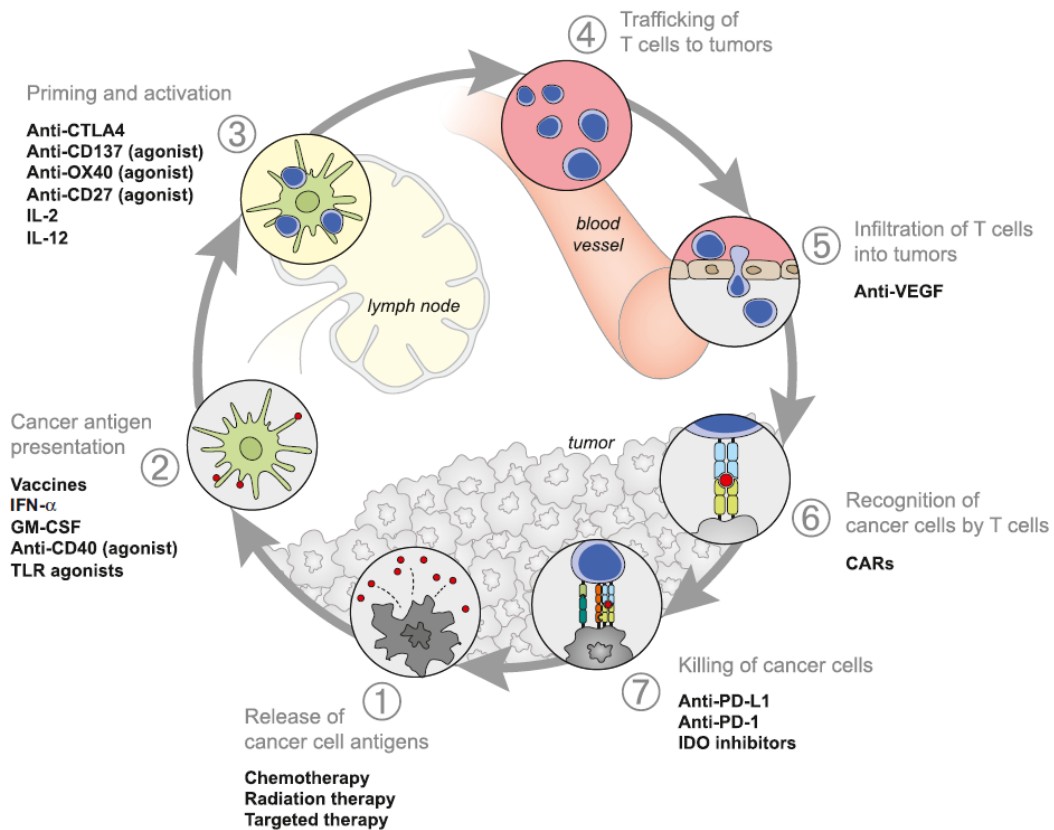


**Figure 8: The Cancer-Immunity Cycle and current (immune-)therapeutic interventions that target each step for reactivation and amplification of the anti-tumor immune response.** Schematic illustration of the seven central steps in the generation of an anti-tumor response by the innate and adaptive immunity (grey). A selection of potential therapeutic strategies to improve each step are listed below (bold black). TLR = Toll-like receptor; IL = interleukin; CARs = chimeric antigen receptor T lymphocytes; IDO = Indoleamine 2,3-dioxygenase. Adapted from [192].

The repertoire of immunotherapeutic approaches compiles a great variety of strategies that each target different steps of the Cancer-Immunity Cycle [192,193]. The currently most extensively studied and targeted steps are the priming and activation phase of tumor-antigen-specific T lymphocytes as well as the recognition and killing phase of neoplastic cells. Here, the targeting of so called immune co-inhibitory checkpoint molecules significantly improved the prognosis for patients suffering from malignant melanoma, non-small cellular lung carcinoma, prostate cancer and many more [194–197]. Hence, James Patrick Allison and Tasuku Honjo were awarded with the Nobel Prize in Physiology or Medicine in 2018 for the discovery of cytotoxic T lymphocyte-associated protein 4 (CTLA-4) and programmed death protein 1 ligand 1 (PD-L1) as well as their contribution to the development of clinically-approved antagonistic antibodies targeting CTLA-4 and programmed death protein 1, the receptor for PD-L1 [198]. Besides CTLA-4, PD-1 and PD-L1, there are currently several other co-inhibitory and co-stimulatory molecules under investigation as potential therapeutic targets [135,136,202–204,137–141,199–201] as well as alternative immunotherapeutic strategies like cancer vaccines [205], immune-stimulatory cytokines [142–145,206–210], synthetic immune-stimulatory molecules and anti-metabolites [211], adoptive immune cell therapy with chimeric antigen receptor T cells [212–214] and oncolytic viruses [215].

In comparison to standard oncological treatment regimens like chemo- and radiotherapy, the major desired benefits of immunotherapeutic approaches are the specific targeting of regulatory mechanisms (1) within a pre-existing endogenous anti-tumor system (2) that potentially exhibits higher specificity (3) and effectiveness (4). However, the greatest challenge for the success of immunotherapy in cancer treatment as well as its danger lies in the fact that cancer cells originate from endogenous cells and, therefore, display a high degree of similarity to healthy cells. Hence, the unwanted induction of severe auto-immune responses constitutes a common side effect in current immunotherapeutic regimens [216]. Moreover, it is still unclear why some patients show extraordinary response towards immunotherapy while others display either pre-existing or secondary acquired resistance [217,218]. This situation is clearly underscored by lack of reliable biomarkers for prediction of patient responses towards the different immunotherapeutic strategies highlighting that immunotherapy in cancer is still in the early stages of development and there are numerous open questions in the field of tumor immunology [219].

### 1.4.1 PD-1 and PD-L1 as targets in cancer therapy

In the last five years, many immunotherapeutic approaches and drugs entered the clinic. In this process, monoclonal antagonistic antibodies targeting either PD-1 or PD-L1 generated special attention, since results from clinical trials indicated outstanding efficiency for the treatment of several highly aggressive malignancies [220]. At present, three therapeutic antibodies either targeting PD-1 or PD-L1 are approved for clinical application in Europe and the United States of America (**Table 2**) [221].

**Table 2: Approved PD-1 or PD-L1 targeting monoclonal agonistic antibodies for cancer immunotherapy.**

| Antibody (Tradename)     | Target | Isotype                    | Distributor            |
|--------------------------|--------|----------------------------|------------------------|
| Pembrolizumab (Keytruda) | PD-1   | humanized IgG <sub>4</sub> | Merck                  |
| Nivolumab (Opdivo)       | PD-1   | human IgG <sub>4</sub>     | Bristol-Myers Squibb   |
| Cemiplimab (Libtayo)     | PD-1   | human IgG <sub>4</sub>     | Sanofi/Regeneron       |
| Durvalumab (Imfinzi)     | PD-L1  | human IgG <sub>1</sub>     | Medimmune/Astra Zeneca |
| Avelumab (Bavencio)      | PD-L1  | human IgG <sub>1</sub>     | Merck/Pfizer           |
| Atezolizumab (Tecentriq) | PD-L1  | humanized IgG <sub>1</sub> | Genentech/Roche        |

Overall, PD-1/PD-L1 antagonistic antibodies have revolutionized the treatment regimens for almost every of the most frequent tumor entities. In order to give just a few prominent examples, Atezolizumab in combination with Bevacizumab (Avastin), a VEGF inhibitor, has been designated as Breakthrough Therapy by the U.S. food and drug administration (FDA) as first-line treatment for advanced and metastatic hepatocellular carcinoma (HCC) [222]. Further Breakthrough Therapy designations have been assigned to Nivolumab for the first-line treatment of Hodgkin lymphoma [223], Pembrolizumab in combination with Lenvatinib for the first-line treatment of advanced unresectable HCC [224], Avelumab in combination with Axitinib for the first-line treatment of patients with advanced renal cell carcinoma [225], Cemiplimab for the first-line treatment of metastatic unresectable cutaneous squamous cell carcinoma [226] as well as Durvalumab as monotherapy for the treatment of stage III unresectable non-small cellular lung carcinoma [227]. However, it should be noted that despite the vast number of granted approvals by the U.S. FDA and the European Medicines Agency (EMA), only a distinct subgroup of patients benefits from therapy with so-called checkpoint inhibitors. One reason for this might be that currently available biomarkers and clinical indications poorly perform in patient stratification [216,218]. Nevertheless, recent studies

addressed various tumor characteristics as potential biomarkers for effective therapy with PD-1 and PD-L1 antagonists, e.g. tumor-associated PD-L1 expression, the tumor mutational burden (TMB) and tumor infiltration by CTLs [29,102,219,228]. In the case of tumor-associated PD-L1 expression, several companion and complementary diagnostics have been developed and approved (**Table 3**). These assays stratify patients based on immunohistochemical staining of PD-L1 in tumor biopsies, which is classified by an assay-specific standardized evaluation scheme. The results from staining evaluation indicate whether a patient might benefit from therapy with the associated PD-1/PD-L1 antagonist or not [229,230].

**Table 3: Approved IHC-based companion and complementary diagnostic assay for evaluation of PD-L1 expression status in tumor tissues.** NSCLC = non-small cellular lung carcinoma; UC = Urothelial cancer; SCCHN = Squamous cell carcinoma of head and neck; mAb = monoclonal antibody

| Assay                  | Tumor                            | Clinical mAb   | Distributor  |
|------------------------|----------------------------------|--|--------------|
| PD-L1 IHC 22C3 pharmDx | NSCLC                            | Pembrolizumab (Keytruda)   | Agilent/Dako |
| Ventana PD-L1 (SP263)  | NSCLC                            | Nivolumab (Opdivo)<br>Durvalumab (Imfinzi)<br>Pembrolizumab (Keytruda) | Roche        |
| Ventana PD-L1 (SP142)  | UC                               | Atezolizumab (Tecentriq)   | Roche        |
| PD-L1 IHC 28-8 pharmDx | NSCLC<br>SCCHN<br>Melanoma<br>UC | Nivolumab (Opdivo)   | Agilent/Dako |
| 73-10 Assay            | NSCLC                            | Avelumab (Bavencio)  | Agilent/Dako |

In the present study, Durvalumab was utilized to examine the effect of PD-L1 inhibition on the phenotype and activity of CD8<sup>+</sup> T lymphocytes in different microenvironmental conditions *in vitro*. Therefore, Durvalumab will be introduced in more detail in the following chapter.

### 1.4.2 Durvalumab (Imfinzi)

Durvalumab (Imfizi) is a human IgG<sub>1</sub> kappa monoclonal PD-L1 targeting antibody that has been developed and marketed by Astra Zeneca and its subsidiary Medimmune. Its therapeutic application is located in the field of oncology where this antagonistic antibody is utilized to block the extracellular binding epitope on PD-L1 that is engaged by PD-1 (**Figure 9**). Thereby, Durvalumab interferes with PD-L1-mediated signaling induction via PD-1, a mechanism by which neoplastic cells terminate anti-tumor immune responses by activated CTLs (introduced in **section 1.3.2**) [231].

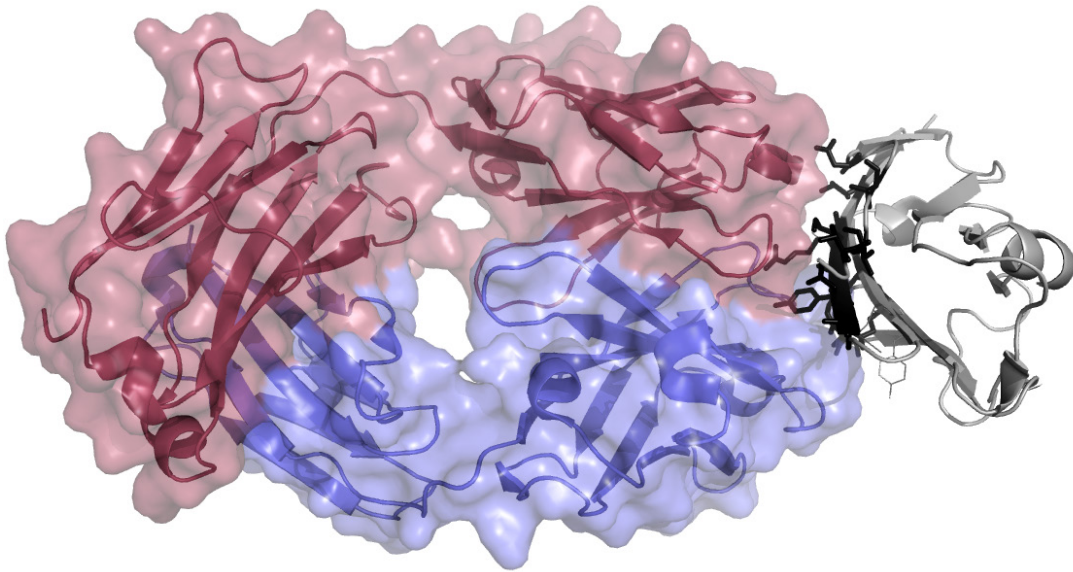


**Figure 9: Durvalumab in complex with human PD-L1.** Surface (transparent) and ribbon diagram of Durvalumab Fab-fragment (blue = heavy chain; red = light chain) in complex with the Immunoglobulin superfamily (IgSF) V-set domain of human PD-L1 (grey) according to the orthorhombic crystal structure determined by X-ray crystallography (pdb entry: 5X8M). Main- and side chains of PD-L1 IgSF V-set domain, which are engaged by Durvalumab via hydrogen bonds, salt bridges and hydrophobic interactions, are presented in black (stick model). Data has been obtained from [232].

In February 2016, Durvalumab received Breakthrough Therapy designation status by the U.S. FDA for the second-line treatment of patients with unresectable or metastatic PD-L1 positive urothelial bladder cancers based on the high response rates and durability observed in phase I and II clinical trials NCT01693562 and NCT02118337 [233–235]. Already two years later in February 2018, Durvalumab received approval by the U.S. FDA for the treatment of patients with stage III unresectable NSCLC, who reveal no tumor progression after chemo- and radiotherapy. Approval was granted based on improved progression-free survival compared to the placebo group observed in the PACIFIC study (NCT02125461) [236]. In April 2019, also the Federal Joint Committee in Germany approved the survival benefits of Durvalumab for the treatment of stage III NSLCL in patients that display no disease progression after platinum-based radio-chemotherapy.

In future perspective, Durvalumab might receive the approval for the treatment of several other tumor entities, e.g. NSCLC, colorectal cancer, head and neck cancer, gastric cancer and HCC, either in mono- or combination-therapy with other checkpoint inhibitors, radio-/chemotherapy or other novel anti-cancer drugs. Hence, at this time (August 27<sup>th</sup>, 2019) the application of Durvalumab is scheduled in 349 trials listed at the U.S. National Library of Medicine (<https://clinicaltrials.gov>). Moreover, in 16 of these trials, the therapeutic potential of Durvalumab for the treatment patients suffering from either resectable or advanced/metastatic PDAC is addressed.

## 1.5 Aim of the study

Despite the enormous progress made in the field of immunotherapy and other targeted therapeutic strategies for the treatment of cancer patients as well as the continuous growing insight into the mechanisms that drive PDAC development and progression, PDAC is estimated to become the second cause of cancer-related death by 2030 [5]. This perspective clearly reflects the poor progress made in the treatment of PDAC within the last three decades since the implementation of Gemcitabine as standard chemotherapeutic agent [237]. In the current age of immunotherapy, PD-1 and PD-L1 antagonistic monoclonal antibodies revolutionized therapy concepts for some tumor entities that either lacked efficient therapeutic options or showed stagnation in clinical progress for a long time. Therefore, first clinical trials utilizing PD-1 and PD-L1 agonists were launched with great enthusiasm. However, expectations soon turned to disappointment when results from these initial trials did not show the desired benefits of monotherapies with checkpoint inhibitors on overall survival but even low response rates [238]. In order to understand why some patients suffering from one malignant disease show remarkable responses to PD-1/PD-L1 targeted therapies while other patients suffering from the same disease or another tumor entity do not benefit from the same therapeutic approach, we have to understand the tumor biological role PD-1/PD-L1 in each individual disease.

Therefore, the first aim of this study was to comprehensively characterize PD-L1 expression in in the tumor and stromal compartment of pancreatic tumor tissues from a cohort of 59 PDAC patients by immunohistochemistry as well as correlate the findings with tumor, stromal and patient-specific clinic-pathological parameters. The second aim of this study was to translate findings from *in situ* analyses into *in vitro* settings, in order to investigate the cellular interplay of tumor and immune cell populations as well as the role of PD-L1 in phenotypic alterations mediated in co-culture settings. For the latter purpose, the PD-L1 targeting monoclonal antagonistic antibody Durvalumab, kindly provided by AstraZeneca, was applied for inhibiting PD-1/PD-L1 interaction.

## 2. Materials

### 2.1 Chemicals and Reagents

| Compound   | Manufacturer                                   |
|--|--|
| 2-mercaptoethanol  | Sigma-Aldrich, München, DE                     |
| Accutase solution  | Pan-Biotech GmbH, Aidenbach, DE                |
| Acetic acid  | Carl Roth GmbH, Karlsruhe, DE                  |
| Ammonium chloride  | Merck Millipore, Darmstadt, DE                 |
| Ammonium persulfate (APS)                                  | Merck Millipore, Darmstadt, DE                 |
| BlueBlock PF (10x)   | Serva, Heidelberg, DE                          |
| Bovine pituitary extract (BPE)                             | Life Technologies, Darmstadt, DE               |
| Bovine serum albumin (BSA), fraction V                     | Biomol, Hamburg, DE                            |
| Bromophenol blue   | Merck Millipore, Darmstadt, DE                 |
| Calcein AM   | BioLegend, Fell, DE                            |
| Carboxyfluorescein succinimidyl ester (CFSE)               | Thermo Scientific, Schwerte, DE                |
| CellTracker CMTPX Red                                      | Thermo Scientific, Schwerte, DE                |
| Citric acid  | Sigma-Aldrich, München, DE                     |
| Dithiothreitol (DTT)                                       | Sigma-Aldrich, München, DE                     |
| Dimethyl sulfoxide (DMSO)                                  | Th.Geyer GmbH, Renningen, DE                   |
| Dulbecco's Modified Eagle Medium (DMEM)                    | Biochrom, Berlin, DE                           |
| Ethanol  | Merck Millipore, Darmstadt, DE                 |
| Ethylenediaminetetraacetic acid (EDTA)                     | Carl Roth GmbH, Karlsruhe, DE                  |
| FcR blocking reagent human                                 | Miltenyi Biotec GmbH,<br>Bergisch Gladbach, DE |
| Fetal calf serum (FCS)                                     | Pan-Biotech GmbH, Aidenbach, DE                |
| Fixation/Permeabilization Concentrate                      | eBioscience, Frankfurt, DE                     |
| Fixation/Permeabilization Diluent                          | eBioscience, Frankfurt, DE                     |
| Fluoro-Gel   | Electron Microscopy Science, Hatfield, UK      |
| Glycerol 80 %  | Sigma-Aldrich, München, DE                     |
| Glycine  | Carl Roth GmbH, Karlsruhe, DE                  |
| 4-(2-hydroxyethyl)-1-piperazineethanesulfonic acid (HEPES) | Pan-Biotech GmbH, Aidenbach, DE                |
| Hoechst 33258  | Sigma-Aldrich, München, DE                     |
| Horse serum  | Thermo Scientific, Schwerte, DE                |



|   |  |
|---|--|
| Potassium bicarbonate   | Merck Millipore, Darmstadt, DE           |
| Keratinocyte serum-free medium  | Life Technologies, Darmstadt, DE         |
| L-glutamine (L-Gln)   | Biochrom, Berlin, DE                     |
| LightCycler480 SYBR Green I Master                                    | Roche, Basel, CH                         |
| Methanol  | Th.Geyer GmbH, Renningen, DE             |
| Milk powder   | Carl Roth GmbH, Karlsruhe, DE            |
| PageRuler prestained protein ladder                                   | Thermo Scientific, Schwerte, DE          |
| Pancoll, 1.077 g/l  | Pan-Biotech GmbH, Aidenbach, DE          |
| Paraformaldehyde (PFA) 4.0 %  | Thermo Scientific, Schwerte, DE          |
| Penicillin-streptomycin (Pen/Strep)                                   | Biochrom, Berlin, DE                     |
| Permeabilization Buffer (10x)   | eBioscience, Frankfurt, DE               |
| Phosphate-buffered saline (PBS) Dulbecco                              | Biochrom, Berlin, DE                     |
| Propidium iodide  | BioLegend, Fell, DE                      |
| Puromycin (10 mg/ml)  | Invivo Gen, San Diego, US                |
| Roswell Park Memorial Institute (RPMI) 1640 medium                    | Biochrom, Berlin, DE                     |
| Rotiphorese gel 40 (37.5:1)<br>acrylamide/bisacrylamide 40 % solution | Carl Roth GmbH, Karlsruhe, DE            |
| Sodium chloride   | Carl Roth GmbH, Karlsruhe, DE            |
| Sodium dodecyl sulfate (SDS) ultra-pure                               | Carl Roth GmbH, Karlsruhe, DE            |
| Sodium orthovanadate  | Santa Cruz Biotechnology, Heidelberg, DE |
| Sodium pyruvate   | Biochrom, Berlin, DE                     |
| Solution 555  | Beckmann Coulter GmbH, Krefeld, DE       |
| Tetramethyl ethylenediamine (TEMED)                                   | Carl Roth GmbH, Karlsruhe, DE            |
| Trans-Blot Turbo 5x Transfer Buffer                                   | Bio-Rad Laboratories, München, DE        |
| Tris(hydroxymethyl)aminomethane (Tris)                                | Carl Roth GmbH, Karlsruhe, DE            |
| Triton X-100  | Sigma-Aldrich, München, DE               |
| Trypan blue solution Fluka 0.4 %                                      | Sigma-Aldrich, München, DE               |
| Trypsin-EDTA  | Biowest, Riverside, US                   |
| Tween 20  | Serva, Heidelberg, DE                    |
| Western Bright ECL substrate  | Advansta, San Jose, US                   |
| Xylene  | Th.Geyer GmbH, Renningen, DE             |

## 2.2 Buffers

| Buffer   | Formulation  |
|--|--|
| <b>— Density gradient &amp; counterflow centrifugation —</b> |  |
| Erythrocyte lysis buffer                                     | 155 mM NH <sub>4</sub> Cl<br>10 mM KHCO <sub>3</sub><br>0.1 mM EDTA<br>in ddH <sub>2</sub> O |
| Elutriation buffer   | 0.1 % (v/v) FCS<br>10 mM EDTA<br>in PBS<br>pH 7.4  |
| <b>— Flow Cytometry —</b>                                    |  |
| Fixation solution  | 1 % (v/v) PFA<br>in MACS buffer  |
| FixPerm Solution   | 25 % (v/v) Fixation/Permeabilization Concentrate<br>in Fixation/Permeabilization Diluent     |
| MACS buffer  | 0.5 % (w/v) BSA<br>2 mM EDTA<br>in PBS<br>pH 7.4<br>sterile-filtered and vacuum-degassed     |
| Perm Washing buffer  | 10 % (v/v) Permeabilization buffer (10x)<br>in ddH <sub>2</sub> O                            |
| <b>— Western Blotting —</b>                                  |  |
| Blotto   | 5 % (w/v) milk powder<br>in TBS-T  |
| Lämmli buffer  | 128 mM Tris<br>4.6 % (w/v) SDS<br>10 % (v/v) glycerol<br>in ddH <sub>2</sub> O<br>pH 7.6     |

|                             |   |
|-----------------------------|---|
| Loading Dye (4x)            | 0.005 % (w/v) bromophenol blue<br>10 % (v/v) 2-mercaptoethanol<br>in Lämmli buffer    |
| Running gel buffer          | 1.5 M Tris<br>0.4 % (w/v) SDS<br>in ddH <sub>2</sub> O<br>pH 8.8                      |
| Stacking gel buffer         | 0.5 M Tris<br>0.4 % (w/v) SDS<br>in ddH <sub>2</sub> O<br>pH 6.8                      |
| TBS-Tween (TBS-T)           | 20 mM Tris<br>140 mM NaCl<br>0.05 % (v/v) Tween 20<br>in ddH <sub>2</sub> O<br>pH 7.6 |
| Western blot running buffer | 25 mM Tris<br>192 mM glycine<br>0.1 % (w/v) SDS<br>in ddH <sub>2</sub> O              |

## 2.3 Cell culture material

### 2.3.1 Cell lines

Authentication of all cell lines was carried out by short tandem repeat analysis in the Institute of Forensic Medicine in Kiel.

| Cell line | Information  | Reference |
|-----------|--|-----------|
| BxPc3     | Moderately differentiated human PDAC cell line isolated from the primary tumor of a 61-year-old Caucasian female.<br><br>They exhibit a driver mutation in <i>p53</i> (Y220) along with homozygous <i>p16</i> and <i>dpc4</i> deletion but display wildtype <i>k-ras</i> status. BxPc3 cells were purchased from ATCC. | [239–241] |

|             |  |                   |
|-------------|--|-------------------|
| Capan-1     | Well differentiated human PDAC cell line isolated from liver metastasis of a 40-year-old Caucasian male. They exhibit driver mutations in <i>p53</i> (A159V) and <i>k-ras</i> (G12V) as well as point-nonsense mutation in exon 8 of <i>dpc4</i> and homozygous <i>p16</i> deletion. Capan-1 cells were purchased from ATCC.   | [240,242–246]     |
| Colo357     | Moderately differentiated human PDAC cell line isolated from lymph node metastasis of a 77-year-old Caucasian female. They exhibit a driver mutation in <i>k-ras</i> (G12V) as well as homozygous <i>dpc4</i> deletion but wildtype <i>p53</i> and <i>p16</i> status.  | [240,242,247,248] |
| H6c7eR-kras | HPV-16 E6/E7 immortalized HPDE cell line expressing murine ecotropic retroviral receptor (eR) transduced with retroviral pBabepuro- <i>K-ras4B</i> <sup>G12V</sup> vector. These cells were used as an <i>in vitro</i> model for premalignant PDCECs harboring only a <i>k-ras</i> mutation. H6c7eR-kras cells were kindly provided by M.-S. Tsao (Ontario Cancer Institute, Toronto, Canada). | [249–252]         |
| H6c7eR-pBp  | HPV-16 E6/E7 immortalized HPDE cell line expressing murine ecotropic retroviral receptor (eR) transduced with empty retroviral pBabepuro vector. These cells were used as an <i>in vitro</i> model for benign PDECs with a near normal genotype and phenotype. H6c7eR-pBp cells were kindly provided by M.-S. Tsao (Ontario Cancer Institute, Toronto, Canada).                                | [249–252]         |
| MIA PaCa-2  | Poorly differentiated human PDAC cell line isolate from the primary tumor of a 65-year-old Caucasian male. They exhibit driver mutations in <i>k-ras</i> (G12C) and <i>p53</i> (R248W) as well as homozygous <i>p16</i> deletion but <i>dpc4</i> wild type status. MIA PaCa-2 cells were purchased from ATCC.  | [240,241,253,254] |

|          |   |               |
|----------|---|---------------|
| Panc1    | Poorly differentiated human PDAC cell line isolated from the primary tumor of a 56-year-old Caucasian male. They exhibit driver mutations in <i>k-ras</i> (G12D), <i>p53</i> (R273H) and <i>p16</i> (homozygous deletion) but show wildtype <i>dpc4</i> status. Panc1 cells were purchased from ATCC.   | [240,254,255] |
| Panc89   | Moderately differentiated human PDAC cell line isolated from lymph node metastasis of 64-year-old Caucasian male. They exhibit a <i>p53</i> mutation (Y220C) and methylated <i>p16</i> 5' CpG island but show <i>k-ras</i> and <i>dpc4</i> wild type status. Panc89 cells were kindly provided by K. Keiichi (Kyoto Prefectural University of Medicine, Japan).                         | [240,254,256] |
| PancTu-I | Poorly differentiated human PDAC cell line isolated from the primary tumor of a Caucasian female patient. They exhibit driver mutations in <i>k-ras</i> (G12V) and <i>p53</i> (C176S) as well as a methylated 5' CpG island within the <i>p16</i> locus leading to its transcriptional inactivation. PancTu-I cells were kindly provided by M. v. Bülow (University of Mainz, Germany). | [240,254]     |

### 2.3.2 Culture media

| Usage                      | Formulation  |
|----------------------------|--|
| H6c7eR-pBp<br>H6c7eR-kras  | 50 % (v/v) keratinocyte serum-free medium supplemented with 50 µg/ml BPE, 5 ng/ml EGF, 4 µg/ml puromycin   |
| Macrophage differentiation | 50 % (v/v) RPMI 1640 supplemented with 10 % (v/v) FCS, 2 mM L-Gln<br>RPMI 1640 medium supplemented with 1 % (v/v) FCS, 2 mM L-Gln, 100 U/ml Penicillin, 100 µg/ml Streptomycin |

|   |  |
|---|--|
| Panc1, PancTu-I, Panc89,<br>Colo357, BxPC3, Capan-1 | RPMI 1640 medium<br>supplemented with 10 % (v/v) FCS, 2 mM L-Gln,<br>1 mM sodium pyruvate  |
| T cell activation<br>Co-culture                     | RPMI 1640 medium<br>supplemented with 10 % (v/v) FCS, 20 mM HEPES,<br>2 mM L-Gln, 1 mM sodium pyruvate,<br>100 U/ml Penicillin, 100 µg/ml Streptomycin |
| MIA PaCa-2  | DMEM (4.5 g/l D-glucose) medium<br>supplemented with 10 % (v/v) FCS, 2 mM L-Gln,<br>2.5 % (v/v) horse serum  |

### 2.3.3 Growth factors and cytokines

| Compound                          | Concentration (ng/ml) | Manufacturer                    |
|-----------------------------------|-----------------------|---------------------------------|
| EGF, human recombinant            | 20                    | Thermo Scientific, Schwerte, DE |
| GM-CSF, human recombinant         | 2.4                   | BioLegend, Fell, DE             |
| IFN $\gamma$ , human recombinant  | 10                    | BioLegend, Fell, DE             |
| IL-2, human recombinant           | 60                    | BioLegend, Fell, DE             |
| IL-6, human recombinant           | 10                    | BioLegend, Fell, DE             |
| M-CSF, human recombinant          | 50                    | BioLegend, Fell, DE             |
| TGF- $\beta$ 1, human recombinant | 20                    | BioLegend, Fell, DE             |
| TNF $\alpha$ , human recombinant  | 10                    | BioLegend, Fell, DE             |

## 2.4 Patient derived material

### 2.4.1 Ethics statement

Utilization of pancreatic tissues from PDAC patients for research purposes was carried out in accordance with the World Medical Association's Declaration of Helsinki. The research project was approved by the ethics committee of the University Hospital Schleswig-Holstein (reference number: D430/09). Written informed consent was obtained from all patients.

## 2.4.2 Histopathology and study cohort

Pancreatic tissues were obtained from patients during oncological surgery at the university hospital Schleswig-Holstein (UKSH) in Kiel. Tissue specimens were gross sectioned, fixed in formalin and embedded in paraffin (FFPE). Deparaffinized sections were stained with haematoxylin and eosin. Tumor grade and stage were classified according to the 7<sup>th</sup> edition of the UICC guidelines by board certified surgical pathologists in the Institute of Pathology, UKSH Campus Kiel. Overall, 59 pancreatic tumor tissues und 18 peritumoral tissues, of which 13 corresponded to available tumor specimens, were included in this study. Clinic-pathological data were obtained from the hospital records and the *Epidemiological Cancer Registry* of the state of Schleswig-Holstein, Germany. All patient data were pseudonymized prior to study inclusion.

## 2.5 Molecular biological material

### 2.5.1 Primer

| Target         | 5' - 3' Sequence   | Annealing (°C) |
|----------------|--|----------------|
| E-Cadherin*    | fw - TTA GAG GTC AGC GTG TGT GA<br>rv - CAG TAA GGG CTC TTT GAC CA         | 55             |
| GAPDH          | fw - TCC ATG ACA ACT TTG GTA TCG TGG<br>rv - GAC GCC TGC TTC ACC ACC TTC T | 58             |
| IFN $\gamma$ * | fw - TCC CAT GGG TTG TGT GTT TA<br>rv - AAG CAC CAG GCA TGA AAT CT         | 58             |
| IL-1 $\beta$ * | fw - TTC GAC ACA TGG GAT AAC GA<br>rv - TCT TTC AAC ACG CAG GAC AG         | 58             |
| IL-2*          | fw - AAT GTA CAG GAT GCA ACT CC<br>rv - TTC TTG GGC ATG TAA AAC TT         | 58             |
| IL-6*          | fw - ATG CAA TAA CCA CCC CTG AC<br>rv - GAG GTG CCC ATG CTA CAT TT         | 58             |
| IL-8           | fw - GTG TGA AGG TGC AGT TTT GCC<br>rv - AAC TTC TCC ACA ACC CTC TGC       | 55             |
| IL-10*         | fw - AAG CCT GAC CAC GCT TTC TA<br>rv - ATG AAG TGG TTG GGG AAT GA         | 58             |
| L1CAM*         | fw - GAA CTG GAT GTG GTG GAG AG<br>rv - GAG GGT GGT AGA GGT CTG GT         | 58             |

|                |  |    |
|----------------|--|----|
| TGF- $\beta$ 1 | fw - CGT GGA GCT GTA CCA GAA ATA<br>rv - TCC GGT GAC ATC AAA AGA TAA         | 58 |
| TNF- $\alpha$  | fw - TCC TTC AGA CAC CCT CAA CC<br>rv - AGG CCC CAG TTT GAA TTC TT           | 58 |
| VEGF-A*        | fw - CGC TTA CTC TCA CCT GCT TC<br>rv - GGA AGG TCA ACC ACT CAC AC           | 58 |
| Vimentin*      | fw - TCC AAG TTT GCT GAC CTC TC<br>rv - TCA ACG GCA AAG TTC TCT TC           | 58 |
| Zeb-1          | fw - TCC ATG CTT AAG AGC GCT AGC T<br>rv - ACC GTA GTT GAG TAG GTG TAT GCC A | 61 |

\* = Primers purchased from Real Time Primers, LCC (Elkins Park, Pennsylvania, US). Provided as 50  $\mu$ M stocks of forward and reverse primer mix in nuclease-free ddH<sub>2</sub>O supplemented with 10 mM Tris-HCl, 0.1 mM EDTA (pH 7.5)

Other primers were purchased from Eurofins Genomics GmbH (Ebersberg, DE). Stocks of forward and reverse primers were diluted at 1 pmol/ $\mu$ l in nuclease-free ddH<sub>2</sub>O.

## 2.5.2 Antibodies

| Target (-Conjugate)<br>[Clone] | Host<br>[Isotype]           | Stock ( $\mu$ g/ml)<br>[Dilution] | Manufacturer                       |
|--------------------------------|-----------------------------|-----------------------------------|------------------------------------|
| — Isotype controls —           |                             |                                   |                                    |
| Isotype<br>[SP137]             | rabbit<br>[IgG]             | 200<br>[conditional]              | Abcam, Cambridge, UK               |
| Isotype<br>[11711]             | mouse<br>[IgG1]             | 1000<br>[conditional]             | R&D Systems GmbH,<br>Wiesbaden, DE |
| Isotype                        | human<br>[IgG1, $\kappa$ ]  | 5000<br>[conditional]             | MedImmune, Gaithersburg, US        |
| Isotype-APC<br>[MOPC-21]       | mouse<br>[IgG1, $\kappa$ ]  | 200<br>[conditional]              | BioLegend, Fell, DE                |
| Isotype-APC<br>[MPC-11]        | mouse<br>[IgG2b, $\kappa$ ] | 100<br>[conditional]              | BioLegend, Fell, DE                |
| Isotype-BV510<br>[MOPC-21]     | mouse<br>[IgG1, $\kappa$ ]  | 200<br>[conditional]              | BioLegend, Fell, DE                |
| Isotype-FITC<br>[MOPC-21]      | mouse<br>[IgG1, $\kappa$ ]  | 500<br>[conditional]              | BioLegend, Fell, DE                |



|                            |                     |                      |                     |
|----------------------------|---------------------|----------------------|---------------------|
| Isotype-FITC<br>[MOPC-173] | mouse<br>[IgG2a, κ] | 200<br>[conditional] | BioLegend, Fell, DE |
| Isotype-PE<br>[MOPC-21]    | mouse<br>[IgG1, κ]  | 200<br>[conditional] | BioLegend, Fell, DE |
| Isotype-PE<br>[MOPC-173]   | mouse<br>[IgG2a, κ] | 200<br>[conditional] | BioLegend, Fell, DE |
| Isotype-PECy7<br>[MOPC-21] | mouse<br>[IgG1, κ]  | 200<br>[conditional] | BioLegend, Fell, DE |

— **Primary Antibodies** —

|                               |                     |  |  |
|-------------------------------|---------------------|--|--|
| CD14-PE<br>[M5E2]             | mouse<br>[IgG2a, κ] | 200<br>[FC: 1:10]                                  | BioLegend, Fell, DE                            |
| CD163-PE<br>[REA812]          | mouse<br>[IgG1, κ]  | 250<br>[FC: 1:10]                                  | Miltenyi Biotec GmbH,<br>Bergisch Gladbach, DE |
| CD206-FITC<br>[15-2]          | mouse<br>[IgG1, κ]  | 200<br>[FC: 1:10]                                  | BioLegend, Fell, DE                            |
| CD274<br>[E1L3N]              | rabbit<br>[IgG]     | 874<br>[IHC: 1:100]<br>[IF: 1:200]<br>[WB: 1:1000] | Cell Signaling, Frankfurt, DE                  |
| CD274 / Durvalumab            | human<br>[IgG1, κ]  | 5000<br>[CC: 1:500]                                | MedImmune, Gaithersburg, US                    |
| CD274-PECy7<br>[MIH1]         | mouse<br>[IgG1, κ]  | 200<br>[FC: 1:10]                                  | BD Bioscience, San Jose, US                    |
| CD279<br>[4H4D1]              | mouse<br>[IgG2b, κ] | 1213.3<br>[WB: 1:1000]                             | Proteintech, Manchester, UK                    |
| CD279-APC<br>[EH12.2H7]       | mouse<br>[IgG1, κ]  | 50<br>[FC: 1:10]                                   | BioLegend, Fell, DE                            |
| CD279-PE<br>[EH12.2H7]        | mouse<br>[IgG1, κ]  | 100<br>[FC: 1:20]                                  | BioLegend, Fell, DE                            |
| CD28 (Ultra LEAF)<br>[CD28.2] | mouse<br>[IgG1, κ]  | 1000<br>[CC: 1:666.7]                              | BioLegend, Fell, DE                            |
| CD3 (Ultra LEAF)<br>[OKT3]    | mouse<br>[IgG2a, κ] | 1000<br>[CC: 1:666.7]                              | BioLegend, Fell, DE                            |

|   |                     |                      |  |
|---|---------------------|----------------------|--|
| CD45-BV510<br>[HI30]                          | mouse<br>[IgG1, κ]  | 100<br>[FC: 1:25]    | BioLegend, Fell, DE                            |
| CD4-APC<br>[RPA-T4]                           | mouse<br>[IgG1, κ]  | 50<br>[FC: 1:10]     | BioLegend, Fell, DE                            |
| CD68<br>[514H12]                              | mouse<br>[IgG2a, κ] | 37<br>[IF: 1:100]    | Leica Biosystems, Wetzlar, DE                  |
| CD68-APC<br>[Y1/82A]                          | mouse<br>[IgG2b, κ] | 100<br>[FC: 1:200]   | BioLegend, Fell, DE                            |
| CD80-APC<br>[2D10]                            | mouse<br>[IgG1, κ]  | 200<br>[FC: 1:10]    | BioLegend, Fell, DE                            |
| CD8a-FITC<br>[RPA-T8]                         | mouse<br>[IgG1, κ]  | 200<br>[FC: 1:10]    | BioLegend, Fell, DE                            |
| CD8a-PE<br>[RPA-T8]                           | mouse<br>[IgG1, κ]  | 200<br>[FC: 1:10]    | BioLegend, Fell, DE                            |
| Cytokeratin-FITC<br>[CK3-6H5]                 | mouse<br>[IgG1, κ]  | 33<br>[FC: 1:82.5]   | Miltenyi Biotec GmbH,<br>Bergisch Gladbach, DE |
| E-Cadherin<br>[32A8]                          | mouse<br>[IgG1, κ]  | 28<br>[WB: 1:1000]   | Cell Signaling, Frankfurt, DE                  |
| ERK1/2<br>[polyclonal]                        | rabbit              | 19<br>[WB: 1:1000]   | Cell Signaling, Frankfurt, DE                  |
| HLA-DR-FITC<br>[L243]                         | mouse<br>[IgG2a, κ] | 50<br>[FC: 1:10]     | BioLegend, Fell, DE                            |
| HSP 90α/β<br>[F-8]                            | mouse<br>[IgG2a, κ] | 200<br>[WB: 1:2000]  | Santa Cruz, Heidelberg, DE                     |
| L1CAM<br>[L1-9.3]                             | mouse<br>[IgG]      | 1000<br>[WB: 1:1000] | DKFZ, Heidelberg, DE<br>Reference [257]        |
| phospho-ERK1/2<br>(T202/Y204)<br>[polyclonal] | rabbit              | 177<br>[WB: 1:1000]  | Cell Signaling, Frankfurt, DE                  |
| phospho-Stat1 (Y701)<br>[D4A7]                | rabbit<br>[IgG]     | 42<br>[WB: 1:1000]   | Cell Signaling, Frankfurt, DE                  |
| Stat1<br>[polyclonal]                         | rabbit              | 125<br>[WB: 1:1000]  | Cell Signaling, Frankfurt, DE                  |

|                       |                    |                       |                            |
|-----------------------|--------------------|-----------------------|----------------------------|
| Tubulin<br>[B-5-1-2]  | mouse<br>[IgG1, κ] | 3800<br>[WB: 1:10000] | Sigma-Aldrich, München, DE |
| Vimentin<br>[V9]      | mouse<br>[IgG1, κ] | 200<br>[WB: 1:200]    | Santa Cruz, Heidelberg, DE |
| α/βTCR-FITC<br>[IP26] | mouse<br>[IgG1, κ] | 400<br>[FC: 1:10]     | BioLegend, Fell, DE        |
| β-Actin<br>[AC-15]    | mouse<br>[IgG1, κ] | 2000<br>[WB: 1:10000] | Sigma-Aldrich, München, DE |

— Secondary Antibodies —

|                                       |       |                     |                                 |
|---------------------------------------|-------|---------------------|---------------------------------|
| mouse IgG (H+L)-AF546<br>[polyclonal] | goat  | 2000<br>[IF: 1:500] | Thermo Scientific, Schwerte, DE |
| mouse IgG-HRP<br>[polyclonal]         | horse | 170<br>[WB: 1:2000] | Cell Signaling, Frankfurt, DE   |
| rabbit IgG-HRP<br>[polyclonal]        | goat  | 83<br>[WB: 1:2000]  | Cell Signaling, Frankfurt, DE   |

## 2.6 Consumables

| Consumable  | Manufacturer                            |
|---|---|
| 0.1 - 10 µl, 10 - 200 µl, 100 - 1000 µl<br>pipette tips | Sarstedt, Nümbrecht, DE                 |
| 1.25 ml, 5.0 ml Ritips                                  | Ritter, Schwabmünchen, DE               |
| 1.5 ml, 2.0 ml Eppendorf tubes                          | Eppendorf, Hamburg, DE                  |
| 12-/24-/96-well flat-bottom plates                      | Sarstedt, Nümbrecht, DE                 |
| 12-well transwell inserts, pore size 0.4 µm             | Sarstedt, Nümbrecht, DE                 |
| 15 ml, 20 ml centrifuge tubes                           | Sarstedt, Nümbrecht, DE                 |
| 18 mm coverslips  | Menzel, Braunschweig, DE                |
| 5 ml, 10 ml, 50 ml serological pipettes                 | Greiner Bio-One GmbH, Frickenhausen, DE |
| 75 cm <sup>2</sup> cell culture flasks                  | Greiner Bio-One GmbH, Frickenhausen, DE |
| 96-well PCR plates, white                               | Roche, Basel, CH                        |
| 96-well V-bottom plates                                 | Greiner Bio-One GmbH, Frickenhausen, DE |
| Cell scraper 25 cm                                      | Sarstedt, Nümbrecht, DE                 |
| CryoPure tube, 1.0 ml, white                            | Sarstedt, Nümbrecht, DE                 |

|   |  |
|---|--|
| Cyto-chamber with gasket, 8 ml, 240 mm <sup>2</sup> | Hettich, Tuttlingen, DE                        |
| FACS tubes  | Thermo Scientific, Schwerte, DE                |
| Filter cartridges #1676                             | Hettich, Tuttlingen, DE                        |
| Immune-Blot PVDF membrane                           | Bio-Rad Laboratories, München, DE              |
| MACS LD Columns                                     | Miltenyi Biotec GmbH,<br>Bergisch Gladbach, DE |
| Micro-Touch nitrile examination gloves              | Ansell GmbH, München, DE                       |
| Parafilm M sealing film                             | Brand GmbH & Co. KG, Wertheim, DE              |
| Scalpel   | Feather, Osaka, JPN                            |
| SuperFrost Plus object slide 76x26 mm               | Menzel, Braunschweig, DE                       |
| Thermanox plastic coverslip, 15 mm                  | Thermo Scientific, Schwerte, DE                |
| Trans-Blot Turbo Mini-size Transfer Stacks          | Bio-Rad Laboratories, München, DE              |
| Transfer pipettes 3.5 ml                            | Sarstedt, Nümbrecht, DE                        |
| VueLife Closed Culture System, 32 ml                | Süd-Laborbedarf, Gauting, DE                   |
| WatchMaker Forcep No. 6                             | Thermo Scientific, Schwerte, DE                |

## 2.7 Kit systems

| Kit   | Manufacturer                                   |
|---|--|
| Alexa Fluor 488 Tyramide SuperBoost, goat anti-rabbit Kit | Thermo Scientific, Schwerte, DE                |
| Bond Polymer Refine Detection Kit                         | Leica Biosystems, Wetzlar, DE                  |
| CD8+ T cell isolation kit, human                          | Miltenyi Biotec GmbH,<br>Bergisch Gladbach, DE |
| Click-iT Plus EdU Alexa Fluor 488 Imaging Kit             | Thermo Scientific, Schwerte, DE                |
| DC Protein Assay  | Bio-Rad Laboratories, München, DE              |
| LEGENDplex, custom human panel                            | BioLegend, Fell, DE                            |
| peqGOLD Total RNA Kit                                     | PeqLab, Erlangen, DE                           |
| RevertAid First Strand cDNA Synthesis Kit                 | Thermo Scientific, Schwerte, DE                |
| Tumor Dissociation Kit                                    | Miltenyi Biotec GmbH,<br>Bergisch Gladbach, DE |

## 2.8 Software

| Software                             | Manufacturer                       |
|--------------------------------------|------------------------------------|
| Axiovision 4.6                       | Carl Zeiss AG, Jena, DE            |
| BD FACSDiva Software                 | Becton Dickinson, Heidelberg DE    |
| FACScalibur CellQuest Pro            | BD Bioscience, San Jose, US        |
| FlowJo 10.1r3                        | FlowJo, LCC, Oregon, US            |
| FUSION-CAPT 16.06                    | Vilber Lourmat, Eberhardzell, DE   |
| Gen5 Data Analysis Software          | BioTek, Bad Friedrichshall, DE     |
| i-control Microplate Reader Software | Tecan, Crailsheim, DE              |
| ImageJ                               | National Institute of Health, US   |
| LEGENDplex Data Analysis software v8 | VigeneTech Inc., Carlisle, US      |
| LightCycler480 Software              | Roche, Basel, CH                   |
| Mendeley Desktop, V1.19.4            | Mendeley Ltd, New York, US         |
| Microsoft Office 2016                | Microsoft Corporation, Redmond, US |
| PyMOL v1.3                           | Schrödinger, LLC, München, DE      |
| SigmaPlot 12.5                       | Systat Software Inc., Chicago, US  |

## 2.9 Laboratory Devices

| Centrifuges / Rotors      | Manufacturer                          |
|---------------------------|---------------------------------------|
| Avanti J-20 XP centrifuge | Beckmann Coulter GmbH, Krefeld, DE    |
| Heraeus Biofuge pico      | Thermo Scientific, Schwerte, DE       |
| Heraeus Fresco 17         | Thermo Scientific, Schwerte, DE       |
| Heraeus Multifuge 3 S-R   | Thermo Scientific, Schwerte, DE       |
| Heraeus Multifuge X1      | Thermo Scientific, Schwerte, DE       |
| Heraeus Pico 17           | Thermo Scientific, Schwerte, DE       |
| JE-5.0 Elutriator Rotor   | Beckmann Coulter GmbH, Krefeld, DE    |
| Rotino 420 R              | Hettich, Tuttlingen, DE               |
| Sprout mini-centrifuge    | Heathrow Scientific, Vernon Hills, US |

**Incubators / Shaker**

|                                    |                                  |
|------------------------------------|----------------------------------|
| BBD 6220 CO <sub>2</sub> incubator | Thermo Scientific, Schwerte, DE  |
| GyroTwister 3D shaker              | Labnet, Woodbridge, US           |
| HERA Cell 240 incubator            | Thermo Scientific, Schwerte, DE  |
| PMS 1000 microplate shaker         | Grant bio, Essex, UK             |
| QBA1 block heater                  | Grant, Cambridge, UK             |
| Stuart SRT9 tube roller            | Bibby Scientific Ltd., Stone, UK |
| WNB 7-45 water bath                | Memmert, Schwabach, DE           |
| WTC ED-53 incubator                | Binder, Tuttlingen, DE           |

**Measuring devices**

|                                   |   |
|-----------------------------------|---|
| BD FACScalibur flow cytometer     | Beckton Dickinson, Heidelberg DE                            |
| BD FACVerse flow cytometer        | Beckton Dickinson, Heidelberg DE                            |
| BD LSRFortessa flow cytometer     | Beckton Dickinson, Heidelberg DE                            |
| Fusion SL detection system        | Vilber Lourmat, Eberhardzell, DE                            |
| Infinite 200PRO microplate reader | Tecan, Crailsheim, DE                                       |
| LightCycler 480 II                | Roche, Basel, CH  |
| NanoQuant Plate                   | Tecan, Crailsheim, DE                                       |
| Neubauer counting chamber         | Marienfeld Superior GmbH & Co. KG,<br>Lauda-Königshofen, DE |
| pH 7110 pH-meter                  | inoLab, Weilheim, DE  |

**Microscopes**

|                                   |                                |
|-----------------------------------|--------------------------------|
| AE2000                            | Motic, Wetzlar, DE             |
| Axio Scope A.1                    | Carl Zeiss AG, Jena, DE        |
| Axiovert 25                       | Zeiss, Jena, DE                |
| Evos XL Core Cell Imaging System  | AMG, Bothell, US               |
| Lionheart FX Automated Microscope | BioTek, Bad Friedrichshall, DE |

**Other devices**

|                                   |                                   |
|-----------------------------------|-----------------------------------|
| ARPEGE 110, liquid nitrogen tank  | Air Liquide GmbH, Düsseldorf, DE  |
| BOND-MAX Autostainer              | Leica Biosystems, Wetzlar, DE     |
| Buffer Tank and Lid               | Bio-Rad Laboratories, München, DE |
| Clamping plate with clamping ring | Hettich, Tuttlingen, DE           |

|  |   |
|--|---|
| CS-300V power supply                           | Cleaver Scientific, West Sussex, UK                         |
| Cyto hygiene carrier, HET1660                  | Hettich, Tuttlingen, DE                                     |
| Freezer  | Liebherr, Ochsenhausen, DE                                  |
| Fridge   | Liebherr, Ochsenhausen, DE                                  |
| HERAfreeze basic freezer (-80°C)               | Thermo Scientific, Schwerte, DE                             |
| Laboport vacuum pump                           | KNF Neuberger, Freiburg, DE                                 |
| MACS MultiStand                                | Miltenyi Biotec GmbH,<br>Bergisch Gladbach, DE              |
| Masterflex L/S tubing pump                     | Cole Parmer Instruments,<br>Novodirect GmbH, Kehl/Rhein, DE |
| Mini PROTEAN Short plates                      | Bio-Rad Laboratories, München, DE                           |
| Mini PROTEAN Glass plates<br>(1.5 mm spacers)  | Bio-Rad Laboratories, München, DE                           |
| Mini PROTEAN Tetra Cell                        | Bio-Rad Laboratories, München, DE                           |
| Mini PROTEAN Tetra Cell Casting Module         | Bio-Rad Laboratories, München, DE                           |
| Mini PROTEAN Tetra Companion Running<br>Module | Bio-Rad Laboratories, München, DE                           |
| Mini PROTEAN Tetra Electrode Assembly          | Bio-Rad Laboratories, München, DE                           |
| MR Hei-Mix S magnetic stirrer                  | Heidolph Instruments, Schwabach, DE                         |
| Sonicator Sonopuls                             | Bandelin, Berlin, DE  |
| Sunrise remote control                         | Tecan, Crailsheim, DE                                       |
| Trans-Blot Turbo Transfer System               | Bio-Rad Laboratories, München, DE                           |
| VORTEX Genius 3 vortex shaker                  | IKA-Werke, Staufen, DE                                      |

### Pipettes

|                              |                                   |
|------------------------------|-----------------------------------|
| Finnpipette F1 0.2 - 2 µl    | Thermo Scientific, Schwerte, DE   |
| Finnpipette F1 1 - 10 µl     | Thermo Scientific, Schwerte, DE   |
| Finnpipette F1 2 - 20 µl     | Thermo Scientific, Schwerte, DE   |
| Finnpipette F1 20- 200 µl    | Thermo Scientific, Schwerte, DE   |
| Finnpipette F1 100 - 1000 µl | Thermo Scientific, Schwerte, DE   |
| Macro Pipette Controlle      | Brand, Wertheim, DE               |
| PIPETBOY acu                 | Integra Biosciences, Fernwald, DE |
| Ripette                      | Ritter, Schwabmünchen, DE         |

---

**Sterile benches**

|              |                                 |
|--------------|---------------------------------|
| HERA Safe    | Thermo Scientific, Schwerte, DE |
| HERA Safe KS | Thermo Scientific, Schwerte, DE |

**Scales**

|                  |                                       |
|------------------|---------------------------------------|
| Precisa BJ 2100D | Precisa Gravimetrics AG, Dietikon, CH |
| Precisa XB120A   | Precisa Gravimetrics AG, Dietikon, CH |



## 3. Methods

### 3.1 Cell biological methods

#### 3.1.1 Cultivation of human pancreatic ductal epithelial cells

Human pancreatic ductal epithelial cells (PDECs) were routinely cultured in 75 cm<sup>2</sup> cell culture flasks filled with 10 ml of their respective medium (**section 2.3.2**). For maintenance and expansion, cultures were split at ratios of 1:3 to 1:5 twice a week when cultures reached a confluency of 70 – 90 %. For this purpose, adherent growing PDECs were detached by incubation in 5 ml Trypsin/EDTA or Accutase solution for 15 min at 37°C. Proteolytic reaction was stopped by adding 7 ml of pre-warmed medium. Subsequently, the cell suspension was transferred into a 50 ml tube and cells were sedimented *via* centrifugation for 10 min at 300 ·g and room temperature (RT). Afterwards, supernatants were aspirated and cells were resuspended in 10 ml of their respective medium, diluted at the respective ratio and transferred into 75 cm<sup>2</sup> cell culture flasks. All PDEC lines were cultured for maintenance, expansion and experiments at 37°C, 5 % CO<sub>2</sub> and 86 % humidity.

#### 3.1.2 Cell counting

Cell numbers were manually counted making use of a Neubauer counting chamber to seed appropriate cells numbers in experiments or determine vital cell numbers after experiments. In brief, respective cell suspensions were mixed at a ratio of 1:10 with trypan blue to identify and exclude non-viable cells from counting. Hereafter, 10 µl of the sample were filled into the Neubauer counting chamber. Cell numbers were calculated by the following formula:

$$\frac{\text{counted cell number}}{\text{counted squares}} \cdot 10^4 = \frac{\text{cell number}}{\text{ml}}$$

#### 3.1.3 Isolation of peripheral mononuclear blood cells

Peripheral blood mononuclear cells (PBMCs) were isolated from lymphocyte retaining systems (LRS), a leftover of whole blood donations provided by the Institute of Transfusion Medicine in Kiel. Informed consent from healthy donors was obtained. Isolation was performed *via* density gradient centrifugation depleting remaining erythrocytes, granulocytes and cellular debris. For this purpose, the content of one LRS was transferred into a 75 cm<sup>2</sup> cell culture flask containing 20 ml sterile PBS. Afterwards, the flask was filled up to a volume of 140 ml with PBS. The resulting suspension was mixed by gently shaking. Subsequently, 15 ml of Pancoll

separating solution were pipetted into each of four 50 ml tubes, respectively. At the next step, each prepared Pancoll solution was carefully overlaid with 35 ml of the blood suspension establishing two separated phases. The prepared samples were centrifuged for 25 min at 350 ·g slowly accelerating and without mechanical deceleration to prevent mixing of the resulting buffy coat. Next, the supernatant was aspirated up to 1 cm above the white interphase ring and PBMCs were transferred into new 50 ml tubes that were filled up with ice-cold sterile PBS and centrifuged for 10 min at 300 ·g and 4°C. In order to remove remaining erythrocytes from the PBMC fraction, the resulting cell sediments were resuspended in 10 ml erythrocyte lysis buffer (**section 2.2**), incubated for 6 min in the dark at RT, filled up with ice-cold PBS and centrifuged for 10 min at 175 ·g and 4°C. Finally, sedimented cells were resuspended in 50 ml ice-cold elutriation buffer (**section 2.2**) and cell count was determined (**section 3.1.2**).

### 3.1.4 Counterflow centrifugation

Counterflow centrifugation was performed to separate lymphocytes from monocytes within the isolated PBMCs based on their differential sedimentation potential. For this purpose, isolated PBMCs (**section 3.1.3**) were adjusted to a maximum of  $1.2 \cdot 10^9$  PBMCs/50 ml elutriation buffer. Before loading PBMCs into the system, the tubing system and the elutriation chamber had been washed first with 70 % ethanol in ddH<sub>2</sub>O, then with pure ddH<sub>2</sub>O and finally they were equilibrated with ice-cold elutriation buffer. PBMCs were loaded *via* the tubing system into the elutriation chamber of a JE-5.0 rotor at 3,500 rpm, 4°C and a flowrate of 26 ml/min (**Figure 10**).

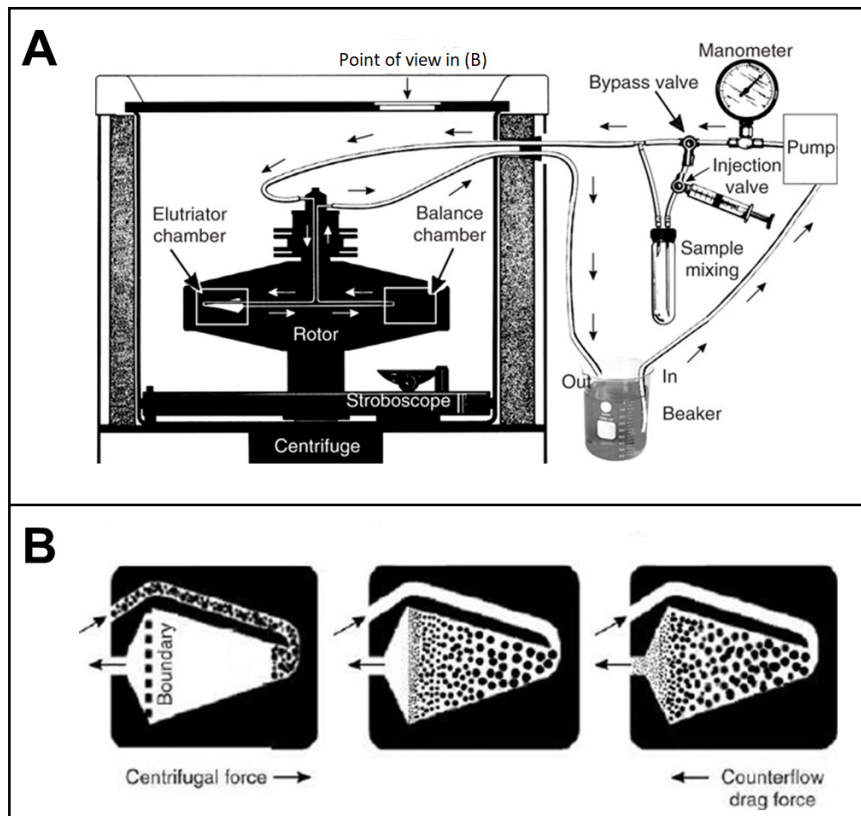


**Figure 10: Schematic illustration of the counterflow centrifugation system (A) and the separation principle in the elutriation chamber in detail (B).** Cell populations are separated by counterflow centrifugation due to their differences in sedimentation potential. During this process cells are exposed to a constant centrifugal force and opposing increasing counterflow. Adapted from [258].

After loading and rinsing with additional 100 ml of elutriation buffer, three fractions of each 50 ml (fractions 26A, B and C) were collected before the flowrate was increased stepwise by 2 ml/min up to 32 ml/min collecting a fraction of each 50 ml after every increase of the flowrate (fractions 28, 30 and 32). At a flowrate of 32 ml/min, step size of the flowrate increase per fraction was decreased to 1 ml/min until a maximum of 45 ml/min (fractions 33, 34, 35, 36, 37, 38, 39, 40, 41, 42, 43 and 44). Immediately after reaching a flowrate of 45 ml/min, the centrifuge was switched off and the final fraction was collected (fraction 45). Lymphocyte and monocyte purity within fractions 26A to 45 were determined by flow cytometry *via* forward/side scatter analysis.

Finally, lymphocyte-enriched fractions (lymphocyte purity  $\geq 90\%$ ) were prepared for storage in liquid nitrogen (**section 3.1.5**) and monocyte-enriched fractions (monocyte purity  $\geq 90\%$ ) were subjected to differentiation culture (**section 3.1.9**).

### 3.1.5 Long-term storage of PDEC lines and primary human lymphocytes in liquid nitrogen

For long-term storage of PDEC lines and isolated human primary lymphocytes, cells were stocked in liquid nitrogen. For this purpose, cell suspension was centrifuged for 10 min at 300 ·g and RT. Thereafter, supernatant was aspirated, and cells were resuspended in FCS supplemented with 10 % (v/v) DMSO. Cell suspension was transferred into a cryo tube and stored for 24 h at -80°C. Finally, cryo tubes were transferred into an ARPEGE 110 tank filled with liquid nitrogen.

In order to bring cells back into culture, frozen cell suspension was rapidly thawed by adding pre-warmed culture medium (37°C) and unfrozen cell suspension was immediately diluted in 10 ml/cryo tube pre-warmed fresh culture medium. Finally, cell suspension was centrifuged for 5 min at 300 ·g and sedimented cells were resuspended either in their respective culture medium (**section 2.3.2**) or in ice-cold MACS buffer (**section 2.2**) for subsequent isolation of naïve CD8<sup>+</sup> T cells (**section 3.1.6**).

### 3.1.6 Isolation of primary human naïve CD8<sup>+</sup> T cells

Activated CD8<sup>+</sup> T lymphocytes represent the major T cell subpopulation with considerable cytostatic and cytotoxic properties [68]. In this study, naïve CD8<sup>+</sup> T cells were isolated from lymphocyte-enriched fractions after counterflow centrifugation (**section 3.1.4**) for *in vitro* activation followed by co-culture and PD-L1 blocking experiments.

For this purpose, lymphocyte-enriched fractions from counterflow centrifugation were unfrozen as described in **section 3.1.5**. Afterwards, cell number of pooled lymphocytes was determined. Noteworthy, also trypan blue positive cells were included in cell count to avoid an overloading of the paramagnetic separation columns in the subsequent isolation process. Unlabeled human naïve CD8<sup>+</sup> T cells were obtained by negative selection with the CD8<sup>+</sup> T isolation kit purchased from Miltenyi Biotec according to the manufacturer's instructions (with adapted antibody concentration). The following steps were carried out under sterile conditions with pre-cooled and degassed buffers (2-8°C). The formation of air bubbles was avoided in every step to ensure an optimal isolation process. Briefly, lymphocytes were centrifuged for 10 min at 200 ·g and 4°C. Subsequently, cells were resuspended in MACS buffer at a concentration of 10<sup>7</sup> cells per 40 µl with a maximum of 4 · 10<sup>8</sup> lymphocytes in total. Then, 5 µl of Biotin-Antibody Cocktail per 1 · 10<sup>7</sup> cells were added, well mixed and incubated for 7 min 30 s at 4°C in the refrigerator. Hereafter, 30 µl of MACS buffer and 10 µl MicroBead

Cocktail per  $1 \cdot 10^7$  cells were added to the suspension, well mixed and incubated for 15 min at 4°C in the refrigerator. Meanwhile, MACS LD columns (1 column per maximal  $10^8$  cells) were placed in the magnetic field of a MACS MultiStand and equilibrated with 3 ml MACS buffer. In the following steps, a constant head of liquid on top of the LD columns was ensured to prevent the columns from running dry. After the incubation with MicroBead Cocktail and column equilibration, labeled cell suspension was evenly distributed onto the LD columns. Fresh 50 ml tubes containing 5 ml MACS buffer were placed under each LD column and cell suspension was allowed to run completely into the paramagnetic matrix by gravity. Subsequently, additional 3 ml MACS buffer were added onto each column and allowed to run through the columns by gravity. Finally, the eluates of all LD columns were pooled, and vital cell number was determined. In order to assess the quality of the isolation process, an immunofluorescence co-staining of  $\alpha\beta$  T cell receptor ( $\alpha\beta$ TCR), CD4 and CD8a was performed for subsequent flow cytometric analysis (**section 3.2.1**).

### 3.1.7 Carboxyfluorescein succinimidyl ester staining

Carboxyfluorescein succinimidyl ester (CFSE) staining was performed to track the proliferation of lymphocytes and isolated CD8<sup>+</sup> T cells after activation culture and under the applied culture conditions as well as after blockade of PD-L1. Excessive staining with CFSE is toxic for cells, since the dye covalently binds to lysine residues and other amine groups within the cell and, therefore, potentially impairs the function of essential molecules. Hence, following exactly the protocol is highly recommended.

CFSE staining was carried out under prevention of excessive light exposure, if possible, in the dark. First, CFSE (Stock: 5  $\mu$ M) was diluted to a concentration of 5 mM in 1 ml T cell medium. Secondly, cells were sedimented by centrifugation for 10 min at 300  $\cdot$ g and RT in a conical 50 ml tube. Thirdly, supernatant was discarded, and cells were rapidly resuspended in pre-diluted CFSE medium avoiding the formation of air bubbles to ensure a homogenous staining. Then, the cell suspension was incubated for 5 min at RT in the dark. Afterwards, cells were carefully but thoroughly washed thrice with 25 ml T cell medium at each step and centrifugation for 10 min at 300  $\cdot$ g and RT in between. Finally, vital cell count was determined prior to seeding for activation culture (**section 3.1.8**).

### 3.1.8 Activation and cultivation of primary human naïve (CD8<sup>+</sup>) T cells

Activation of primary human naïve lymphocytes and isolated CD8<sup>+</sup> T cells was performed *via* administration of immobilized CD28 and soluble CD3 antibodies. This stimulation causes the artificial clustering of the CD3-TCR complex with CD28 at the cell membrane and, thereby, polyclonal activation of TCR downstream signaling [259].

For this purpose, an uncoated polystyrene 24-well cell culture plate was coated with CD3 antibody by adding 200 µl of 1.5 µg/ml CD3 antibody (**section 2.5.2**) diluted in sterile PBS in each well. Afterwards, the culture plate was sealed with Parafilm and incubated for 3 h at 37°C in the incubator. Afterwards, the coated wells were rinsed twice with sterile PBS to remove unbound antibody. Then, CFSE-labeled lymphocytes or isolated CD8<sup>+</sup> T cells (**section 3.1.7**) were seeded at a density of  $1.5 \cdot 10^6$  cells per well in T cell medium and 1.5 µg/ml soluble CD28 antibody were added to each well. Isolated CD8<sup>+</sup> T cells were additionally stimulated with 60 ng/ml ( $\cong$  1200 U/ml) recombinant human IL-2. Activation status of lymphocytes was analyzed after culture durations of 3 and 5 days, respectively. Hence, an activation culture duration of 4 days, including a restimulation after 72 h with 60 ng/ml ( $\cong$  1200 U/ml) recombinant human IL-2, was established for subsequent co-culture experiments of CD8<sup>+</sup> T cells with PDECs and/or polarized macrophages.

### 3.1.9 Differentiation and cultivation of primary human polarized macrophages

Macrophages displaying an M1- or M2-like polarized phenotype were generated *in vitro* from isolated monocytes (**section 3.1.4**) by stimulation with Granulocyte-Macrophage Colony Stimulating Factor (GM-CSF) and Macrophage Colony-Stimulating Factor (M-CSF), respectively.

Briefly, monocyte-enriched fractions (monocyte purity  $\geq$  90 %) from counterflow centrifugation were centrifuged for 10 min at 300 ·g, sedimented monocytes were resuspended in macrophage medium (**section 2.3.2**) and pooled. Afterwards, monocytes were counted, and  $15 \cdot 10^6$  cells were transferred into a 50 ml tube. Subsequently, the monocyte suspension was filled up to a volume of 27 ml with macrophage medium and either 2.4 ng/ml GM-CSF ( $\cong$  240 U/ml) or 50 ng/ml M-CSF ( $\cong$  100 U/ml) were added. Avoiding the accumulation of air bubbles, the monocyte suspension was transferred into VueLife culture bags. Differentiation cultures were incubated for 7 days at 37 °C, 5 % CO<sub>2</sub> and 86 % humidity before polarized macrophages were used for experiments.

For harvesting *in vitro* polarized macrophages, culture bags were incubated on ice for 30 min before macrophages were carefully mechanically detached. The content of a culture bag was transferred into a 50 ml tube. Afterwards, culture bag was rinsed with sterile PBS to optimize the cell yield. Subsequently, the cell suspension was centrifuged for 10 min at 300  $\cdot$ g. Sedimented macrophages were resuspended in co-culture medium and counted for seeding the appropriate number of cells. The phenotype of M1-like and M2-like polarized macrophages generated by GM-CSF and M-CSF stimulation, respectively, has been characterized in previous studies and regularly verified before subsequent experiments in the present study [58,260,261].

### 3.1.10 *In vitro* mono- and co-culture settings

For *in vitro* mono- and co-culture experiments, all PDEC lines, polarized macrophages and lymphocytes as well as isolated CD8<sup>+</sup> T cells were seeded in 2 ml of their respective medium (section 2.3.2) into 12-well flat bottom cell culture plates and cultured under standard cell culture conditions at 37°C, 5 % CO<sub>2</sub> and 86 % humidity. PD-L1 blocking antibody Durvalumab or its respective human IgG<sub>1</sub> isotype control antibody was applied at a concentration of 10  $\mu$ g/ml in culture settings. Any variations are stated in the following part.

#### Day 1

PDECs were seeded at a density of  $5 \cdot 10^4$  cells per well and allowed to adhere and grow for 24 h. Isolated CD8<sup>+</sup> T cells were restimulated with recombinant human IL-2 (section 3.1.8).

#### Day 2

PDEC's medium was replaced by fresh culture medium and cells were stimulated with either human IgG<sub>1</sub> isotype control antibody or Durvalumab in mono-culture settings.

M1- and M2-like polarized human macrophages were seeded at a density of  $1 \cdot 10^6$  cells per well either directly into a 12-well flat bottom cell culture plate or into a 12-well transwell insert that has been placed into a 12-well flat bottom culture plate. Then, the macrophages were allowed to acclimate for 6 h until medium was replaced by fresh culture medium and cells were stimulated with either human IgG<sub>1</sub> isotype control antibody or Durvalumab in mono-culture settings.

Pre-activated lymphocytes or isolated CD8<sup>+</sup> T cells were seeded at a density of  $1 \cdot 10^6$  cells per well and left unstimulated or stimulated with human IgG<sub>1</sub> isotype control and Durvalumab, respectively, in mono-culture settings. For direct co-culture with either PDECs or polarized human macrophages, the culture medium from PDECs and macrophages was aspirated and  $1 \cdot 10^6$  pre-activated CD8<sup>+</sup> T cells were added. Afterwards, the cells were left unstimulated or

stimulated with human IgG<sub>1</sub> isotype control antibody and Durvalumab, respectively. For the triple co-culture setting, the culture medium from PancTu-I cells in the culture plates as well as the culture medium from M1-like polarized macrophages in the transwell inserts was aspirated. Then,  $1 \cdot 10^6$  pre-activated CD8<sup>+</sup> T cells were added to the PancTu-I cells in direct co-culture in 1 ml co-culture medium. Finally, transwell inserts containing M1-like polarized macrophages were added and filled with 1 ml co-culture medium. For all co-culture and triple co-culture experiments respective mono- and co-culture control settings were run in parallel. A schematic illustration of the triple co-culture system is depicted in **Figure 11**.

#### Day 4

The culture duration of triple co-cultures and respective control groups ended after 48 h.

#### Day 5

The culture duration of mono-cultures as well as co-cultures and respective control groups ended after 72 h.

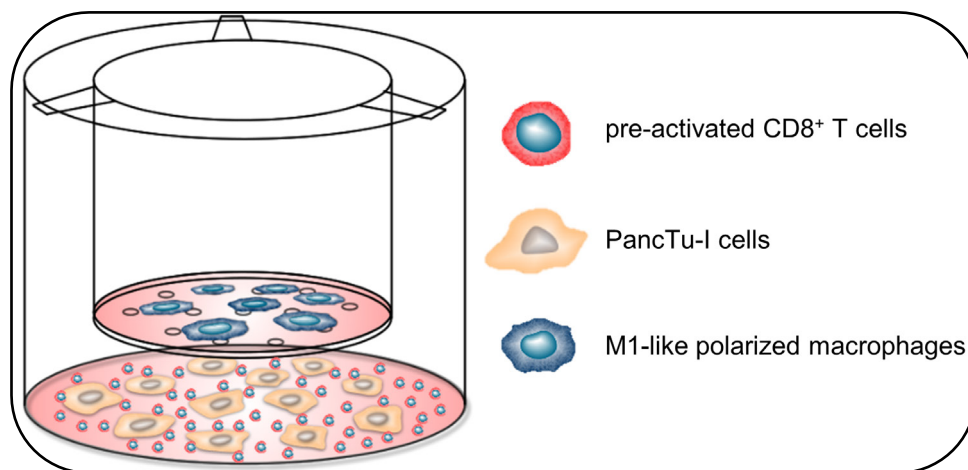


**Figure 11:** Schematic illustration of the setting for co-culture of pre-activated CD8<sup>+</sup> T lymphocytes, M1-polarized macrophages and PancTu-I cells. PancTu-I cells and CD8<sup>+</sup> T lymphocytes are seeded in the lower well of a 12-well culture plate for direct co-culture. M1-polarized macrophages are seeded in transwell inserts with a pore size of 0.4  $\mu\text{m}$ .

### 3.1.11 Single-cell dissociation from human PDAC tissues

Freshly isolated tumor tissues were obtained from PDAC patients during surgery at the community hospital in Kiel. Written and informed consent was obtained from all patients. Histopathological diagnosis was performed by board certified surgical pathologists in the pathology of the community hospital in Kiel. Isolation of vital tumor and stromal cells from PDAC tissues was performed with the human Tumor Dissociation Kit purchased from Miltenyi Biotec. Briefly, tumor tissue was cut with a scalpel into pieces of approximately 0.5 mm<sup>3</sup> in size and incubated in 10 ml RPMI 1640 supplemented with an enzyme mix provided by the kit



for 1 h at 37°C on a roller mixer. Afterwards, remaining undissociated tissue pieces were filtered out with cell strainers (mesh sizes: 100 µm and 30 µm). Finally, the cells were centrifuged for 10 min at 300 ·g and 4°C, washed with cold MACS buffer and counted for subsequent immunofluorescence staining (**section 3.2.1.1**)

## 3.2 Immunobiological methods

### 3.2.1 Immunofluorescence staining

#### 3.2.1.1 Flow cytometry

Intracellular and cell surface proteins were detected on single-cell level by immunofluorescence staining followed by flow cytometric analysis. Unless otherwise stated, the following staining procedure was performed cold either on ice or in the refrigerator at 4°C. In case of intracellular and cell surface co-staining approaches, cell surface staining was performed first. Briefly, up to  $1 \cdot 10^7$  cells were resuspended in 80 µl cold MACS buffer. Then, 20 µl human FcR Blocking Reagent were added, the cell suspension was well mixed and incubated for 10 min at 4°C in the refrigerator. Afterwards,  $2 - 4 \cdot 10^5$  cells per staining were transferred to a 96-well V-bottom plate, cold MACS was added to a total volume of 200 µl and the cell suspension was centrifuged for 10 min at 300 ·g and 4°C. Subsequently, the supernatant was dumped and the sedimented cells were carefully resuspended in 25 µl cold MACS buffer supplemented with respective antibodies at indicated concentrations (**section 2.5.2**). Incubation was carried out for 20 min at 4°C in the refrigerator. Hereafter, the cells were washed twice with ice-cold MACS buffer by centrifugation for 10 min at 300 ·g and 4°C. If no additional intracellular staining was intended, the cells were resuspended in 100 µl fixation solution, transferred into FACS tubes, sealed with Parafilm and wrapped in aluminum foil for storage of up to 7 days until flow cytometric measurement. For additional intracellular staining, the cells were resuspended in 50 µl FixPerm solution after the second washing step and incubated for 10 min at RT in the dark. Afterwards, 150 µl cold Perm Washing buffer were added and the cell suspension was centrifuged for 10 min at 300 ·g and 4°C. Then, the supernatant was dumped, and the cells were resuspended in 25 µl cold Perm Washing buffer supplemented with respective antibodies at indicated concentrations (**section 2.5.2**). Incubation was performed for 20 min at 4°C in the refrigerator. Finally, the cells were washed twice, once with ice-cold Perm Washing buffer and once with ice-cold MACS buffer, as described before, resuspended in 100 µl fixation solution, transferred into FACS tubes, sealed with Parafilm and wrapped in aluminum foil for storage of up to 7 days until flow cytometric measurement. Data acquisition was performed with a FACScalibur or

LSRFortessa flow cytometer making use of the CellQuest Pro and FACSDiva software, respectively. For each measurement at least signals of  $2 - 3 \cdot 10^5$  cells were acquired. Specificity of each staining was verified by additional staining with respective isotype control antibody. Final data evaluation was carried out with FlowJo 10 software. Relative cell surface expression levels of PD-1, PD-L1, CD163 and CD206 were evaluated by calculation of the median fluorescence intensity (MFI) ratio, which is calculated by the following formula:

$$\text{MFI Ratio} = \frac{\text{MFI (specific staining)}}{\text{MFI (respective isotype control)}}$$

### 3.2.1.2 Immunofluorescence staining for PD-L1 on coverslip-seeded cells and cytopins

For immunofluorescence staining (IF) of cell surface-associated PD-L1 expression in PDECs and polarized macrophages, PDECs and macrophages were seeded into a 12-well culture plate as described in **section 3.1.10** onto sterile 18 mm glass coverslips and Thermanox plastic coverslips, respectively. After cultivation, the medium was aspirated, and the cells were rinsed with cold PBS.

Cytopins were generated from naive and activated lymphocytes for subsequent immunofluorescence staining of cell surface located PD-L1 and PD-1. For this purpose, a SuperFrost Plus adhesion slide was inserted with a filter cartridge and an 8 ml cyto-chamber on top in a cyto-clamping plate. Then,  $2.5 \cdot 10^5$  cells in 500  $\mu$ l PBS were transferred into the cyto-chamber and centrifuged for 3 min at 340  $\cdot$ g and RT with an acceleration of 1/9 and deceleration 7/9. Finally, the cyto-chamber was removed, and the slides were centrifuged for 1 min at 1380  $\cdot$ g with acceleration 3/9 and deceleration 9/9. Hereafter, cytopins were subjected to IF staining for PD-L1 and PD-1.

For this purpose, the cells on coverslips and cytopins were fixed by incubation in 4.0 % PFA for 10 min at RT. Afterwards, the cells were washed thrice with PBS for 5 min. IF staining for PD-L1 was carried out with the Alexa Fluor 488 Tyramide SuperBoost, goat anti-rabbit IgG Kit provided by Thermo Scientific according to the manufacturer's instructions. Briefly, coverslip/adhesion slide-attached cells were incubated with stabilized 3 % Hydrogen Peroxide Solution (Component C2) for 1 h at RT in a humified chamber. Hereafter, the cells were thoroughly rinsed and incubated with Blocking buffer (Component A) for 1 h at RT in a humified chamber. Then, the cells were incubated with anti-PD-L1 antibody (clone E1L3N, Cell Signaling) diluted at 4.37  $\mu$ g/ml in PBS supplemented with 1 % (w/v) BSA overnight in a

humified chamber. Subsequently, the cells were thoroughly washed thrice with PBS for 5 min and incubated with goat anti-rabbit poly-HRP-conjugated secondary antibody (Component B) for 1 h at RT in a humified chamber. Afterwards, the cells were again thoroughly washed three-times with PBS for 5 min and incubated with freshly prepared Tyramide working solution for 10 min at RT in the dark. Thereafter, Tyramide working solution was aspirated, an equal volume of freshly prepared Reaction Stop Reagent was added and incubated for 5 min at RT in the dark. For subsequent nuclei staining, the cells were rinsed and incubated in Hoechst 33258 diluted at 2 µg/ml in PBS supplemented with 1 % (w/v) BSA for 45 min at RT in a humified chamber. Finally, the cells were thoroughly rinsed thrice with PBS and once with ddH<sub>2</sub>O before the coverslips were sealed upside-down in a drop of Fluoro-Gel onto an object slide with clear nail polish. After drying of the nail polish, slides were stored at 4°C in the refrigerator. Fluorescence signals were detected, acquired and evaluated with a Lionheart FX Automated Microscope.

### **3.2.1.3 Immunofluorescence co-staining of PD-L1 and CD68 in pancreatic tissue sections**

For IF staining, formalin-fixed paraffin-embedded (FFPE) pancreatic tumor tissue sections from PDAC patients were deparaffinized with Xylene and rehydrated with a descending alcohol series. Afterwards, tissue sections were washed in PBS before antigen-retrieval was performed by incubation in a steamer for 20°C in pre-warmed citrate buffer pH 6.0. After cool-down to RT, quenching of tissue autofluorescence was performed *via* incubation in 70 % (v/v) ethanol in ddH<sub>2</sub>O supplemented with 0.1 % (w/v) Sudan Black B for 20 min at RT. Then, IF staining of PD-L1 with the Alexa Fluor 488 Tyramide SuperBoost, goat anti-rabbit IgG Kit was carried out as described in **section 3.2.1.2**. For co-staining, an anti-human CD68 antibody was applied at the indicated concentration (**section 2.5.2**) simultaneously with the anti-human PD-L1 antibody. Moreover, a goat anti-mouse IgG (H+L)-AF546 antibody (**section 2.5.2**) was added to the secondary antibody incubation step. Image acquisition and staining evaluation was performed with a Lionheart FX Automated Microscope.

### 3.2.2 Immunohistochemistry

Immunohistochemical PD-L1 staining in FFPE pancreatic tumor tissue sections from PDAC patients was carried out on a BOND-MAX Automated IHC/ISH Stainer in the Institute of Pathology at the UK-SH in Kiel. For this purpose, FFPE tissue sections were deparaffinized with xylene and rehydrated in a descending alcohol series. Afterwards, heat-induced epitope retrieval was performed by incubation for 20 min at 100°C in BOND Epitope Retrieval ER2 solution (pH 9.0). Subsequent staining was conducted with the Polymer Refine Detection Kit provided by Leica according to the program listed in **Table 4**.

**Table 4: BOND-MAX Automated IHC/ISH Stainer program for immunohistochemical detection of PD-L1 in deparaffinized, rehydrated formalin-fixed tissue sections.**

| Step             | Reagent  | Time (min) |
|------------------|--|------------|
| Peroxide block   | Polymer Refine Detection Kit, Peroxide Block   | 5          |
| Primary antibody | anti-PD-L1 (E1L3N) diluted at 8.76 µg/ml       | 20         |
| Linker antibody  | Polymer Refine Detection Kit, Post-Primary     | 8          |
| Polymer antibody | Polymer Refine Detection Kit, Polymer          | 8          |
| Imaging          | Polymer Refine Detection Kit; Mixed DAB Refine | 10         |
| Counterstaining  | Polymer Refine Detection Kit, Hematoxylin      | 5          |

Finally, stained tissue sections were dehydrated by incubation in ascending alcohol series and xylene before conservation with SignalStain Mounting Medium. Specificity of the staining was ensured by application of a respective rabbit IgG isotype control antibody revealing no staining. Immunohistochemical staining for CD3, CD4, CD8, CD25, FoxP3,  $\gamma\delta$ TCR, CD68, HLA-DR, CD163,  $\alpha$ -SMA, Vimentin, E-Cadherin, L1CAM, PanCK and Ki67 referred to in this study have been performed and described in a previous study [88].

### 3.2.3 Multiplex analysis of culture supernatants

Supernatants from lymphocyte and CD8<sup>+</sup> T cell cultures were analyzed for the abundance of cytokines, chemokines and effector molecules related to a cytostatic/cytotoxic T cell activation status. For this purpose, cell culture supernatants were collected and centrifuged for 10 min at 15000 ·g and 4°C to remove remaining cells and cellular debris. Resulting supernatants were stored at -80°C until further processing. Analysis of supernatants was performed with a customized human LEGENDplex panel, a bead-based flow cytometric multiplex assay,

purchased from BioLegend and carried out with adapted antibody concentrations according to the manufacturer's instructions. The compiled custom panel included antibodies for the detection of human VEGF-A, TNF $\alpha$ , IL-6, IL-8, IL-17A, soluble Fas, soluble Fas ligand, Granzyme A, Granzyme B, IFN $\gamma$ , Granulysin and Perforin. Prior to assay procedure, all reagents were pre-warmed at RT, supplied pre-mixed beads and antibodies were incubated for 10 min in an ultrasonic bath and Wash Buffer was diluted with ddH<sub>2</sub>O. Then, the provided lyophilized standard was reconstituted in 250  $\mu$ l Assay Buffer by briefly vortexing and incubation for 10 min at RT. Afterwards, the solubilized standard stock (standard C7) was diluted in a serial dilution with Assay Buffer to 1:4 (C6), 1:16 (C5), 1:64 (C4), 1:256 (C3), 1:1024 (C2) and 1:4096 (C1). Assay Buffer was used as blank sample (C0). First, 50  $\mu$ l of Assay Buffer were added to each well of a 96-well V-bottom plate. Secondly, 12.5  $\mu$ l of standard dilutions (C7 to C0) were added to the respective standard wells and 12.5  $\mu$ l of cell culture supernatants were added to the respective sample wells. Thirdly, 12.5  $\mu$ l of sonicated pre-mixed bead cocktail were added to each well, the plate was sealed with a plate sealer, wrapped in aluminum foil and incubated for 2 h at 800 rpm and RT on a plate shaker. Hereafter, the plate was centrifuged for 5 min at 250  $\cdot$ g and RT. Then, the supernatant was dumped by quickly inverting and flicking the plate before 200  $\mu$ l 1X Wash Buffer were added to each well. Then, beads were resuspended by incubating the plate for 1 min at 800 rpm on a shaker. Afterwards, beads were sedimented again by centrifugation for 5 min at 250  $\cdot$ g and RT. Then, 12.5  $\mu$ l Assay Buffer and 12.5  $\mu$ l Detection Antibody Cocktail were added to each well, beads were carefully resuspended, and the plate was sealed with a plate sealer, wrapped in aluminum foil and incubated for 1 h at 800 rpm and RT on a plate shaker. Subsequently, 12.5  $\mu$ l Assay Buffer and 12.5  $\mu$ l SA-PE Cocktail were added to each well, thoroughly mixed and the plate was sealed with a plate sealer, wrapped in aluminum foil and incubated for 10 min at 800 rpm and RT on a plate shaker. Finally, the plate was centrifuged for 5 min at 250  $\cdot$ g and RT, the supernatant was dumped, the beads were resuspended in 200  $\mu$ l 1X Wash Buffer and transferred to a 1.5 ml Eppendorf tube for subsequent analysis. Data acquisition was carried out with a FACSverse flow cytometer and FACSDiva software (Beckton Dickinson). Data processing and analysis was performed with the LEGENDplex Data Analysis software v8 (VigeneTech) according to the provided manual.

### 3.3 Molecular biological methods

#### 3.3.1 RNA Isolation and quantification

Isolation of RNA from PDECs, macrophages and lymphocytes was performed making use of the peqGOLD Total RNA Kit purchased from peqLab according to manufacturer's instructions. Briefly, adherent cells (PDECs and macrophages) were washed with PBS directly in the culture plate, lysed in 300  $\mu$ l lysis buffer T and lysates were transferred into a 1.5 ml Eppendorf tube. Lymphocytes were centrifuged for 10 min at 300  $\cdot$ g and 4°C, resuspended in PBS and again sedimented by centrifugation. Then, lymphocytes were resuspended in 300  $\mu$ l lysis buffer T. Lysates were either frozen at -80 °C for storage or immediately subjected to RNA isolation. In the latter case, the lysates were transferred onto DNA removing column. After centrifugation for 1 min at 11.000  $\cdot$ g and RT, 300  $\mu$ l 70 % (v/v) ethanol were added to RNA in the flow through. Gently mixed RNA suspension was transferred onto PerfectBind column and centrifuged for 1 min at 11.000  $\cdot$ g and RT. Subsequently, the column with bound RNA was washed once with 500  $\mu$ l RNA washing buffer I and once with 600  $\mu$ l RNA washing buffer II. Finally, the empty binding column was centrifuged for 2 min at 11.000  $\cdot$ g before 40  $\mu$ l RNase-free water were pipetted onto the membrane. After incubation for 2 min, RNA was eluted by centrifugation for 2 min at 8.000  $\cdot$ g into a 1.5 ml Eppendorf tube. RNA samples were stored at -80 °C.

Nucleic acid concentrations were determined using a Tecan Infinite 200PRO spectrophotometer in combination with NanoQuant plate application.

#### 3.3.2 Complementary DNA synthesis *via* reverse transcription

In this study, the RevertAid First Strand cDNA Synthesis Kit provided by Fermentas was used for synthesis of complementary DNA (cDNA) from isolated RNA according to the manufacturer's instructions.

Briefly, 0.1 - 500 ng of RNA template were prepositioned in a 1.5 ml Eppendorf tube. Then, 1  $\mu$ l of oligo dT primer was added and suspension filled up to a volume of 12.5  $\mu$ l with nuclease-free water. Afterwards, suspension was incubated for 5 min at 65 °C, spun-down and again cooled down on ice. Following this, 7.5  $\mu$ l of the prepared master mix (**Table 5**) were added, gently mixed and incubated for 1 h at 42 °C in a block heater.

**Table 5: Master Mix composition per sample for complementary DNA synthesis from mRNA templates.**

| Reagent                                  | Volume ( $\mu$ l) |
|--|-------------------|
| Reaction buffer (5x)                     | 4                 |
| RiboLock RNase inhibitor (20 U/ $\mu$ l) | 0.5               |
| 10 mM dNTP Mix                           | 2                 |
| RevertAid M-MuLV RvT (200 U/ $\mu$ l)    | 1                 |

Finally, the reaction was stopped by heating the sample for 5 min at 70 °C. Resulting single stranded cDNA was stored at -20 °C.

### 3.3.3 Quantitative real-time polymerase chain reaction

Quantitative real-time polymerase chain reaction (qPCR) was performed for relative quantification of activation- and differentiation-associated cytokine and chemokine expression in lymphocytes and polarized macrophages as well as EMT-related marker expression in PDECs.

For this purpose, synthesized cDNA (**section 3.3.2**) was diluted at 1:3 with nuclease-free water and 2.5  $\mu$ l of this dilution were pipetted into wells of a 96-well PCR plate. In order to detect variances due to pipetting inaccuracies, each sample was analyzed in technical triplicates. Afterwards, 7.5  $\mu$ l of the respective master mix (**Table 6**) were added to each well. For appropriate mixture of cDNA template and master mix, PCR plates were centrifuged for 2 min at 300  $\cdot$ g and 4 °C.

**Table 6: Master Mix composition per sample for quantitative real-time polymerase chain reaction from cDNA templates.**

| Reagent                          | Volume ( $\mu$ l)<br>(Eurofins primer) | Volume ( $\mu$ l)<br>(RealTime primer) |
|----------------------------------|--|--|
| Light Cycler SYBR Green I Master | 5                                      | 5                                      |
| Forward Primer                   | 1                                      | -                                      |
| Reverse Primer                   | 1                                      | -                                      |
| Forward/Reverse Primer Mix       | -                                      | 1                                      |
| Nuclease-free distilled water    | 0.5                                    | 1.5                                    |

Light Cycler SYBR Green I Master is endowed with FastStart Taq DNA polymerase, SYBR Green I dye, dNTPs as well as appropriate ionic concentrations and components for hot start reaction. Template amplification and measurement were carried out with a LightCycler 480 II applying the program listed in **Table 7**.

**Table 7: Light Cycler program for cDNA amplification and analysis in quantitative real-time polymerase chain reaction.**

| Step No. | Time   | Temperature (°C)         | Step                 |
|----------|--------|--------------------------|----------------------|
| 1        | 5 min  | 95                       | Initial Denaturation |
| 2        | 10 s   | 95                       | Denaturation         |
| 3        | 20 s   | <b>2.4.1</b>             | Annealing            |
| 4        | 30 s   | 72                       | Elongation           |
| 5        | —      | Steps 2-4 (40-50 cycles) | —                    |
| 6        | 10 min | 72                       | Final elongation     |
| 7        | 5 min  | 72 to 95                 | Melting curve        |
| 8        | ∞      | 4                        | Cooling              |

Evaluation of qPCR results was accomplished by  $2^{-\Delta\Delta C_t}$ -method. Therefore, cycle threshold (Ct) was defined and mean Ct-value of technical triplicates was calculated. As internal quality controls technical replicates were excluded from further analysis when Ct-values differed by more than  $\pm 0.5$  from each other and specificity of amplification process was verified by melting curve analysis. Finally, gene of interest's (GOI) Ct-values were referred to respective Ct-value of the housekeeper gene according to the following formula:

$$relative\ expression = 2^{-\left(\frac{Ct(GOI)}{Ct(housekeeper)}\right)}$$



## 3.4 Biochemical methods

### 3.4.1 Isolation and quantification of proteins

For analyses of alterations in cellular protein synthesis, whole cell lysates were prepared, and protein content was determined followed by SDS-PAGE (**section 3.4.2**) and western blotting (**section 3.4.3**). For this purpose, culture medium was aspirated, cells were washed with PBS and 100 - 150  $\mu$ l Lämmli buffer supplemented with 1 mM sodium orthovanadate were added to the cells dependent on the cellular confluency and cell number, respectively. After detachment of the cells, cell lysates were transferred into a 1.5 ml Eppendorf tube and treated with a sonicator to ensure protein solubilization by cellular decomposition. Whole cell lysates were stored at -20 °C.

Protein concentrations were determined making use of the colorimetric DC<sup>TM</sup> Protein Assay kit provided by Bio-Rad according to the manufacturer's instructions. This kit endows all components for a modified protein assay according to Lowry [262]. For calibration, a standard row containing defined concentrations of BSA solved in Lämmli buffer was applied. For this purpose, the provided BSA standard with a concentration of 1.55 mg/ml was diluted at 1:2, 1:4 and 1:8. Additionally, samples containing only Lämmli buffer (zero value) and only reaction mix (blank value) were prepared. First, a volume of 5  $\mu$ l for protein samples and standard row samples were applied in technical duplicates into the wells of 96-well transparent flat-bottom plate. Then, 25  $\mu$ l of a 1:50 dilution of reagent S in reagent A were added to each well followed by additional 200  $\mu$ l of reagent B. Reaction was incubated for 15 min in darkness at RT before light absorption was measured at  $\lambda = 750$  nm using a Tecan Infinite 200PRO spectrophotometer. Protein concentrations were calculated based on the resulting linear regression formula for standard samples values.

### 3.4.2 Sodium dodecyl sulfate polyacrylamide gel electrophoresis

Sodium dodecyl sulfate polyacrylamide gel electrophoresis (SDS-PAGE) was carried out for pre-separation of proteins in whole cell lysates for subsequent western blot analysis (**section 3.4.3**).

For this purpose, whole cell lysate samples were adjusted to an equal protein content with Lämmli buffer. Then, loading dye (4x) was added at a dilution of 1:4 and samples were mixed. Finally, lysates were heated for 10 min at 95°C in a heating block and spun-down before they were applied to the polyacrylamide gel. Buffers and gel system for SDS-PAGE were applied according to Lämmli as indicated in **section 2.2** [263]. Polyacrylamide content in running gels

varied in a range from 10 to 15 % according to the intended resolution of proteins at low or high molecular weight, respectively. Electrophoresis was performed with a MINI-Protean Tetra Cell system at constant voltage of 90 V.

### 3.4.3 Western blotting

Western blotting (WB) was performed with the semi-dry Trans-Blot Turbo Transfer System provided by Bio-Rad. Therefore, PVDF membrane was activated by deposition in methanol for 10 s. Afterwards, gel was removed from the electrophoresis chamber and Whatman filter papers were soaked in Trans-Blot Turbo 5x Transfer buffer diluted 1:5 in ethanol/ddH<sub>2</sub>O (1:3). Finally, Whatman filter papers, PVDF membrane, polyacrylamide gel and again Whatman filter papers were air bubble-free stacked onto the anode of the transfer chamber. Protein transfer onto the PVDF membrane was performed at 2.5 mA (constant) and 25 V (maximum) for 10 min. Afterwards, the PVDF membrane was washed with TBS-T for 10 min before the membrane was blocked by incubation in TBS-T supplemented with 5 % (w/v) milk powder (Blotto) on a 3D shaker for 1 h at RT. Then, the membrane was incubated in primary antibodies solved at respective dilutions (**section 2.5.2**) in BlueBlock PF (10x), pre-diluted 1:10 in ddH<sub>2</sub>O, overnight at 4°C on a roller mixer. Hereafter, the membrane was washed with TBS-T three times for 10 min, before it was incubated in secondary antibody solution at appropriate dilutions (**section 2.5.2**) for 1 h at RT on a roller mixer. Finally, the membrane was washed thrice with TBS-T for 10 min and incubated in Western Bright ECL substrate for 2 min in the dark. Chemiluminescence signals were recorded with the Fusion SL detection system and processed with the corresponding FUSION-CAPT 16.06 software. Densitometric analyses were performed with ImageJ. In this process, signals for proteins of interest were normalized to examined signal intensities of respective loading controls.

## 3.5 Microscopical analysis

### 3.5.1 Evaluation of PD-L1 staining in pancreatic tissue sections from PDAC patients

Evaluation of immunohistochemical PD-L1 staining in pancreatic tumor and peritumoral tissue sections from PDAC patients was carried out with an Axioplan 2.0 microscope (Zeiss). Briefly, whole tissue sections (1-6 cm<sup>2</sup>) were screened at 200-fold magnification and each microscopic field of view (FoV,  $\varnothing$  0.87 mm) was rated with regard to the percentage of PD-L1 positive cells and the mean staining intensity of stained cells. Notably, only membranous staining was assessed in epithelial/tumor cells while stromal cells were rated positive for any staining. Moreover, only ductal epithelial, tumor and stromal cells as well as tumor-associated lymph follicles were included in the rating. Fat and neural tissue as well as acinus and endothelial cells were excluded from evaluation. The following immunoreactivity scoring system (IRS) was applied for each microscopic FoV as previously published in [264]: (I) the presence and percentage of PD-L1<sup>+</sup> cells were graded as 0 (negative), 1 ( $\leq$  1% positive) or 2 ( $>$  1% positive), (II) the mean staining intensity of FoV comprising PD-L1<sup>+</sup> cells were graded as 1 (weak), 2 (moderate) or 3 (strong). The total number of graded FoV (30-600) depended on the size of the tumor tissue section. Hereafter, the IRS for each FoV was calculated by summation of both scores resulting in values ranging from 0 to 5. Finally, the „Tissue Score“ for each specimen was determined by calculating the mean value of its total IRS scores. In order to characterize the intratumoral/local scattering of PD-L1 positive cells within each tissue section, the proximity of PD-L1 expressing cells towards each other within FoV with an IRS  $>$ 0 was graded as 0 (PD-L1 positive cells are widely distributed) or 1 (formation of PD-L1<sup>+</sup> cell cluster). The resulting „Cluster Score“ for each specimen represents the mean value of all rated FoV resulting in values between 0 and 1. In order to score PD-L1 expression in tumor-associated lymph follicles, staining intensity within each follicle was graded as 0 (negative), 1 (weak) or 2 (strong). The resulting „Lymph Score“ for each specimen represents the median value of all rated tumor-associated lymph follicles. Correlation of Tissue Scores with post-surgical patient survival resulted in classification of PD-L1<sup>low</sup> and PD-L1<sup>high</sup> tissue sections. Hereafter, proportion of PD-L1<sup>+</sup> PanCK<sup>+</sup> and PD-L1<sup>+</sup> PanCK<sup>-</sup> cells within PD-L1<sup>high</sup> tissue sections was evaluated by immunohistochemical PanCK/PD-L1 staining. Therefore, tissue sections were screened at 400-fold magnification to count the number of PanCK<sup>+</sup> PD-L1<sup>+</sup> and PanCK<sup>-</sup> PD-L1<sup>+</sup> cells within each FoV. FoV comprising more PanCK<sup>+</sup> PD-L1<sup>+</sup> cells were graded as 1 and FoV comprising more PanCK<sup>-</sup> PD-L1<sup>+</sup> cells were rated as 2. Cell Scores 1 ( $\geq$  90% FoV rated as 1), 2 ( $\geq$  90% FoV rated as 2) and 3 ( $\sum$ FoV=1  $\approx$   $\sum$ FoV=2) are based on the overall proportion

of FoV graded as 1 or 2 within the tissue section. All evaluations were performed twice in a blinded manner. In case of discrepant results, sections were additionally evaluated by a second investigator.

### 3.5.2 Cellular confluency analysis

PDECs seeded on coverslips were stained with CellTracker Red CMPTX dye and Hoechst 33258 for subsequent microscopical analysis. Therefore, the culture medium was aspirated, and cells were incubated in fresh culture medium supplemented with 5  $\mu$ M CellTracker Red CMTPX dye for 30 min at 37°C, 5 % CO<sub>2</sub> and 86 % humidity. Afterwards, cells were rinsed twice with PBS and fixed with 4.0 % PFA for 10 min at RT in the dark. Then, cells were washed three-times with PBS for 5 min and stained with Hoechst 33528 diluted at 2  $\mu$ g/ml in PBS supplemented with 1 % (w/v) BSA for 45 min at RT in a humidified chamber. Finally, coverslips were washed thrice with PBS, once with ddH<sub>2</sub>O and sealed upside down in a drop of Fluoro-Gel onto a microscopic slide with clear nail polish. Staining was stored at 4°C in the refrigerator until analysis.

For analysis, coverslips with stained PDECs were scanned with a Lionheart FX Automated Microscope at 4-fold magnification and images were stitched with Gen5 Data Analysis Software in “Process” mode. Afterwards, a representative square area (Plug) with a size of 64000000  $\mu$ m<sup>2</sup> was selected *via* implemented “Cellular Analysis” tool of the “Analyze” mode. Finally, cellular area was discriminated from cell-free area based on acquired signals in DAPI (LED 356 nm | EX 377/50 | EM 447/60) and RFP (LED 523 nm | EX 531/40 | EM 593/40) filter channels by parameter settings listed in **Table 8**.

**Table 8:** Parameters for cellular confluency analysis with Gen5 software “cell analysis” application.

| Parameter                    | Value         |
|------------------------------|---------------|
| Threshold                    | 5000 - 7000   |
| Background                   | Dark          |
| Split touching objects       | Unchecked     |
| Fill holes in the mask       | Checked       |
| Min. object size             | 5 $\mu$ m     |
| Max. object size             | 10000 $\mu$ m |
| Include primary edge objects | Checked       |
| Analyze entire Image         | Unchecked     |

## — Advanced detection options —

|                          |                                 |
|--------------------------|---------------------------------|
| Background flattening    | Checked                         |
| Auto                     | Unchecked                       |
| Rolling Ball diameter    | 5 $\mu\text{m}$<br>4 pixels     |
| Image smoothing strength | 10 Cycles of 3x3 average filter |
| Evaluate background on   | 1 % of lowest pixels            |
| Primary mask             | Use threshold mask              |

Cellular confluency in the Plug was calculated by following formula:

$$\text{Cellular confluency (\%)} = \left( \frac{\text{Object sum area } (\mu\text{m}^2)}{\text{Plug size } (\mu\text{m}^2)} \right) \cdot 100$$

### 3.6 Statistical analysis

Statistical analyses were performed using SigmaPlot v12.5. First, data were tested for normality and equal variance by Shapiro-Wilk and Equal Variance test, respectively. For comparison of two-groups comprising parametric distributed datasets, t-test was applied. Two groups of datasets that failed normality or equal variance test were analyzed with Mann-Whitney Rank Sum test. Parametric data including multiple groups were tested by one-way analysis of variance (one-way ANOVA) for statistical significance. Non-parametrical datasets of multiple groups were analyzed with Kruskal-Wallis one-way ANOVA on ranks test. Statistically significant differences between the groups were assumed at p-values < 0.05 according to Student-Newman-Keuls method (parametric data) and Dunn's method (non-parametric data), respectively.

Data acquired by histological analyses were examined as raw scores, categorized by dichotomization and resulting values were compared between groups by Chi-square or Fisher Exact test. Survival curves were estimated according to Kaplan-Meier method and potential influence factors were identified by Log-Rank test.

## 4. Results

### 4.1 *In situ* characterization of PD-L1 expression in PDAC tissue

The immunohistochemical detection and pathological classification of PD-L1 expression status in tumor biopsies *via* companion diagnostics is a common method for identification of patients that potentially benefit from therapeutic approaches targeting either PD-1 or PD-L1 by monoclonal antibodies [229,230]. In the case of PDAC, several studies already reported the expression of PD-L1 in pancreatic tumor tissue [98,265–268]. However, PDAC is well known for its exceptional intra- and inter-tumoral heterogeneity and none of the previously published studies elaborated this topic in detail. Therefore, the first aim of this study was to comprehensively characterize PD-L1 expression status in tumoral and stromal compartment *via* IHC in a well-characterized cohort of 59 PDAC tissues and 18 peritumoral pancreatic tissues. The study cohort comprised mainly patients with malignant diseases staged T3N1M0 (86.4%), the most common PDAC stage subjected to curative surgical resection. Further patient characteristics are listed in **Table 9**.

**Table 9: Clinic-pathological characteristics of PDAC patients included in the study cohort**

| Parameter                                 | Number of cases |
|---|-----------------|
| Patients                                  | 59              |
| Median age (range)                        | 66 (46-85)      |
| Sex (male/female)                         | 34 / 25         |
| Tumor stage T1/T2/T3/T4                   | 0 / 0 / 58 / 1  |
| Nodal stage N0/N1                         | 8 / 51          |
| Metastasis stage M0/M1                    | 57 / 2          |
| Tumor grade 1 (well differentiated)       | 7               |
| Tumor grade 2 (moderately differentiated) | 27              |
| Tumor grade 3 (poorly differentiated)     | 24              |
| Post-surgical survival in months (range)  | 13 (0-108)      |

#### 4.1.1 Pancreatic tumor tissues from PDAC patients displays high heterogeneity in terms of PD-L1 staining in various tumor compartments

In order to consider intra-tumoral heterogeneity, whole sections of pancreatic tumor tissues were analyzed for PD-L1 staining in neoplastic and stromal cells as well as tumor-associated lymph follicles. First screenings revealed prominent intra- and intertumoral differences in PD-L1 staining with respect to staining intensity and relative proportion of PD-L1<sup>+</sup> cells. Therefore, staining intensities in each microscopic FoV were scored from 1 to 3 (weak, moderate and strong) (**Figure 12 A-C**) and the proportion of PD-L1<sup>+</sup> cells was rated from 0 to 2 (0%,  $\leq 1\%$  and  $> 1\%$  PD-L1<sup>+</sup> cells) (**Figure 12 D-F**). In order to compare the different PDAC tissue sections within the cohort with each other, Intensity and Quantity Scores were generated for each PDAC tissue by calculating the median value of scored microscopic FoV.

Tumor-associated lymph follicles are tertiary lymphoid structures that are formed *de novo* by local infiltration of leukocytes. Since these structures represent an access point into the tumor for cells like CTLs, PD-L1 staining in tumor-associated lymph follicles was rated separately from the remaining tumor tissue. Here, three distinct staining patterns were discriminated: 0 (negative), 1 (weak) and 2 (strong) (**Figure 12 G-I**). For following comparison of PDAC tissues, Lymph Score was generated for each tissue by calculating the median value of all tumor-associated lymph follicles within each tissue section.

Besides the prominent local clustering of PD-L1 staining observed within tumor-associated lymph follicles, some areas within the remaining tumor tissue also showed notable clusters of PD-L1<sup>+</sup> neoplastic and/or stromal cells while other areas displayed rather a scattered distribution of PD-L1 staining. Therefore, the respective staining pattern in each microscopic FoV was scored as 0 (scattered) or 1 (clustered) (**Figure 12 J+K**). Again, for subsequent comparison of PDAC tissue sections, Cluster Scores were generated by calculating the mean value of all rated FoV within each tissue section.

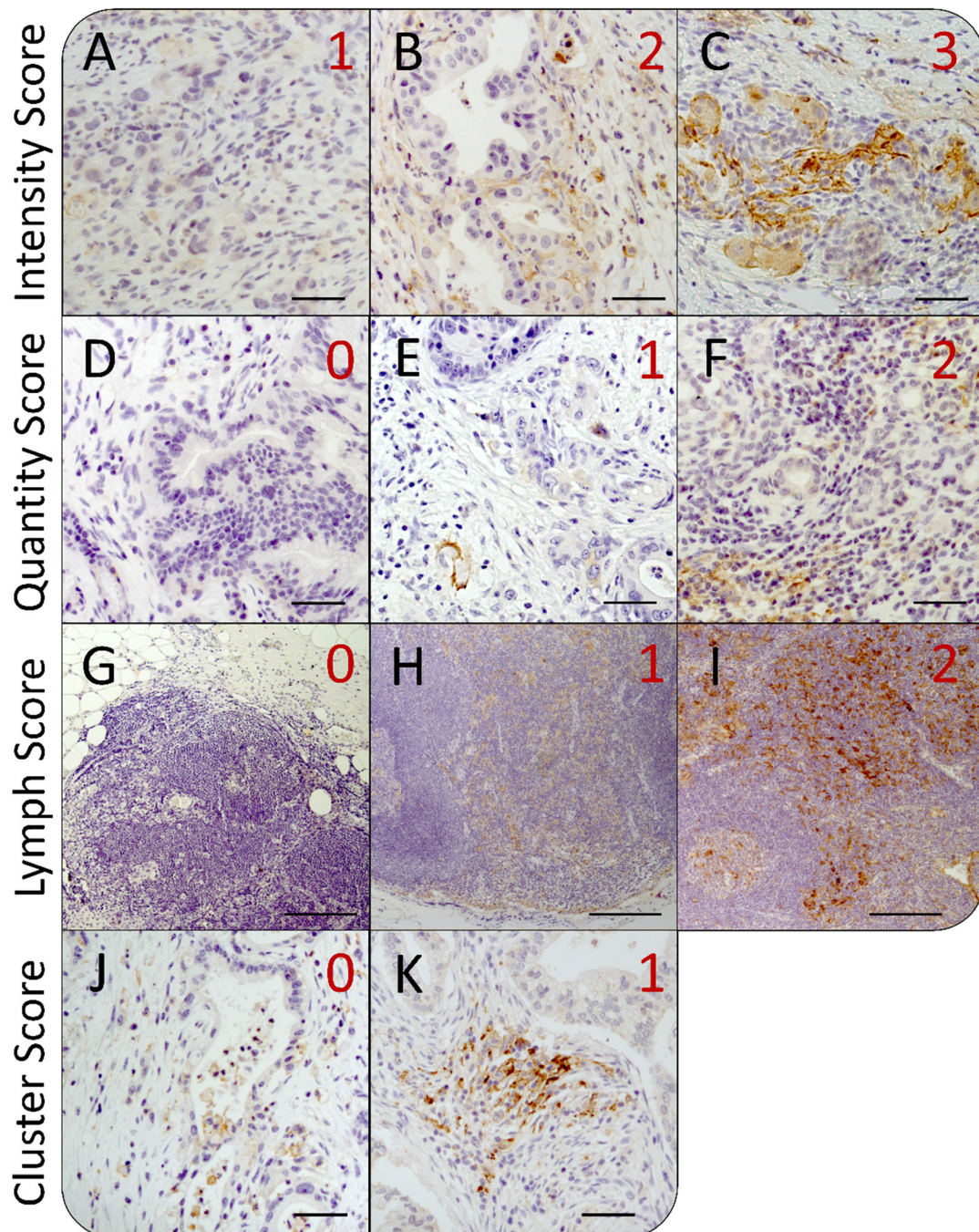


**Figure 12: Heterogeneity of intra-tumoral PD-L1 expression in pancreatic tissue sections from PDAC patients.** Representative images of immunohistochemical PD-L1 staining in pancreatic tissues of PDAC patients for different scoring values (red numbers) with regard to (A-C) the staining intensity, (D-F) the proportion of PD-L1<sup>+</sup> cells, (G-I) the expression in tumor-associated lymph follicles as well as (J+K) the local distribution of PD-L1<sup>+</sup> cells within the tumor. According to the evaluation system, PD-L1 mean staining intensity in fields of view (FoV) showing PD-L1<sup>+</sup> cells was rated as (A) weak (1), (B) moderate (2) or (C) strong (3). The proportion of PD-L1<sup>+</sup> cells within FoV was scored as (D) negative (0), (E) < 1% PD-L1<sup>+</sup> cells (1) or (F) > 1% PD-L1<sup>+</sup> cells (2). PD-L1 expression in tumor-associated lymph follicles was rated as (G) negative (0), (H) weak/moderate (1) or (I) strong (2). Finally, distribution of PD-L1<sup>+</sup> cells within FoV was categorized as (J) „diffuse/patternless“ (0) and (K) „cluster formation“ (1). Original magnification/scale bar: 100-fold/200  $\mu$ m (G-I); 200-fold/50  $\mu$ m (A-F; J+K). (published data [264])



Implementation of this scoring system to all PDAC tissue sections within the cohort revealed that 3 of 59 tissues exhibited mainly tumor-associated lymph follicles and no neoplastic cells within the small proportion of adjacent tissue. Therefore, these sections were excluded from Intensity, Quantity and Cluster scoring. Moreover, 44 of the remaining 56 cases (78.6%) showed scarce overall PD-L1 staining causing Quantity and Intensity Scores of 0. However, some of these tissues exhibited small areas with pronounced PD-L1 staining in terms of quantity and/or intensity. In order to cope with this intra-tumoral heterogeneity, an immunoreactivity scoring (IRS) system was applied. Therefore, Quantity and Intensity Scores were summed up for each rated microscopic FoV and mean instead of median value was calculated for the whole tissue section (Tissue Score).

In summary, Tissue Scores revealed values in the range from 0 to 2.65 with a mean score of 0.55. Lymph and Cluster Scores of PDAC tissue sections ranged from 0 to 2 with a median of 1 (Lymph Score) and from 0 to 0.52 with a median of 0.14 (Cluster Score), respectively. As an additional indicator for overall PD-L1 staining within each tumor tissue section, the proportion of microscopic FoV containing at least one PD-L1<sup>+</sup> cell (%FoV<sup>+</sup>) has been recorded for each tissue section. The proportion of PD-L1<sup>+</sup> FoV within PDAC tissue sections ranged from 0 to 92.4% with a median proportion of 22.9%. The overall results from staining evaluations are summarized in **Supplementary Table 10**.

#### **4.1.2 PD-L1 staining is characteristic for malignancy-associated desmoplastic but not healthy pancreatic tissue**

In pathological conditions pronounced PD-L1 expression in tissues is attributed to local inflammation and/or malignant disease formation [269]. However, in certain tissues PD-L1 is commonly expressed under physiological conditions, e.g. lymph nodes, tonsils, lung, placenta and liver [270,271]. In order to investigate whether PD-L1 is primarily or even exclusively expressed under pathological conditions in the pancreas or also expressed in physiological pancreatic tissues, 18 peritumoral tissue sections were evaluated by the established scoring system. Staining evaluations showed that PD-L1 is rarely expressed within tumor-distant acini, pancreatic ducts, islets of Langerhans as well as blood and lymph vessels. Therefore, these tissue areas were excluded from the scoring system. Instead an area around 2 mm from the tumor margin into the healthy tissue as well as the desmoplastic tumor tissue was included for scoring (peritumoral tissue) (**Figure 13**). Comparative examination of the staining revealed a significantly lower proportion of PD-L1<sup>+</sup> FoV in peritumoral pancreatic tissue sections

compared to tumor tissue sections (12.2% vs. 22.9%) (**Figure 13 A**). In line with this, comparing the results from scoring of PD-L1 staining in 13 peritumoral tissue sections and their corresponding tumor sections showed significantly higher Tissue Scores in tumor tissues compared to peritumoral tissues (Median Peritumoral/Tumor Tissue Score = 0.144) (**Figure 13 B**). However, in 4 of 18 peritumoral tissues comparatively high Tissue Scores ( $\geq 0.8$ ) and high proportions of PD-L1<sup>+</sup> FoV ( $> 30\%$ ) were identified. Notably, these peritumoral tissues exhibited either only a small or no neoplastic-cell-free tumor margin (**Figure 13 C**). Moreover, all peritumoral but not tumoral located lymph follicles displayed PD-L1 staining (Lymph Score  $> 0$ ) and Cluster Scores  $> 0.4$  were exclusively found in neoplastic pancreatic tissues (**Supplementary Table 10**).

#### 4.1.3 PD-L1 staining correlates with patient survival and tumor differentiation grade

Tissue Score results from scoring of PD-L1 staining revealed marked differences between tumor and peritumoral tissues and but also within each group (**Figure 13 D**). On the search for a reasonable threshold within the established scoring system that identifies a tumor biological or clinically relevant PD-L1 expression status in PDAC tissue, Tissue Scores and respective post-surgical patient life span were subjected to Log-Rank test according to Kaplan-Meier method. Indeed, analysis showed a significant correlation between a higher Tissue Score  $> 0.8$  (PD-L1<sup>high</sup>) and decreased overall survival (Median survival 23 vs. 7 months) (**Figure 13 E**). Notably, despite the pathological homogeneity within the present cohort (98% T3 and 87% T3N1M0), post-surgical survival markedly differed between patients (**Table 9**), a common problem for correlation of TNM status and disease prognostics in PDAC. Interestingly, statistical analysis of Tissue Scores with regard to the respective pathological tumor grade indicated a correlation between a high overall PD-L1 staining and a poor tumor differentiation status (Median Tissue Scores (Tumor grade): 0.255 (1) vs. 0.481 (2) vs. 0.588 (3)) (**Figure 13 F**).

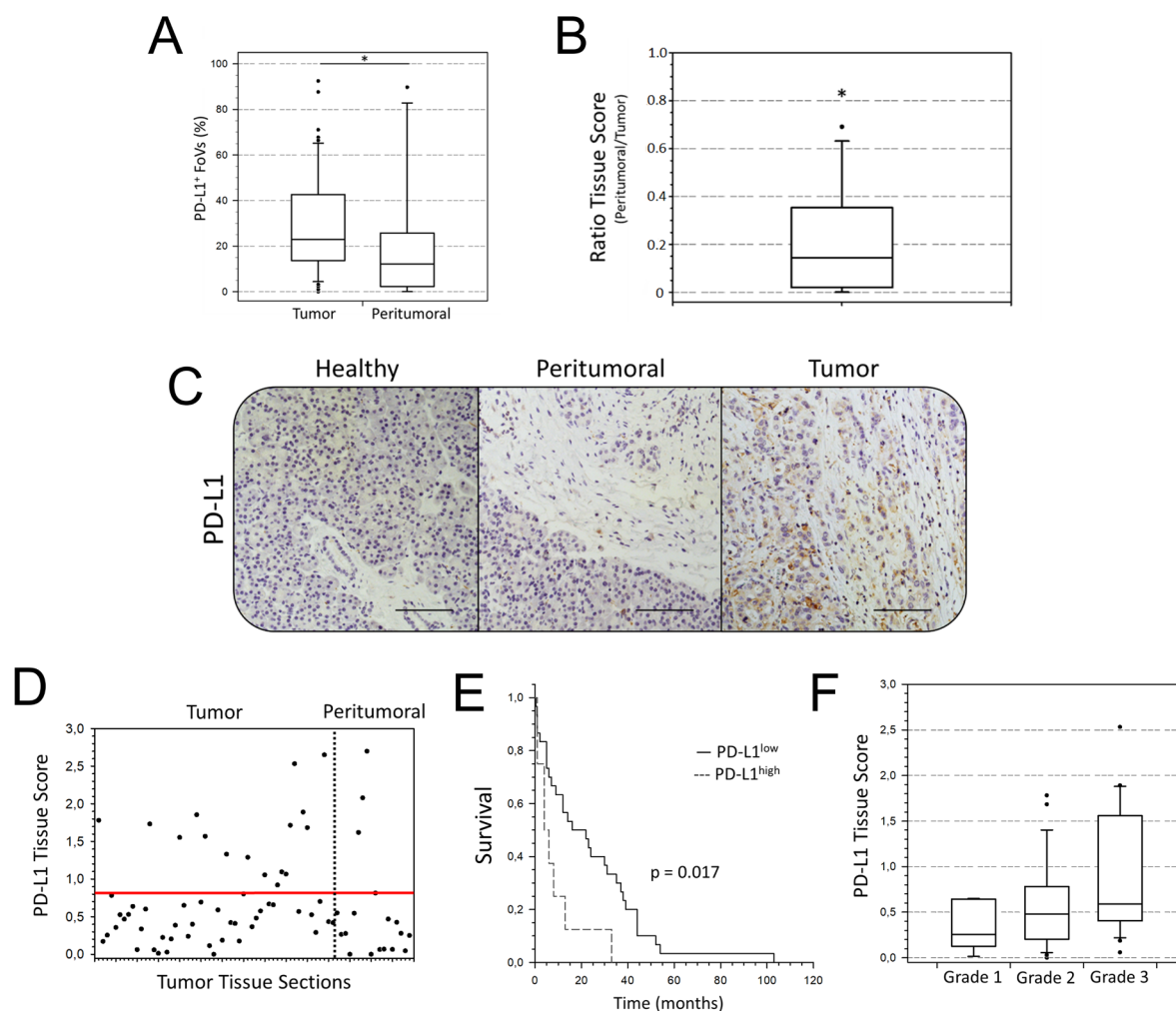


**Figure 13: PD-L1 expression is enhanced in PDAC tumor area compared to peritumoral tissue and correlates with clinic-pathological patient characteristics.** (A) Proportion of analyzed microscopic fields of view (FoV) with at least one PD-L1<sup>+</sup> cell in PDAC tumor and peritumoral tissue sections presented as Box-and-whisker plot. (B) Ratio of PD-L1 Tissue Scores in PDAC tumor tissue and respective peritumoral pancreatic tissue presented as Box-and-whisker plot. (C) Representative images of immunohistochemical PD-L1 staining in different areas of pancreatic tissue from a PDAC patient. Shown are adjacent healthy acinus tissue (left, “Healthy”), peritumoral margin with desmoplastic stroma (middle, “Peritumoral”) and intratumoral tissue (right, “Tumor”). (D) Tissue Scores of each PDAC tumor and peritumoral tissue section are presented as dots by a scatter plot. Red line at a value of 0.8 indicates the identified threshold between PD-L1<sup>low</sup> and PD-L1<sup>high</sup> tissue sections. (E) Survival LogRank analysis correlates overall survival time (months) of PDAC patients with intratumoral PD-L1 expression (Tissue Score: PD-L1<sup>low</sup> vs. PD-L1<sup>high</sup>). Considering surgery-related mortality, patients with survival times of less than 4 months were excluded from analysis. (F) PD-L1 Tissue Scores are presented as Box-and-whisker plots with regard to the pathological defined tumor grade. n = 56 (D, F); 39 (E). Original magnification/scale bar: 200-fold/100  $\mu$ m. n = 56 vs. 18 (A); 13 (B). \* = p<0.05. (published data [264])

#### 4.1.4 PD-L1 staining is predominantly located to stromal but not neoplastic cells in PDAC

Aberrant PD-L1 expression by neoplastic cells is regarded as one of the central immune escape mechanisms in other tumor entities like malignant melanoma or some cases of non-small cellular lung carcinoma [129,272,273]. However, in the last years the awareness grew that PD-L1 expression by various non-neoplastic cell populations like TAMs, MDSCs, Tregs, endothelial cells and fibroblasts also represents a factor for an impaired anti-tumor response [128,274].

In order to address this topic by precise discrimination of stromal- and neoplastic cell-associated PD-L1 staining, PD-L1/PanCK IHC co-staining of PD-L1<sup>high</sup> classified PDAC tissue sections was performed. Cell Scores resulting from this analysis indicate whether PD-L1 is primarily expressed by PanCK<sup>+</sup> epithelial/cancer cells (Cell Score 1; **Figure 14 A-C**), PanCK<sup>-</sup> stromal cells (Cell Score 2; **Figure 14 D-F**) or whether PD-L1 is expressed by both populations to a similar extent (Cell Score 3; **Figure 14 G-I**). Staining evaluations showed that only 4 cases (23.5%) displayed PD-L1 staining exclusively located in PanCK<sup>+</sup> cells (Cell Score 1). In contrast, 53% of PD-L1<sup>high</sup> classified PDAC sections exhibited PD-L1 staining primarily in stromal cells (Cell Score 2). Noteworthy, 5 of these tissue sections showed in less than 10% of all cells stained for PD-L1 a co-localisation of PD-L1 and PanCK. A nearly equal ratio (40:60 to 60:40) of PanCK<sup>-</sup> to PanCK<sup>+</sup> cells positively stained for PD-L1 was found in 4 cases (23.5%) (Cell Score 3) (**Figure 14 J**).

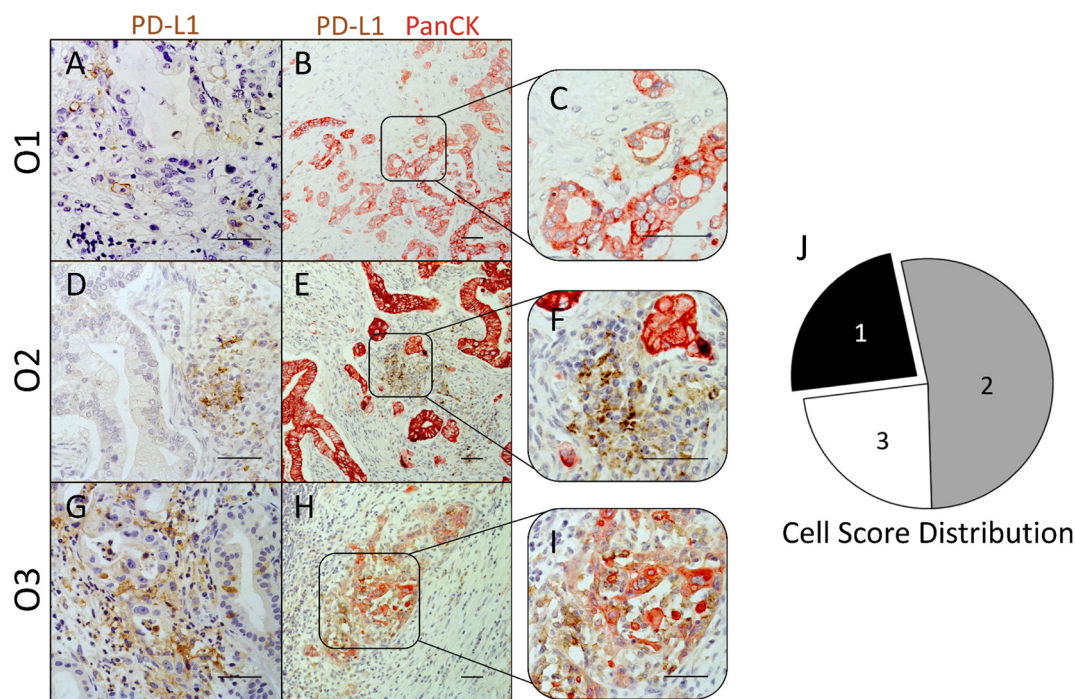


**Figure 14: PD-L1 expression in PDAC is not restricted to epithelial/tumor cells but is localized to a large extent within the tumor stroma.** (A-I) Representative images of immunohistochemical PD-L1 (brown)/PanCK (red) staining in PD-L1<sup>high</sup> graded pancreatic tissues of PDAC patients. Cellular origin of PD-L1 expression observed in single staining (A, D+G) was evaluated in PD-L1/PanCK double staining (B+C, E+F, H+I). Tissues were classified into 3 groups with regard to the prevalent cellular origin of PD-L1 expression: Cell Score 1 (PanCK<sup>+</sup>PD-L1<sup>+</sup>), Cell Score 2 (PanCK<sup>-</sup>PD-L1<sup>+</sup>) and Cell Score 3 (PanCK<sup>+/-</sup>PD-L1<sup>+</sup>). (J) Pie chart illustrates the proportion of PDAC tissues rated as Cell Score 1 (black), 2 (grey) and 3 (white) within PD-L1<sup>high</sup> graded tissues. Original magnification/scale bar: 200-fold/100  $\mu$ m (B, E+H); 400-fold/100  $\mu$ m (A, C, D, F, G+I). (published data [264]).

In summary, examined Cell Scores revealed that within this PDAC cohort PD-L1 is predominantly expressed by stromal cell populations and only to a minor proportion either partially or exclusively by neoplastic cells.

#### 4.1.5 Comprehensive IHC-based determination of PD-L1 status in PDAC by POLE Score

In order to comprehensively consider all data obtained from the evaluation of immunohistochemical PD-L1 staining in the PDAC cohort, a scoring system that resembles the structure of the TNM system was established. For this purpose, compiled Tissue, Cell, Lymph and Cluster Scores were converted into a four-letter code (**POLE** Score) that comprises intra-tumoral overall PD-L1 staining (**P**), cellular **O** rigin of PD-L1 staining (**O**), PD-L1 status in tumor-associated **L** ymph follicles (**L**) and the **E** umerated spatial distribution of PD-L1<sup>+</sup> cells (**E**) by single digits. Definition criteria of POLE Score parameters are listed in **Supplementary Table 11**.

According to these definition criteria, collected data were converted into respective POLE Scores (**Figure 15 A**). In summary, P-Score proportions highlight that strong PD-L1 staining is observed in only 30.4% (P2) of PDAC tissues, while most specimens show either weak (25.0%; P1) or absent (44.6%; P0) PD-L1 staining. Since O-Score represents one-to-one the former Cell Score, it indicates that 76.5% of P2 rated PDAC tissue sections exhibit either exclusive (O2, 53.0%) or prominent (O3, 23.5%) PD-L1 staining located in stromal cells. Noteworthy, L0 rated tissue sections were only found within the P0 subgroup. Finally, remarkable formation of clusters comprising neoplastic and/or stromal cells stained for PD-L1 were only detected within the P2 subgroup (**Figure 15 B**).

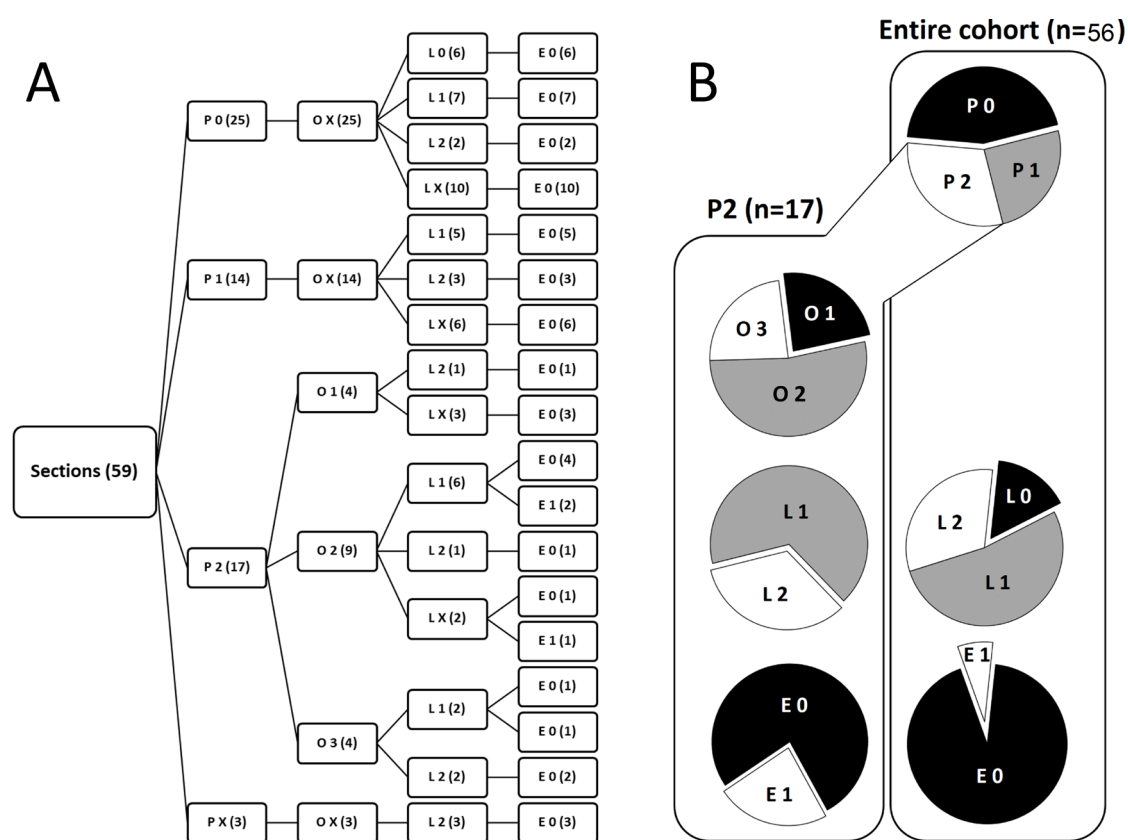


**Figure 15: Characterization of PD-L1 expression in PDAC by the POLE Score system.**

(A) Tree diagram illustrates the distribution of POLE Scores for PD-L1 expression in pancreatic tissue sections of PDAC patients. Scoring values P0-2 (overall PD-L1 expression), O1-3 (PD-L1 cellular Origin), L0-2 (PD-L1 expression in tumor-associated Lymph follicles) and E0-1 (Enumerated spatial distribution of PD-L1<sup>+</sup> cells) are depicted at the end of the branches. Number of cases are indicated in brackets. (B) Pie charts illustrate the proportion of compiled POLE Scores within the entire cohort (right, n=56) and subset of P2 scored (left, n=17) PDAC tissues. X = not rated (excluded in pie charts). (published data [264]).

#### 4.1.6 POLE Score correlates with a pattern of immunological markers that characterizes a distinct cellular tumor stroma composition

Data from IHC analyses indicate that marked PD-L1 expression is mainly attributed to stromal cell populations in PDAC tissue and correlates with malignancy-associated histopathological alterations. The tumor stroma of PDAC commonly consists of a wide variety of different non-neoplastic cell populations, e.g. CD4<sup>+</sup>, CD8<sup>+</sup> and regulatory T lymphocytes as well as TAMs and fibroblasts [62,65,88]. In order to investigate whether there is an interrelationship between POLE Score parameters and tumor stroma composition, data obtained on PD-L1 expression in the present study were correlated with IHC-based data of a former study, which used serial tissue sections of the same cohort [88]. These data included markers for infiltration of various T lymphocyte populations, macrophage infiltration and polarization, fibroblast proportion and activation status as well as proportion, differentiation and proliferation of neoplastic cells [88]. For this purpose, POLE Scores (except for E-Score) were dichotomized prior to statistical analyses into:

- I) +P1 vs. +P2 (P0 + P1 vs. P2)
- II) +O1 vs. +O2 (O1 vs. O2 + O3)
- III) +L1 vs. +L2 (L0 vs. L1 + L2)

This form of dichotomization was chosen to explicitly separate specimens with strikingly high overall PD-L1 staining from those with low/absent PD-L1 staining, specimens with exclusively PanCK<sup>+</sup> PD-L1<sup>+</sup> cells from those with high stromal attributed PD-L1 staining as well as specimens with absent PD-L1 staining in tumor-associated lymph follicles from those that show PD-L1 staining in the majority of tumor-associated lymph follicles.

Subsequent statistical analyses of dichotomized POLE Score parameters and markers related to the infiltration of T lymphocytes in general (CD3<sup>+</sup>), T helper lymphocytes (CD3<sup>+</sup> CD4<sup>+</sup>), cytotoxic T lymphocytes (CD3<sup>+</sup> CD8<sup>+</sup>), regulatory T cells (CD3<sup>+</sup> CD4<sup>+</sup>, CD25<sup>+</sup>, FoxP3<sup>+</sup>) and  $\gamma\delta$  T cells ( $\gamma\delta$  TCR<sup>+</sup>) revealed significant interrelations between the cellular origin of PD-L1 staining and overall T cell infiltration as well as PD-L1 staining in tumor-associated lymph follicles and the presence of T helper lymphocytes (**Figure 16 A**). In detail, dominant PD-L1 staining in PanCK<sup>-</sup> cells exclusively correlated with high stromal infiltration by CD3<sup>+</sup> T cells. Conversely, all specimens with PD-L1 staining restricted to epithelial cells were characterized by a low abundance of CD3<sup>+</sup> T cells (**Figure 16 B**). Likewise, PD-L1 staining in tumor-associated lymph follicles positively correlated with the presence of CD4<sup>+</sup> cells. Thus, 18 of 23

cases (78.2%) showed either +L1/CD4<sup>low</sup> or +L2/CD4<sup>high</sup> status (**Figure 16 C**).

Moreover, a significant coherence between PD-L1 staining in tumor-associated lymph follicles and the local abundance of markers for TAMs (CD68<sup>+</sup>, CD163<sup>+</sup>, HLA-DR) was found (**Figure 16 A**). In detail, 16 of 23 specimens (69.5%) rated as +L2 were associated with a high proportion of CD68<sup>+</sup> or CD163<sup>+</sup> cells in close proximity to epithelial cells (duct-associated) (**Figure 16 D**).

Indicating a link between cellular origin of PD-L1 staining and the proportion of stromal myofibroblasts, an exclusive correlation between +O1/ $\alpha$ -SMA<sup>low</sup> and +O2/ $\alpha$ -SMA<sup>high</sup> rated specimens was identified (**Figure 16 E**).

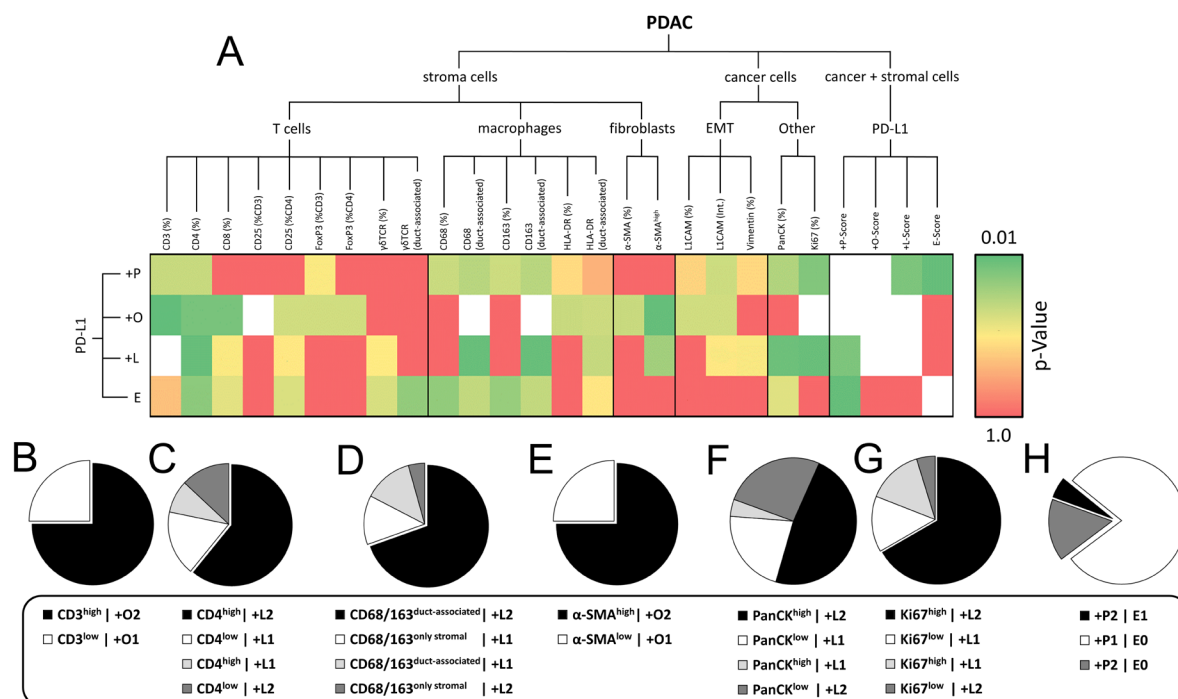


**Figure 16: PD-L1 expression characterized by POLE Score correlates with intra-tumoral proportion of distinct immune cell populations.** (A) Heatmap illustrates results from statistical correlation of dichotomized POLE Scores, markers for stromal cell populations, EMT and Ki67 status assessed by immunohistochemical staining. Dichotomization was performed according to the following pattern: +P1 (=P0+P1) vs. +P2 (=P2); +O1 (=O1) vs. +O2 (=O2+O3); +L1 (=L0) vs. +L2 (=L1+L2). P-values from statistical analyses are illustrated by color gradient (dark green:  $p=0.01$  to dark red:  $p=1.0$ ; white: statistical analysis not possible). Pie charts show proportion of subgroups within correlations of (B) +O-Score vs. CD3 (% stroma), (C) +L-Score vs. CD4 (% stroma), (D) +L-Score vs. CD68/CD163 (duct-associated), (E) +O-Score vs.  $\alpha$ -SMA (intensity), (F) +O-Score vs. PanCK (% section), (G) +O-Score vs. Ki67 (% epithelium) and (H) +P-Score vs. E-Score. Statistical analyses were performed by Chi-square/Fisher exact test. (published data [264]).

Moreover, the overall proportion of PanCK<sup>+</sup> cells and PanCK<sup>+</sup> Ki67<sup>+</sup> epithelial cells in PDAC tissue sections tended to correlate with respective PD-L1 staining in tumor-associated lymph follicles ( $p=0.069$ ;  $p=0.053$ ) (**Figure 16 A**). In detail, 16 of 23 specimens showed either +L1/PanCK<sup>low</sup> or +L2/PanCK<sup>high</sup> status and 17 of 23 cases displayed either +L1/Ki67<sup>low</sup> or +L2/Ki67<sup>high</sup> status (**Figure 16 F+G**). Indeed, spot-checking areas in PDAC tissues with low or



absent stromal PD-L1 staining for Ki67 staining in respective serial tissue sections verified the coincidentally low proportion of Ki67<sup>+</sup> epithelial cells. In contrast strong stromal PD-L1 staining was associated with a high proportion of Ki67<sup>+</sup> PanCK<sup>+</sup> cells in serial tissue section (**Figure 17**).

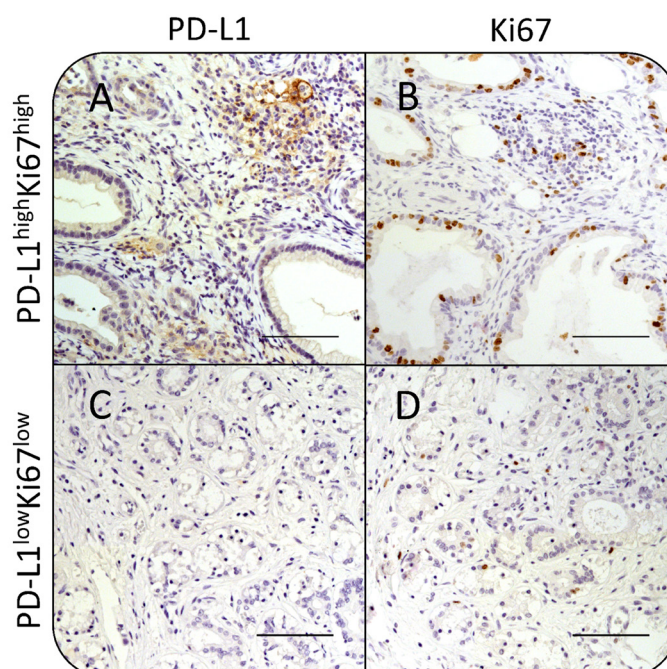


**Figure 17: Intratumoral areas enriched for PD-L1<sup>+</sup> stromal cells show high proportion of Ki67<sup>+</sup> cells within the epithelial tumor compartment.** Representative images of (A+C) PD-L1 and (B+D) Ki67 immunohistochemical staining in serial pancreatic tissue sections from PDAC patients. Original magnification/scale bar: 200-fold/100  $\mu$ m (published data [264]).

Finally, PDAC tissue sections exhibiting prominent formation of PD-L1<sup>+</sup> cell clusters (E1) were only found within the subgroup of tissue sections exhibiting strong overall PD-L1 staining. Hence, 30 of 36 E0 rated specimens showed low overall PD-L1 staining (**Figure 16 H**).

Taken together, these data show that PD-L1 expression in PDAC markedly varies in terms of the tumor compartment (neoplastic vs. stromal cells vs. tumor-associated lymph follicles) and correlates with distinct patterns of tumor stroma composition. Furthermore, data indicate that strong PD-L1 staining in the stromal compartment is associated with high tumor infiltration by CD3<sup>+</sup> T lymphocytes and presence of activated myofibroblasts. Interestingly, most correlations were identified between strong PD-L1 staining within tumor-associated lymph follicles and the presence of CD4<sup>+</sup> and CD8<sup>+</sup> T lymphocytes as well as a high proportion of proliferative epithelial cells.

#### 4.1.7 PD-L1 staining in PDAC tissues is predominantly found within distinct tumor regions and associated with a local accumulation of specific immune cell populations

As outlined in **section 4.1.1** immunohistochemical detection of PD-L1 in PDAC tissues displayed a very heterogenous staining pattern characterized by low overall and locally strong PD-L1 staining in P2 scored specimens. In order to investigate whether PD-L1 enriched areas are located in distinct tumor regions and display a particular stromal composition as indicated by the results from statistical analyses, PD-L1<sup>high</sup> areas in P2 tissues were examined in more detail in serial tissue sections stained for CD3, CD4, CD68, CD163,  $\alpha$ -SMA and PanCK.

The first type of tumor area that frequently showed remarkable PD-L1 staining was located at the tumor-lymph follicle interface. A representative example of this type of area is depicted in **Figure 18**. This type of area exhibiting notable PD-L1 staining (**Figure 18 B+D**) was characterized by a high proportion of PanCK<sup>+</sup> neoplastic cells in close proximity or even surrounded by a tumor-associated lymph follicle (**Figure 18 A+C**). Neoplastic ductal structures were surrounded by tumor stroma primarily streaked by  $\alpha$ -SMA<sup>+</sup> cells (**Figure 18 G+J**). CD68<sup>+</sup> cells predominantly accumulated at the tumor-lymph follicle interphase coinciding with PD-L1 staining (**Figure 18 F+I**, arrow heads). Interestingly, PD-L1 staining appeared to be polarized towards adjacent tissue comprising neoplastic PanCK<sup>+</sup> cells. Thus, the tumor-lymph follicle interface but not tumor-averted border of the lymph follicle showed strong PD-L1 staining (**Figure 18 B**, arrow heads). Notably, this correlation between the local presence of malignant cells and strong PD-L1 staining had been observed previously in the comparison of tumor and peritumoral tissue sections (**section 4.1.2**) as well as in the statistical analyses of tumor stroma composition and POLE Score parameters in **section 4.1.6**. Furthermore, CD4<sup>+</sup> cell clusters showed overlapping areas with PD-L1 staining inside the tumor-associated lymph follicle but not within the tumor tissue (**Figure 18 E+H**, arrow heads).

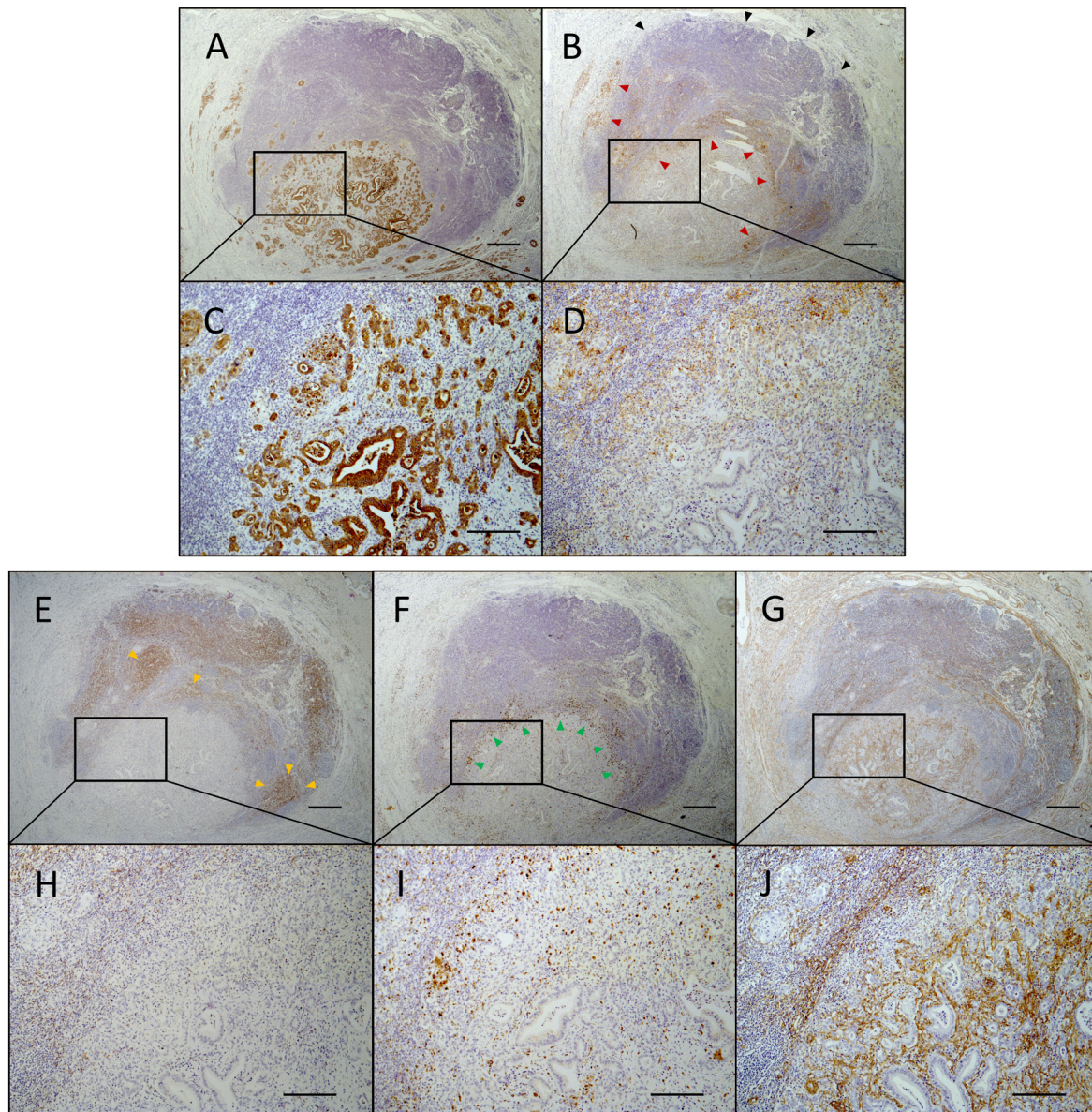


**Figure 18: Polarized PD-L1 expression at the tumor-lymph follicle interface coincides with the presence of CD68<sup>+</sup> macrophages.** Representative images of (A+C) pan-cytokeratin (PanCK), (B+D) PD-L1, (E+H) CD4, (F+I) CD68 and (G+J)  $\alpha$ -SMA immunohistochemical staining in serial pancreatic tissue sections from a PDAC patient. (B) Shown is an infiltrated tumor-associated lymph follicle exhibiting high proportion of PD-L1<sup>+</sup> cells at the tumor margin (red arrow heads) and absence of PD-L1 expression at the tumor-averted border (black arrow heads). PD-L1 expression is co-localized with (E) CD4 (yellow arrow heads) and (F) CD68 staining (green arrow heads). Original magnification/scale bar: 25-fold/500  $\mu$ m (overviews; A+B, E-G); 100-fold/200  $\mu$ m (detail; C+D, H-J). (published data [264]).

The second type of tumor area that frequently exhibited high accumulation of PD-L1<sup>+</sup> cells was located at the tumor margin comprising neoplastic cells in close proximity to remaining adjacent acinus tissue. A representative example of this type of area is presented in **Figure 19**. This type of area displayed a wide tumor margin with invasive growing neoplastic cells (**Figure 19 A+E**) being associated with pronounced PD-L1 staining (**Figure 19 B+F**). Additionally, this area coincided with dense infiltration of CD3<sup>+</sup> T lymphocytes (**Figure 19 C+G**) being not CD4<sup>+</sup> (**Figure 19 D+H**) but CD8<sup>+</sup> (**Figure 19 I+M**). Moreover, CD68<sup>+</sup> TAMs (**Figure 19 J+N**) and

especially a CD163<sup>+</sup> subpopulation (**Figure 19 K+O**) were found at high frequency and tightly associated with neoplastic cells. In contrast, local  $\alpha$ -SMA staining was weak compared to the inner tumor area (**Figure 19 L+P**, compare upper area vs. marked area). Notably, PD-L1 staining co-localized within this type of area with both neoplastic and stromal cell populations.

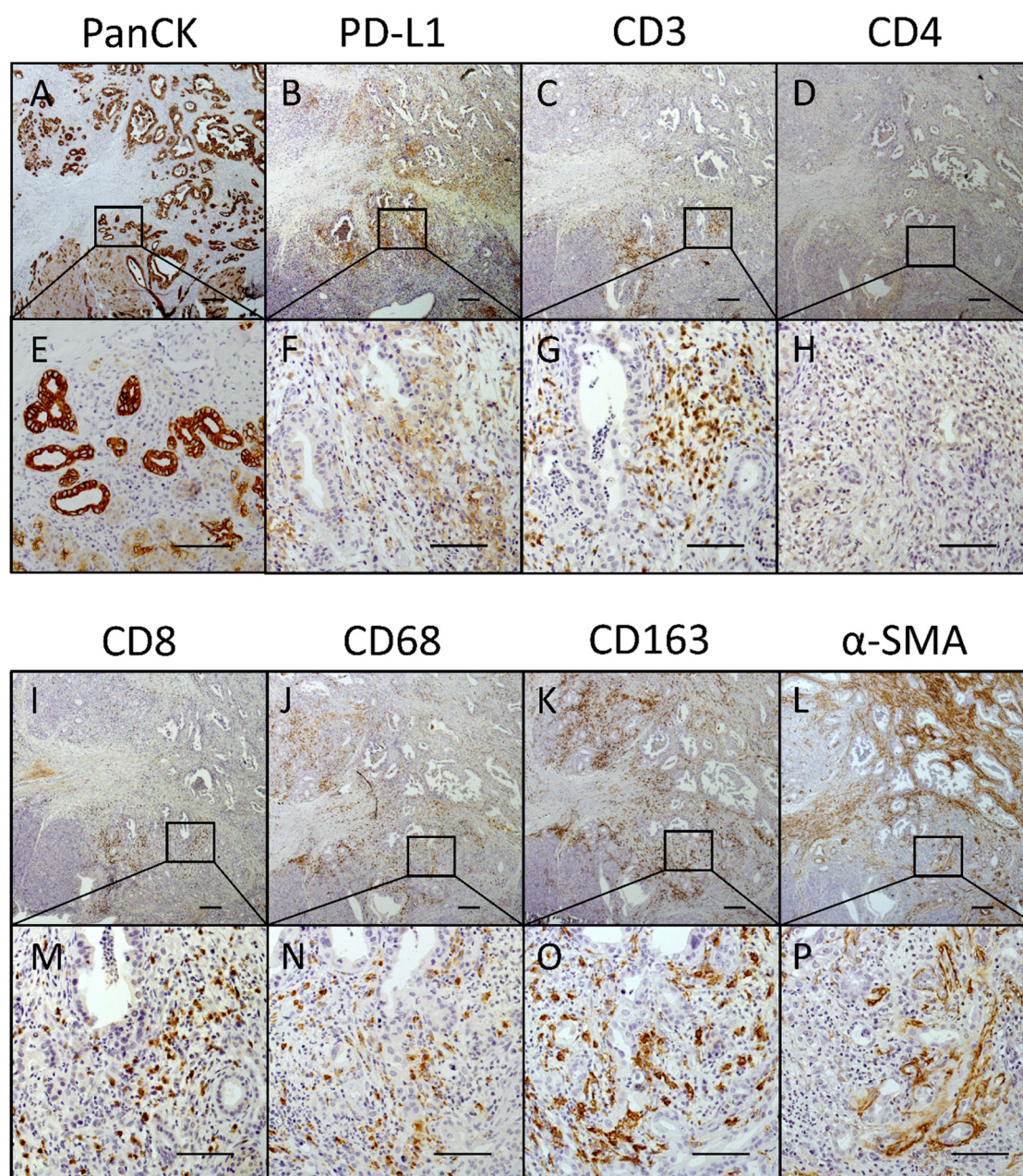


**Figure 19: PD-L1 is markedly expressed within tumor areas that show high proportion of CD8<sup>+</sup> T cells and macrophages.** Representative images of (A+E) PanCK, (B+F) PD-L1, (C+G) CD3, (D+H) CD4, (I+M) CD8, (J+N) CD68, (K+O) CD163 and (L+P)  $\alpha$ -SMA immunohistochemical staining in serial pancreatic tissue sections from a PDAC patient. Original magnification/scale bar: 25-fold/200  $\mu$ m (overviews; A-D+I-L); 200-fold/100  $\mu$ m (detail; E-H+M-P). (published data [264]).

Overall, the analyses on serial tissue sections confirmed the results from previous statistical analyses correlating POLE Score parameters with tumor stroma composition (**section 4.1.6**). While it has been highlighted that PD-L1 is very heterogeneously expressed in PDAC, it has been also shown that pronounced accumulation of PD-L1<sup>+</sup> cells is restricted to tumor areas, which are associated with a high infiltration by CD8<sup>+</sup> T lymphocytes and CD68<sup>+</sup> CD163<sup>+</sup> TAMs.

#### **4.1.8 Tumor-associated macrophages represent one of the major PD-L1 expressing stromal cell populations in PDAC**

Analysis of various lineage markers by IHC in serial sections of PDAC tissues suggested that not epithelial/neoplastic cells but rather leukocytes represent the major cellular origin of intra-tumoral PD-L1 expression. Particularly, T lymphocytes and myeloid cells accumulated within tumor regions of strong PD-L1 staining indicated by prominent local CD3 and CD68 staining in serial sections.

In order to specify PD-L1 expressing cell populations in PDAC in more detail, multicolour flow cytometric analysis of freshly isolated cells from enzymatically dissociated PDAC specimens was performed. The established staining panel allowed the discrimination of cell surface expressed PD-L1 on cells of epithelial origin (panCK<sup>+</sup> PD-L1<sup>+</sup>), leukocytes (CD45<sup>+</sup> PD-L1<sup>+</sup>) as well as TAMs (CD45<sup>+</sup> SSC<sup>high</sup> CD68<sup>+</sup> PD-L1<sup>+</sup>) (**Figure 20 A**). The results from flow cytometric analyses of tumor specimens from three PDAC patients very well reflected both tumor heterogeneity and cellular origin of PD-L1 staining previously described in IHC-based analyses. In detail, PD-L1<sup>+</sup> cells within the subgroup of panCK<sup>+</sup> cells were either absent or represented a minor proportion (3.27%, 0.78 % and 0.0%) (**Figure 20 B**). Moreover, median fluorescence ratios (MFI Ratio) of panCK<sup>+</sup> PD-L1<sup>+</sup> cells indicated very low surface expression levels (MFI Ratio 1.42, 1.27 and 1.05) (**Figure 20 C**). TAMs were found in two of three specimens at varying proportion. Hence, one of these specimens possessed a high proportion of PD-L1<sup>+</sup> TAMs (87.9% PD-L1<sup>+</sup>) (**Figure 20 B**) along with high surface expression level (MFI Ratio 2.53) (**Figure 20 C**). In contrast, the other specimen exhibited just a minor population of PD-L1<sup>+</sup> TAMs (7.2%) (**Figure 20 B**) along with low cell surface expression levels (MFI Ratio 1.55) (**Figure 20 C**). In addition to flow cytometric analyses, PD-L1 expression by TAMs was also verified by co-localization of CD68 and PD-L1 in immunofluorescence staining of P2 rated PDAC tissue sections (**Figure 20 D**). Notably, both flow cytometry and immunofluorescence staining highlighted that not all TAMs show PD-L1 expression and that other leukocyte populations clearly contribute to intra-tumoral PD-L1 expression in PDAC. Thus, PD-L1<sup>+</sup> non-

myeloid leukocytes ( $CD45^+ CD68^- PD-L1^+$ ) were identified in every specimen, at varying proportions (62.1%, 11.6% and 35.9%) (**Figure 20 B**) with considerable surface levels (MFI Ratio 2.42, 2.96 and 1.53) (**Figure 20 C**). Moreover, additional staining of PD-1 within the flow cytometry panel revealed that only non-myeloid leukocytes ( $CD45^+ CD68^-$ ) exhibited detectable cell surface expression levels of PD-1 (data not shown).

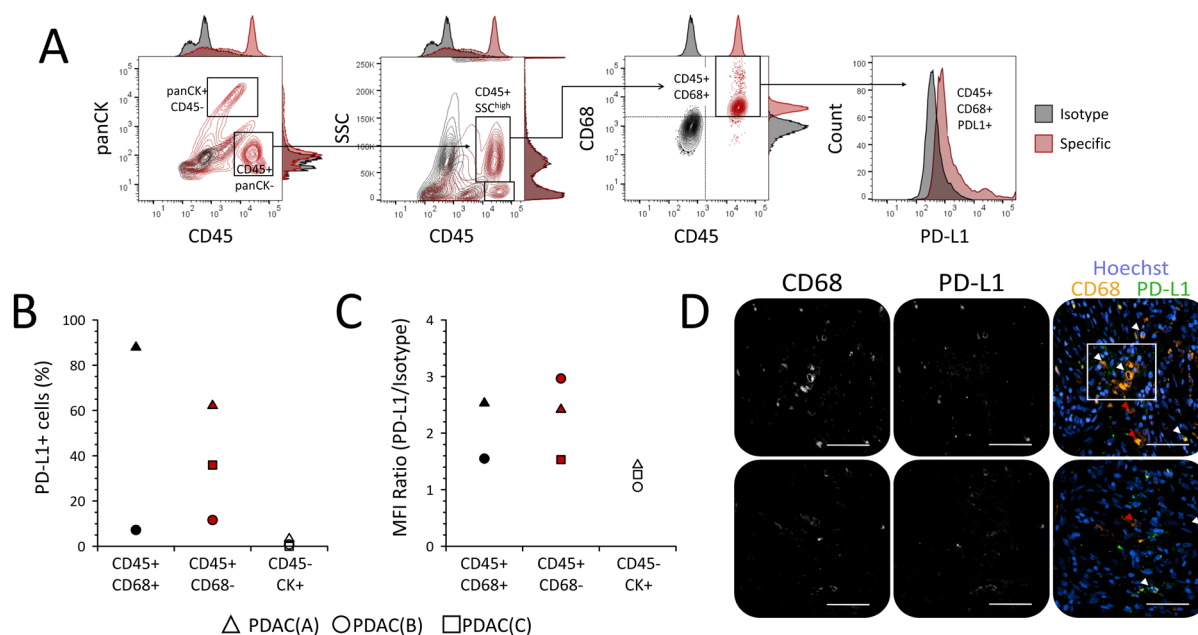


**Figure 20: Tumor-associated macrophages represent a PD-L1 expressing stromal cell population in some PDAC patients or distinct tumor areas.** (A) Gating strategy for detection of cell surface PD-L1 expression by flow cytometry in distinct populations of freshly isolated cells in resected PDAC specimens. Epithelial/tumor cells were discriminated from leukocytes by panCK/CD45 staining. Tumor-associated macrophages (TAMs) within the  $CD45^+$  leukocyte populations were discriminated from other leukocyte populations *via* side scatter (SSC) and CD68 expression. Specificity of staining (red contour plots/histograms) was ensured by detection of signals from respective isotype staining (black contour plots/histograms) in parallel. (B, C) Scatter plots summarize results from flow cytometric detection of PD-L1 cell surface expression in freshly isolated TAMs ( $CD45^+ CD68^+$ ; black symbols), non-TAM leukocytes ( $CD45^+ CD68^-$ ; red symbols) and epithelial/tumor cells ( $CD45^- panCK^+$ ; white symbols) of PDAC specimens from three different patients with regard to (B) proportion of PD-L1<sup>+</sup> cells and (C) median fluorescence intensity (MFI) ratio ( $MFI^{PD-L1}/MFI^{isotype}$ ). (D) Representative images of CD68 and PD-L1 immunofluorescence co-staining in PDAC tissue sections from two different patients. Shown are grey scale signals from single channels for detection of CD68 (left) and PD-L1 (middle) staining as well as overlay (right) of CD68 (orange), PD-L1 (green) and nuclei staining by Hoechst (blue) for analysis of co-localization. Marked are PD-L1<sup>+</sup> CD68<sup>+</sup> (white arrow heads) and PD-L1<sup>-</sup> CD68<sup>+</sup> (red arrow heads) TAMs as well as a cluster of PD-L1<sup>+</sup> CD68<sup>+</sup> TAMs (white quadrant). Original magnification/scale bar: 200-fold/50  $\mu m$ . (published data [264]).

Taken together, the findings from *in situ* analyses clearly show that PD-L1 expression in the present cohort of PDAC tissues is very heterogenous and mainly absent or at low overall level. Moreover, hot spots for accumulation of PD-L1<sup>+</sup> cells are located within distinct tumor regions, namely tumor-lymph follicle interfaces and the tumor margin. Finally, these areas are characterized by a distinct cellular composition that includes proliferative neoplastic cells along with high infiltration by T lymphocytes and TAMs. By trend, PD-L1 expression was mostly

attributed to stromal cell populations like TAMs and other leukocytes rather than epithelial/neoplastic cells.

## 4.2 *In vitro* analyses on the immune-regulatory role of PD-L1 in co-culture settings that resemble cellular compositions in PDAC tissues

In order to investigate the immune-regulatory potential of PD-L1 expression within areas of PDAC that are characterized by a cellular composition of neoplastic cells, T lymphocytes and macrophages, the next aim of this study was the establishment of an *in vitro* co-culture system that mimics the cellular composition with variable PD-L1 expression. For this purpose, different PDAC cell lines and human primary polarized macrophages were screened for basal levels and inducibility of PD-L1 expression. Moreover, an experimental setup for isolation, activation and characterization of human primary T lymphocytes has been developed.

### 4.2.1 Premalignant pancreatic ductal epithelial cell lines and most PDAC cell lines exhibit basal surface expression of PD-L1 but not PD-1

*In situ* analyses indicated that just a minor proportion of neoplastic cells in PDAC exhibit considerable PD-L1 cell surface expression. In order to examine whether this also applies to well-established PDAC cell lines, benign, premalignant and malignant pancreatic ductal epithelial cell (PDEC) lines were analyzed for basal PD-L1 expression by flow cytometry and western blotting (**Figure 21**). For this initial screening, H6c7eR-pBp and H6c7eR-kras cells, models for benign and premalignant PDEC, respectively, as well as the PDAC cell lines Panc1, PancTu-I, Panc89, MIA PaCa-2, BxPc3 and Colo357 were chosen. Western blot analyses of whole-cell lysates revealed that H6c7eR-pBp and H6c7-eR-kras cells exhibited the highest basal PD-L1 levels (**Figure 21 A**). Notably, H6c7eR-kras cells, showed the highest PD-L1 expression. Within the group of PDAC cell lines PancTu-I cells displayed the highest PD-L1 expression level. While BxPc3 and Colo357 cells showed both an intermediate basal PD-L1 expression, Panc89 and MIA PaCa-2 cells exhibited a low basal PD-L1 level. In contrast, PD-L1 was not detectable by western blotting in whole-cell lysates of Panc1 cells (**Figure 21 A**). Flow cytometric analyses of PD-L1 cell surface levels verified relative PD-L1 levels detected in whole-cell lysates. Hence, flow cytometry showed the highest PD-L1 signal intensity for

H6c7eR-kras cells (MFI Ratio 6.46) (**Figure 21 B**) and comparatively lower signal intensities for PanTu-I cells (MFI Ratio  $3.35 \pm 0.35$ ) (**Figure 21 B+C**). In line with western blotting results, PD-L1 was not detectable by flow cytometry on the cell surface of Panc1 cells (**Figure 21 B**). Notably, PD-1 was not detectable at the cell surface of H6c7eR-kras, PanTu-I and Panc1 cells (**Figure 21 B+C**).

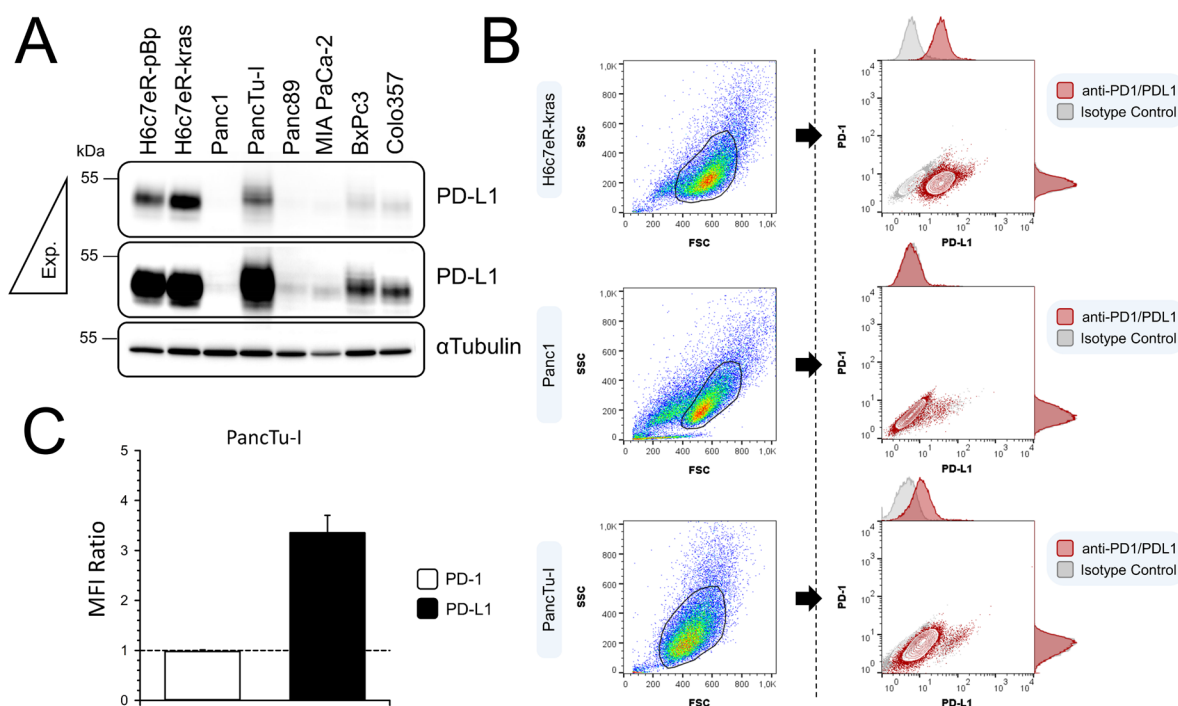


**Figure 21: Basal PD-1 and PD-L1 expression in various PDEC cell lines.** Cells for analyses were obtained from standard culture conditions of respective cell lines. (C) Representative western blot of whole-cell lysates from various pancreatic ductal epithelial cell lines from three independent experiments. Alpha tubulin was detected as loading control. Molecular weights in kDa are indicated according to the applied standard. Exp. = decreased/increased time of light exposure for signal detection. (B) Representative dot plots from flow cytometric analyses of H6c7eR-kras (top), Panc-1 (middle) and PanTu-I cells (bottom). Shown are the gating strategy in FSC/SSC dot plots (left) as well as signals detected by PD-1/PD-L1 antibody staining (red) and respective isotype control staining (grey) in dot plots with attached histograms. (C) PD-1 (white) and PD-L1 (black) cell surface expression levels in PanTu-I cells detected by immunofluorescence staining and subsequent flow cytometric analysis. Bar chart presents mean values and SEM of median fluorescence intensity ratios detected in three independent experiments. The dashed line marks an MFI ratio of “1”.

#### 4.2.2 IFN $\gamma$ is the strongest inducer of PD-L1 expression in pre-malignant PDEC and most PDAC cell lines

Besides the basal cellular levels, potential inducers for PD-L1 expression in PDAC cells are even more relevant for the qualitative and comparative evaluation of different PD-L1 expression levels within the tumor. As outlined, up to 80% of the PDAC tumor mass consists of non-neoplastic cells. Within this non-neoplastic compartment infiltrating leukocytes and activated fibroblasts generate a complex tumor microenvironment composed of various cytokines, chemokines and other paracrine active factors that essentially affect the proliferation, differentiation, polarization and activation status of each cell population in the tumor [62,65].



In order to gain a better understanding of intra-tumoral differences in PD-L1 expression and interrelate these with the respective local cellular composition, several cytokines and growth factors, which are well-known to be present in the tumor microenvironment of PDAC, have been checked for their potential to induce PD-L1 expression in PDECs.

IFN $\gamma$  is a key mediator of activated T lymphocytes and a well-known potent inducer for PD-L1 expression *via* downstream activation of Stat1. Stimulation of H6c7eR-kras, Panc1, PancTu-I, Panc89, Colo357 and BxPc3 cells with 10 ng/ml recombinant human IFN $\gamma$  for 72 h caused considerable upregulation of total Stat1 levels as well as phosphorylation of Stat1, its transcriptional regulatory active form (**Figure 22 A+B**). At the same time, markedly increased PD-L1 expression was detected in whole-cell lysates of all tested cell lines, except for Panc1 cells (**Figure 22 A+B**).

EGF is a prominent mitogen secreted by neoplastic cells and macrophages in PDAC. Binding to its receptor causes downstream activation of MAPK signaling commonly detected by phosphorylation of ERK1/2. Stimulation of H6c7eR-kras, Panc1, PancTu-I, Panc89, Colo357 and BxPc3 cells with 20 ng/ml recombinant human EGF for 72 h did hardly affect total ERK1/2 levels and markedly increased levels of phosphorylated ERK1/2 only in H6c7-kras, Panc1 and BxPc3 cells (**Figure 22 A+B**). Noteworthy, simultaneous slightly increased PD-L1 expression levels were observed only in H6c7eR-kras cells in biological replicates (**Figure 22 A+B**).

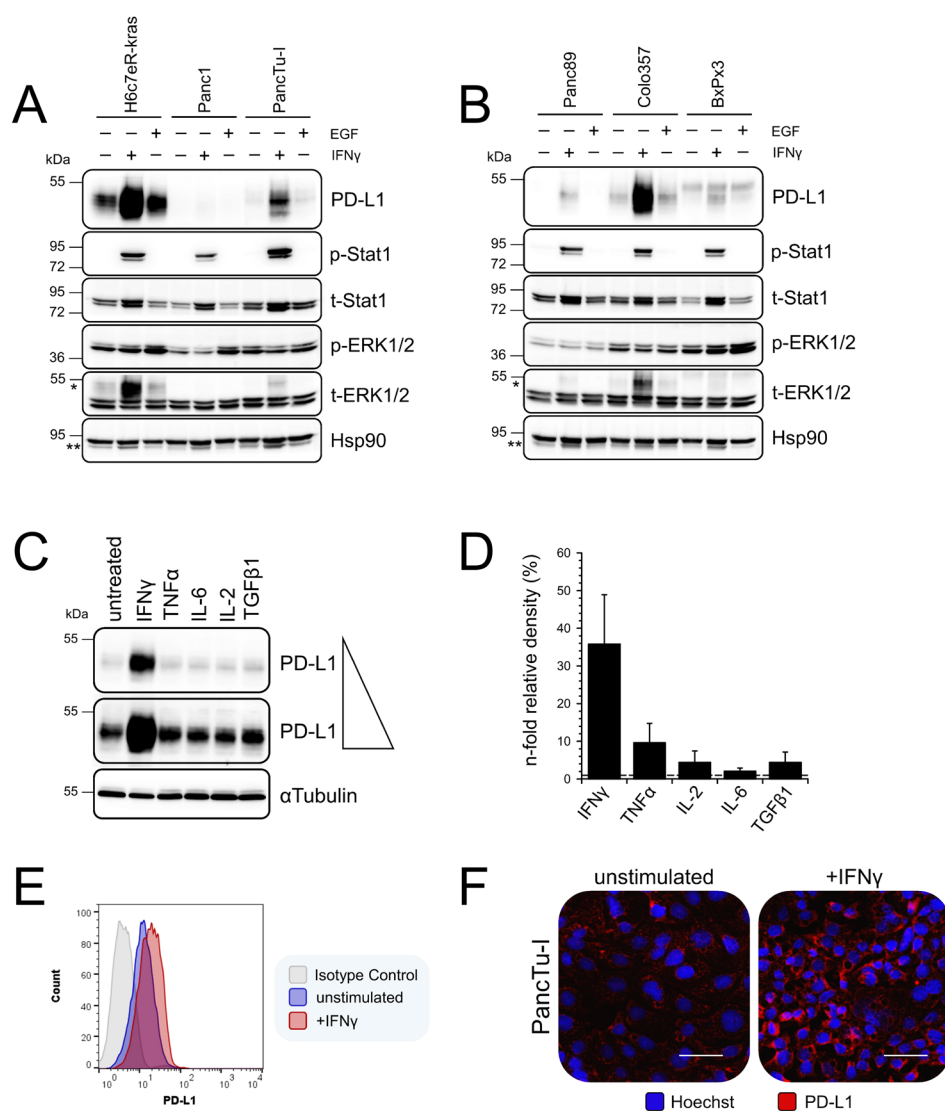


**Figure 22: Induction of PD-L1 expression by various cytokines and growth factors in premalignant PDEC and PDAC cell lines.** H6c7eR-kras, Panc-1, PancTu-I, Panc89, Colo357 and BxPc3 cells were cultured for 72 h in respective standard culture medium supplemented with 10 ng/ml IFN $\gamma$ , 20 ng/ml EGF, 10 ng/ml TNF $\alpha$ , 10 ng/ml IL-6, 60 ng/ml IL-2 or 20 ng/ml TGF- $\beta$ 1. **(A+B)** Representative western blots of whole-cell lysates from **(A)** H6c7eR-kras, Panc-1 and PancTu-I as well as **(B)** Panc89, Colo357 and BxPc3 cells after stimulation (+) with recombinant human EGF or IFN $\gamma$  in comparison to unstimulated (-) cells. Hsp90 was detected as loading control. \* = PD-L1 signal, \*\* = p-Stat1 signal **(C)** Representative western blot of whole-cell lysates from PancTu-I cells after indicated stimulations. Alpha tubulin was detected as loading control. Molecular weights in kDa are indicated according to the applied standard. **(D)** Densitometric analysis of PD-L1 levels detected by western blotting in whole-cell lysates of PancTu-I cells after stimulation with indicated cytokines. Relative PD-L1 signal intensities were normalized to unstimulated PancTu-I cells. Bar chart presents mean values and SEM from three independent experiments. **(E)** Representative histograms from flow cytometric analysis of unstimulated (blue) and IFN $\gamma$  stimulated (red) PancTu-I cells stained with fluorochrome-conjugated PD-L1 antibody (blue and red) or respective isotype control antibody (grey). **(F)** Representative fluorescence microscopical images of immunofluorescence PD-L1 (red) staining in unstimulated and IFN $\gamma$  stimulated PancTu-I cells. Nuclei were stained with Hoechst (blue). Scale bar = 50  $\mu$ m

Further stimulation experiments included only PancTu-I and Panc1 cells, because of their contrary basal and IFN $\gamma$ -inducible PD-L1 expression levels.

TNF $\alpha$  and IL-6 are two major pro-inflammatory cytokines in PDAC predominantly secreted by TAMs and to some extent by neoplastic cells and activated myofibroblasts [275,276]. In

contrast, TGF- $\beta$ 1 represents an anti-inflammatory cytokine secreted by TAMs and neoplastic cells [58,62]. IL-2 is an essential cytokine for T lymphocyte activation and survival secreted by activated CD4<sup>+</sup> T lymphocytes [277]. Western blotting and subsequent densitometric analysis verified IFN $\gamma$  as the most potent inducer of PD-L1 expression in PancTu-I cells (**Figure 22 C+D**). In line with western blotting results, increased PD-L1 cell surface levels in IFN $\gamma$  stimulated compared to unstimulated PancTu-I cells were also detected by flow cytometry (**Figure 22 E**) and immunofluorescence staining (**Figure 22 F**). While stimulation of PancTu-I cells with 10 ng/ml TNF $\alpha$  or 20 ng/ml TGF- $\beta$ 1 for 72 h slightly increased PD-L1 levels, stimulation with 10 ng/ml IL-6 and 60 ng/ml IL-2 for 72 h did not affect PD-L1 expression levels (**Figure 22 C+D**). Notably, none of the tested cytokines resulted in PD-L1 expression levels detectable by western blotting, flow cytometry or immunofluorescence in Panc1 cells (data not shown).

In summary, the results from these initial screening experiments suggest PancTu-I cells as a suitable *in vitro* model for PDAC cells exhibiting notable basal and inducible PD-L1 cell surface expression levels.

#### **4.2.3 GM-CSF differentiated M1-like polarized primary human macrophages exhibit remarkable PD-L1 surface expression levels**

Tumor-associated macrophages have been identified as a major source for intra-tumoral PD-L1 expression in the present PDAC cohort. In order to generate macrophages for *in vitro* studies, human primary monocytes were isolated from leukocyte retaining systems *via* density gradient centrifugation (**section 3.1.3**) followed by counterflow centrifugation (**section 3.1.4**). Finally, monocytes were differentiated into either M1-like polarized pro-inflammatory (M1 M $\Phi$ ) or M2-like polarized anti-inflammatory macrophages (M2 M $\Phi$ ) by stimulation with human recombinant GM-CSF and M-CSF, respectively (**section 3.1.9**). Resulting phenotypes of GM-CSF and M-CSF derived macrophages have been extensively characterized in previously published studies and regularly verified in this study by flow cytometry and qPCR analysis of differentiation markers and gene expression profiles [58,260,261].

After differentiation culture, polarized macrophages were analyzed by flow cytometry for PD-1 and PD-L1 cell surface expression levels. Immunofluorescence co-staining of the lineage marker CD14 was performed as internal control for differentiation of monocytes into macrophages and not dendritic cells (**Figure 23 A**). Flow cytometric analyses showed that PD-

L1 is highly expressed at the cell surface of both M1 MΦ (MFI Ratio  $7.84 \pm 1.29$ ) and M2 MΦ (MFI Ratio  $3.01 \pm 0.92$ ) (**Figure 23 B**). Notably, M1 MΦ exhibited significantly higher PD-L1 cell surface levels than M2 MΦ ( $p=0.001$ ). PD-1 was not detectable by flow cytometry at the cell surface of both M1 and M2 MΦ (**Figure 23 B**). In line with flow cytometry results, western blotting revealed higher PD-L1 levels in M1 MΦ than in M2 MΦ. Moreover, macrophages of both polarizations showed markedly higher basal PD-L1 levels than PDAC cell lines Panc1, PancTu-I, Panc89, MIA PaCa-2, BxPc3, Colo357 and Capan-1 (**Figure 23 C**).

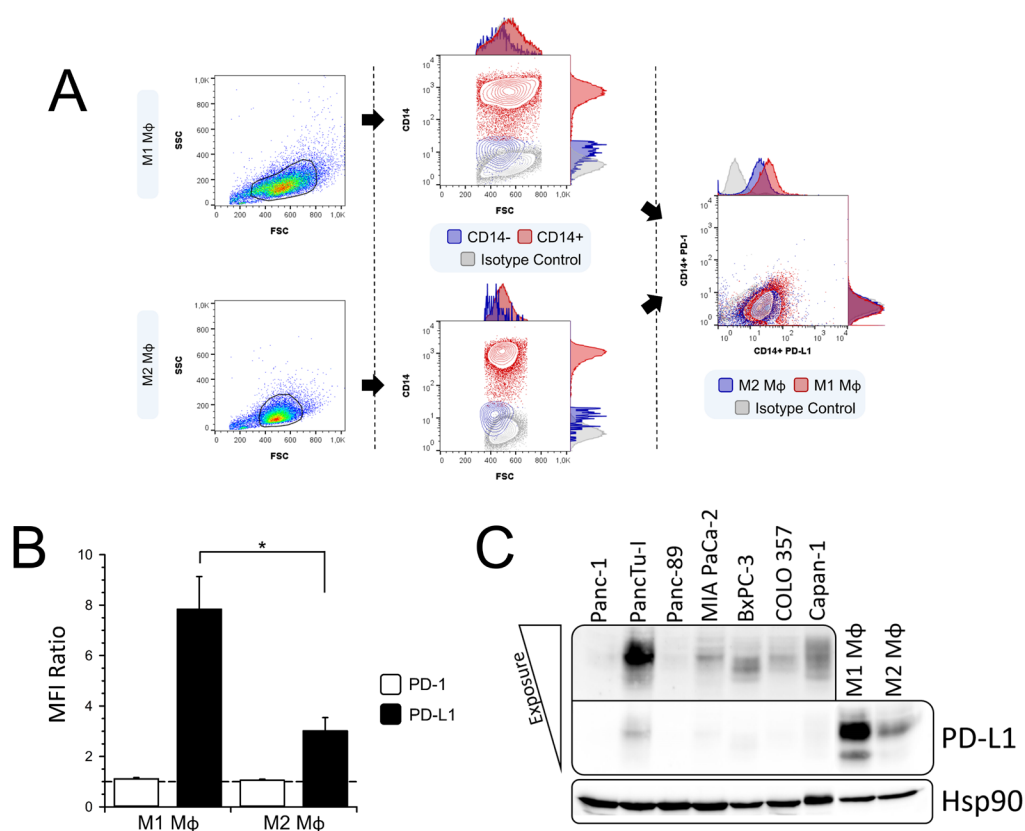


**Figure 23: Basal PD-1 and PD-L1 expressions levels in M1- and M2-polarized macrophages.** Polarized primary human macrophages were generated by *in vitro* stimulation of monocytes with either GM-CSF (M1 MΦ) or M-CSF (M2 MΦ) for seven days. (**A**) Representative dot plots from flow cytometric analyses of M1 MΦ (top) and M2 MΦ (bottom). Shown are the gating strategy in FSC/SSC dot plots (left) and discrimination of CD14<sup>+</sup> macrophages (red) from CD14<sup>-</sup> cells (blue) (middle) as well as signals detected by PD-1/PD-L1 antibody staining in M1 MΦ (red) and M2 MΦ (blue). Signal specificities were verified by staining with respective isotype control antibodies (grey). (**B**) PD-1 (white) and PD-L1 (black) cell surface expression levels in M1- and M2 MΦ detected by immunofluorescence staining and subsequent flow cytometric analysis. Bar chart presents mean values and SEM of median fluorescence intensity ratios detected in three independent experiments. The dashed line marks an MFI ratio of “1”. (**C**) Representative western blot of whole-cell lysates from M1- and M2 MΦ as well as various PDAC cell lines. Hsp90 was detected as loading control. Exposure = decreased/increased time of light exposure for signal detection; \* =  $p<0.05$

#### 4.2.4 GM-CSF, M-CSF and IFN $\gamma$ are potent inducers of PD-L1 expression in human macrophages

Macrophages represent a leukocyte population characterized by high cellular plasticity; a property owed to their great immune-regulatory functional diversity. Therefore, gene expression in macrophages is exceptionally strong affected by extracellular stimuli [70,79]. In order to examine which cytokines have the potential to induce PD-L1 expression in TAMs, M1- and M2-like polarized macrophages were stimulated *in vitro* with cytokines that are commonly found in the tumor microenvironment of PDAC. Besides IFN $\gamma$ , TNF $\alpha$  and TGF- $\beta$ 1, whose cellular origin and function have been briefly outlined in **section 4.2.2**, macrophages were stimulated with either 2.4 ng/ml recombinant human GM-CSF or 50 ng/ml recombinant human M-CSF for 72 h. GM-CSF is commonly secreted by a variety of cell populations like T lymphocytes, endothelial cells fibroblasts, tumor cells and macrophages and exhibits immune-stimulatory properties [278–280]. An immune-stimulatory function also applies to M-CSF, which is primarily secreted by endothelial cells, fibroblasts, tumor cells and macrophages [260,280,281].

Flow cytometric analysis of M1 M $\Phi$  and M2 M $\Phi$  after 72 h of stimulation followed by cell surface staining of PD-L1 was performed as depicted in **Figure 23 A**. Flow cytometry results for M1 M $\Phi$  showed an increase of relative PD-L1 cell surface levels after stimulation with GM-CSF (+14.5%), M-CSF (+8.7%) and IFN $\gamma$  (+11.6%) compared to unstimulated macrophages. In contrast, relative PD-L1 cell surface levels were decreased due to stimulation with TNF $\alpha$  (-9.9%) and TGF- $\beta$ 1 (-11.0%) (**Figure 24 A**). In line with flow cytometric measurements, the same effects of GM-CSF, M-CSF, IFN $\gamma$ , TNF $\alpha$  and TGF- $\beta$ 1 on PD-L1 expression levels in M1 M $\Phi$  were detected by immunofluorescence staining followed by microscopical analysis (**Figure 24 B**) as well as western blotting analysis of whole-cell lysates (**Figure 24 E**).

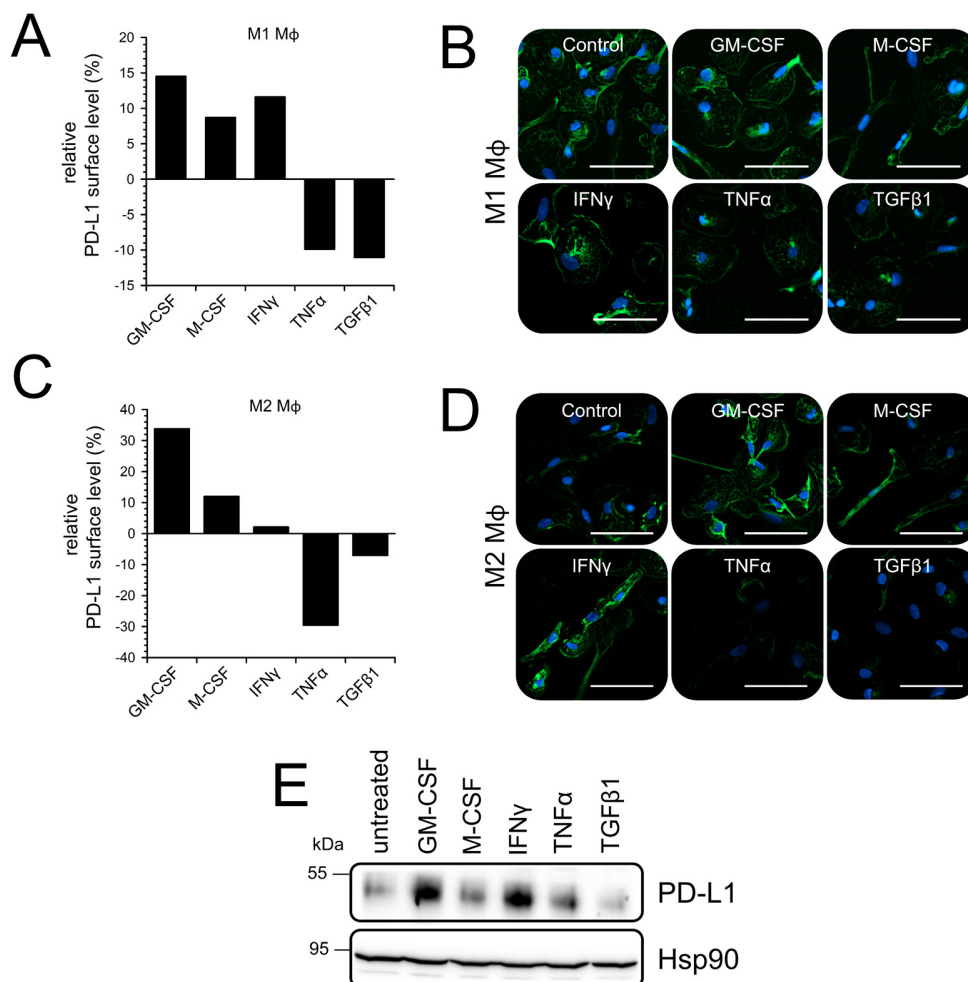


**Figure 24: Induction of PD-L1 expression by various cytokines in M1- and M2-polarized macrophages.** Polarized primary human macrophages were generated by *in vitro* stimulation of monocytes with either GM-CSF (M1 M $\Phi$ ) or M-CSF (M2 M $\Phi$ ) for seven days. Macrophages were cultured for 72 h in respective standard culture medium supplemented with 2.4 ng/ml GM-CSF, 50 ng/ml M-CSF, 10 ng/ml IFN $\gamma$ , 10 ng/ml TNF $\alpha$  or 20 ng/ml TGF- $\beta$ 1. (A+C) Relative PD-L1 cell surface expression levels in (A) M1- and (C) M2 M $\Phi$  after stimulation with indicated cytokines in comparison to unstimulated macrophages. Bar charts present percentage changes in median fluorescence intensity ratios resulting from single flow cytometric analysis of PD-L1 immunofluorescence staining. (B+D) Representative fluorescence microscopical images of immunofluorescence PD-L1 (green) staining in (B) M1- and (D) M2 M $\Phi$  after stimulation with indicated cytokines. Nuclei were stained with Hoechst (blue) (Scale bar = 50  $\mu$ m). (E) Representative western blot of whole-cell lysates from M1 M $\Phi$  after indicated stimulations. Hsp90 was detected as loading control. Molecular weights in kDa are indicated according to the applied standard.

Similar effects on relative PD-L1 cell surface expression levels were detected in M2 M $\Phi$ . Flow cytometric analysis after PD-L1 staining of M2 M $\Phi$  revealed an increase in relative PD-L1 surface levels after stimulation with GM-CSF (33.8%), M-CSF (11.9%) and IFN $\gamma$  (2.1%) compared to unstimulated M2 M $\Phi$ . Stimulation with TNF $\alpha$  or TGF- $\beta$ 1 decreased relative PD-L1 cell surface levels by 29.6% and 7.0%, respectively (Figure 24 C). Immunofluorescence staining of PD-L1 followed by microscopical analysis verified effects of GM-CSF, M-CSF, IFN $\gamma$ , TNF $\alpha$  and TGF- $\beta$ 1 stimulation on PD-L1 expression in M2 M $\Phi$  (Figure 24 D).

Taken together, GM-CSF, M-CSF and IFN $\gamma$  have been identified as potent inducers of PD-L1 expression in both M1 and M2 M $\Phi$ . However, answering the question, which macrophage

polarization status is predominantly found within the areas of the tumor margin and tumor lymphatics interface that exhibit high accumulation of PD-L1<sup>+</sup> cells, is hard to determine based on the available *in situ* data. In this context, Helm and colleagues reported that TAMs in PDAC exhibit both M1- and M2-associated properties [58]. Since monocyte differentiation *via* GM-CSF stimulation generated macrophages with a significantly higher PD-L1 expression than M-CSF stimulation and both GM-CSF as well as IFN $\gamma$  are cytokines secreted by CD8<sup>+</sup> cytotoxic tumor-infiltrating T lymphocytes, a cell population shown to be highly enriched within PDAC areas exhibiting pronounced PD-L1 expression, M1 M $\Phi$  were chosen as a model for TAMs in the following *in vitro* settings.

#### 4.2.5 Characterization of T lymphocyte activation status after stimulation with CD3- and CD28-targeting antibodies

The third cell population that has been identified to be present at high abundance in PDAC tissues exhibiting high PD-L1 staining were T lymphocyte subsets. In order to generate pre-activated T lymphocytes for the following *in vitro* experiments, a protocol for isolation and *in vitro* activation of human primary T lymphocytes has been developed.

In the first step, lymphocytes were isolated from leukocyte retaining system via density gradient centrifugation (**section 3.1.3**) and subsequently separated from monocytes via counterflow centrifugation (**section 3.1.4**). Then, lymphocyte fraction containing  $\alpha\beta$ - and  $\gamma\delta$ -T lymphocyte subsets as well as B cells and NK cells were stimulated with immobilized CD3- and soluble CD28-targeting antibodies. Microscopical analysis in the time course of five days revealed the formation of activation clusters, centers for clonal expansion of activated T lymphocytes, already after 24 h. Activation clusters of anti-CD3/CD28 stimulated lymphocytes showed continuous growth within the whole cultivation duration of five days. In contrast, unstimulated lymphocytes did not form any activation clusters even after five days (**Figure 25 A**). Western blotting analysis of whole-cell lysates after days 3 and 5 revealed markedly increased levels of phosphorylated ERK1/2 and Stat1 in anti-CD3/CD28 stimulated but not in unstimulated lymphocytes compared to initially seeded cells (d0) (**Figure 25 B**). Moreover, anti-CD3/CD28 stimulated lymphocytes showed clearly increased PD-L1 expression levels compared to unstimulated as well as initially seeded cells (**Figure 25 B**). Notably, both pStat1 and PD-L1 expression levels were highest in anti-CD3/CD28 stimulated lymphocytes after three days and decreased at day 5 (**Figure 25 B**). Immunofluorescence staining of PD-L1 and PD-1 in cytopins of unstimulated and anti-CD3/CD28 stimulated lymphocytes after day 5 of culture

verified higher PD-L1 expression levels in stimulated cells and, additionally, showed concomitantly elevated levels of PD-1 (**Figure 25 C**).

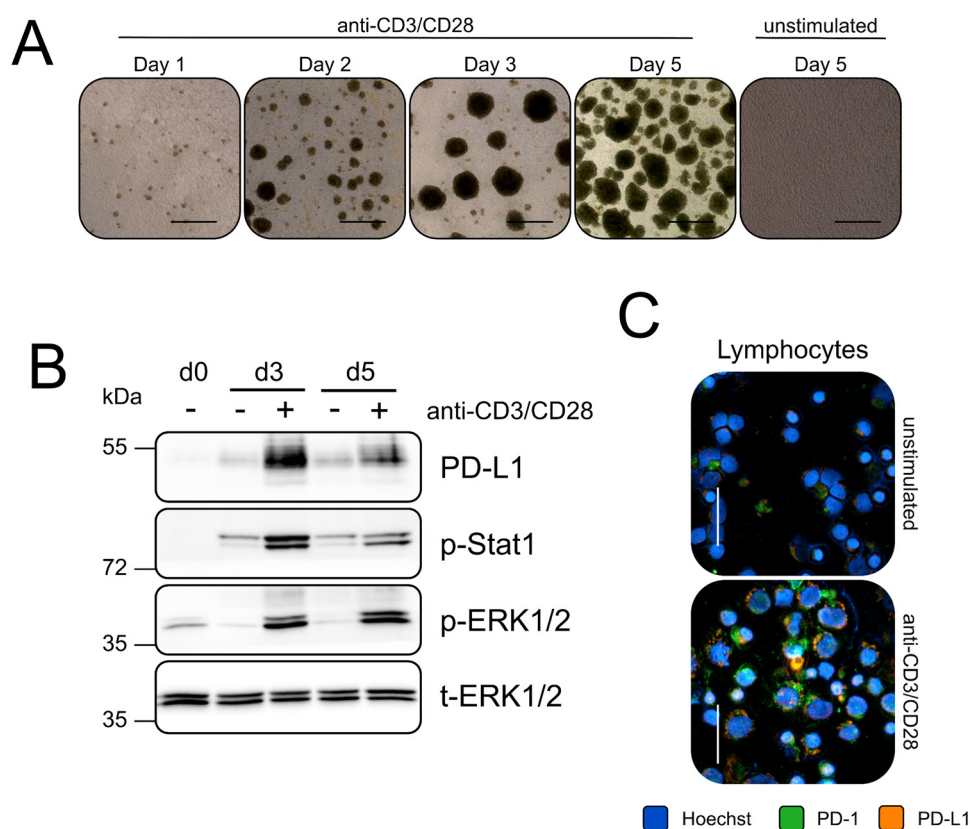


**Figure 25: Lymphocyte activation by anti-CD3/CD28 stimulation.** Primary human lymphocytes were isolated from leukocyte retaining systems by density gradient centrifugation followed by counterflow centrifugation. Afterwards, lymphocytes were seeded in standard culture medium and either left unstimulated or were stimulated with immobilized CD3- and soluble CD28-targeting antibodies for 3 to 5 days. **(A)** Representative light microscopical images of unstimulated and anti-CD3/CD28 stimulated lymphocytes after indicated culture durations (Scale bar = 500  $\mu$ m). **(B)** Representative western blot of whole-cell lysates from unstimulated (-) and anti-CD3/CD28 stimulated (+) lymphocytes after seeding (d0) and three (d3) and five (d5) days of culture, respectively. Molecular weights in kDa are indicated according to the applied standard. **(C)** Representative fluorescence microscopical images of immunofluorescence PD-1 (green) and PD-L1 (orange) staining in cytopins of unstimulated or anti-CD3/CD28 stimulated lymphocytes after five days of culture. Nuclei were stained with Hoechst (blue). Scale bar = 30  $\mu$ m

In order to characterize lymphocytes activated by stimulation with anti-CD3/CD28 antibodies in more detail, flow cytometric analyses of CFSE, CD4, CD8, PD1 and PD-L1 co-staining was performed on days 3 and 5 after seeding of lymphocytes. The gating strategy of flow cytometric analysis is depicted in **Figure 26**.



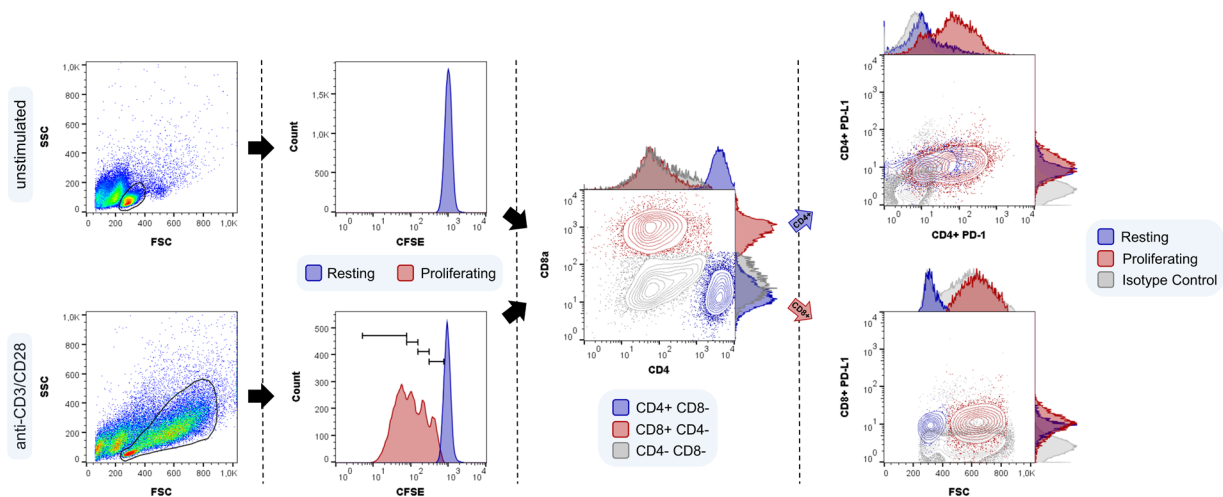


**Figure 26: Schematic illustration of the gating strategy for flow cytometric analyses of lymphocyte populations.** Primary human lymphocytes were isolated from leukocyte retaining systems by density gradient centrifugation followed by counterflow centrifugation. Afterwards, lymphocytes were stained with CFSE, seeded in standard culture medium and were either left unstimulated or were stimulated with immobilized CD3- and soluble CD28-targeting antibodies. First, vital lymphocytes were discriminated in FSC/SSC plot. Secondly, resting (blue) and proliferating (red) population were identified via CFSE staining intensity. Thirdly, CD4<sup>+</sup> (blue) CD8<sup>+</sup> (red) and CD4<sup>-</sup> CD8<sup>-</sup> (grey) populations were discriminated by staining with fluorochrome-conjugated antibodies targeting CD4 and CD8, respectively. Finally, PD-1 and PD-L1 cell surface levels were quantified within resting (blue) and proliferating (red) populations of CD4<sup>+</sup> (top) and CD8<sup>+</sup> (bottom) lymphocytes by respective immunofluorescence signals. Signal specificities were verified by staining with respective isotype control antibodies (grey).

In detail, anti-CD3/CD28 stimulated lymphocytes showed in FSC/SSC plots the formation of an additional population larger in size and markedly more granulated than unstimulated lymphocytes, a characteristic phenotype of lymphoblasts (**Figure 26**). Flow cytometric evaluation of CFSE staining revealed a typical pattern for proliferating lymphocytes resulting from 1:2 dye dilution in every cell division. Gating for proliferating CFSE<sup>low</sup> cells showed a significantly higher proportion of proliferating cells in anti-CD3/CD28 stimulated lymphocytes compared to unstimulated lymphocytes after 3 (0.2% vs. 18.7%) and 5 (1.2% vs. 72.9%) days of culture duration. Moreover, the proportion of proliferating cells in both stimulated and unstimulated lymphocytes significantly increased in the time course of day 3 to 5 (**Figure 27 A**). However, an increased number of vital cells was detected first at day 5 in anti-CD3/CD28 stimulated lymphocytes ( $1.93 \pm 0.30$  (day 5) vs.  $1.13 \pm 0.09$  (day 3)  $\cdot 10^6$  cells;  $p=0.046$ ) (**Figure 27 B**). In order to examine whether anti-CD3/CD28 stimulation caused activation of CD4<sup>+</sup> and CD8<sup>+</sup> lymphocyte subsets to a similar extent, CFSE profiles of pre-gated proliferating CD4<sup>+</sup> and CD8<sup>+</sup> lymphocytes were analyzed. CFSE profiles at day 3 after stimulation revealed up to three distinguishable cell divisions within both CD4<sup>+</sup> and CD8<sup>+</sup> lymphocyte populations with the majority of cells having divided once or twice. Notably, CD4<sup>+</sup> and CD8<sup>+</sup> showed very similar CFSE profiles at day 3 (CD4/CD8: 47.0/48.0 vs. 36.6/35.5 vs. 16.6/16.4 % of proliferating cell population in CFSE peaks 1 to 3) (**Figure 27 C**). At day 5 after anti-

CD3/CD28 stimulation up to 5 distinguishable cell divisions were detected for both CD4<sup>+</sup> and CD8<sup>+</sup> lymphocytes. Most lymphocytes were located in CFSE peaks of low median fluorescence intensity indicating that lymphocytes had divided four to five times. Thus, these data suggest that initially activated cells continuously proliferate during a course of 5 days. Again, CD4<sup>+</sup> and CD8<sup>+</sup> lymphocytes showed similar CFSE profiles at day 5 (CD4/CD8: 10.6/8.0 vs. 12.6/12.6 vs. 18.6/20.3 vs. 23.3/26.7 vs. 34.7/27.3 % of proliferating cell population in CFSE peaks 1 to 5) (Figure 27 D).

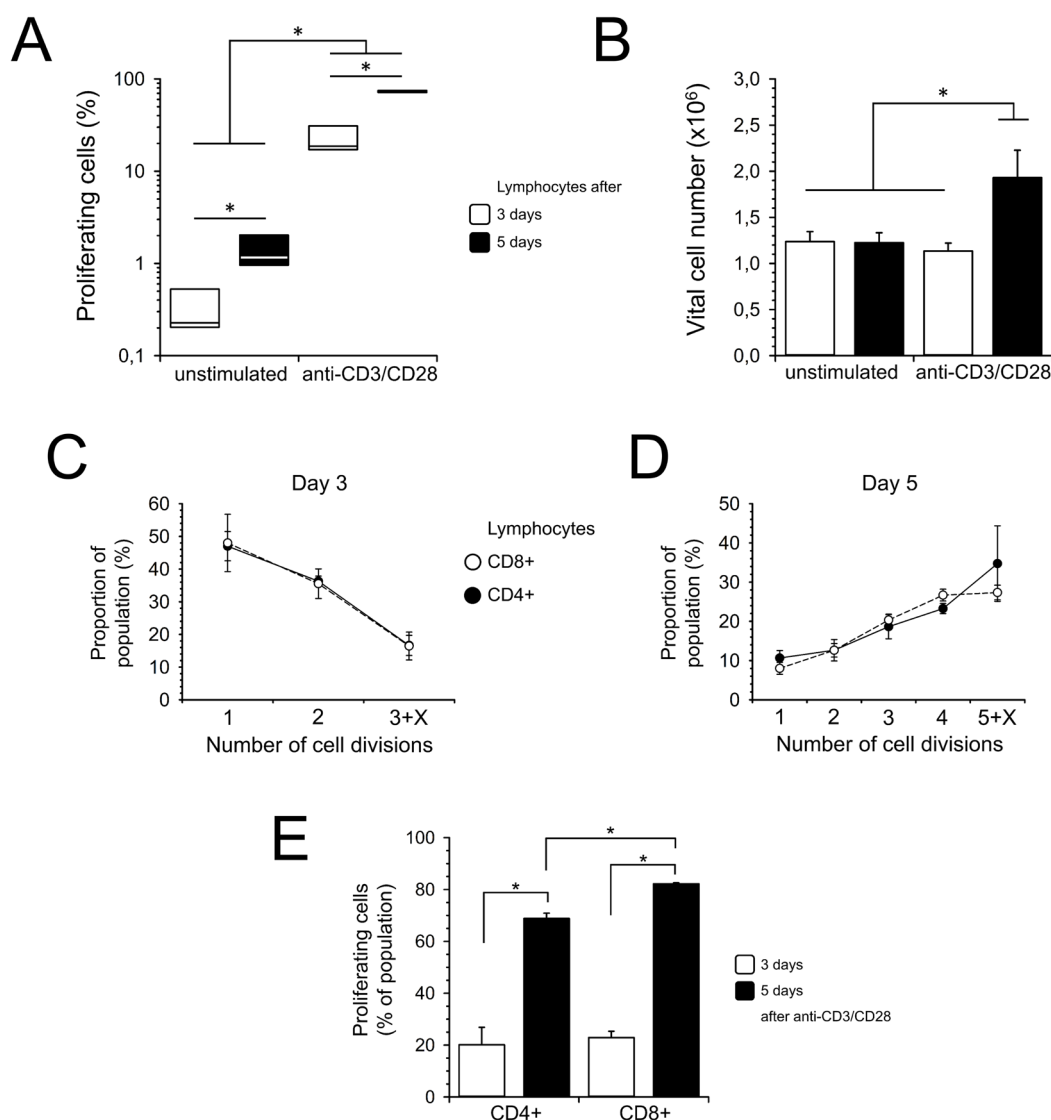


**Figure 27: Proliferation within CD4<sup>+</sup> and CD8<sup>+</sup> lymphocyte populations after anti-CD3/CD28 stimulation.** Primary human lymphocytes were isolated from leukocyte retaining systems by density gradient centrifugation followed by counterflow centrifugation. Afterwards, lymphocytes were CFSE stained, seeded in standard culture medium and either left unstimulated or were stimulated with immobilized CD3- and soluble CD28-targeting antibodies for 3 to 5 days. (A) Proportion of proliferating cells and (B) vital cell numbers in unstimulated and anti-CD3/CD28 stimulated lymphocyte populations after three (white) and five (black) days. (C+D) CFSE profiles of proliferating lymphocytes within the CD4<sup>+</sup> (black) and CD8<sup>+</sup> (white) population after (C) three and (D) five days of anti-CD3/CD28 stimulation. Data presents mean values and SEM of lymphocytes having divided 1 to 5 times. The maximum numbers of clearly distinguishable peaks in respective CFSE profiles are indicated by “+X”. (E) Proportion of proliferating lymphocytes within the CD4<sup>+</sup> and CD8<sup>+</sup> population after three (white) and five (black) days of anti-CD3/CD28 stimulation. Box plots present median values with quartiles (Q<sub>0.75</sub> as upper, Q<sub>0.25</sub> as lower deviation) and bar charts present mean values with SEM of three independent experiments. \* = p<0.05

Verifying the similar effectiveness of anti-CD3/CD28 stimulation in terms of cell proliferation in CD4<sup>+</sup> and CD8<sup>+</sup> T lymphocyte subsets, no significant differences in proportions of proliferating CD4<sup>+</sup> and CD8<sup>+</sup> lymphocytes were observed at day 3 ( $20.12 \pm 6.74\%$  vs.  $22.90 \pm 2.40\%$ ) and a significant increase of proliferating cells in the time course from day 3 to day 5 after stimulation was shown for both CD4<sup>+</sup> ( $p < 0.001$ ) and CD8<sup>+</sup> ( $p < 0.001$ ) lymphocytes. Interestingly, a significantly higher proportion of proliferation cells within CD8<sup>+</sup> compared to CD4<sup>+</sup> lymphocytes was detected at day 5 ( $82.23 \pm 0.23\%$  vs.  $68.83 \pm 2.06\%$ ;  $p = 0.035$ ) (**Figure 27 E**).

Analyzing how lymphocyte activation by anti-CD3/CD28 stimulation alters cell surface levels of PD-1 and PD-L1 in CD4<sup>+</sup> and CD8<sup>+</sup> T cell subsets, flow cytometric analyses revealed significantly increased PD-1 surface levels within the proliferating population of the CD4<sup>+</sup> lymphocyte subset compared resting cells that was constant from day 3 (MFI Ratio  $8.06 \pm 0.27$  vs.  $1.85 \pm 0.08$ ;  $p < 0.001$ ) up to day 5 (MFI Ratio  $8.53 \pm 1.17$  vs.  $1.70 \pm 0.06$ ;  $p < 0.001$ ) after stimulation (**Figure 28 A**). Similarly, PD-L1 cell surface levels were significantly increased in the proliferating compared to the resting CD4<sup>+</sup> lymphocyte subset at day 3 (MFI Ratio  $8.68 \pm 0.19$  vs.  $2.00 \pm 0.16$ ;  $p < 0.001$ ) and day 5 (MFI Ratio  $4.69 \pm 0.23$  vs.  $2.49 \pm 0.17$ ;  $p < 0.001$ ) after stimulation. In contrast to PD-1, PD-L1 cell surface expression levels were not stable over the course of time but significantly decreased in the proliferating CD4<sup>+</sup> lymphocyte subset at day 5 compared to levels at day 3 after anti-CD3/CD28 stimulation ( $p < 0.001$ ) (**Figure 28 B**). Similar, results were observed for the CD8<sup>+</sup> T cell population in response to anti-CD3/CD28 stimulation (**section 4.2.6**).

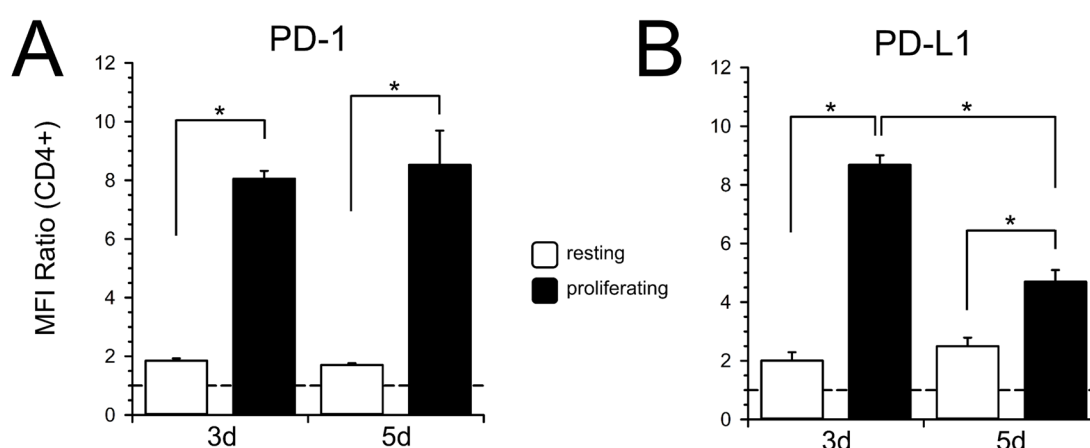


**Figure 28: PD-1 and PD-L1 cell surface levels in the CD4<sup>+</sup> T lymphocyte population after anti-CD3/CD28 stimulation.** Primary human lymphocytes were isolated from leukocyte retaining systems by density gradient centrifugation followed by counterflow centrifugation. Afterwards, lymphocytes were seeded in standard culture medium and stimulated with immobilized CD3- and soluble CD28-targeting antibodies for 3 to 5 days until immunofluorescence staining followed by flow cytometric analysis. (A) PD-1 and (B) PD-L1 cell surface expression levels in the resting (white) and proliferating (black) population of CD4<sup>+</sup> lymphocytes after indicated culture durations. Bar charts present mean values and SEM of median fluorescence intensity ratios detected in three independent experiments. The dashed line marks an MFI ratio of “1”. \* =  $p < 0.05$

T lymphocyte activation is accompanied by an increased expression of general (IFN $\gamma$  and IL-2) as well as various subset-specific (TNF $\alpha$ , TGF- $\beta$ 1, IL-10, IL-17A, sFasL, Perforin, Granulysin, Granzyme A and Granzyme B) cytokines and effector molecules [68]. Therefore, intracellular mRNA levels and supernatant protein levels of cytokines and chemokines associated with activation of T lymphocytes and other leukocyte populations (IL-1 $\beta$ , IL-6 and IL-8) were examined via qPCR (**Figure 29**) and multiplex assay (**Figure 30**).

Quantitative real-time PCR analysis revealed significantly increased levels of IFN $\gamma$  (3702.71 vs. 1.58-fold; **Figure 29 A**) and IL-2 (651.52 vs. 128.5-fold; **Figure 29 B**) in anti-CD3/CD28 stimulated lymphocytes compared to unstimulated lymphocytes at day 3. However, while still significantly increased mRNA levels of IFN $\gamma$  in stimulated lymphocytes (880.26 vs. 1.19-fold; **Figure 29 A**) decreased from day 3 to 5, IL-2 mRNA levels (1165.88 vs. 651.52-fold; **Figure 29 B**) were increased by trend in stimulated lymphocytes at day 5 after stimulation compared to day 3. By trend, a similar expression pattern over the course of 5 days as for IFN $\gamma$  was detected for TNF $\alpha$  mRNA levels. TNF $\alpha$  levels were constantly higher in anti-CD3/CD28 stimulated lymphocytes compared to unstimulated lymphocytes at day 3 (28.72 vs. 0.84-fold) and day 5 (22.04 vs. 1.55-fold) but slightly decreased from day 3 to day 5 after stimulation (**Figure 29 C**). TGF- $\beta$ 1 mRNA levels in anti-CD3/CD28 stimulated lymphocytes remained unchanged over the period of 5 days ( $1.23 \pm 0.20$  (d3) vs.  $1.03 \pm 0.32$ -fold (d5)) compared to basal levels in freshly isolated lymphocytes. In contrast, unstimulated lymphocytes showed by trend constantly lower TGF- $\beta$ 1 mRNA levels ( $0.46 \pm 0.06$  (d3) vs.  $0.48 \pm 0.08$ -fold (d5)) in comparison to levels in freshly isolated lymphocytes (**Figure 29 D**). IL-6 (d3: 23.25 vs. 3.73-fold; **Figure 29 E**) and IL-10 (d3: 58.46 vs. 8.58-fold; **Figure 29 F**) mRNA levels were significantly higher in anti-CD3/CD28 stimulated lymphocytes compared to unstimulated lymphocytes after day 3, but both IL-6 (d5: 6.49 vs. 3.73-fold; **Figure 29 E**) and IL-10 (d5: 28.88 vs. 26.02-fold; **Figure 29 F**) levels dropped in the course of time to levels detected in unstimulated lymphocytes at day 5. Macrophage-associated cytokines IL-1 $\beta$  (d3:  $7.54 \pm 1.44$  vs.  $3.10 \pm 0.77$ -fold; **Figure 29 G**) and IL-8 (d3:  $6.35 \pm 3.55$  vs.  $1.11 \pm 0.52$ -fold; **Figure 29 H**) showed markedly higher mRNA levels in unstimulated compared to stimulated lymphocytes at day 3, but both mRNA levels, IL-1 $\beta$  (d5:  $3.38 \pm 0.36$  vs.  $1.54 \pm 0.94$ -fold; **Figure 29 G**) more than IL-8 (d5:  $4.64 \pm 1.94$  vs.  $1.20 \pm 0.45$ -fold; **Figure 29 H**) levels, markedly dropped in the course of time from day 3 to day 5 in unstimulated lymphocytes.

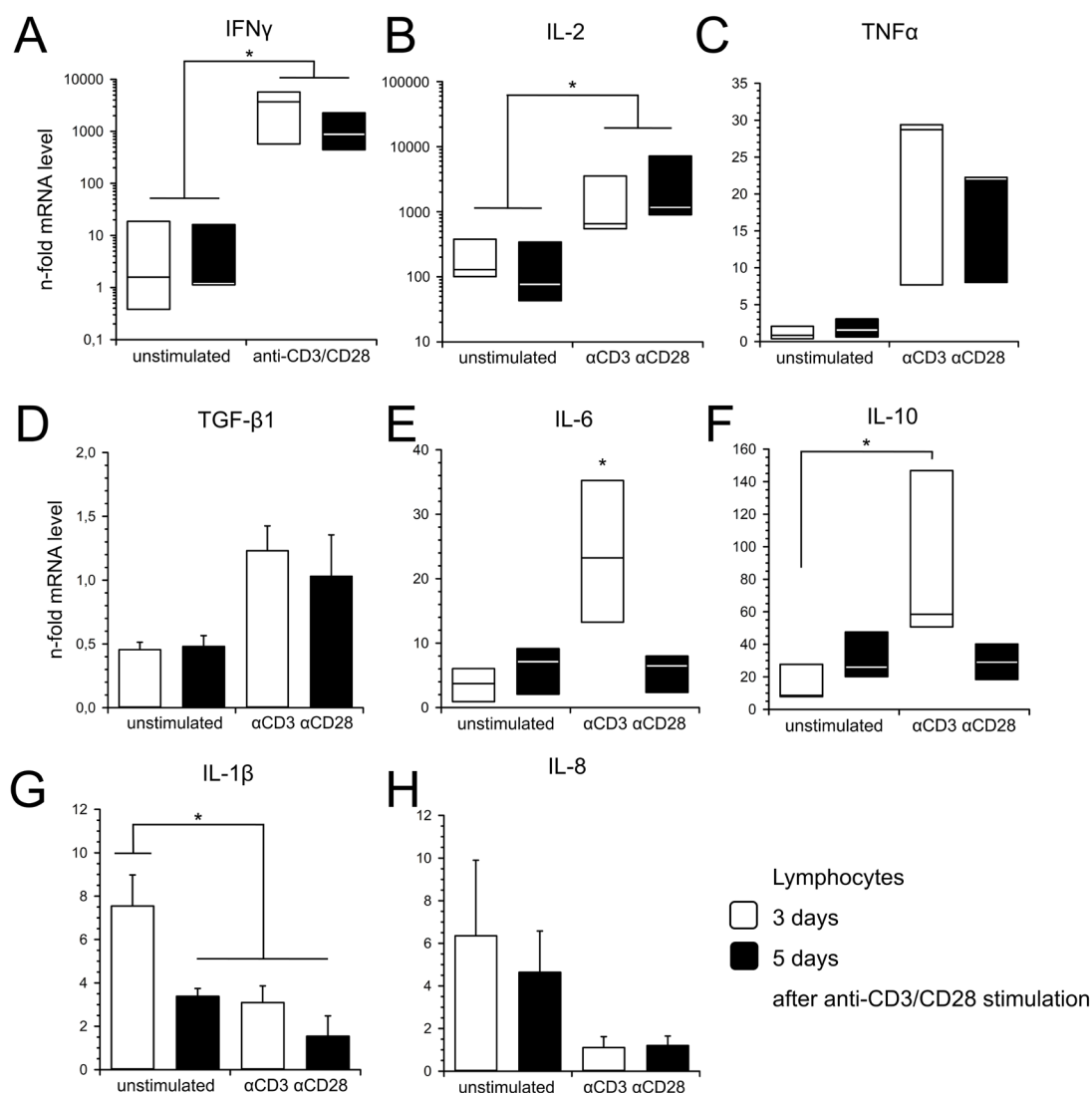


**Figure 29: Gene expression profile of cytokines and chemokines associated with various lymphocyte populations after anti-CD3/CD28 stimulation of whole lymphocyte populations.** Primary human lymphocytes were isolated from leukocyte retaining systems by density gradient centrifugation followed by counterflow centrifugation. Afterwards, lymphocytes were seeded in standard culture medium and were either left unstimulated or stimulated with immobilized CD3- and soluble CD28-targeting antibodies for 3 (white) to 5 days (black). Relative mRNA levels of (A) IFN $\gamma$ , (B) IL-2, (C) TNF $\alpha$ , (D) TGF- $\beta$ 1, (E) IL-6, (F) IL-10, (G) IL-1 $\beta$  and (H) IL-8 in unstimulated and anti-CD3/CD28 stimulated lymphocytes after three (white) and five (black) days of culture. Box plots present median values with quartiles (Q<sub>0.75</sub> as upper, Q<sub>0.25</sub> as lower deviation) and bar charts present mean values with SEM of three independent experiments. Messenger RNA levels were normalized to respective GAPDH levels as well as levels detected in freshly isolated lymphocytes prior to seeding (= 1). \* = p < 0.05

Detection of cytokines associated with T lymphocyte activation *via* multiplex assay revealed significantly elevated levels of every analyte within the cytokine panel, except for IL-6 that was only increased by trend, in culture supernatants of anti-CD3/CD28 stimulated lymphocytes compared to unstimulated cells (Figure 30). Additionally, all cytokines detected in the supernatants of anti-CD3/CD28 stimulated lymphocytes, except for IFN $\gamma$ , showed an increase in concentration over the culture duration of five days. In detail, IFN $\gamma$  levels in supernatants of stimulated lymphocytes were increased at day three by 28.14 ng/ml (29.32 vs. 1.18 ng/ml) and at day five by 28.43 ng/ml (29.60 vs. 1.17 ng/ml) compared to unstimulated lymphocytes

(**Figure 30 A**). IL-6 levels were increased at day three by 3.39 ng/ml (4.06 vs. 0.67 ng/ml) and at day five by 5.20 ng/ml (5.76 vs. 0.56 ng/ml) (**Figure 30 B**). TNF $\alpha$  levels were increased after three days by 6207.84 pg/ml (6214.35 vs. 6.51 pg/ml) and after five days by 10.8 ng/ml (10809.36 vs. 9.10 pg/ml) (**Figure 30 C**). IL-17A supernatant levels were increased at day 3 by 1306.79 pg/ml (1330.74 vs. 23.95 pg/ml) and after day 5 by 4.00 ng/ml (4090.96 vs. 87.70 pg/ml) (**Figure 30 D**). Soluble FasL levels were increased at day 3 by 966.82 pg/ml (973.63 vs. 6.81 pg/ml) and at day 5 after stimulation by 3.38 ng/ml (3406.36 vs. 22.27 pg/ml) (**Figure 30 E**). Perforin levels were increased in supernatants of stimulated lymphocytes at day 3 by 3.25 ng/ml (3.60 vs. 0.35 ng/ml) and at day 5 by 8.79 ng/ml (9.55 vs. 0.76 ng/ml) (**Figure 30 F**). Granzyme A levels were increased at day 3 by 9.87 ng/ml (10.50 vs. 0.63 ng/ml) and at day 5 by 30.02 ng/ml (32.00 vs. 1.98 ng/ml) compared to unstimulated lymphocytes (**Figure 30 G**). Granzyme B levels were increased at day 3 by 75.77 ng/ml (76.32 vs. 0.55 ng/ml) and at day 5 by 82.45 ng/ml (82.96 vs. 0.51 ng/ml) (**Figure 30 H**). Finally, Granulysin levels in supernatants of anti-CD3/CD28 stimulated lymphocytes were elevated by 21.39 ng/ml (22.14 vs. 0.75 ng/ml) and at day 5 by 82.01 ng/ml (85.05 vs. 3.04 ng/ml) compared to unstimulated lymphocytes (**Figure 30 I**).

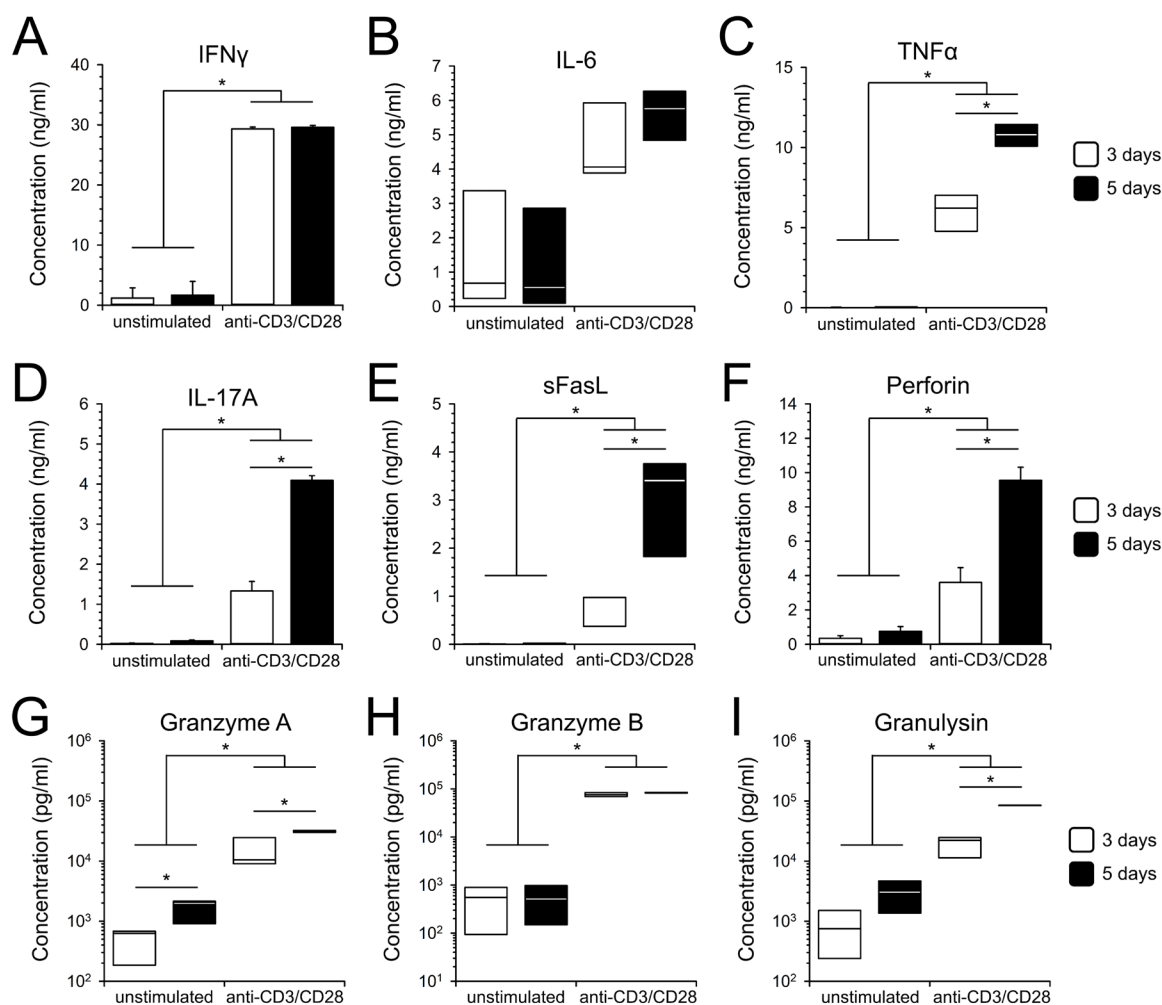


**Figure 30: Supernatant levels of T lymphocyte-associated cytokines after anti-CD3/CD28 stimulation of whole lymphocyte populations.** Primary human lymphocytes were isolated from leukocyte retaining systems by density gradient centrifugation followed by counterflow centrifugation. Afterwards, lymphocytes were seeded in standard culture medium and were either left unstimulated or were stimulated with immobilized CD3- and soluble CD28-targeting antibodies for 3 to 5 days. Concentrations of (A) IFN $\gamma$ , (B) IL-6, (C) TNF $\alpha$ , (D) IL-17A, (E) soluble Fas ligand, (F) Perforin, (G) Granzyme A, (H) Granzyme B and (I) Granulysin were measured by multiplex assay in the culture supernatant of unstimulated and anti-CD3/CD28 stimulated lymphocytes after three (white) and five (black) days of culture. Box plots present median values with quartiles (Q<sub>0.75</sub> as upper, Q<sub>0.25</sub> as lower deviation) and bar charts present mean values with SEM of three independent experiments. \* = p < 0.05

Taken together, these data show that the established protocol for activation of isolated primary human T lymphocytes via CD3- and CD28-targeting antibodies leads to specific activation of both CD4<sup>+</sup> and CD8<sup>+</sup> T lymphocyte subsets. Moreover, activation status of T lymphocytes progresses over the whole culture duration of five days. Notably, within the CD8<sup>+</sup> T lymphocyte subset proliferating cells reached a proportion of almost 90%. Finally, both PD-1 and PD-L1 cell surface levels have been shown to be upregulated exclusively in proliferating lymphocytes. In order to obtain a pre-activated T lymphocyte population that still possesses activation capacity and, therefore, might be susceptible to stimuli provided by PDAC cells and M1 M $\Phi$ ,

an activation culture duration of 4 days was assumed to be ideal for subsequent co-culture experiments.

#### 4.2.6 Isolation and activation of CD8<sup>+</sup> T lymphocytes from whole lymphocyte population for subsequent co-culture experiments

*In situ* identified areas of high PD-L1 expression have been shown to be enriched for CD3<sup>+</sup> T lymphocytes, especially CD8<sup>+</sup> subsets. CD8<sup>+</sup> TILs are part of the adaptive anti-tumor response exhibiting cytotoxic potential [68]. Therefore, the cytotoxic activity of activated CD8<sup>+</sup> TILs within tissues has to be tightly regulated. Besides their T cell receptor antigen-specificity, PD-1 signaling in TILs *via* binding to target cell-expressed PD-L1 represents one central mechanism for escape from lysis and induction of anergy in TILs [175]. In order to evaluate whether PD-L1 expression by PDAC cells, macrophages and/or CD8<sup>+</sup> T lymphocytes themselves represents a factor that negatively affects CD8<sup>+</sup> T lymphocyte activation status *in vitro*, a protocol for isolation of primary human CD8<sup>+</sup> T lymphocytes and subsequent activation has been developed.

Briefly, lymphocytes were isolated from leukocyte retaining systems as already described in **section 4.2.5**. Then, CD8<sup>+</sup> T lymphocytes were isolated by magnetic-activated cell separation negative selection (**section 3.1.6**). Afterwards, CD8<sup>+</sup> T lymphocyte purity was controlled by  $\alpha\beta$ TCR, CD4 and CD8 co-staining. Subsequent flow cytometric analyses revealed initial proportions of  $\alpha\beta$ TCR<sup>+</sup> cells in the range of about 60-80% and CD8<sup>+</sup> T cells within the  $\alpha\beta$ TCR<sup>+</sup> population of about 18-30% (**Figure 31 A**). After magnetic-activated cell separation, proportions of >90%  $\alpha\beta$ TCR<sup>+</sup> CD8<sup>+</sup> T lymphocytes were detected (92.50  $\pm$  2.05%) (**Figure 31 B**).



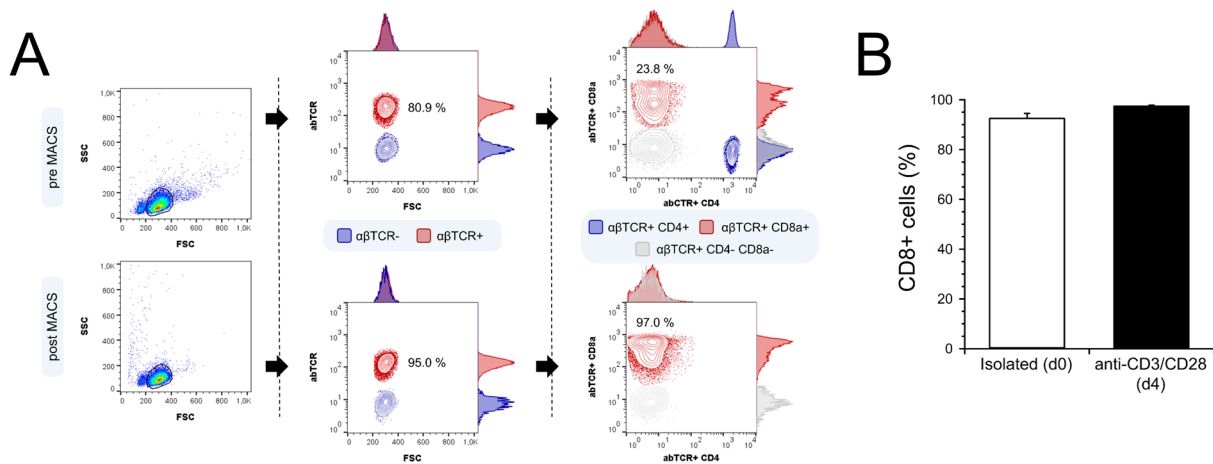


**Figure 31: Isolation of primary human CD8<sup>+</sup> T lymphocytes from peripheral blood mononuclear cells.** Primary human lymphocytes were isolated from leukocyte retaining systems by density gradient centrifugation followed by counterflow centrifugation. **(A)** Schematic illustration of the staining panel and gating strategy in flow cytometric analysis before (pre MACS) and after (post MACS) magnetic-activated cell separation. First, vital lymphocytes were gated in FSC/SSC plot. Secondly,  $\alpha\beta$  T cell receptor ( $\alpha\beta$ TCR) positive (red) were discriminated from  $\alpha\beta$ TCR negative cells (blue). Finally, the proportion of CD4<sup>+</sup> (blue), CD8<sup>+</sup> (red) and CD4<sup>-</sup>CD8<sup>-</sup> (grey)  $\alpha\beta$ TCR<sup>+</sup> T lymphocytes were examined. **(B)** Proportion of CD8<sup>+</sup> T lymphocytes after isolation by MACS separation (white) and after 4 days of anti-CD3/CD28 stimulation (black). Bar chart presents mean values with SEM of six independent experiments.

Finally, cells were stained with CFSE (**section 3.1.7**) and activated by stimulation with immobilized CD3- and soluble CD28-targeting antibodies. Since CD8<sup>+</sup> T lymphocytes do not produce sufficient levels of IL-2 for self-preservation, recombinant human IL-2 was added to the activation culture (**section 3.1.8**). Flow cytometric phenotypic after 4 days of activation culture revealed a purity of  $\alpha\beta$ TCR<sup>+</sup> CD8<sup>+</sup> T lymphocytes of >95% ( $97.47 \pm 0.38\%$ ) (**Figure 31 B**).

Further characterization of anti-CD3/CD28 stimulated CD8<sup>+</sup> T lymphocytes after 4 days of activation culture showed in FSC/SSC plots the formation of a dominant population with increased size and higher granularity than isolated cells (**Figure 32 A**). CFSE profile analysis revealed up to five distinguishable cell divisions within the population (**Figure 32 B**). However, the major proportion of CD8<sup>+</sup> T lymphocytes within the proliferating population had undergone one ( $30.28 \pm 4.25\%$ ;  $p < 0.001$ ) or two ( $29.85 \pm 2.00\%$ ;  $p < 0.001$ ) cell divisions and more than 80% of the population did not exceed three cell divisions 4 days after stimulation (**Figure 32 C**). Overall, the proportion of proliferating cells within the population was >50% ( $53.14 \pm 4.46\%$ ) (**Figure 32 D**). Quantitative real-time PCR analysis showed markedly increased mRNA levels for IFN $\gamma$  (3.19-fold) and TNF $\alpha$  (2.24-fold), while IL-2 (0.09-fold) and IL-6 (0.30-fold) mRNA levels were clearly decreased in comparison to levels in whole lymphocyte populations (**Figure 32 E**). Finally, western blotting analysis revealed markedly elevated levels of phosphorylated ERK1/2 as well as total and phosphorylated Stat1 in whole-cell lysates of CD8<sup>+</sup> T lymphocytes stimulated for four days with CD3- and CD28-targeting antibodies

compared to unstimulated cells underscoring high proliferative activity of CD8<sup>+</sup> T lymphocytes after anti-CD3/CD28 stimulation (**Figure 32 F**).

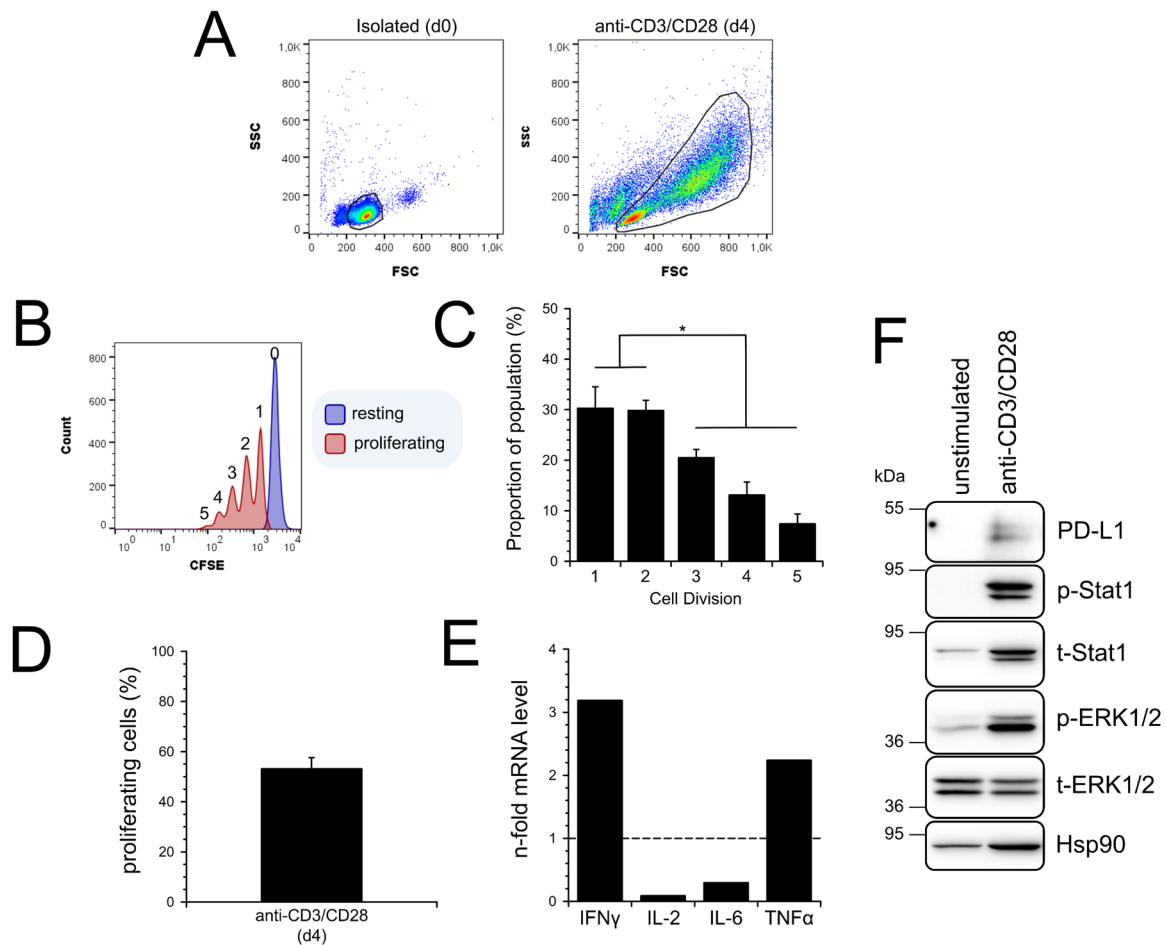


**Figure 32: Activation of human CD8<sup>+</sup> T lymphocytes by anti-CD3/CD28 stimulation.** Primary human lymphocytes were isolated from leukocyte retaining systems by density gradient centrifugation followed by counterflow centrifugation. Afterwards, CD8<sup>+</sup> T lymphocytes were isolated by negative MACS selection, stained with CFSE and stimulated with immobilized CD3- and soluble CD28-targeting antibodies as well as IL-2 for 4 days. **(A)** Representative FSC/SSC dot plots of CD8<sup>+</sup> T lymphocyte populations directly after MACS isolation (d0) and four days of anti-CD3/CD28 stimulation. **(B)** Representative histogram of CFSE staining in CD8<sup>+</sup> T lymphocytes after four days of anti-CD3/CD28 stimulation. The resting (blue) and proliferating (red) population are discriminated by CFSE dilution. The numbers indicate the quantity of cell divisions each population characterized by the respective peak has progressed through. **(C)** CFSE profile of proliferating CD8<sup>+</sup> T lymphocytes after four days of anti-CD3/CD28 stimulation. Bar chart presents mean proportions with SEM of lymphocytes having divided 1 to 5 times in six independent experiments. **(D)** Overall proportion of proliferating CD8<sup>+</sup> T lymphocytes after four days of anti-CD3/CD28 stimulation. Bar chart presents mean value with SEM of six independent experiments. **(E)** Relative mRNA levels of IFN $\gamma$ , IL-2, IL-6 and TNF $\alpha$  in anti-CD3/CD28 stimulated CD8<sup>+</sup> T lymphocytes after four days of culture. Bar chart presents mean values of technical triplicates from one representative experiment. Messenger RNA levels were normalized to respective GAPDH levels as well as levels detected in whole lymphocyte population after four days of anti-CD3/CD28 stimulation (= 1). **(F)** Representative western blot of whole-cell lysates from unstimulated CD8<sup>+</sup> T lymphocytes and after four days of anti-CD3/CD28 stimulation. Hsp90 was detected as loading control. Molecular weights in kDa are indicated according to the applied standard. \* = p<0.05

In order to interrelate PD-1 and PD-L1 surface expression levels with cell proliferation, CFSE stained CD8<sup>+</sup> T lymphocytes were additionally stained for PD-1 (**Figure 33 A**) and PD-L1 (**Figure 33 B**). Subsequent flow cytometric analysis revealed significantly higher cell surface levels of PD-1 in the proliferating population of CD8<sup>+</sup> T lymphocytes compared to both the initial levels in freshly isolated resting CD8<sup>+</sup> T cells (MFI Ratio  $9.70 \pm 0.90$  vs.  $2.66 \pm 0.22$ ;  $p=0.001$ ) and the whole population of anti-CD3/CD28 stimulated cells on day 4 (MFI Ratio  $9.70 \pm 0.90$  vs.  $4.17 \pm 0.82$ ;  $p=0.002$ ) (**Figure 33 C**). Correlation of PD-1 cell surface levels with the number of passed cell divisions indicated clearly lower PD-1 levels on the cell surface of CD8<sup>+</sup> T lymphocyte clones having divided thrice or more (MFI Ratio  $7.89$  vs.  $6.88$  vs.  $8.04$ ) compared to those having divided only once or twice (MFI Ratio  $16.63$  vs.  $11.80$ ) (**Figure 33 E**). Similar but less pronounced tendencies were observed for PD-L1 cell surface expression levels. In detail, flow cytometric analysis showed significantly higher PD-L1 cell surface levels in the proliferating population of anti-CD3/CD28 stimulated CD8<sup>+</sup> T lymphocytes compared to levels detected in freshly isolated resting cells (MFI Ratio  $3.44 \pm 0.48$  vs.  $1.22 \pm 0.18$ ;  $p=0.007$ ). In contrast to PD-1 levels, the cell surface levels of PD-L1 in the proliferating population showed hardly any differences in comparison to the overall population of stimulated CD8<sup>+</sup> T lymphocytes (MFI Ratio  $3.44 \pm 0.48$  vs.  $3.27 \pm 0.43$ ) (**Figure 33 D**). Moreover, correlation of PD-L1 cell surface levels with CFSE dilution showed a minor decrease in populations having divided once to populations having divided up to 5 times (MFI Ratio  $3.62$  vs.  $3.23$  vs.  $2.94$  vs.  $2.71$  vs.  $2.63$ ) (**Figure 33 F**).

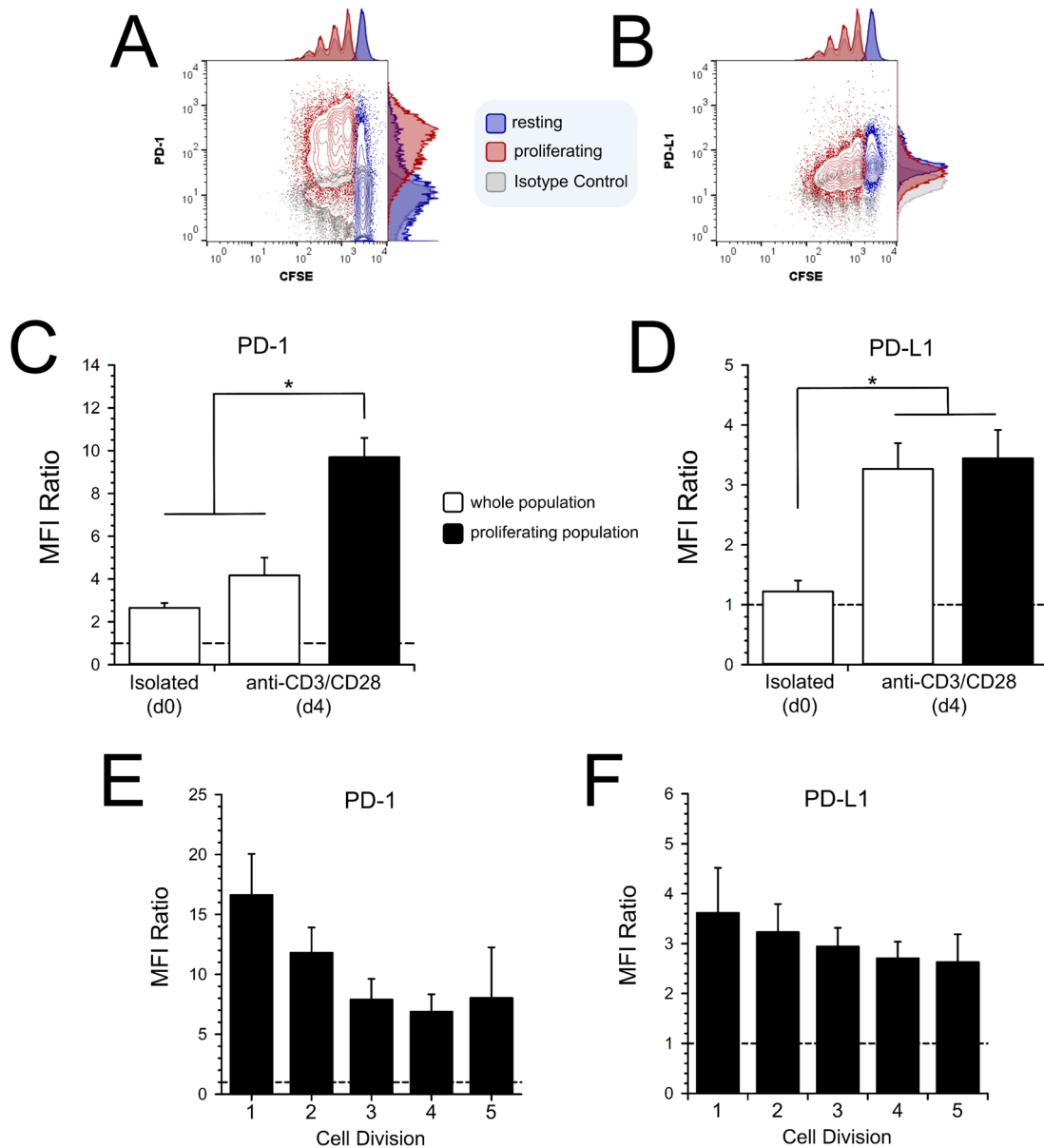


**Figure 33: PD-1 and PD-L1 cell surface expression levels in CD8<sup>+</sup> T lymphocytes after anti-CD3/CD28 stimulation.** Primary human lymphocytes were isolated from leukocyte retaining systems by density gradient centrifugation followed by counterflow centrifugation. Afterwards, CD8<sup>+</sup> T lymphocytes were isolated by negative MACS selection, stained with CFSE and stimulated with immobilized CD3- and soluble CD28-targeting antibodies as well as IL-2 for 4 days. (A+B) Representative contour plots with attached histograms showing correlation between CFSE staining and (A) PD-1 or (B) PD-L1 staining within the resting (blue) and proliferating (red) population of anti-CD3/CD28 stimulated CD8<sup>+</sup> T lymphocytes. Signal specificities were verified by staining with respective isotype control antibodies (grey). (C) PD-1 and (D) PD-L1 cell surface expression levels in the whole (white) and proliferating (black) population of CD8<sup>+</sup> lymphocytes after indicated stimulations and culture durations. Bar charts present mean values and SEM of median fluorescence intensity ratios examined in six independent experiments. (E) PD-1 and (F) PD-L1 cell surface expression levels in anti-CD3/CD28 stimulated CD8<sup>+</sup> T lymphocytes having divided one to five times. Bar charts present mean values and SEM of median fluorescence intensity ratios examined in six independent experiments. The dashed lines mark an MFI ratio of “1”. \* = p<0.05

In summary, these data show that sufficient amounts of highly purified CD8<sup>+</sup> T lymphocytes can be isolated from whole lymphocytes population by magnetic-activated cell separation. Moreover, the established stimulation protocol generates an activated population of CD8<sup>+</sup> T lymphocytes that is suitable for subsequent co-culture experiments.

#### 4.2.7 M1 MΦ and activated autologous CD8<sup>+</sup> T lymphocytes exhibit a more distinct phenotype after direct co-culture compared to mono-culture conditions

In order to investigate how M1 MΦ affect the activation status of activated CD8<sup>+</sup> T lymphocytes and *vice versa*, direct co-culture experiments have been performed.

First, the activation status of mono- compared to co-cultured CD8<sup>+</sup> T lymphocytes was analyzed. Flow cytometric analysis showed marked differences between mono- and co-cultured CD8<sup>+</sup> T lymphocytes after three days of culture duration (**Figure 34 A**). In detail, CD8<sup>+</sup> T lymphocytes co-cultured with M1 MΦ were larger in size and revealed higher granularity than mono-cultured cells, indicated by higher FSC (Mean  $512.78 \pm 53.15$  vs.  $403.17 \pm 19.70$ ; **Figure 34 B**) and SSC (Mean  $262.22 \pm 23.50$  vs.  $204.33 \pm 23.35$ ; **Figure 34 C**) median values. Moreover, CD8<sup>+</sup> T lymphocyte populations exhibited higher vital cell numbers by trend after co-culture with M1 MΦ than after mono-culture ( $1.56 \pm 0.63$  vs.  $1.16 \pm 0.20 \cdot 10^6$  cells; **Figure 34 D**). In line with results from vital cell counting, flow cytometric analyses of CFSE profiles revealed a higher proportion of proliferating CD8<sup>+</sup> T lymphocytes after co-culture with M1 MΦ compared to those from mono-cultures ( $58.86 \pm 20.42\%$  vs.  $37.45 \pm 12.54\%$ ; **Figure 34 E**). Additionally, western blotting analysis showed markedly lower levels of phosphorylated ERK1/2 in mono-cultured but not co-cultured CD8<sup>+</sup> T lymphocytes compared to levels in T lymphocytes directly after activation culture (**Figure 35 C**). CFSE profiles of both mono- and co-cultured T lymphocyte populations revealed a spectrum of up to seven distinguishable cell divisions. Interestingly, CFSE profiles of CD8<sup>+</sup> T lymphocyte populations after mono- and co-culture with M1 MΦ displayed only minor differences, predominantly within the proportion of proliferating cells having divided either only once or three to five times. By trend, T lymphocyte populations from co-culture conditions exhibited a higher proportion of cells having gone through only one cell division ( $30.03 \pm 11.47\%$  vs.  $17.29 \pm 6.48\%$ ) but lower proportions of cells having progressed through 3 ( $10.49 \pm 1.89\%$  vs.  $13.3 \pm 0.99\%$ ), 4 ( $10.87 \pm 2.87\%$  vs.  $16.00 \pm 1.39\%$ ) and 5 ( $12.95 \pm 0.01\%$  vs.  $18.05 \pm 0.81\%$ ) cell divisions in comparison to mono-cultured cells (**Figure 34 F**).

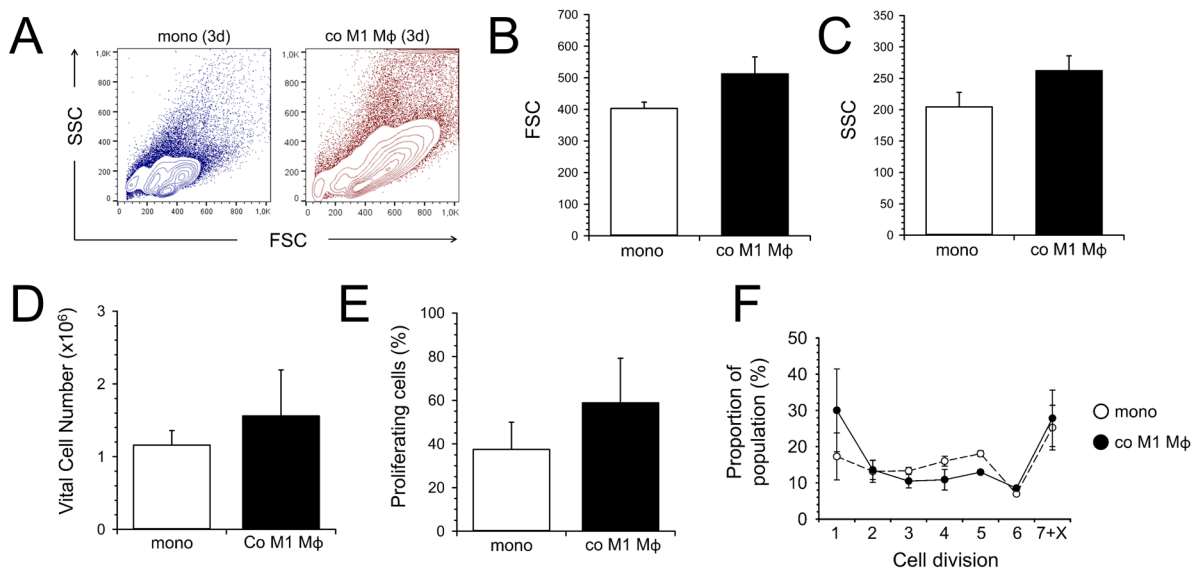


**Figure 34: Phenotype and proliferation of CD8<sup>+</sup> T lymphocytes after direct co-culture with autologous M1-polarized macrophages.** Activated primary human CD8<sup>+</sup> T lymphocytes were mono-cultured or directly co-cultured for 72 h with M1-like polarized macrophages, which were differentiated from autologous monocytes by GM-CSF stimulation. (A) Representative FSC/SSC contour plots from flow cytometric analysis of CD8<sup>+</sup> T lymphocytes after 72 h of mono- and co-culture with M1 Mφ, respectively. Comparison of (B) FSC medians, (C) SSC medians, (D) vital cell numbers and (E) the proportion of proliferating lymphocytes within CD8<sup>+</sup> T lymphocytes populations after mono- or direct co-culture with M1 Mφ for 72 h. Data present mean values with SEM of three independent experiments. (F) CFSE profiles of proliferating lymphocytes within CD8<sup>+</sup> T lymphocyte populations after mono- (white) or co-culture with M1 Mφ (black) for 72 h. Data presents mean proportions and SEM of lymphocytes having divided 1 to 7 times examined in three independent experiments. The maximum numbers of clearly distinguishable peaks in respective CFSE profiles are indicated by “+X”.

Considering cell surface expression levels of PD-1 and PD-L1, CD8<sup>+</sup> T lymphocytes exhibited markedly higher PD-1 levels in both resting (MFI Ratio  $2.86 \pm 0.95$  vs.  $1.26 \pm 0.24$ ) and proliferating (MFI Ratio  $4.73 \pm 1.35$  vs.  $1.91 \pm 0.15$ ) populations after co-culture with M1 Mφ compared to cells after mono-culture (**Figure 35 A**). However, in comparison to proliferating CD8<sup>+</sup> T cells after activation culture (MFI Ratio  $9.70 \pm 0.90$ ; **Figure 33 C**) PD-1 cell surface levels in both mono- and co-cultured CD8<sup>+</sup> T lymphocytes markedly decreased after 72 h of both mono- and co-culture. Similarly, PD-L1 cell surface levels in both the resting (MFI Ratio  $3.62 \pm 1.07$  vs.  $1.92 \pm 0.42$ ) and the proliferating (MFI Ratio  $2.45 \pm 0.10$  vs.  $1.65 \pm 0.08$ ) population of co-cultured T lymphocytes were higher compared to respective populations in mono-cultured cells (**Figure 35 B**). Interestingly, in contrast to PD-1 levels, PD-L1 cell surface expression was higher in the resting than in the proliferating lymphocyte population. Notably, western blotting analysis revealed higher PD-L1 levels in CD8<sup>+</sup> T lymphocytes after co-culture with M1 Mφ than in mono-cultured cells as well as in CD8<sup>+</sup> T lymphocytes directly after activation culture (**Figure 35 C**).

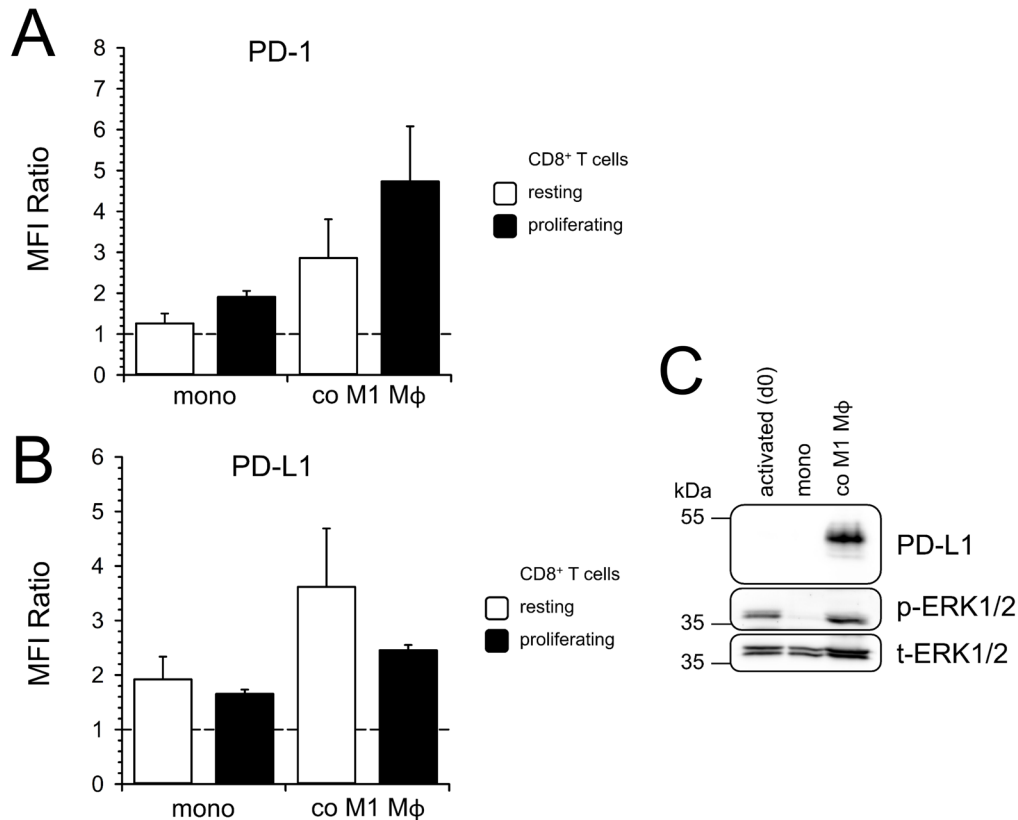


**Figure 35: PD-1 and PD-L1 cell surface levels in CD8<sup>+</sup> T lymphocytes after direct co-culture with autologous M1-polarized macrophages.** Pre-activated primary human CD8<sup>+</sup> T lymphocytes were mono-cultured or directly co-cultured for 72 h with M1-like polarized macrophages, which were differentiated from autologous monocytes by GM-CSF stimulation. (A) PD-1 and (B) PD-L1 cell surface expression levels in the resting (white) and proliferating (black) population of CD8<sup>+</sup> lymphocytes after indicated culture conditions. Bar charts present mean values and SEM of median fluorescence intensity ratios examined in three independent experiments. The dashed lines mark an MFI ratio of “1”. (C) Representative western blot of whole-cell lysates from CD8<sup>+</sup> T lymphocytes directly after four days of anti-CD3/CD28 stimulation (activated (d0)) as well as after following 72 h of either mono- or co-culture with M1 Mφ. Molecular weights in kDa are indicated according to the applied standard.

Besides the effects observed on the phenotype and proliferation of CD8<sup>+</sup> T lymphocytes after co-culture conditions, the phenotype of mono- and co-cultured macrophages was examined, too, by staining of PD-L1, CD206 and CD163 followed by flow cytometric analysis (**Figure 36 A**). Cell surface levels of PD-L1 were markedly higher in M1 Mφ after co-culture with CD8<sup>+</sup> T lymphocytes compared to mono-cultured cells (MFI Ratio  $10.77 \pm 3.21$  vs.  $1.76 \pm 0.46$ ;  $p=0.05$ ; **Figure 36 A**). While CD206 levels were not altered (MFI Ratio  $3.43 \pm 0.54$  vs.  $3.05 \pm 0.02$ ; **Figure 36 B**), CD163 cell surface levels were notably lower in co-cultured compared to mono-cultured M1 Mφ (MFI Ratio  $2.12 \pm 0.52$  vs.  $14.30 \pm 7.07$ ; **Figure 36 C**).

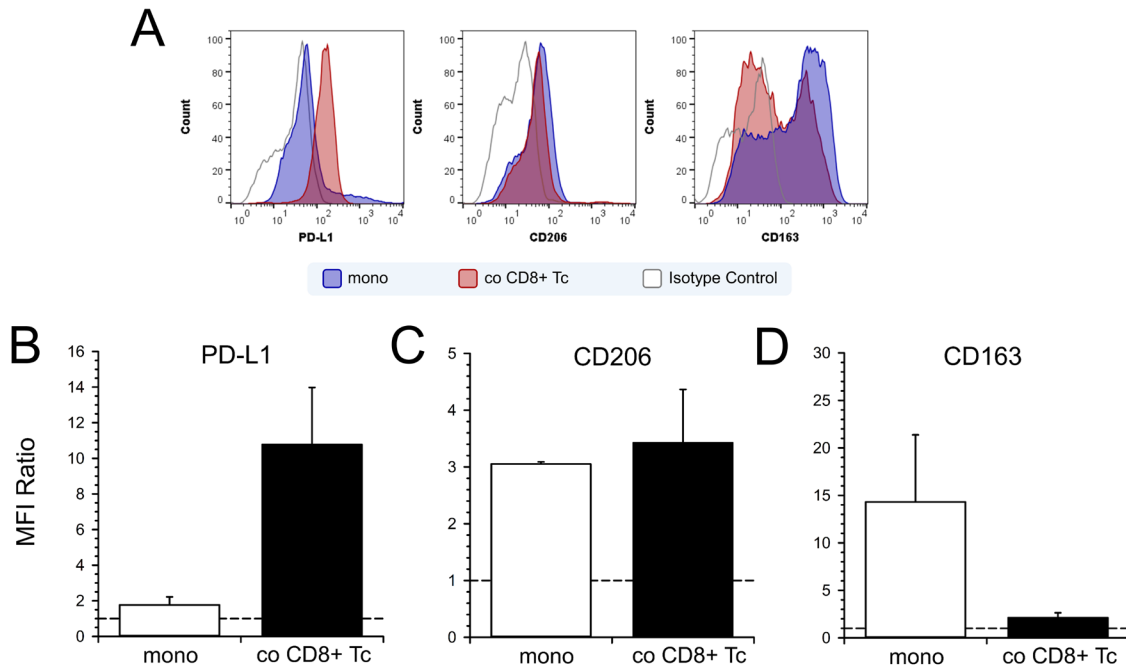


**Figure 36: Cell surface expression levels of PD-L1, CD206 and CD163 in M1-polarized macrophages after co-culture with autologous activated CD8<sup>+</sup> T lymphocytes.** M1-polarized primary human macrophages were mono-cultured or directly co-cultured for 72 h with autologous pre-activated CD8<sup>+</sup> T lymphocytes. (A) Representative histograms from flow cytometric analysis of PD-L1 (left), CD206 (middle) and CD163 (right) cell surface immunofluorescence staining in M1 MΦ after mono- (blue) or co-culture with CD8<sup>+</sup> T lymphocytes (red). Signal specificities were verified by staining with respective isotype control antibodies (white/grey). (B) PD-L1, (C) CD206 and (D) CD163 cell surface levels in M1 MΦ after indicated culture conditions. Bar charts present mean values and SEM of median fluorescence intensity ratios examined in three independent experiments. The dashed lines mark an MFI ratio of “1”.

Finally, the concentrations of various cytokines secreted by macrophages (IL-6, IL-8 and VEGF) were detected in supernatants of mono- and co-cultures. Thus, IL-8 as well as VEGF showed significantly higher levels in culture settings comprising M1 MΦ compared to mono-cultured CD8<sup>+</sup> T lymphocytes. Moreover, IL-6 was exclusively detected in cultures containing M1 MΦ. In detail, IL-8 concentrations in supernatants of M1 MΦ and CD8<sup>+</sup> T lymphocyte co-cultures were slightly higher than in M1 MΦ mono-cultures and both significantly exceeded concentrations detected in T lymphocyte mono-cultures (21.81 vs. 20.30 vs. 0.22 ng/ml;  $p < 0.001$ ) (Figure 37 A). The same proportions were detected for VEGF levels in supernatants of co-/mono-cultured M1 MΦ and CD8<sup>+</sup> T lymphocyte mono-cultures (282.48 vs. 239.79 vs. 15.16 pg/ml;  $p < 0.001$ ) (Figure 37 B). By trend, IL-6 levels were higher in supernatants of co-cultured M1 MΦ than in those of mono-cultured M1 MΦ (3624.47 ± 3154.86 pg/ml vs. 244.12 ± 218.20 pg/ml) (Figure 37 C).

Same as macrophage-associated cytokines, levels of T lymphocyte-associated cytokines (TNFα, IFNγ, IL-17A, soluble Fas ligand, Perforin, Granulysin, Granzyme A and Granzyme B) in co-culture settings either significantly or at least by trend exceeded those detected in mono-culture supernatants. In detail, supernatants of M1 MΦ and CD8<sup>+</sup> T lymphocyte co-



cultures contained 61.63 pg/ml TNF $\alpha$  while in mono-cultures of either CD8<sup>+</sup> T lymphocytes or macrophages only 3.23 pg/ml and 2.59 pg/ml were measured, respectively ( $p=0.011$ ; **Figure 37 D**). IFN $\gamma$  was not detectable in supernatants of mono-cultured M1 M $\Phi$ . However, mono-cultures of CD8<sup>+</sup> T lymphocytes contained IFN $\gamma$  concentrations of 623.51 pg/ml and significantly higher levels of IFN $\gamma$  under co-culture conditions (12.78 ng/ml;  $p=0.004$ ; **Figure 37 E**). IL-17A concentrations in supernatants of co-cultures markedly exceeded levels detected in those of mono-cultured T lymphocytes (183.74 vs. 37.85 pg/ml) while IL-17A was hardly detectable in supernatants of mono-cultured M1 M $\Phi$  (5.80 pg/ml) (**Figure 37 F**). Soluble FasL levels in co-culture supernatants were clearly higher than in mono-cultures of CD8<sup>+</sup> T lymphocytes or M1 M $\Phi$  (492.45 vs. 54.65 vs. 2.45 pg/ml) (**Figure 37 G**). The same trend applied to concentrations of Perforin (3846.59 vs. 1493.22 vs. 20.59 pg/ml) (**Figure 37 H**), Granulysin (37.96 vs. 5.87 vs. 0.03 ng/ml) (**Figure 37 I**) and Granzyme A (7189.51 vs. 829.27 vs. 19.85 pg/ml;  $p=0.011$ ) (**Figure 37 J**). Finally, Granzyme B concentrations were also significantly higher in supernatants of co-cultured than mono-cultured CD8<sup>+</sup> T lymphocytes or M1 M $\Phi$  (64.97 vs. 0.34 vs. 0.54 ng/ml;  $p=0.025$ ) (**Figure 37 K**).

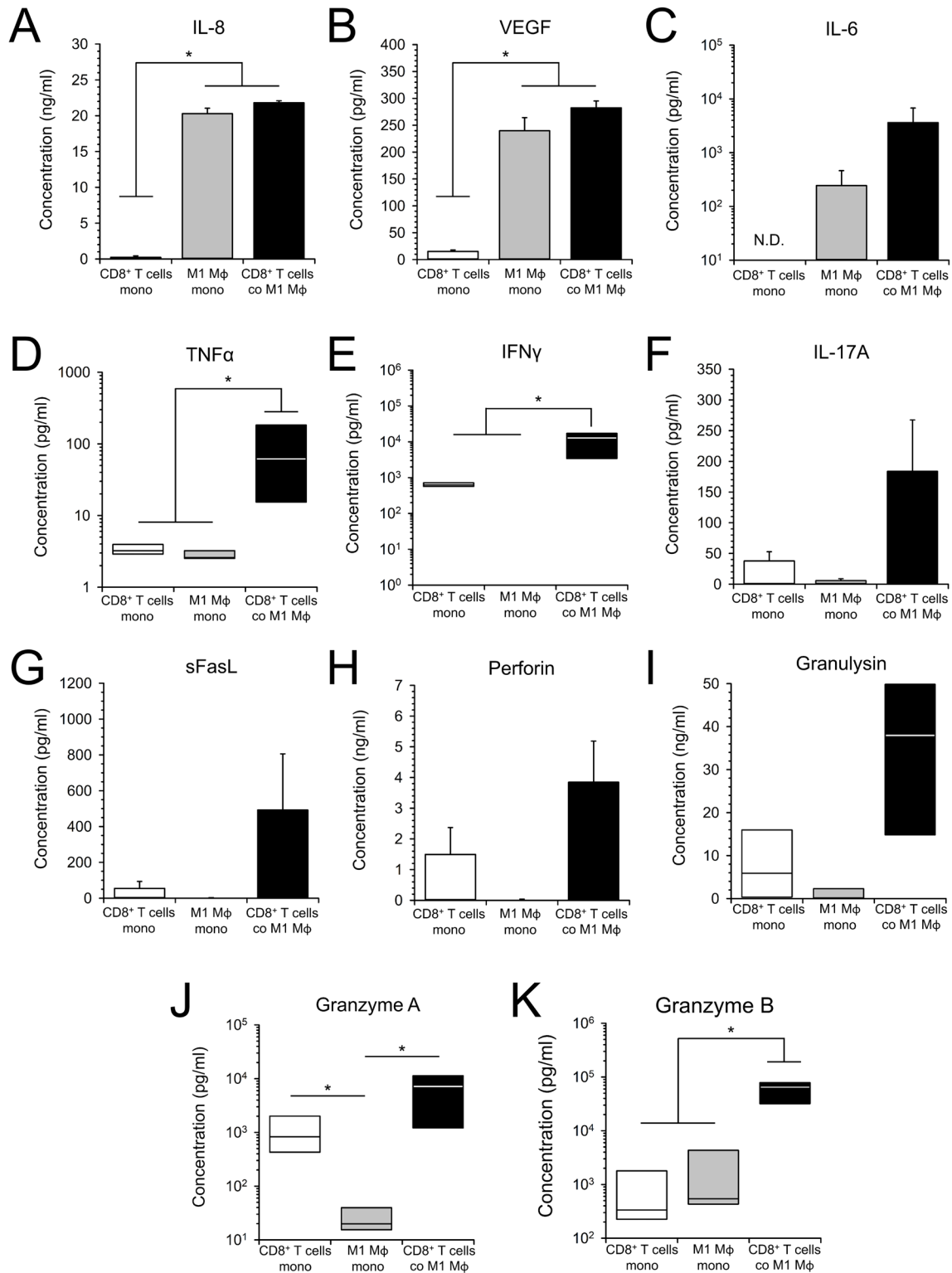


**Figure 37: Supernatant levels of T lymphocyte- and macrophage-associated cytokines, chemokines, growth factors and effector molecules after direct co-culture of activated CD8<sup>+</sup> T lymphocytes with autologous M1-polarized macrophages.** Pre-activated primary human CD8<sup>+</sup> T lymphocytes and autologous M1-polarized macrophages were either mono-cultured or directly co-cultured for 72 h. Concentrations of (A) IL-8, (B) VEGF, (C) IL-6, (D) TNFα, (E) IFNγ, (F) IL-17A, (G) soluble Fas ligand, (H) Perforin, (I) Granulysin, (J) Granzyme A and (K) Granzyme B were measured by multiplex assay in the culture supernatant of mono-cultured CD8<sup>+</sup> T lymphocytes (white) and M1 Mφ (grey) as well as direct co-cultures (black) after 72 h. Box plots present median values with quartiles (Q<sub>0.75</sub> as upper, Q<sub>0.25</sub> as lower deviation) and bar charts present mean values with SEM of three independent experiments. N.D. = not detectable; \* = p < 0.05;

In summary, these results indicate that both M1 MΦ and pre-activated CD8<sup>+</sup> T lymphocytes exhibit a more pronounced pro-inflammatory and activated phenotype, respectively, after direct co-culture compared to respective phenotypes after mono-culture conditions.

#### 4.2.8 PD-L1 cell surface levels of PDAC cells might affect activation the status of pre-activated CD8<sup>+</sup> T lymphocytes

Next, it has been investigated whether and how different PDAC cell lines affect the activation status of activated CD8<sup>+</sup> T lymphocyte populations in direct co-culture settings. For this purpose, three different PDAC cell lines were used that had shown neither basal and nor inducible PD-L1 cell surface expression levels (Panc1), moderate basal and inducible PD-L1 expression (Panc89) or high basal and strongly inducible PD-L1 cell surface levels in previous experiments (**section 4.2.1** and **section 4.2.2**).

Flow cytometric analyses showed no differences between mono- and co-cultured CD8<sup>+</sup> T lymphocytes in terms of size and granularity (data not shown). However, the overall proportion of proliferating CD8<sup>+</sup> T lymphocytes was lower after co-culture with Panc89 or PancTu-I cells compared to CD8<sup>+</sup> T lymphocytes after co-culture with Panc1 cells or mono-culture (55.40 % vs. 57.45 % vs. 70.15 % vs. 68.40%) (**Figure 38 A**). In line, the median values for CFSE fluorescence intensities within the whole (MFI 554.00 vs. 422.50 vs. 165.50 vs. 190.00) and the proliferating (MFI 162.50 vs. 144.00 vs. 85.55 vs. 91.10) CD8<sup>+</sup> T lymphocyte populations were higher after co-culture with Panc89 or PancTu-I cells than after co-culture with Panc1 cells or mono-cultured CD8<sup>+</sup> T lymphocytes (**Figure 38 B**). Subsequent analyses of CFSE profiles revealed that the CD8<sup>+</sup> T lymphocyte populations from mono-cultures and co-culture with Panc1 cells showed very similar profiles with up to 5 distinguishable cell divisions and over 50 % of the population having progressed through 4 or more cell divisions (**Figure 38 C**). In contrast, CFSE profiles of CD8<sup>+</sup> T lymphocytes after co-culture with Panc89 and PancTu-I cells, respectively, showed that the majority of cells had only passed one to three cell divisions and the proportion of cells having proceeded through five cell divisions was markedly lower in lymphocyte populations co-cultured with Panc89 or PancTu-I cells compared to those after co-culture with Panc1 cells or mono-culture (**Figure 38 D+E**).

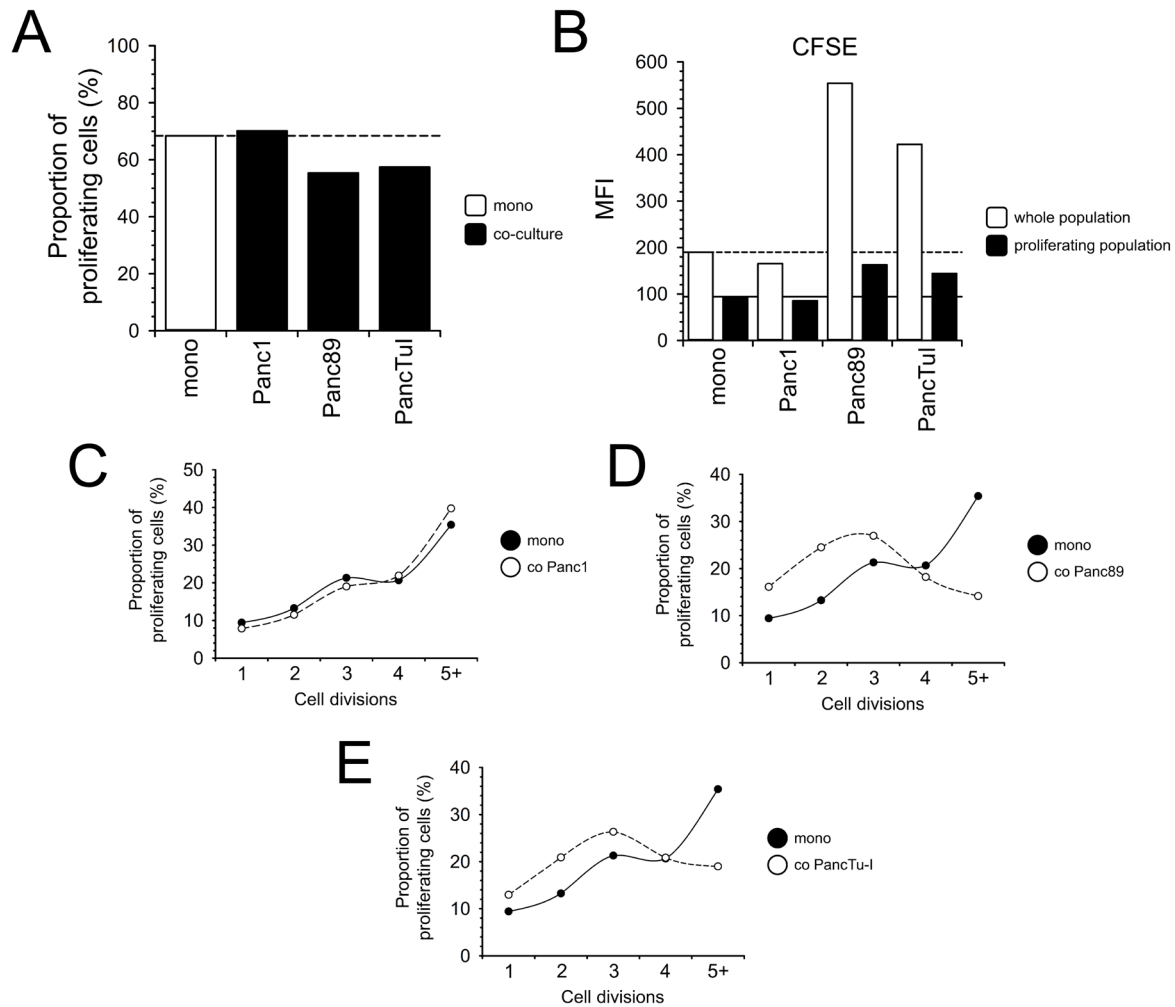


**Figure 38: Proliferation of activated CD8<sup>+</sup> T lymphocytes after direct co-culture with various PDAC cell lines.** Pre-activated primary human CD8<sup>+</sup> T lymphocytes were either mono- or directly co-cultured for 72 h with Panc1, Panc89 and PancTu-I cells, respectively. (A) Proportion of proliferating cells within CD8<sup>+</sup> T lymphocytes after mono- (white) or indicated co-culture (black) conditions. Dashed line marks the proportion of proliferating cells in mono-cultured T lymphocytes. (B) Median fluorescence intensity (MFI) of CFSE staining in the whole (white) and proliferating (black) population of CD8<sup>+</sup> T lymphocytes after indicated mono- and co-culture settings with PDAC cell lines. Dashed line indicates the CFSE MFI in the whole lymphocyte population and drawn through line indicates the CFSE MFI of the proliferating lymphocyte population of mono-cultured CD8<sup>+</sup> T lymphocytes. (C-E) CFSE profiles of proliferating CD8<sup>+</sup> T lymphocytes after mono-culture (white) and direct co-culture with (C) Panc1, (D) Panc89 and (E) PancTu-I cells. Data present proportions of lymphocytes having divided 1 to 5 times. The maximum numbers of clearly distinguishable peaks in respective CFSE profiles are indicated by “+”. (A-E) Graphs present data from one experiment.

Interestingly, the observed alterations in terms of T lymphocytes’ proliferation after co-culture with either Panc89 or PancTu-I cells were associated with changes of PD-1 cell surface expression levels in CD8<sup>+</sup> T lymphocytes as well as PD-L1 expression in Panc89 and PancTu-I cells, respectively (Figure 39). In detail, PD-1 cell surface levels in CD8<sup>+</sup> T lymphocytes co-cultured with Panc1 cells were similar to those levels detected in the whole (MFI Ratio 2.53 vs. 2.74) and proliferating (MFI Ratio 2.64 vs. 2.94) population of mono-cultured CD8<sup>+</sup> T lymphocytes (Figure 39 A). In contrast, PD-1 levels at the cell surface of T lymphocytes co-cultured with Panc89 cells were clearly higher in the proliferating population

compared to the expression levels in the whole population (MFI Ratio 5.22 vs. 3.47) and, therefore, 26.6% higher in the whole and 77.6% higher in the proliferating population compared to mono-cultured CD8<sup>+</sup> T lymphocytes (**Figure 39 A**). Similar but less pronounced, PD-1 cell surface levels in CD8<sup>+</sup> T lymphocytes after co-culture with PancTu-I cells were higher in the proliferating population compared to expression levels of the whole population (MFI Ratio 4.10 vs. 3.18). Hence, PD-1 cell surface levels in CD8<sup>+</sup> T lymphocytes from PancTu-I co-cultures exceeded levels detected in mono-cultured T lymphocytes by 16.1% and 39.5% comparing expression levels in the whole and proliferating population, respectively (**Figure 39 A**). While PD-L1 expression was absent or at very low level on the cell surface of CD8<sup>+</sup> T lymphocytes after both mono- and co-culture with each PDAC cell line (**Figure 39 B**), PD-L1 levels in both Panc89 and PancTu-I cells but not Panc1 cells were clearly elevated after co-culture with CD8<sup>+</sup> T lymphocytes compared to mono-cultured cells (**Figure 39 C**).

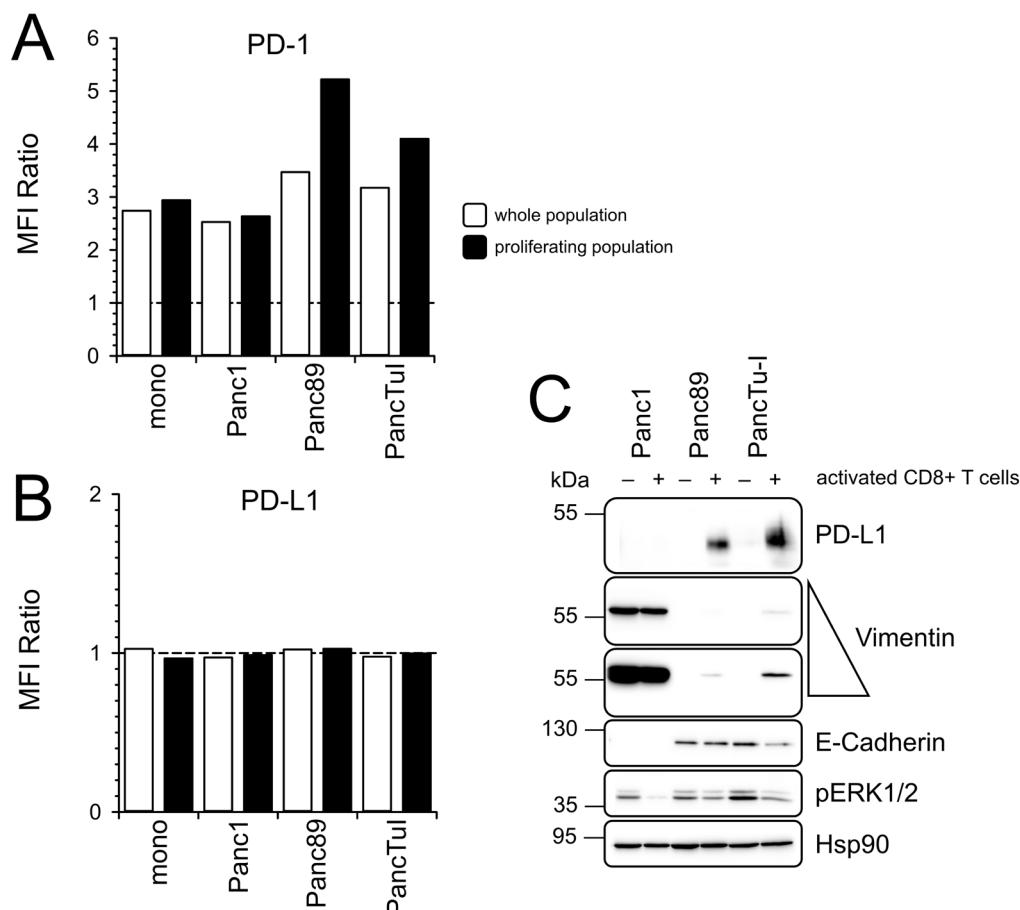


**Figure 39: PD-1 and PD-L1 cell surface expression levels in CD8<sup>+</sup> T lymphocytes as well as levels of proteins associated with differentiation and proliferation status in various PDAC cell lines after direct co-culture.** Pre-activated primary human CD8<sup>+</sup> T lymphocytes were either mono- or directly co-cultured for 72 h with Panc1, Panc89 and PancTu-I cells, respectively. (A) PD-1 and (B) PD-L1 cell surface levels in the whole (white) and proliferating (black) population of CD8<sup>+</sup> T lymphocytes after indicated culture conditions. Bar charts present median fluorescence intensity ratios examined in one experiment. The dashed lines mark an MFI ratio of “1”. (C) Representative western blot of whole-cell lysates from Panc1, Panc89 and PancTu-I cells after mono- (-) or co-culture with activated CD8<sup>+</sup> T lymphocytes (+). Hsp90 was detected as loading control. Molecular weights in kDa are indicated according to the applied standard. Triangle indicates decreased/increased time of light exposure for vimentin signal detection.

In **section 4.2.6**, it has been shown that CD8<sup>+</sup> T lymphocytes express and secrete various pro-inflammatory cytokines upon activation by anti-CD3/CD28 stimulation. Notably, it has been reported that tumor cells upon stimulation by some of these cytokines, e.g. IFN $\gamma$  and IL-6, acquire a more mesenchymal phenotype due to cytokine-induced EMT-associated signaling pathways [48,52]. In order to investigate whether PDAC cell lines in the present co-culture setting show EMT-related alterations, the expression of E-cadherin and vimentin has been examined by western blotting. Indeed, western blotting analysis revealed increased vimentin and decreased E-cadherin expression in co-cultured Panc89 and PancTu-I cells. In contrast, Panc1 cells exhibited unaltered high vimentin and absent E-cadherin expression after both mono- and co-culture conditions (**Figure 39 C**). Notably, all PDAC cell lines showed markedly lower levels of phosphorylated ERK1/2 after co-culture with CD8<sup>+</sup> T lymphocytes in comparison to levels detected in mono-cultured cells (**Figure 39 C**).

In summary, these data indicate a link between proliferation and PD-1 cell surface levels of CD8<sup>+</sup> T lymphocytes as well as PD-L1 expression and EMT-associated alterations in PDAC cells in direct co-culture settings. Supporting the assumption that PDAC cells in the present co-culture system affect the phenotype of CD8<sup>+</sup> T lymphocytes and *vice versa*, results from multiplex quantitative analysis of cytokines revealed that culture supernatant concentrations of cytokines predominantly secreted by PDAC cells (VEGF, IL-6 and IL-8) or CD8<sup>+</sup> T lymphocytes (IFN $\gamma$ , IL-17A, sFasL, Perforin, Granulysin, Granzyme A and Granzyme B) markedly differ in co-culture settings compared to mono-cultures (**Supplementary Figure 58**). Moreover, microscopical time-lapse analyses indicated that CD8<sup>+</sup> T lymphocytes get in contact with PancTu-I cells by directed cell-cell interactions (**Supplementary Figure 59**). Based on these and previous results (**section 4.2.1** and **section 4.2.2**), PancTu-I cells were chosen as *in vitro* model for subsequent triple co-culture experiments with activated CD8<sup>+</sup> T lymphocytes and M1 M $\Phi$ .

#### **4.2.9 Co-culture of activated CD8<sup>+</sup> T lymphocytes with PancTu-I cells and M1 M $\Phi$**

The next step was to examine phenotypic alterations in CD8<sup>+</sup> T lymphocytes, PancTu-I cells and M1 M $\Phi$  after co-culture in a setting that comprises all three populations, a scenario that mostly resembles the situation in PDAC. In contrast to the previous setting, a direct co-culture of CD8<sup>+</sup> T lymphocytes and PancTu-I cells combined with an indirect co-culture with M1 M $\Phi$  was applied (**Figure 11**). This modified experimental setup was made in order to enable

additional gene expression profile analyses in M1 M $\Phi$  macrophages by qPCR, which otherwise would not be possible without effortful separation of adherent growing M1 M $\Phi$  from PancTu-I cells. Moreover, this setting allowed to investigate whether effects on T lymphocytes' activation status in co-culture with M1 M $\Phi$  are mediated by paracrine interactions or whether direct cell-cell contact is necessary.

Flow cytometric analysis of CD8<sup>+</sup> T lymphocytes in FSC/SSC plots revealed slightly larger cells after co-culture with M1 M $\Phi$  or PancTu-I cells compared to mono-cultures (Mean 476.50  $\pm$  5.81 *vs.* 485.88  $\pm$  3.67 *vs.* 471.75  $\pm$  5.88). After co-culture with both PancTu-I cells and M1 M $\Phi$  highest median FSC values were detected in CD8<sup>+</sup> T lymphocyte populations by trend (Mean 490.38  $\pm$  1.56) (**Figure 40 A**). In terms of cellular granularity, only minor differences in T lymphocyte populations were detected after co-culture with PancTu-I cells (Mean 248.88  $\pm$  9.58) or M1 M $\Phi$  (Mean 250.13  $\pm$  11.62) in comparison to mono-cultured cells (Mean 252.88  $\pm$  8.96). In contrast, CD8<sup>+</sup> T lymphocytes from co-culture with both M1 M $\Phi$  and PancTu-I cells showed clearly the lowest SSC values compared to the other culture settings (Mean 238.38  $\pm$  10.90) (**Figure 40 B**). By trend, vital cell counting revealed higher cell numbers in CD8<sup>+</sup> T lymphocytes co-cultured with M1 M $\Phi$  (1.11  $\pm$  0.08-fold) and lower number of vital cells after co-culture with PancTu-I cells (0.92  $\pm$  0.06-fold) compared to mono-cultured cells. After co-culture including all three cell populations, vital cell numbers of CD8<sup>+</sup> T lymphocytes were similar to those detected in populations of mono-cultured CD8<sup>+</sup> T lymphocytes (1.04  $\pm$  0.6-fold) (**Figure 40 C**).

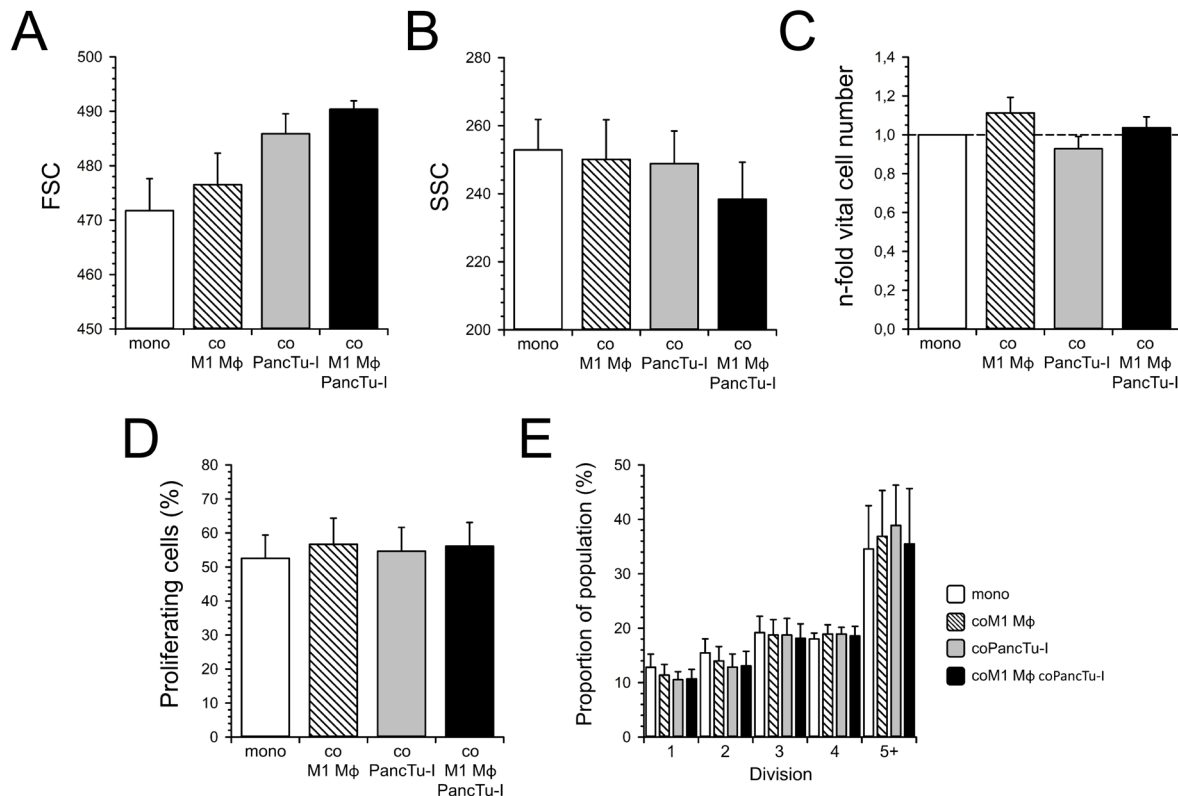


**Figure 40: Phenotype and proliferation of CD8<sup>+</sup> T lymphocytes after co-culture with PancTu-I cells and autologous M1-polarized macrophages.** Pre-activated primary human CD8<sup>+</sup> T lymphocytes were either mono-cultured (white), indirectly co-cultured with autologous M1 MΦ (banded), directly co-cultured with PancTu-I cells (grey) or co-cultured with both autologous M1 MΦ (indirect) and PancTu-I cells (direct) (black) for 48 h. Comparison of (A) FSC medians, (B) SSC medians, (C) relative vital cell numbers and (D) the proportion of proliferating cells within CD8<sup>+</sup> T lymphocytes from indicated culture settings. Bar charts present mean values with SEM of three independent experiments. (E) CFSE profiles of proliferating CD8<sup>+</sup> T lymphocytes after 48 h of indicated mono- and co-culture conditions. Bar chart presents mean proportions with SEM of T lymphocytes having divided 1 to 5 times in three independent experiments. The maximum numbers of clearly distinguishable peaks in respective CFSE profiles are indicated by “+”.

Analyses of CFSE staining in CD8<sup>+</sup> T lymphocytes after mono-culture, indirect co-culture with M1 MΦ, direct co-culture with PancTu-I cells or co-culture with both M1 MΦ and PancTu-I cells showed neither significant nor by trend any differences with respect to the proportion of proliferating cells ( $52.57 \pm 6.91\%$  vs.  $56.68 \pm 7.68\%$  vs.  $54.67 \pm 6.98\%$  vs.  $56.13 \pm 6.99\%$ ) (Figure 40 D) and the respective CFSE profiles (Figure 40 E). In detail, CFSE profiles of CD8<sup>+</sup> T lymphocytes after each culture condition revealed a spectrum of up to 5 distinguishable cell divisions with most cells having passed four (~20%) to five (>35%) cell divisions.

Flow cytometric analysis of PD-1 (Figure 41 A) and PD-L1 (Figure 41 B) cell surface expression levels in CD8<sup>+</sup> T lymphocytes after mono-culture or different co-culture settings showed no notable differences between CD8<sup>+</sup> T lymphocytes from each culture condition. Noteworthy, in comparison to the levels detected in the whole population, PD-1 cell surface levels were markedly higher in the proliferating subset of CD8<sup>+</sup> T lymphocytes after each culture setting (Figure 41 A), while PD-L1 levels were hardly differed in the proliferating



population from the whole population (**Figure 41 B**). Correlation of PD-1 cell surface levels and CFSE profiles showed only minor differences in CD8<sup>+</sup> T lymphocytes from mono- and co-culture settings (**Figure 41 C**). Thus, PD-1 cell surface levels in CD8<sup>+</sup> T lymphocytes after co-culture with PancTu-I cells as well as triple co-culture tended to be slightly higher in CD8<sup>+</sup> T lymphocyte populations having divided one to six times (**Figure 41 C**). Correlation of PD-L1 surface levels and CFSE profiles revealed neither significant nor by trend any differences between different culture settings (data not shown).

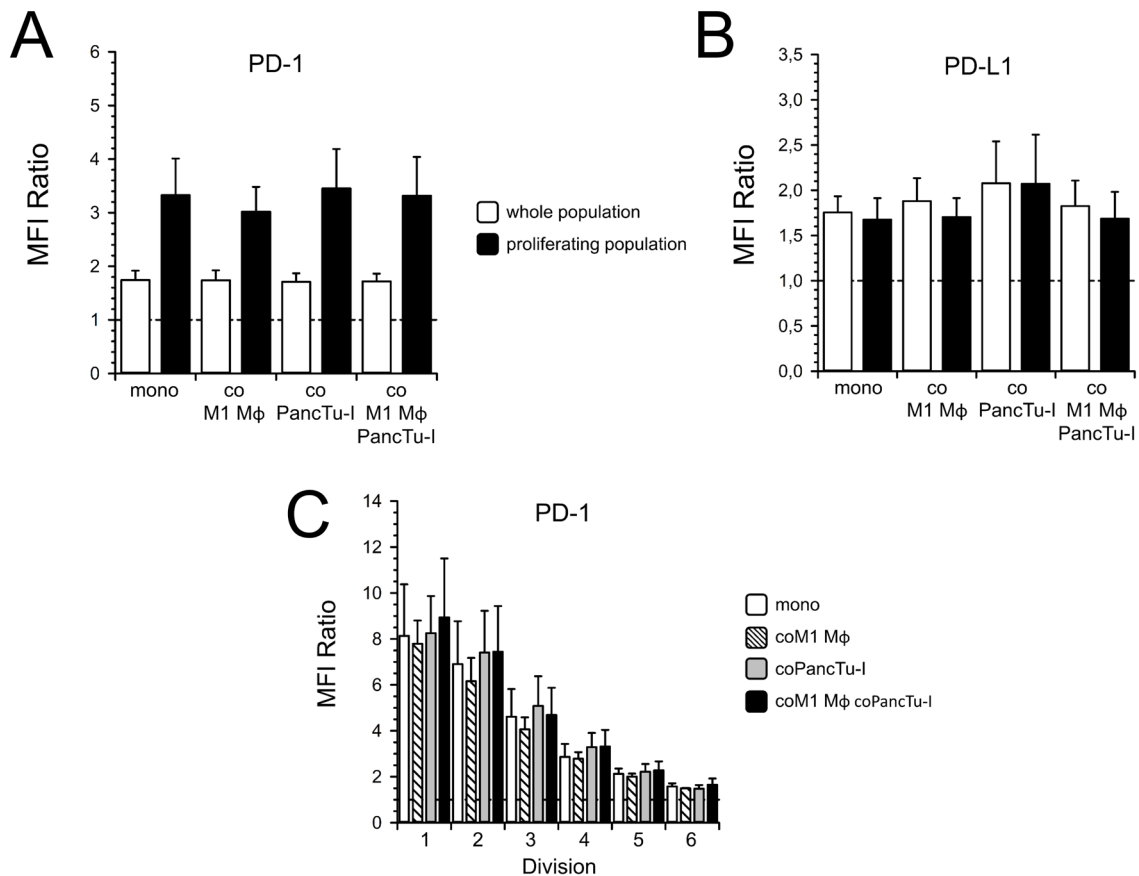


**Figure 41: PD-1 and PD-L1 cell surface expression levels in CD8<sup>+</sup> T lymphocytes after co-culture with PancTu-I cells and autologous M1-polarized macrophages.** Pre-activated primary human CD8<sup>+</sup> T lymphocytes were either mono-cultured (white), indirectly co-cultured with autologous M1 MΦ (banded), directly co-cultured with PancTu-I cells (grey) or co-cultured with both autologous M1 MΦ (indirect) and PancTu-I cells (direct) (black) for 48 h. (A) PD-1 and (B) PD-L1 cell surface levels in the whole (white) and proliferating (black) population of CD8<sup>+</sup> T lymphocytes after indicated culture conditions. (C) PD-1 cell surface expression levels in populations of CD8<sup>+</sup> T lymphocytes having divided one to six times after indicated mono- and co-culture conditions. (A-C) Bar charts present mean values with SEM of median fluorescence intensity ratios examined in three independent experiments. The dashed lines mark an MFI ratio of “1”.

In order to characterize the phenotype of M1 MΦ after mono-culture as well as indirect co-culture with CD8<sup>+</sup> T lymphocytes, PancTu-I cells or both T lymphocytes and PancTu-I cells, macrophages were stained for PD-L1, CD206 or CD163. Subsequent flow cytometric analysis revealed minor differences in PD-L1 cell surface levels between M1 MΦ from different culture conditions (MFI Ratio  $2.40 \pm 0.42$  vs.  $2.54 \pm 0.43$  vs.  $2.36 \pm 0.39$  vs.  $2.55 \pm 0.36$ ) (**Figure 42 A**).

Likewise, CD206 cell surface levels varied only marginally between M1 MΦ from mono- and co-culture settings. By trend, lower CD206 levels were detected on the cell surface of macrophages from co-culture with CD8<sup>+</sup> T lymphocytes (MFI Ratio 5.74 ±0.79), PancTu-I cells (MFI Ratio 5.55 ±0.66) and co-cultures with both CD8<sup>+</sup> T lymphocytes and PancTu-I cells (MFI Ratio 5.32 ±0.82) in comparison to mono-cultured M1 MΦ (MFI Ratio 6.40 ±0.81) (**Figure 42 B**). Cell surface levels of CD163 tended to be lower in M1 MΦ after co-culture with CD8<sup>+</sup> T lymphocytes (MFI Ratio 8.36 ±2.60) but higher after co-culture with PancTu-I cells (MFI Ratio 10.99 ±4.11) compared to M1 MΦ from mono-cultures (MFI Ratio 9.56 ±3.16) (**Figure 42 C**). In contrast, M1 MΦ from co-cultures with both CD8<sup>+</sup> T lymphocytes and PancTu-I cells showed CD163 cell surface levels comparable to mono-cultured macrophages (MFI Ratio 9.61 ±3.58 vs. 9.56 ±3.16) (**Figure 42 C**).

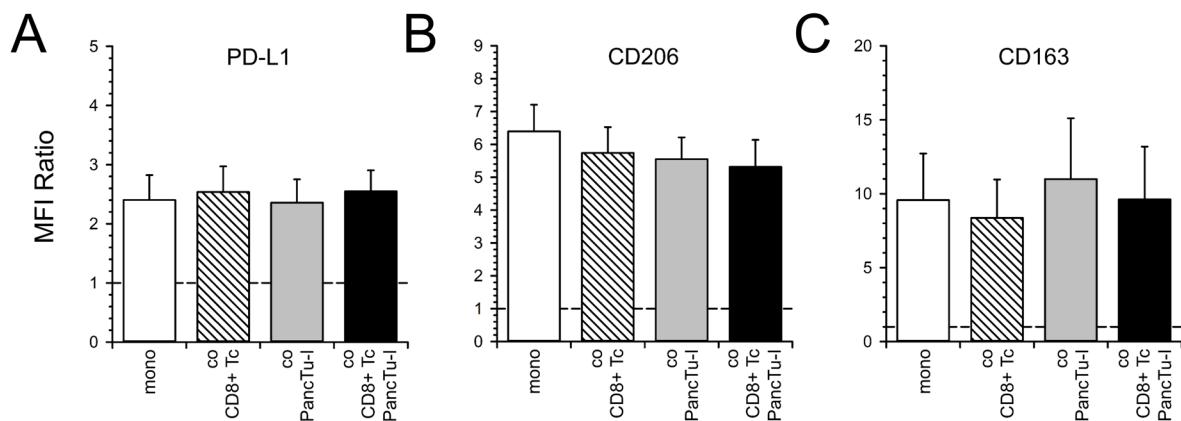


**Figure 42: Cell surface expression levels of PD-L1, CD206 and CD163 in M1-polarized macrophages after co-culture with PancTu-I cells and autologous activated CD8<sup>+</sup> T lymphocytes.** Primary human M1-polarized macrophages were either mono-cultured (white), indirectly co-cultured with autologous pre-activated CD8<sup>+</sup> T lymphocytes (banded), PancTu-I cells (grey) or both autologous CD8<sup>+</sup> T lymphocytes and PancTu-I cells (black) for 48 h. (A) PD-L1, (B) CD206 and (C) CD163 cell surface levels in M1 MΦ after indicated culture conditions. Bar charts present mean values with SEM of median fluorescence intensity ratios examined in three independent experiments. The dashed lines mark an MFI ratio of “1”.

Furthermore, relative mRNA levels of cytokines, chemokines and growth factors associated with an M1- (IL-1β, IL-6, IL-8 and TNFα) or M2-like (IL-10, TGF-β1 and VEGF) polarization were analyzed by qPCR in M1 MΦ after respective culture conditions (**Figure 43**). In comparison to macrophages from mono-cultures, mRNA levels of pro-inflammatory cytokines IL-1β, IL-6 and TNFα were either markedly or even significantly lower in M1 MΦ from each co-culture setting. In detail, IL-1β mRNA were significantly lower in M1 MΦ from co-cultures with CD8<sup>+</sup> T lymphocytes (0.58 ±0.14-fold; p=0.017), PancTu-I cells (0.63 ±0.03-fold; p=0.013) and co-cultures with both CD8<sup>+</sup> T lymphocytes and PancTu-I cells (0.48 ±0.08-fold; p=0.010) compared to levels in mono-cultured M1 MΦ (**Figure 43 A**). IL-6 mRNA levels were lower by trend in M1 MΦ co-cultured with CD8<sup>+</sup> T lymphocytes (0.59 ±0.25-fold) and

significantly lower after co-culture with PancTu-I cells ( $0.31 \pm 0.03$ -fold;  $p=0.011$ ) as well as co-culture with both  $CD8^+$  T lymphocytes and PancTu-I cells ( $0.29 \pm 0.03$ -fold;  $p=0.017$ ) in comparison to M1  $M\Phi$  from mono-culture conditions (**Figure 43 B**). By trend,  $TNF\alpha$  mRNA levels were lower in M1  $M\Phi$  from co-cultures with  $CD8^+$  T lymphocytes ( $0.56 \pm 0.27$ -fold), PancTu-I cells ( $0.50 \pm 0.20$ -fold) as well as after co-culture with both  $CD8^+$  T lymphocytes and PancTu-I cells ( $0.50 \pm 0.17$ -fold) compared to levels detected in mono-cultured macrophages (**Figure 43 C**). In contrast, IL-8 mRNA levels in M1  $M\Phi$  from co-cultures with both  $CD8^+$  T lymphocytes and PancTu-I cells ( $1.27 \pm 0.22$ -fold) by trend exceeded those detected in mono-cultured macrophages while being comparatively lower in M1  $M\Phi$  after co-culture with  $CD8^+$  T lymphocytes alone ( $0.69 \pm 0.11$ -fold) (**Figure 43 D**). In terms of cytokines associated with an M2-polarized phenotype, mRNA levels were lower in M1  $M\Phi$  from each co-culture condition compared to levels in mono-cultured macrophages. In detail, IL-10 mRNA levels were slightly lower by trend in M1  $M\Phi$  after co-culture with  $CD8^+$  T lymphocytes ( $0.86 \pm 0.11$ -fold) and PancTu-I cells ( $0.81 \pm 0.14$ -fold) but markedly lower after co-culture with both  $CD8^+$  T lymphocytes and PancTu-I cells ( $0.50 \pm 0.15$ -fold) compared to levels detected in mono-cultured macrophages (**Figure 43 E**).  $TGF-\beta 1$  mRNA levels were more or less pronounced lower in M1  $M\Phi$  from co-cultures with  $CD8^+$  T lymphocytes ( $0.49 \pm 0.22$ -fold), PancTu-I cells ( $0.73 \pm 0.27$ -fold) or triple co-culture settings ( $0.67 \pm 0.08$ -fold) in comparison to mono-cultured M1  $M\Phi$  (**Figure 43 F**). Finally, VEGF mRNA levels revealed least differences in M1  $M\Phi$  co-cultured with  $CD8^+$  T lymphocytes ( $0.79 \pm 0.11$ -fold), PancTu-I cells ( $0.92 \pm 0.20$ -fold) or both  $CD8^+$  T lymphocytes and PancTu-I cells ( $0.84 \pm 0.21$ -fold) in comparison to levels detected in M1  $M\Phi$  from mono-cultures conditions (**Figure 43 G**).

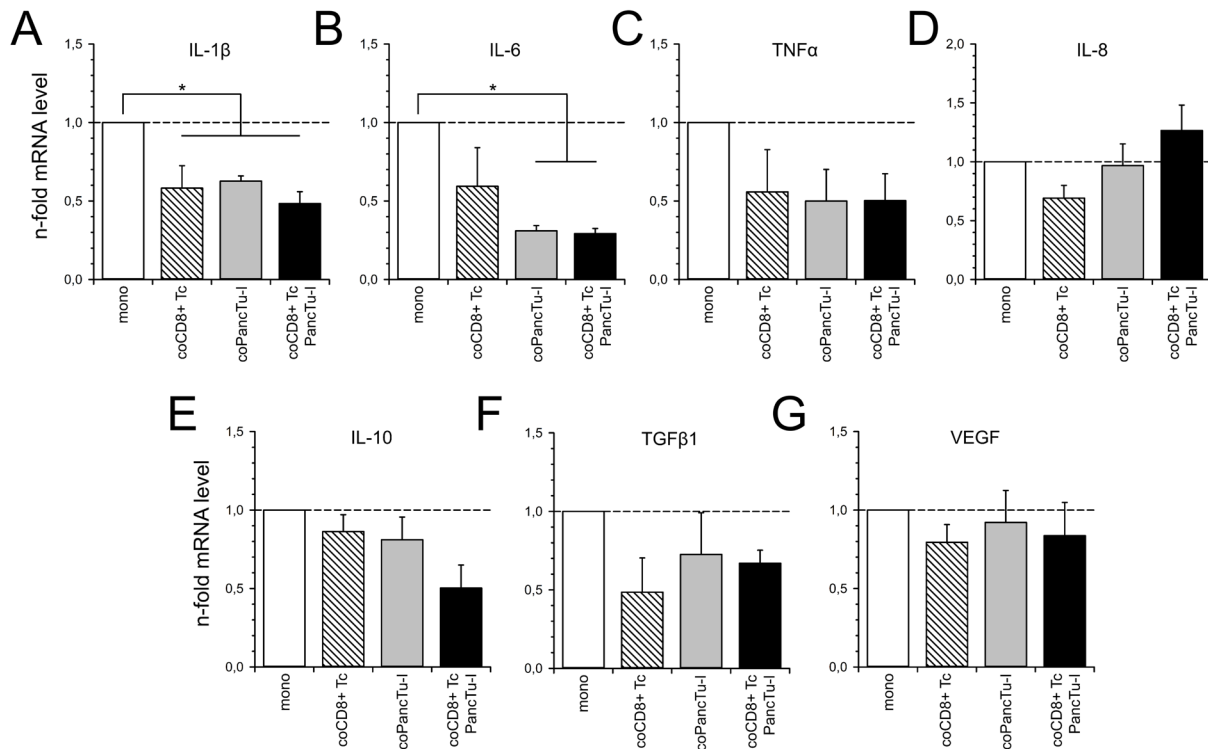


**Figure 43: Gene expression profiles of cytokines, chemokines and growth factors in M1-polarized macrophages after co-culture with PancTu-I cells and autologous activated CD8<sup>+</sup> T lymphocytes.** Primary human M1-polarized macrophages were either mono-cultured (white) or indirectly co-cultured with autologous pre-activated CD8<sup>+</sup> T lymphocytes (banded), PancTu-I cells (grey) or both autologous CD8<sup>+</sup> T lymphocytes and PancTu-I cells (black) for 48 h. Relative mRNA levels of (A) IL-1 $\beta$ , (B) IL-6, (C) TNF $\alpha$ , (D) IL-8, (E) IL-10, (F) TGF- $\beta$ 1 and (G) VEGF in M1 M $\Phi$  after indicated mono- and indirect co-culture conditions. Messenger RNA levels were normalized to respective GAPDH levels as well as levels detected in M1 M $\Phi$  from mono-cultures, indicated by dashed lines. Bar charts present mean values with SEM of three independent experiments. \* =  $p < 0.05$

In order to examine the effect of each co-culture setting on the growth of PancTu-I cells, confluency analyses of phase-contrast pictures was performed after removal of CD8<sup>+</sup> T lymphocytes and M1 M $\Phi$  (**Figure 44 A**). Analyses revealed a significantly lower cellular confluency after co-culture with CD8<sup>+</sup> T lymphocytes ( $34.67 \pm 3.84$  %;  $p = 0.041$ ) but not M1 M $\Phi$  ( $43.46 \pm 2.86$  %) in comparison to PancTu-I mono-cultures ( $50.11 \pm 2.57$  %). Interestingly, the confluency of PancTu-I cells was even lower after triple co-culture with both CD8<sup>+</sup> T lymphocytes and M1 M $\Phi$  ( $28.94 \pm 4.83$  %) (**Figure 44 B**).

Concerning the differentiation status of PancTu-I cells after co-culture settings, western blot analysis of whole-cell lysates indicated synergistic effects of co-culture with both CD8<sup>+</sup> T lymphocytes and M1 M $\Phi$  on protein levels associated with an epithelial and mesenchymal phenotype, respectively. Hence, levels of the mesenchymal protein vimentin were higher in PancTu-I cells after co-culture with CD8<sup>+</sup> T lymphocytes in comparison to levels detected in mono-cultured cells but even exceeded by expression levels in triple co-cultures (**Figure 44 C**). While levels of the epithelial protein E-cadherin were lower in PancTu-I cells after co-culture with CD8<sup>+</sup> T lymphocytes compared to mono-cultured cells, higher expression levels were

detected after co-culture with M1 MΦ. Interestingly, E-cadherin expression levels detected after co-culture of PancTu-I cells with both CD8<sup>+</sup> T lymphocytes and M1 MΦ were similar to those in mono-cultured cells. (**Figure 44 C**). Finally, PD-L1 levels were markedly higher in PancTu-I cells after any co-culture condition comprising CD8<sup>+</sup> T lymphocytes in comparison to mono-culture and co-culture conditions with only M1 MΦ (**Figure 44 C**).

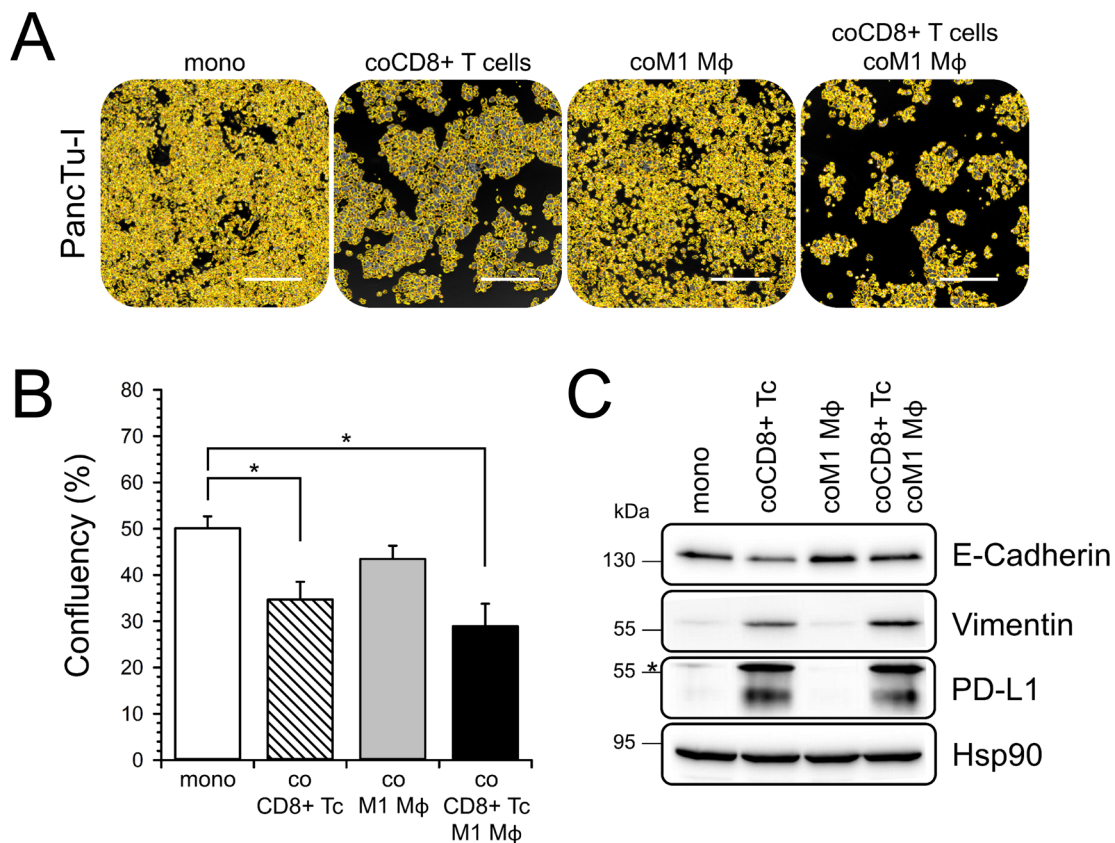


**Figure 44: Cell growth and differentiation of PancTu-I cells after co-culture with activated CD8<sup>+</sup> T lymphocytes and M1-polarized macrophages.** PancTu-I cells were either mono-cultured (white), directly co-cultured with primary human pre-activated CD8<sup>+</sup> T lymphocytes (banded), indirectly co-cultured with M1-polarized macrophages (grey) or co-cultured with both CD8<sup>+</sup> T lymphocytes and M1 MΦ (black) for 48 h. (**A**) Representative images of confluency analysis on light microscopical phase contrast pictures of PancTu-I cells after indicated culture conditions. (**B**) Confluency of PancTu-I cell after indicated mono- and co-culture conditions. Bar chart presents mean values with SEM of three independent experiments. (**C**) Representative western blot of whole-cell lysates from PancTu-I cells after indicated culture conditions. Hsp90 was detected as loading control. Molecular weights in kDa are indicated according to the applied standard. (**B**) \* =  $p < 0.05$ ; (**C**) \* = vimentin signal; Scale bar = 500  $\mu$ m

At last, concentrations of proteins secreted by activated CD8<sup>+</sup> T lymphocytes (IFN $\gamma$ , IL-17A, soluble FasL, Granulysin, Perforin, Granzyme A and Granzyme B) as well as macrophages and PancTu-I cells (VEGF, IL-6 and IL-8) were measured in the culture supernatant of each mono- and co-culture setting (**Figure 45**).

In detail, VEGF concentrations were higher in culture supernatants of settings comprising M1 MΦ than in cultures including only PancTu-I cells (>450 pg/ml vs. <350 pg/ml). Notably,

highest VEGF levels were measured in culture supernatants of triple co-cultures ( $572.71 \pm 78.03$  pg/ml) but not co-cultures of M1 M $\Phi$  and PancTu-I cells ( $457.30 \pm 15.05$  pg/ml) (**Figure 45 A**). Even more pronounced differences were found in terms of IL-8 concentrations. IL-8 levels in supernatants of culture settings comprising M1 M $\Phi$  ( $>16.8$  ng/ml) were at least 32-fold higher than in those settings, in which PancTu-I cells but no M1 M $\Phi$  were present ( $<0.53$  ng/ml). However, the presence of CD8<sup>+</sup> T lymphocytes and/or PancTu-I cells did hardly affect IL-8 concentrations in M1 M $\Phi$  co-cultures compared to mono-culture conditions ( $\pm 4.17\%$ ) (**Figure 45 B**). Moreover, IL-6 levels were higher in culture settings comprising M1 M $\Phi$  than in those including only PancTu-I cells but no M1 M $\Phi$  ( $>770$  pg/ml vs.  $<200$  pg/ml). Similarly to VEGF, IL-6 concentrations revealed highest levels in supernatants of co-cultures containing M1 M $\Phi$ , CD8<sup>+</sup> T lymphocytes and PancTu-I cells ( $1100.92 \pm 380.56$  pg/ml) (**Figure 45 C**). With respect to T lymphocyte-associated cytokines, considerable concentrations of all analytes were exclusively detected in culture settings including CD8<sup>+</sup> T lymphocytes. Since IFN $\gamma$  concentrations in supernatants greatly varied between biological replicates and even normalization revealed no clear tendencies between the applied culture conditions (data not shown), multiplex analysis indicated no effects of co-culture with M1 M $\Phi$  ( $2.48 \pm 1.60$  ng/ml), PancTu-I cells ( $3.82 \pm 3.15$  ng/ml) or both M1 M $\Phi$  and PancTu-I cells ( $2.60 \pm 2.07$  ng/ml) on IFN $\gamma$  secretion by CD8<sup>+</sup> T lymphocytes compared to mono-culture conditions ( $2.72 \pm 1.57$  ng/ml) (**Figure 45 D**). By trend, IL-17A concentrations were slightly lower in supernatants of CD8<sup>+</sup> T lymphocytes after co-culture with M1 M $\Phi$  ( $126.03 \pm 33.20$  pg/ml), PancTu-I cells ( $133.97 \pm 46.78$  pg/ml) and triple co-culture ( $115.15 \pm 40.35$  pg/ml) compared to levels detected in mono-cultures ( $156.41 \pm 39.63$  pg/ml) (**Figure 45 E**). In contrast, cytokine levels of soluble FasL were comparatively higher in supernatants of CD8<sup>+</sup> T lymphocytes co-cultured with M1 M $\Phi$  ( $82.22 \pm 7.22$  pg/ml), PancTu-I cells ( $77.10 \pm 25.77$  pg/ml) and both M1 M $\Phi$  and PancTu-I cells ( $96.58 \pm 23.02$  pg/ml) than in supernatants of mono-cultured CD8<sup>+</sup> T lymphocytes ( $54.25 \pm 14.62$  pg/ml) (**Figure 45 F**). Same as for IFN $\gamma$ , due to high variations between biological replicates no trends for supernatant levels of Granulysin were examined in co-cultures of CD8<sup>+</sup> T lymphocytes with M1 M $\Phi$  ( $4.00 \pm 2.50$  ng/ml), PancTu-I cells ( $8.81 \pm 6.87$  ng/ml) or both M1 M $\Phi$  and PancTu-I cells ( $5.83 \pm 3.78$  ng/ml) in comparison to concentrations detected in mono-cultures ( $5.98 \pm 4.16$  ng/ml) (**Figure 45 G**).

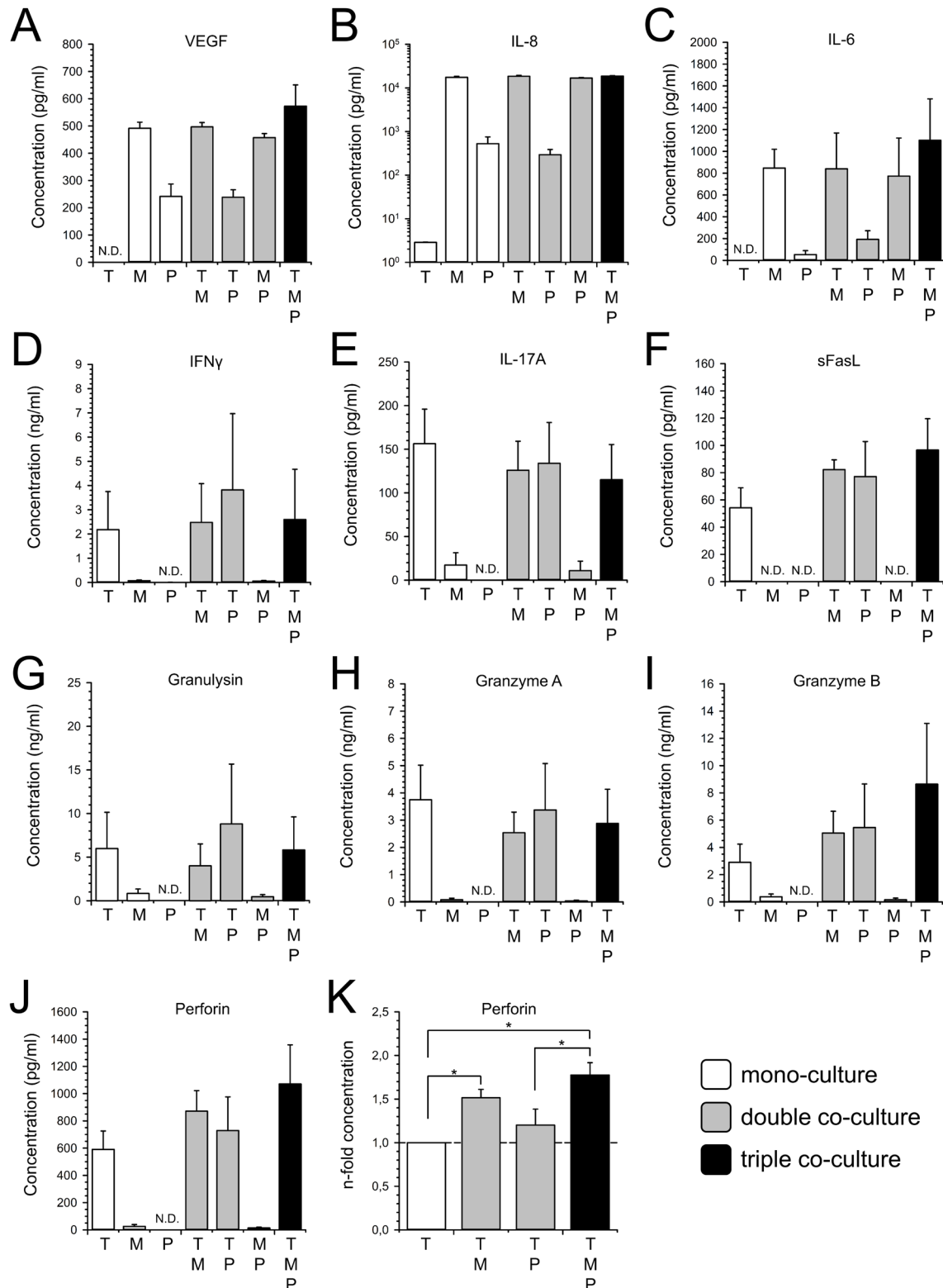


**Figure 45: Supernatant levels of various cytokines, chemokines and growth factors after co-culture of activated CD8<sup>+</sup> T lymphocytes with autologous M1-polarized macrophages and PancTu-I cells.** Pre-activated primary human CD8<sup>+</sup> T lymphocytes (T), M1 M $\Phi$  (M) and PancTu-I cells (P) were either mono-cultured (white), co-cultured with a second cell population (grey) or co-cultured all together (black: direct co-culture of PancTu-I cells and CD8<sup>+</sup> T lymphocytes and indirectly co-cultured with M1 M $\Phi$ ). Concentrations of (A) VEGF, (B) IL-8, (C) IL-6, (D) IFN $\gamma$ , (E) IL-17A, (F) soluble Fas ligand, (G) Granulysin, (H) Granzyme A, (I) Granzyme B and (J) Perforin were measured by multiplex assay in the culture supernatant of indicated mono- and culture settings. Bar charts present mean values with SEM of three independent experiments. (K) Relative Perforin levels in supernatants of T lymphocyte mono- and co-culture settings normalized to levels detected in supernatants of mono-cultured CD8<sup>+</sup> T lymphocytes indicated by the dashed line. N.D. = not detectable; \* = p < 0.05

Granzyme A concentrations were lower by trend in each biological replicate of CD8<sup>+</sup> T lymphocyte co-cultures with M1 MΦ compared to levels detected in mono-cultured T lymphocytes ( $2.54 \pm 0.75$  vs.  $3.75 \pm 1.27$  ng/ml) but not in supernatants of T lymphocytes co-cultured with PancTu-I cells ( $3.37 \pm 1.71$  ng/ml) or both M1 MΦ and PancTu-I cells ( $2.88 \pm 1.26$  ng/ml) (**Figure 45 H**). In contrast, Granzyme B detection revealed by trend higher levels in supernatants of CD8<sup>+</sup> T lymphocytes co-cultured with M1 MΦ ( $5.05 \pm 1.60$  ng/ml), PancTu-I cells ( $5.46 \pm 3.20$  ng/ml) as well as triple co-culture ( $8.64 \pm 4.46$  ng/ml) in comparison to levels in mono-cultured CD8<sup>+</sup> T lymphocytes ( $2.90 \pm 1.33$  ng/ml) (**Figure 45 I**). The same tendencies applied to Perforin concentrations, which markedly exceeded those levels measured in T lymphocyte mono-cultures ( $590.47 \pm 135.25$  pg/ml) when CD8<sup>+</sup> T lymphocytes were co-cultured with M1 MΦ ( $871.10 \pm 150.92$  pg/ml), PancTu-I cells ( $728.46 \pm 247.70$ ) or both of them ( $1070.92 \pm 287.38$  pg/ml) (**Figure 45 J**). Moreover, comparison of normalized levels revealed that Perforin concentrations were statistically significant higher in supernatants of CD8<sup>+</sup> T lymphocytes co-cultured with M1 MΦ (1.52-fold;  $p=0.047$ ) than in those of mono-cultures. Notably, this trend was even more pronounced in supernatants of triple co-cultures (1.78-fold;  $p=0.010$ ) (**Figure 45 K**).

Taken together, in review of the results from **section 4.2.7** and **section 4.2.8**, the differences in the phenotype, proliferation as well as PD-1 and PD-L1 cell surface expression levels of CD8<sup>+</sup> T lymphocytes were less pronounced under indirect co-culture with M1 MΦ or both M1 MΦ and PancTu-I cells compared to direct co-culture with M1 MΦ or PancTu-I cells. The same tendency applied to results regarding the phenotypical alterations of M1 macrophages from indirect co-culture settings compared to results from direct co-cultures with CD8<sup>+</sup> T lymphocytes. These results suggest that besides paracrine interactions also direct cell-cell contacts play an essential role in the present co-culture setting. However, considering the culture supernatant concentrations of VEGF, IL-6, soluble Fas ligand, Granzyme B and Perforin as well as the growth and differentiation status of PancTu-I cells, results from triple co-culture conditions indicated a synergy of effects mediated by the presence of each population.



#### 4.2.10 Application of Durvalumab does not affect the phenotype and proliferation but PD-L1 cell surface levels and cytokine secretion profile of mono-cultured activated CD8<sup>+</sup> T lymphocytes

Having identified some notable alterations in CD8<sup>+</sup> T lymphocytes' phenotype, proliferation and cytokine secretion profile as well as the differentiation status of M1 MΦ and PancTu-I cells due to the reciprocal interplay of these cell populations, it was next elucidated whether availability of PD-L1 as ligand for PD-1, the latter being exclusively expressed by CD8<sup>+</sup> T lymphocytes in this system, plays a causal role. For this purpose, PD-L1 binding domain for PD-1 was blocked by application of Durvalumab (kindly provided by Astra Zeneca) in the following experimental settings.

First, it was investigated whether PD-L1 blockade by Durvalumab affects the phenotype, proliferation and cytokine secretion of CD8<sup>+</sup> T lymphocytes after activation culture. Flow cytometric analysis of FSC/SSC plots indicated no differences between activated CD8<sup>+</sup> T lymphocyte populations treated with either human IgG<sub>1</sub> isotype control antibody or Durvalumab in terms of cell size (Mean FSC 441.50 ±16.76 vs. 441.67 ±18.45) and granularity (Mean SSC 177.33 ±11.62 vs. 177.00 ±11.57), respectively (**Figure 46 A+B**). Moreover, neither vital cell numbers (1.04 ±0.04-fold) (**Figure 46 C**) nor the overall proportion of proliferating cells in the CD8<sup>+</sup> T lymphocyte population treated with Durvalumab markedly varied in comparison to isotype control antibody treated cells (81.50 ±4.53 % vs. 81.36 ±4.74 %) (**Figure 46 D**). In line with this, CFSE profiles of both control isotype and Durvalumab treated CD8<sup>+</sup> T lymphocyte populations revealed up to five distinguishable cell divisions and no differences in distribution patterns (**Figure 46 E**).

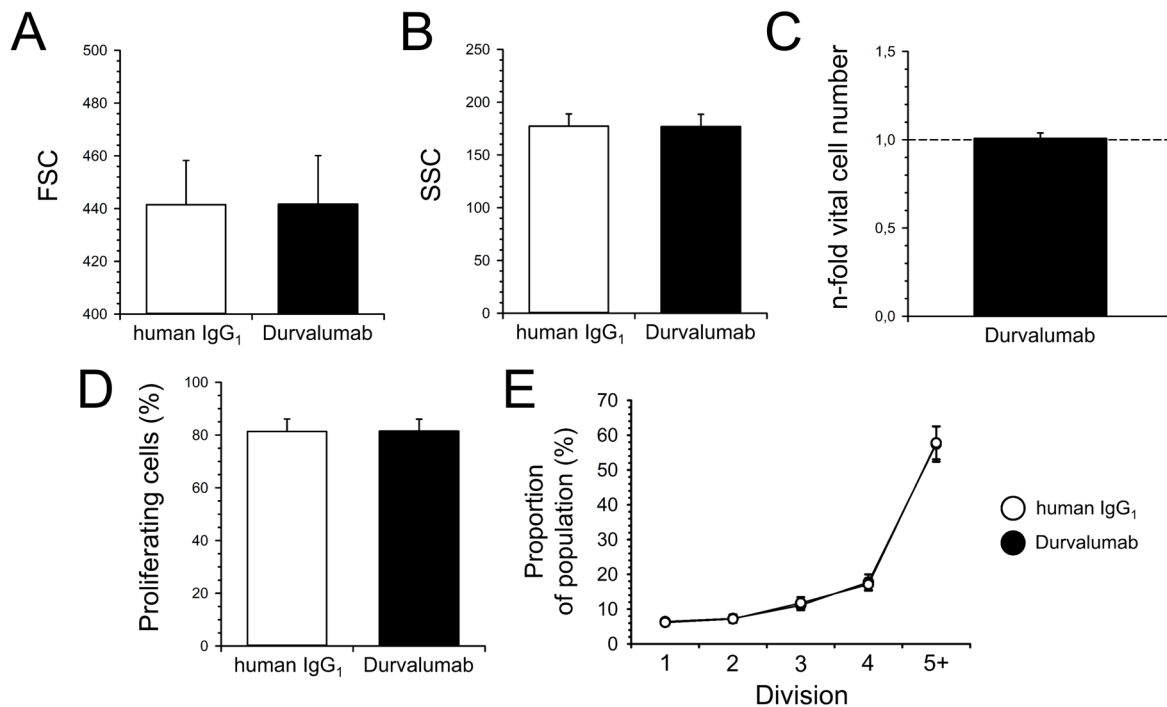


**Figure 46: Phenotype and proliferation of activated CD8<sup>+</sup> T lymphocytes after treatment with Durvalumab.** Anti-CD3/CD28 pre-activated CD8<sup>+</sup> T lymphocytes were treated with 10  $\mu$ g/ml Durvalumab (black) or respective IgG<sub>1</sub> isotype control antibody (white) for 72h. Comparison of (A) FSC medians, (B) SSC medians, (C) n-fold vital cell numbers and (D) the proportion of proliferating cells within CD8<sup>+</sup> T lymphocyte populations after indicated treatment. Bar charts present mean values with SEM of three independent experiments. (E) CFSE profiles of proliferating CD8<sup>+</sup> T lymphocytes after 72 h of indicated treatment. Data present mean proportions with SEM of T lymphocytes having divided 1 to 5 times in three independent experiments. The maximum numbers of clearly distinguishable peaks in respective CFSE profiles are indicated by “+”.

Flow cytometric analysis of PD-1 cell surface levels revealed no differences between IgG<sub>1</sub> and Durvalumab treated CD8<sup>+</sup> T lymphocyte populations (MFI Ratio  $4.42 \pm 0.83$  vs.  $4.37 \pm 0.79$ ) (Figure 47 A). Moreover, correlations of PD-1 cell surface levels with CFSE cell division profiles showed no variations between IgG<sub>1</sub> and Durvalumab treated CD8<sup>+</sup> T lymphocytes (Figure 47 B). In contrast, PD-L1 cell surface levels were significantly lower in CD8<sup>+</sup> T lymphocytes after Durvalumab treatment in comparison to IgG<sub>1</sub> isotype control antibody treated cells (MFI Ratio  $1.26 \pm 0.09$  vs.  $1.84 \pm 0.17$ ;  $p=0.014$ ) (Figure 47 A).

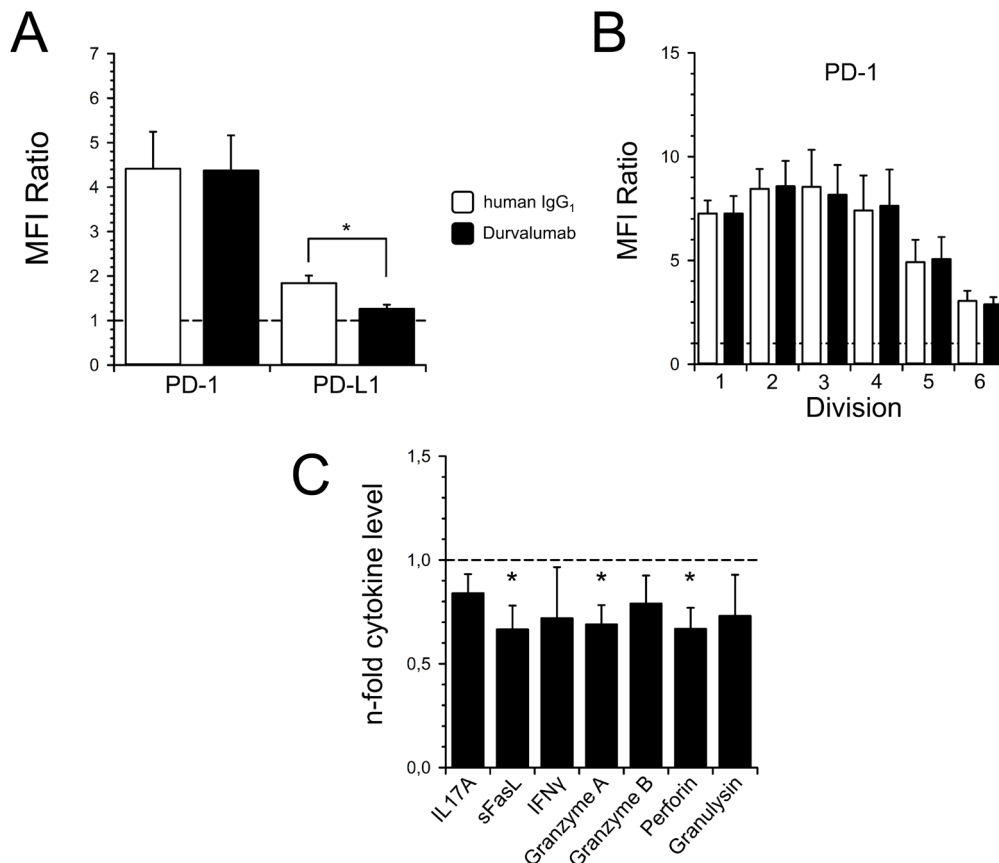


**Figure 47: PD-1 and PD-L1 surface expression in CD8<sup>+</sup> T lymphocytes as well as cytokine levels in culture supernatants after treatment with Durvalumab.** Anti-CD3/CD28 activated CD8<sup>+</sup> T lymphocytes were treated with 10  $\mu$ g/ml Durvalumab (black) or respective IgG<sub>1</sub> isotype control antibody (white) for 72h. **(A)** PD-1 and PD-L1 cell surface expression levels in the IgG<sub>1</sub> isotype control antibody (white) and Durvalumab (black) treated CD8<sup>+</sup> lymphocytes. **(B)** PD-1 cell surface expression levels in CD8<sup>+</sup> T lymphocytes having dived one to six times after indicated treatment. **(A+B)** Bar charts present mean values and SEM of median fluorescence intensity ratios examined in six independent experiments. The dashed lines mark an MFI ratio of “1”. **(C)** N-fold supernatant levels of cytokines and effector molecules. Concentrations have been measured by multiplex assay and normalized to levels detected in culture supernatants of CD8<sup>+</sup> T lymphocytes treated with IgG<sub>1</sub> isotype control antibody, indicated by the dashed line. Bar chart presents mean values and SEM of six independent experiments. \* =  $p < 0.05$

Interestingly, multiplex analysis of CTL-associated cytokines revealed lower concentrations of IL-17A ( $0.84 \pm 0.09$ -fold), IFN $\gamma$  ( $0.72 \pm 0.25$ -fold), Granzyme B ( $0.79 \pm 0.14$ -fold) and Granulysin ( $0.74 \pm 0.20$ -fold) by trend as well as significantly lower levels of soluble Fas ligand ( $0.66 \pm 0.12$ -fold;  $p = 0.044$ ), Granzyme A ( $0.69 \pm 0.09$ -fold;  $p = 0.029$ ) and Perforin ( $0.67 \pm 0.10$ -fold;  $p = 0.031$ ) in culture supernatants of CD8<sup>+</sup> T lymphocytes after treatment with Durvalumab in comparison to CD8<sup>+</sup> T lymphocytes treated with IgG<sub>1</sub> isotype control antibody (**Figure 47 C**).

In summary, these data show that treatment of activated CD8<sup>+</sup> T lymphocytes in mono-culture does not affect the phenotype, proliferation and PD-1 cell surface levels, but is accompanied by markedly reduced PD-L1 cell surface expression levels in CD8<sup>+</sup> T lymphocytes as well as decreased levels of major CTL-associated effector molecules in culture supernatants.

#### 4.2.11 Durvalumab application in direct co-cultures markedly alters PD-1 cell surface levels of CD8<sup>+</sup> T lymphocytes and PD-L1 cell surface levels in both M1 MΦ and T lymphocytes

Next, it was investigated whether blocking of PD-L1 affects the previously observed differences in the phenotypes of CD8<sup>+</sup> T lymphocytes and M1 MΦ after direct co-culture of both populations (**section 4.2.7**).

Flow cytometric analysis indicated no differences in terms of size and granularity as well as proliferation of activated CD8<sup>+</sup> T lymphocytes due to the application of Durvalumab in comparison to mono- and co-cultures stimulated with human IgG<sub>1</sub> isotype control antibody (**Figure 48**). In detail, after co-coculture with M1 MΦ accompanied by treatment with human IgG<sub>1</sub> or Durvalumab both CD8<sup>+</sup> T lymphocyte populations were larger in size (Mean FSC 520.50 ±47.64 vs. 526.67 ±49.52) and showed higher granularity (Mean SSC 257.50 ±28.80 vs. 264.50 ±27.52) in comparison to respective mono-cultured CD8<sup>+</sup> T lymphocytes treated with human IgG<sub>1</sub> isotype control antibody (Mean FSC: 451.67 ±20.85; Mean SSC: 191.00 ±11.93) or Durvalumab (Mean FSC: 453.67 ±22.67; Mean SSC: 192.00 ±10.54) (**Figure 48 A+B**). Moreover, CD8<sup>+</sup> T lymphocyte populations from co-cultures with M1 MΦ supplemented with either human IgG<sub>1</sub> control antibody (81.57 ±8.31 vs. 77.02 ±9.58%) or Durvalumab (81.10 ±8.62 vs. 77.27 ±9.15%) both showed slightly higher proportions of proliferating cells than respective CD8<sup>+</sup> T lymphocytes from mono-cultures (**Figure 48 C**). CFSE profiles of CD8<sup>+</sup> T lymphocytes from mono- and co-cultures supplemented with Durvalumab showed no prominent differences in comparison to CFSE profiles of lymphocytes from respective IgG<sub>1</sub> treated cultures (**Figure 48 D**). CD8<sup>+</sup> T lymphocyte populations after mono- and M1 MΦ co-cultures with both treatments showed the same range of 5 to 6 distinguishable cell divisions, which only varied between biological replicates. However, CD8<sup>+</sup> T lymphocyte populations from both IgG<sub>1</sub> and Durvalumab treated co-cultures revealed by trend a higher proportion of cells having divided once to thrice and a lower proportion of cells having divided five times or more in comparison to CD8<sup>+</sup> T lymphocyte populations from respective mono-cultures. Lastly, western blotting analysis revealed markedly higher levels of phosphorylated ERK1/2 in CD8<sup>+</sup> T lymphocytes from co-culture setting with either treatment in comparison to respective mono-cultures (**Figure 48 E**). Notably, all these findings for IgG<sub>1</sub> isotype control antibody treated CD8<sup>+</sup> T lymphocytes from mono- and co-cultures are in line with previous results from direct co-culture experiments of CD8<sup>+</sup> T lymphocytes and M1 MΦ (**section 4.2.7**).

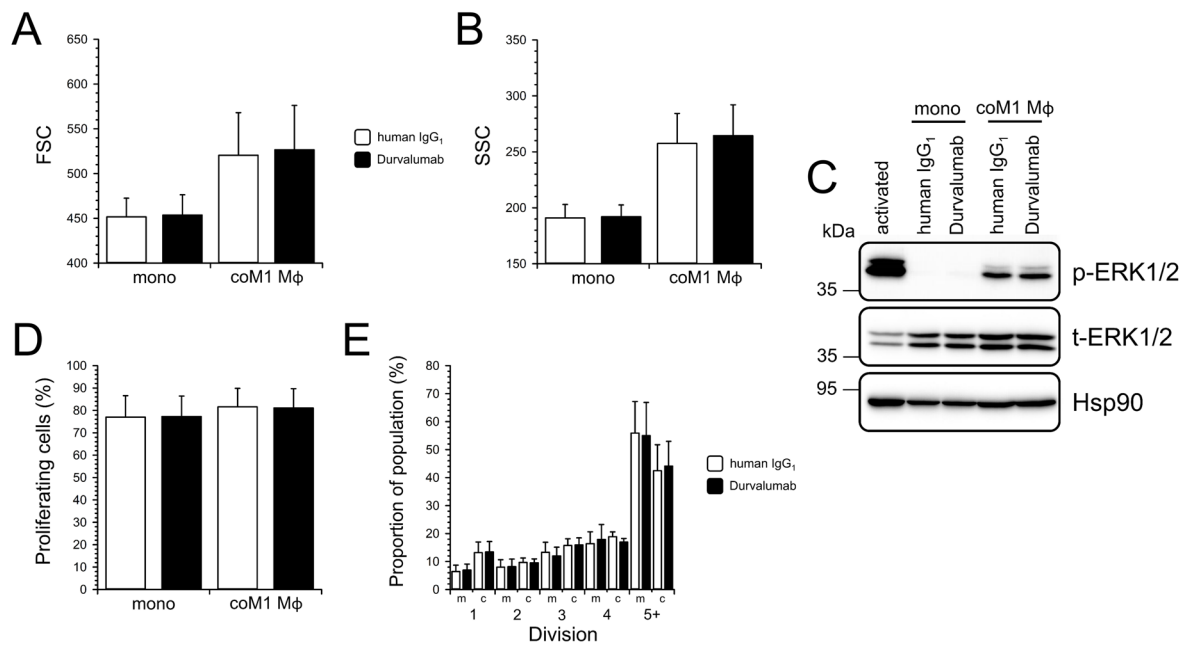


**Figure 48: Phenotype and proliferation of activated CD8<sup>+</sup> T lymphocytes after direct co-culture with autologous M1-polarized macrophages and treatment with Durvalumab.** Pre-activated primary human CD8<sup>+</sup> T lymphocytes were mono-cultured or directly co-cultured for 72 h with autologous M1-like polarized macrophages and treated with 10 $\mu$ g/ml of either human IgG<sub>1</sub> isotype control antibody (white) or Durvalumab (black). Comparison of (A) FSC medians, (B) SSC medians and (C) the proportion of proliferating cells within CD8<sup>+</sup> T lymphocyte populations after indicated culture settings and treatments. Bar charts present mean values with SEM of three independent experiments. (D) CFSE profiles of proliferating CD8<sup>+</sup> T lymphocytes after 72 h of mono- (m) or co-culture (c) and indicated treatment. Data present mean proportions with SEM of T lymphocytes having divided one to five times in three independent experiments. The maximum numbers of clearly distinguishable peaks in respective CFSE profiles are indicated by “+”. (E) Representative western blot of whole-cell lysates from activated CD8<sup>+</sup> T lymphocytes directly after four days of anti-CD3/CD28 stimulation and activated CD8<sup>+</sup> T lymphocytes after indicated culture settings and treatments. Hsp90 was detected as loading control. Molecular weights in kDa are indicated according to the applied standard.

Next, cell surface expression levels of PD-1 and PD-L1 in CD8<sup>+</sup> T lymphocytes after mono- and co-cultures supplemented with IgG<sub>1</sub> isotype control antibody or Durvalumab were analyzed by flow cytometry (Figure 49 A). In line with results from previous experiments (section 4.2.7), human IgG<sub>1</sub> treated proliferating CD8<sup>+</sup> T lymphocytes from M1 M $\Phi$  co-cultures showed markedly higher PD-1 cell surface levels than respective CD8<sup>+</sup> T lymphocytes from mono-culture conditions (MFI Ratio 10.31  $\pm$  2.44 vs. 3.62  $\pm$  1.50). Interestingly, this trend was even more pronounced in Durvalumab treated co-culture settings (MFI Ratio 12.59  $\pm$  3.20 vs. 3.53  $\pm$  1.46) (Figure 49 B). Correlations with CFSE profiles showed that PD-1 cell surface levels in CD8<sup>+</sup> T lymphocytes from Durvalumab supplemented M1 M $\Phi$  co-culture settings exceeded by trend PD-1 levels in CD8<sup>+</sup> T lymphocytes from respective IgG<sub>1</sub> treated co-cultures throughout the spectrum of lymphocytes having divided up to six times (Figure 49 A+C). Similar to previous results (section 4.2.6 and 4.2.7), PD-1 cell surface levels tended to be decreased in relation to progressive number of divisions CD8<sup>+</sup> T lymphocytes have passed. Cell surface expression levels of PD-L1 were significantly higher in the proliferating population of CD8<sup>+</sup>

T lymphocytes after IgG<sub>1</sub> supplemented co-culture with M1 MΦ compared to respective mono-cultured lymphocytes (MFI Ratio  $2.88 \pm 0.19$  vs.  $2.01 \pm 0.29$ ;  $p=0.007$ ) (**Figure 49 D**). However, application of Durvalumab to the cultures was associated with markedly lower PD-L1 cell surface levels in proliferating CD8<sup>+</sup> T lymphocytes from both mono- (MFI Ratio  $1.39 \pm 0.01$  vs.  $2.01 \pm 0.29$ ) and co-culture (MFI Ratio  $1.42 \pm 0.05$  vs.  $2.88 \pm 0.19$ ;  $p<0.001$ ) in comparison to respective IgG<sub>1</sub> isotype control treated cells (**Figure 49 D**). Notably, PD-L1 surface expression of Durvalumab stimulated T lymphocytes from mono- and co-cultures dropped to very similar levels.

In summary, IgG<sub>1</sub> isotype control treated CD8<sup>+</sup> T lymphocytes showed the same alterations in phenotype and proliferation as well as PD-1 and PD-L1 cell surface expression levels after direct co-culture with M1 MΦ as observed in previous experiments (**section 4.2.7**). Durvalumab treatment only affected PD-1 and PD-L1 cell surface expression levels in CD8<sup>+</sup> T lymphocytes. Hence, Durvalumab treated CD8<sup>+</sup> T lymphocytes from both mono- and co-culture settings showed markedly decreased PD-L1 cell surface levels while PD-1 cell surface levels in Durvalumab treated CD8<sup>+</sup> T lymphocytes were even more elevated exclusively after direct co-culture with M1 MΦ in comparison to respective IgG<sub>1</sub> isotype control treated CD8<sup>+</sup> T lymphocytes.

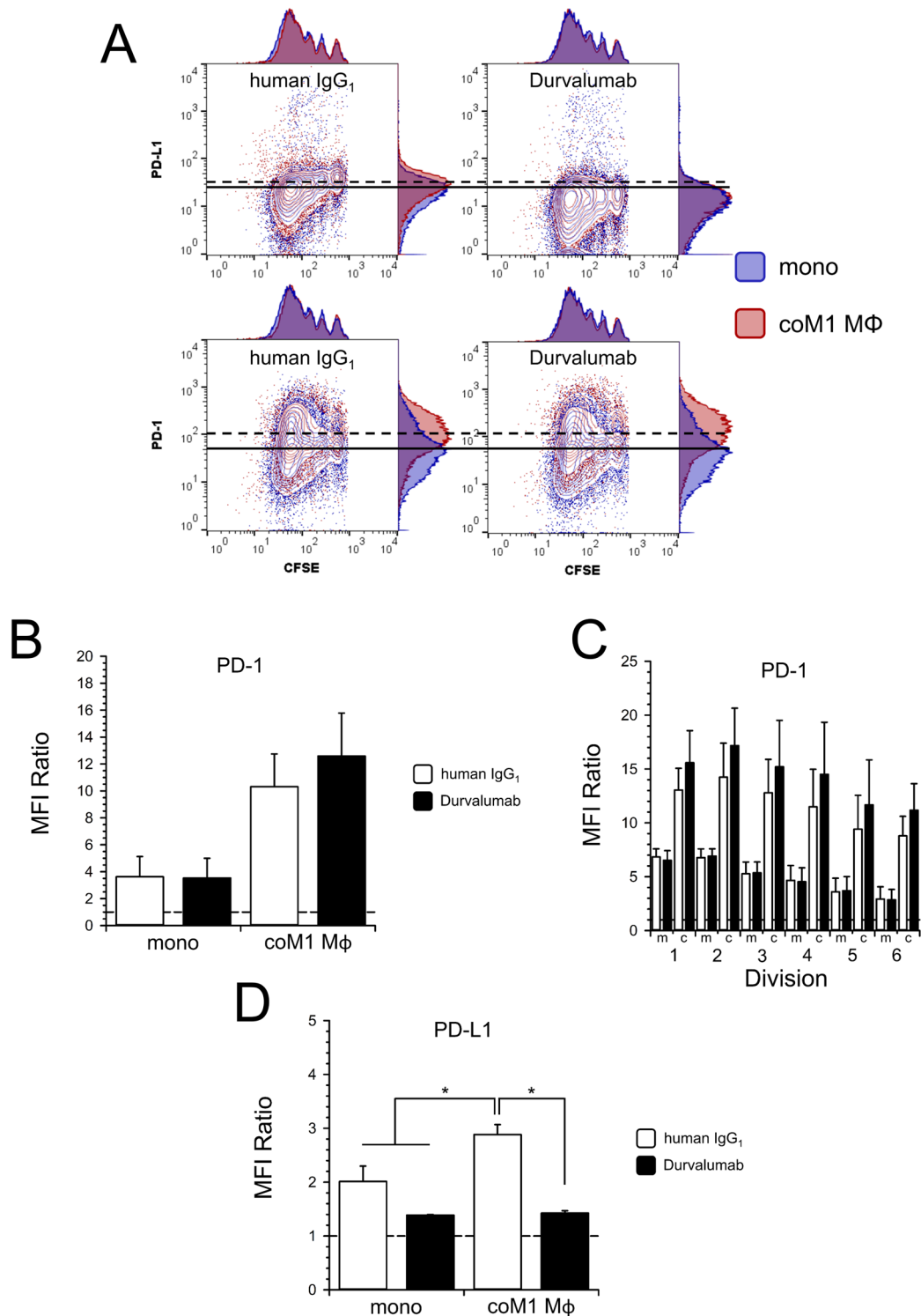


**Figure 49: PD-1 and PD-L1 cell surface expression levels in CD8<sup>+</sup> T lymphocytes after direct co-culture with autologous M1-polarized macrophages and treatment with Durvalumab.** Pre-activated primary human CD8<sup>+</sup> T lymphocytes were mono-cultured or directly co-cultured for 72 h with autologous M1-like polarized macrophages and treated with 10 $\mu$ g/ml of either human IgG<sub>1</sub> isotype control antibody (white) or Durvalumab (black). (A) Representative contour plots with attached histograms correlating CFSE with PD-L1 (top panel) and PD-1 (bottom panel) staining in CD8<sup>+</sup> T lymphocytes from mono- (blue) and M1 M $\Phi$  co-cultures (red) treated with either human IgG<sub>1</sub> isotype control antibody (left panel) or Durvalumab (right panel). Drawn through (mono-cultured CD8<sup>+</sup> T lymphocytes) and dashed lines (co-cultured CD8<sup>+</sup> T lymphocytes) indicate median fluorescence intensities detected for PD-L1 and PD-1 staining. (B) PD-1 and (D) PD-L1 cell surface expression levels in CD8<sup>+</sup> T lymphocytes after indicated culture settings and treatments. (C) PD-1 cell surface expression levels in populations of CD8<sup>+</sup> T lymphocytes having divided one to six times after indicated culture settings and treatments. (B-D) Bar charts present mean values with SEM of median fluorescence intensity ratios examined in three independent experiments. The dashed lines mark an MFI ratio of "1". \* =  $p < 0.05$

In order to examine the effects of co-culture conditions and PD-L1 blockade by Durvalumab on the phenotype of M1 MΦ, immunofluorescence staining of PD-L1, CD206 and CD163 were performed (**Figure 50 A**) as well as mRNA levels of various macrophage-associated cytokines and chemokines were analyzed by qPCR (**Figure 51**).

In line with results from previous co-culture experiments (**section 4.2.7**), flow cytometric analysis revealed significantly higher PD-L1 cell surface levels in M1 MΦ from IgG<sub>1</sub> supplemented co-cultures with CD8<sup>+</sup> T lymphocytes than levels detected in respective mono-cultured M1 MΦ (MFI Ratio  $6.35 \pm 1.04$  vs.  $2.95 \pm 0.75$ ;  $p=0.006$ ) (**Figure 50 B**). Similar to the observation for CD8<sup>+</sup> T lymphocytes, adding Durvalumab to the culture media resulted in significantly reduced and similar PD-L1 cell surface levels in macrophages from both mono- (MFI Ratio  $1.26 \pm 0.03$  vs.  $2.95 \pm 0.75$ ) and co-culture conditions (MFI Ratio  $1.29 \pm 0.18$  vs.  $6.35 \pm 1.04$ ) compared to M1 MΦ from IgG<sub>1</sub> isotype control treated cultures (**Figure 50 B**). However, western blotting analyses of whole-cell lysates showed only a minor decrease in overall cellular PD-L1 level in M1 MΦ treated with Durvalumab compared to M1 MΦ treated with human IgG<sub>1</sub> isotype control (**Supplementary Figure 60 A**). In accordance with flow cytometry results, mRNA levels of PD-L1 were lower by trend in mono-cultured M1 MΦ treated with Durvalumab (0.71-fold) than in control antibody treated macrophages but higher in M1 MΦ from co-cultures supplemented with IgG<sub>1</sub> antibody (1.56-fold) in comparison to M1 MΦ from respective mono-cultures (**Supplementary Figure 60 B**). Interestingly, relative mRNA levels of PD-L1 in M1 MΦ after co-culture with CD8<sup>+</sup> T lymphocytes and addition of Durvalumab showed the highest value (3.18-fold), a clear contradiction to cell surface levels detected by flow cytometry (**Supplementary Figure 60 B**). CD206 cell surface levels were marginally lower in M1 MΦ after co-culture with CD8<sup>+</sup> T lymphocytes and IgG<sub>1</sub> isotype control antibody treatment in comparison to respective mono-cultured macrophages (MFI Ratio  $4.81 \pm 0.79$  vs.  $5.81 \pm 1.13$ ). PD-L1 blockade by Durvalumab did not affect CD206 surface levels in M1 MΦ from mono- (MFI Ratio  $5.50 \pm 1.17$ ) and co-culture conditions (MFI Ratio  $4.72 \pm 0.63$ ) compared to IgG<sub>1</sub> isotype control treated macrophages (**Figure 50 C**). Lastly, CD163 cell surface expression was very low in M1 MΦ from co-cultures with CD8<sup>+</sup> T lymphocytes supplemented with either IgG<sub>1</sub> control antibody (MFI Ratio  $2.42 \pm 0.73$ ) or Durvalumab (MFI Ratio  $2.29 \pm 0.32$ ) while CD163 was highly expressed to a similar extent at the cell surface of both control IgG<sub>1</sub> isotype control (MFI Ratio  $37.80 \pm 10.40$ ) and Durvalumab (MFI Ratio  $33.81 \pm 14.27$ ) treated macrophages from mono-cultures (**Figure 50 D**).



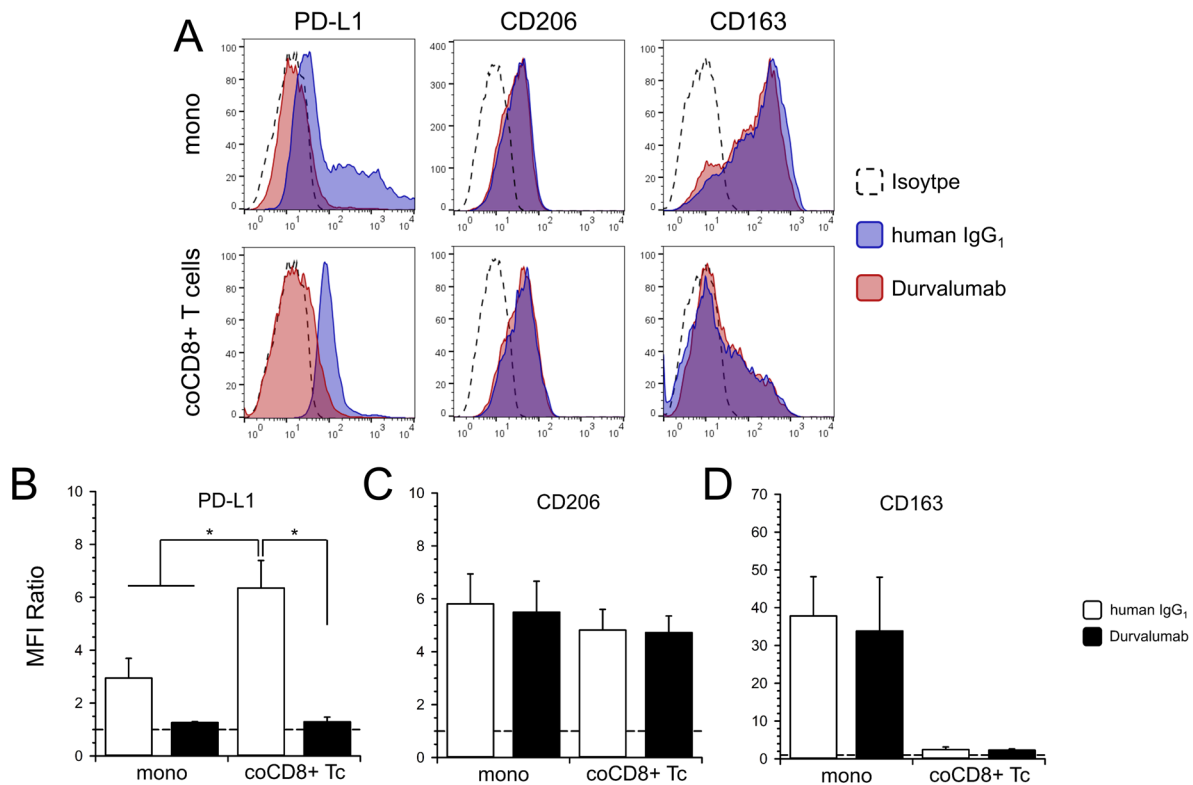


**Figure 50:** Cell surface expression levels of PD-L1, CD206 and CD163 in M1-polarized macrophages after co-culture with autologous activated CD8<sup>+</sup> T lymphocytes and treatment with Durvalumab. Primary human M1-polarized macrophages were mono-cultured or directly co-cultured with anti-CD3/CD28 pre-activated autologous CD8<sup>+</sup> T lymphocytes and treated with 10 $\mu$ g/ml of either human IgG<sub>1</sub> isotype control antibody (white, blue) or Durvalumab (black, red) for 72 h. (A) Representative histograms from flow cytometric analysis of PD-L1 (left), CD206 (middle) and CD163 (right) cell surface immunofluorescence staining in M1 M $\Phi$  after the indicated culture conditions and treatment. Signal specificities were verified by staining with respective isotype control antibodies (dashed). (B) PD-L1, (C) CD206 and (D) CD163 cell surface levels in M1 M $\Phi$  after indicated culture settings and treatments. Bar charts present mean values and SEM of median fluorescence intensity ratios examined in three independent experiments. The dashed lines mark an MFI ratio of “1”. \* = p<0.05

Relative quantification of macrophage-associated cytokine, chemokine and growth factor mRNA levels revealed markedly lower levels of IL-1 $\beta$  (0.42-fold; **Figure 51 A**), IL-6 (0.26-fold; **Figure 51 B**), IL-8 (0.19-fold; **Figure 51 C**), IL-10 (0.13-fold; **Figure 51 D**), TGF- $\beta$ 1 (0.24-fold; **Figure 51 E**) and VEGF (0.28-fold; **Figure 51 F**) in M1 M $\Phi$  from co-cultures with CD8<sup>+</sup> T lymphocytes that were supplemented with isotype control IgG<sub>1</sub> antibody than in respective M1 M $\Phi$  from mono-cultures. In contrast, TNF $\alpha$  mRNA levels in co-cultured M1 M $\Phi$  treated with human IgG<sub>1</sub> isotype control antibody were higher than in respective mono-cultured cells (3.33-fold; **Figure 51 G**). Interestingly, addition of Durvalumab to the medium of M1 M $\Phi$  mono-cultures resulted in higher mRNA levels of IL-1 $\beta$  (1.50-fold; **Figure 51 A**), IL-6 (2.06-fold; **Figure 51 B**), IL-8 (1.32-fold; **Figure 51 C**) and VEGF (1.11-fold; **Figure 51 F**) but lower levels of IL-10 (0.73-fold; **Figure 51 D**) and TGF- $\beta$ 1 (0.12-fold; **Figure 51 E**) in comparison to respective IgG<sub>1</sub> isotype control antibody treated M1 M $\Phi$ . In co-culture settings with CD8<sup>+</sup> T lymphocytes, Durvalumab treatment was associated with even higher TNF $\alpha$

mRNA levels in M1 M $\Phi$  than those detected in respective IgG<sub>1</sub> treated M1 M $\Phi$  (8.57-fold vs. 3.33-fold; **Figure 51 G**). TGF- $\beta$ 1 mRNA levels in Durvalumab treated M1 M $\Phi$  from co-culture conditions were also higher than levels in respective IgG<sub>1</sub> treated macrophages but still markedly lower than those levels detected in IgG<sub>1</sub> control antibody treated M1 M $\Phi$  from mono-cultures (0.62-fold vs. 0.24-fold; **Figure 51 E**). Durvalumab treatment in co-cultures with CD8<sup>+</sup> T lymphocytes did hardly affect the mRNA levels of IL1- $\beta$  (0.42-fold vs. 0.41-fold; **Figure 51 A**), IL-6 (0.37-fold vs. 0.24-fold; **Figure 51 B**), IL-8 (0.17-fold vs. 0.19-fold; **Figure 51 C**), IL-10 (0.11-fold vs. 0.13-fold; **Figure 51 D**) and VEGF (0.32-fold vs. 0.28-fold; **Figure 51 F**) in M1 M $\Phi$  compared to levels detected in macrophages from co-cultures supplemented with IgG<sub>1</sub> isotype control antibody.

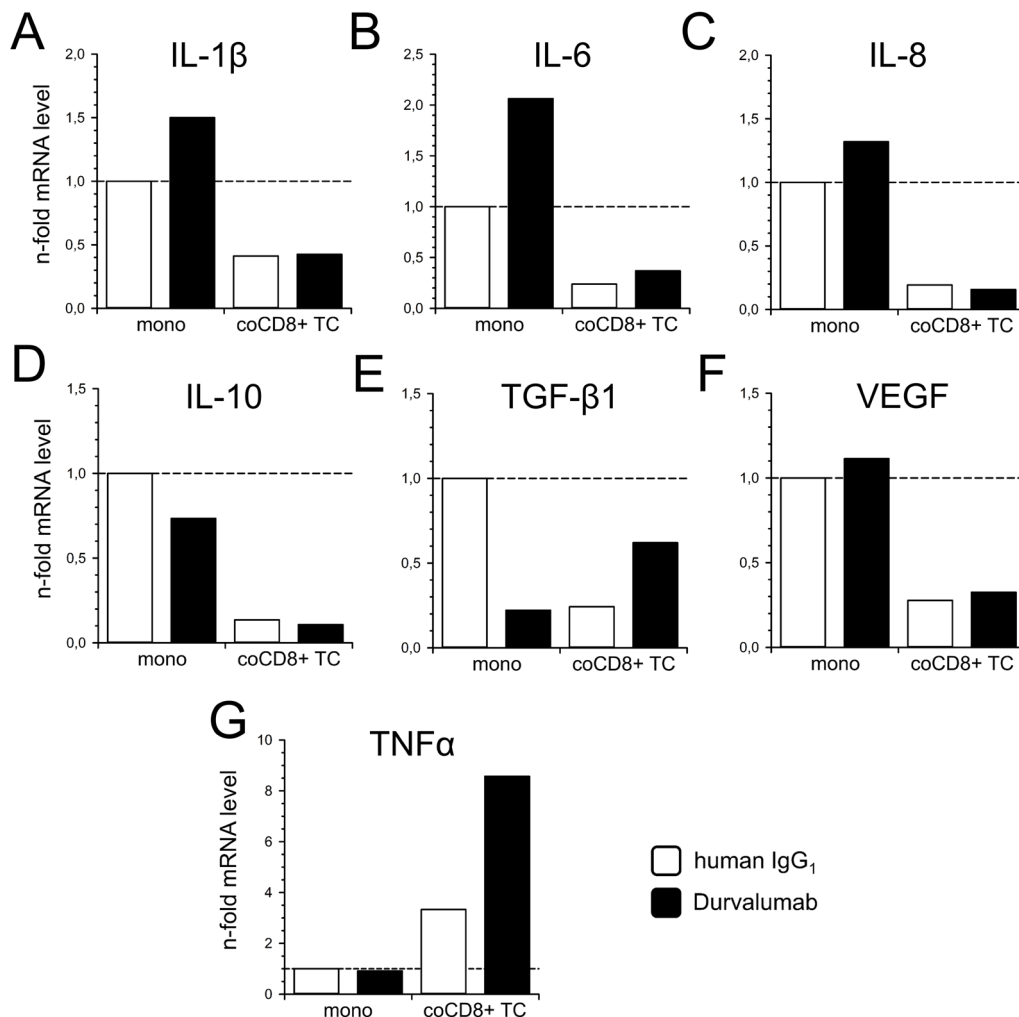


**Figure 51: Gene expression profiles of cytokines, chemokines and growth factors in M1-polarized macrophages after co-culture with autologous activated CD8<sup>+</sup> T lymphocytes and treatment with Durvalumab.** Primary human M1-polarized macrophages were mono-cultured or directly co-cultured with anti-CD3/CD28 pre-activated autologous CD8<sup>+</sup> T lymphocytes and treated with 10 $\mu$ g/ml of either human IgG<sub>1</sub> isotype control antibody (white) or Durvalumab (black) for 72 h. Relative mRNA levels of (A) IL-1 $\beta$ , (B) IL-6, (C) IL-8, (D) IL-10, (E) TGF- $\beta$ 1, (F) VEGF and (G) TNF $\alpha$  in M1 M $\Phi$  after indicated culture settings and treatments. Messenger RNA levels were normalized to respective GAPDH levels as well as levels detected in M1 M $\Phi$  from mono-cultures treated with IgG<sub>1</sub> isotype control antibody, indicated by dashed lines. Bar charts present mean values of technical triplicates resulting from one experiment.

Finally, it was investigated whether Durvalumab treatment in mono- and co-cultures of CD8<sup>+</sup> T lymphocytes and M1 MΦ affects the levels of cytokines, chemokines, effector molecules and growth factors secreted by macrophages (VEGF, IL-6 and IL-8) and CD8<sup>+</sup> T lymphocytes (IL-17A, soluble Fas ligand, Perforin, Granulysin, Granzyme A and Granzyme B) (**Figure 52**). Considering the macrophage-associated soluble factors, VEGF levels tended to be lower in supernatants of control IgG<sub>1</sub> antibody supplemented M1 MΦ co-cultures compared to respective mono-cultures (579.59 ±18.68 vs. 647.47 ±70.50 pg/ml). Moreover, Durvalumab treatment was associated with slightly lower VEGF levels in both M1 MΦ from mono- (605.92 ±46.76 vs. 647.47 ±70.50 pg/ml) and co-cultures (564.20 ±24.53 vs. 579.59 ±18.68 pg/ml) (**Figure 52 A**). IL-8 concentrations did not markedly differ between M1 MΦ from mono- and co-cultures supplemented with either IgG<sub>1</sub> control antibody (20.00 vs. 19.80 ng/ml) or Durvalumab (18.91 vs. 19.51 ng/ml) (**Figure 52 B**). In contrast to VEGF, IL-6 levels in co-culture supernatants were clearly higher in both IgG<sub>1</sub> (9.40 vs. 2.21 ng/ml) and Durvalumab (10.56 vs. 2.08 ng/ml) treated M1 MΦ cultures than in respective M1 MΦ mono-cultures (**Figure 52 C**). Notably, Durvalumab treatment did not affect IL-6 levels in culture supernatants of M1 MΦ mono- and co-cultures.

In terms of CTL-associated cytokines, concentrations of soluble Fas ligand were higher by 89.06 pg/ml in IgG<sub>1</sub> and by 129.40 pg/ml in Durvalumab treated CD8<sup>+</sup> T lymphocyte co-cultures compared to respective CD8<sup>+</sup> T lymphocyte mono-cultures (**Figure 52 D**). Similarly, Granulysin levels were clearly higher in supernatants of both IgG<sub>1</sub> (45.21 vs. 11.62 ng/ml) and Durvalumab (24.55 vs. 6.23 ng/ml) supplemented CD8<sup>+</sup> T lymphocyte co-cultures with M1 MΦ than in respective mono-cultures of CD8<sup>+</sup> T lymphocytes (**Figure 52 E**). The same trend applied to Granzyme B concentrations. Here, Granzyme B levels in co-culture supernatants of IgG<sub>1</sub> isotype antibody and Durvalumab treated CD8<sup>+</sup> T lymphocytes and M1 MΦ exceeded those levels detected in respective CD8<sup>+</sup> T lymphocyte mono-cultures by 7.31 ng/ml and 15.24 ng/ml, respectively (**Figure 52 F**). By trend, Perforin concentrations in supernatants of CD8<sup>+</sup> T lymphocytes co-cultured with M1 MΦ were higher than levels detected in CD8<sup>+</sup> T lymphocyte mono-culture supernatants irrespective of the treatment (IgG<sub>1</sub> isotype: 2.61 vs. 2.22 ng/ml; Durvalumab: 2.69 vs. 1.4 ng/ml) (**Figure 52 G**).

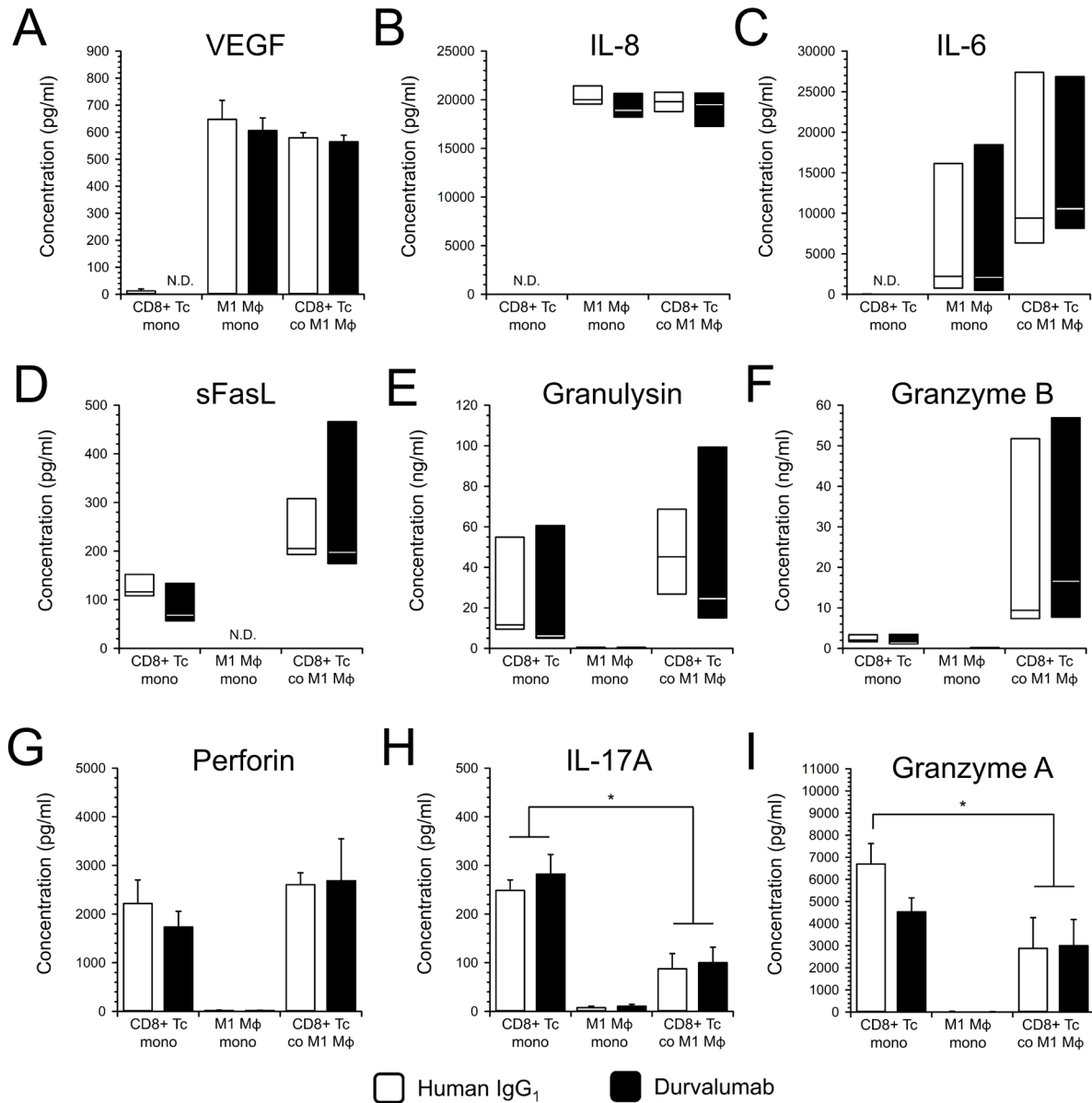


**Figure 52: Levels of T lymphocyte- and macrophage-associated cytokines, chemokines, growth factors and effector molecules in supernatants of directly co-cultured activated CD8<sup>+</sup> T lymphocytes and autologous M1-polarized macrophages treated with Durvalumab.** Pre-activated primary human CD8<sup>+</sup> T lymphocytes (CD8<sup>+</sup> Tc) and M1 Mφ were mono-cultured or directly co-cultured for 72 h and treated with 10 μg/ml of either human IgG<sub>1</sub> isotype control antibody (white) or Durvalumab (black). Concentrations of (A) VEGF, (B) IL-8, (C) IL-6, (D) soluble Fas ligand, (E) Granulysin, (F) Granzyme B, (G) Perforin, (H) IL-17A and (I) Granzyme A were measured by multiplex assay in the culture supernatant of indicated culture settings and treatments. Box plots present median values with quartiles (Q<sub>0.75</sub> as upper, Q<sub>0.25</sub> as lower deviation) and bar charts present mean values with SEM of three independent experiments. N.D. = not detectable; \* = p<0.05

In contrast to sFasL, Granulysin and Granzyme B levels, IL-17A concentrations were significantly lower in supernatants of both IgG<sub>1</sub> isotype control ( $87.48 \pm$  vs.  $248.60 \pm$  pg/ml;  $p=0.022$ ) and Durvalumab ( $100.09 \pm$  vs.  $282.24 \pm$  pg/ml;  $p=0.004$ ) treated co-culture settings compared to levels detected in respective CD8<sup>+</sup> T lymphocytes mono-cultures (Figure 52 H). The same applied to Granzyme A concentrations, which were lower by 3.82 ng/ml ( $p=0.041$ ) in IgG<sub>1</sub> and by 1.53 ng/ml in Durvalumab supplemented co-cultures than in supernatants of

mono-cultured CD8<sup>+</sup> T lymphocytes (**Figure 52 I**).

Taken together, having a closer look on the effects of Durvalumab on cytokine secretion by M1 MΦ and CD8<sup>+</sup> T lymphocytes, results described in **section 4.2.10** showed that Durvalumab treatment of activated CD8<sup>+</sup> T lymphocytes in mono-culture was associated with markedly decreased levels of effector molecules in culture supernatants. In contrast, analyses of normalized cytokine levels revealed elevated levels of IL-6, IFN $\gamma$ , IL17-A, sFasL, Granzyme A and Granzyme B in supernatants of CD8<sup>+</sup> T lymphocytes co-cultured with M1 MΦ and treated with Durvalumab in comparison to levels detected in supernatants of IgG<sub>1</sub> treated co-cultures (**Supplementary Figure 61**). Hence, data indicate that effects of Durvalumab on CD8<sup>+</sup> T lymphocytes differ in mono- and co-culture setting with M1 MΦ. Notably, same applied to the effect of Durvalumab on M1 MΦ, since mRNA levels of IL-1 $\beta$ , IL-6, IL-10, TGF- $\beta$ 1 and TNF $\alpha$  in M1 MΦ were differentially altered after Durvalumab treatment in mono- and co-culture with CD8<sup>+</sup> T lymphocytes (**Figure 51**).

#### **4.2.12 Durvalumab treatment has only minor effects on CD8<sup>+</sup> T lymphocytes and PancTu-I cells in direct co-culture settings**

Finally, it was investigated whether blocking of PD-L1 by application of Durvalumab in direct co-culture settings comprising activated CD8<sup>+</sup> T lymphocytes and PancTu-I cells causes alterations in the phenotype and/or proliferation of CD8<sup>+</sup> T lymphocytes (**Figure 53** and **Figure 54**), the differentiation and/or growth of PancTu-I cells (**Figure 55** and **Figure 56**) as well as release of selected effector molecules in the cell culture supernatants (**Figure 57**).

Starting with examinations of the phenotype and proliferation of CD8<sup>+</sup> T lymphocytes, flow cytometric analysis revealed no differences between the size of either IgG<sub>1</sub> isotype control or Durvalumab treated CD8<sup>+</sup> T lymphocytes after mono- (Mean FSC 431.33  $\pm$ 29.43 vs. 429.67  $\pm$ 32.30) and co-culture (Mean FSC 433.83  $\pm$ 28.67 vs. 433.00  $\pm$ 28.29) with PancTu-I cells (**Figure 53 A**). However, the granularity of CD8<sup>+</sup> T lymphocytes was lower by trend, but to a similar extent, in population from both IgG<sub>1</sub> control antibody (Mean SSC 151.33  $\pm$ 16.45 vs. 163.67  $\pm$ 18.59) and Durvalumab (Mean SSC 151.17  $\pm$ 16.66 vs. 162.00  $\pm$ 18.26) treated co-culture settings compared to those of CD8<sup>+</sup> T lymphocytes from respective mono-cultures (**Figure 53 B**). In terms of CD8<sup>+</sup> T lymphocyte proliferation, vital cell counting revealed significantly lower vital cell numbers of CD8<sup>+</sup> T lymphocytes after co-culture with PancTu-I cells and treatment with both IgG<sub>1</sub> (0.87  $\pm$ 0.02-fold) and Durvalumab (0.91  $\pm$ 0.06-fold) compared to mono-cultured and IgG<sub>1</sub> isotype control treated CD8<sup>+</sup> T lymphocytes (**Figure 53 C**). In line, the proportion of proliferating CD8<sup>+</sup> T lymphocytes from co-cultures treated with

IgG<sub>1</sub> isotype control ( $83.83 \pm 1.87\%$  vs.  $85.70 \pm 1.25\%$ ) or Durvalumab ( $83.57 \pm 1.94\%$  vs.  $85.73 \pm 1.02\%$ ) was lower by trend than in CD8<sup>+</sup> T lymphocyte populations from respective mono-cultures (**Figure 53 D**). However, western blotting did not show marked differences between total and phosphorylated ERK1/2 levels in CD8<sup>+</sup> T lymphocyte population from each culture setting (**Figure 53 E**). Analysis of CFSE profiles revealed that predominantly the proportion of CD8<sup>+</sup> T lymphocytes that had divided five to six times was lower in both IgG<sub>1</sub> and Durvalumab treated populations from co-cultures than those from respective mono-culture settings (**Figure 53 F**).

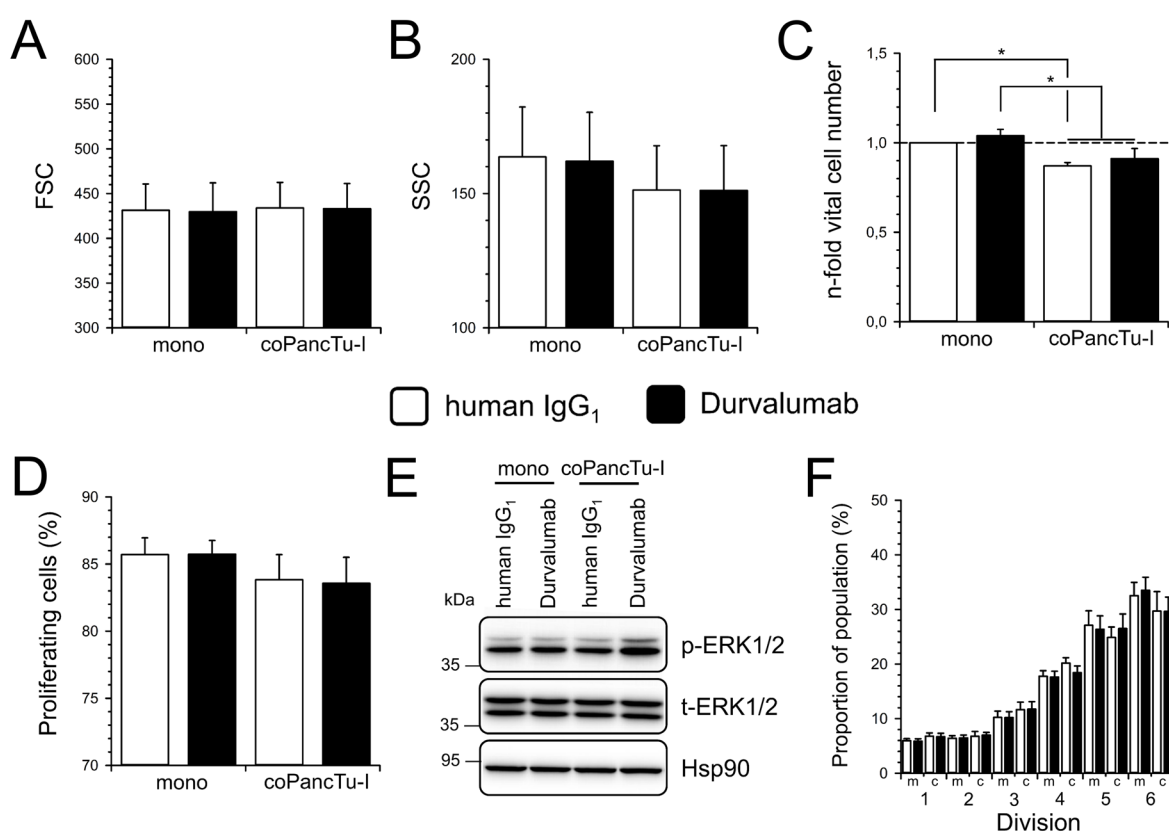


**Figure 53: Phenotype and proliferation of activated CD8<sup>+</sup> T lymphocytes after direct co-culture with PancTu-I cells and treatment with Durvalumab.** Pre-activated primary human CD8<sup>+</sup> T lymphocytes were mono-cultured or directly co-cultured for 72 h with PancTu-I cells and treated with 10 μg/ml of either human IgG<sub>1</sub> isotype control antibody (white) or Durvalumab (black). Comparison of (A) FSC medians, (B) SSC medians, (C) n-fold vital cell numbers and (D) the proportion of proliferating cells within CD8<sup>+</sup> T lymphocyte populations after indicated culture settings and treatments. Bar charts present mean values with SEM of three independent experiments. (E) Representative western blot of whole-cell lysates from CD8<sup>+</sup> T lymphocytes after indicated culture settings and treatments. Hsp90 was detected as loading control. Molecular weights in kDa are indicated according to the applied standard. (F) CFSE profiles of proliferating CD8<sup>+</sup> T lymphocytes after 72 h of mono- (m) or co-culture (c) and indicated treatment. Data present mean proportions with SEM of T lymphocytes having divided one to six times in three independent experiments. \* =  $p < 0.05$

Moreover, subsequent flow cytometric analysis revealed no remarkable changes of PD-1 cell surface expression levels in the proliferating population of CD8<sup>+</sup> T lymphocytes from IgG<sub>1</sub> or Durvalumab treated mono- (MFI Ratio  $5.21 \pm 0.75$  vs.  $5.05 \pm 0.74$ ) and co-cultures with PancTu-

I cells (MFI Ratio  $5.22 \pm 0.51$  vs.  $4.64 \pm 0.13$ ) (**Figure 54 A**). Correlation of CFSE profiles with PD-1 staining showed that PD-1 cell surface levels in both IgG<sub>1</sub> antibody and Durvalumab treated T lymphocyte populations from co-culture with PancTu-I cells tended to be lower than those detected in populations from respective mono-cultures, especially in CD8<sup>+</sup> T lymphocytes having divided one to five times. Notably, this tendency applied to a similar extent in CD8<sup>+</sup> T lymphocyte populations from both IgG<sub>1</sub> isotype control and Durvalumab treated co-cultures (**Figure 54 B**). With respect to PD-L1 expression, co-culture with PancTu-I cells did not affect PD-L1 cell surface levels in the proliferating population of IgG<sub>1</sub> control antibody treated CD8<sup>+</sup> T lymphocytes compared to respective CD8<sup>+</sup> T lymphocytes from mono-cultures (MFI Ratio  $1.84 \pm 0.13$  vs.  $1.67 \pm 0.18$ ). In contrast, Durvalumab treatment was associated with markedly lower but still similar PD-L1 cell surface expression level in CD8<sup>+</sup> T lymphocytes from both mono- (MFI Ratio  $1.14 \pm 0.17$ ;  $p=0.073$ ) and co-culture settings (MFI Ratio  $1.24 \pm 0.08$ ;  $p=0.037$ ;  $p=0.046$ ) compared to levels detected in respective IgG<sub>1</sub> supplemented cultures (**Figure 54 C**).

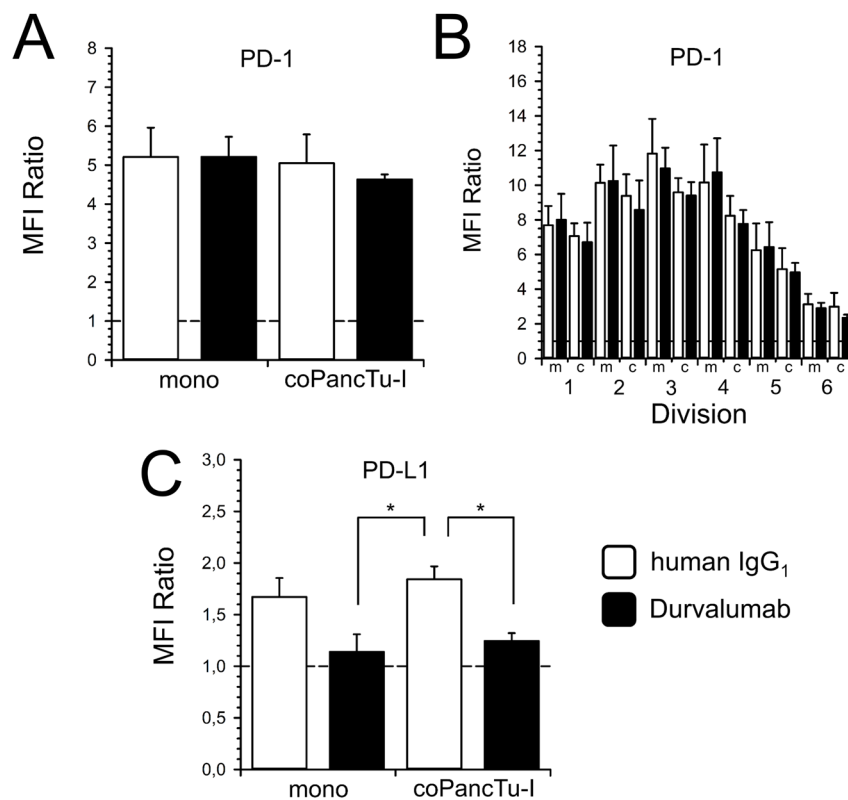


**Figure 54: PD-1 and PD-L1 cell surface expression levels in activated CD8<sup>+</sup> T lymphocytes after direct co-culture with PancTu-I cells and treatment with Durvalumab.** Pre-activated primary human CD8<sup>+</sup> T lymphocytes were mono-cultured (m) or directly co-cultured (c) for 72 h with PancTu-I cells and treated with 10 $\mu$ g/ml of either human IgG<sub>1</sub> isotype control antibody (white) or Durvalumab (black). (A) PD-1 and (C) PD-L1 cell surface expression levels in CD8<sup>+</sup> T lymphocytes after indicated culture settings and treatments. (B) PD-1 cell surface expression levels in populations of CD8<sup>+</sup> T lymphocytes having divided one to six times after indicated culture settings and treatments. (A-C) Bar charts present mean values with SEM of median fluorescence intensity ratios examined in three independent experiments. The dashed lines mark an MFI ratio of “1”. \* =  $p < 0.05$

Next, the effect of Durvalumab on growth and differentiation status of mono- and co-cultured PancTu-I was examined. As observed in previous experiments (**section 4.2.9**), the confluency of PancTu-I cells after co-culture with activated CD8<sup>+</sup> T lymphocytes was significantly lower than in mono-cultures ( $p < 0.001$ ) (**Figure 55 A+B**). However, PancTu-I cells from IgG<sub>1</sub> isotype control and Durvalumab treated mono- ( $64.30 \pm 2.80\%$  vs.  $67.06 \pm 6.86\%$ ) and co-cultures ( $17.68 \pm 3.47\%$  vs.  $15.16 \pm 2.73\%$ ) showed very similar levels of confluency (**Figure 55 B**). In line, both IgG<sub>1</sub> ( $0.60 \pm 0.16$ -fold;  $p = 0.018$ ) and Durvalumab ( $0.65 \pm 0.11$ -fold;  $p = 0.018$ ) treated PancTu-I cell populations co-cultured with CD8<sup>+</sup> T lymphocytes showed significantly and similarly lower vital cell numbers compared to respective PancTu-I cells from mono-cultures (**Figure 55 C**).

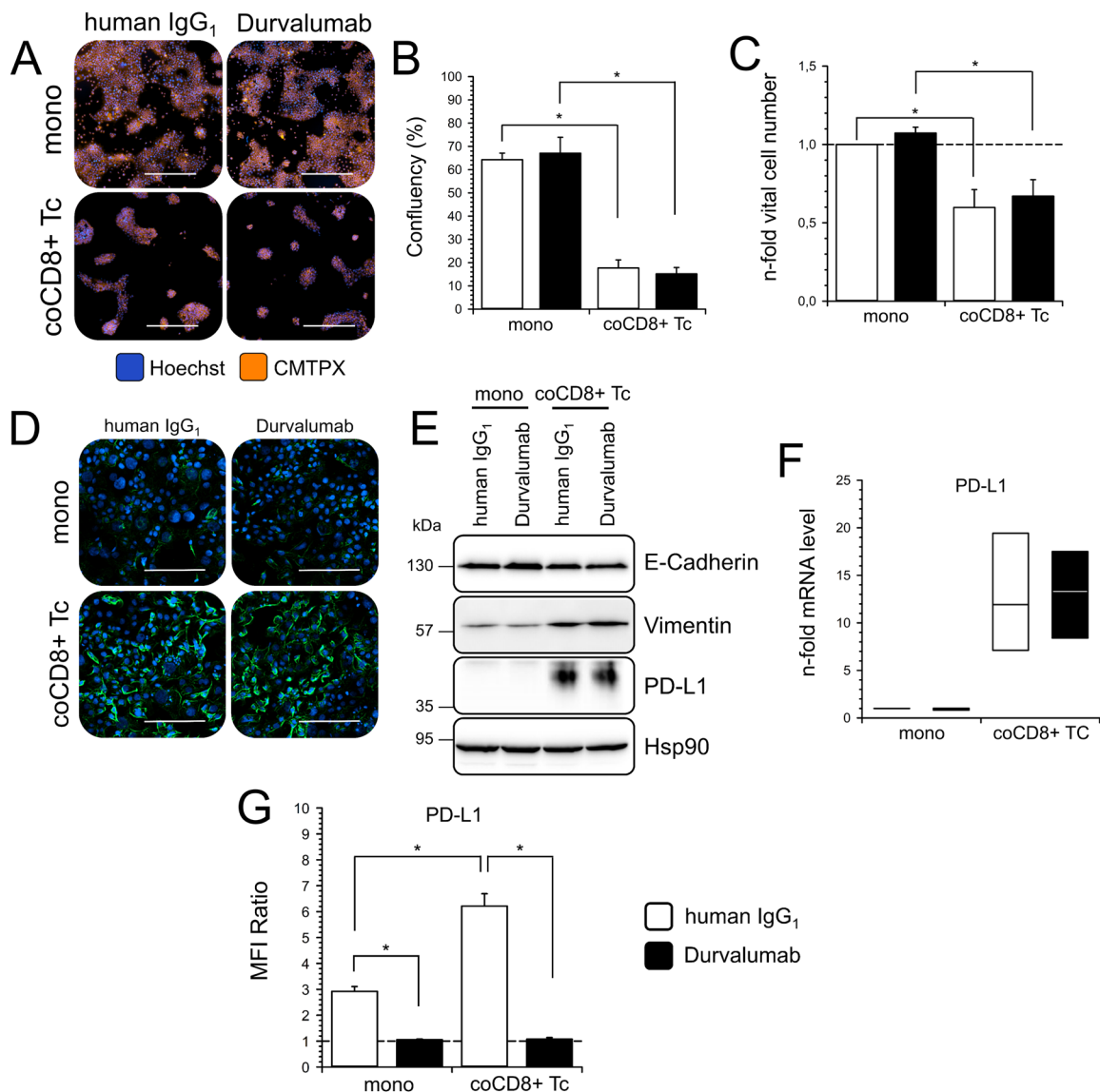


**Figure 55: Cell growth, phenotype and PD-L1 expression levels of PancTu-I cells after direct co-culture with activated CD8<sup>+</sup> T lymphocytes and Durvalumab treatment.** PancTu-I cells were mono-cultured or directly co-cultured for 72 h with anti-CD3/CD28 pre-activated CD8<sup>+</sup> T lymphocytes and treated with 10 µg/ml of either human IgG<sub>1</sub> isotype control antibody (white) or Durvalumab (black). (A) Representative fluorescence microscopical images of PancTu-I cells stained with CellTracker Red CMTPIX dye (orange) and Hoechst (blue) after indicated culture settings and treatments. Scale bar = 500 µm



(B) Confluency and (C) n-fold vital cell numbers of PancTu-I cell after indicated culture settings and treatments. Bar charts presents mean values with SEM of three independent experiments. (D) Representative fluorescence microscopical images of PancTu-I cells stained for PD-L1 (green) after indicated culture settings and treatments. Nuclei were stained with Hoechst. Scale bar = 200  $\mu\text{m}$ . (E) Representative western blot of whole-cell lysates from PancTu-I cells after indicated culture settings and treatments. Hsp90 was detected as loading control. Molecular weights in kDa are indicated according to the applied standard. (F) Relative PD-L1 mRNA levels in PancTu-I cells after indicated culture settings and treatments. Messenger RNA levels were normalized to respective GAPDH levels as well as levels detected in PancTu-I cells from mono-cultures treated with IgG<sub>1</sub> isotype control antibody. Box plots present median values with quartiles (Q<sub>0.75</sub> as upper, Q<sub>0.25</sub> as lower deviation) of three independent experiments. (G) PD-L1 cell surface expression levels in PancTu-I cells after indicated culture settings and treatments. Bar chart presents mean values with SEM of median fluorescence intensity ratios examined in three independent experiments. \* =  $p < 0.05$

Subsequent analysis of PD-L1 protein levels by immunofluorescence staining (**Figure 55 D**) and western blotting (**Figure 55 E**) revealed clearly higher levels in PancTu-I cells after direct co-culture with activated CD8<sup>+</sup> T lymphocytes than after mono-culture. Notably, both detection methods indicated no remarkable difference concerning PD-L1 levels between treatments with IgG<sub>1</sub> isotype control antibody and Durvalumab, respectively. The same trend applied to results from qPCR analysis on PD-L1 mRNA levels, which were markedly increased to a similar extent in both IgG<sub>1</sub> (11.92-fold) and Durvalumab (13.32-fold) treated PancTu-I cells from co-culture compared to detected levels in mono-cultured PancTu-I cells (**Figure 55 F**). However, while flow cytometric analysis verified significantly higher PD-L1 cell surface levels in PancTu-I cells from co-cultures treated with IgG<sub>1</sub> isotype control antibody compared to PancTu-I cells from respective mono-cultures (MFI Ratio  $6.22 \pm 0.48$  vs.  $2.92 \pm 0.19$ ), treatment with Durvalumab was associated with almost complete loss of PD-L1 signal at the cell surface in both mono- (MFI Ratio  $1.05 \pm 0.03$ ) and co-cultured PancTu-I cells (MFI Ratio  $1.07 \pm 0.06$ ) (**Figure 55 G**). Since the antibody clone E1L3N, which has been used for immunostaining and western blotting, binds to the cytoplasmic domain of PD-L1, these controversial findings from flow cytometric analysis to western blotting, immunostaining and qPCR analysis indicate that antibody clone MIH1, which has been used for immunostaining in flow cytometric analyses, competes with Durvalumab for a similar epitope within the extracellular variable immunoglobulin region of PD-L1. Noteworthy, these findings clearly disprove the statement by Karzai and colleagues, who reported that the clone MIH1 does not compete with Durvalumab and, therefore, can be used for PD-L1 detection subsequent to Durvalumab treatment [282]. Notably, these findings also suggest that decreased PD-L1 cell surface expression levels in CD8<sup>+</sup> T lymphocytes and M1 M $\Phi$  after Durvalumab treatment observed in **section 4.2.10** and **4.2.11** are based on the blockade of the detection antibody's binding epitope by Durvalumab. However, overall these data show that Durvalumab treatment of PancTu-I cells in mono- and co-culture with activated CD8<sup>+</sup> T lymphocytes does not affect the proliferation and PD-L1 cell surface expression levels in PancTu-I cells.

Analyses of the expression profiles of genes coding for proteins that are associated with a mesenchymal (vimentin, L1CAM, Zeb-1) or epithelial (E-Cadherin) differentiation status of PDAC cells, revealed no differences between vimentin mRNA levels in IgG<sub>1</sub> control antibody treated PancTu-I cells from mono- and co-culture with CD8<sup>+</sup> T lymphocytes (**Figure 56 A**). Addition of Durvalumab was associated by trend with lower vimentin mRNA levels in PancTu-I cells from mono-cultures (0.82 ±0.04-fold) while slightly higher expression levels were detected in PancTu-I cells from co-cultures treated with Durvalumab in comparison to IgG<sub>1</sub> treated PancTu-I cells from co-cultures (1.10 ±0.19-fold vs. 0.99 ±0.13-fold) (**Figure 56 A**). Interestingly, results from western blotting analysis of vimentin levels showed clearly higher levels in PancTu-I cells from co-culture with CD8<sup>+</sup> T lymphocytes, but indicated no effect of Durvalumab on vimentin expression levels (**Figure 55 E**). L1CAM was not detectable on protein level by western blotting of PancTu-I whole-cell lysates, but mRNA levels were significantly higher in both IgG<sub>1</sub> (1.60 ±0.21-fold; p=0.018) and Durvalumab (1.54 ±0.10-fold; p=0.028) treated PancTu-I cells after co-culture with CD8<sup>+</sup> T lymphocyte compared to those levels detected in PancTu-I cells from respective mono-cultures (**Figure 56 B**). Similarly, Zeb-1 mRNA levels were significantly higher in IgG<sub>1</sub> control antibody (5.32 ±0.71-fold; p=0.015) and markedly higher in Durvalumab (3.43 ±1.31-fold) treated PancTu-I cells from co-cultures with CD8<sup>+</sup> T lymphocytes in comparison to PancTu-I cells from respective mono-cultures (**Figure 56 C**). Moreover, significantly higher E-cadherin mRNA levels were detected in PancTu-I cells from IgG<sub>1</sub> supplemented co-culture settings than in IgG<sub>1</sub> isotype control treated mono-cultured PancTu-I cells (1.86 ±0.15-fold; p=0.002) (**Figure 56 D**). Interestingly, Durvalumab treatment was associated with contrary effects on E-cadherin expression in PancTu-I cells from mono- and co-culture settings. Thus, E-Cadherin mRNA levels in PancTu-I cells from mono-cultures were lower by trend (0.70 ±0.12-fold) while being significantly higher in Durvalumab treated PancTu-I cells from co-culture (2.53 ±0.17-fold vs. 1.86 ±0.15-fold; p=0.006) in comparison to levels detected in respective IgG<sub>1</sub> isotype control treated PancTu-I cells (**Figure 56 D**). Notably, relative E-cadherin mRNA levels in PancTu-I from each culture setting correlated diametrically with E-cadherin protein levels detected by western blotting in respective culture and treatment settings (**Figure 55 E**).

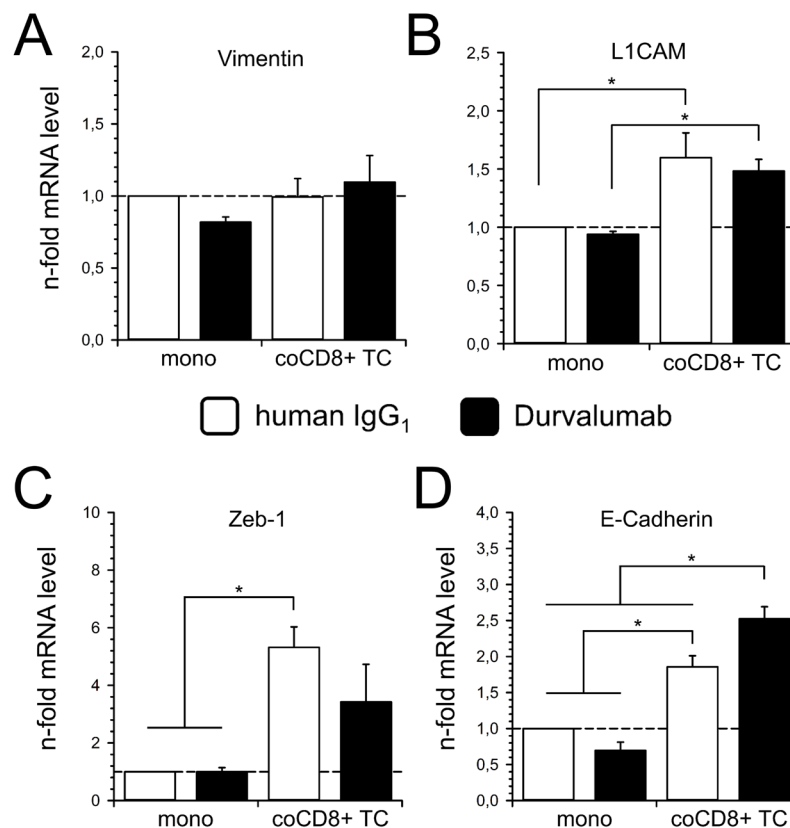


**Figure 56: Gene expression profiles of EMT-associated proteins in PancTu-I cells after co-culture with activated CD8<sup>+</sup> T lymphocytes and treatment with Durvalumab.** PancTu-I cells were mono-cultured or directly co-cultured for 72 h with anti-CD3/CD28 pre-activated CD8<sup>+</sup> T lymphocytes and treated with 10 μg/ml of either human IgG<sub>1</sub> isotype control antibody (white) or Durvalumab (black). Relative mRNA levels of (A) Vimentin, (B) L1CAM, (C) Zeb-1 and (D) E-cadherin in PancTu-I cells after indicated culture settings and treatments. Messenger RNA levels were normalized to respective GAPDH levels as well as levels detected in PancTu-I cells from mono-cultures treated with IgG<sub>1</sub> isotype control antibody, indicated by dashed lines. Box plots present median values with quartiles (Q<sub>0.75</sub> as upper, Q<sub>0.25</sub> as lower deviation) and bar charts present mean values with SEM of three independent experiments. \* = p<0.05

Lastly, the effects of Durvalumab treatment on the release of selected cytokines, chemokines, effector molecules and growth factors secreted by PancTu-I cells (VEGF, IL-6 and IL-8) or activated CD8<sup>+</sup> T lymphocytes (IL-17A, soluble Fas ligand, Perforin, Granzyme A and Granzyme B) in mono- and co-culture settings were investigated by multiplex analysis of the cell culture supernatants (Figure 57).

In line with results from previous experiments (section 4.2.8 and Supplementary Figure 58), VEGF (905.17 ± 114.95 vs. 524.60 ± 87.62 pg/ml) and IL-6 (509.70 ± 141.11 vs. 138.48 ± 23.19 pg/ml; p=0.007) levels were markedly higher, but IL-8 (305.74 ± 35.94 vs. 612.80 ± 72.64 pg/ml; p=0.002) concentrations were significantly lower in supernatants of IgG<sub>1</sub> isotype control treated co-cultures than in respective PancTu-I cell mono-cultures (Figure 57 A-C). Interestingly, Durvalumab treatment was associated with elevated levels of VEGF (1011.45 ± 209.23 pg/ml; Figure 57 A), IL-6 (596.10 ± 138.35 pg/ml; Figure 57 B) and IL-8 (360.61 ± 64.42 pg/ml;

**Figure 57 C)** in co-cultures but not in mono-cultures of PancTu-I cells.

Considering T cell-associated effector molecule concentrations, multiplex analyses revealed even opposing effects of Durvalumab treatment in mono- and co-cultures of CD8<sup>+</sup> T lymphocytes. In line with results shown in **section 4.2.10**, IL-17A, soluble Fas ligand, Perforin, Granzyme A and Granzyme B levels were markedly decreased in mono-cultures of Durvalumab treated CD8<sup>+</sup> T lymphocytes compared to levels detected in supernatants of IgG<sub>1</sub> isotype control treated CD8<sup>+</sup> T lymphocytes. In contrast, elevated concentrations of IL-17-A ( $188.35 \pm 78.29$  vs.  $152.42 \pm 47.41$  pg/ml; **Figure 57 D**), soluble Fas ligand ( $213.45 \pm 55.74$  vs.  $154.08 \pm 15.90$  pg/ml; **Figure 57 E**), Perforin ( $2.82 \pm 0.73$  vs.  $2.02 \pm 0.27$  ng/ml; **Figure 57 F**), Granzyme A ( $6.65 \pm 4.00$  vs.  $4.51 \pm 2.11$  ng/ml; **Figure 57 G**) and Granzyme B ( $8.96 \pm 2.71$  vs.  $6.69 \pm 1.01$  ng/ml; **Figure 57 H**) were detected in Durvalumab treated co-cultures of CD8<sup>+</sup> T lymphocytes and PancTu-I cells in comparison to IgG<sub>1</sub> isotype control treated co-cultures.

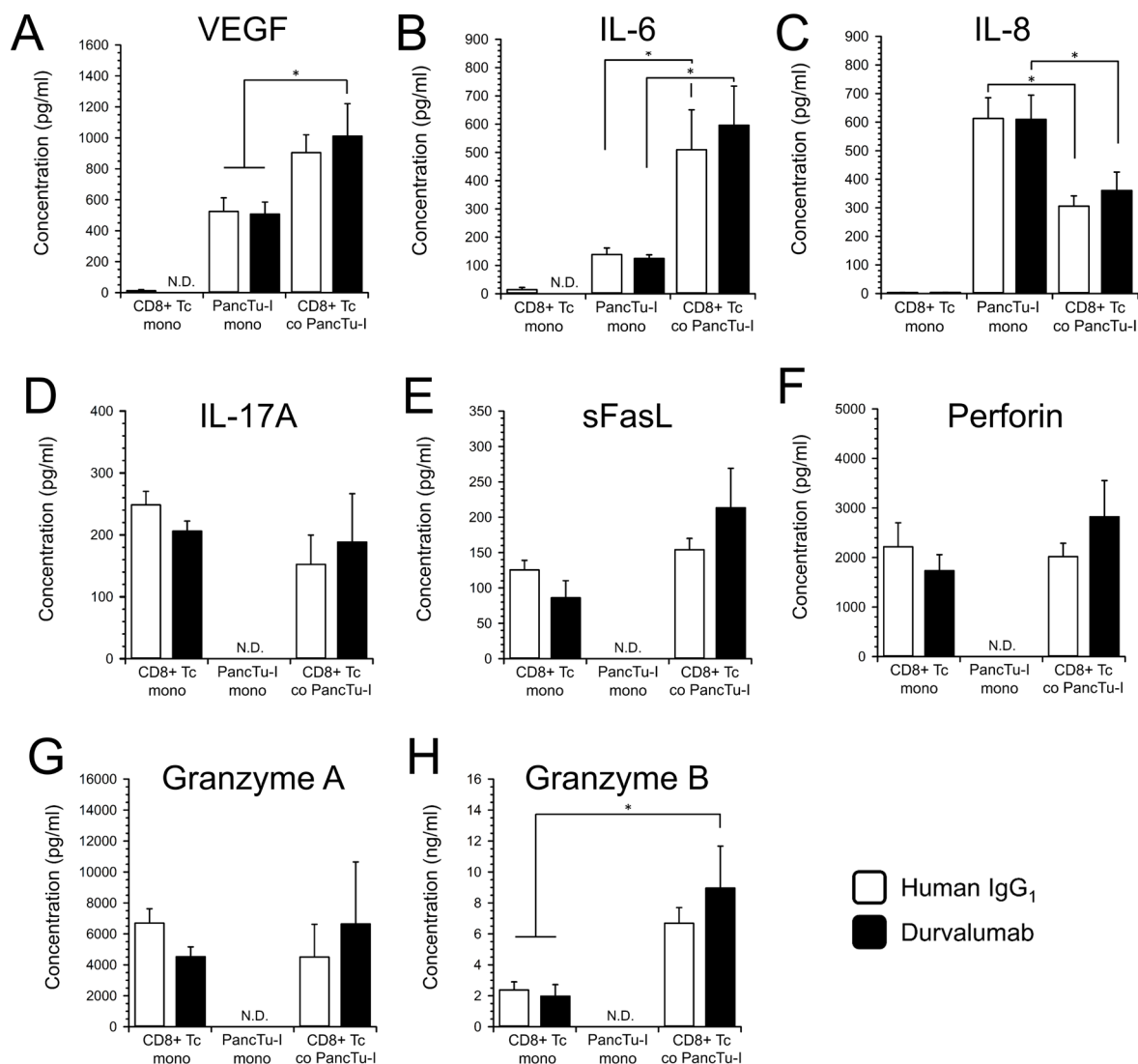


**Figure 57: Levels of cytokines, chemokines, growth factors and effector molecules in supernatants of directly co-cultured activated CD8<sup>+</sup> T lymphocytes and PancTu-I cells treated with Durvalumab.** Pre-activated primary human CD8<sup>+</sup> T lymphocytes (CD8<sup>+</sup> Tc) and PancTu-I cells were mono-cultured or directly co-cultured for 72 h and treated with 10µg/ml of either human IgG<sub>1</sub> isotype control antibody (white) or Durvalumab (black). Levels of (A) VEGF, (B) IL-6, (C) IL-8, (D) IL-17A, (E) soluble Fas ligand, (F) Perforin, (G) Granzyme A and (H) Granzyme B were measured by multiplex assay in the culture supernatant of indicated culture settings and treatments. Bar charts present mean values with SEM of three independent experiments. N.D. = not detectable; \* = p<0.05

Taken together, effects due to co-culture of activated CD8<sup>+</sup> T lymphocytes with PancTu-I cells on the proliferation and cytokine secretion of CD8<sup>+</sup> T lymphocytes as well as the proliferation, differentiation status and PD-L1 expression levels in PancTu-I cells that had been shown in previous experiments (section 4.2.8 and 4.2.9) were also observed in IgG<sub>1</sub> isotype control treated co-culture settings. However, gene expression and multiplex analyses indicated that the expression of EMT markers in PancTu-I cells as well as the cytokine secretion by PancTu-I and CD8<sup>+</sup> T lymphocytes are diametrically affected by Durvalumab treatment in mono-cultures compared to co-culture settings.

## 5. Discussion

### 5.1 Classification of the PD-L1 status by immunohistochemistry in general and as a prognostic biomarker in PDAC

Antagonistic monoclonal antibodies inhibiting the binding site between PD-1 and PD-L1 started to enter clinical application in 2014 and today progressively supplement standard cancer therapy regimens due to the impressive results from clinical trials [283,284]. However, the increasing amount of data from clinical trials also highlights that the molecular mechanisms behind the effect of PD-1/PD-L1 antagonists are rather poorly understood and, therefore, not as simple as proposed [219]. Currently, the answer to the central question “Which cancer patient benefits from immune checkpoint inhibitor therapy” is always attributed with a “might” and clinical trials are predominantly guided by the trial-and-error principle in the hope to get an optimal positioning on the market for checkpoint inhibitors. The reason for this dilemma is the lack of biomarkers that allow a reliable prediction of patient responses. To date, classification of PD-L1 status in tumor biopsies with certified companion or complementary diagnostics (**Table 3**) represents the only approved method for patient stratification [285,286]. Like in this study, these assays are based on the immunohistochemical detection of PD-L1 in tumor tissues followed by rating of PD-L1 staining according to a standardized scheme. Next to *in situ* hybridization for the analysis of genomic aberrations, immunohistochemistry (IHC) has become the gold standard for the disease-associated analysis of antigens in tissues. In this context, the fast performance and high sensitivity as well as the potential to directly correlate antigen presence with pathohistological alterations *in situ* are the main advantages of IHC-based analyses [287]. Nevertheless, at the same time IHC exhibits serious pitfalls that especially complicate the inquiry of tumor-markers like PD-L1. One of the main problems is given by the tumor heterogeneity. Commonly, PD-L1 is detected in whole tissue sections or tumor micro arrays (TMA) from a single tumor biopsy, which represent just a small area of the whole tumor. In the present study, it has been shown that notable PD-L1 staining is located in distinct tumor areas while it is mainly low or even absent in the rest of the tumor mass. In order to consider tumor heterogeneity in the best possible way, in this study whole tissue sections with an area of up to 6 cm<sup>2</sup> were analyzed. Moreover, taking the low overall PD-L1 staining into account, an immunoreactivity scoring system (IRS) was applied, which combines data from grading of both the proportion of PD-L1<sup>+</sup> cells and the staining intensity and, therefore, generates an in-depth scoring of PD-L1 staining. Finally, Tissue Scores were generated by calculating the mean instead of the median values of all rated microscopic fields of view in each tissue section.

Thereby, even small PD-L1<sup>+</sup> tumor areas contributed to the resulting Tissue Scores. The restricted diagnostic conclusiveness of single-biopsies for the determination of PD-L1 status has been addressed in several other studies. Thus, Gniadek and colleagues reported that immunohistochemical analysis of PD-L1 expression in just one biopsy from different areas of pulmonary squamous cell carcinoma and adenocarcinoma leads to different status classifications within the same tumor [288]. Similar findings were reported by Ilie and colleagues who showed that in 48% of NSCLC biopsies PD-L1 expression does not match with levels detected in respective resected tumors [289]. However, in the case of unresectable and/or advanced disease stages biopsies are the only available tumor specimens and material is often limited in view of the numerous following tests.

Another major problem of IHC-based PD-L1 classification in tumor biopsies is the timing of probing. As shown in this and other studies and discussed in more detail in **section 5.4**, PD-L1 expression is strongly inducible in tumor and stromal cell populations by various cytokines like IFN $\gamma$ , TNF $\alpha$  and GM-CSF [290–292]. Moreover, recent studies reported that PD-L1 expression in neoplastic cells is upregulated via NF- $\kappa$ B signaling in response to chemotherapeutic treatment [293]. Therefore, both changes in the local microenvironment and therapeutic interventions after biopsy withdrawal may markedly affect tumoral PD-L1 status.

Besides these tumor biological obstacles, IHC as the method of choice represents a critical variable for the performance of PD-L1 detection. The four U.S. FDA approved companion and complementary diagnostics each utilize different PD-L1 targeting antibody clones (28-8, 22C3, SP142 and SP263) that bind to different epitopes. Furthermore, each kit has been optimized for a specific staining protocol and different staining platforms, either the Autostainer Link 48 developed by Dako or the VENTANA BenchMark Ultra series by Roche [285,294]. For the immunohistochemical detection of PD-L1 in this study, the anti-PD-L1 clone E1L3N from Cell Signaling was used and staining was performed on the BOND-MAX Autostainer system with the Polymer Refine Kit, both provided by Leica. Although not implicated in any approved complementary diagnostic kit, the E1L3N clone is well accepted for its specificity and has been used in numerous studies (31<sup>st</sup> August 2019: 161 citations listed at CiteAb.com) as well as laboratory-developed tests [228,295]. Interestingly, several studies investigated the performance of the E1L3N anti-PD-L1 antibody in comparison to the performance of the anti-PD-L1 clones 28-8, 22C3, SP142 and SP263. Overall, the E1L3N clone showed comparable performance and high specificity [296–300]. Nevertheless, it has to be emphasized that all of these studies used different IHC protocols. Moreover, in some studies staining was performed manually while others used autostainer platforms. In general, IHC performance is highly

susceptible to any variations in the sample preparation and staining procedure, e.g. differences in the antigen retrieval buffer's pH value, the use of different signal amplification kits or secondary antibodies and even differences in tissue sampling, preparation and storage of FFPE tissues. Therefore, comparative analysis of antibody performances under non-standardized conditions have to be considered critically. Underscoring this fact, own efforts to establish PD-L1 staining with the SP142 clone on the BOND-MAX autostainer system were not satisfactory in terms of sensitivity and staining intensity (data not shown).

Finally, staining evaluation represents the most controversially discussed step in the assessment of tissue-based PD-L1 status. In this study, the POLE Score has been established, which characterizes PD-L1 staining in all tumor compartments (tumor and stroma) exhibiting marked intra- and inter-tumoral heterogeneity. The POLE Score includes the overall PD-L1 staining in the tumor (P-Score), the proportion of PD-L1 staining located to stromal and epithelial/neoplastic cells (O-Score), the PD-L1 staining in tumor-associated lymph follicles (L-Score) as well as the local distribution and clustering of cells stained for PD-L1 (E-Score). Comparing the POLE Score with the approved complementary and companion diagnostic assays, the P-Score mostly resembles the central statement of the established assays displaying both similarities and differences. Here, each microscopic field of view has been rated by applying cutoffs of  $\leq 1\%$  and  $\geq 1\%$  to classify PD-L1 staining. Similarly, a cutoff of  $\geq 1\%$  is also applied in the 28-8, 22C3 and SP142 assays in order to discriminate PD-L1 negative from PD-L1 positive specimens [301]. In contrast to the POLE Score procedure, the marketed assays directly evaluate the tissue sections in total instead of each microscopic field. However, the resulting larger size of the area of interest makes the assessment more sophisticated especially when it comes to the discrimination of PD-L1 staining in tumor and stromal cells as well as when tumor tissues exhibit a high proportion of areas that are excluded from grading, e.g. necroses. Nevertheless, from a "time investment" point of view, the analysis of tissues sections in total is much faster than the POLE Score procedure and, therefore, more applicable in diagnostic routine for experienced pathologists. Furthermore, the approved assays discriminate more than the three grades, 0%,  $< 1\%$  and  $\geq 1\%$ , assessed in this study. For example, the Ventana SP142 assay discriminates between 0-1% (negative), 1-5% (low/weak), 5-50% (medium) and  $> 50\%$  (high/strong) of total area stained for PD-L1, grades that have been proven to be still well distinguishable by eye [301]. In the procedure of Tissue Score assessment, the putative lack of complexity in the rating of microscopic fields of view is compensated by application of the IRS system and calculation of mean values. Therefore, the Tissue Score classifies overall PD-L1 staining even more differentiated than commercial assays.



In the initial phase of PD-L1 status evaluation for diagnostic purposes only tumor cell-associated PD-L1 expression was regarded as a prognostic factor. However, in the recent two to three years descriptive and functional studies highlighted that in some tumor entities PD-L1 is rather expressed in stromal cell populations than tumor cells and stromal PD-L1 also contributes to the suppression of anti-tumor immune responses [228,274,302,303]. A pronounced stromal participation in PDAC-associated PD-L1 expression has been also identified in the present study. Therefore, tumor- and stromal-associated PD-L1 staining has been quantified separately and rated by the O-Score that indicates whether PD-L1 staining is predominantly located to tumor or stromal cells or to both by a similar extent. Although several other studies already reported on PD-L1 expression in PDAC [267,268,304–306], this study is the first one which showed that PD-L1 staining is predominantly located in the stromal compartment of PDAC [264,307]. Even though the diagnostic significance of stromal PD-L1 is still controversially discussed, the Ventana SP142 and SP263 assay provided by Roche as well as the 22C3 pharmDx assay by Dako recently implicated the scoring of stromal PD-L1 staining at least for the assessment of PD-L1 status in specimens from distinct tumor entities like urothelial carcinoma and NSCLC [301]. Notably, both POLE Score and all diagnostically approved assays only rate membranous PD-L1 staining in tumor cells while stromal cells are rated as PD-L1 positive independent of the cellular localization, a fact that is owed to the much smaller cytoplasmatic compartment in stromal cells and especially immune cell populations. Therefore, staining resolution makes it not possible to discriminate cytoplasmatic from membranous IHC staining in stromal cell population. In the present study, *in vitro* experiments indicated that PD-L1 expression by stromal cell populations like macrophages is not necessarily associated with an immunosuppressive phenotype but rather a stimulatory phenotype, a finding that is discussed in more detail in **section 5.3**. In contrast, Zhang and colleagues showed in a genetically-modified PDAC mouse model that PD-L1 expression by tumor infiltrating myeloid cell populations contributes to tumor progression [274]. Similar findings were reported by Lau and colleagues, who showed in an orthotopic tumor genetically-modified mouse model that PD-L1 expression by both tumor and tumor-infiltrating immune cells represents a negative regulator of T cell-mediated anti-tumor responses [308]. However, these and many other recent studies just started to consider stromal PD-L1 expression and, therefore, its various facets in the regulation of anti-tumor responses are still poorly understood. Taken together, a better understanding of the impact of tumor and/or stroma related PD-L1 expression might help to explain why some patients do not respond to anti-PD-1/PD-L1 therapies and, therefore, will be

important for the patient-specific optimization of checkpoint inhibitor-based immunotherapy [265,303,309].

The third component of the POLE Score, the L-Score, addressed PD-L1 staining in tumor-associated lymph follicles. These *de novo* formed tertiary lymphoid organs (TLOs) are commonly found within or at the periphery of chronically inflamed tissues associated with autoimmune diseases and tumors [310,311]. On the histological level, TLOs resemble the structure of secondary lymphoid organs with B cell follicles, T cell zones and high endothelial venules as well as scattered distribution of APCs like dendritic cells [312,313]. In the present study, tumor-associated lymph follicles have been identified in 66.1% of PDAC tumor tissues and 50% of peritumoral tissues showing remarkable intra- and inter-tumoral differences in terms of PD-L1 staining. Interestingly, numerous studies in various tumor entities, e.g. colorectal cancer, lung cancer, malignant melanoma and breast cancer, reported that the presence of TLOs within, in the periphery or at the invasive margin of tumors correlates with high levels of TILs. Moreover, the presence of TLOs have been associated with a better prognosis in terms of overall-survival and tumor relapse [314–317]. In line with the assumption that TLOs represent a source for TILs, PD-L1<sup>-</sup> tumor-associated lymph follicles were only found in tissues with absent overall PD-L1 staining (P0) in the present study. Notably, the role of PD-1/PD-L1 signaling has been only investigated in the context of secondary lymphoid organs and T cell priming but not in TLOs so far. However, *in situ* results from the present study indicate that PD-L1 staining is primarily located in T cell zones as well as the follicles margin and co-localizes with the presence of CD3<sup>+</sup> and CD68<sup>+</sup> cells. In line with this observation, *in vitro* results revealed that high PD-L1 expression is associated with a pro-inflammatory macrophage polarization and T lymphocyte activation. Moreover, this and other studies previously showed that secretion of IFN $\gamma$ , the most potent inducer of PD-L1 expression, is a surrogate marker for T cell activation [318]. Therefore, strong PD-L1 staining in tumor-associated lymph follicles might be rather associated with an activated pro-inflammatory response than an immunosuppressive microenvironment, which causes T cell exhaustion prior to tumor infiltration. Noteworthy, none of the approved complementary and companion diagnostics currently determines TLO-associated PD-L1 status, another fact highlighting the uncertainty of its prognostic value for immune checkpoint-targeted therapy.

At last, the present study revealed differences in the spatial distribution of PD-L1 stained cells, which appeared to be either randomly spread or locally clustered, an observation that is graded by the E-Score. The rationale for the assessment of PD-L1<sup>+</sup> cell clusters is quite reasonable. Since PD-L1 signaling *via* PD-1 requires cell-cell contact, these clusters might represent hot

spots for PD-1/PD-L1-mediated immune suppression [133]. In order to foster this assumption, it would be necessary to examine via PD-1/PD-L1 co-staining whether also PD-1<sup>+</sup> cells are located within these clusters. However, indicating that PD-L1 clusters indeed have prognostic relevance, the Ventana SP142 assay routinely assesses whether PD-L1<sup>+</sup> immune cell clusters are present or not in urothelial cancer tissues. According to the manufacturer's information, these clusters are primarily composed of lymphocytes, macrophages, dendritic cells and granulocytes. In line with this, co-staining of CD68 and PD-L1 in the context of the present study demonstrated that TAMs are frequently present within PD-L1<sup>+</sup> cell clusters.

In 2016, when the present study started, PD-L1 was the most considered biomarker for stratification of patients that might benefit from therapy with PD-1/PD-L1 antagonists. Therefore, the aforementioned assays (**Table 3**) have been developed in parallel and, thereby, caused great confusion in the diagnostic community. Considering the afore discussed methodical obstacles and the marked differences in terms of evaluation criteria between the assays, major concerns were raised about the diagnostic interchangeability of these assays. In order to evaluate the performance comparability of these four assays, the Pathology Committee of the International Association for the Study of Lung Cancer initiated the Blueprint study in cooperation with industrial stakeholders, namely AstraZeneca, Roche, Bristol Myers-Squibb, Dako and Merck [294,319]. Results from Phase I of the Blueprint project showed similar performance of 22C3, 28-8 and SP263 assays. However, staining intensities markedly varied between the assays and the SP142 assay even showed overall lower proportions of cells stained for PD-L1 [294]. Thus, this feasibility study revealed that PD-L1 classification varied in 37% of the cases depending on which assay and scoring system was applied [229]. In phase II of the Blueprint study, the interchangeability of the pharmDx 22C3, pharmDx 28-8, Ventana SP142, Ventana SP263 and Dako 73-10 assay were tested by the analysis of 81 lung cancer specimens according to each assay's indicated scoring system. Noteworthy, analyses were simultaneously performed by independent pathologists from different institutes in order to assess observer variances. In brief, results from the phase II Blueprint study showed high comparability regarding PD-L1 staining of tumor cells in the 22-C3, 28-8 and SP263 assay as well as very strong interobserver assay-specific concordance. However, while the SP142 assay showed lower sensitivity, the 73-10 revealed higher sensitivity for the staining of tumor cell-associated PD-L1 in comparison to the 22-C3, 28-8 and SP263 assay. Moreover, the comparability and assay-specific interobserver concordance in terms of immune cell-associated PD-L1 staining was very poor [230]. In the ongoing phase IIB of the Blueprint study, results from PD-L1 classification in large tumor specimens will be compared to those obtained in small biopsies

and cytologies from the same tumor. The final phase of the Blueprint study plans to investigate the comparability of the approved assays in predicting the response rates and outcomes in a patient cohort treated with PD-1 or PD-L1 antagonists. However, already at the present stages it has been clearly shown that PD-L1 status classification markedly varies between the available assays and reliable assay evaluation requires qualified and experienced pathologists. Notably, similar results were reported by the German equivalent to the Blueprint study, the “Harmonisierungsstudie” [320].

Having provided an overview on the major difficulties in the assessment of PD-L1 expression in tumor tissues, the major question is: “What is the prognostic relevance of currently available companion diagnostics for the treatment with PD-1 and PD-L1 antagonists?”. Addressing this question, several studies, e.g. KEYNOTE-001, CheckMate-057 and CheckMate-067 trial, reported that PD-L1 positivity determined by IHC correlates with improved response rates as well as prolonged overall and progression-free survival in comparison to the PD-L1 negative subgroup, [321–323]. Hence, the KEYNOTE-001 trial revealed an objective response rate of 45% towards treatment with Pembrolizumab in NSCLC patients if  $\geq 50\%$  of the tumor cells showed PD-L1 staining [324]. Nevertheless, in the same study, 11% of patients showing PD-L1 expression in less than 1% of the tumor cells, and thereby regarded as PD-L1 negative tumors, also displayed objective responses towards Pembrolizumab treatment [324]. Noteworthy, the results from KEYNOTE-001 do not represent an individual case but rather a general observation. Thus, Gibney and colleagues summarized in 2016 that no study has reported an IHC-based PD-L1 status thresholding that consistently predicted both positive and negative responses towards PD-1 or PD-L1 antagonist treatment in any tumor entity [325]. At present (2<sup>nd</sup> September 2019), the assessment of the PD-L1 status by U.S. FDA approved companion diagnostics has been declared to be indicative for the treatment of triple-negative breast cancer and urothelial carcinoma patients with Atezolizumab as well as the treatment of NSCLC, Head & Neck squamous cell carcinoma, urothelial carcinoma, gastric cancer, cervical cancer and esophageal cancer patients with Pembrolizumab (<https://www.fda.gov/drugs/resources-information-approved-drugs>).

In contrast, the application of Atezolizumab and Pembrolizumab in other tumor entities as well as all approvals for Durvalumab, Nivolumab, Avelumab and Cemiplimab are independent of the tissue-based PD-L1 status (Data source: <https://reference.medscape.com/>, 02.09.2019 11:40). Nevertheless, three years ago a PD-L1 positive tissue status was only required for the treatment of NSCLC patients with Pembrolizumab [325]. Therefore, the predictive relevance of PD-L1 assessment has markedly increased.

In respect of the present study, the central question is: “Does the POLE Score add any potential diagnostically relevant information to the established assays?”. As already outlined, the P- and O-Score are equivalent to the Tumor Proportion Score (TPS) and the Immune Cell Score (IC) assessed by most of the available companion and complementary diagnostics. Moreover, grading of the overall presence of PD-L1<sup>+</sup> cell clusters (presented by the E-Score) is also implicated in the Ventana SP142 assay. All in all, the POLE Score includes all parameters of PD-L1 staining that are assessed by the available U.S. FDA approved assays. In addition, the POLE Score also classifies PD-L1 staining in tumor-associated lymph follicles, a variable that is not included in any other assay. However, according to the current literature and the results from the present study, TLOs might indeed have prognostic significance. Here, it has been shown *in situ* that PD-L1 staining in tumor-associated lymph follicles correlates with high T cell infiltration as well as strong intra-tumoral overall PD-L1 staining, which is predominantly located to stromal cells. Furthermore, *in vitro* experiments revealed that PD-L1 expression is predominantly induced by cytokines like IFN $\gamma$ , which is characteristic for a pro-inflammatory immune response, as well as that high PD-L1 levels are associated with an activated T lymphocyte status and pro-inflammatory macrophages polarization. In turn, these results suggest that PD-L1 staining in tumor-associated lymph follicles represents a surrogate marker for tumor infiltration by activated T lymphocytes. Interestingly, besides tumor mutational burden, tumor infiltration by CTLs, which is discussed on more detail in **section 5.4**, currently represents one of the most promising markers that might improve the diagnostic conclusiveness for patient stratification in combination with the assessment of the tumor PD-L1 status [325,326].

Summarizing all these tumor-specific and methodical-related factors that have been shown to markedly affect the assessment of tumor PD-L1 status, the best way to examine the predictive significance of the POLE Score would be its application on tumor tissue specimens obtained from patients prior to treatment with one of the approved PD-1 or PD-L1 targeting antagonistic antibodies followed by correlation of the POLE Score parameters with objective response rates, progression-free and overall survival. Moreover, it would be interesting to investigate whether different POLE Scores are assessed in pre-treated patients, who underwent chemo-/radiotherapy or other therapeutic interventions that do not include tumor resection, compared to treatment-naive patients and whether POLE Scores change in the course of therapy, a factor that is widely discussed but poorly investigated. In this context, a major challenge will be the threshold finding for each parameter, since evaluation of PD-L1 is not a simple yes-or-no question. In the present study, only the Tissue Score threshold (PD-L1<sup>high</sup>  $\geq 0.8$ ), which is based

on the significant correlation with post-surgical patient survival, has been set in dependence on a clinic-pathological parameter, while all other thresholds were either based on median values or presence and absence of a marker. However, the general validity of patient survival as a suitable marker for correlational analysis is uncertain, since mortality of PDAC patients that undergo curative surgical resection are essentially affected by the patient's recovery from surgery as well as the pre-existence of clinically undetectable micro metastases [60,327]. The major relevance of these factors for survival of PDAC patients is supported on the one hand by the marked differences in post-surgical survival, ranging from 0 to 103 months within the present cohort, despite the homogeneity in TNM staging (86.4% T3N1M0) and on the other hand by the fact that even patients with T3N0M0 tumor stages, who underwent R0 resection, often develop tumor relapses at secondary sites like the liver or the lung [328]. Additionally highlighting the questionable validity of PD-L1 status as a prognostic marker for patient survival, a positive correlation between PD-L1 expression and patient prognosis in PDAC and other tumor entities was also reported [228,265,329]. Taken together, the most accurate way for thresholding of PD-L1 staining and assessing its tumor-biological value is based on multiple-marker staining, which allows to evaluate PD-L1 expression within a cellular context, a topic that is discussed in more detail in **section 5.4**.

## **5.2 The clinical potential PD-1 and PD-L1 antagonists for the treatment of PDAC patients**

Due to the asymptomatic initiation and progression in early stages and the lack of reliable markers for preventive screening, less than 20% of PDAC patients exhibit disease stages suitable for curative surgical resection at the time of diagnosis. The major proportion of PDAC patients show either locally advanced or metastatic disease stages. The only available treatment options for these patients are palliative chemotherapeutic regimens that according to the patient's physical status include gemcitabine monotherapy, gemcitabine in combination with nanoparticle albumin-bound paclitaxel (nab-paclitaxel) as well as FOLFIRINOX, a combination of 5-fluorouracil, irinotecan, leucovorin and oxaliplatin [65,330]. The fact that gemcitabine represents the standard treatment option in the palliative setting since almost 20 years and no efficient strategies for the treatment of advanced disease stages have been developed so far, clearly highlights the poor clinical progress in the treatment of PDAC [237]. Therefore, the impressive results from clinical trials using monoclonal antagonistic antibodies to target co-inhibitory immune checkpoint molecules CTLA-4 (Tremelimumab and Ipilimumab), PD-1 (Nivolumab, Pembrolizumab and Cemiplimab) or PD-L1 (Durvalumab,

Atezolizumab and Avelumab) for the therapy of various hard-to-treat tumor entities raised the hope for soon clinical progression in the treatment of PDAC [197,224,235,272].

In comparison other tumor entities like NSCLC or malignant melanoma, analyses of PD-L1 staining in the present cohort indicated that overall PD-L1 expression in PDAC is rather low, since only 30.3% of the specimens were graded with a Tissue Score of  $\geq 0.8$  (Tissue Score maximum value = 5). In line with this, Nomi and colleagues analyzed a cohort of 51 human PDAC cases and reported that PD-L1 staining was found in only 39.2% of the cases [304]. Moreover, in a large cohort of 453 human PDAC cases, Birnbaum and colleagues found up-regulated PD-L1 mRNA levels even only in 19% of the specimens [266]. In view of these results, PD-1 or PD-L1 targeted therapy might be beneficial only for a subgroup of PDAC patients. However, the present study also showed that marked PD-L1 expression in PDAC is restricted to distinct tumor areas, namely the tumor invasive margin and the tumor-lymph follicle interface. Considering this, it has to be noted that both areas were not found in every tissue section of the present cohort and, therefore, PD-L1 absence in the respective tissue section certainly is not a verification for the lack of PD-L1 expression in the tumor. As discussed in **section 5.1**, tumor heterogeneity as well as dynamic regulation of PD-L1 expression are the main reasons for the limited significance of PD-L1 status assessment in biopsies. Aggravating this situation, in PDAC patients even tumor material from biopsies is rare, because only few studies analyzed tissue samples from primary and/or secondary site in advanced or metastasized disease stages. Therefore, most of the current knowledge on PD-L1 expression in advanced stages of PDAC is acquired from analyses of endogenous PDAC mouse models. Considering this situation, the question is whether PD-L1 is a suitable target in over 80% of PDAC patients or not. Indeed, the results from this and other studies indicate that PD-L1 expression is related to malignancy-associated alterations in the pancreas and goes along with the dedifferentiation of neoplastic PDECs, an essential step in the process of tumor cell dissemination. Hence, similar to the findings presented in this study, Wang and colleagues reported that PD-L1 expression is absent in healthy pancreatic tissue, except for pancreatic islets, while PD-L1 was expressed in pancreatic tumor tissue and high expression levels correlated with poor tumor differentiation [267]. Notably, increased PD-L1 expression in malignant compared to healthy tissue has been reported for several other tumor entities, e.g. sarcoma, cervical cancers, prostate cancer, gastric cancer and melanoma [331]. Moreover, preliminary data on IHC-based PD-L1 staining analyses in a cohort of PDAC patients exhibiting already metastasized disease stages revealed that PD-L1 is expressed in both primary tumor tissues and liver metastases (unpublished data). Taken together, according the results from the present study, PD-L1 is expressed in both early

and advanced/metastatic stages of PDAC in primary and secondary tumors, especially in tumor areas that are markedly encountered by immune cell populations, and, therefore, represents a potential target for the treatment with antagonistic antibodies. In line with this, several pre-clinical studies making use of endogenous PDAC mouse models reported that targeting the PD-1/PD-L1 axis fosters anti-tumor responses and, thereby, causes either notable tumor regression or even complete remission in some cases [274,304,332].

However, results from clinical trials evaluating the therapeutic benefit of PD-1 and PD-L1 antagonists for the treatment of locally restricted and advanced/metastasized stage PDAC patients are rare or disappointing so far [333]. Briefly summarized, clinical trials testing anti-PD-L1 antibodies in monotherapy for the treatment patient with advanced/metastasized stages of PDAC failed to show any therapeutic benefit [334,335]. For example, a randomized phase II study investigating the potential of Durvalumab either in monotherapy or combination with Tremelimumab as second-line treatment of metastatic PDAC revealed poor overall survival of 3.6 vs. 3.1 months and low disease control rates (partial responses + stable disease + complete remission) of 6% and 9%, respectively [335]. Furthermore, PD-1 and PD-L1 antagonist are currently tested in ongoing clinical trials for the treatment of borderline resectable PDAC and advanced/metastatic stages in combination with common chemotherapeutic agents like gemcitabine or nab-paclitaxel, stereotactic radiation therapy, other checkpoint inhibitors targeting CTLA-4 or Lag-3, cancer vaccines like CRS-207 and GVAX, oncolytic viruses like reolysin as well as small molecule inhibitors and many more [333]. Here, especially the combination of chemotherapeutic regimens with checkpoint inhibitors targeting PD-1, PD-L1 and/or CTLA-4 appears promising, since PDAC is characterized by a relatively low tumor mutational burden in comparison to other tumor entities like malignant melanomas that show high response rates towards immune checkpoint inhibitors [29,98]. Such a strategy intends to prime the release of neoantigens from tumor cells by chemotherapeutic drugs, in order to generate anti-tumor immune responses that are supported by the application of checkpoint inhibitors. In view of this, Renouf and colleagues reported promising preliminary results from a randomized phase II study on the benefit of adding Durvalumab and Tremelimumab to the first-line treatment of metastatic PDAC with gemcitabine and nab-paclitaxel. This combinatorial regimen was associated with partial responses in 73% of the patients and a disease control rate of 100%. Moreover, median progression-free survival was 7.9 months. Therefore, this phase II study is still ongoing and a phase III trial is planned [336].

Another promising combinatorial treatment strategy represents the combination of PD-1/PD-L1 antagonists with GVAX, a whole tumor vaccine consisting of irradiated, GM-CSF secreting



PDECs [209]. In other studies, this immune-stimulatory vaccine has been shown induce a pro-inflammatory M1-like macrophage polarization, which is characterized by the increased capability for antigen-presentation and co-stimulation as well as the secretion of cytokines that support T<sub>H</sub>1 responses [58,73,260,261]. Since PDAC is characterized by a marked infiltration with TAMs with both pro- and anti-inflammatory properties and GM-CSF is a potent inducer of PD-L1 expression in both M1- and M2-like polarized human macrophages as shown in the present study, the combination of GVAX with PD-1/PD-L1 antagonists for the treatment of PDAC patients represents a rational concept [58,80,87]. Notably, the anti-tumoral efficiency of checkpoint inhibitors in combination with GVAX has been already reported in two pre-clinical studies using PDAC mouse models [210,337]. In general, PDAC is regarded as a poorly immunogenic tumor entity which is characterized by low overall CTL infiltration and high stromal abundance of immune suppressive cell populations like MDSCs, TAMs and Tregs [62,63,338]. With respect to the potential therapeutic efficiency of checkpoint inhibitors, recent concepts indicate that so-called “cold” or “immune-excluded” tumors have to be converted into “hot” tumors [339]. Therefore, a major obstacle for the success of checkpoint inhibitors in PDAC might be the preparation of the tumor to enable CTLs and other cytotoxic immune cell populations to infiltrate into the tumor. Besides the aforementioned low tumor mutational burden and the immune suppressive stromal immune cell populations in PDAC, the entire stromal compartment, meaning both the cellular and acellular compartment, is discussed as a key factor that impairs tumor infiltration by CTLs [62]. However, the stromal barrier function is a highly controversial discussed topic in PDAC progression, since there are studies that support the “barrier” hypothesis while other studies indicate that the stromal compartment encapsulates the tumor and, thereby, prevents its faster progression and more aggressive invasion [62,67,276].

In summary, the results obtained in the present study in context with the current literature suggest that PD-L1 represents a druggable target in PDAC. However, the results from first clinical trials show that blocking of the PD-1/PD-L1 signaling axis in monotherapy is not an effective strategy to generate a clinically relevant anti-tumor response. Instead, combinatorial strategies that aim at impairing PDAC-specific immune exclusion and suppression characteristics are more promising [333]. In view of these strategies, it has to be noted that especially the combination of PD-1/PD-L1 antagonists with CTLA-4 has been shown to be associated with severe immune-related adverse events, a concern that has to be taken into serious consideration since many PDAC patients display a poor physical state [216,234]. Moreover, a recent study by De Sousa Linares and colleagues indicated that the PD-L1

antagonists Avelumab, Atezolizumab and Durvalumab display a better performance than PD-1 antagonists Nivolumab and Pembrolizumab in blocking PD-1/PD-L1 signaling [340]. However, PD-L1 antagonists do not interfere with PD-L2 signaling, whose role in PDAC is poorly understood. Finally, it has to be highlighted that recent studies suggest a cell-specific, PD-1 independent role for PD-L1, a topic that is discussed in more detail in **section 5.3**.

### 5.3 Intrinsic regulation and cell-specific role of PD-L1

PD-L1 is a type I transmembrane protein that specifically binds via its complementary determining-like regions (CDRs) within the membrane immunoglobulin variable domain to PD-1 [341]. The subsequent initiation of PD-1/PD-L1-mediated co-inhibitory signaling in T lymphocytes has been assumed for a long time to be the only function of PD-L1. However, recently growing evidence has emerged that PD-L1 also exerts intrinsic functions that are independent of its binding to PD-1 and even cell type-specific. Therefore, some of these PD-1-dependent and -independent PD-L1 functions, which have been reported in tumor cells, macrophages and CD8<sup>+</sup> T lymphocytes, are discussed in the following with respect to their relevance for the findings presented in this study.

PD-L1 expression and stability is highly regulated by extrinsic and intrinsic factors. On the genetic level, aberrant PD-L1 expression in tumor cells has been reported to be associated with copy number amplifications of chromosome 9p24, the genetic locus of PD-L1 [342,343]. Interestingly, in PDAC 9p24 amplifications and deletions as well as translocations have been identified (Dessen P., & Huret JL., <http://atlasgeneticsoncology.org/Bands/9p24.html>, 04.09.2019 11:20). Epigenetically, PD-L1 expression has been shown to be regulated by DNA methylation and histone modifications as well as various micro RNAs, which either cause stabilization or destabilization of PD-L1 mRNA [344,345]. Moreover, in several tumor entities the disruption of the 3' untranslated region (UTR) has been identified as an essential mechanism that fosters PD-L1 mRNA stability [346]. Each of these mechanisms represents a reasonable explanation for the aberrant expression as well as differences in levels and inducibility of PD-L1 in PDAC cell lines that have been analyzed in the present study. However, which of the proposed mechanism applies to which PDAC cell line has to be clarified in future studies by genome sequencing as well as analyses of histone modifications and DNA methylation patterns. In the case of H6c7eR-pBp and H6c7eR-kras cells that represent models for benign and premalignant PDECs, respectively, aberrant PD-L1 expression is not attributed to endogenous acquired genomic alterations but to immortalization with human papillomavirus 16 (HPV16)

oncoproteins E6 and E7, which have been reported to induce strong PD-L1 expression [347]. Notably, on the transcriptional level PD-L1 expression is regulated by various signaling pathways, which are either induced *via* extracellular signals or due to genetic alterations that cause constitutive activation of oncogenic signaling pathways [331]. The role of these predominantly extrinsic PD-L1 inducing pathways are extensively discussed **in section 5.4**.

Protein stability of PD-L1 is regulated by various post-translational modifications (PTMs) including phosphorylation, N-glycosylation and ubiquitination as well as protein-protein interactions [348]. N-glycosylation is exclusively found in the extracellular domain at asparagine residues N35, N192, N200 and N219 [349]. In this context, Li and colleagues showed that especially N-glycosylation at N192, N200 and N219 prevents the binding of GSK3 $\beta$ , which otherwise phosphorylates PD-L1 at T180 and S184 and, thereby marks PD-L1 for ubiquitination and subsequent degradation [349]. Therefore, N-glycosylation has been revealed to be an important regulator of PD-L1 stability during maturation and subcellular transportation via the ER/Golgi system as well as for internalization and subsequent degradation of membrane located PD-L1 [349,350]. In the latter case, the four lysine residues within the cytoplasmic domain represent targets for ubiquitination by E3 ligases [348,351]. In contrast, PD-L1 interaction with CMTM4/-6 has been shown to inhibit ubiquitination and, thereby, leads to PD-L1 stabilization as well as increased cell surface levels [352]. In regard to the impact of PTMs on PD-L1 binding capacity, structural analyses indicated that N-glycosylation does neither affect the binding of PD-1 nor the binding of therapeutic antagonistic antibodies to PD-L1 [232,341]. However, the fact that only functional, membrane-associated PD-L1 displays N-glycosylation at multiple sites suggests that the broad signal detected by western blotting at ~ 45 kDa in the present study predominantly refers to the cellular level of mature membrane-associated PD-L1.

In view of these complex regulatory mechanisms that control PD-L1 expression, protein stability and degradation, several studies support the evidence that PD-L1 exhibits PD-1 independent cell-specific intrinsic functions [351,353]. On the search for potential intrinsic signaling motifs, Gato-Cañas and colleagues identified three conserved amino acid sequences within the cytoplasmic domain of mammalian PD-L1. Among these conserved sequences, they reported that the membrane proximal RMLDVEKC motif is essential for PD-L1-mediated resistance towards IFN $\beta$ -related cytotoxicity. Moreover, the membrane distal DTSSK motif, which is frequently mutated in neoplastic cells, has been shown to be a negative regulator of PD-L1-mediated protection against IFN $\beta$ -induced apoptosis [353]. However, the molecular mechanism by which these motifs modulate the protective function of PD-L1 against harmful

interferon signaling are poorly understood and the identified motifs do not display similarity to any known signaling motif or adaptor site [351]. However, data provided by high-throughput affinity purification mass spectrometry analyses in HEK293T cells, performed by Huttlin and colleagues, indeed indicate that PD-L1 independent of PD-1 participates in an intracellular signalosome that regulates interferon signaling, apoptosis and DNA damage responses [351,354]. Taken together, these findings add substantial information to the way we might have to interpret the function of tumor cell-associated PD-L1 expression, which is proposed by the following model: Chronic exposure of neoplastic cells to high levels of interferons secreted by tumor infiltrating T lymphocytes might cause the selection for tumor cell clones that due to genetic alterations aberrantly express high levels of PD-L1, which in turn protects the tumor cells from interferons-induced cell cycle arrest and apoptosis induction [351,353]. Notably, Gato-Cañas and colleagues also showed that PD-L1 antagonistic antibodies sensitized melanoma cells towards interferons, an effect that according to findings by Contreras-Sandoval and colleagues might be attributed to the internalization and subsequent degradation of PD-L1 upon blockade [353,355]. In line with the proposed model, results from the present study showed that all tested PDAC cell lines, except for Panc1 cells, displayed markedly increased PD-L1 expression levels upon IFN $\gamma$  stimulation as well as after co-culture with pre-activated CD8<sup>+</sup> T cells, which secrete high levels of IFN $\gamma$  upon anti-CD3/CD28 activation. Interestingly, PD-L1 deficient Panc1 cells showed the lowest confluency levels and vital numbers (data not shown) as well as markedly lower levels of phosphorylated ERK1/2 compared to Panc89 and PancTu-I cells after co-culture with CD8<sup>+</sup> T lymphocytes, indicating a protective function of PD-L1 in PDAC cells. However, these effects cannot be exclusively attributed to potential intrinsic functions of PD-L1, since CD8<sup>+</sup> T lymphocytes showed reduced growth under co-culture with PD-L1 expressing Panc89 and PancTu-I cells. Therefore, the present results indicate that in the established *in vitro* setting PD-L1 expression by PDAC cells exerts T cell suppressive functions via stimulation of PD-1 signaling in CD8<sup>+</sup> T lymphocytes. However, PD-L1 blockade by Durvalumab in mono- and co-cultures did not affect the growth and differentiation status of PancTu-I cells in comparison to respective IgG<sub>1</sub> isotype control settings, a finding that is discussed in more detail in **section 5.5**. Noteworthy, PD-L1-associated signaling pathways have been implicated to regulate several other cellular features in neoplastic cells that have been not addressed in the present study due to reasons of complexity. These features include cell death induction, caspase activation, DNA damage response, metabolic reprogramming, chemoresistance, metastatic potential and cancer stem cell properties [331,351]. For PDAC cells, findings of the present study indicate that EMT-related alterations

in tumor cells are associated with PD-L1 expression. These findings will be discussed in more detail in **section 5.4**.

Macrophages represent besides CD8<sup>+</sup> T cells the second immune cell population that has been analyzed in the present study. In regard to the protocol used for monocyte differentiation in the present study, previously studies validated that M1 MΦ generated by the current protocol are characterized by markedly higher cell surface levels of HLA-DR as well as superior expression and secretion of pro-inflammatory cytokines like IL-1β, IL-6, TNFα and IL-8 in comparison to M2 MΦ. In contrast, M-CSF differentiated M2 MΦ are characterized by higher cell surface levels of CD163 and superior secretion of anti-inflammatory cytokines IL-10 and TGF-β1 [58,73]. Interestingly, results from *in vitro* setups indicate that high PD-L1 expression levels in macrophages are rather associated with a pro-inflammatory than an anti-inflammatory phenotype. Hence, GM-CSF differentiated M1 MΦ revealed higher PD-L1 expression levels than M-CSF differentiated M2 MΦ. Moreover, M1 MΦ showed an even more pronounced pro-inflammatory phenotype after co-culture with pre-activated CD8<sup>+</sup> T lymphocytes in comparison to mono-cultured M1 MΦ. While pro-inflammatory polarization of macrophages in response to GM-CSF stimulation is a well-known effect, the amplification of M1-like polarization during co-culture is presumably attributed to paracrine signals mediated *via* IFNγ and TNFα, which are both secreted at high levels by pre-activated CD8<sup>+</sup> T lymphocytes [356,357]. In line with the present study, Herbst and colleagues showed that prominent PD-L1 expression by macrophages is a common phenomenon in PDAC and other tumor entities like colorectal cancer, gastric cancer and malignant melanoma [358]. In view of these observations, the question arises whether high PD-L1 expression levels in pro-inflammatory macrophages are associated with an increased capability to suppress activated T lymphocytes *via* induction of PD-1 signaling. Considering the results from the present study, high PD-L1 expression by macrophages has been shown to be associated rather with a T lymphocyte supportive than a suppressive phenotype. Compared to the previously discussed results for tumor cell-related expression of PD-L1, these data indicate that the function of PD-L1 depends on its cellular context. The role of PD-L1 in macrophages might be explained in the context of their biological function. M1 MΦ represent one of the central sources for pro-inflammatory cytokines and chemokines, which both initiate and foster a pro-inflammatory immune response. At the same time macrophages adapt to local changes within the microenvironment and, thereby, orchestrate the activity of other immune cells like T lymphocytes, NK cells and neutrophils [70,74]. In this context, PD-L1 might exert different functions in macrophages. PD-L1 intrinsic signaling has been shown to protect cells from apoptosis induction due to interferons, which are secreted at

high levels by T lymphocytes in inflamed tissues [353]. Moreover, PD-L1 intrinsic signaling has been linked to the activation of mTOR pathway that regulates the expression of glycolysis-associated enzymes [359] and, thereby, fosters the induction of a glycolytic phenotype, which has been reported to be functionally linked with a pro-inflammatory M1-like macrophage polarization [360,361]. Interestingly, Wang and colleagues reported a link between IFN $\gamma$  signaling in macrophages and M1-like polarization, a finding that substantially underscores the observations reported in the present study and supports the link between M1 polarization and high PD-L1 expression levels [362]. Besides these potential intrinsic functions, PD-L1 expressed by M1 M $\Phi$  presumably also regulates T cell activity in inflamed tissues *via* binding to PD-1 and, thereby, induces peripheral self-tolerance. Moreover, PD-1/PD-L1 signaling might protect M1 M $\Phi$  from T cell-mediated lysis, since macrophages are able to present foreign antigens in the context of MHC I molecules *via* cross presentation and, therefore, signals are needed by which macrophages identify themselves as APCs in interaction with activated T cells [120]. Notably, based on a previous study [363], Sugiura and colleagues recently reported that PD-L1 capability for binding to PD-1 is highly regulated by cis interaction of CD80 and PD-L1 in APCs [364]. In detail, Sugiura and colleagues showed that CD80 on the cell surface of APCs binds to proximate PD-L1 and, thereby, prevents PD-L1 signaling *via* PD-1 [364]. Noteworthy, this finding represents a reasonable explanation for the observation that high PD-L1 expression by M1 M $\Phi$  is not associated with CD8<sup>+</sup> T cell suppression in the present study, since M1 M $\Phi$  displayed high cell surface expression levels of PD-L1 but also of CD80 (data not shown). Nevertheless, results from the present and other recent studies indicate that PD-L1 in macrophages intrinsically exerts also inhibitory functions. Hence, as a result of PD-L1 blockade by Durvalumab, markedly higher mRNA levels of IL-1 $\beta$ , IL-6 and IL-8 in mono-cultured as well as higher TNF $\alpha$  mRNA levels in co-cultured M1 M $\Phi$  were detected in comparison to respective isotype control treated macrophages in the present study. Coincidentally, IL-10 and TGF- $\beta$ 1 mRNA levels in Durvalumab treated M1 M $\Phi$  were lower than in control antibody treated M1 M $\Phi$ . Moreover, preliminary data showed that cell surface expression levels of HLA-DR and CD86 in Durvalumab treated M1 M $\Phi$  are elevated in comparison to IgG<sub>1</sub> isotype control treated M1 M $\Phi$  (data not shown). In line with these results, Hartley and colleagues reported that treatment of murine and human macrophages with PD-L1 antagonists is associated with upregulation of the mTOR signaling pathway, increased cell surface levels of CD86 and MHC II as well as elevated synthesis of TNF $\alpha$  and IL-12 [365]. Interestingly, Hartley and colleagues also showed that this phenotypic shift in macrophages due to PD-L1 blockade is linked to enhanced anti-tumor responses in an orthotopic mouse model

[365]. Besides these associations between PD-L1 expression and macrophage function, Gordon and colleagues recently reported that PD-1/PD-L1 signaling in TAMs impairs tumor phagocytotic ability and, therefore, attenuates their immune-stimulatory potential in the initiation of anti-tumor responses [366]. However, these and other studies reported that macrophages also express PD-1 and suggest that PD-1 signaling in macrophages has a functional relevance for phagocytotic activity and IL-10 secretion [366–368]. In this context, it has to be noted that PD-1 was not detectable by the applied methods in primary human monocytes, M-CSF and GM-CSF differentiated macrophages as well as TAMs isolated from fresh PDAC tissues in the present study. Overall, the results obtained in the present study showed that GM-CSF differentiated M1 MΦ despite their high PD-L1 cell surface levels exhibit rather T cell-supportive than suppressive abilities. Moreover, the present study indicates that these supportive abilities are mediated either by direct cell-cell contact or very close spatial proximity between macrophages and T cells, since observed effects on both populations were markedly stronger in direct than in indirect co-culture settings, a finding that is discussed in more detail in **section 5.5**. Notably, PD-L1 blockade by Durvalumab did neither foster nor dampen this stimulatory capacity indicating that the observed effects on CD8<sup>+</sup> T lymphocyte proliferation and effector molecule secretion after co-culture with M1 MΦ are independent of PD-1/PD-L signaling.

The third and last cell population, which has been investigated with respect to its phenotypical changes under the established co-culture conditions as well as PD-L1 blockade, are CD8<sup>+</sup> T lymphocytes that were chosen as a model for tumor-infiltrating CTLs in the present study. As already discussed, CD8<sup>+</sup> T lymphocytes represent the only cell population within the present culture settings that are potentially affected by PD-L1 signaling via PD-1, because they have been shown to be the only population with detectable cell surface expression of PD-1. In this context, it has been already extensively discussed why PD-L1 expression in PDAC cells but not M1 MΦ exerts inhibitory effects on CD8<sup>+</sup> T lymphocytes. Noteworthy, the inhibitory role of PD-L1 expressed by PancTu-I cells during co-culture is underlined by the analysis of T cell-associated effector molecules in culture supernatants. Hence, the presented data showed that PD-L1 blockade by Durvalumab in co-culture settings was associated with elevated levels of IL-17A, Granzyme A, Perforin, soluble Fas ligand and Granzyme B in culture supernatants in comparison to control treatment. However, the present study also indicates an intrinsic role for PD-L1 in CD8<sup>+</sup> T lymphocytes that is independent of PD-1. Hence, it has been shown that PD-L1 expression is upregulated specifically in the proliferating population of CD8<sup>+</sup> T lymphocytes. This observation might be attributed to the activation by anti-CD3/CD28

stimulation itself as well as autocrine stimulation by secreted interferons upon activation [369]. Indicating an intrinsic role of PD-L1 in activated CD8<sup>+</sup> T lymphocytes, supernatant levels of all analyzed effector molecules were either significantly or by trend lower in Durvalumab than in IgG<sub>1</sub> treated CD8<sup>+</sup> T lymphocytes from mono-cultures. In line with these results, Saha and colleagues revealed in a murine graft-versus-host disease model, that PD-L1<sup>-/-</sup> donor CD8<sup>+</sup> T cells show a diminished cytokine secretion [370]. Moreover, they and others reported that PD-L1<sup>-/-</sup> CTLs exhibit decreased expression levels of anti-apoptotic proteins like Bcl-xL as well as reduced glycolytic activity in comparison to wildtype CTLs [370,371]. Considering the anti-apoptotic intrinsic function of PD-L1, Azuma and colleagues reported that PD-L1 expression desensitizes cancer cells to Fas ligand-induced apoptosis [372]. Since Fas ligand is highly secreted upon T cell activation and represents a well-known important mediator of activation-induced cell death during T cell priming as well as a regulator of CD4<sup>+</sup> T cell expansion and CD8<sup>+</sup> T cell activity, PD-L1 might also play a protective role in T lymphocytes upon activation [373,374]. Considering the metabolic switch in PD-L1 deficient CD8<sup>+</sup> T lymphocytes, it has been previously discussed that PD-L1 expression is associated with activation of the mTOR signaling pathway, a central regulator for glycolytic activity [351]. Notably, similar to pro-inflammatory macrophages CD8<sup>+</sup> T lymphocytes' function is also associated with active mTOR signaling and high glycolytic activity, which is attributed to the increased need of glucose for maintenance of the anabolic metabolism in CTLs [375]. However, in the present study neither differences in proliferation have been observed nor metabolic alterations in CD8<sup>+</sup> T lymphocytes have been investigated in response to Durvalumab treatment. Furthermore, the mode of action by which antagonistic antibody binding to PD-L1 alters its intrinsic signaling are poorly understood. Therefore, it can only be speculated whether Durvalumab binding to PD-L1 causes structural changes within its cytoplasmic domain or whether binding causes the internalization and degradation of PD-L1.

Taken together, the present study adds valuable indications to the current literature that the function of PD-L1 is not only determined by its expression level but highly depends on the cellular context. Moreover, PD-L1 has been shown to exert both intercellular as well as intrinsic signaling potential even though the latter is poorly understood so far. In view of these evidences, it might be not surprising that PD-1 and PD-L1 antagonists in cancer therapy have been shown to exhibit non-redundant performance [340]. Finally, supporting the assumption that particularly macrophage- and CTL-associated PD-L1 expression represents an indicator for active immune responses, Pollari and colleagues reported that PD-L1<sup>+</sup> TAMs and PD-1<sup>+</sup> TILs are prognostic markers for a favorable prognosis for patients with testicular lymphoma [376].



## 5.4 Correlation between tumor infiltration by CTLs, PD-L1 expression and efficiency of PD-1/PD-L1 targeted therapies as well as tumor progression

As already extensively outlined in **section 5.1**, the prognostic and predictive relevance of the IHC-based PD-L1 status in tumor tissues is controversially discussed. Therefore, it is suggested that the combination of tumor PD-L1 status with other biomarkers significantly improves patient stratification for immune checkpoint-targeted therapies [325]. Based on the proposed mode of action, tumor infiltration by CTLs represents one of the most promising markers for the efficiency of immune checkpoint inhibitors. However, the assumption that the pre-existence of an immunological anti-tumor response represents a requisite for the therapeutic efficiency of immune checkpoint antagonists will be addressed in more detail in **section 5.5**.

In the present study, it has been shown that high PD-L1 expression in PDAC is predominantly located at the tumor invasive margin as well as the interface between tumor tissue and tumor-associated lymph follicles. Notably, both areas were characterized by high local abundance of CD8<sup>+</sup> T lymphocytes and TAMs, a finding that led to the establishment of the respective coculture system. In view of these results, the question arises what might be the reason for particularly high local PD-L1 expression within these distinct tumor areas. As outlined in **section 5.3**, aberrant PD-L1 expression in neoplastic cells is assumed as a protective mechanism, which is a consequence of adaptation to recurrent or chronic confrontation with cytotoxic immune mediators *via* genetic and epigenetic alterations in the process of immunoediting [191]. However, the initial mediators that cause this later on intrinsic PD-L1 expression in neoplastic cells, are most likely the same that cause high PD-L1 expression within tumor areas identified in the present study, namely cytokines. Hence, it has been shown in the present study that PD-L1 expression is highly inducible by IFN $\gamma$ , GM-CSF and M-CSF in monocytes, M1 M $\Phi$  and M2 M $\Phi$  as well as by IFN $\gamma$  and TNF $\alpha$  in pancreatic ductal epithelial cells. In line with this, it has been shown that in various cell types IFN $\gamma$  is the most potent inducer of PD-L1 expression *via* activation of the JAK-STAT signaling pathway, which leads to phosphorylation of Stat1 and downstream activation of interferon regulatory factors, a subgroup of transcription factors that regulate gene expression *via* interferon response elements [290,318,377]. Moreover, Yamazaki and colleagues reported that GM-CSF is a potent inducer of PD-L1 expression in macrophages [378]. In this context, Thorn and colleagues reported that GM-CSF-mediated PD-L1 expression in myeloid cells is controlled *via* JAK2 signaling and downstream activation of STAT3 [292]. The link between M-CSF induced signaling and PD-L1 expression currently remains unclear. One reasonable explanation for induction of PD-L1

expression in monocytes and macrophages due to M-CSF stimulation might be the induction of Ras signaling, which has been reported to cause stabilization of PD-L1 mRNA at least in tumor cells [379–381]. In contrast, Zhu and colleagues reported that blockade of CSF1R, the receptor for M-CSF, in a PDAC mouse model was associated with increased PD-L1 expression [382]. However, whether these findings are directly or indirectly linked to the blockade of M-CSF signaling is poorly understood. With regard to the proposed mediators of PD-L1 induction and the cellular composition that has been identified to be associated with high PD-L1 expression in the present cohort, it has to be noted that IFN $\gamma$  is predominantly secreted by activated T lymphocytes while GM-CSF and M-CSF are secreted by different cell populations relevant in PDAC including T cells, macrophages and fibroblasts [92,383]. Noteworthy, several studies indicate that GM-CSF is also secreted by PDAC cells at high levels due to constitutive activation of Kras signaling [278,279,384]. In the context of TNF $\alpha$  induced PD-L1 expression, Lim and colleagues showed that TNF $\alpha$  signaling induces NF $\kappa$ B activation in tumor cells, which in turn causes the expression CSN5 that deubiquitinates PD-L1 and, therefore, leads to its stabilization [385]. Nevertheless, PD-L1 expression has been reported to be regulated *via* several other cytokines and downstream signaling pathways that either have not been investigated in the present study or did not show an effect, an observation that might be attributed to cell-specific differences like the lack of respective receptors or genetic alterations [386,387]. In the latter context, it has to be noted that most PDAC cells exhibit mutations in codon 12 of the *k-Ras* gene, which causes constitutive K-ras protein activation and, therefore, leads to epidermal growth factor stimulation-independent Ras signaling, which has been reported as a key driver of PD-L1 expression in tumor cells [65]. Other mutations that have been associated with impaired PD-L1 expression in response to IFN $\gamma$  as well as resistance towards PD-1 inhibitors are located within the JAK/STAT signaling pathway [388,389]. With regard to negative regulators of PD-L1, Ou and colleagues reported that TGF- $\beta$  downstream signaling represents a potent inhibitor of PD-L1 expression in monocytic cells, which is in line with the findings of the present study [390].

Summarizing the findings from *in situ* and *in vitro* analyses of the present study in the context of the current literature, the high PD-L1 expression levels that have been frequently observed at the invasive margin and tumor-lymphatics interface in PDAC tissues and the identified cellular composition within these areas are certainly linked to the local cytokine levels. However, in order to verify this assumption, locally elevated levels of PD-L1-inducing cytokines, have to be validated, e.g. by multiplex or ELISA analyses on comparative tumor microdissections.

Having discussed the cause for elevated PD-L1 levels, the question arises whether similar patterns for PD-L1 expression are also found in other tumor entities and, secondly, what might be the tumor biological relevance. Considering the first question, indeed several studies reported that pronounced PD-L1 expression at the tumor invasive margin and tumor-lymphatics interface is associated with local high abundance of immune cell populations and in particular TILs and macrophages [228,303,391]. In this context, Thompson and colleagues examined PD-L1 expression in a cohort of gastric cancer patients. They reported that PD-L1 is predominantly expressed within the stromal compartment at the tumor margin and tumor-immune cell interface. Moreover Thompson and colleagues showed that high PD-L1 expression correlates with locally enriched CD8<sup>+</sup> T lymphocyte infiltration [303]. In line with the present study, Gani and colleagues also reported that PD-L1 is frequently expressed at high levels at the tumor margin of intrahepatic cholangiocarcinoma and correlates with local infiltration by TAMs [391]. Noteworthy, these are just two examples of numerous studies on different tumor entities, which indicate that elevated PD-L1 expression is commonly found in tumor areas that are confronted with an active immune response characterized by marked local infiltration with TILs and TAMs. However, only in some of these studies marked PD-L1 expression within the tumor-immune interface has been reported to correlate with a favorable prognosis while most studies reported a dismal prognosis [392–396]. In the present study, higher overall PD-L1 expression correlated with shorter post-surgical survival of PDAC patients, a finding that has to be critically judged as discussed in **section 5.1**. In contrast, *in vitro* results provided by the present study indicated that high PD-L1 expression in macrophages is associated with T cell supportive pro-inflammatory phenotype and PD-L1/PD-1 positivity does not obligatory indicate a suppressed T cell status.

Therefore, the central question arises: “How can we explain these findings, which appear to be controversial at first sight?”. It has to be noted that marked tumor-infiltration by CD8<sup>+</sup> T lymphocytes in general is correlated with a favorable patient prognosis in every tumor entity, since it indicates an activated anti-tumor immune response. Therefore, tumor infiltration by CTLs is regarded as a good predictive marker for the efficiency of immune checkpoint targeted therapies [397]. However, the fundamental problem with most of the studies, including the present one, is that tumor complexity and especially precise immune cell function is very difficult to assess. The growing knowledge on immune cell subset diversity highlights that optimal classifications need to implicate cell surface markers in combination with multiple -omics analyses including genomics, proteomics and transcriptomics. Prominent examples for oversimplified concepts are the common analyses of FoxP3 as a marker for regulatory T cells,

although it has been shown that several other cells also express FoxP3 [398,399], as well as the strict classification of macrophages into either M1 or M2 polarization based on single marker analyses [78]. Moreover, the spatial distribution of each stromal population and different tumor cell clones within the tumor also represents an important factor within the concept of “immunologically hot vs. cold tumors”. In principle, this concept discriminates tumors based on the presence of different immune cell populations as well as their spatial distribution. Thereby, four tumor subtypes can be classified, namely (1) inflamed/hot, (2) non-inflamed/cold, (3) immune-excluded and (4) immune-suppressed subtype [400]. Therefore, the combination of immune signatures with histological data is regarded as the next generation approach for reliable patient stratification for immunotherapy [401]. Underscoring the rethinking within the scientific community towards a more comprehensive analyses of tumor composition, in recent years several novel classification systems have been proposed that integrate data from different molecular biological approaches [98,402]. For example, Knudsen and colleagues reported a promising novel approach that predicts PDAC patient response to immunotherapy based on gene expression data, multiple tissue-based lineage marker analysis, metabolic characteristics and whole-exome sequencing data on mutational burden [98]. In view of the current state of research, the presented POLE Score lacks essential information on the spatial distribution of PD-L1 in context of the whole tumor. However, in order to add an assessable spatial component to the POLE Score, it would be necessary to obtain and analyze samples from different areas of the tumor, a task that is ambitious to perform by IHC and not feasible with respect to the sample limitation.

Lastly, the efficiency of innate and especially adaptive immunity highly depends on the duration of the immune response, a factor that is very difficult to address in patient stratification. Statistically every fifth malignant disease is associated with chronic infections, e.g. infections with *Helicobacter pylori*, *Hepatitis virus B* and *Human herpesvirus type 8*, which in turn cause chronic inflammation. Furthermore, well known risk factors of various cancer types are tightly linked to the establishment of a chronically inflamed microenvironment, e.g. tobacco abuse, excessive alcohol consumption and obesity [403,404]. Therefore, it is not surprising that chronic inflammation has been classified as a hallmark of cancer [405]. In this context, it has to be noted that chronic inflammation exhibits the potential to cause malignant transformation as well as promote tumor progression [406]. As already discussed, aberrant PD-L1 expression has been proposed to be an adaptive mechanism of neoplastic cells towards chronic exposure to interferons [407]. Besides the induction of co-inhibitory regulators such as PD-L1, prominent inflammation-associated cytokines like type I and II interferons, TNF $\alpha$  and IL-6 have been

shown to be central drivers of a cellular process in neoplastic cells that promotes tumor progression and therapy resistance, namely EMT [48,49,52]. Interestingly, numerous recent studies suggested a link between PD-L1 expression or its intrinsic signaling and EMT program in various tumor entities [408–410]. Therefore, in the present study the expression of markers associated with an epithelial and mesenchymal differentiation status, respectively, have been investigated in PancTu-I cells after co-culture with pre-activated CD8<sup>+</sup> T lymphocytes. It has been shown that PancTu-I cells from co-culture settings exhibited lower protein levels of E-cadherin and markedly higher levels of vimentin in comparison to mono-cultured PancTu-I cells. On mRNA level, co-cultured PancTu-I cells exhibited significantly higher levels of both L1CAM and E-cadherin as well as Zeb-1, a central transcription factor in the EMT program [411]. Notably, PancTu-I cells from co-culture with CD8<sup>+</sup> T lymphocytes concomitantly showed markedly increased expression of PD-L1 on both mRNA and protein level. In line with these findings, Imai and colleagues just recently reported a link between IFN $\gamma$  signaling, PD-L1 expression and EMT induction in pancreatic cancer [52]. In detail, they showed *in situ* that strong PD-L1 expression in PDAC is associated with increased vimentin and snail levels as well as decreased E-cadherin levels. Moreover, Imai and colleagues validated *in vitro* that similar alterations in PD-L1 and EMT marker expression are attributed to IFN $\gamma$  levels in a dose-dependent manner *via* Stat1 signaling induction in PK-45P cells [52]. Noteworthy, besides CD8<sup>+</sup> T lymphocytes, several other common stromal cell populations have been shown to contribute to EMT induction in PDAC *via* paracrine interactions, e.g. CD4<sup>+</sup> T lymphocytes, TAMs and fibroblasts [58,412,413]. Hence, in view of the present study, Helm and colleagues reported that both M1- and M2-like polarized macrophages as well as TAMs isolated from PDAC specimens mediate EMT induction in benign and malignant PDECs in a paracrine manner [58]. However, in the present study PancTu-I cells from indirect co-culture with M1 M $\Phi$  revealed no alterations in E-cadherin and vimentin expression levels in comparison to mono-cultured cells. One reasonable explanation for these difference between these results and the results reported by Helm and colleagues might be the varying culture duration (2 days vs. 5 days) [58]. Hence, these findings highlight the fact that short-time effects of inflammatory mediators drastically differ from long-time effects. Regarding the link between PD-L1 expression and EMT, results from the present study indicated minor effects of PD-L1 blockade *via* Durvalumab on the differentiation status of PancTu-I cells. Thus, protein levels of E-cadherin, vimentin and L1CAM were unaffected in Durvalumab treated PancTu-I cells from mono-cultures and also co-culture with CD8<sup>+</sup> T lymphocytes in comparison to the respective IgG<sub>1</sub> isotype control treated cells. Interestingly, mRNA levels analyses revealed that PD-L1

blockade in co-culture but not mono-culture was associated by trend with lower Zeb-1 and L1CAM levels as well as significantly higher E-cadherin mRNA levels in PancTu-I cells. While this varying effect of Durvalumab in mono- and co-culture settings is discussed in more detail in **section 5.5**, these results indicate a potential role of PD-L1 in the regulation of EMT in PDAC cells. However, according to the current literature it is controversially discussed whether PD-L1 represents a direct regulator of EMT program or whether PD-L1 upregulation is just a cause of EMT induction. Thus, it has been shown that PD-L1 expression is induced by various cytokines, signaling pathways and other extrinsic factors like tumor-associated hypoxia that are tightly linked to the induction of EMT, but an intrinsic mechanism by which PD-L1 itself regulates EMT induction has not been identified yet [31,36,331,414]. Moreover, Dong and colleagues reported that PD-L1 copy number amplifications are commonly associated with copy number amplifications of genes associated with EMT program, e.g. snail and N-cadherin [331]. Nevertheless, recent studies reported that interfering with PD-L1 expression *via* CRISPR/Cas9-mediated knockout or siRNA-mediated knockdown also affects the migratory and invasive capabilities of cancer cells [409,410,415]. For example, Chen and colleagues reported that RNA interference-mediated PD-L1 knockdown and ablation of the cytoplasmic domain of PD-L1 in Eca-109 cells attenuated cell viability as well as the expression of mesenchymal markers and migratory capacity of the cells, while overexpression of wildtype PD-L1 and stimulation with PD-1 fusion protein was associated with elevated expression levels of EMT markers and an increased migratory potential [410]. In view of these results, data provided by the present study indicate that PD-L1 rather exerts reverse signaling potential upon binding to PD-1 than the intrinsic ability to potentiate EMT induction. This assumption is based on the finding that Durvalumab-mediated blockade of PD-L1 only affected differentiation status of PancTu-I cells in co-culture settings, when PD-1 as a receptor was provided by CD8<sup>+</sup> T lymphocytes and PD-L1 expression levels were upregulated by T cell-secreted cytokines like IFN $\gamma$ . Nevertheless, the differentiation status of PancTu-I cells as well as EMT-associated alterations upon the applied culture and treatment settings were not characterized in more detail and, therefore, these assumptions have to be validated in following studies that characterize cell morphology, expression of further EMT markers and assess the migratory and invasive abilities of PancTu-I cells both *in vitro* and *in vivo* in dependence of Durvalumab treatment.

Taken together and in view of the current state of research, the present study indicates that PD-L1 expression is regulated by numerous extrinsic, intrinsic and genetic factors. Moreover, the function of PD-L1 highly depends on its cellular context. TILs and TAMs are prominent source for paracrine mediators that induce PD-L1 expression and, therefore, commonly localized in

tumor areas that exhibiting high PD-L1 expression. According to the present study, elevated PD-L1 expression levels in TAMs and TILs do not necessarily correlate with an immunosuppressive and exhausted phenotype, respectively. Overall, the predominant localization of PD-L1 expression at the tumor margin and tumor-lymphatics interface as well as its absence in the tumor core correlates with the general assumption that PDAC represents an immune excluded tumor entity. Noteworthy, the immune cell composition in these areas indicate the presence of local tumor-associated inflammation processes, which poses a serious risk that neoplastic cells adapt a more resistant and aggressive phenotype, e.g. by EMT induction.

### **5.5 Qualitative assessment of the established *in vitro* setting's capacity to resemble *in vivo* relevant cellular phenotypes and cellular interactions**

In the present study, a well-characterized cohort of PDAC tissues has been analyzed for PD-L1 expression *via* IHC staining and findings were integrated into a novel comprehensive scoring system, the POLE Score. Afterwards, POLE Score parameters were correlated by multiple-marker analyses in serial tissue section with lineage markers for different stromal cell population as well as markers indicating the differentiation and proliferation status of epithelial/neoplastic cells. Resulting findings showed that PD-L1 is predominantly expressed by stromal cell populations in PDAC and suggested that locally elevated PD-L1 expression levels correlate with a high abundance of TAMs and CD8<sup>+</sup> T lymphocytes at the tumor margin as well as the tumor-tumor lymph follicle interface. In order to investigate which role PD-L1 plays within this cellular context, an *in vitro* co-culture setting has been established, which comprises the most common cell populations within PD-L1<sup>high</sup> tumor areas identified *in situ*, namely, PDAC cells, macrophages and CD8<sup>+</sup> T lymphocytes. *In vitro* settings represent a common tool, which aims to provide a simplified, manipulable model of the *in vivo* situation in order to analyze cellular interactions and reactions towards distinct stimuli on a mechanistic level. However, despite the numerous advantages of *in vitro* models, they notably lack complexity in comparison to *in vivo* models. Therefore, in the following section the established *in vitro* system, will be discussed with respect to its functional and *in vivo* relevance according the current state of research.

Starting with the choice of cell lines, the well-established PDAC cell lines Panc1, Panc89, PancTu-I, Colo357, MIA PaCa-2, BxPc3 and Capan-1 have been analyzed with regard to their

basal and inducible PD-L1 expression. Interestingly, only Panc1 cells showed neither detectable basal nor inducible PD-L1 expression, a finding that might be attributed to genetic or epigenetic alterations as discussed in **section 5.3**. All other PDAC cell lines exhibited at least weak basal PD-L1 expression levels and strongly responded towards IFN $\gamma$  stimulation with PD-L1 induction. However, this finding is contradictory to the observation made in *in situ* analyses, which indicated that PD-L1 is rarely expressed in PDAC cells. One reasonable explanation for this discrepancy might be the fact that within the process of tumor cell isolation and cell line establishment those cells are selected, which show anchorage-independent survival and growth in commonly hyperglycemic conditions. Since recent studies indicate that PD-L1 expression is linked by currently unknown mechanisms with mTOR signaling as well as the induction of EMT and the acquisition of a cancer stem cell phenotype, PD-L1 expression by PDAC cells might be the cause or the consequence of a tumor cell phenotype that displays selection advantages in the isolation process [331,351]. PancTu-I cells have been chosen as model for the present study, since this cell line originates from the primary site, displays a poor differentiation status, a factor that correlated by trend with overall PD-L1 staining *in situ*, exhibits common PDAC driver mutations in *p53* and *k-ras* as well as transcriptional silencing of *p16* [240,254]. Moreover, PancTu-I cells showed notable basal cell surface PD-L1 expression levels and appeared to be highly responsive towards IFN $\gamma$  stimulation. Another important aspect for choosing PancTu-I cells was the fact that this cell line lacks expression of CD80 and CD86 (data not shown), which represent potential co-stimulatory molecules as well as negative regulators of PD-L1 in direct co-culture settings and, therefore, both molecules are able to initiate TCR-independent T cell responses against tumor cells that display high cell surface levels of CD80 or CD86 (unpublished data) [364,416]. However, in the context of tumor heterogeneity in PDAC, results obtained in the present study using PancTu-I cells as model system might not be transferable to all other cell lines. Therefore, other PDAC cell lines have to be tested in the future in order to validate whether the observed alterations after co-culture with CD8<sup>+</sup> T lymphocytes and/or treatment with Durvalumab are not cell line-specific. In this context, it has to be noted that even cell lines do not exhibit a homogenous phenotype throughout the population, but rather comprise different subclones [417]. In line with this, microscopical analyses revealed marked heterogeneity within the PancTu-I cell population in respect to cell morphology and PD-L1 cell surface expression levels.

The second cell population that has been used in the presented experimental settings are macrophages, which were differentiated *in vitro* from isolated primary human monocytes. There are several available protocols for isolation of primary human monocytes from blood



samples. These techniques are commonly based on monocyte characteristics like adherence to the surface of culture dishes or the expression of monocyte-specific surface molecules for targeted isolation. In the present study, monocytes were isolated *via* density gradient and counterflow centrifugation. The major advantage of this procedure is that monocytes are obtained at high purity without the use of antibodies or other selection markers. Since monocytes are highly responsive towards any provided stimuli, like culture material or endotoxins in culture medium, only those so called “untouched” monocytes ensure the reproducible differentiation by subsequent stimulation protocols. In the present study, GM-CSF and M-CSF were used for monocyte differentiation into M1-like and M2-like polarized phenotypes, respectively. However, the question is which of these phenotypes best resembles the phenotype of TAMs in PDAC. In general, the determination of macrophage polarization status and functional classification is a very complex topic and the precise analysis requires more parameters than just the commonly applied cell surface markers. For example, most studies conduct M2 macrophage classification based on the expression of CD206 and CD163 [74,418]. However, CD206 is induced *via* GM-CSF stimulation and CD206 as well as CD163 have been shown to be expressed by both M1- and M2-like polarized macrophages albeit at different expression levels underscoring that rather CD163/CD206 expression levels than expression status indicates macrophage polarization [73,280]. Helm and colleagues have analyzed freshly isolated TAMs from PDAC tissues by a combination of subset-specific cell surface molecules as well as gene expression profile analyses and reported that TAMs in PDAC display both pro- and anti-inflammatory characteristics [58]. However, as outlined in **section 1.2.1** macrophages exhibit high cellular plasticity and, therefore, TAM polarization certainly varies between different tumor areas in dependence on the local microenvironment. With regard to the high local abundance of predominantly CD8<sup>+</sup> T lymphocytes in PDAC tumor areas that displayed strong PD-L1 staining, it has been assumed that local macrophage polarization is rather dominated by pro-inflammatory cytokines like IFN $\gamma$ , which represents a strong driver for M1-like polarization [74,76]. In view of these *in situ* findings, GM-CSF instead of M-CSF differentiated macrophages have been used in the present as model for TAMs. Moreover, the high PD-L1 basal cell surface expression levels in GM-CSF differentiated macrophages as well as their responsiveness towards IFN $\gamma$  stimulation supported this decision. However, whether results obtained in the present study depended on the initial monocyte differentiation stimuli has to be investigated in following studies using other common stimuli for monocyte differentiation like IFN $\gamma$  and LPS for M1-polarized macrophages or M-CSF and IL-10 for generation of M2-polarized macrophages, respectively. Noteworthy, GM-CSF differentiated

M1 MΦ exhibited pronounced CD80 and CD86 cell surface expression levels, co-stimulatory molecules that have been reported to be commonly expressed by macrophages (data not shown) [68,73]. Overall, the phenotype of macrophages certainly represents one of most inconstant and variable characteristics of mono- and co-culture settings in the present study since it is highly affected by donor variabilities as well as efficiency of macrophage differentiation and T cell activation. A reasonable alternative to the common protocols for *in vitro* generation of macrophages that resemble TAMs in PDAC might be the use of tumor-conditioned medium for monocyte differentiation.

As a model for TILs, CD8<sup>+</sup> T lymphocytes have been isolated in the present study from PBMCs of healthy donors *via* density gradient and counterflow centrifugation followed by magnetic-activated cell sorting in negative selection mode. This procedure provides several advantages for the subsequent steps of the experimental setup. First, CD8<sup>+</sup> T lymphocytes and monocytes can be isolated from the same donors, an important factor to circumvent allogenic reaction in the co-culture settings. Second, this procedure enables the isolation of “untouched” CD8<sup>+</sup> T cells, which is important for the efficiency of subsequent T cell activation *via* CD3- and CD28-targeting antibodies. As for macrophage differentiation, there are several available methods for activation of primary human T cells. However, all these methods have in common that they activate downstream mediators of the TCR, since primary T lymphocyte populations from human blood in contrast to T lymphocytes from genetically-modified mouse models, like the OT-1 and OT-2 model, exhibit a vast variety of different TCR clones that cannot be triggered by a TCR-specific stimulus. Noteworthy, this applies to T cell activation in the absence of APCs like it has been performed in the present study. In the presence of APCs, T cells can be activated *via* TCR-targeting by stimulation with so called superantigens like staphylococcal enterotoxins [419]. The most common and effective methods for TCR-independent activation of T cells *in vitro* include the stimulation with phorbol-12-myristate 13-acetate (PMA), an activator of PKC, or phytohemagglutinin (PHA) in combination with ionomycin, a bacterial calcium ionophore, or pervanadate, a phosphatase inhibitor [259,277,420,421]. In contrast to these methods, the stimulation of T cells *via* CD3- and CD28-targeting antibodies represents a more physiological way for T cell activation. In principle, this method causes the artificial clustering of the TCR-CD3 complex with CD28 and, thereby, locally enriches adaptor sites for kinases. These kinases reside in a pre-activated state in the cytoplasm, catalyze upon recruitment the phosphorylation of CD3 ITAMs and, thereby, initiate TCR downstream signaling [259]. In hypothesis, the CD3-/CD28-targeting activation model, therefore, represents a suitable model to investigate potential inhibitory effects of PD-1/PD-L1

signaling on T cell activation status, since PD-1/PD-L1 signaling has been proposed to mainly compete with TCR and CD28 signaling *via* recruitment of phosphatases SHP1/2, which cause the inactivation of adaptor kinases by dephosphorylation [133,180]. Overall, anti-CD3/CD28 in combination with IL-2 stimulation has been validated as an effective way for activation of CD8<sup>+</sup> T lymphocytes by demonstrating the induction of proliferation, lymphoblasts differentiation as well as expression and secretion of activation-related cytokines and effector molecules. Moreover, the expression of activation-associated cell surface molecules CD25 and CD69 upon anti-CD3/CD28 stimulation has been detected (data not shown). Nevertheless, it has to be noted that the respective protocol for artificial T cell activation markedly impacts the resulting cytokine profile of activated T cell, which thereby essentially affects subsequent experiments [420]. In line with the current literature, both PD-1 and PD-L1 have been shown to be expressed at markedly higher levels at the cell surface of activated proliferating CD8<sup>+</sup> T lymphocytes than resting cells, indicating that both molecules represent early activation markers [422]. Moreover, correlations of CFSE profiles with PD-1 cell surface levels indicated that PD-1 levels decrease in T lymphocyte populations in dependence on the number of cell divisions they have passed. In this context, it has been reported that PD-1 cell surface levels indeed decrease in the course from activation to effector function to differentiation into memory T cells [422,423]. However, while the role of initial PD-1 upregulation and subsequent stepwise downregulation is poorly understood so far, it has been reported that constantly high PD-1 cell surface levels are commonly found in virus infected T cells and correlate with an exhausted phenotype [422,424]

The fact that the biological relevance of differential PD-1 expression during T cell activation and effector function is poorly understood, highlights that is has not been yet clearly solved whether PD-1/PD-L1 signaling predominantly regulates T lymphocytes' priming or effector function. Generally, it is assumed that PD-1 and PD-L1 antagonists in cancer therapy are only effective for the treatment of patients with a pre-existing anti-tumor response, implying that PD-1/PD-L1 signaling mediates peripheral tolerance in the effector phase [189,425]. However, while there is great evidence that PD-1/PD-L1 additionally regulates positive and negative selection in the thymus, a recently published study by Mizuno and colleagues indicated that PD-1/PD-L1 signaling also prominently participates in the regulation of T cell priming by direct interference with TCR signaling instead of solely competing with CD28 co-stimulatory signaling [190]. According to the findings obtained in the present study, PD-1 expression is strongly upregulated in proliferating T lymphocytes after anti-CD3/CD28 stimulation indicating that PD-1 has a function in regulating the clonal expansion of T cells upon priming.

However, the provided data allow no conclusion about the exact time point of PD-1 functional relevance in T cell priming in the present activation model. Nevertheless, preliminary data indicate that a higher proportion of vital CD8<sup>+</sup> T lymphocytes can be obtained from activation cultures after anti-CD3/CD28 and IL-2 stimulation when culture medium is supplemented with Durvalumab instead of IgG<sub>1</sub> isotype control (data not shown). Interestingly, flow cytometric analyses of freshly isolated CD8<sup>+</sup> T lymphocyte populations prior to activation culture reproducibly revealed the existence of a small PD-1<sup>+</sup> subpopulation. However, whether this subpopulation might be the responsive towards PD-L1 blockade by Durvalumab during activation culture cannot be deduced from the present data and, therefore, needs to be addressed in further studies. In CD8<sup>+</sup> T lymphocyte mono-cultures after activation culture, Durvalumab treatment showed no effects on the proportion of proliferating cells, CFSE profiles, the proportion of vital/dead cells and cell morphology compared to IgG<sub>1</sub> isotype control treated cells, but Durvalumab treatment was associated with significantly decreased supernatant levels of activation-related cytokines and effector molecules. In view of the findings obtained in the present study and current literature, the underlying mechanism for this observation can only be assumed. A reasonable explanation for the decreased effector molecule levels in Durvalumab treated T lymphocyte cultures despite the lack of alterations within the proportion of vital and dead cells could implicate rather intrinsic PD-L1 functions than signaling *via* PD-1. Since several studies provide evidence that intrinsic PD-L1 signaling is a regulator of mTOR and mTOR signaling essentially promotes a glycolytic metabolism that is needed to maintain the effector function-associated anabolic pathways of T cells, blockade of PD-L1 might indirectly interfere with mTOR signaling and, therefore, attenuates protein biosynthesis of effector molecules. However, this hypothesis is based on the assumption that PD-L1 indeed exerts intrinsic signaling that regulates mTOR activation, which has not been proven on a mechanistic level so far. Moreover, it is questionable how Durvalumab could affect the intrinsic function PD-L1. In this context, it can only be speculated that Durvalumab binding to PD-L1 either causes structural changes with the cytoplasmic domain or PD-L1 internalization. According to the current state of research, there is great evidence that the biological relevance of PD-1/PD-L1 signaling for the regulation of T cell activation status is not exclusively restricted to the effector phase and maintenance of peripheral tolerance. Moreover, PD-1/PD-L1 signaling has been shown to be tightly regulated on several levels. Noteworthy, preliminary data shows that besides PD-L1 also CD80 cell surface expression levels are significantly upregulated in CD8<sup>+</sup> T lymphocytes upon anti-CD3/CD28 stimulation and, therefore, CD80-PD-L1 cis-interaction

might play an essential role for the regulation of PD-1/PD-L1 signaling in clonal expansion of T cells (data not shown).

The central question addressed by the *in vitro* experimental setup in the present study has been whether the *in situ* identified tumor areas at the tumor margin and tumor-lymphatics interface, which have been characterized by high abundance of TAMs and T lymphocytes as well as remarkable PD-L1 expression in both tumor and stromal cell populations, rather provide a T cell suppressive or promoting microenvironment and whether PD-L1 plays a regulating role in this context. Based on the already discussed assumption that the *in situ* identified cellular composition favors an M1-like macrophage polarization, the results obtained in the present study clearly suggest a T cell activation promoting role of TAMs within these areas. This finding might be attributed to several characteristics of M1 MΦ in the present setup. First, M1 MΦ secrete high levels of TNFα and IL-6. These pro-inflammatory cytokines potentially foster T cell activation and prevent the differentiation into regulatory T cells by the induction of NFκB and JAK/Stat signaling, respectively [426,427]. Vice versa, pro-inflammatory cytokines secreted by T cells like IFNγ foster M1-like polarization of macrophages causing a positive feedback loop, a potential mechanism that is also supported by the present study. Secondly, preliminary data show that M1 MΦ express high cell surface levels of co-stimulatory molecules CD80 and CD86, a finding that might explain why T cell supportive function of M1 MΦ was more pronounced in direct than in indirect co-culture settings. Moreover, CD80 cell surface levels in M1 MΦ might interfere with the binding capacity of macrophage expressed PD-L1 to T cell localized PD-1 *via* cis-interaction [364,416], a mechanism that could explain why Durvalumab treatment does not foster the T cell supportive abilities of M1 MΦ despite their high PD-L1 expression levels. Notably, the finding that CD8<sup>+</sup> T lymphocyte proliferation was hardly affected by co-culture with M1 MΦ might be attributed to the fact that IL-2, which is essential for maintenance of T cell proliferation and survival, is neither secreted by M1 MΦ nor to sufficient amounts by CD8<sup>+</sup> T lymphocytes [68]. Moreover, this finding highlights the *in vivo* relevance of CD4<sup>+</sup> T lymphocytes for a sustained anti-tumor response, which has been reported in several studies [89,99,102–104]. In the context of this study, it has been shown *in situ* that especially the tumor margin is characterized by high infiltration with CD8<sup>+</sup> but not CD4<sup>+</sup> T lymphocytes, a finding that does not suggest a favorable microenvironment for a durable anti-tumor response. As discussed in the previous sections, most studies reported a negative correlation between PD-L1 expression and the presence of TAMs with respect to patient prognosis in PDAC and other tumor entities [80,392,393,395,396]. However, as outlined in this and the previous section, in most of the studies macrophage characterization is

oversimplified and important factors like spatial separation within the tumor as well as the overall cellular stromal composition are poorly addressed. In the latter context, multi-marker co-staining panels combined with subsequent computer-based staining evaluation, like the PhenoOptics™ approach provided by Perkin Elmer, certainly represent one of the best methods for precise characterization of the tumor-stromal composition as well as for implementation of spatial cellular distribution. With regard to the role of PD-L1 expression by tumor and stromal cell populations, a major problem for putting results of the present study into the context of their *in vivo* relevance is the fact that currently available data on the prognostic value of tumor infiltration by CTLs, the presence of TAMs and tumor PD-L1 status almost exclusively originate from retrospective studies. Hence, at present in many tumor entities it is completely unknown how the tumor and stromal compartment develops under PD-1 or PD-L1-targeting immunotherapy. Having a closer look at the role of TAMs for the efficiency of immune checkpoint antagonists, Arlauckas and colleagues reported that TAMs efficiently impede the function of PD-1 antagonists by capturing antibodies *via* FC $\gamma$  receptors [428]. Furthermore, Vargas and colleagues reported that CTLA-4 antagonists induce antibody-mediated cytotoxicity against intra-tumoral regulatory T cells *via* targeting FC $\gamma$  receptor expressing TAMs and, thereby, causing tumor rejection [429]. In the present study, it has been shown that PD-1 cell surface levels in CD8<sup>+</sup> T lymphocytes were markedly increased after co-culture with M1 M $\Phi$  and this effect was even more pronounced in Durvalumab treated culture settings. Similar to the present findings, which indicate that PD-L1 targeted therapies affect the expression levels of PD-1 in T cells, Sasse and colleagues reported that classical Hodgkin lymphoma patients that relapsed under therapy with PD-1 antagonists showed a markedly increase in PD-1<sup>+</sup> T cells and decrease of PD-L1<sup>+</sup> macrophages in tissue biopsies after relapse in comparison to biopsies, which were sampled before treatment [430]. Searching for a reasonable explanation for increased PD-1 expression levels in CD8<sup>+</sup> T cells upon co-culture with M1 M $\Phi$ , Austin and colleagues reported that IL-6 signaling *via* Stat3 activation induces PD-1 expression in T cells [431]. Since it has been shown that M1 M $\Phi$  secrete high levels of IL-6 whose expression is even elevated in Durvalumab treated M1 M $\Phi$ , IL-6 likely represents the mediator for increased PD-1 expression in CD8<sup>+</sup> T lymphocytes upon co-culture with M1 M $\Phi$  in the present study.

In line with the findings of numerous other studies [274,332,337], it has been shown in the present study that increased PD-L1 expression by PDAC cell lines correlates with suppressive effect on CD8<sup>+</sup> T lymphocyte proliferation and cytokine secretion. However, despite it has been demonstrated that CD8<sup>+</sup> T lymphocytes indeed interact with PancTu-I cells in the present co-

culture settings, major points of concern within the established co-culture system are allogenic reactions as well as the fact that isolated, activated CD8<sup>+</sup> T lymphocyte populations only to a very low probability comprise TCR clones, which react antigen-specific against PancTu-I cells. Therefore, growth inhibition of PancTu-I under co-culture settings with CD8<sup>+</sup> T lymphocytes was certainly mainly mediated by T cell-secreted interferons that cause cell cycle arrest but not cell-specific lysis *via* cytotoxic effector molecules like perforin, granzymes and granulysin. However, it cannot be excluded with certainty that also antigen-specific T cell clones are isolated and activated by chance. Nevertheless, in order to validate whether reduced vital cell numbers and confluency resulted from T cell-mediated induction of cell cycle arrest or apoptosis, further experiments have to be performed which assess e.g. caspase activities, DNA fragmentation and histone H2AX $\gamma$  formation as well as Ki67 and cyclin-dependent kinases status. Another interesting finding obtained in the present study are the changes in the cytokine secretion profile of IL-8, IL-6 and VEGF in PancTu-I cells from co-culture with pre-activated CD8<sup>+</sup> T lymphocytes. Concerning the decreased levels of IL-8 in supernatants of PancTu-I co-cultures with CD8<sup>+</sup> T lymphocytes, Hess and colleagues identified a CXCR1 expressing CD8<sup>+</sup> T cell subset [432]. However, whether CD8<sup>+</sup> T lymphocytes generated in the present study express CXCR1 and, therefore, are able to remove PancTu-I secreted IL-8 from the culture medium has to be proven. Elevated IL-6 levels in co-culture supernatants might be attributed to lymphocyte-secreted TNF $\alpha$  which induces IL-6 expression in PancTu-I cells *via* activation of NF $\kappa$ B [433]. Frequent binding of soluble TNF $\alpha$  to TNFR1 or TNFR2 expressed by PancTu-I cells might be also a reasonable explanation for the low supernatant concentrations of TNF $\alpha$  in co-cultures. These findings might be even relevant from a therapeutic point of view. Considering that TNF $\alpha$  secreted by TILs or TAMs activates IL-6 expression in PDAC cells and, in turn, IL-6/Stat3 signaling-mediated upregulation of PD-1 expression in CD8<sup>+</sup> T lymphocytes sensitizes T lymphocytes for PD-1/PD-L1 signaling induced anergy, both TNF $\alpha$  and IL-6 represent reasonable therapeutic targets in combinatorial therapeutic regimens. Notably, therapeutic antagonists targeting TNF $\alpha$  and IL-6 are already available, namely Etanercept [434], Tocilizumab [435] and soluble gp130, respectively [436]. Finally, the higher cellular density in co-culture settings might cause increased VEGF secretion by PancTu-I cells in two separate ways. First, the high number of lymphocytes surrounding PancTu-I cells might cause a decrease of local oxygen levels. The lower oxygen levels in turn could cause the activation of hypoxia-inducible factor 1 alpha (HIF1 $\alpha$ ) signaling, which leads to the elevated expression, synthesis and secretion of VEGF [437]. Moreover, activated CD8<sup>+</sup> T lymphocytes exhibit a highly glycolytic metabolism, which even in buffered cell culture medium stepwise

leads to medium acidification due to secretion of metabolic intermediates like lactate. These acids release protons that bind available oxygen and, therefore, can cause a marked reduction of oxygen levels. Interestingly, both tumor acidification and tumor hypoxia in combination with increased VEGF secretion by neoplastic cells have been reported to suppress the effector function of VEGFR-1/2 positive T cells as well as promote cancer stemness and tumor cell invasion [438,439]. However, whether these mechanisms also apply to the present *in vitro* setting has to be investigated in further studies. Nevertheless, the present results indicate that already approved VEGF inhibitors like Bevacizumab [440] and Aflibercept [441] represent interesting supplements for combinatorial therapeutic regimens in PDAC.

As already discussed in **section 5.4**, the present study might indicate another tumor progression-promoting ability of CD8<sup>+</sup> T lymphocytes, namely EMT induction in PDAC cells *via* interferons and other pro-inflammatory mediators. Considering these findings, it would be interesting to examine the correlation between local PD-L1 expression, differentiation status of tumor cells and stromal composition *in situ* by the analysis of EMT markers, PD-L1, cytokeratin and leukocyte lineage markers in co-staining. Moreover, the present co-culture system might provide the basis for tumor evolutionary experiments by phenotypic analysis of PancTu-I cells that have been repeatedly challenged by co-culture with CD8<sup>+</sup> T lymphocytes and treatment with Durvalumab or IgG<sub>1</sub> isotype control.

Taken together, results obtained from the *in vitro* co-culture settings resemble numerous findings that have been reported by other pre-clinical studies as well as coincide with proposed mechanisms *in vivo*. Noteworthy, the present findings underscore that the local cellular composition has to be considered as an important factor for predicting the effect of PD-L1 blockade by Durvalumab. Therefore, it is likely that Durvalumab effects might vary between organs and even different tumor areas. Moreover, the presented results indicate that PD-1/PD-L1 co-inhibitory signaling represents not the only way PDAC cells interfere with T cell effector function and, in turn, CD8<sup>+</sup> T lymphocytes themselves might induce immune-modulating responses and escape mechanisms in PDAC cells, like VEGF secretion and EMT induction. In this context, the established co-culture system might be helpful to identify and test combinatorial therapeutic approaches that synergize with Durvalumab effects. However, it has to be noted that the present co-culture system is certainly limited in its ability to model the complex tumor biology in PDAC. Hence, *in vivo* relevant obstacles in other phases of the anti-tumor response like the role of macrophages and extracellular matrix composition in blocking tumor infiltration by T cells, the role of PD-L1 expression in lymphatic vessels as well as T cell



priming in secondary and tertiary lymphoid structures could not be addressed [107,275,311,442].

## 6. Conclusion

In conclusion, the present study clearly highlights that overall tumor-associated PD-L1 expression is not an obligatory marker for an immune suppressive state. Instead, the provided data along with the current state of research emphasize that the precise functional relevance of PD-L1 has to be considered in the context of (1) its subcellular origin, (2) co-expressed regulatory molecules like CD80, (3) the cellular population in which PD-L1 is expressed, (4) the tumor compartment PD-L1<sup>+</sup> cells are located in and (5) the cellular composition as well as microenvironment PD-L1<sup>+</sup> cells are nestled. Some of these variables have been already implicated in the presented POLE Score, but others might have to be addressed by alternative molecular biological methods due to the technical- and material-related limitations of IHC-based analysis. Moreover, in the present study an *in vitro* co-culture setting has been established which simulated to a large extent the tumor situation identified *in situ*, provided molecular evidences for PD-L1 and PD-1 expression in macrophages, CD8<sup>+</sup> T lymphocytes and PDAC cells as well as coincided in many parts with data from other pre-clinical studies and *in vivo* findings.

Considering the therapeutic potential of PD-1/PD-L1 inhibitors for the treatment of PDAC in view of the present study and current literature, it has to be noted that PD-1/PD-L1 signaling-mediated suppression of T cell-based anti-tumor responses seems not to represent the central mechanism of tumor immune escape in PDAC. Commonly, PDAC is an immune excluded tumor and, therefore, future combinatorial therapies have to face the problem of CTL mobilization into the tumor across the cellular and acellular barriers of the tumor. From the predictive point of view, future diagnostic assays have to deal with tumor complexity and integrate data from various resources in order to reliably predict patient responses towards PD-1 and PD-L1 antagonists. Noteworthy, since the present study started in 2016, PD-L1 based companion diagnostics markedly have improved and included several additional variables of PD-L1 expression like the assessment of stromal PD-L1 expression and clustering of PD-L1<sup>+</sup> cells. However, translation of current knowledge into clinical application commonly takes a long time. Furthermore, it is not clear whether the assay complexity that is needed for reliable patient stratification will enter clinical routine in near future, since such sophisticated assays require the collaboration of experts from different fields as well as different technical applications and, thereby, are hardly economic.

---

## References

- [1] F. Bray, J. Ferlay, I. Soerjomataram, R.L. Siegel, L.A. Torre, A. Jemal, Global cancer statistics 2018: GLOBOCAN estimates of incidence and mortality worldwide for 36 cancers in 185 countries, *CA. Cancer J. Clin.* (2018). doi:10.3322/caac.21492.
- [2] T.P. Yeo, A.B. Lowenfels, Demographics and epidemiology of pancreatic cancer, *Cancer J. (United States)*. (2012). doi:10.1097/PPO.0b013e3182756803.
- [3] A.E. Becker, Y.G. Hernandez, H. Frucht, A.L. Lucas, Pancreatic ductal adenocarcinoma: Risk factors, screening, and early detection, *World J. Gastroenterol.* 20 (2014) 11182–11198. doi:10.3748/wjg.v20.i32.11182.
- [4] K.Y. Bilimoria, D.J. Bentrem, C.Y. Ko, J. Ritchey, A.K. Stewart, D.P. Winchester, M.S. Talamonti, Validation of the 6th edition AJCC pancreatic cancer staging system: Report from the National Cancer Database, *Cancer*. (2007). doi:10.1002/cncr.22852.
- [5] L. Rahib, B.D. Smith, R. Aizenberg, A.B. Rosenzweig, J.M. Fleshman, L.M. Matrisian, Projecting cancer incidence and deaths to 2030: The unexpected burden of thyroid, liver, and pancreas cancers in the united states, *Cancer Res.* (2014). doi:10.1158/0008-5472.CAN-14-0155.
- [6] D.K. Bartsch, T.M. Gress, P. Langer, Familial pancreatic cancer current knowledge, *Nat. Rev. Gastroenterol. Hepatol.* (2012). doi:10.1038/nrgastro.2012.111.
- [7] S. Raimondi, A.B. Lowenfels, A.M. Morselli-Labate, P. Maisonneuve, R. Pezzilli, Pancreatic cancer in chronic pancreatitis; Aetiology, incidence, and early detection, *Best Pract. Res. Clin. Gastroenterol.* (2010). doi:10.1016/j.bpg.2010.02.007.
- [8] S. Iodice, S. Gandini, P. Maisonneuve, A.B. Lowenfels, Tobacco and the risk of pancreatic cancer: A review and meta-analysis, *Langenbeck's Arch. Surg.* 393 (2008) 535–545. doi:10.1007/s00423-007-0266-2.
- [9] P.J. Villeneuve, K.C. Johnson, Y. Mao, A.J. Hanley, B. Paulse, R. Dewar, D. Dryer, N. Kreiger, E. Kliewer, D. Robson, S. Fincham, N. Le, Environmental tobacco smoke and the risk of pancreatic cancer: Findings from a Canadian population-based case-control study, *Can. J. Public Heal.* (2004).
- [10] E.J. Duell, Epidemiology and potential mechanisms of tobacco smoking and heavy alcohol consumption in pancreatic cancer, *Mol. Carcinog.* (2012). doi:10.1002/mc.20786.
- [11] J.M. Genkinger, D. Spiegelman, K.E. Anderson, L. Bergkvist, L. Bernstein, P.A. Van Den Brandt, D.R. English, J.L. Freudenheim, C.S. Fuchs, G.G. Giles, E. Giovannucci, S.E. Hankinson, P.L. Horn-Ross, M. Leitzmann, S. Männistö, J.R. Marshall, M.L. McCullough, A.B. Miller, D.J. Reding, K. Robien, T.E. Rohan, A. Schatzkin, V.L. Stevens, R.Z. Stolzenberg-Solomon, B.A.J. Verhage, A. Wolk, R.G. Ziegler, S.A. Smith-Warner, Alcohol intake and pancreatic cancer risk: A pooled analysis of fourteen cohort studies, *Cancer Epidemiol. Biomarkers Prev.* (2009). doi:10.1158/1055-9965.EPI-08-0880.
- [12] S.J. Pandol, M. Raraty, Pathobiology of alcoholic pancreatitis, in: *Pancreatology*, 2007. doi:10.1159/000104235.
- [13] L. Bonelli, H. Aste, P. Bovo, G. Cavallini, M. Felder, R. Gusmaroli, E. Morandini, P. Ravelli, R. Briglia, L. Lombardo, A. De Micheli, V. Pugliese, Exocrine pancreatic

- cancer, cigarette smoking, and diabetes mellitus: A case-control study in Northern Italy, *Pancreas*. (2003). doi:10.1097/00006676-200308000-00007.
- [14] E.E. Calle, C. Rodriguez, K. Walker-Thurmond, M.J. Thun, Overweight, obesity, and mortality from cancer in a prospectively studied cohort of U.S. Adults, *N. Engl. J. Med.* (2003). doi:10.1056/NEJMoa021423.
- [15] R.H. Hruban, A. Maitra, S.E. Kern, M. Goggins, Precursors to Pancreatic Cancer, *Gastroenterol. Clin. North Am.* (2007). doi:10.1016/j.gtc.2007.08.012.
- [16] R.H. Hruban, M. Goggins, J. Parsons, S.E. Kern, Progression model for pancreatic cancer, *Clin. Cancer Res.* (2000).
- [17] H. Han, D.D. Von Hoff, SnapShot: Pancreatic cancer, *Cancer Cell*. (2013). doi:10.1016/j.ccr.2013.03.008.
- [18] T. Furukawa, R. Chiba, M. Kobari, S. Matsuno, H. Nagura, T. Takahashi, Varying grades of epithelial atypia in the pancreatic ducts of humans: Classification based on morphometry and multivariate analysis and correlated with positive reactions of carcinoembryonic antigen, *Arch. Pathol. Lab. Med.* (1994).
- [19] R.H. Hruban, N.V. Adsay, J. Albores-Saavedra, C. Compton, E.S. Garrett, S.N. Goodman, S.E. Kern, D.S. Klimstra, G. Klöppel, D.S. Longnecker, J. Lüttges, G.J.A. Offerhaus, Pancreatic intraepithelial neoplasia: A new nomenclature and classification system for pancreatic duct lesions, *Am. J. Surg. Pathol.* (2001). doi:10.1097/00000478-200105000-00003.
- [20] B.B. Friday, A.A. Adjei, K-ras as a target for cancer therapy, *Biochim. Biophys. Acta - Rev. Cancer*. (2005). doi:10.1016/j.bbcan.2005.08.001.
- [21] C. Almoguera, D. Shibata, K. Forrester, J. Martin, N. Arnheim, M. Perucho, Most human carcinomas of the exocrine pancreas contain mutant c-K-ras genes, *Cell*. (1988). doi:10.1016/0092-8674(88)90571-5.
- [22] B.J. Raphael, R.H. Hruban, A.J. Aguirre, R.A. Moffitt, J.J. Yeh, C. Stewart, A.G. Robertson, A.D. Cherniack, M. Gupta, G. Getz, S.B. Gabriel, M. Meyerson, C. Cibulskis, S.S. Fei, T. Hinoue, H. Shen, P.W. Laird, S. Ling, Y. Lu, G.B. Mills, R. Akbani, P. Loher, E.R. Londin, I. Rigoutsos, A.G. Telonis, E.A. Gibb, A. Goldenberg, A.M. Mezlini, K.A. Hoadley, E. Collisson, E. Lander, B.A. Murray, J. Hess, M. Rosenberg, L. Bergelson, H. Zhang, J. Cho, G. Tiao, J. Kim, D. Livitz, I. Leshchiner, B. Reardon, E. Van Allen, A. Kamburov, R. Beroukhim, G. Saksena, S.E. Schumacher, M.S. Noble, D.I. Heiman, N. Gehlenborg, J. Kim, M.S. Lawrence, V. Adsay, G. Petersen, D. Klimstra, N. Bardeesy, M.D.M. Leiserson, R. Bowlby, K. Kasaian, I. Birol, K.L. Mungall, S. Sadeghi, J.N. Weinstein, P.T. Spellman, Y. Liu, L.T. Amundadottir, J. Tepper, A.D. Singhi, R. Dhir, D. Paul, T. Smyrk, L. Zhang, P. Kim, J. Bowen, J. Frick, J.M. Gastier-Foster, M. Gerken, K. Lau, K.M. Leraas, T.M. Lichtenberg, N.C. Ramirez, J. Renkel, M. Sherman, L. Wise, P. Yena, E. Zmuda, J. Shih, A. Ally, M. Balasundaram, R. Carlsen, A. Chu, E. Chuah, A. Clarke, N. Dhalla, R.A. Holt, S.J.M. Jones, D. Lee, Y. Ma, M.A. Marra, M. Mayo, R.A. Moore, A.J. Mungall, J.E. Schein, P. Sipahimalani, A. Tam, N. Thiessen, K. Tse, T. Wong, D. Brooks, J.T. Auman, S. Balu, T. Bodenheimer, D.N. Hayes, A.P. Hoyle, S.R. Jefferys, C.D. Jones, S. Meng, P.A. Mieczkowski, L.E. Mose, C.M. Perou, A.H. Perou, J. Roach, Y. Shi, J. V. Simons, T. Skelly, M.G. Soloway, D. Tan, U. Veluvolu, J.S. Parker, M.D. Wilkerson, A. Korkut, Y. Senbabaoglu, P. Burch, R. McWilliams, K. Chaffee, A. Oberg, W. Zhang, M.C. Gingras, D.A. Wheeler, L. Xi, M. Albert, J. Bartlett, H. Sekhon, Y. Stephen, Z. Howard, M. Judy, A. Breggia, R.T.

- Shroff, S. Chudamani, J. Liu, L. Lolla, R. Naresh, T. Pihl, Q. Sun, Y. Wan, Y. Wu, S. Jennifer, K. Roggin, K.F. Becker, M. Behera, J. Bennett, L. Boice, E. Burks, C.G. Carlotti Junior, J. Chabot, D. Pretti da Cunha Tirapelli, J. Sebastião dos Santos, M. Dubina, J. Eschbacher, M. Huang, L. Huelsenbeck-Dill, R. Jenkins, A. Karpov, R. Kemp, V. Lyadov, S. Maithel, G. Manikhas, E. Montgomery, H. Noushmehr, A. Osunkoya, T. Owonikoko, O. Paklina, O. Potapova, S. Ramalingam, W.K. Rathmell, K. Rieger-Christ, C. Saller, G. Setdikova, A. Shabunin, G. Sica, T. Su, T. Sullivan, P. Swanson, K. Tarvin, M. Tavobilov, L.B. Thorne, S. Urbanski, O. Voronina, T. Wang, D. Crain, E. Curley, J. Gardner, D. Mallery, S. Morris, J. Paulauskis, R. Penny, C. Shelton, T. Shelton, K.P. Janssen, O. Bathe, N. Bahary, J. Slotta-Huspenina, A. Johns, H. Hibshoosh, R.F. Hwang, A. Sepulveda, A. Radenbaugh, S.B. Baylin, M. Berrios, M.S. Bootwalla, A. Holbrook, P.H. Lai, D.T. Maglinte, S. Mahurkar, T.J. Triche, D.J. Van Den Berg, D.J. Weisenberger, L. Chin, R. Kucherlapati, M. Kucherlapati, A. Pantazi, P. Park, G. Saksena, D. Voet, P. Lin, S. Frazer, T. Defreitas, S. Meier, L. Chin, S.Y. Kwon, Y.H. Kim, S.J. Park, S.S. Han, S.H. Kim, H. Kim, E. Furth, M. Tempero, C. Sander, A. Biankin, D. Chang, P. Bailey, A. Gill, J. Kench, S. Grimmond, A. Johns, A.P. Cancer Genome Initiative (APGI), R. Postier, R. Zuna, H. Sicotte, J.A. Demchok, M.L. Ferguson, C.M. Hutter, K.R. Mills Shaw, M. Sheth, H.J. Sofia, R. Tarnuzzer, Z. Wang, L. Yang, J. (Julia) Zhang, I. Felau, J.C. Zenklusen, Integrated Genomic Characterization of Pancreatic Ductal Adenocarcinoma, *Cancer Cell.* (2017). doi:10.1016/j.ccell.2017.07.007.
- [23] J.D. Day, J.A. Digiuseppe, C. Yeo, M. Lai-Goldman, S.M. Anderson, S.N. Goodman, S.E. Kern, R.H. Hruban, Immunohistochemical evaluation of HER-2/neu expression in pancreatic adenocarcinoma and pancreatic intraepithelial neoplasms, *Hum. Pathol.* (1996). doi:10.1016/S0046-8177(96)90364-0.
- [24] N.T. Van Heek, A.K. Meeker, S.E. Kern, C.J. Yeo, K.D. Lillemoe, J.L. Cameron, G.J.A. Offerhaus, J.L. Hicks, R.E. Wilentz, M.G. Goggins, A.M. De Marzo, R.H. Hruban, A. Maitra, Telomere shortening is nearly universal in pancreatic intraepithelial neoplasia, *Am. J. Pathol.* (2002). doi:10.1016/S0002-9440(10)64432-X.
- [25] H. Ying, P. Dey, W. Yao, A.C. Kimmelman, G.F. Draetta, A. Maitra, R.A. Depinho, Genetics and biology of pancreatic ductal adenocarcinoma, *Genes Dev.* (2016). doi:10.1101/gad.275776.115.
- [26] C.A. Lacobuzio-Donahue, B. Fu, S. Yachida, M. Luo, H. Abe, C.M. Henderson, F. Vilardell, Z. Wang, J.W. Keller, P. Banerjee, J.M. Herman, J.L. Cameron, C.J. Yeo, M.K. Halushka, J.R. Eshleman, M. Raben, A.P. Klein, R.H. Hruban, M. Hidalgo, D. Laheru, DPC4 gene status of the primary carcinoma correlates with patterns of failure in patients with pancreatic cancer, *J. Clin. Oncol.* (2009). doi:10.1200/JCO.2008.17.7188.
- [27] A. V. Biankin, N. Waddell, K.S. Kassahn, M.C. Gingras, L.B. Muthuswamy, A.L. Johns, D.K. Miller, P.J. Wilson, A.M. Patch, J. Wu, D.K. Chang, M.J. Cowley, B.B. Gardiner, S. Song, I. Harliwong, S. Idrisoglu, C. Nourse, E. Nourbakhsh, S. Manning, S. Wani, M. Gongora, M. Pajic, C.J. Scarlett, A.J. Gill, A. V. Pinho, I. Rooman, M. Anderson, O. Holmes, C. Leonard, D. Taylor, S. Wood, Q. Xu, K. Nones, J.L. Fink, A. Christ, T. Bruxner, N. Cloonan, G. Kolle, F. Newell, M. Pinese, R.S. Mead, J.L. Humphris, W. Kaplan, M.D. Jones, E.K. Colvin, A.M. Nagrial, E.S. Humphrey, A. Chou, V.T. Chin, L.A. Chantrill, A. Mawson, J.S. Samra, J.G. Kench, J.A. Lovell, R.J. Daly, N.D. Merrett, C. Toon, K. Epari, N.Q. Nguyen, A. Barbour, N. Zeps, N. Kakkar, F. Zhao, Y.Q. Wu, M. Wang, D.M. Muzny, W.E. Fisher, F.C. Brunicardi, S.E. Hodges, J.G. Reid, J. Drummond, K. Chang, Y. Han, L.R. Lewis, H. Dinh, C.J. Buhay, T. Beck, L. Timms,

- M. Sam, K. Begley, A. Brown, D. Pai, A. Panchal, N. Buchner, R. De Borja, R.E. Denroche, C.K. Yung, S. Serra, N. Onetto, D. Mukhopadhyay, M.S. Tsao, P.A. Shaw, G.M. Petersen, S. Gallinger, R.H. Hruban, A. Maitra, C.A. Iacobuzio-Donahue, R.D. Schulick, C.L. Wolfgang, R.A. Morgan, R.T. Lawlor, P. Capelli, V. Corbo, M. Scardoni, G. Tortora, M.A. Tempero, K.M. Mann, N.A. Jenkins, P.A. Perez-Mancera, D.J. Adams, D.A. Largaespada, L.F.A. Wessels, A.G. Rust, L.D. Stein, D.A. Tuveson, N.G. Copeland, E.A. Musgrove, A. Scarpa, J.R. Eshleman, T.J. Hudson, R.L. Sutherland, D.A. Wheeler, J. V. Pearson, J.D. McPherson, R.A. Gibbs, S.M. Grimmond, Pancreatic cancer genomes reveal aberrations in axon guidance pathway genes, *Nature*. (2012). doi:10.1038/nature11547.
- [28] E.A. Collisson, A. Sadanandam, P. Olson, W.J. Gibb, M. Truitt, S. Gu, J. Cooc, J. Weinkle, G.E. Kim, L. Jakkula, H.S. Feiler, A.H. Ko, A.B. Olshen, K.L. Danenberg, M.A. Tempero, P.T. Spellman, D. Hanahan, J.W. Gray, Subtypes of pancreatic ductal adenocarcinoma and their differing responses to therapy, *Nat. Med.* (2011). doi:10.1038/nm.2344.
- [29] M. Yarchoan, L.A. Albacker, A.C. Hopkins, M. Montesion, K. Murugesan, T.T. Vithayathil, N. Zaidi, N.S. Azad, D.A. Laheru, G.M. Frampton, E.M. Jaffee, PD-L1 expression and tumor mutational burden are independent biomarkers in most cancers, *JCI Insight*. (2019). doi:10.1172/jci.insight.126908.
- [30] D. Shook, R. Keller, Mechanisms, mechanics and function of epithelial-mesenchymal transitions in early development, *Mech. Dev.* (2003). doi:10.1016/j.mod.2003.06.005.
- [31] R. Kalluri, R.A. Weinberg, The basics of epithelial-mesenchymal transition, *J. Clin. Invest.* (2009). doi:10.1172/JCI39104.
- [32] M.A. Nieto, R.Y.Y.J. Huang, R.A.A. Jackson, J.P.P. Thiery, EMT: 2016, *Cell*. (2016). doi:10.1016/j.cell.2016.06.028.
- [33] A. Soltermann, V. Tischler, S. Arbogast, J. Braun, N. Probst-Hensch, W. Weder, H. Moch, G. Kristiansen, Prognostic significance of epithelial-mesenchymal and mesenchymal-epithelial transition protein expression in non-small cell lung cancer, *Clin. Cancer Res.* (2008). doi:10.1158/1078-0432.CCR-08-0935.
- [34] Z.A. Rasheed, J. Yang, Q. Wang, J. Kowalski, I. Freed, C. Murter, S.M. Hong, J.B. Koorstra, N. V. Rajeshkumar, X. He, M. Goggins, C. Iacobuzio-Donahue, D.M. Berman, D. Laheru, A. Jimeno, M. Hidalgo, A. Maitra, W. Matsui, Prognostic significance of tumorigenic cells with mesenchymal features in pancreatic adenocarcinoma, *J. Natl. Cancer Inst.* (2010). doi:10.1093/jnci/djp535.
- [35] S. Spaderna, O. Schmalhofer, F. Hlubek, G. Berx, A. Eger, S. Merkel, A. Jung, T. Kirchner, T. Brabletz, A Transient, EMT-Linked Loss of Basement Membranes Indicates Metastasis and Poor Survival in Colorectal Cancer, *Gastroenterology*. (2006). doi:10.1053/j.gastro.2006.06.016.
- [36] J.H. Taube, J.I. Herschkowitz, K. Komurov, A.Y. Zhou, S. Gupta, J. Yang, K. Hartwell, T.T. Onder, P.B. Gupta, K.W. Evans, B.G. Hollier, P.T. Ram, E.S. Lander, J.M. Rosen, R.A. Weinberg, S.A. Mani, Core epithelial-to-mesenchymal transition interactome gene-expression signature is associated with claudin-low and metaplastic breast cancer subtypes, *Proc. Natl. Acad. Sci. U. S. A.* (2010). doi:10.1073/pnas.1004900107.
- [37] M. Yilmaz, G. Christofori, EMT, the cytoskeleton, and cancer cell invasion, *Cancer Metastasis Rev.* (2009). doi:10.1007/s10555-008-9169-0.

- 
- [38] B. De Craene, G. Berx, Regulatory networks defining EMT during cancer initiation and progression, *Nat. Rev. Cancer*. (2013). doi:10.1038/nrc3447.
- [39] A. Díaz-López, G. Moreno-Bueno, A. Cano, Role of microRNA in epithelial to mesenchymal transition and metastasis and clinical perspectives, *Cancer Manag. Res.* (2014). doi:10.2147/CMAR.S38156.
- [40] H. Gabbert, R. Wagner, R. Moll, C.D. Gerharz, Tumor dedifferentiation: An important step in tumor invasion, *Clin. Exp. Metastasis*. (1985). doi:10.1007/BF01585081.
- [41] A. Aghdassi, M. Sendler, A. Guenther, J. Mayerle, C.O. Behn, C.D. Heidecke, H. Friess, M. Büchler, M. Evert, M.M. Lerch, F.U. Weiss, Recruitment of histone deacetylases HDAC1 and HDAC2 by the transcriptional repressor ZEB1 downregulates E-cadherin expression in pancreatic cancer, *Gut*. (2012). doi:10.1136/gutjnl-2011-300060.
- [42] S. Nakajima, R. Doi, E. Toyoda, S. Tsuji, M. Wada, M. Koizumi, S.S. Tulachan, D. Ito, K. Kami, T. Mori, Y. Kawaguchi, K. Fujimoto, R. Hosotani, M. Imamura, N-cadherin expression and epithelial-mesenchymal transition in pancreatic carcinoma, *Clin. Cancer Res.* (2004). doi:10.1158/1078-0432.CCR-0578-03.
- [43] A. Sparmann, D. Bar-Sagi, Ras-induced interleukin-8 expression plays a critical role in tumor growth and angiogenesis, *Cancer Cell*. (2004). doi:10.1016/j.ccr.2004.09.028.
- [44] M.A. Huber, N. Kraut, H. Beug, Molecular requirements for epithelial-mesenchymal transition during tumor progression, *Curr. Opin. Cell Biol.* (2005). doi:10.1016/j.ceb.2005.08.001.
- [45] T. Shibue, R.A. Weinberg, EMT, CSCs, and drug resistance: The mechanistic link and clinical implications, *Nat. Rev. Clin. Oncol.* (2017). doi:10.1038/nrclinonc.2017.44.
- [46] M.A. Esteban, M.G.B. Tran, S.K. Harten, P. Hill, M.C. Castellanos, A. Chandra, R. Raval, T.S. O'Brien, P.H. Maxwell, Regulation of E-cadherin expression by VHL and hypoxia-inducible factor, *Cancer Res.* (2006). doi:10.1158/0008-5472.CAN-05-2670.
- [47] H. Kim, J.A. Choi, J.H. Kim, Ras promotes transforming growth factor- $\beta$ (TGF- $\beta$ )-induced epithelial-mesenchymal transition via a leukotriene B4 receptor-2-linked cascade in mammary epithelial cells, *J. Biol. Chem.* (2014). doi:10.1074/jbc.M114.556126.
- [48] Y. Wu, J. Deng, P.G. Rychahou, S. Qiu, B.M. Evers, B.P. Zhou, Stabilization of Snail by NF- $\kappa$ B Is Required for Inflammation-Induced Cell Migration and Invasion, *Cancer Cell*. (2009). doi:10.1016/j.ccr.2009.03.016.
- [49] N.J. Sullivan, A.K. Sasser, A.E. Axel, F. Vesuna, V. Raman, N. Ramirez, T.M. Oberyszyn, B.M. Hall, Interleukin-6 induces an epithelial-mesenchymal transition phenotype in human breast cancer cells, *Oncogene*. (2009). doi:10.1038/onc.2009.180.
- [50] Y. Li, L. Wang, L. Pappan, A. Galliher-Beckley, J. Shi, IL-1 $\beta$  promotes stemness and invasiveness of colon cancer cells through Zeb1 activation, *Mol. Cancer*. (2012). doi:10.1186/1476-4598-11-87.
- [51] A.K. Bonde, V. Tischler, S. Kumar, A. Soltermann, R.A. Schwendener, Intratumoral macrophages contribute to epithelial-mesenchymal transition in solid tumors, *BMC Cancer*. (2012). doi:10.1186/1471-2407-12-35.

- 
- [52] D. Imai, T. Yoshizumi, S. Okano, S. Itoh, T. Ikegami, N. Harada, S. Aishima, Y. Oda, Y. Maehara, IFN- $\gamma$  Promotes Epithelial-Mesenchymal Transition and the Expression of PD-L1 in Pancreatic Cancer, *J. Surg. Res.* (2019). doi:10.1016/j.jss.2019.02.038.
- [53] M. Beuran, I. Negoï, S. Paun, A.D. Ion, C. Bleotu, R.I. Negoï, S. Hostiuc, The epithelial to mesenchymal transition in pancreatic cancer: A systematic review, *Pancreatology.* (2015). doi:10.1016/j.pan.2015.02.011.
- [54] M. Zeisberg, E.G. Neilson, Biomarkers for epithelial-mesenchymal transitions, *J. Clin. Invest.* (2009). doi:10.1172/JCI36183.
- [55] U. Burk, J. Schubert, U. Wellner, O. Schmalhofer, E. Vincan, S. Spaderna, T. Brabletz, A reciprocal repression between ZEB1 and members of the miR-200 family promotes EMT and invasion in cancer cells, *EMBO Rep.* (2008). doi:10.1038/embor.2008.74.
- [56] A.D. Rhim, E.T. Mirek, N.M. Aiello, A. Maitra, J.M. Bailey, F. McAllister, M. Reichert, G.L. Beatty, A.K. Rustgi, R.H. Vonderheide, S.D. Leach, B.Z. Stanger, EMT and dissemination precede pancreatic tumor formation, *Cell.* 148 (2012) 349–361. doi:10.1016/j.cell.2011.11.025.
- [57] E. Grage-Griebenow, E. Jerg, A. Gorys, D. Wicklein, D. Wesch, S. Freitag-Wolf, L. Goebel, I. Vogel, T. Becker, M. Ebsen, C. Röcken, P. Altevogt, U. Schumacher, H. Schäfer, S. Sebens, L1CAM promotes enrichment of immunosuppressive T cells in human pancreatic cancer correlating with malignant progression, *Mol. Oncol.* (2014). doi:10.1016/j.molonc.2014.03.001.
- [58] O. Helm, J. Held-Feindt, E. Grage-Griebenow, N. Reiling, H. Ungefroren, I. Vogel, U. Krüger, T. Becker, M. Ebsen, C. Röcken, D. Kabelitz, H. Schäfer, S. Sebens, Tumor-associated macrophages exhibit pro- and anti-inflammatory properties by which they impact on pancreatic tumorigenesis, *Int. J. Cancer.* 135 (2014) 843–861. doi:10.1002/ijc.28736.
- [59] H. Kiefel, S. Bondong, M. Pfeifer, U. Schirmer, N. Erbe-Hoffmann, H. Schäfer, S. Sebens, P. Altevogt, EMT-associated up-regulation of L1CAM provides insights into L1CAM-mediated integrin signalling and NF- $\kappa$ B activation, *Carcinogenesis.* (2012). doi:10.1093/carcin/bgs220.
- [60] A.D. Rhim, F.I. Thege, S.M. Santana, T.B. Lannin, T.N. Saha, S. Tsai, L.R. Maggs, M.L. Kochman, G.G. Ginsberg, J.G. Lieb, V. Chandrasekhara, J.A. Drebin, N. Ahmad, Y.X. Yang, B.J. Kirby, B.Z. Stanger, Detection of circulating pancreas epithelial cells in patients with pancreatic cystic lesions, *Gastroenterology.* 146 (2014) 647–651. doi:10.1053/j.gastro.2013.12.007.
- [61] J. Kleeff, P. Beckhove, I. Esposito, S. Herzig, P.E. Huber, J.M. Löhr, H. Friess, Pancreatic cancer microenvironment, *Int. J. Cancer.* 121 (2007) 699–705. doi:10.1002/ijc.22871.
- [62] S. Lunardi, R.J. Muschel, T.B. Brunner, The stromal compartments in pancreatic cancer: Are there any therapeutic targets?, *Cancer Lett.* (2014). doi:10.1016/j.canlet.2013.09.039.
- [63] H. Miyamoto, T. Murakami, K. Tsuchida, H. Sugino, H. Miyake, S. Tashiro, Tumor-Stroma Interaction of Human Pancreatic Cancer: Acquired Resistance to Anticancer Drugs and Proliferation Regulation Is Dependent on Extracellular Matrix Proteins, *Pancreas.* (2004). doi:10.1097/00006676-200401000-00006.



- 
- [64] L.M. Coussens, Z. Werb, Inflammation and cancer, *Nature*. 420 (2002) 860–867. doi:10.1038/nature01322.
- [65] E. Fokas, E. O’Neill, A. Gordon-Weeks, S. Mukherjee, W.G. McKenna, R.J. Muschel, Pancreatic ductal adenocarcinoma: From genetics to biology to radiobiology to oncoimmunology and all the way back to the clinic, *Biochim. Biophys. Acta - Rev. Cancer*. (2015). doi:10.1016/j.bbcan.2014.12.001.
- [66] M. Erkan, C.W. Michalski, S. Rieder, C. Reiser-Erkan, I. Abiatari, A. Kolb, N.A. Giese, I. Esposito, H. Friess, J. Kleeff, The Activated Stroma Index Is a Novel and Independent Prognostic Marker in Pancreatic Ductal Adenocarcinoma, *Clin. Gastroenterol. Hepatol*. (2008). doi:10.1016/j.cgh.2008.05.006.
- [67] A.D. Rhim, P.E. Oberstein, D.H. Thomas, E.T. Mirek, C.F. Palermo, S.A. Sastra, E.N. Dekleva, T. Saunders, C.P. Becerra, I.W. Tattersall, C.B. Westphalen, J. Kitajewski, M.G. Fernandez-Barrena, M.E. Fernandez-Zapico, C. Iacobuzio-Donahue, K.P. Olive, B.Z. Stanger, Stromal elements act to restrain, rather than support, pancreatic ductal adenocarcinoma, *Cancer Cell*. (2014). doi:10.1016/j.ccr.2014.04.021.
- [68] K. Murphy, P. Travers, M. Walport, *Janeway Immunologie*, 2009. doi:10.1007/978-3-8274-2219-4.
- [69] C. Shi, E.G. Pamer, Monocyte recruitment during infection and inflammation, *Nat. Rev. Immunol*. (2011). doi:10.1038/nri3070.
- [70] A. Sica, M. Erreni, P. Allavena, C. Porta, Macrophage polarization in pathology, *Cell. Mol. Life Sci*. (2015). doi:10.1007/s00018-015-1995-y.
- [71] S.D. Wright, R.A. Ramos, P.S. Tobias, R.J. Ulevitch, J.C. Mathison, CD14, a receptor for complexes of lipopolysaccharide (LPS) and LPS binding protein, *Science* (80- ). (1990). doi:10.1126/science.1698311.
- [72] C. Buechler, M. Ritter, E. Orsó, T. Langmann, J. Klucken, G. Schmitz, Regulation of scavenger receptor CD163 expression in human monocytes and macrophages by pro- and antiinflammatory stimuli, *J. Leukoc. Biol*. (2000). doi:10.1002/jlb.67.1.97.
- [73] C.A. Ambarus, S. Krausz, M. van Eijk, J. Hamann, T.R.D.J. Radstake, K.A. Reedquist, P.P. Tak, D.L.P. Baeten, Systematic validation of specific phenotypic markers for in vitro polarized human macrophages, *J. Immunol. Methods*. (2012). doi:10.1016/j.jim.2011.10.013.
- [74] P.J. Murray, J.E. Allen, S.K. Biswas, E.A. Fisher, D.W. Gilroy, S. Goerdt, S. Gordon, J.A. Hamilton, L.B. Ivashkiv, T. Lawrence, M. Locati, A. Mantovani, F.O. Martinez, J.L. Mege, D.M. Mosser, G. Natoli, J.P. Saeij, J.L. Schultze, K.A. Shirey, A. Sica, J. Suttles, I. Udalova, J.A. vanGinderachter, S.N. Vogel, T.A. Wynn, Macrophage Activation and Polarization: Nomenclature and Experimental Guidelines, *Immunity*. (2014). doi:10.1016/j.immuni.2014.06.008.
- [75] B. Ruffell, L.M. Coussens, Macrophages and therapeutic resistance in cancer, *Cancer Cell*. 27 (2015) 462–472. doi:10.1016/j.ccell.2015.02.015.
- [76] A. Sica, T. Schioppa, A. Mantovani, P. Allavena, Tumour-associated macrophages are a distinct M2 polarised population promoting tumour progression: Potential targets of anti-cancer therapy, *Eur. J. Cancer*. (2006). doi:10.1016/j.ejca.2006.01.003.
- [77] S. Gordon, F.O. Martinez, Alternative activation of macrophages: Mechanism and functions, *Immunity*. (2010). doi:10.1016/j.immuni.2010.05.007.

- 
- [78] O. Helm, J. Held-Feindt, H. Schafer, S. Sebens, M1 and M2: there is no “good” and “bad”-How macrophages promote malignancy-associated features in tumorigenesis, *Oncoimmunology*. 3 (2014) e946818. doi:10.4161/21624011.2014.946818.
- [79] A. Mantovani, S. Sozzani, M. Locati, P. Allavena, A. Sica, Macrophage polarization: Tumor-associated macrophages as a paradigm for polarized M2 mononuclear phagocytes, *Trends Immunol.* (2002). doi:10.1016/S1471-4906(02)02302-5.
- [80] H. Kurahara, H. Shintchi, Y. Mataka, K. Maemura, H. Noma, F. Kubo, M. Sakoda, S. Ueno, S. Natsugoe, S. Takao, Significance of M2-polarized tumor-associated macrophage in pancreatic cancer, *J. Surg. Res.* (2011). doi:10.1016/j.jss.2009.05.026.
- [81] A. Mielgo, M.C. Schmid, Impact of tumour associated macrophages in pancreatic cancer, *BMB Rep.* (2013). doi:10.5483/BMBRep.2013.46.3.036.
- [82] D.M. Richards, J. Hettinger, M. Feuerer, Monocytes and macrophages in cancer: Development and functions, *Cancer Microenviron.* (2013). doi:10.1007/s12307-012-0123-x.
- [83] A. Zlotnik, Chemokines and cancer, *Int. J. Cancer.* (2006). doi:10.1002/ijc.22024.
- [84] P. Monti, B.E. Leone, F. Marchesi, G. Balzano, A. Zerbi, F. Scaltrini, C. Pasquali, G. Calori, F. Pessi, C. Sperti, V. Di Carlo, P. Allavena, L. Piemonti, The CC Chemokine MCP-1/CCL2 in Pancreatic Cancer Progression: Regulation of Expression and Potential Mechanisms of Antimalignant Activity, *Cancer Res.* (2003).
- [85] Y. Zhu, B.L. Knolhoff, M.A. Meyer, T.M. Nywening, B.L. West, J. Luo, A. Wang-Gillam, S.P. Goedegebuure, D.C. Linehan, D.G. De Nardo, CSF1/CSF1R blockade reprograms tumor-infiltrating macrophages and improves response to T-cell checkpoint immunotherapy in pancreatic cancer models, *Cancer Res.* 74 (2014) 5057–5069. doi:10.1158/0008-5472.CAN-13-3723.
- [86] D.E. Sanford, B.A. Belt, R.Z. Panni, A. Mayer, A.D. Deshpande, D. Carpenter, J.B. Mitchem, S.M. Plambeck-Suess, L.A. Worley, B.D. Goetz, A. Wang-Gillam, T.J. Eberlein, D.G. Denardo, S.P. Goedegebuure, D.C. Linehan, Inflammatory monocyte mobilization decreases patient survival in pancreatic cancer: A role for targeting the CCL2/CCR2 axis, *Clin. Cancer Res.* (2013). doi:10.1158/1078-0432.CCR-13-0525.
- [87] J.B. Mitchem, D.J. Brennan, B.L. Knolhoff, B.A. Belt, Y. Zhu, D.E. Sanford, L. Belaygorod, D. Carpenter, L. Collins, D. Piwnica-Worms, S. Hewitt, G.M. Udipi, W.M. Gallagher, C. Wegner, B.L. West, A. Wang-Gillam, P. Goedegebuure, D.C. Linehan, D.G. DeNardo, Targeting tumor-infiltrating macrophages decreases tumor-initiating cells, relieves immunosuppression, and improves chemotherapeutic responses, *Cancer Res.* (2013). doi:10.1158/0008-5472.CAN-12-2731.
- [88] O. Helm, R. Mennrich, D. Petrick, L. Goebel, S. Freitag-Wolf, C. Röder, H. Kalthoff, C. Röcken, B. Sipos, D. Kabelitz, H. Schäfer, H.H. Oberg, D. Wesch, S. Sebens, Comparative characterization of stroma cells and ductal epithelium in chronic pancreatitis and pancreatic ductal adenocarcinoma, *PLoS One.* 9 (2014). doi:10.1371/journal.pone.0094357.

- [89] A. Fukunaga, M. Miyamoto, Y. Cho, S. Murakami, Y. Kawarada, T. Oshikiri, K. Kato, T. Kurokawa, M. Suzuoki, Y. Nakakubo, K. Hiraoka, T. Itoh, T. Morikawa, S. Okushiba, S. Kondo, K. Hiroyuki, CD8<sup>+</sup>tumor-infiltrating lymphocytes together with CD4<sup>+</sup>tumor-infiltrating lymphocytes and dendritic cells improve the prognosis of patients with pancreatic adenocarcinoma, *Pancreas*. (2004). doi:10.1097/00006676-200401000-00023.
- [90] C.E. Clark, S.R. Hingorani, R. Mick, C. Combs, D.A. Tuveson, R.H. Vonderheide, Dynamics of the immune reaction to pancreatic cancer from inception to invasion, *Cancer Res*. (2007). doi:10.1158/0008-5472.CAN-07-0175.
- [91] M.J.M. Gooden, G.H. De Bock, N. Leffers, T. Daemen, H.W. Nijman, The prognostic influence of tumour-infiltrating lymphocytes in cancer: A systematic review with meta-analysis, *Br. J. Cancer*. (2011). doi:10.1038/bjc.2011.189.
- [92] K. Schroder, P.J. Hertzog, T. Ravasi, D.A. Hume, Interferon- $\gamma$ : an overview of signals, mechanisms and functions, *J. Leukoc. Biol*. (2004). doi:10.1189/jlb.0603252.
- [93] F. Burke, N. East, C. Upton, K. Patel, F.R. Balkwill, Interferon gamma induces cell cycle arrest and apoptosis in a model of ovarian cancer: Enhancement of effect by batimastat, *Eur. J. Cancer Part A*. (1997). doi:10.1016/S0959-8049(97)88065-3.
- [94] S. Nakayamada, H. Takahashi, Y. Kanno, J.J. O'Shea, Helper T cell diversity and plasticity, *Curr. Opin. Immunol*. (2012). doi:10.1016/j.coi.2012.01.014.
- [95] B. Alberts, A. Johnson, J. Lewis, Helper T cells and Lymphocyte Activation, in: *Mol. Biol. Cell*, 2002.
- [96] D.A.A. Vignali, L.W. Collison, C.J. Workman, How regulatory T cells work, *Nat. Rev. Immunol*. (2008). doi:10.1038/nri2343.
- [97] B.E. Russ, J.E. Prier, S. Rao, S.J. Turner, T cell immunity as a tool for studying epigenetic regulation of cellular differentiation, *Front. Genet*. (2013). doi:10.3389/fgene.2013.00218.
- [98] E.S. Knudsen, P. Vail, U. Balaji, H. Ngo, I.W. Botros, V. Makarov, N. Riaz, V. Balachandran, S. Leach, D.M. Thompson, T.A. Chan, A.K. Witkiewicz, Stratification of Pancreatic Ductal Adenocarcinoma: Combinatorial Genetic, Stromal, and Immunologic Markers, *Clin. Cancer Res*. 23 (2017) 4429–4440. doi:10.1158/1078-0432.CCR-17-0162.
- [99] J.L. Carstens, P.C. De Sampaio, D. Yang, S. Barua, H. Wang, A. Rao, J.P. Allison, V.S. Le Bleu, R. Kalluri, Spatial computation of intratumoral T cells correlates with survival of patients with pancreatic cancer, *Nat. Commun*. (2017). doi:10.1038/ncomms15095.
- [100] A. Ene-Obong, A.J. Clear, J. Watt, J. Wang, R. Fatah, J.C. Riches, J.F. Marshall, J. Chin-Aleong, C. Chelala, J.G. Gribben, A.G. Ramsay, H.M. Kocher, Activated pancreatic stellate cells sequester CD8<sup>+</sup> T cells to reduce their infiltration of the juxtatumoral compartment of pancreatic ductal adenocarcinoma, *Gastroenterology*. (2013). doi:10.1053/j.gastro.2013.07.025.
- [101] N. Tewari, A.M. Zaitoun, A. Arora, S. Madhusudan, M. Ilyas, D.N. Lobo, The presence of tumour-associated lymphocytes confers a good prognosis in pancreatic ductal adenocarcinoma: An immunohistochemical study of tissue microarrays, *BMC Cancer*. (2013). doi:10.1186/1471-2407-13-436.

- 
- [102] Y. Ino, R. Yamazaki-Itoh, K. Shimada, M. Iwasaki, T. Kosuge, Y. Kanai, N. Hiraoka, Immune cell infiltration as an indicator of the immune microenvironment of pancreatic cancer, *Br. J. Cancer*. (2013). doi:10.1038/bjc.2013.32.
- [103] A.L. Marzo, B.F. Kinnear, R.A. Lake, J.J. Frelinger, E.J. Collins, B.W.S. Robinson, B. Scott, Tumor-Specific CD4 + T Cells Have a Major “Post-Licensing” Role in CTL Mediated Anti-Tumor Immunity, *J. Immunol.* (2000). doi:10.4049/jimmunol.165.11.6047.
- [104] H. Huang, F. Li, J.R. Gordon, J. Xiang, Synergistic enhancement of antitumor immunity with adoptively transferred tumor-specific CD4 + and CD8 + T cells and intratumoral lymphotactin transgene expression, *Cancer Res.* (2002).
- [105] N. Hiraoka, K. Onozato, T. Kosuge, S. Hirohashi, Prevalence of FOXP3+ regulatory T cells increases during the progression of pancreatic ductal adenocarcinoma and its premalignant lesions, *Clin. Cancer Res.* (2006). doi:10.1158/1078-0432.CCR-06-0369.
- [106] L. De Monte, M. Reni, E. Tassi, D. Clavenna, I. Papa, H. Recalde, M. Braga, V. Di Carlo, C. Doglioni, M.P. Protti, Intratumor T helper type 2 cell infiltrate correlates with cancer-associated fibroblast thymic stromal lymphopoietin production and reduced survival in pancreatic cancer, *J. Exp. Med.* (2011). doi:10.1084/jem.20101876.
- [107] G.L. Beatty, R. Winograd, R.A. Evans, K.B. Long, S.L. Luque, J.W. Lee, C. Clendenin, W.L. Gladney, D.M. Knoblock, P.D. Guirnalda, R.H. Vonderheide, Exclusion of T Cells From Pancreatic Carcinomas in Mice Is Regulated by Ly6Clow F4/80+ Extratumoral Macrophages, *Gastroenterology*. (2015). doi:10.1053/j.gastro.2015.04.010.
- [108] W. Von Bernstorff, M. Voss, S. Freichel, A. Schmid, I. Vogel, C. Jöhnk, D. Henne-Bruns, B. Kremer, H. Kalthoff, Systemic and local immunosuppression in pancreatic cancer patients, *Clin. Cancer Res.* (2001).
- [109] A. Bhandoola, A. Sambandam, From stem cell to T cell: One route or many?, *Nat. Rev. Immunol.* (2006). doi:10.1038/nri1778.
- [110] J.B. Tan, I. Visan, J.S. Yuan, C.J. Guidos, Requirement for Notch1 signals at sequential early stages of intrathymic T cell development, *Nat. Immunol.* (2005). doi:10.1038/ni1217.
- [111] R. Vanhanen, N. Heikkilä, K. Aggarwal, D. Hamm, H. Tarkkila, T. Pätilä, T.S. Jokiranta, J. Saramäki, T.P. Arstila, T cell receptor diversity in the human thymus, *Mol. Immunol.* (2016). doi:10.1016/j.molimm.2016.07.002.
- [112] A.I. Garbe, A. Krueger, F. Gounari, J.C. Zuniga-Pflucker, H. von Boehmer, Differential synergy of Notch and T cell receptor signaling determines alpha beta versus gamma delta lineage fate, *J. Exp. Med.* (2006).
- [113] R.N. Germain, t-cell development and the CD4-CD8 lineage decision, *Nat. Rev. Immunol.* (2002). doi:10.1038/nri798.
- [114] M. Huesmann, B. Scott, P. Kisielow, H. von Boehmer, Kinetics and efficacy of positive selection in the thymus of normal and T cell receptor transgenic mice, *Cell*. (1991). doi:10.1016/0092-8674(81)90016-7.
- [115] C.D. Surh, J. Sprent, T-cell apoptosis detected in situ during positive and negative selection in the thymus, *Nature*. (1994). doi:10.1038/372100a0.

- 
- [116] H. von Boehmer, P. Kisielow, H. Kishi, B. Scott, P. Borgulya, H.S. Teh, The Expression of CD4 and CD8 Accessory Molecules on Mature T Cells is not Random but Correlates with the Specificity of the  $\alpha\beta$  Receptor for Antigen, *Immunol. Rev.* (1989). doi:10.1111/j.1600-065X.1989.tb00023.x.
- [117] L. Klein, B. Kyewski, P.M. Allen, K.A. Hogquist, Positive and negative selection of the T cell repertoire: What thymocytes see (and don't see), *Nat. Rev. Immunol.* (2014). doi:10.1038/nri3667.
- [118] M. Wieczorek, E.T. Abualrous, J. Sticht, M. Álvaro-Benito, S. Stolzenberg, F. Noé, C. Freund, Major histocompatibility complex (MHC) class I and MHC class II proteins: Conformational plasticity in antigen presentation, *Front. Immunol.* (2017). doi:10.3389/fimmu.2017.00292.
- [119] J. Neefjes, M.L.M. Jongsma, P. Paul, O. Bakke, Towards a systems understanding of MHC class I and MHC class II antigen presentation, *Nat. Rev. Immunol.* (2011). doi:10.1038/nri3084.
- [120] S. Burgdorf, C. Schölz, A. Kautz, R. Tampé, C. Kurts, Spatial and mechanistic separation of cross-presentation and endogenous antigen presentation, *Nat. Immunol.* (2008). doi:10.1038/ni.1601.
- [121] P.A. Van Der Merwe, O. Dushek, Mechanisms for T cell receptor triggering, *Nat. Rev. Immunol.* (2011). doi:10.1038/nri2887.
- [122] J. Borst, T. Ahrends, N. Bąbała, C.J.M. Melief, W. Kastenmüller, CD4<sup>+</sup> T cell help in cancer immunology and immunotherapy, *Nat. Rev. Immunol.* (2018). doi:10.1038/s41577-018-0044-0.
- [123] X. Zang, J.P. Allison, The B7 family and cancer therapy: Costimulation and coinhibition, *Clin. Cancer Res.* (2007). doi:10.1158/1078-0432.CCR-07-1030.
- [124] A.M. Paterson, V.K. Vanguri, A.H. Sharpe, SnapShot: B7/CD28 Costimulation, *Cell.* (2009). doi:10.1016/j.cell.2009.05.015.
- [125] D.L. Mueller, Mechanisms maintaining peripheral tolerance, *Nat. Immunol.* (2010). doi:10.1038/ni.1817.
- [126] A. Ribas, Tumor immunotherapy directed at PD-1, *N. Engl. J. Med.* (2012). doi:10.1056/NEJMe1205943.
- [127] I. Akhmetzyanova, G. Zelinsky, E. Littwitz-Salomon, A. Malyskina, K.K. Dietze, H. Streeck, S. Brandau, U. Dittmer, CD137 Agonist Therapy Can Reprogram Regulatory T Cells into Cytotoxic CD4<sup>+</sup> T Cells with Antitumor Activity, *J. Immunol.* (2016). doi:10.4049/jimmunol.1403039.
- [128] S. Chen, L.F. Lee, T.S. Fisher, B. Jessen, M. Elliott, W. Evering, K. Logronio, G.H. Tu, K. Tsaparikos, X. Li, H. Wang, C. Ying, M. Xiong, T. Van Arsdale, J.C. Lin, Combination of 4-1BB agonist and PD-1 antagonist promotes antitumor effector/memory CD8 T cells in a Poorly Immunogenic Tumor Model, *Cancer Immunol. Res.* (2015). doi:10.1158/2326-6066.CIR-14-0118.
- [129] C. Robert, J. Schachter, G. V. Long, A. Arance, J.J. Grob, L. Mortier, A. Daud, M.S. Carlino, C. McNeil, M. Lotem, J. Larkin, P. Lorigan, B. Neyns, C.U. Blank, O. Hamid, C. Mateus, R. Shapira-Frommer, M. Kosh, H. Zhou, N. Ibrahim, S. Ebbinghaus, A. Ribas, Pembrolizumab versus Ipilimumab in Advanced Melanoma, *N. Engl. J. Med.* 372 (2015) 2521–2532. doi:10.1056/NEJMoa1503093.

- 
- [130] S. Tahara-Hanaoka, K. Shibuya, Y. Onoda, H. Zhang, S. Yamazaki, A. Miyamoto, S.I. Honda, L.L. Lanier, A. Shibuya, Functional characterization of DNAM-1 (CD226) interaction with its ligands PVR (CD155) and nectin-2 (PRR-2/CD112), *Int. Immunol.* (2004). doi:10.1093/intimm/dxh059.
- [131] J. Hendriks, L.A. Gravestien, K. Tesselaar, R.A.W. Van Lier, T.N.M. Schumacher, J. Borst, CD27 is required for generation and long-term maintenance of T cell immunity, *Nat. Immunol.* (2000). doi:10.1038/80877.
- [132] C. Dong, A.E. Juedes, U.A. Temann, S. Shresta, J.P. Allison, N.H. Ruddle, R.A. Flavell, ICOS co-stimulatory receptor is essential for T-cell activation and function, *Nature.* (2001). doi:10.1038/35051100.
- [133] H. Arasanz, M. Gato-Cañas, M. Zuazo, M. Ibañez-Vea, K. Breckpot, G. Kochan, D. Escors, PD1 signal transduction pathways in T cells, *Oncotarget.* (2017). doi:10.18632/oncotarget.17232.
- [134] W.C. Dougall, S. Kurtulus, M.J. Smyth, A.C. Anderson, TIGIT and CD96: new checkpoint receptor targets for cancer immunotherapy, *Immunol. Rev.* (2017). doi:10.1111/imr.12518.
- [135] S. Ronchetti, O. Zollo, S. Bruscoli, M. Agostini, R. Bianchini, G. Nocentini, E. Ayroldi, C. Riccardi, Frontline: GITR, a member of the TNF receptor superfamily, is costimulatory to mouse T lymphocyte subpopulations, *Eur. J. Immunol.* (2004). doi:10.1002/eji.200324804.
- [136] C.J. Workman, K.J. Dugger, D.A.A. Vignali, Cutting Edge: Molecular Analysis of the Negative Regulatory Function of Lymphocyte Activation Gene-3, *J. Immunol.* (2002). doi:10.4049/jimmunol.169.10.5392.
- [137] C.E. Ruby, W.L. Redmond, D. Haley, A.D. Weinberg, Anti-OX40 stimulation in vivo enhances CD8<sup>+</sup> memory T cell survival and significantly increases recall responses, *Eur. J. Immunol.* (2007). doi:10.1002/eji.200636428.
- [138] R.J. Johnston, L. Comps-Agrar, J. Hackney, X. Yu, M. Huseni, Y. Yang, S. Park, V. Javinal, H. Chiu, B. Irving, D.L. Eaton, J.L. Grogan, The Immunoreceptor TIGIT Regulates Antitumor and Antiviral CD8<sup>+</sup>T Cell Effector Function, *Cancer Cell.* (2014). doi:10.1016/j.ccell.2014.10.018.
- [139] C. Zhu, A.C. Anderson, A. Schubart, H. Xiong, J. Imitola, S.J. Khoury, X.X. Zheng, T.B. Strom, V.K. Kuchroo, The Tim-3 ligand galectin-9 negatively regulates T helper type 1 immunity, *Nat. Immunol.* (2005). doi:10.1038/ni1271.
- [140] J.L. Lines, E. Pantazi, J. Mak, L.F. Sempere, L. Wang, S. O'Connell, S. Ceeraz, A.A. Suriawinata, S. Yan, M.S. Ernstoff, R. Noelle, VISTA is an immune checkpoint molecule for human T cells, *Cancer Res.* (2014). doi:10.1158/0008-5472.CAN-13-1504.
- [141] L. Wang, R. Rubinstein, J.L. Lines, A. Wasiuk, C. Ahonen, Y. Guo, L.F. Lu, D. Gondek, Y. Wang, R.A. Fava, A. Fiser, S. Almo, R.J. Noelle, VISTA, a novel mouse Ig superfamily ligand that negatively regulates T cell responses, *J. Exp. Med.* (2011). doi:10.1084/jem.20100619.
- [142] R.I. Fisher, S.A. Rosenberg, G. Fyfe, Long-term survival update for high-dose recombinant interleukin-2 in patients with renal cell carcinoma, *Cancer J. Sci. Am.* (2000).

- 
- [143] C. Krieg, S. Létourneau, G. Pantaleo, O. Boyman, Improved IL-2 immunotherapy by selective stimulation of IL-2 receptors on lymphocytes and endothelial cells, *Proc. Natl. Acad. Sci. U. S. A.* (2010). doi:10.1073/pnas.1002569107.
- [144] T.M. Petrella, R. Tozer, K. Belanger, K.J. Savage, R. Wong, M. Smylie, S. Kamel-Reid, V. Tron, B.E. Chen, N.N. Hunder, L. Hagerman, W. Walsh, E.A. Eisenhauer, Interleukin-21 has activity in patients with metastatic melanoma: A phase II study, *J. Clin. Oncol.* (2012). doi:10.1200/JCO.2011.40.0655.
- [145] M. Epardaud, K.G. Elpek, M.P. Rubinstein, A.R. Yonekura, A. Bellemare-Pelletier, R. Bronson, J.A. Hamerman, A.W. Goldrath, S.J. Turley, Interleukin-15/interleukin-15R $\alpha$  complexes promote destruction of established tumors by reviving tumor-resident CD8<sup>+</sup> T cells, *Cancer Res.* (2008). doi:10.1158/0008-5472.CAN-08-0045.
- [146] J.M. Curtsinger, M.F. Mescher, Inflammatory cytokines as a third signal for T cell activation, *Curr. Opin. Immunol.* (2010). doi:10.1016/j.coi.2010.02.013.
- [147] M.F. Krummel, F. Bartumeus, A. Gérard, T cell migration, search strategies and mechanisms, *Nat. Rev. Immunol.* (2016). doi:10.1038/nri.2015.16.
- [148] N. Miskov-Zivanov, M.S. Turner, L.P. Kane, P.A. Morel, J.R. Faeder, The duration of T cell stimulation is a critical determinant of cell fate and plasticity, *Sci. Signal.* (2013). doi:10.1126/scisignal.2004217.
- [149] R. Obst, The timing of T cell priming and cycling, *Front. Immunol.* (2015). doi:10.3389/fimmu.2015.00563.
- [150] F. Macián, S.H. Im, F.J. García-Cózar, A. Rao, T-cell anergy, *Curr. Opin. Immunol.* (2004). doi:10.1016/j.coi.2004.01.013.
- [151] M. Dominguez-Villar, D.A. Hafler, Regulatory T cells in autoimmune disease, *Nat. Immunol.* (2018). doi:10.1038/s41590-018-0120-4.
- [152] A. Scholer, S. Hugues, A. Boissonnas, L. Fetler, S. Amigorena, Intercellular Adhesion Molecule-1-Dependent Stable Interactions between T Cells and Dendritic Cells Determine CD8<sup>+</sup> T Cell Memory, *Immunity.* (2008). doi:10.1016/j.immuni.2007.12.016.
- [153] E.O. Long, ICAM-1: Getting a Grip on Leukocyte Adhesion, *J. Immunol.* (2011). doi:10.4049/jimmunol.1100646.
- [154] M. Marski, S. Kandula, J.R. Turner, C. Abraham, CD18 Is Required for Optimal Development and Function of CD4 + CD25 + T Regulatory Cells, *J. Immunol.* (2005). doi:10.4049/jimmunol.175.12.7889.
- [155] J.B. Huppa, M.M. Davis, T-cell-antigen recognition and the immunological synapse, *Nat. Rev. Immunol.* (2003). doi:10.1038/nri1245.
- [156] M.N. Artyomov, M. Lis, S. Devadas, M.M. Davis, A.K. Chakraborty, CD4 and CD8 binding to MHC molecules primarily acts to enhance Lck delivery, *Proc. Natl. Acad. Sci. U. S. A.* (2010). doi:10.1073/pnas.1010568107.
- [157] H. Ike, A. Kosugi, A. Kato, R. Iino, H. Hirano, T. Fujiwara, K. Ritchie, A. Kusumi, Mechanism of Lck recruitment to the T-cell receptor cluster as studied by single-molecule-fluorescence video imaging, *ChemPhysChem.* (2003). doi:10.1002/cphc.200300670.

- 
- [158] P.E. Love, S.M. Hayes, ITAM-mediated signaling by the T-cell antigen receptor., *Cold Spring Harb. Perspect. Biol.* (2010). doi:10.1101/cshperspect.a002485.
- [159] H. Wang, T.A. Kadlecsek, B.B. Au-Yeung, H.E.S. Goodfellow, L.Y. Hsu, T.S. Freedman, A. Weiss, ZAP-70: an essential kinase in T-cell signaling., *Cold Spring Harb. Perspect. Biol.* (2010). doi:10.1101/cshperspect.a002279.
- [160] E.H. Palacios, A. Weiss, Function of the Src-family kinases, Lck and Fyn, in T-cell development and activation, *Oncogene*. (2004). doi:10.1038/sj.onc.1208074.
- [161] A.C. Chan, M. Dalton, R. Johnson, G.H. Kong, T. Wang, R. Thoma, T. Kurosaki, Activation of ZAP-70 kinase activity by phosphorylation of tyrosine 493 is required for lymphocyte antigen receptor function., *EMBO J.* (1995). doi:10.1002/j.1460-2075.1995.tb07247.x.
- [162] V. Di Bartolo, D. Mège, V. Germain, M. Pelosi, E. Dufour, F. Michel, G. Magistrelli, A. Isacchi, O. Acuto, Tyrosine 319, a newly identified phosphorylation site of ZAP-70, plays a critical role in T cell antigen receptor signaling, *J. Biol. Chem.* (1999). doi:10.1074/jbc.274.10.6285.
- [163] J. Wu, Q. Zhao, T. Kurosaki, A. Weiss, The Vav binding site (Y315) in ZAP-70 is critical for antigen receptor-mediated signal transduction, *J. Exp. Med.* (1997). doi:10.1084/jem.185.10.1877.
- [164] G. Gaud, R. Lesourne, P.E. Love, Regulatory mechanisms in T cell receptor signalling, *Nat. Rev. Immunol.* (2018). doi:10.1038/s41577-018-0020-8.
- [165] R.T. Abraham, A. Weiss, Jurkat T cells and development of the T-cell receptor signalling paradigm, *Nat. Rev. Immunol.* (2004). doi:10.1038/nri1330.
- [166] T. Yokosuka, T. Saito, Dynamic regulation of T-cell costimulation through TCR-CD28 microclusters, *Immunol. Rev.* (2009). doi:10.1111/j.1600-065X.2009.00779.x.
- [167] J.H. Esensten, Y.A. Helou, G. Chopra, A. Weiss, J.A. Bluestone, CD28 Costimulation: From Mechanism to Therapy, *Immunity*. (2016). doi:10.1016/j.immuni.2016.04.020.
- [168] K. Okkenhaug, B. Vanhaesebroeck, PI3K in lymphocyte development, differentiation and activation, *Nat. Rev. Immunol.* (2003). doi:10.1038/nri1056.
- [169] D.K. Finlay, E. Rosenzweig, L. V. Sinclair, F.C. Carmen, J.L. Hukelmann, J. Rolf, A.A. Panteleyev, K. Okkenhaug, D.A. Cantrell, PDK1 regulation of mTOR and hypoxia-inducible factor 1 integrate metabolism and migration of CD8<sup>+</sup> T cells, *J. Exp. Med.* (2012). doi:10.1084/jem.20112607.
- [170] B.D. Manning, A. Toker, AKT/PKB Signaling: Navigating the Network, *Cell*. (2017). doi:10.1016/j.cell.2017.04.001.
- [171] L.F. Reynolds, C. De Bettignies, T. Norton, A. Beeser, J. Chernoff, V.L.J. Tybulewicz, Vav1 Transduces T Cell Receptor Signals to the Activation of the Ras/ERK Pathway via LAT, Sos, and RasGRP1, *J. Biol. Chem.* (2004). doi:10.1074/jbc.M400257200.
- [172] K. Hayashi, A. Altman, Filamin A Is Required for T Cell Activation Mediated by Protein Kinase C- $\theta$ , *J. Immunol.* (2006). doi:10.4049/jimmunol.177.3.1721.
- [173] R. Tavano, R.L. Contento, S.J. Baranda, M. Soligo, L. Tuosto, S. Manes, A. Viola, CD28 interaction with filamin-A controls lipid raft accumulation at the T-cell immunological synapse, *Nat. Cell Biol.* (2006). doi:10.1038/ncb1492.



- [174] K.D. Fischer, Y.Y. Kong, H. Nishina, K. Tedford, L.E.M. Marengère, I. Koziaradzki, T. Sasaki, M. Starr, G. Chan, S. Gardener, M.P. Nghiem, D. Bouchard, M. Barbacid, A. Bernstein, J.M. Penninger, Vav is a regulator of cytoskeletal reorganization mediated by the T-cell receptor, *Curr. Biol.* (1998).
- [175] T. Okazaki, T. Honjo, PD-1 and PD-1 ligands: From discovery to clinical application, *Int. Immunol.* (2007). doi:10.1093/intimm/dxm057.
- [176] M.E. Keir, M.J. Butte, G.J. Freeman, A.H. Sharpe, PD-1 and Its Ligands in Tolerance and Immunity, *Annu. Rev. Immunol.* (2008). doi:10.1146/annurev.immunol.26.021607.090331.
- [177] W. Zou, L. Chen, Inhibitory B7-family molecules in the tumour microenvironment, *Nat. Rev. Immunol.* (2008). doi:10.1038/nri2326.
- [178] D.M. Pardoll, The blockade of immune checkpoints in cancer immunotherapy., *Nat. Rev. Cancer.* 12 (2012) 252–64. doi:10.1038/nrc3239.
- [179] J.M. Chemnitz, R. V. Parry, K.E. Nichols, C.H. June, J.L. Riley, SHP-1 and SHP-2 Associate with Immunoreceptor Tyrosine-Based Switch Motif of Programmed Death 1 upon Primary Human T Cell Stimulation, but Only Receptor Ligation Prevents T Cell Activation, *J. Immunol.* (2004). doi:10.4049/jimmunol.173.2.945.
- [180] K.A. Sheppard, L.J. Fitz, J.M. Lee, C. Benander, J.A. George, J. Wooters, Y. Qiu, J.M. Jussif, L.L. Carter, C.R. Wood, D. Chaudhary, PD-1 inhibits T-cell receptor induced phosphorylation of the ZAP70/CD3zeta signalosome and downstream signaling to PKCtheta, *FEBS Lett.* 574 (2004) 37–41. doi:10.1016/j.febslet.2004.07.083.
- [181] G. Rota, C. Niogret, A.T. Dang, C.R. Barros, N.P. Fonta, F. Alfei, L. Morgado, D. Zehn, W. Birchmeier, E. Vivier, G. Guarda, Shp-2 Is Dispensable for Establishing T Cell Exhaustion and for PD-1 Signaling In Vivo, *Cell Rep.* (2018). doi:10.1016/j.celrep.2018.03.026.
- [182] T. Yokosuka, M. Takamatsu, W. Kobayashi-Imanishi, A. Hashimoto-Tane, M. Azuma, T. Saito, Programmed cell death 1 forms negative costimulatory microclusters that directly inhibit T cell receptor signaling by recruiting phosphatase SHP2, *J. Exp. Med.* (2012). doi:10.1084/jem.20112741.
- [183] N. Patsoukis, L. Li, D. Sari, V. Petkova, V.A. Boussiotis, PD-1 Increases PTEN Phosphatase Activity While Decreasing PTEN Protein Stability by Inhibiting Casein Kinase 2, *Mol. Cell. Biol.* (2013). doi:10.1128/mcb.00319-13.
- [184] K. Karwacz, C. Bricogne, D. MacDonald, F. Arce, C.L. Bennett, M. Collins, D. Escors, PD-L1 co-stimulation contributes to ligand-induced T cell receptor down-modulation on CD8 + T cells, *EMBO Mol. Med.* (2011). doi:10.1002/emmm.201100165.
- [185] H. Huang, M. shin Jeon, L. Liao, C. Yang, C. Elly, J.R. Yates, Y.C. Liu, K33-linked polyubiquitination of T cell receptor- $\zeta$  regulates proteolysis-independent T cell signaling, *Immunity.* (2010). doi:10.1016/j.immuni.2010.07.002.
- [186] D. Fang, Y.C. Liu, Proteolysis-independent regulation of P13K by Cbl-b-mediated ubiquitination in T cells, *Nat. Immunol.* (2001). doi:10.1038/ni0901-870.
- [187] N. Patsoukis, K. Bardhan, P. Chatterjee, D. Sari, B. Liu, L.N. Bell, E.D. Karoly, G.J. Freeman, V. Petkova, P. Seth, L. Li, V.A. Boussiotis, PD-1 alters T-cell metabolic reprogramming by inhibiting glycolysis and promoting lipolysis and fatty acid oxidation, *Nat. Commun.* (2015). doi:10.1038/ncomms7692.

- [188] J.M. Michot, C. Bigenwald, S. Champiat, M. Collins, F. Carbonnel, S. Postel-Vinay, A. Berdelou, A. Varga, R. Bahleda, A. Hollebecque, C. Massard, A. Fuerea, V. Ribrag, A. Gazzah, J.P. Armand, N. Amellal, E. Angevin, N. Noel, C. Boutros, C. Mateus, C. Robert, J.C. Soria, A. Marabelle, O. Lambotte, Immune-related adverse events with immune checkpoint blockade: A comprehensive review, *Eur. J. Cancer.* (2016). doi:10.1016/j.ejca.2015.11.016.
- [189] C. Blank, I. Brown, A.C. Peterson, M. Spiotto, Y. Iwai, T. Honjo, T.F. Gajewski, PD-L1/B7H-1 Inhibits the Effector Phase of Tumor Rejection by T Cell Receptor (TCR) Transgenic CD8+ T Cells, *Cancer Res.* (2004). doi:10.1158/0008-5472.CAN-03-3259.
- [190] R. Mizuno, D. Sugiura, K. Shimizu, T. Maruhashi, M. Watada, I. mi Okazaki, T. Okazaki, PD-1 primarily targets TCR signal in the inhibition of functional T cell activation, *Front. Immunol.* (2019). doi:10.3389/fimmu.2019.00630.
- [191] R. Kim, Cancer Immunoediting: From Immune Surveillance to Immune Escape, in: *Cancer Immunother.*, 2007. doi:10.1016/B978-012372551-6/50066-3.
- [192] D.S. Chen, I. Mellman, Oncology meets immunology: The cancer-immunity cycle, *Immunity.* (2013). doi:10.1016/j.immuni.2013.07.012.
- [193] V. Velcheti, K. Schalper, Basic Overview of Current Immunotherapy Approaches in Cancer, *Am. Soc. Clin. Oncol. Educ. B.* (2016). doi:10.14694/edbk\_156572.
- [194] M. Reck, D. Rodriguez-Abreu, A.G. Robinson, R. Hui, T. Csöszi, A. Fülöp, M. Gottfried, N. Peled, A. Tafreshi, S. Cuffe, M. O'Brien, S. Rao, K. Hotta, M.A. Leiby, G.M. Lubiniecki, Y. Shentu, R. Rangwala, J.R. Brahmer, Pembrolizumab versus Chemotherapy for PD-L1-Positive Non-Small-Cell Lung Cancer, *N. Engl. J. Med.* (2016). doi:10.1056/NEJMoa1606774.
- [195] L. Gandhi, D. Rodríguez-Abreu, S. Gadgeel, E. Esteban, E. Felip, F. De Angelis, M. Domine, P. Clingan, M.J. Hochmair, S.F. Powell, S.Y.S. Cheng, H.G. Bischoff, N. Peled, F. Grossi, R.R. Jennens, M. Reck, R. Hui, E.B. Garon, M. Boyer, B. Rubio-Viqueira, S. Novello, T. Kurata, J.E. Gray, J. Vida, Z. Wei, J. Yang, H. Raftopoulos, M.C. Pietanza, M.C. Garassino, Pembrolizumab plus chemotherapy in metastatic non-small-cell lung cancer, *N. Engl. J. Med.* (2018). doi:10.1056/NEJMoa1801005.
- [196] J.D. Wolchok, V. Chiarion-Sileni, R. Gonzalez, P. Rutkowski, J.J. Grob, C.L. Cowey, C.D. Lao, J. Wagstaff, D. Schadendorf, P.F. Ferrucci, M. Smylie, R. Dummer, A. Hill, D. Hogg, J. Haanen, M.S. Carlino, O. Bechter, M. Maio, I. Marquez-Rodas, M. Guidoboni, G. McArthur, C. Lebbé, P.A. Ascierto, G. V. Long, J. Cebon, J. Sosman, M.A. Postow, M.K. Callahan, D. Walker, L. Rollin, R. Bhore, F.S. Hodi, J. Larkin, Overall Survival with Combined Nivolumab and Ipilimumab in Advanced Melanoma, *N. Engl. J. Med.* (2017). doi:10.1056/NEJMoa1709684.
- [197] M. Rijnders, R. de Wit, J.L. Boormans, M.P.J. Lolkema, A.A.M. van der Veldt, Systematic Review of Immune Checkpoint Inhibition in Urological Cancers, *Eur. Urol.* (2017). doi:10.1016/j.eururo.2017.06.012.
- [198] J. Wolchok, Putting the Immunologic Brakes on Cancer, *Cell.* (2018). doi:10.1016/j.cell.2018.11.006.
- [199] S. Hannier, F. Triebel, The MHC class II ligand lymphocyte activation gene-3 is co-distributed with CD8 and CD3-TCR molecules after their engagement by mAb or peptide-MHC class I complexes, *Int. Immunol.* (1999). doi:10.1093/intimm/11.11.1745.

- 
- [200] K. Sakuishi, L. Apetoh, J.M. Sullivan, B.R. Blazar, V.K. Kuchroo, A.C. Anderson, Targeting Tim-3 and PD-1 pathways to reverse T cell exhaustion and restore anti-tumor immunity, *J. Exp. Med.* (2010). doi:10.1084/jem.20100643.
- [201] J.K. Petty, K. He, C.L. Corless, J.T. Vetto, A.D. Weinberg, Survival in human colorectal cancer correlates with expression of the T-cell costimulatory molecule OX-40 (CD134), in: *Am. J. Surg.*, 2002. doi:10.1016/S0002-9610(02)00831-0.
- [202] G.L. Beatty, E.G. Chiorean, M.P. Fishman, B. Saboury, U.R. Teitelbaum, W. Sun, R.D. Huhn, W. Song, D. Li, L.L. Sharp, D.A. Torigian, P.J. O'Dwyer, R.H. Vonderheide, CD40 agonists alter tumor stroma and show efficacy against pancreatic carcinoma in mice and humans., *Science*. 331 (2011) 1612–6. doi:10.1126/science.1198443.
- [203] R.H. Vonderheide, K.T. Flaherty, M. Khalil, M.S. Stumacher, D.L. Bajor, N.A. Hutnick, P. Sullivan, J.J. Mahany, M. Gallagher, A. Kramer, S.J. Green, P.J. O'Dwyer, K.L. Running, R.D. Huhn, S.J. Antonia, Clinical activity and immune modulation in cancer patients treated with CP-870,893, a novel CD40 agonist monoclonal antibody, *J. Clin. Oncol.* (2007). doi:10.1200/JCO.2006.08.3311.
- [204] L. Lu, X. Xu, B. Zhang, R. Zhang, H. Ji, X. Wang, Combined PD-1 blockade and GITR triggering induce a potent antitumor immunity in murine cancer models and synergizes with chemotherapeutic drugs, *J. Transl. Med.* (2014). doi:10.1186/1479-5876-12-36.
- [205] P.J. DeMaria, M. Bilusic, *Cancer Vaccines*, *Hematol. Oncol. Clin. North Am.* (2019). doi:10.1016/j.hoc.2018.12.001.
- [206] L.H. Kasper, A.T. Reder, Immunomodulatory activity of interferon-beta, *Ann. Clin. Transl. Neurol.* (2014). doi:10.1002/acn3.84.
- [207] S.A. Rosenberg, C. Sportès, M. Ahmadzadeh, T.J. Fry, L.T. Ngo, S.L. Schwarz, M. Stetler-Stevenson, K.E. Morton, S.A. Mavroukakis, M. Morre, R. Buffet, C.L. Mackall, R.E. Gress, IL-7 administration to humans leads to expansion of CD8+ and CD4+ cells but a relative decrease of CD4+ T-regulatory cells, *J. Immunother.* (2006). doi:10.1080/03601270600564088.
- [208] C. Sportès, R.R. Babb, M.C. Krumlauf, F.T. Hakim, S.M. Steinberg, C.K. Chow, M.R. Brown, T.A. Fleisher, P. Noel, I. Maric, M. Stetler-Stevenson, J. Engel, R. Buffet, M. Morre, R.J. Amato, A. Pecora, C.L. Mackall, R.E. Gress, Phase I study of recombinant human interleukin-7 administration in subjects with refractory malignancy, *Clin. Cancer Res.* (2010). doi:10.1158/1078-0432.CCR-09-1303.
- [209] J. Nemunaitis, Vaccines in cancer: GVAX, a GM-CSF gene vaccine., *Expert Rev. Vaccines*. 4 (2005) 259–74. doi:10.1586/14760584.4.3.259.
- [210] D.T. Le, E. Lutz, J.N. Uram, E.A. Sugar, B. Onners, S. Solt, L. Zheng, L.A. Diaz, R.C. Donehower, E.M. Jaffee, D.A. Laheru, Evaluation of ipilimumab in combination with allogeneic pancreatic tumor cells transfected with a GM-CSF gene in previously treated pancreatic cancer, *J. Immunother.* (2013). doi:10.1097/CJI.0b013e31829fb7a2.
- [211] M. Dougan, G. Dranoff, S.K. Dougan, *Cancer Immunotherapy: Beyond Checkpoint Blockade*, *Annu. Rev. Cancer Biol.* (2019). doi:10.1146/annurev-cancerbio-030518-055552.

- [212] S.A. Rosenberg, J.C. Yang, R.M. Sherry, U.S. Kammula, M.S. Hughes, G.Q. Phan, D.E. Citrin, N.P. Restifo, P.F. Robbins, J.R. Wunderlich, K.E. Morton, C.M. Laurencot, S.M. Steinberg, D.E. White, M.E. Dudley, Durable complete responses in heavily pretreated patients with metastatic melanoma using T-cell transfer immunotherapy, *Clin. Cancer Res.* (2011). doi:10.1158/1078-0432.CCR-11-0116.
- [213] C.M. Bollard, S. Gottschalk, A.M. Leen, H. Weiss, K.C. Straathof, G. Carrum, M. Khalil, M.F. Wu, M.H. Huls, C.C. Chang, M.V. Gresik, A.P. Gee, M.K. Brenner, C.M. Rooney, H.E. Heslop, Complete responses of relapsed lymphoma following genetic modification of tumor-antigen presenting cells and T-lymphocyte transfer, *Blood.* (2007). doi:10.1182/blood-2007-05-091280.
- [214] H. Dai, Y. Wang, X. Lu, W. Han, Chimeric antigen receptors modified T-cells for cancer therapy, *J. Natl. Cancer Inst.* (2016). doi:10.1093/jnci/djv439.
- [215] H.L. Kaufman, F.J. Kohlhapp, A. Zloza, Oncolytic viruses: A new class of immunotherapy drugs, *Nat. Rev. Drug Discov.* (2015). doi:10.1038/nrd4663.
- [216] L.A. Emens, P.A. Ascierto, P.K. Darcy, S. Demaria, A.M.M. Eggermont, W.L. Redmond, B. Seliger, F.M. Marincola, Cancer immunotherapy: Opportunities and challenges in the rapidly evolving clinical landscape, *Eur. J. Cancer.* (2017). doi:10.1016/j.ejca.2017.01.035.
- [217] P. Sharma, S. Hu-Lieskovan, J.A. Wargo, A. Ribas, Primary, Adaptive, and Acquired Resistance to Cancer Immunotherapy, *Cell.* (2017). doi:10.1016/j.cell.2017.01.017.
- [218] N.P. Restifo, M.J. Smyth, A. Snyder, Acquired resistance to immunotherapy and future challenges, *Nat. Rev. Cancer.* (2016). doi:10.1038/nrc.2016.2.
- [219] J.J. Havel, D. Chowell, T.A. Chan, The evolving landscape of biomarkers for checkpoint inhibitor immunotherapy, *Nat. Rev. Cancer.* (2019). doi:10.1038/s41568-019-0116-x.
- [220] J. Gong, A. Chehrazi-Raffle, S. Reddi, R. Salgia, Development of PD-1 and PD-L1 inhibitors as a form of cancer immunotherapy: A comprehensive review of registration trials and future considerations, *J. Immunother. Cancer.* (2018). doi:10.1186/s40425-018-0316-z.
- [221] K.C. Ohaegbulam, A. Assal, E. Lazar-Molnar, Y. Yao, X. Zang, Human cancer immunotherapy with antibodies to the PD-1 and PD-L1 pathway, *Trends Mol. Med.* 21 (2015) 24–33. doi:10.1016/j.molmed.2014.10.009.
- [222] S. Stein, M.J. Pishvaian, M.S. Lee, K.-H. Lee, S. Hernandez, A. Kwan, B. Liu, W. Grossman, K. Iizuka, B.-Y. Ryoo, Safety and clinical activity of 1L atezolizumab + bevacizumab in a phase Ib study in hepatocellular carcinoma (HCC)., *J. Clin. Oncol.* (2018). doi:10.1200/jco.2018.36.15\_suppl.4074.
- [223] Y.L. Kasamon, R.A. de Claro, Y. Wang, Y.L. Shen, A.T. Farrell, R. Pazdur, FDA Approval Summary: Nivolumab for the Treatment of Relapsed or Progressive Classical Hodgkin Lymphoma, *Oncologist.* (2017). doi:10.1634/theoncologist.2017-0004.
- [224] M. Ikeda, M.W. Sung, M. Kudo, M. Kobayashi, A.D. Baron, R.S. Finn, S. Kaneko, A.X. Zhu, T. Kubota, S. Kraljevic, K. Ishikawa, A.B. Siegel, H. Kumada, T. Okusaka, A phase 1b trial of lenvatinib (LEN) plus pembrolizumab (PEM) in patients (pts) with unresectable hepatocellular carcinoma (uHCC)., *J. Clin. Oncol.* (2018). doi:10.1200/jco.2018.36.15\_suppl.4076.

- [225] T.K. Choueiri, J.M.G. Larkin, M. Oya, F.C. Thistlethwaite, M. Martignoni, P.D. Nathan, T. Powles, D.F. McDermott, P.B. Robbins, D.D. Chism, D.C. Cho, M.B. Atkins, M.S. Gordon, S. Gupta, H. Uemura, Y. Tomita, A. Compagnoni, A. di Pietro, B.I. Rini, First-line avelumab + axitinib therapy in patients (pts) with advanced renal cell carcinoma (aRCC): Results from a phase Ib trial., *J. Clin. Oncol.* (2017). doi:10.1200/jco.2017.35.15\_suppl.4504.
- [226] A. Markham, S. Duggan, Cemiplimab: First Global Approval, *Drugs.* (2018). doi:10.1007/s40265-018-1012-5.
- [227] S.J. Antonia, A. Villegas, D. Daniel, D. Vicente, S. Murakami, R. Hui, T. Kurata, A. Chiappori, K.H. Lee, M. De Wit, B.C. Cho, M. Bourhaba, X. Quantin, T. Tokito, T. Mekhail, D. Planchard, Y.C. Kim, C.S. Karapetis, S. Hired, G. Ostoros, K. Kubota, J.E. Gray, L. Paz-Ares, J. De Castro Carpeño, C. Faivre-Finn, M. Reck, J. Vansteenkiste, D.R. Spigel, C. Wadsworth, G. Melillo, M. Taboada, P.A. Dennis, M. Özgüroğlu, Overall survival with durvalumab after chemoradiotherapy in stage III NSCLC, *N. Engl. J. Med.* (2018). doi:10.1056/NEJMoa1809697.
- [228] C. Böger, H. Behrens, M. Mathiak, S. Krüger, H. Kalthoff, C. Röcken, PD-L1 is an independent prognostic predictor in gastric cancer of Western patients., *Oncotarget.* 7 (2016) 24269–83. doi:10.18632/oncotarget.8169.
- [229] F.R. Hirsch, A. McElhinny, D. Stanforth, J. Ranger-Moore, M. Jansson, K. Kulangara, W. Richardson, P. Towne, D. Hanks, B. Vennapusa, A. Mistry, R. Kalamegham, S. Averbuch, J. Novotny, E. Rubin, K. Emancipator, I. McCaffery, J.A. Williams, J. Walker, J. Longshore, M.S. Tsao, K.M. Kerr, PD-L1 Immunohistochemistry Assays for Lung Cancer: Results from Phase 1 of the Blueprint PD-L1 IHC Assay Comparison Project, *J. Thorac. Oncol.* 12 (2017) 208–222. doi:10.1016/j.jtho.2016.11.2228.
- [230] M.S. Tsao, K.M. Kerr, M. Kockx, M.B. Beasley, A.C. Borczuk, J. Botling, L. Bubendorf, L. Chirieac, G. Chen, T.Y. Chou, J.H. Chung, S. Dacic, S. Lantuejoul, M. Mino-Kenudson, A.L. Moreira, A.G. Nicholson, M. Noguchi, G. Pelosi, C. Poleri, P.A. Russell, J. Sauter, E. Thunnissen, I. Wistuba, H. Yu, M.W. Wynes, M. Pintilie, Y. Yatabe, F.R. Hirsch, PD-L1 Immunohistochemistry Comparability Study in Real-Life Clinical Samples: Results of Blueprint Phase 2 Project, *J. Thorac. Oncol.* (2018). doi:10.1016/j.jtho.2018.05.013.
- [231] H.D. Finnes, Durvalumab (Imfinzi™), *Oncol. Times.* (2017). doi:10.1097/01.cot.0000527389.56587.3c.
- [232] H.T. Lee, J.Y. Lee, H. Lim, S.H. Lee, Y.J. Moon, H.J. Pyo, S.E. Ryu, W. Shin, Y.S. Heo, Molecular mechanism of PD-1/PD-L1 blockade via anti-PD-L1 antibodies atezolizumab and durvalumab, *Sci. Rep.* (2017). doi:10.1038/s41598-017-06002-8.
- [233] C. Massard, M.S. Gordon, S. Sharma, S. Rafii, Z.A. Wainberg, J. Luke, T.J. Curiel, G. Colon-Otero, O. Hamid, R.E. Sanborn, P.H. O'Donnell, A. Drakaki, W. Tan, J.F. Kurland, M.C. Rebelatto, X. Jin, J.A. Blake-Haskins, A. Gupta, N.H. Segal, Safety and efficacy of durvalumab (MEDI4736), an anti-programmed cell death ligand-1 immune checkpoint inhibitor, in patients with advanced urothelial bladder cancer, *J. Clin. Oncol.* (2016). doi:10.1200/JCO.2016.67.9761.

- [234] T. Powles, P.H. O'Donnell, C. Massard, H.-T. Arkenau, T.W. Friedlander, C. Hoimes, J.-L. Lee, M. Ong, S.S. Sridhar, N.J. Vogelzang, M.N. Fishman, J. Zhang, S. Srinivas, J. Parikh, J. Antal, X. Jin, A.K. Gupta, N.M. Hahn, Updated efficacy and tolerability of durvalumab in locally advanced or metastatic urothelial carcinoma., *J. Clin. Oncol.* (2017). doi:10.1200/jco.2017.35.6\_suppl.286.
- [235] J.R. Brahmer, S.S. Tykodi, L.Q.M. Chow, W.-J. Hwu, S.L. Topalian, P. Hwu, C.G. Drake, L.H. Camacho, J. Kauh, K. Odunsi, H.C. Pitot, O. Hamid, S. Bhatia, R. Martins, K. Eaton, S. Chen, T.M. Salay, S. Alaparthi, J.F. Grosso, A.J. Korman, S.M. Parker, S. Agrawal, S.M. Goldberg, D.M. Pardoll, A. Gupta, J.M. Wigginton, Safety and activity of anti-PD-L1 antibody in patients with advanced cancer., *N. Engl. J. Med.* 366 (2012) 2455–65. doi:10.1056/NEJMoal200694.
- [236] S.J. Antonia, A. Villegas, D. Daniel, D. Vicente, S. Murakami, R. Hui, T. Yokoi, A. Chiappori, K.H. Lee, M. De Wit, B.C. Cho, M. Bourhaba, X. Quantin, T. Tokito, T. Mekhail, D. Planchard, Y.C. Kim, C.S. Karapetis, S. Hired, G. Ostoros, K. Kubota, J.E. Gray, L. Paz-Ares, J. De Castro Carpeño, C. Wadsworth, G. Melillo, H. Jiang, Y. Huang, P.A. Dennis, M. Özgüroğlu, Durvalumab after chemoradiotherapy in stage III non-small-cell lung cancer, *N. Engl. J. Med.* (2017). doi:10.1056/NEJMoal709937.
- [237] M.L. Rothenberg, M.J. Moore, M.C. Cripps, J.S. Andersen, R.K. Portenoy, H.A. Burris, M.R. Green, P.G. Tarassoff, T.D. Brown, E.S. Casper, A.M. Storniolo, D.D. Von Hoff, A phase II trial of gemcitabine in patients with 5-FU-refractory pancreas cancer, *Ann. Oncol.* (1996). doi:10.1093/oxfordjournals.annonc.a010600.
- [238] H. Johansson, R. Andersson, M. Bauden, S. Hammes, S. Holdenrieder, D. Ansari, Immune checkpoint therapy for pancreatic cancer, *World J. Gastroenterol.* (2016). doi:10.3748/wjg.v22.i43.9457.
- [239] M.H. Tan, N.J. Nowak, R. Loo, H. Ochi, A.A. Sandberg, C. Lopez, J.W. Pickren, R. Berjian, H.O. Douglass, T.M. Chu, Characterization of a new primary human pancreatic tumor line, *Cancer Invest.* (1986). doi:10.3109/07357908609039823.
- [240] B. Sipos, S. Möser, H. Kalthoff, V. Török, M. Löhr, G. Klöppel, A comprehensive characterization of pancreatic ductal carcinoma cell lines: towards the establishment of an in vitro research platform., *Virchows Arch.* 442 (2003) 444–452. doi:10.1007/s00428-003-0784-4.
- [241] C. Sun, T. Yamato, T. Furukawa, Y. Ohnishi, H. Kijima, A. Horii, Characterization of the mutations of the K-ras, p53, p16, and SMAD4 genes in 15 human pancreatic cancer cell lines, *Oncol. Rep.* (2001).
- [242] H. Kalthoff, W. Schmiegell, C. Roeder, D. Kasche, A.S. and G. Lauer, H.G. Thiele, G. Honold, K. Pantel, G. Riethmueller, p53 and K-RAS alterations in pancreatic epithelial cell lesions., *Oncogene.* (1993).
- [243] D. Bartsch, P. Barth, D. Bastian, A. Ramaswamy, B. Gerdes, B. Chaloupka, Y. Deiss, B. Simon, A. Schudy, Higher frequency of DPC4/Smad4 alterations in pancreatic cancer cell lines than in primary pancreatic adenocarcinomas, *Cancer Lett.* (1999). doi:10.1016/S0304-3835(98)00380-2.
- [244] M. Schutte, R.H. Hruban, L. Hedrick, K.R. Cho, G.M. Nadasdy, C.L. Weinstein, G.S. Bova, W.B. Isaacs, P. Cairns, H. Nawroz, D. Sidransky, R.A. Casero, P.S. Meltzer, S.A. Hahn, S.E. Kern, DPC4 gene in various tumor types, *Cancer Res.* (1996).

- [245] G. Berrozpe, J. Schaeffer, M.A. Peinado, F.X. Real, M. Perucho, Comparative analysis of mutations in the p53 and K-ras genes in pancreatic cancer, *Int. J. Cancer*. (1994). doi:10.1002/ijc.2910580207.
- [246] E.L. Deer, J. González-Hernández, J.D. Coursen, J.E. Shea, J. Ngatia, C.L. Scaife, M.A. Firpo, S.J. Mulvihill, Phenotype and genotype of pancreatic cancer cell lines, *Pancreas*. (2010). doi:10.1097/MPA.0b013e3181c15963.
- [247] R.T. Morgan, L.K. Woods, G.E. Moore, L.A. Quinn, L. McGavran, S.G. Gordon, Human cell line (COLO 357) of metastatic pancreatic adenocarcinoma, *Int. J. Cancer*. (1980). doi:10.1002/ijc.2910250507.
- [248] C.M. Barton, S.L. Staddon, C.M. Hughes, C. O'Sullivan, N.R. Lemoine, P.A. Hall, G. Klöppel, B. Theis, R.C.G. Russell, J. Neoptolemos, R.C.N. Williamson, D.P. Lane, Abnormalities of the p53 tumour suppressor gene in human pancreatic cancer, *Br. J. Cancer*. (1991). doi:10.1038/bjc.1991.467.
- [249] J. Qian, J. Niu, M. Li, P.J. Chiao, M.S. Tsao, In vitro modeling of human pancreatic duct epithelial cell transformation defines gene expression changes induced by K-ras oncogenic activation in pancreatic carcinogenesis, *Cancer Res.* 65 (2005) 5045–5053. doi:10.1158/0008-5472.CAN-04-3208.
- [250] T. Furukawa, W.P. Duguid, L. Rosenberg, J. Viallet, D.A. Galloway, M.S. Tsao, Long-term culture and immortalization of epithelial cells from normal adult human pancreatic ducts transfected by the E6E7 gene of human papilloma virus 16., *Am. J. Pathol.* (1996).
- [251] N. Liu, T. Furukawa, M. Kobari, M.S. Tsao, Comparative phenotypic studies of duct epithelial cell lines derived from normal human pancreas and pancreatic carcinoma, *Am. J. Pathol.* (1998). doi:10.1016/S0002-9440(10)65567-8.
- [252] H. Ouyang, L.J. Mou, C. Luk, N. Liu, J. Karaskova, J. Squire, M.S. Tsao, Immortal human pancreatic duct epithelial cell lines with near normal genotype and phenotype, *Am. J. Pathol.* (2000). doi:10.1016/S0002-9440(10)64800-6.
- [253] A.A. Yunis, G.K. Arimura, D.J. Russin, Human pancreatic carcinoma (mia paca-2) in continuous culture: Sensitivity to asparaginase, *Int. J. Cancer*. (1977). doi:10.1002/ijc.2910190118.
- [254] P.S. Moore, B. Sipos, S. Orlandini, C. Sorio, F.X. Real, N.R. Lemoine, T. Gress, C. Bassi, G. Klöppel, H. Kalthoff, H. Ungefroren, M. Lohr, A. Scarpa, Genetic profile of 22 pancreatic carcinoma cell lines. Analysis of K-ras, p53, p16 and DPC4/Smad4, *Virchows Arch.* 439 (2001) 798–802. doi:10.1007/s004280100474.
- [255] M. Lieber, J. Mazzetta, W. Nelson-Rees, M. Kaplan, G. Todaro, Establishment of a continuous tumor-cell line (PANC-1) from a human carcinoma of the exocrine pancreas, *Int. J. Cancer*. (1975). doi:10.1002/ijc.2910150505.
- [256] T. Okabe, N. Yamaguchi, N. Ohsawa, Establishment and characterization of a carcinoembryonic antigen (CEA)-producing cell line from a human carcinoma of the exocrine pancreas, *Cancer*. 51 (1983) 662–668. doi:10.1002/1097-0142(19830215)51:4<662::AID-CNCR2820510419>3.0.CO;2-X.
- [257] S. Wolterink, G. Moldenhauer, M. Fogel, H. Kiefel, M. Pfeifer, S. Lüttgau, R. Gouveia, J. Costa, J. Endell, U. Moebius, P. Altevogt, Therapeutic antibodies to human L1CAM: Functional characterization and application in a mouse model for ovarian carcinoma, *Cancer Res.* (2010). doi:10.1158/0008-5472.CAN-09-3730.

- [258] G. Banfalvi, Cell cycle synchronization of animal cells and nuclei by centrifugal elutriation, *Nat. Protoc.* (2008). doi:10.1038/nprot.2008.34.
- [259] A. Trickett, Y.L. Kwan, T cell stimulation and expansion using anti-CD3/CD28 beads, *J. Immunol. Methods.* (2003). doi:10.1016/S0022-1759(03)00010-3.
- [260] D.C. Lacey, A. Achuthan, A.J. Fleetwood, H. Dinh, J. Roiniotis, G.M. Scholz, M.W. Chang, S.K. Beckman, A.D. Cook, J.A. Hamilton, Defining GM-CSF- and Macrophage-CSF-Dependent Macrophage Responses by In Vitro Models, *J. Immunol.* (2012). doi:10.4049/jimmunol.1103426.
- [261] A.J. Fleetwood, T. Lawrence, J.A. Hamilton, A.D. Cook, Granulocyte-macrophage colony-stimulating factor (CSF) and macrophage CSF-dependent macrophage phenotypes display differences in cytokine profiles and transcription factor activities: implications for CSF blockade in inflammation., *J. Immunol.* (2007).
- [262] O.H. LOWRY, N.J. Rosebrough, A.L. Farr, R.J. Randall, A. Lewis, Protein measurement with the folin, *J. Biol. Chem.* (1951). doi:10.1007/s10982-008-9035-9.
- [263] U.K. Laemmli, Cleavage of structural proteins during the assembly of the head of bacteriophage T4, *Nature.* (1970). doi:10.1038/227680a0.
- [264] S. Rahn, S. Krüger, R. Mennrich, L. Goebel, D. Wesch, H.-H. Oberg, I. Vogel, M. Ebsen, C. Röcken, O. Helm, S. Sebens, POLE Score: a comprehensive profiling of programmed death 1 ligand 1 expression in pancreatic ductal adenocarcinoma, *Oncotarget.* 10 (2019) 1572–1588. doi:10.18632/oncotarget.26705.
- [265] A. Diana, L.M. Wang, Z. D’Costa, P. Allen, A. Azad, M.A. Silva, Z. Soonawalla, S. Liu, W.G. McKenna, R.J. Muschel, E. Fokas, Prognostic value, localization and correlation of PD-1/PD-L1, CD8 and FOXP3 with the desmoplastic stroma in pancreatic ductal adenocarcinoma., *Oncotarget.* 7 (2016) 40992–41004. doi:10.18632/oncotarget.10038.
- [266] D.J. Birnbaum, P. Finetti, A. Lopresti, M. Gilabert, F. Poizat, O. Turrini, J. Raoul, J. Delpero, V. Moutardier, D. Birnbaum, E. Mamessier, F. Bertucci, Prognostic value of PDL1 expression in pancreatic cancer., *Oncotarget.* 7 (2016) 71198–71210. doi:10.18632/oncotarget.11685.
- [267] L. Wang, Q. Ma, X. Chen, K. Guo, J. Li, M. Zhang, Clinical significance of B7-H1 and B7-1 expressions in pancreatic carcinoma, *World J. Surg.* 34 (2010) 1059–1065. doi:10.1007/s00268-010-0448-x.
- [268] L. Geng, D. Huang, J. Liu, Y. Qian, J. Deng, D. Li, Z. Hu, J. Zhang, G. Jiang, S. Zheng, B7-H1 up-regulated expression in human pancreatic carcinoma tissue associates with tumor progression, *J. Cancer Res. Clin. Oncol.* 134 (2008) 1021–1027. doi:10.1007/s00432-008-0364-8.
- [269] M. Loos, N.A. Giese, J. Kleeff, T. Giese, M.M. Gaida, F. Bergmann, M. Laschinger, M. W.Büchler, H. Friess, Clinical significance and regulation of the costimulatory molecule B7-H1 in pancreatic cancer, *Cancer Lett.* 268 (2008) 98–109. doi:10.1016/j.canlet.2008.03.056.
- [270] H. Dong, G. Zhu, K. Tamada, L. Chen, B7-H1, a third member of the B7 family, co-stimulates T-cell proliferation and interleukin-10 secretion, *Nat. Med.* (1999). doi:10.1038/70932.



- [271] G.J. Freeman, A.J. Long, Y. Iwai, K. Bourque, T. Chernova, H. Nishimura, L.J. Fitz, N. Malenkovich, T. Okazaki, M.C. Byrne, H.F. Horton, L. Fouser, L. Carter, V. Ling, M.R. Bowman, B.M. Carreno, M. Collins, C.R. Wood, T. Honjo, Engagement of the PD-1 immunoinhibitory receptor by a novel B7 family member leads to negative regulation of lymphocyte activation, *J. Exp. Med.* (2000). doi:10.1084/jem.192.7.1027.
- [272] E. Giroux Leprieur, C. Dumenil, C. Julie, V. Giraud, J. Dumoulin, S. Labrune, T. Chinet, Immunotherapy revolutionises non-small-cell lung cancer therapy: Results, perspectives and new challenges, *Eur. J. Cancer.* (2017). doi:10.1016/j.ejca.2016.12.041.
- [273] L. Zitvogel, G. Kroemer, Targeting PD-1/PD-L1 interactions for cancer immunotherapy., *Oncoimmunology.* 1 (2012) 1223–1225. doi:10.4161/onci.21335.
- [274] Y. Zhang, A. Velez-Delgado, E. Mathew, D. Li, F.M. Mendez, K. Flannagan, A.D. Rhim, D.M. Simeone, G.L. Beatty, M. Pasca di Magliano, Myeloid cells are required for PD-1/PD-L1 checkpoint activation and the establishment of an immunosuppressive environment in pancreatic cancer, *Gut.* 66 (2017) 124–136. doi:10.1136/gutjnl-2016-312078.
- [275] S.K. Dougan, The pancreatic cancer microenvironment, *Cancer J. (United States).* (2017). doi:10.1097/PPO.0000000000000288.
- [276] S. Mürköster, K. Wegehenkel, A. Arlt, M. Witt, B. Sipos, M.L. Kruse, T. Sebens, G. Klöppel, H. Kalthoff, U.R. Fölsch, H. Schäfer, Tumor Stroma Interactions Induce Chemoresistance in Pancreatic Ductal Carcinoma Cells Involving Increased Secretion and Paracrine Effects of Nitric Oxide and Interleukin-1beta, *Cancer Res.* 64 (2004) 1331–1337. doi:10.1158/0008-5472.CAN-03-1860.
- [277] T. Chatila, L. Silverman, R. Miller, R. Geha, Mechanisms of T cell activation by the calcium ionophore ionomycin., *J. Immunol.* (1989).
- [278] L.J. Bayne, G.L. Beatty, N. Jhala, C.E. Clark, A.D. Rhim, B.Z. Stanger, R.H. Vonderheide, Tumor-Derived Granulocyte-Macrophage Colony-Stimulating Factor Regulates Myeloid Inflammation and T Cell Immunity in Pancreatic Cancer, *Cancer Cell.* (2012). doi:10.1016/j.ccr.2012.04.025.
- [279] B. Becher, S. Tugues, M. Greter, GM-CSF: From Growth Factor to Central Mediator of Tissue Inflammation, *Immunity.* (2016). doi:10.1016/j.immuni.2016.10.026.
- [280] A. Lescoat, A. Ballerie, Y. Augagneur, C. Morzadec, L. Vernhet, O. Fardel, P. Jégo, S. Jouneau, V. Lecureur, Distinct properties of human M-CSF and GM-CSF monocyte-derived macrophages to simulate pathological lung conditions in vitro: Application to systemic and inflammatory disorders with pulmonary involvement, *Int. J. Mol. Sci.* (2018). doi:10.3390/ijms19030894.
- [281] M. Green, M.A. Harrington, A Comparison of Macrophage Colony-Stimulating Factor (M-CSF) Gene Expression in Primary and Immortalized Endothelial Cells, *J. Hematother. Stem Cell Res.* 9 (2000) 237–246. doi:10.1089/152581600319450.
- [282] F. Karzai, D. VanderWeele, R.A. Madan, H. Owens, L.M. Cordes, A. Hankin, A. Couvillon, E. Nichols, M. Bilusic, M.L. Beshiri, K. Kelly, V. Krishnasamy, S. Lee, M.-J. Lee, A. Yuno, J.B. Trepel, M.J. Merino, R. Dittamore, J. Marté, R.N. Donahue, J. Schlom, K.J. Killian, P.S. Meltzer, S.M. Steinberg, J.L. Gulley, J.-M. Lee, W.L. Dahut, Activity of durvalumab plus olaparib in metastatic castration-resistant prostate cancer in men with and without DNA damage repair mutations, *J. Immunother. Cancer.* (2018). doi:10.1186/s40425-018-0463-2.

- [283] A. Ribas, J.D. Wolchok, Cancer immunotherapy using checkpoint blockade, *Science* (80-. ). (2018). doi:10.1126/science.aar4060.
- [284] G. Abril-Rodriguez, A. Ribas, SnapShot: Immune Checkpoint Inhibitors, *Cancer Cell*. (2017). doi:10.1016/j.ccell.2017.05.010.
- [285] G.M. Blumenthal, R. Pazdur, Approvals in 2016: the march of the checkpoint inhibitors, *Nat. Rev. Clin. Oncol.* 14 (2017) 131–132. doi:10.1038/nrclinonc.2017.15.
- [286] J.T. Jørgensen, Companion diagnostic assays for PD-1/PD-L1 checkpoint inhibitors in NSCLC, *Expert Rev. Mol. Diagn.* (2016). doi:10.1586/14737159.2016.1117389.
- [287] D.J. Dabbs, *Diagnostic Immunohistochemistry*, 2010. doi:10.1016/B978-1-4160-5766-6.X0001-5.
- [288] T.J. Gniadek, Q.K. Li, E. Tully, S. Chatterjee, S. Nimmagadda, E. Gabrielson, Heterogeneous expression of PD-L1 in pulmonary squamous cell carcinoma and adenocarcinoma: implications for assessment by small biopsy, *Mod. Pathol.* (2017) 1–9. doi:10.1038/modpathol.2016.213.
- [289] M. Ilie, E. Long-Mira, C. Bence, C. Butori, S. Lassalle, L. Bouhlel, L. Fazzalari, K. Zahaf, S. Lalvée, K. Washetine, J. Mouroux, N. Vénissac, M. Poudenx, J. Otto, J.C. Sabourin, C.H. Marquette, V. Hofman, P. Hofman, Comparative study of the PD-L1 status between surgically resected specimens and matched biopsies of NSCLC patients reveal major discordances: A potential issue for anti-PD-L1 therapeutic strategies, *Ann. Oncol.* (2016). doi:10.1093/annonc/mdv489.
- [290] A. Garcia-Diaz, D.S. Shin, B.H. Moreno, J. Saco, H. Escuin-Ordinas, G.A. Rodriguez, J.M. Zaretsky, L. Sun, W. Hugo, X. Wang, G. Parisi, C.P. Saus, D.Y. Torrejon, T.G. Graeber, B. Comin-Anduix, S. Hu-Lieskovan, R. Damoiseaux, R.S. Lo, A. Ribas, Interferon Receptor Signaling Pathways Regulating PD-L1 and PD-L2 Expression, *Cell Rep.* (2017). doi:10.1016/j.celrep.2017.04.031.
- [291] X. Wang, L. Yang, F. Huang, Q. Zhang, S. Liu, L. Ma, Z. You, Inflammatory cytokines IL-17 and TNF- $\alpha$  up-regulate PD-L1 expression in human prostate and colon cancer cells, *Immunol. Lett.* (2017). doi:10.1016/j.imlet.2017.02.006.
- [292] M. Thorn, P. Guha, M. Cunetta, N.J. Espat, G. Miller, R.P. Junghans, S.C. Katz, Tumor-associated GM-CSF overexpression induces immunoinhibitory molecules via STAT3 in myeloid-suppressor cells infiltrating liver metastases, *Cancer Gene Ther.* (2016). doi:10.1038/cgt.2016.19.
- [293] J. Peng, J. Hamanishi, N. Matsumura, K. Abiko, K. Murat, T. Baba, K. Yamaguchi, N. Horikawa, Y. Hosoe, S.K. Murphy, I. Konishi, M. Mandai, Chemotherapy induces programmed cell death-ligand 1 overexpression via the nuclear factor- $\kappa$ B to foster an immunosuppressive tumor microenvironment in Ovarian Cancer, *Cancer Res.* (2015). doi:10.1158/0008-5472.CAN-14-3098.
- [294] F.R. Hirsch, A. McElhinny, D. Stanforth, J. Ranger-Moore, M. Jansson, K. Kulangara, W. Richardson, P. Towne, D. Hanks, B. Vennapusa, A. Mistry, R. Kalamegham, S. Averbuch, J. Novotny, E. Rubin, K. Emancipator, I. McCaffery, J.A. Williams, J. Walker, J. Longshore, M.S. Tsao, K.M. Kerr, PD-L1 Immunohistochemistry Assays for Lung Cancer: Results from Phase 1 of the Blueprint PD-L1 IHC Assay Comparison Project, *J. Thorac. Oncol.* (2017). doi:10.1016/j.jtho.2016.11.2228.

- [295] J. McLaughlin, G. Han, K.A. Schalper, D. Carvajal-Hausdorf, V. Pelekanou, J. Rehman, V. Velcheti, R. Herbst, P. LoRusso, D.L. Rimm, Quantitative assessment of the heterogeneity of PD-L1 expression in non-small-cell lung cancer, *JAMA Oncol.* (2016). doi:10.1001/jamaoncol.2015.3638.
- [296] S. Ahn, Y. Lee, J. Kim, J. Lee, J. Hwang, Y. Yoon, J.Y. Cho, H. Han, Y. Choi, H. Kim, Programmed cell death ligand-1 (PD-L1) expression in extrahepatic biliary tract cancers: a comparative study using 22C3, SP263 and E1L3N anti-PD-L1 antibodies, *Histopathology.* (2019). doi:10.1111/his.13901.
- [297] J. Cogswell, H.D. Inzunza, Q. Wu, J.N. Feder, G. Mintier, J. Novotny, D.M. Cardona, An Analytical Comparison of Dako 28-8 PharmDx Assay and an E1L3N Laboratory-Developed Test in the Immunohistochemical Detection of Programmed Death-Ligand 1, *Mol. Diagnosis Ther.* (2017). doi:10.1007/s40291-016-0237-9.
- [298] E.R. Parra, P. Villalobos, B. Mino, J. Rodriguez-Canales, Comparison of Different Antibody Clones for Immunohistochemistry Detection of Programmed Cell Death Ligand 1 (PD-L1) on Non-Small Cell Lung Carcinoma, *Appl. Immunohistochem. Mol. Morphol.* (2018). doi:10.1097/PAI.0000000000000531.
- [299] K. Schats, E. van Vre, S. De Schepper, B. Neyns, I. De Meester, M. Kockx, 23P \* PD-L1 IHC validation and comparison of E1L3N & SP142 mAbs in melanoma, *Ann. Oncol.* (2015). doi:10.1093/annonc/mdv514.13.
- [300] R.A. Soo, J.S.Y. Lim, B.R. Asuncion, Z. Fazreen, M.C. Herrera, M.F.M. Omar, N.H.D. Phuong, J.E. Seet, B. Amanuel, B. Iacopetta, D. Byrne, S. Hendry, S. Fox, R. Soong, Determinants of variability of five programmed death ligand-1 immunohistochemistry assays in non-small cell lung cancer samples, *Oncotarget.* (2018). doi:10.18632/oncotarget.23827.
- [301] G. Baretton, PD-L1 als neuer Biomarker, *Diagnostik Im Dialog.* (2016).
- [302] J.W. Kleinovink, K.A. Marijt, M.J.A. Schoonderwoerd, T. van Hall, F. Ossendorp, M.F. Franssen, PD-L1 expression on malignant cells is no prerequisite for checkpoint therapy, *Oncoimmunology.* 6 (2017). doi:10.1080/2162402X.2017.1294299.
- [303] E.D. Thompson, M. Zahurak, A. Murphy, T. Cornish, N. Cuka, E. Abdelfatah, S. Yang, M. Duncan, N. Ahuja, J.M. Taube, R.A. Anders, R.J. Kelly, Patterns of PD-L1 expression and CD8 T cell infiltration in gastric adenocarcinomas and associated immune stroma, *Gut.* 66 (2017) 794–801. doi:10.1136/gutjnl-2015-310839.
- [304] T. Nomi, M. Sho, T. Akahori, K. Hamada, A. Kubo, H. Kanehiro, S. Nakamura, K. Enomoto, H. Yagita, M. Azuma, Y. Nakajima, Clinical significance and therapeutic potential of the programmed death-1 ligand/programmed death-1 pathway in human pancreatic cancer, *Clin. Cancer Res.* 13 (2007) 2151–2157. doi:10.1158/1078-0432.CCR-06-2746.
- [305] X.-L. Chen, S.-X. Yuan, C. Chen, Y.-X. Mao, G. Xu, X.-Y. Wang, Expression of B7-H1 protein in human pancreatic carcinoma tissues and its clinical significance., *Ai Zheng.* 28 (2009) 1328–1332.
- [306] X. Song, J. Liu, Y. Lu, H. Jin, D. Huang, Overexpression of B7-H1 correlates with malignant cell proliferation in pancreatic cancer, *Oncol. Rep.* 31 (2014) 1191–1198. doi:10.3892/or.2013.2955.

- 
- [307] S. Rahn, S. Krüger, C. Röcken, O. Helm, S. Sebens, Response to: “Patterns of PD-L1 expression and CD8 T cell infiltration in gastric adenocarcinomas and associated immune stroma”. *Gut*. 68 (2019) 179–180. doi:10.1136/gutjnl-2017-315843.
- [308] J. Lau, J. Cheung, A. Navarro, S. Lianoglou, B. Haley, K. Totpal, L. Sanders, H. Koeppen, P. Caplazi, J. McBride, H. Chiu, R. Hong, J. Grogan, V. Javinal, R. Yauch, B. Irving, M. Belvin, I. Mellman, J.M. Kim, M. Schmidt, Tumour and host cell PD-L1 is required to mediate suppression of anti-tumour immunity in mice, *Nat. Commun.* (2017). doi:10.1038/ncomms14572.
- [309] J.W. Kleinovink, K.A. Marijt, M.J.A. Schoonderwoerd, T. van Hall, F. Ossendorp, M.F. Franssen, PD-L1 expression on malignant cells is no prerequisite for checkpoint therapy, *Oncoimmunology*. (2017). doi:10.1080/2162402X.2017.1294299.
- [310] M.P. Armengol, M. Juan, A. Lucas-Martín, M.T. Fernández-Figueras, D. Jaraquemada, T. Gallart, R. Pujol-Borrell, Thyroid autoimmune disease: Demonstration of thyroid antigen -specific B cells and recombination-activating gene expression in chemokine-containing active intrathyroidal germinal centers, *Am. J. Pathol.* (2001). doi:10.1016/S0002-9440(10)61762-2.
- [311] M.C. Dieu-Nosjean, J. Goc, N.A. Giraldo, C. Sautès-Fridman, W.H. Fridman, Tertiary lymphoid structures in cancer and beyond, *Trends Immunol.* (2014). doi:10.1016/j.it.2014.09.006.
- [312] A. Ager, High endothelial venules and other blood vessels: Critical regulators of lymphoid organ development and function, *Front. Immunol.* (2017). doi:10.3389/fimmu.2017.00045.
- [313] L. Lin, X. Hu, H. Zhang, H. Hu, Tertiary Lymphoid Organs in Cancer Immunology: Mechanisms and the New Strategy for Immunotherapy, *Front. Immunol.* (2019). doi:10.3389/fimmu.2019.01398.
- [314] T.P.W. McMullen, R. Lai, L. Dabbagh, T.M. Wallace, C.J. De Gara, Survival in rectal cancer is predicted by T cell infiltration of tumour-associated lymphoid nodules, *Clin. Exp. Immunol.* (2010). doi:10.1111/j.1365-2249.2010.04147.x.
- [315] M.C. Dieu-Nosjean, M. Antoine, C. Danel, D. Heudes, M. Wislez, V. Poulot, N. Rabbe, L. Laurans, E. Tartour, L. De Chaisemartin, S. Lebecque, W.H. Fridman, J. Cadranel, Long-term survival for patients with non-small-cell lung cancer with intratumoral lymphoid structures, *J. Clin. Oncol.* (2008). doi:10.1200/JCO.2007.15.0284.
- [316] X. Liu, J.Y.S. Tsang, T. Hlaing, J. Hu, Y. Ni, S.K. Chan, S.Y. Cheung, G.M. Tse, Distinct Tertiary Lymphoid Structure Associations and Their Prognostic Relevance in HER2 Positive and Negative Breast Cancers, *Oncologist*. (2017). doi:10.1634/theoncologist.2017-0029.
- [317] A. Ladányi, J. Kiss, B. Somlai, K. Gilde, Z. Fejős, A. Mohos, I. Gaudi, J. Tímár, Density of DC-LAMP + mature dendritic cells in combination with activated T lymphocytes infiltrating primary cutaneous melanoma is a strong independent prognostic factor, *Cancer Immunol. Immunother.* (2007). doi:10.1007/s00262-007-0286-3.

- [318] N. Karachaliou, M. Gonzalez-Cao, G. Crespo, A. Drozdowskyj, E. Aldeguer, A. Gimenez-Capitan, C. Teixido, M.A. Molina-Vila, S. Viteri, M.D.L.L. Gil, S.M. Algarra, E. Perez-Ruiz, I. Marquez-Rodas, D. Rodriguez-Abreu, R. Blanco, T. Puertolas, M.A. Royo, R. Rosell, Interferon gamma, an important marker of response to immune checkpoint blockade in non-small cell lung cancer and melanoma patients, *Ther. Adv. Med. Oncol.* (2018). doi:10.1177/1758834017749748.
- [319] K.M. Kerr, F.R. Hirsch, Programmed death ligand-1 immunohistochemistry: Friend or foe?, *Arch. Pathol. Lab. Med.* 140 (2016) 326–331. doi:10.5858/arpa.2015-0522-SA.
- [320] A.H. Scheel, M. Dietel, L.C. Heukamp, K. Jöhrens, T. Kirchner, S. Reu, J. Rüschoff, H.U. Schildhaus, P. Schirmacher, M. Tiemann, A. Warth, W. Weichert, R.N. Fischer, J. Wolf, R. Büttner, Prädiktive PD-L1-Immunhistochemie beim nichtkleinzelligen Bronchialkarzinom, *Pathologe.* (2016). doi:10.1007/s00292-016-0189-1.
- [321] R. Hui, E.B. Garon, J.W. Goldman, N.B. Leighl, M.D. Hellmann, A. Patnaik, L. Gandhi, J.P. Eder, M.J. Ahn, L. Horn, E. Felip, E. Carcereny, R. Rangwala, G.M. Lubiniecki, J. Zhang, K. Emancipator, C. Roach, N.A. Rizvi, Pembrolizumab as first-line therapy for patients with PD-L1-positive advanced non-small cell lung cancer: A phase 1 trial, *Ann. Oncol.* (2017). doi:10.1093/annonc/mdx008.
- [322] H. Borghaei, L. Paz-Ares, L. Horn, D.R. Spigel, M. Steins, N.E. Ready, L.Q. Chow, E.E. Vokes, E. Felip, E. Holgado, F. Barlesi, M. Kohlhüfl, O. Arrieta, M.A. Burgio, J. Fayette, H. Lena, E. Poddubskaya, D.E. Gerber, S.N. Gettinger, C.M. Rudin, N. Rizvi, L. Crina, G.R. Blumenschein, S.J. Antonia, C. Dorange, C.T. Harbison, F. Graf Finckenstein, J.R. Brahmer, Nivolumab versus docetaxel in advanced nonsquamous non-small-cell lung cancer, *N. Engl. J. Med.* (2015). doi:10.1056/NEJMoa1507643.
- [323] J. Larkin, V. Chiarion-Sileni, R. Gonzalez, J.J. Grob, C.L. Cowey, C.D. Lao, D. Schadendorf, R. Dummer, M. Smylie, P. Rutkowski, P.F. Ferrucci, A. Hill, J. Wagstaff, M.S. Carlino, J.B. Haanen, M. Maio, I. Marquez-Rodas, G.A. McArthur, P.A. Ascierto, G. V. Long, M.K. Callahan, M.A. Postow, K. Grossmann, M. Sznol, B. Dreno, L. Bastholt, A. Yang, L.M. Rollin, C. Horak, F.S. Hodi, J.D. Wolchok, Combined nivolumab and ipilimumab or monotherapy in untreated Melanoma, *N. Engl. J. Med.* (2015). doi:10.1056/NEJMoa1504030.
- [324] E.B. Garon, N.A. Rizvi, R. Hui, N. Leighl, A.S. Balmanoukian, J.P. Eder, A. Patnaik, C. Aggarwal, M. Gubens, L. Horn, E. Carcereny, M. Ahn, E. Felip, J. Lee, M.D. Hellmann, O. Hamid, J.W. Goldman, J. Soria, M. Dolled-Filhart, R.Z. Rutledge, J. Zhang, J.K. Luceford, R. Rangwala, G.M. Lubiniecki, C. Roach, K. Emancipator, L. Gandhi, KEYNOTE-001 Investigators, Keynote-001 NSCLC appendix, *N. Engl. J. Med.* (2015). doi:10.1056/NEJMoa1501824.
- [325] G.T. Gibney, L.M. Weiner, M.B. Atkins, Predictive biomarkers for checkpoint inhibitor-based immunotherapy, *Lancet Oncol.* (2016). doi:10.1016/S1470-2045(16)30406-5.
- [326] B. Farhood, M. Najafi, K. Mortezaee, CD8 + cytotoxic T lymphocytes in cancer immunotherapy: A review, *J. Cell. Physiol.* (2019). doi:10.1002/jcp.27782.
- [327] F. Puleo, R. Maréchal, P. Demetter, M.A. Bali, A. Calomme, J. Closset, J.B. Bachet, J. Deviere, J.L. Van Laethem, New challenges in perioperative management of pancreatic cancer, *World J. Gastroenterol.* (2015). doi:10.3748/wjg.v21.i8.2281.

- [328] A. Barhli, J. Cros, L. Bartholin, C. Neuzillet, Prognostic stratification of resected pancreatic ductal adenocarcinoma: Past, present, and future, *Dig. Liver Dis.* (2018). doi:10.1016/j.dld.2018.08.009.
- [329] J. Hutcheson, U. Balaji, M.R. Porembka, M.B. Wachsmann, P.A. McCue, E.S. Knudsen, A.K. Witkiewicz, Immunologic and metabolic features of pancreatic ductal adenocarcinoma define prognostic subtypes of disease, *Clin. Cancer Res.* 22 (2016) 3606–3617. doi:10.1158/1078-0432.CCR-15-1883.
- [330] T. Conroy, F. Desseigne, M. Ychou, O. Bouché, R. Guimbaud, Y. Bécouarn, A. Adenis, J.L. Raoul, S. Gourgou-Bourgade, C. De La Fouchardière, J. Bennouna, J.B. Bachet, F. Khemissa-Akouz, D. Péré-Vergé, C. Delbaldo, E. Assenat, B. Chauffert, P. Michel, C. Montoto-Grillot, M. Ducreux, FOLFIRINOX versus gemcitabine for metastatic pancreatic cancer, *N. Engl. J. Med.* (2011). doi:10.1056/NEJMoa1011923.
- [331] P. Dong, Y. Xiong, J. Yue, S.J.B. Hanley, H. Watari, Tumor-intrinsic PD-L1 signaling in cancer initiation, development and treatment: Beyond immune evasion, *Front. Oncol.* (2018). doi:10.3389/fonc.2018.00386.
- [332] R. Winograd, K.T. Byrne, R.A. Evans, P.M. Odorizzi, A.R.L. Meyer, D.L. Bajor, C. Clendenin, B.Z. Stanger, E.E. Furth, E.J. Wherry, R.H. Vonderheide, Induction of T-cell Immunity Overcomes Complete Resistance to PD-1 and CTLA-4 Blockade and Improves Survival in Pancreatic Carcinoma., *Cancer Immunol. Res.* 3 (2015) 399–411. doi:10.1158/2326-6066.CIR-14-0215.
- [333] A. Henriksen, A. Dyhl-Polk, I. Chen, D. Nielsen, Checkpoint inhibitors in pancreatic cancer, *Cancer Treat. Rev.* (2019). doi:10.1016/j.ctrv.2019.06.005.
- [334] J.R. Brahmer, S.S. Tykodi, L.Q.M. Chow, W.J. Hwu, S.L. Topalian, P. Hwu, C.G. Drake, L.H. Camacho, J. Kauh, K. Odunsi, H.C. Pitot, O. Hamid, S. Bhatia, R. Martins, K. Eaton, S. Chen, T.M. Salay, S. Alaparthi, J.F. Grosso, A.J. Korman, S.M. Parker, S. Agrawal, S.M. Goldberg, D.M. Pardoll, A. Gupta, J.M. Wigginton, Safety and activity of anti-PD-L1 antibody in patients with advanced cancer, *N. Engl. J. Med.* (2012). doi:10.1056/NEJMoa1200694.
- [335] E.M. O'Reilly, D.-Y. Oh, N. Dhani, D.J. Renouf, M.A. Lee, W. Sun, G.A. Fisher, A.F. Hezel, S.-C. Chang, G. Vlahovic, O. Takahashi, Y. Yang, P.A. Philip, A randomized phase 2 study of durvalumab monotherapy and in combination with tremelimumab in patients with metastatic pancreatic ductal adenocarcinoma (mPDAC): ALPS study., *J. Clin. Oncol.* (2018). doi:10.1200/jco.2018.36.4\_suppl.217.
- [336] D.J. Renouf, N.C. Dhani, P. Kavan, D.J. Jonker, A.C. Wei, T. Hsu, P.A. Tang, B. Graham, L. Gallinaro, T. Hasan, W. Li, K. Hart, D. Tu, C.J. O'Callaghan, The Canadian Cancer Trials Group PA.7 trial: Results from the safety run in of a randomized phase II study of gemcitabine (GEM) and nab-paclitaxel (Nab-P) versus GEM, nab-P, durvalumab (D), and tremelimumab (T) as first-line therapy in metastatic pancreat, *J. Clin. Oncol.* (2018). doi:10.1200/jco.2018.36.4\_suppl.349.
- [337] K.C. Soares, A.A. Rucki, A.A. Wu, K. Olino, Q. Xiao, Y. Chai, A. Wamwea, E. Bigelow, E. Lutz, L. Liu, S. Yao, R.A. Anders, D. Laheru, C.L. Wolfgang, B.H. Edil, R.D. Schulick, E.M. Jaffee, L. Zheng, PD-1/PD-L1 blockade together with vaccine therapy facilitates effector T-cell infiltration into pancreatic tumors., *J. Immunother.* 38 (2015) 1–11. doi:10.1097/CJI.0000000000000062.

- 
- [338] E.S. Knudsen, P. Vail, U. Balaji, H. Ngo, I.W. Botros, V. Makarov, N. Riaz, V. Balachandran, S. Leach, D.M. Thompson, T.A. Chan, A.K. Witkiewicz, Stratification of pancreatic ductal adenocarcinoma: Combinatorial genetic, stromal, and immunologic markers, *Clin. Cancer Res.* (2017). doi:10.1158/1078-0432.CCR-17-0162.
- [339] P. Bonaventura, T. Shekarian, V. Alcazer, J. Valladeau-Guilemond, S. Valsesia-Wittmann, S. Amigorena, C. Caux, S. Depil, Cold tumors: A therapeutic challenge for immunotherapy, *Front. Immunol.* (2019). doi:10.3389/fimmu.2019.00168.
- [340] A. De Sousa Linhares, C. Battin, S. Jutz, J. Leitner, C. Hafner, J. Tobias, U. Wiedermann, M. Kundi, G.J. Zlabinger, K. Grabmeier-Pfistershammer, P. Steinberger, Therapeutic PD-L1 antibodies are more effective than PD-1 antibodies in blocking PD-1/PD-L1 signaling, *Sci. Rep.* 9 (2019) 11472. doi:10.1038/s41598-019-47910-1.
- [341] K.M. Zak, R. Kitel, S. Przetocka, P. Golik, K. Guzik, B. Musielak, A. Dömling, G. Dubin, T.A. Holak, Structure of the Complex of Human Programmed Death 1, PD-1, and Its Ligand PD-L1, *Structure.* (2015). doi:10.1016/j.str.2015.09.010.
- [342] J. George, M. Saito, K. Tsuta, R. Iwakawa, K. Shiraishi, A.H. Scheel, S. Uchida, S.I. Watanabe, R. Nishikawa, M. Noguchi, M. Peifer, S.J. Jang, I. Petersen, R. Buttner, C.C. Harris, J. Yokota, R.K. Thomas, T. Kohno, Genomic amplification of CD274 (PD-L1) in small-cell lung cancer, *Clin. Cancer Res.* (2017). doi:10.1158/1078-0432.CCR-16-1069.
- [343] M.T. Barrett, K.S. Anderson, E. Lenkiewicz, M. Andreozzi, H.E. Cunliffe, C.L. Klassen, A.C. Dueck, A.E. McCullough, S.K. Reddy, R.K. Ramanathan, D.W. Northfelt, B.A. Pockaj, Genomic amplification of 9p24.1 targeting JAK2, PD-L1, and PD-L2 is enriched in high-risk triple negative breast cancer, *Oncotarget.* (2015). doi:10.18632/oncotarget.4494.
- [344] J. Dunn, S. Rao, Epigenetics and immunotherapy: The current state of play, *Mol. Immunol.* (2017). doi:10.1016/j.molimm.2017.04.012.
- [345] Q. Wang, W. Lin, X. Tang, S. Li, L. Guo, Y. Lin, H.F. Kwok, The roles of microRNAs in regulating the expression of PD-1/PD-11 immune checkpoint, *Int. J. Mol. Sci.* (2017). doi:10.3390/ijms18122540.
- [346] K. Kataoka, Y. Shiraishi, Y. Takeda, S. Sakata, M. Matsumoto, S. Nagano, T. Maeda, Y. Nagata, A. Kitanaka, S. Mizuno, H. Tanaka, K. Chiba, S. Ito, Y. Watatani, N. Kakiuchi, H. Suzuki, T. Yoshizato, K. Yoshida, M. Sanada, H. Itonaga, Y. Imaizumi, Y. Totoki, W. Munakata, H. Nakamura, N. Hama, K. Shide, Y. Kubuki, T. Hidaka, T. Kameda, K. Masuda, N. Minato, K. Kashiwase, K. Izutsu, A. Takaori-Kondo, Y. Miyazaki, S. Takahashi, T. Shibata, H. Kawamoto, Y. Akatsuka, K. Shimoda, K. Takeuchi, T. Seya, S. Miyano, S. Ogawa, Aberrant PD-L1 expression through 3'-UTR disruption in multiple cancers, *Nature.* (2016). doi:10.1038/nature18294.
- [347] C. Liu, J. Lu, H. Tian, W. Du, L. Zhao, J. Feng, D. Yuan, Z. Li, Increased expression of PD-L1 by the human papillomavirus 16 E7 oncoprotein inhibits anticancer immunity, *Mol. Med. Rep.* (2017). doi:10.3892/mmr.2017.6102.
- [348] Y. Wang, H. Wang, H. Yao, C. Li, J.Y. Fang, J. Xu, Regulation of PD-L1: Emerging routes for targeting tumor immune evasion, *Front. Pharmacol.* (2018). doi:10.3389/fphar.2018.00536.

- [349] C.W. Li, S.O. Lim, W. Xia, H.H. Lee, L.C. Chan, C.W. Kuo, K.H. Khoo, S.S. Chang, J.H. Cha, T. Kim, J.L. Hsu, Y. Wu, J.M. Hsu, H. Yamaguchi, Q. Ding, Y. Wang, J. Yao, C.C. Lee, H.J. Wu, A.A. Sahin, J.P. Allison, D. Yu, G.N. Hortobagyi, M.C. Hung, Glycosylation and stabilization of programmed death ligand-1 suppresses T-cell activity, *Nat. Commun.* (2016). doi:10.1038/ncomms12632.
- [350] C.W. Li, S.O. Lim, E.M. Chung, Y.S. Kim, A.H. Park, J. Yao, J.H. Cha, W. Xia, L.C. Chan, T. Kim, S.S. Chang, H.H. Lee, C.K. Chou, Y.L. Liu, H.C. Yeh, E.P. Perillo, A.K. Dunn, C.W. Kuo, K.H. Khoo, J.L. Hsu, Y. Wu, J.M. Hsu, H. Yamaguchi, T.H. Huang, A.A. Sahin, G.N. Hortobagyi, S.S. Yoo, M.C. Hung, Eradication of Triple-Negative Breast Cancer Cells by Targeting Glycosylated PD-L1, *Cancer Cell.* (2018). doi:10.1016/j.ccell.2018.01.009.
- [351] D. Escors, M. Gato-Cañas, M. Zuazo, H. Arasanz, M.J. García-Granda, R. Vera, G. Kochan, The intracellular signalosome of PD-L1 in cancer cells, *Signal Transduct. Target. Ther.* (2018). doi:10.1038/s41392-018-0022-9.
- [352] R. Mezzadra, C. Sun, L.T. Jae, R. Gomez-Eerland, E. De Vries, W. Wu, M.E.W. Logtenberg, M. Slagter, E.A. Rozeman, I. Hofland, A. Broeks, H.M. Horlings, L.F.A. Wessels, C.U. Blank, Y. Xiao, A.J.R. Heck, J. Borst, T.R. Brummelkamp, T.N.M. Schumacher, Identification of CMTM6 and CMTM4 as PD-L1 protein regulators, *Nature.* (2017). doi:10.1038/nature23669.
- [353] M. Gato-Cañas, M. Zuazo, H. Arasanz, M. Ibañez-Vea, L. Lorenzo, G. Fernandez-Hinojal, R. Vera, C. Smerdou, E. Martisova, I. Arozarena, C. Wellbrock, D. Llopiz, M. Ruiz, P. Sarobe, K. Breckpot, G. Kochan, D. Escors, PDL1 Signals through Conserved Sequence Motifs to Overcome Interferon-Mediated Cytotoxicity, *Cell Rep.* (2017). doi:10.1016/j.celrep.2017.07.075.
- [354] E.L. Huttlin, L. Ting, R.J. Bruckner, F. Gebreab, M.P. Gygi, J. Szpyt, S. Tam, G. Zarraga, G. Colby, K. Baltier, R. Dong, V. Guarani, L.P. Vaites, A. Ordureau, R. Rad, B.K. Erickson, M. Wühr, J. Chick, B. Zhai, D. Kolippakkam, J. Mintseris, R.A. Obar, T. Harris, S. Artavanis-Tsakonas, M.E. Sowa, P. De Camilli, J.A. Paulo, J.W. Harper, S.P. Gygi, The BioPlex Network: A Systematic Exploration of the Human Interactome, *Cell.* (2015). doi:10.1016/j.cell.2015.06.043.
- [355] A.M. Contreras-Sandoval, M. Merino, M. Vasquez, I.F. Trocóniz, P. Berraondo, M.J. Garrido, Correlation between anti-PD-L1 tumor concentrations and tumor-specific and nonspecific biomarkers in a melanoma mouse model, *Oncotarget.* (2016). doi:10.18632/oncotarget.12727.
- [356] X. Wu, W. Xu, X. Feng, Y. He, X. Liu, Y. Gao, S. Yang, Z. Shao, C. Yang, Z. Ye, TNF- $\alpha$  mediated inflammatory macrophage polarization contributes to the pathogenesis of steroid-induced osteonecrosis in mice, *Int. J. Immunopathol. Pharmacol.* (2015). doi:10.1177/0394632015593228.
- [357] N. Parameswaran, S. Patial, Tumor necrosis factor- $\alpha$  signaling in macrophages, *Crit. Rev. Eukaryot. Gene Expr.* (2010). doi:10.1615/CritRevEukarGeneExpr.v20.i2.10.
- [358] R.S. Herbst, J.C. Soria, M. Kowanetz, G.D. Fine, O. Hamid, M.S. Gordon, J.A. Sosman, D.F. McDermott, J.D. Powderly, S.N. Gettinger, H.E.K. Kohrt, L. Horn, D.P. Lawrence, S. Rost, M. Leabman, Y. Xiao, A. Mokatrín, H. Koeppen, P.S. Hegde, I. Mellman, D.S. Chen, F.S. Hodi, Predictive correlates of response to the anti-PD-L1 antibody MPDL3280A in cancer patients, *Nature.* (2014). doi:10.1038/nature14011.



- [359] A.S. Strimpakos, E.M. Karapanagiotou, M.W. Saif, K.N. Syrigos, The role of mTOR in the management of solid tumors: An overview, *Cancer Treat. Rev.* (2009). doi:10.1016/j.ctrv.2008.09.006.
- [360] J. Van den Bossche, J. Baardman, M.P.J. de Winther, Metabolic characterization of polarized M1 and M2 bone marrow-derived macrophages using real-time extracellular flux analysis, *J. Vis. Exp.* (2015). doi:10.3791/53424.
- [361] S. Galván-Peña, L.A.J. O'Neill, Metabolic reprogramming in macrophage polarization, *Front. Immunol.* (2014). doi:10.3389/fimmu.2014.00420.
- [362] F. Wang, S. Zhang, R. Jeon, I. Vuckovic, X. Jiang, A. Lerman, C.D. Folmes, P.D. Dzeja, J. Herrmann, Interferon Gamma Induces Reversible Metabolic Reprogramming of M1 Macrophages to Sustain Cell Viability and Pro-Inflammatory Activity, *EBioMedicine.* (2018). doi:10.1016/j.ebiom.2018.02.009.
- [363] A. Chaudhri, Y. Xiao, A.N. Klee, X. Wang, B. Zhu, G.J. Freeman, PD-L1 Binds to B7-1 Only In Cis on the Same Cell Surface , *Cancer Immunol. Res.* (2018). doi:10.1158/2326-6066.cir-17-0316.
- [364] D. Sugiura, T. Maruhashi, I.M. Okazaki, K. Shimizu, T.K. Maeda, T. Takemoto, T. Okazaki, Restriction of PD-1 function by cis-PD-L1/CD80 interactions is required for optimal T cell responses, *Science* (80-. ). (2019). doi:10.1126/science.aav7062.
- [365] G.P. Hartley, L. Chow, D.T. Ammons, W.H. Wheat, S.W. Dow, Programmed cell death ligand 1 (PD-L1) signaling regulates macrophage proliferation and activation, *Cancer Immunol. Res.* (2018). doi:10.1158/2326-6066.CIR-17-0537.
- [366] S.R. Gordon, R.L. Maute, B.W. Dulken, G. Hutter, B.M. George, M.N. McCracken, R. Gupta, J.M. Tsai, R. Sinha, D. Corey, A.M. Ring, A.J. Connolly, I.L. Weissman, PD-1 expression by tumour-associated macrophages inhibits phagocytosis and tumour immunity, *Nature.* (2017). doi:10.1038/nature22396.
- [367] A.P.R. Bally, P. Lu, Y. Tang, J.W. Austin, C.D. Scharer, R. Ahmed, J.M. Boss, NF- $\kappa$ B Regulates PD-1 Expression in Macrophages, *J. Immunol.* (2015). doi:10.4049/jimmunol.1402550.
- [368] E.A. Said, F.P. Dupuy, L. Trautmann, Y. Zhang, Y. Shi, M. El-Far, B.J. Hill, A. Noto, P. Ancuta, Y. Peretz, S.G. Fonseca, J. Van Grevenynghe, M.R. Boulassel, J. Bruneau, N.H. Shoukry, J.P. Routy, D.C. Douek, E.K. Haddad, R.P. Sekaly, Programmed death-1-induced interleukin-10 production by monocytes impairs CD4 + T cell activation during HIV infection, *Nat. Med.* (2010). doi:10.1038/nm.2106.
- [369] R.M.G. Johnson, H. Dong, Functional expression of programmed death-ligand 1 (B7-H1) by immune cells and tumor cells, *Front. Immunol.* (2017). doi:10.3389/fimmu.2017.00961.
- [370] A. Saha, R.S. O'Connor, G. Thangavelu, S.B. Lovitch, D.B. Dandamudi, C.B. Wilson, B.G. Vincent, V. Tkachev, J.M. Pawlicki, S.N. Furlan, L.S. Kean, K. Aoyama, P.A. Taylor, A. Panoskaltsis-Mortari, R. Foncea, P. Ranganathan, S.M. Devine, J.S. Burrill, L. Guo, C. Sacristan, N.W. Snyder, I.A. Blair, M.C. Milone, M.L. Dustin, J.L. Riley, D.A. Bernlohr, W.J. Murphy, B.T. Fife, D.H. Munn, J.S. Miller, J.S. Serody, G.J. Freeman, A.H. Sharpe, L.A. Turka, B.R. Blazar, Programmed death ligand-1 expression on donor T cells drives graft-versus-host disease lethality, *J. Clin. Invest.* (2016). doi:10.1172/JCI85796.

- [371] V. Pulko, K.J. Harris, X. Liu, R.M. Gibbons, S.M. Harrington, C.J. Krco, E.D. Kwon, H. Dong, B7-H1 Expressed by Activated CD8 T Cells Is Essential for Their Survival, *J. Immunol.* (2011). doi:10.4049/jimmunol.1003976.
- [372] T. Azuma, S. Yao, G. Zhu, A.S. Flies, S.J. Flies, L. Chen, B7-H1 is a ubiquitous antiapoptotic receptor on cancer cells, *Blood.* (2008). doi:10.1182/blood-2007-11-123141.
- [373] D.R. Green, N. Droin, M. Pinkoski, Activation-induced cell death in T cells, *Immunol. Rev.* (2003). doi:10.1034/j.1600-065X.2003.00051.x.
- [374] I. Puliaeva, R. Puliaev, A. Shustov, M. Haas, C.S. Via, Fas Expression on Antigen-Specific T Cells Has Costimulatory, Helper, and Down-Regulatory Functions In Vivo for Cytotoxic T Cell Responses but Not for T Cell-Dependent B Cell Responses, *J. Immunol.* (2008). doi:10.4049/jimmunol.181.9.5912.
- [375] D.K. Finlay, MTORC1 regulates CD8+ T-cell glucose metabolism and function independently of PI3K and PKB, *Biochem. Soc. Trans.* (2013). doi:10.1042/BST20120359.
- [376] M. Pollari, O. Brück, T. Pellinen, P. Vähämurto, M.L. Karjalainen-Lindsberg, S. Mannisto, O. Kallioniemi, P.L. Kellokumpu-Lehtinen, S. Mustjoki, S.K. Leivonen, S. Leppä, PD-L1+ tumor-associated macrophages and PD-1+ tumor-infiltrating lymphocytes predict survival in primary testicular lymphoma, *Haematologica.* (2018). doi:10.3324/haematol.2018.197194.
- [377] K. Abiko, N. Matsumura, J. Hamanishi, N. Horikawa, R. Murakami, K. Yamaguchi, Y. Yoshioka, T. Baba, I. Konishi, M. Mandai, IFN- $\gamma$  from lymphocytes induces PD-L1 expression and promotes progression of ovarian cancer., *Br. J. Cancer.* 1 (2015) 1–9. doi:10.1038/bjc.2015.101.
- [378] T. Yamazaki, H. Akiba, H. Iwai, H. Matsuda, M. Aoki, Y. Tanno, T. Shin, H. Tsuchiya, D.M. Pardoll, K. Okumura, M. Azuma, H. Yagita, Expression of Programmed Death 1 Ligands by Murine T Cells and APC, *J. Immunol.* (2002). doi:10.4049/jimmunol.169.10.5538.
- [379] F. Guidez, A.C. Li, A. Horvai, J.S. Welch, C.K. Glass, Differential Utilization of Ras Signaling Pathways by Macrophage Colony-Stimulating Factor (CSF) and Granulocyte-Macrophage CSF Receptors during Macrophage Differentiation, *Mol. Cell. Biol.* (1998). doi:10.1128/mcb.18.7.3851.
- [380] E.R. Stanley, V. Chitu, CSF-1 receptor signaling in myeloid cells, *Cold Spring Harb. Perspect. Biol.* (2014). doi:10.1101/cshperspect.a021857.
- [381] M.A. Coelho, S. de Carné Trécesson, S. Rana, D. Zecchin, C. Moore, M. Molina-Arcas, P. East, B. Spencer-Dene, E. Nye, K. Barnouin, A.P. Snijders, W.S. Lai, P.J. Blackshear, J. Downward, Oncogenic RAS Signaling Promotes Tumor Immuno-resistance by Stabilizing PD-L1 mRNA, *Immunity.* (2017). doi:10.1016/j.immuni.2017.11.016.
- [382] Y. Zhu, B.L. Knolhoff, M.A. Meyer, T.M. Nywening, B.L. West, J. Luo, A. Wang-Gillam, S.P. Goedegebuure, D.C. Linehan, D.G. De Nardo, CSF1/CSF1R blockade reprograms tumor-infiltrating macrophages and improves response to T-cell checkpoint immunotherapy in pancreatic cancer models, *Cancer Res.* (2014). doi:10.1158/0008-5472.CAN-13-3723.

- 
- [383] Y. Shi, C.H. Liu, A.I. Roberts, J. Das, G. Xu, G. Ren, Y. Zhang, L. Zhang, R.Y. Zeng, H.S.W. Tan, G. Das, S. Devadas, Granulocyte-macrophage colony-stimulating factor (GM-CSF) and T-cell responses: What we do and don't know, in: *Cell Res.*, 2006. doi:10.1038/sj.cr.7310017.
- [384] Y. Pylayeva-Gupta, K.E. Lee, C.H. Hajdu, G. Miller, D. Bar-Sagi, Oncogenic Kras-Induced GM-CSF Production Promotes the Development of Pancreatic Neoplasia, *Cancer Cell.* (2012). doi:10.1016/j.ccr.2012.04.024.
- [385] S.O. Lim, C.W. Li, W. Xia, J.H. Cha, L.C. Chan, Y. Wu, S.S. Chang, W.C. Lin, J.M. Hsu, Y.H. Hsu, T. Kim, W.C. Chang, J.L. Hsu, H. Yamaguchi, Q. Ding, Y. Wang, Y. Yang, C.H. Chen, A.A. Sahin, D. Yu, G.N. Hortobagyi, M.C. Hung, Deubiquitination and Stabilization of PD-L1 by CSN5, *Cancer Cell.* (2016). doi:10.1016/j.ccell.2016.10.010.
- [386] N. Chen, W. Fang, J. Zhan, S. Hong, Y. Tang, S. Kang, Y. Zhang, X. He, T. Zhou, T. Qin, Y. Huang, X. Yi, L. Zhang, Upregulation of PD-L1 by EGFR activation mediates the immune escape in EGFR-driven NSCLC: Implication for optional immune targeted therapy for NSCLC patients with EGFR mutation, *J. Thorac. Oncol.* (2015). doi:10.1097/JTO.0000000000000500.
- [387] N. Zhang, Y. Zeng, W. Du, J. Zhu, D. Shen, Z. Liu, J.A. Huang, The EGFR pathway is involved in the regulation of PDL1 expression via the IL-6/JAK/STAT3 signaling pathway in EGFR-mutated non-small cell lung cancer, *Int. J. Oncol.* (2016). doi:10.3892/ijo.2016.3632.
- [388] T. Doi, T. Ishikawa, T. Okayama, K. Oka, K. Mizushima, T. Yasuda, N. Sakamoto, K. Katada, K. Kamada, K. Uchiyama, O. Handa, T. Takagi, Y. Naito, Y. Itoh, The JAK/STAT pathway is involved in the upregulation of PD-L1 expression in pancreatic cancer cell lines, *Oncol. Rep.* (2017). doi:10.3892/or.2017.5399.
- [389] J.M. Zaretsky, A. Garcia-Diaz, D.S. Shin, H. Escuin-Ordinas, W. Hugo, S. Hu-Lieskovan, D.Y. Torrejon, G. Abril-Rodriguez, S. Sandoval, L. Barthly, J. Saco, B.H. Moreno, R. Mezzadra, B. Chmielowski, K. Ruchalski, I.P. Shintaku, P.J. Sanchez, C. Puig-Saus, G. Cherry, E. Seja, X. Kong, J. Pang, B. Berent-Maoz, B. Comin-Anduix, T.G. Graeber, P.C. Tumeh, T.N.M. Schumacher, R.S. Lo, A. Ribas, Mutations associated with acquired resistance to PD-1 blockade in melanoma, *N. Engl. J. Med.* (2016). doi:10.1056/NEJMoa1604958.
- [390] J.N. Ou, A.E. Wiedeman, A.M. Stevens, TNF- $\alpha$  and TGF- $\beta$  counter-regulate PD-L1 expression on monocytes in systemic lupus erythematosus, *Sci. Rep.* (2012). doi:10.1038/srep00295.
- [391] F. Gani, N. Nagarajan, Y. Kim, Q. Zhu, L. Luan, F. Bhaijje, R.A. Anders, T.M. Pawlik, Program Death 1 Immune Checkpoint and Tumor Microenvironment: Implications for Patients With Intrahepatic Cholangiocarcinoma, *Ann. Surg. Oncol.* (2016). doi:10.1245/s10434-016-5101-y.
- [392] T.S. Nowicki, R. Akiyama, R.R. Huang, I.P. Shintaku, X. Wang, P.C. Tumeh, A. Singh, B. Chmielowski, C. Denny, N. Federman, A. Ribas, Infiltration of CD8 T cells and expression of PD-1 and PD-L1 in synovial sarcoma, *Cancer Immunol. Res.* (2017). doi:10.1158/2326-6066.CIR-16-0148.

- [393] A. Cimino-Mathews, E. Thompson, J.M. Taube, X. Ye, Y. Lu, A. Meeker, H. Xu, R. Sharma, K. Lecksell, T.C. Cornish, N. Cuka, P. Argani, L.A. Emens, PD-L1 (B7-H1) expression and the immune tumor microenvironment in primary and metastatic breast carcinomas, *Hum. Pathol.* (2016). doi:10.1016/j.humpath.2015.09.003.
- [394] S. Liu, M. Gönen, Z.K. Stadler, M.R. Weiser, J.F. Hechtman, E. Vakiani, T. Wang, M. Vyas, U. Joneja, M. Al-Bayati, N.H. Segal, J.J. Smith, S. King, S. Guercio, P. Ntiamoah, A.J. Markowitz, L. Zhang, A. Cercek, J. Garcia-Aguilar, L.B. Saltz, L.A. Diaz, D.S. Klimstra, J. Shia, Cellular localization of PD-L1 expression in mismatch-repair-deficient and proficient colorectal carcinomas, *Mod. Pathol.* (2019). doi:10.1038/s41379-018-0114-7.
- [395] Q. Wang, W. Lou, W. Di, X. Wu, Prognostic value of tumor PD-L1 expression combined with CD8+ tumor infiltrating lymphocytes in high grade serous ovarian cancer, *Int. Immunopharmacol.* (2017). doi:10.1016/j.intimp.2017.08.017.
- [396] S. Tsutsumi, H. Saeki, Y. Nakashima, S. Ito, E. Oki, M. Morita, Y. Oda, S. Okano, Y. Maehara, Programmed death-ligand 1 expression at tumor invasive front is associated with epithelial-mesenchymal transition and poor prognosis in esophageal squamous cell carcinoma, *Cancer Sci.* (2017). doi:10.1111/cas.13237.
- [397] M.W.L. Teng, S.F. Ngiow, A. Ribas, M.J. Smyth, Classifying cancers based on T-cell infiltration and PD-L1, *Cancer Res.* (2015). doi:10.1158/0008-5472.CAN-15-0255.
- [398] S.Z. Manrique, M.A.D. Correa, D.B. Hoelzinger, A.L. Dominguez, N. Mirza, H.H. Lin, J. Stein-Streilein, S. Gordon, J. Lustgarten, Foxp3-positive macrophages display immunosuppressive properties and promote tumor growth, *J. Exp. Med.* (2011). doi:10.1084/jem.20100730.
- [399] V. Karanikas, M. Speletas, M. Zamanakou, F. Kalala, G. Loules, T. Kerenidi, A.K. Barda, K.I. Gourgoulianis, A.E. Germenis, Foxp3 expression in human cancer cells, *J. Transl. Med.* (2008). doi:10.1186/1479-5876-6-19.
- [400] J. Galon, D. Bruni, Approaches to treat immune hot, altered and cold tumours with combination immunotherapies, *Nat. Rev. Drug Discov.* (2019). doi:10.1038/s41573-018-0007-y.
- [401] P. Sharma, J.P. Allison, The future of immune checkpoint therapy, *Science* (80-. ). 348 (2015) 56–61. doi:10.1126/SCIENCE.AAA8172.
- [402] P. Jiang, S. Gu, D. Pan, J. Fu, A. Sahu, X. Hu, Z. Li, N. Traugh, X. Bu, B. Li, J. Liu, G.J. Freeman, M.A. Brown, K.W. Wucherpfennig, X.S. Liu, Signatures of T cell dysfunction and exclusion predict cancer immunotherapy response, *Nat. Med.* (2018). doi:10.1038/s41591-018-0136-1.
- [403] B.B. Aggarwal, R. V. Vijayalekshmi, B. Sung, Targeting inflammatory pathways for prevention and therapy of cancer: Short-term friend, long-term foe, *Clin. Cancer Res.* (2009). doi:10.1158/1078-0432.CCR-08-0149.
- [404] F. Balkwill, A. Mantovani, Inflammation and cancer: Back to Virchow?, *Lancet.* (2001). doi:10.1016/S0140-6736(00)04046-0.
- [405] D. Hanahan, R.A. Weinberg, Hallmarks of cancer: The next generation, *Cell.* 144 (2011) 646–674. doi:10.1016/j.cell.2011.02.013.
- [406] S. Kumar, C.J. Chan, L.M. Coussens, Inflammation and Cancer, in: *Encycl. Immunobiol.*, 2016. doi:10.1016/B978-0-12-374279-7.17002-X.

- [407] J.L. Benci, B. Xu, Y. Qiu, T.J. Wu, H. Dada, C. Twyman-Saint Victor, L. Cucolo, D.S.M. Lee, K.E. Pauken, A.C. Huang, T.C. Gangadhar, R.K. Amaravadi, L.M. Schuchter, M.D. Feldman, H. Ishwaran, R.H. Vonderheide, A. Maity, E.J. Wherry, A.J. Minn, Tumor Interferon Signaling Regulates a Multigenic Resistance Program to Immune Checkpoint Blockade, *Cell*. (2016). doi:10.1016/j.cell.2016.11.022.
- [408] C.Y. Ock, S. Kim, B. Keam, M. Kim, T.M. Kim, J.H. Kim, Y.K. Jeon, J.S. Lee, S.K. Kwon, J. Hun Hah, T.K. Kwon, D.W. Kim, H.G. Wu, M.W. Sung, D.S. Heo, PD-L1 expression is associated with epithelial-mesenchymal transition in head and neck squamous cell carcinoma, *Oncotarget*. (2016). doi:10.18632/oncotarget.7431.
- [409] A. Alsuliman, D. Colak, O. Al-Harazi, H. Fitwi, A. Tulbah, T. Al-Tweigeri, M. Al-Alwan, H. Ghebeh, Bidirectional crosstalk between PD-L1 expression and epithelial to mesenchymal transition: Significance in claudin-low breast cancer cells, *Mol. Cancer*. (2015). doi:10.1186/s12943-015-0421-2.
- [410] L. Chen, Y. Xiong, J. Li, X. Zheng, Q. Zhou, A. Turner, C. Wu, B. Lu, J. Jiang, PD-L1 Expression Promotes Epithelial to Mesenchymal Transition in Human Esophageal Cancer, *Cell. Physiol. Biochem*. (2017). doi:10.1159/000480000.
- [411] A.M. Krebs, J. Mitschke, M.L. Losada, O. Schmalhofer, M. Boerries, H. Busch, M. Boettcher, D. Mougiakakos, W. Reichardt, P. Bronsert, V.G. Brunton, C. Pilarsky, T.H. Winkler, S. Brabletz, M.P. Stemmler, T. Brabletz, The EMT-activator Zeb1 is a key factor for cell plasticity and promotes metastasis in pancreatic cancer, *Nat. Cell Biol*. 19 (2017) 518–529. doi:10.1038/ncb3513.
- [412] L. Goebel, E. Grage-Griebenow, A. Gorys, O. Helm, G. Genrich, L. Lenk, D. Wesch, H. Ungefroren, S. Freitag-Wolf, B. Sipos, C. Röcken, H. Schäfer, S. Sebens, CD4(+) T cells potently induce epithelial-mesenchymal-transition in premalignant and malignant pancreatic ductal epithelial cells-novel implications of CD4(+) T cells in pancreatic cancer development., *Oncoimmunology*. 4 (2015) e1000083. doi:10.1080/2162402X.2014.1000083.
- [413] C. Qu, Q. Wang, Z. Meng, P. Wang, Cancer-Associated Fibroblasts in Pancreatic Cancer: Should They Be Deleted or Reeducated?, *Integr. Cancer Ther*. (2018). doi:10.1177/1534735418794884.
- [414] J. Jiang, Y.L. Tang, X.H. Liang, EMT: A new vision of hypoxia promoting cancer progression, *Cancer Biol. Ther*. (2011). doi:10.4161/cbt.11.8.15274.
- [415] Y. Wang, H. Wang, Q. Zhao, Y. Xia, X. Hu, J. Guo, PD-L1 induces epithelial-to-mesenchymal transition via activating SREBP-1c in renal cell carcinoma, *Med. Oncol*. (2015). doi:10.1007/s12032-015-0655-2.
- [416] A. Chaudhri, Y. Xiao, A.N. Klee, X. Wang, B. Zhu, G.J. Freeman, PD-L1 Binds to B7-1 only in cis on the same cell surface, *Cancer Immunol. Res*. (2018). doi:10.1158/2326-6066.CIR-17-0316.
- [417] H. Knaack, L. Lenk, L.M. Philipp, L. Miarka, S. Rahn, F. Viol, C. Hauser, J.H. Egberts, J.P. Gundlach, O. Will, S. Tiwari, W. Mikulits, U. Schumacher, J.G. Hengstler, S. Sebens, Liver metastasis of pancreatic cancer: The hepatic microenvironment impacts differentiation and self-renewal capacity of pancreatic ductal epithelial cells, *Oncotarget*. (2018). doi:10.18632/oncotarget.25884.
- [418] Y. Komohara, M. Jinushi, M. Takeya, Clinical significance of macrophage heterogeneity in human malignant tumors, *Cancer Sci*. 105 (2014) 1–8. doi:10.1111/cas.12314.

- [419] S.R. Webb, N.R.J. Gascoigne, T-cell activation by superantigens, *Curr. Opin. Immunol.* (1994). doi:10.1016/0952-7915(94)90129-5.
- [420] I. Olsen, L.M. Sollid, Pitfalls in determining the cytokine profile of human T cells, *J. Immunol. Methods.* (2013). doi:10.1016/j.jim.2013.01.015.
- [421] J.P. Secrist, L.A. Burns, L. Karnitz, G.A. Koretzky, R.T. Abraham, Stimulatory effects of the protein tyrosine phosphatase inhibitor, pervanadate, on T-cell activation events, *J. Biol. Chem.* (1993).
- [422] A.H. Sharpe, E.J. Wherry, R. Ahmed, G.J. Freeman, The function of programmed cell death 1 and its ligands in regulating autoimmunity and infection, *Nat. Immunol.* (2007). doi:10.1038/ni1443.
- [423] D.L. Barber, E.J. Wherry, D. Masopust, B. Zhu, J.P. Allison, A.H. Sharpe, G.J. Freeman, R. Ahmed, Restoring function in exhausted CD8 T cells during chronic viral infection, *Nature.* (2006). doi:10.1038/nature04444.
- [424] J. Duraiswamy, C.C. Ibegbu, D. Masopust, J.D. Miller, K. Araki, G.H. Doho, P. Tata, S. Gupta, M.J. Zilliox, H.I. Nakaya, B. Pulendran, W.N. Haining, G.J. Freeman, R. Ahmed, Phenotype, Function, and Gene Expression Profiles of Programmed Death-1 hi CD8 T Cells in Healthy Human Adults, *J. Immunol.* (2011). doi:10.4049/jimmunol.1001783.
- [425] R.H. Vonderheide, The Immune Revolution: A Case for Priming, Not Checkpoint, *Cancer Cell.* (2018). doi:10.1016/j.ccell.2018.03.008.
- [426] T. Korn, M. Mitsdoerffer, A.L. Croxford, A. Awasthi, V.A. Dardalhon, G. Galileos, P. Vollmar, G.L. Stritesky, M.H. Kaplan, A. Waisman, V.K. Kuchroo, M. Oukka, IL-6 controls Th17 immunity in vivo by inhibiting the conversion of conventional T cells into Foxp3+ regulatory T cells, *Proc. Natl. Acad. Sci. U. S. A.* (2008). doi:10.1073/pnas.0809850105.
- [427] S. Paul, B.C. Schaefer, A new look at T cell receptor signaling to nuclear factor- $\kappa$ B, *Trends Immunol.* (2013). doi:10.1016/j.it.2013.02.002.
- [428] S.P. Arlauckas, C.S. Garris, R.H. Kohler, M. Kitaoka, M.F. Cuccarese, K.S. Yang, M.A. Miller, J.C. Carlson, G.J. Freeman, R.M. Anthony, R. Weissleder, M.J. Pittet, In vivo imaging reveals a tumor-associated macrophage-mediated resistance pathway in anti-PD-1 therapy, *Sci. Transl. Med.* (2017). doi:10.1126/scitranslmed.aal3604.
- [429] F.A. Vargas, A.J.S. Furness, K. Litchfield, K. Joshi, R. Rosenthal, E. Ghorani, I. Solomon, M.H. Lesko, N. Ruef, C. Roddie, J.Y. Henry, L. Spain, A. Ben Aissa, A. Georgiou, Y.N.S. Wong, M. Smith, D. Strauss, A. Hayes, D. Nicol, T. O'brien, L. Mårtensson, A. Ljungars, I. Teige, B. Freundéus, M. Pule, T. Marafioti, M. Gore, J. Larkin, S. Turajlic, C. Swanton, K.S. Peggs, S.A. Quezada, K. Harrington, A. Melcher, A. Wotherspoon, N. Francis, B. Challacombe, A. Fernando, S. Hazell, A. Chandra, L. Pickering, J. Lynch, S. Rudman, S. Chowdhury, K. Harri-Son-Phillips, M. Varia, C. Horsfield, A. Polson, G. Stamp, M. O'donnell, W. Drake, P. Hill, D. Hrouda, E. Mayer, J. Olsburgh, G. Kooiman, K. O'connor, G. Stewart, M. Aitchison, M. Tran, N. Fotiadis, H. Verma, J. Lopez, J. Lester, F. Morgan, M. Kornaszewska, R. Attanoos, H. Adams, H. Davies, D. Fennell, J. Shaw, J. Le Quesne, A. Nakas, S. Rathinam, W. Monteiro, H. Marshall, L. Nelson, J. Bennett, J. Riley, L. Primrose, L. Martinson, G. Anand, S. Khan, M. Nicolson, K. Kerr, S. Palmer, H. Remmen, J. Miller, K. Buchan, M. Chetty, L. Gomersall, S. Lock, B. Naidu, G. Langman, S. Trotter, M. Bellamy, H. Bancroft, A. Kerr, S. Kadiri, J. Webb, G. Middleton, M. Djearaman, Y. Summers, R. Califano, P.

- Taylor, R. Shah, P. Krysiak, K. Rammohan, E. Fontaine, R. Booton, M. Evison, P. Crosbie, S. Moss, F. Idries, J. Novasio, L. Joseph, P. Bishop, A. Chaturvedi, A.M. Quinn, H. Doran, A. Leek, P. Harrison, K. Moore, R. Waddington, F. Blackhall, J. Rogan, E. Smith, C. Dive, G. Brady, D. Roth-Well, S. Gulati, F. Chemie, J. Tugwood, J. Pierce, D. Lawrence, M. Hayward, N. Panagiotopoulos, R. George, D. Patrini, M. Falzon, E. Borg, R. Khuroya, M. Jamal-Hanjani, G. Wilson, N.J. Birkbak, T. Watkins, N. McGranahan, C. Abbosh, S. Horswell, R. Mitter, M. Escudero, A. Stewart, A. Rowan, C. Hiley, J. Goldman, A. Ahmed, M. Taylor, J. Choudhary, P. Shaw, R. Veeriah, J. Czyzewska-Khan, D. Johnson, J. Laycock, R. Hynds, M.W. Sunderland, J. Reading, M. Novelli, D. Oukrif, S. Janes, M. Forster, T. Ahmad, S.M. Lee, P. van Loo, J. Herrero, J. Hartley, R.K. Stone, T. Denner, M. Costa, S. Begum, B. Phillimore, T. Chambers, E. Nye, S. Ward, G. Elgar, M. Al-Bakir, D. Carnell, R. Mendes, J. George, N. Navani, D. Papadatos-Pastos, M. Scarci, P. Gorman, H. Lowe, L. Ensell, D. Moore, M. Mackenzie, M. Wilcox, H. Bell, A. Hackshaw, Y. Ngai, S. Smith, N. Gower, C. Ottensmeier, S. Chee, B. Johnson, A. Alzetani, E. Shaw, E. Lim, P. De Sousa, M.T. Barbosa, A. Nicholson, A. Bowman, S. Jordan, A. Rice, H. Raubenheimer, C. Proli, M.E. Cufari, J.C. Ronquillo, A. Kwayie, H. Bhayani, M. Hamilton, Y. Bakar, N. Mensah, L. Ambrose, A. Devaraj, S. Buder, J. Finch, L. Azcarate, H. Chavan, S. Green, H. Mashinga, K. Lau, M. Sheaff, P. Schmid, J. Conibear, V. Ezhil, V. Prakash, S. Danson, J. Bury, J. Edwards, J. Hill, S. Matthews, Y. Kitsanta, K. Suvarna, M. Shackcloth, J. Gosney, P. Postmus, S. Feeney, J. Asante-Siaw, P. Russell, T. Light, T. Horey, K. Blyth, C. Dick, A. Kirk, Fc Effector Function Contributes to the Activity of Human Anti-CTLA-4 Antibodies, *Cancer Cell*. (2018). doi:10.1016/j.ccell.2018.02.010.
- [430] S. Sasse, K. Reddemann, A. Diepstra, I. Oschlies, A. Schnitter, S. Borchmann, A. Engert, P. Borchmann, W. Klapper, Programmed cell death protein-1 (PD-1)-expression in the microenvironment of classical Hodgkin lymphoma at relapse during anti-PD-1-treatment, *Haematologica*. 104 (2019) e21. doi:10.3324/HAEMATOL.2018.196279.
- [431] J.W. Austin, P. Lu, P. Majumder, R. Ahmed, J.M. Boss, STAT3, STAT4, NFATc1, and CTCF Regulate PD-1 through Multiple Novel Regulatory Regions in Murine T Cells, *J. Immunol*. (2014). doi:10.4049/jimmunol.1302750.
- [432] C. Hess, T.K. Means, P. Autissier, T. Woodberry, M. Altfeld, M.M. Addo, N. Frahm, C. Brander, B.D. Walker, A.D. Luster, IL-8 responsiveness defines a subset of CD8 T cells poised to kill, *Blood*. (2004). doi:10.1182/blood-2004-03-1067.
- [433] T.A. Libermann, D. Baltimore, Activation of interleukin-6 gene expression through the NF-kappa B transcription factor., *Mol. Cell. Biol*. (1990). doi:10.1128/mcb.10.5.2327.
- [434] C.T. Molta, Etanercept, in: *Biol. Gen. Med.*, 2007. doi:10.1007/978-3-540-29018-6\_4.
- [435] V. Oldfield, S. Dhillon, G.L. Plosker, Tocilizumab, *Drugs*. 69 (2009) 609–632. doi:10.2165/00003495-200969050-00007.
- [436] T. Jostock, J. Müllberg, S. Özbek, R. Atreya, G. Blinn, N. Voltz, M. Fischer, M.F. Neurath, S. Rose-John, Soluble gp130 is the natural inhibitor of soluble interleukin-6 receptor transsignaling responses, *Eur. J. Biochem*. (2001). doi:10.1046/j.1432-1327.2001.01867.x.
- [437] A.J. Majmundar, W.J. Wong, M.C. Simon, Hypoxia-Inducible Factors and the Response to Hypoxic Stress, *Mol. Cell*. (2010). doi:10.1016/j.molcel.2010.09.022.

- [438] N.G. Gavalas, M. Tsiatas, O. Tsitsilonis, E. Politi, K. Ioannou, A.C. Ziogas, A. Rodolakis, G. Vlahos, N. Thomakos, D. Haidopoulos, E. Terpos, A. Antsaklis, M.A. Dimopoulos, A. Bamias, VEGF directly suppresses activation of T cells from ascites secondary to ovarian cancer via VEGF receptor type 2, *Br. J. Cancer*. (2012). doi:10.1038/bjc.2012.468.
- [439] Y.L. Li, H. Zhao, X.B. Ren, Relationship of VEGF/VEGFR with immune and cancer cells: staggering or forward?, *Cancer Biol. Med.* (2016). doi:10.20892/j.issn.2095-3941.2015.0070.
- [440] N. Ferrara, K.J. Hillan, H.P. Gerber, W. Novotny, Discovery and development of bevacizumab, an anti-VEGF antibody for treating cancer, *Nat. Rev. Drug Discov.* (2004). doi:10.1038/nrd1381.
- [441] K.K. Ciombor, J. Berlin, E. Chan, Aflibercept, *Clin. Cancer Res.* (2013). doi:10.1158/1078-0432.CCR-12-2911.
- [442] L.C. Dieterich, K. Ikenberg, T. Cetintas, K. Kapaklikaya, C. Hutmacher, M. Detmar, Tumor-associated lymphatic vessels upregulate PDL1 to inhibit T-cell activation, *Front. Immunol.* (2017). doi:10.3389/fimmu.2017.00066.



## List of Figures

- Figure 1: Pancreatic ductal adenocarcinoma (PDAC) arises from pancreatic intraepithelial neoplasia (PanINs) in a multi-step progress.** Schematic illustration of increasing cellular dysplasia associated with progressive PanIN grade (above) as well as representative hematoxylin and eosin staining images of respective PanIN stages (below) and fully developed PDAC. Adapted from [16,17]. ..... 3
- Figure 2: Epithelial to Mesenchymal Transition is induced by an inflammatory microenvironment.** Schematic illustration of EMT induction in epithelial tumor cells due to T lymphocyte secreted  $\text{IFN}\gamma$  as well as  $\text{TGF-}\beta$ ,  $\text{TNF}\alpha$ , IL-6 and IL-1 $\beta$  produced by tumor-associated macrophages. EMT progression goes along with the loss/downregulation of epithelial protein expression (E-cadherin and cytokeratin) and simultaneous induction of mesenchymal proteins' expression (vimentin and L1CAM) as well as activation of transcription factors like Zeb-1. Adapted from [45]. ..... 5
- Figure 3: Tumor- and stromal compartment in pancreatic ductal adenocarcinoma. (A)** Schematic illustration of the cellular and non-cellular compartments in PDAC. Adapted from [64]. **(B)** Representative image of a formalin-fixed paraffin-embedded PDAC tissue section stained for pan-cytokeratin (brownish). Nuclei were stained with hematoxylin (violet)..... 6
- Figure 4: Monocytes differentiate into various subsets of macrophages in dependence of the respective microenvironment.** Monocytes differentiate by stimulation with M-CSF, anti-inflammatory cytokines (e.g. IL-4, IL-13 and IL-10) as well as corticosteroids, prostaglandins and vitamin D3 into an anti-inflammatory M2-macrophage type. GM-CSF,  $\text{IFN}\gamma$  as well as LPS or other bacterial products lead to the differentiation of a pro-inflammatory M1-phenotype. Both phenotypes differ regarding their gene expression profile and resulting functions. Adapted from [76]. ..... 8
- Figure 5: Schematic illustration of T helper cell maturation into functionally different subsets by various cytokines.**  $\text{T}_\text{H}0$  helper cells differentiate upon activation in dependence on cytokines present in the respective microenvironment into  $\text{T}_\text{H}1$ ,  $\text{T}_\text{H}2$ ,  $\text{T}_\text{H}17$  or Treg cells. Key transcription factors that render these functional phenotypes are Tbet, Gata-3, RoR $\gamma$ t and FoxP3, respectively. Adapted from [97] ..... 11
- Figure 6: Three types of signals are necessary for the priming of  $\text{CD4}^+$  T helper lymphocytes and  $\text{CD8}^+$  cytotoxic T lymphocytes by antigen-presenting cells in the secondary lymphoid organ.** Schematic illustration of the interaction between antigen-presenting cells (APC) and  $\text{CD4}^+$ / $\text{CD8}^+$  T cells in the process of T lymphocyte priming. The first signal (1) provided by APCs is the pre-processed MHC-loaded antigen, which is presented via MHC-II or MHC-I to  $\text{CD4}^+$  and  $\text{CD8}^+$  T cells, respectively. Binding of peptide-MHC complex to antigen-specific TCR variants is accompanied by CD4 and CD8 co-receptor crosslinking, respectively. The second signal (2) is provided by either co-stimulatory (+) or co-inhibitory (-) receptor-ligand binding. Co-stimulatory signals between APCs and T cells are provided by CD40-CD40L, CD28-CD80/CD86 and CD27/CD70 interaction. In contrast, binding of PD-L1 or PD-L2 to its receptor PD-1 impedes T lymphocyte activation. The third signal (3) is mediated via cytokines like IL-2, IL-12, IL-15 and IL-15 that affect T lymphocyte differentiation, proliferation, survival and functional activity. Adapted from [122]. ..... 14

**Figure 7: Signal transduction downstream of the T cell receptor.** In CD4<sup>+</sup> T lymphocytes, T cell receptor (TCR) binding to a complementary peptide-MHC II complex on the surface of an antigen-presenting cell (APC) leads to the recruitment of CD4 co-receptor, which binds to the conserved region of the MHC complex. Subsequently, the protein kinase Lck is recruited to CD4 and phosphorylates CD3 $\epsilon$ , - $\delta$  and - $\zeta$  chains associated with the TCR. This phosphorylation enables binding of adaptor protein kinases Fyn and Zap70 to CD3 chains. Then, Zap70 is activated by Fyn- and Lck-mediated phosphorylation and in turn phosphorylates the linker for activation of T cells (LAT) at multiple sites. These modifications generate binding sites for several other adaptor molecules like GADS, PLC- $\gamma$ 1 and Grb-2, which in turn recruit other adaptor molecules and protein kinases leading to the activation of downstream signaling pathways that initiate cytoskeletal rearrangements, cell proliferation as well as the expression of genes associated with respective T lymphocyte function. Adapted from [165]. ..... 17

**Figure 8: The Cancer-Immunity Cycle and current (immune-)therapeutic interventions that target each step for reactivation and amplification of the anti-tumor immune response.** Schematic illustration of the seven central steps in the generation of an anti-tumor response by the innate and adaptive immunity (grey). A selection of potential therapeutic strategies to improve each step are listed below (bold black). TLR = Toll-like receptor; IL = interleukin; CARs = chimeric antigen receptor T lymphocytes; IDO = Indoleamine 2,3-dioxygenase. Adapted from [192]. ..... 20

**Figure 9: Durvalumab in complex with human PD-L1.** Surface (transparent) and ribbon diagram of Durvalumab Fab-fragment (blue = heavy chain; red = light chain) in complex with the Immunoglobulin superfamily (IgSF) V-set domain of human PD-L1 (grey) according to the orthorhombic crystal structure determined by X-ray crystallography (pdb entry: 5X8M). Main- and side chains of PD-L1 IgSF V-set domain, which are engaged by Durvalumab via hydrogen bonds, salt bridges and hydrophobic interactions, are presented in black (stick model). Data has been obtained from [232]. ..... 24

**Figure 10: Schematic illustration of the counterflow centrifugation system (A) and the separation principle in the elutriation chamber in detail (B).** Cell populations are separated by counterflow centrifugation due to their differences in sedimentation potential. During this process cells are exposed to a constant centrifugal force and opposing increasing counterflow. Adapted from [258]. ..... 46

**Figure 11: Schematic illustration of the setting for co-culture of pre-activated CD8<sup>+</sup> T lymphocytes, M1-polarized macrophages and PancTu-I cells.** PancTu-I cells and CD8<sup>+</sup> T lymphocytes are seeded in the lower well of a 12-well culture plate for direct co-culture. M1-polarized macrophages are seeded in transwell inserts with a pore size of 0.4  $\mu$ m. .... 51

**Figure 12: Heterogeneity of intra-tumoral PD-L1 expression in pancreatic tissue sections from PDAC patients.** Representative images of immunohistochemical PD-L1 staining in pancreatic tissues of PDAC patients for different scoring values (red numbers) with regard to (A-C) the staining intensity, (D-F) the proportion of PD-L1<sup>+</sup> cells, (G-I) the expression in tumor-associated lymph follicles as well as (J+K) the local distribution of PD-L1<sup>+</sup> cells within the tumor. According to the evaluation system, PD-L1 mean staining intensity in fields of view (FoV) showing PD-L1<sup>+</sup> cells was rated as (A) weak (1), (B) moderate (2) or (C) strong (3). The proportion of PD-L1<sup>+</sup> cells within FoV was scored as (D) negative (0), (E) < 1% PD-L1<sup>+</sup> cells (1) or (F) > 1% PD-L1<sup>+</sup> cells (2). PD-L1 expression in tumor-associated lymph follicles was rated as (G) negative (0), (H) weak/moderate (1) or (I) strong (2). Finally, distribution of PD-L1<sup>+</sup> cells within FoV was categorized as (J) „diffuse/patternless“ (0) and (K) „cluster formation“ (1). Original magnification/scale bar: 100-fold/200  $\mu\text{m}$  (G-I); 200-fold/50  $\mu\text{m}$  (A-F; J+K). (published data [264])..... 67

**Figure 13: PD-L1 expression is enhanced in PDAC tumor area compared to peritumoral tissue and correlates with clinic-pathological patient characteristics.** (A) Proportion of analyzed microscopic fields of view (FoV) with at least one PD-L1<sup>+</sup> cell in PDAC tumor and peritumoral tissue sections presented as Box-and-whisker plot. (B) Ratio of PD-L1 Tissue Scores in PDAC tumor tissue and respective peritumoral pancreatic tissue presented as Box-and-whisker plot. (C) Representative images of immunohistochemical PD-L1 staining in different areas of pancreatic tissue from a PDAC patient. Shown are adjacent healthy acinus tissue (left, “Healthy”), peritumoral margin with desmoplastic stroma (middle, “Peritumoral”) and intratumoral tissue (right, “Tumor”). (D) Tissue Scores of each PDAC tumor and peritumoral tissue section are presented as dots by a scatter plot. Red line at a value of 0.8 indicates the identified threshold between PD-L1<sup>low</sup> and PD-L1<sup>high</sup> tissue sections. (E) Survival LogRank analysis correlates overall survival time (months) of PDAC patients with intratumoral PD-L1 expression (Tissue Score: PD-L1<sup>low</sup> vs. PD-L1<sup>high</sup>). Considering surgery-related mortality, patients with survival times of less than 4 months were excluded from analysis. (F) PD-L1 Tissue Scores are presented as Box-and-whisker plots with regard to the pathological defined tumor grade. n = 56 (D, F); 39 (E). Original magnification/scale bar: 200-fold/100  $\mu\text{m}$ . n = 56 vs. 18 (A); 13 (B). \* = p<0.05. (published data [264])..... 70

**Figure 14: PD-L1 expression in PDAC is not restricted to epithelial/tumor cells but is localized to a large extent within the tumor stroma.** (A-I) Representative images of immunohistochemical PD-L1 (brown)/PanCK (red) staining in PD-L1<sup>high</sup> graded pancreatic tissues of PDAC patients. Cellular origin of PD-L1 expression observed in single staining (A, D+G) was evaluated in PD-L1/PanCK double staining (B+C, E+F, H+I). Tissues were classified into 3 groups with regard to the prevalent cellular origin of PD-L1 expression: Cell Score 1 (PanCK<sup>+</sup> PD-L1<sup>+</sup>), Cell Score 2 (PanCK<sup>-</sup> PD-L1<sup>+</sup>) and Cell Score 3 (PanCK<sup>+/-</sup> PD-L1<sup>+</sup>). (J) Pie chart illustrates the proportion of PDAC tissues rated as Cell Score 1 (black), 2 (grey) and 3 (white) within PD-L1<sup>high</sup> graded tissues. Original magnification/scale bar: 200-fold/100  $\mu\text{m}$  (B, E+H); 400-fold/100  $\mu\text{m}$  (A, C, D, F, G+I). (published data [264])..... 72

**Figure 15: Characterization of PD-L1 expression in PDAC by the POLE Score system. . .** (A) Tree diagram illustrates the distribution of POLE Scores for PD-L1 expression in pancreatic tissue sections of PDAC patients. Scoring values P0-2 (overall PD-L1 expression), O1-3 (PD-L1 cellular Origin), L0-2 (PD-L1 expression in tumor-associated Lymph follicles) and E0-1 (Enumerated spatial distribution of PD-L1<sup>+</sup> cells) are depicted at the end of the branches. Number of cases are indicated in brackets. (B) Pie charts illustrate the proportion of compiled POLE Scores within the entire cohort (right, n=56) and subset of P2 scored (left, n=17) PDAC tissues. X = not rated (excluded in pie charts). (published data [264])..... 73

**Figure 16: PD-L1 expression characterized by POLE Score correlates with intra-tumoral proportion of distinct immune cell populations.** (A) Heatmap illustrates results from statistical correlation of dichotomized POLE Scores, markers for stromal cell populations, EMT and Ki67 status assessed by immunohistochemical staining. Dichotomization was performed according to the following pattern: +P1 (=P0+P1) vs. +P2 (=P2); +O1 (=O1) vs. +O2 (=O2+O3); +L1 (=L0) vs. +L2 (=L1+L2). P-values from statistical analyses are illustrated by color gradient (dark green: p=0.01 to dark red: p=1.0; white: statistical analysis not possible). Pie charts show proportion of subgroups within correlations of (B) +O-Score vs. CD3 (% stroma), (C) +L-Score vs. CD4 (% stroma), (D) +L-Score vs. CD68/CD163 (duct-associated), (E) +O-Score vs.  $\alpha$ -SMA (intensity), (F) +O-Score vs. PanCK (% section), (G) +O-Score vs. Ki67 (% epithelium) and (H) +P-Score vs. E-Score. Statistical analyses were performed by Chi-square/Fisher exact test. (published data [264])..... 75

**Figure 17: Intratumoral areas enriched for PD-L1<sup>+</sup> stromal cells show high proportion of Ki67<sup>+</sup> cells within the epithelial tumor compartment.** Representative images of (A+C) PD-L1 and (B+D) Ki67 immunohistochemical staining in serial pancreatic tissue sections from PDAC patients. Original magnification/scale bar: 200-fold/100  $\mu$ m (published data [264]).. 76

**Figure 18: Polarized PD-L1 expression at the tumor-lymph follicle interface coincides with the presence of CD68<sup>+</sup> macrophages.** Representative images of (A+C) pan-cytokeratin (PanCK), (B+D) PD-L1, (E+H) CD4, (F+I) CD68 and (G+J)  $\alpha$ -SMA immunohistochemical staining in serial pancreatic tissue sections from a PDAC patient. (B) Shown is an infiltrated tumor-associated lymph follicle exhibiting high proportion of PD-L1<sup>+</sup> cells at the tumor margin (red arrow heads) and absence of PD-L1 expression at the tumor-averted border (black arrow heads). PD-L1 expression is co-localized with (E) CD4 (yellow arrow heads) and (F) CD68 staining (green arrow heads). Original magnification/scale bar: 25-fold/500  $\mu$ m (overviews; A+B, E-G); 100-fold/200  $\mu$ m (detail; C+D, H-J). (published data [264])..... 78

**Figure 19: PD-L1 is markedly expressed within tumor areas that show high proportion of CD8<sup>+</sup> T cells and macrophages.** Representative images of (A+E) PanCK, (B+F) PD-L1, (C+G) CD3, (D+H) CD4, (I+M) CD8, (J+N) CD68, (K+O) CD163 and (L+P)  $\alpha$ -SMA immunohistochemical staining in serial pancreatic tissue sections from a PDAC patient. Original magnification/scale bar: 25-fold/200  $\mu$ m (overviews; A-D+I-L); 200-fold/100  $\mu$ m (detail; E-H+M-P). (published data [264])..... 79

**Figure 20: Tumor-associated macrophages represent a PD-L1 expressing stromal cell population in some PDAC patients or distinct tumor areas.** (A) Gating strategy for detection of cell surface PD-L1 expression by flow cytometry in distinct populations of freshly isolated cells in resected PDAC specimens. Epithelial/tumor cells were discriminated from leukocytes by panCK/CD45 staining. Tumor-associated macrophages (TAMs) within the CD45<sup>+</sup> leukocyte populations were discriminated from other leukocyte populations *via* side scatter (SSC) and CD68 expression. Specificity of staining (red contour plots/histograms) was ensured by detection of signals from respective isotype staining (black contour plots/histograms) in parallel. (B, C) Scatter plots summarize results from flow cytometric detection of PD-L1 cell surface expression in freshly isolated TAMs (CD45<sup>+</sup> CD68<sup>+</sup>; black symbols), non-TAM leukocytes (CD45<sup>+</sup> CD68<sup>-</sup>; red symbols) and epithelial/tumor cells (CD45<sup>-</sup> panCK<sup>+</sup>; white symbols) of PDAC specimens from three different patients with regard to (B) proportion of PD-L1<sup>+</sup> cells and (C) median fluorescence intensity (MFI) ratio (MFI<sup>PD-L1</sup>/MFI<sup>isotype</sup>). (D) Representative images of CD68 and PD-L1 immunofluorescence co-staining in PDAC tissue sections from two different patients. Shown are grey scale signals from single channels for detection of CD68 (left) and PD-L1 (middle) staining as well as overlay (right) of CD68 (orange), PD-L1 (green) and nuclei staining by Hoechst (blue) for analysis of co-localization. Marked are PD-L1<sup>+</sup> CD68<sup>+</sup> (white arrow heads) and PD-L1<sup>-</sup> CD68<sup>+</sup> (red arrow heads) TAMs as well as a cluster of PD-L1<sup>+</sup> CD68<sup>+</sup> TAMs (white quadrant). Original magnification/scale bar: 200-fold/50  $\mu$ m. (published data [264]). ..... 81

**Figure 21: Basal PD-1 and PD-L1 expression in various PDEC cell lines.** Cells for analyses were obtained from standard culture conditions of respective cell lines. (C) Representative western blot of whole-cell lysates from various pancreatic ductal epithelial cell lines from three independent experiments. Alpha tubulin was detected as loading control. Molecular weights in kDa are indicated according to the applied standard. Exp. = decreased/increased time of light exposure for signal detection. (B) Representative dot plots from flow cytometric analyses of H6c7eR-kras (top), Panc-1 (middle) and PancTu-I cells (bottom). Shown are the gating strategy in FSC/SSC dot plots (left) as well as signals detected by PD-1/PD-L1 antibody staining (red) and respective isotype control staining (grey) in dot plots with attached histograms. (C) PD-1 (white) and PD-L1 (black) cell surface expression levels in PancTu-I cells detected by immunofluorescence staining and subsequent flow cytometric analysis. Bar chart presents mean values and SEM of median fluorescence intensity ratios detected in three independent experiments. The dashed line marks an MFI ratio of “1”. ..... 83

**Figure 22: Induction of PD-L1 expression by various cytokines and growth factors in premalignant PDEC and PDAC cell lines.** H6c7eR-kras, Panc-1, PancTu-I, Panc89, Colo357 and BxPc3 cells were cultured for 72 h in respective standard culture medium supplemented with 10 ng/ml IFN $\gamma$ , 20 ng/ml EGF, 10 ng/ml TNF $\alpha$ , 10 ng/ml IL-6, 60 ng/ml IL-2 or 20 ng/ml TGF- $\beta$ 1. (A+B) Representative western blots of whole-cell lysates from (A) H6c7eR-kras, Panc-1 and PancTu-I as well as (B) Panc89, Colo357 and BxpC3 cells after stimulation (+) with recombinant human EGF or IFN $\gamma$  in comparison to unstimulated (-) cells. Hsp90 was detected as loading control. \* = PD-L1 signal, \*\* = p-Stat1 signal (C) Representative western blot of whole-cell lysates from PancTu-I cells after indicated stimulations. Alpha tubulin was detected as loading control. Molecular weights in kDa are indicated according to the applied standard. (D) Densitometric analysis of PD-L1 levels detected by western blotting in whole-cell lysates of PancTu-I cells after stimulation with indicated cytokines. Relative PD-L1 signal intensities were normalized to unstimulated PancTu-I cells. Bar chart presents mean values and SEM from three independent experiments. (E) Representative histograms from flow cytometric analysis of unstimulated (blue) and IFN $\gamma$  stimulated (red) PancTu-I cells stained with fluorochrome-

conjugated PD-L1 antibody (blue and red) or respective isotype control antibody (grey). **(F)** Representative fluorescence microscopical images of immunofluorescence PD-L1 (red) staining in unstimulated and IFN $\gamma$  stimulated PancTu-I cells. Nuclei were stained with Hoechst (blue). Scale bar = 50  $\mu$ m..... **85**

**Figure 23: Basal PD-1 and PD-L1 expressions levels in M1- and M2-polarized macrophages.** Polarized primary human macrophages were generated by in vitro stimulation of monocytes with either GM-CSF (M1 M $\Phi$ ) or M-CSF (M2 M $\Phi$ ) for seven days. **(A)** Representative dot plots from flow cytometric analyses of M1 M $\Phi$  (top) and M2 M $\Phi$  (bottom). Shown are the gating strategy in FSC/SSC dot plots (left) and discrimination of CD14<sup>+</sup> macrophages (red) from CD14<sup>-</sup> cells (blue) (middle) as well as signals detected by PD-1/PD-L1 antibody staining in M1 M $\Phi$  (red) and M2 M $\Phi$  (blue). Signal specificities were verified by staining with respective isotype control antibodies (grey). **(B)** PD-1 (white) and PD-L1 (black) cell surface expression levels in M1- and M2 M $\Phi$  detected by immunofluorescence staining and subsequent flow cytometric analysis. Bar chart presents mean values and SEM of median fluorescence intensity ratios detected in three independent experiments. The dashed line marks an MFI ratio of “1”. **(C)** Representative western blot of whole-cell lysates from M1- and M2 M $\Phi$  as well as various PDAC cell lines. Hsp90 was detected as loading control. Exposure = decreased/increased time of light exposure for signal detection; \* = p<0.05 ..... **87**

**Figure 24: Induction of PD-L1 expression by various cytokines in M1- and M2-polarized macrophages.** Polarized primary human macrophages were generated by in vitro stimulation of monocytes with either GM-CSF (M1 M $\Phi$ ) or M-CSF (M2 M $\Phi$ ) for seven days. Macrophages were cultured for 72 h in respective standard culture medium supplemented with 2.4 ng/ml GM-CSF, 50 ng/ml M-CSF, 10 ng/ml IFN $\gamma$ , 10 ng/ml TNF $\alpha$  or 20 ng/ml TGF- $\beta$ 1. **(A+C)** Relative PD-L1 cell surface expression levels in **(A)** M1- and **(C)** M2 M $\Phi$  after stimulation with indicated cytokines in comparison to unstimulated macrophages. Bar charts present percentage changes in median fluorescence intensity ratios resulting from single flow cytometric analysis of PD-L1 immunofluorescence staining. **(B+D)** Representative fluorescence microscopical images of immunofluorescence PD-L1 (green) staining in **(B)** M1- and **(D)** M2 M $\Phi$  after stimulation with indicated cytokines. Nuclei were stained with Hoechst (blue) (Scale bar = 50  $\mu$ m). **(E)** Representative western blot of whole-cell lysates from M1 M $\Phi$  after indicated stimulations. Hsp90 was detected as loading control. Molecular weights in kDa are indicated according to the applied standard..... **89**

**Figure 25: Lymphocyte activation by anti-CD3/CD28 stimulation.** Primary human lymphocytes were isolated from leukocyte retaining systems by density gradient centrifugation followed by counterflow centrifugation. Afterwards, lymphocytes were seeded in standard culture medium and either left unstimulated or were stimulated with immobilized CD3- and soluble CD28-targeting antibodies for 3 to 5 days. **(A)** Representative light microscopical images of unstimulated and anti-CD3/CD28 stimulated lymphocytes after indicated culture durations (Scale bar = 500  $\mu$ m). **(B)** Representative western blot of whole-cell lysates from unstimulated (-) and anti-CD3/CD28 stimulated (+) lymphocytes after seeding (d0) and three (d3) and five (d5) days of culture, respectively. Molecular weights in kDa are indicated according to the applied standard. **(C)** Representative fluorescence microscopical images of immunofluorescence PD-1 (green) and PD-L1 (orange) staining in cytospins of unstimulated or anti-CD3/CD28 stimulated lymphocytes after five days of culture. Nuclei were stained with Hoechst (blue). Scale bar = 30  $\mu$ m..... **91**

**Figure 26: Schematic illustration of the gating strategy for flow cytometric analyses of lymphocyte populations.** Primary human lymphocytes were isolated from leukocyte retaining systems by density gradient centrifugation followed by counterflow centrifugation. Afterwards, lymphocytes were stained with CFSE, seeded in standard culture medium and were either left unstimulated or were stimulated with immobilized CD3- and soluble CD28-targeting antibodies. First, vital lymphocytes were discriminated in FSC/SSC plot. Secondly, resting (blue) and proliferating (red) population were identified via CFSE staining intensity. Thirdly, CD4<sup>+</sup> (blue) CD8<sup>+</sup> (red) and CD4<sup>-</sup> CD8<sup>-</sup> (grey) populations were discriminated by staining with fluorochrome-conjugated antibodies targeting CD4 and CD8, respectively. Finally, PD-1 and PD-L1 cell surface levels were quantified within resting (blue) and proliferating (red) populations of CD4<sup>+</sup> (top) and CD8<sup>+</sup> (bottom) lymphocytes by respective immunofluorescence signals. Signal specificities were verified by staining with respective isotype control antibodies (grey). ..... 92

**Figure 27: Proliferation within CD4<sup>+</sup> and CD8<sup>+</sup> lymphocyte populations after anti-CD3/CD28 stimulation.** Primary human lymphocytes were isolated from leukocyte retaining systems by density gradient centrifugation followed by counterflow centrifugation. Afterwards, lymphocytes were CFSE stained, seeded in standard culture medium and either left unstimulated or were stimulated with immobilized CD3- and soluble CD28-targeting antibodies for 3 to 5 days. (A) Proportion of proliferating cells and (B) vital cell numbers in unstimulated and anti-CD3/CD28 stimulated lymphocyte populations after three (white) and five (black) days. (C+D) CFSE profiles of proliferating lymphocytes within the CD4<sup>+</sup> (black) and CD8<sup>+</sup> (white) population after (C) three and (D) five days of anti-CD3/CD28 stimulation. Data presents mean values and SEM of lymphocytes having divided 1 to 5 times. The maximum numbers of clearly distinguishable peaks in respective CFSE profiles are indicated by “+X”. (E) Proportion of proliferating lymphocytes within the CD4<sup>+</sup> and CD8<sup>+</sup> population after three (white) and five (black) days of anti-CD3/CD28 stimulation. Box plots present median values with quartiles (Q<sub>0.75</sub> as upper, Q<sub>0.25</sub> as lower deviation) and bar charts present mean values with SEM of three independent experiments. \* = p<0.05 ..... 93

**Figure 28: PD-1 and PD-L1 cell surface levels in the CD4<sup>+</sup> T lymphocyte population after anti-CD3/CD28 stimulation.** Primary human lymphocytes were isolated from leukocyte retaining systems by density gradient centrifugation followed by counterflow centrifugation. Afterwards, lymphocytes were seeded in standard culture medium and stimulated with immobilized CD3- and soluble CD28-targeting antibodies for 3 to 5 days until immunofluorescence staining followed by flow cytometric analysis. (A) PD-1 and (B) PD-L1 cell surface expression levels in the resting (white) and proliferating (black) population of CD4<sup>+</sup> lymphocytes after indicated culture durations. Bar charts present mean values and SEM of median fluorescence intensity ratios detected in three independent experiments. The dashed line marks an MFI ratio of “1”. \* = p<0.05 ..... 94

**Figure 29: Gene expression profile of cytokines and chemokines associated with various lymphocyte populations after anti-CD3/CD28 stimulation of whole lymphocyte populations.** Primary human lymphocytes were isolated from leukocyte retaining systems by density gradient centrifugation followed by counterflow centrifugation. Afterwards, lymphocytes were seeded in standard culture medium and were either left unstimulated or stimulated with immobilized CD3- and soluble CD28-targeting antibodies for 3 (white) to 5 days (black). Relative mRNA levels of (A) IFN $\gamma$ , (B) IL-2, (C) TNF $\alpha$ , (D) TGF- $\beta$ 1, (E) IL-6, (F) IL-10, (G) IL-1 $\beta$  and (H) IL-8 in unstimulated and anti-CD3/CD28 stimulated lymphocytes after three (white) and five (black) days of culture. Box plots present median values with quartiles (Q<sub>0.75</sub> as upper, Q<sub>0.25</sub> as lower deviation) and bar charts present mean values with SEM of three independent experiments. Messenger RNA levels were normalized to respective GAPDH levels as well as levels detected in freshly isolated lymphocytes prior to seeding (= 1). \* = p<0.05 ..... 96

**Figure 30: Supernatant levels of T lymphocyte-associated cytokines after anti-CD3/CD28 stimulation of whole lymphocyte populations.** Primary human lymphocytes were isolated from leukocyte retaining systems by density gradient centrifugation followed by counterflow centrifugation. Afterwards, lymphocytes were seeded in standard culture medium and were either left unstimulated or were stimulated with immobilized CD3- and soluble CD28-targeting antibodies for 3 to 5 days. Concentrations of (A) IFN $\gamma$ , (B) IL-6, (C) TNF $\alpha$ , (D) IL-17A, (E) soluble Fas ligand, (F) Perforin, (G) Granzyme A, (H) Granzyme B and (I) Granulysin were measured by multiplex assay in the culture supernatant of unstimulated and anti-CD3/CD28 stimulated lymphocytes after three (white) and five (black) days of culture. Box plots present median values with quartiles (Q<sub>0.75</sub> as upper, Q<sub>0.25</sub> as lower deviation) and bar charts present mean values with SEM of three independent experiments. \* = p<0.05 ..... 98

**Figure 31: Isolation of primary human CD8<sup>+</sup> T lymphocytes from peripheral blood mononuclear cells.** Primary human lymphocytes were isolated from leukocyte retaining systems by density gradient centrifugation followed by counterflow centrifugation. (A) Schematic illustration of the staining panel and gating strategy in flow cytometric analysis before (pre MACS) and after (post MACS) magnetic-activated cell separation. First, vital lymphocytes were gated in FSC/SSC plot. Secondly,  $\alpha\beta$  T cell receptor ( $\alpha\beta$ TCR) positive (red) were discriminated from  $\alpha\beta$ TCR negative cells (blue). Finally, the proportion of CD4<sup>+</sup> (blue), CD8<sup>+</sup> (red) and CD4<sup>-</sup>CD8<sup>-</sup> (grey)  $\alpha\beta$ TCR<sup>+</sup> T lymphocytes were examined. (B) Proportion of CD8<sup>+</sup> T lymphocytes after isolation by MACS separation (white) and after 4 days of anti-CD3/CD28 stimulation (black). Bar chart presents mean values with SEM of six independent experiments. .... 100

**Figure 32: Activation of human CD8<sup>+</sup> T lymphocytes by anti-CD3/CD28 stimulation.** Primary human lymphocytes were isolated from leukocyte retaining systems by density gradient centrifugation followed by counterflow centrifugation. Afterwards, CD8<sup>+</sup> T lymphocytes were isolated by negative MACS selection, stained with CFSE and stimulated with immobilized CD3- and soluble CD28-targeting antibodies as well as IL-2 for 4 days. (A) Representative FSC/SSC dot plots of CD8<sup>+</sup> T lymphocyte populations directly after MACS isolation (d0) and four days of anti-CD3/CD28 stimulation. (B) Representative histogram of CFSE staining in CD8<sup>+</sup> T lymphocytes after four days of anti-CD3/CD28 stimulation. The resting (blue) and proliferating (red) population are discriminated by CFSE dilution. The numbers indicate the quantity of cell divisions each population characterized by the respective peak has progressed through. (C) CFSE profile of proliferating CD8<sup>+</sup> T lymphocytes after four



days of anti-CD3/CD28 stimulation. Bar chart presents mean proportions with SEM of lymphocytes having divided 1 to 5 times in six independent experiments. **(D)** Overall proportion of proliferating CD8<sup>+</sup> T lymphocytes after four days of anti-CD3/CD28 stimulation. Bar chart presents mean value with SEM of six independent experiments. **(E)** Relative mRNA levels of IFN $\gamma$ , IL-2, IL-6 and TNF $\alpha$  in anti-CD3/CD28 stimulated CD8<sup>+</sup> T lymphocytes after four days of culture. Bar chart presents mean values of technical triplicates from one representative experiment. Messenger RNA levels were normalized to respective GAPDH levels as well as levels detected in whole lymphocyte population after four days of anti-CD3/CD28 stimulation (= 1). **(F)** Representative western blot of whole-cell lysates from unstimulated CD8<sup>+</sup> T lymphocytes and after four days of anti-CD3/CD28 stimulation. Hsp90 was detected as loading control. Molecular weights in kDa are indicated according to the applied standard. \* = p<0.05 ..... 101

**Figure 33: PD-1 and PD-L1 cell surface expression levels in CD8<sup>+</sup> T lymphocytes after anti-CD3/CD28 stimulation.** Primary human lymphocytes were isolated from leukocyte retaining systems by density gradient centrifugation followed by counterflow centrifugation. Afterwards, CD8<sup>+</sup> T lymphocytes were isolated by negative MACS selection, stained with CFSE and stimulated with immobilized CD3- and soluble CD28-targeting antibodies as well as IL-2 for 4 days. **(A+B)** Representative contour plots with attached histograms showing correlation between CFSE staining and **(A)** PD-1 or **(B)** PD-L1 staining within the resting (blue) and proliferating (red) population of anti-CD3/CD28 stimulated CD8<sup>+</sup> T lymphocytes. Signal specificities were verified by staining with respective isotype control antibodies (grey). **(C)** PD-1 and **(D)** PD-L1 cell surface expression levels in the whole (white) and proliferating (black) population of CD8<sup>+</sup> lymphocytes after indicated stimulations and culture durations. Bar charts present mean values and SEM of median fluorescence intensity ratios examined in six independent experiments. **(E)** PD-1 and **(F)** PD-L1 cell surface expression levels in anti-CD3/CD28 stimulated CD8<sup>+</sup> T lymphocytes having divided one to five times. Bar charts present mean values and SEM of median fluorescence intensity ratios examined in six independent experiments. The dashed lines mark an MFI ratio of “1”. \* = p<0.05 ..... 103

**Figure 34: Phenotype and proliferation of CD8<sup>+</sup> T lymphocytes after direct co-culture with autologous M1-polarized macrophages.** Activated primary human CD8<sup>+</sup> T lymphocytes were mono-cultured or directly co-cultured for 72 h with M1-like polarized macrophages, which were differentiated from autologous monocytes by GM-CSF stimulation. **(A)** Representative FSC/SSC contour plots from flow cytometric analysis of CD8<sup>+</sup> T lymphocytes after 72 h of mono- and co-culture with M1 M $\Phi$ , respectively. Comparison of **(B)** FSC medians, **(C)** SSC medians, **(D)** vital cell numbers and **(E)** the proportion of proliferating lymphocytes within CD8<sup>+</sup> T lymphocytes populations after mono- or direct co-culture with M1 M $\Phi$  for 72 h. Data present mean values with SEM of three independent experiments. **(F)** CFSE profiles of proliferating lymphocytes within CD8<sup>+</sup> T lymphocyte populations after mono- (white) or co-culture with M1 M $\Phi$  (black) for 72 h. Data presents mean proportions and SEM of lymphocytes having divided 1 to 7 times examined in three independent experiments. The maximum numbers of clearly distinguishable peaks in respective CFSE profiles are indicated by “+X” ..... 105

**Figure 35: PD-1 and PD-L1 cell surface levels in CD8<sup>+</sup> T lymphocytes after direct co-culture with autologous M1-polarized macrophages.** Pre-activated primary human CD8<sup>+</sup> T lymphocytes were mono-cultured or directly co-cultured for 72 h with M1-like polarized macrophages, which were differentiated from autologous monocytes by GM-CSF stimulation. (A) PD-1 and (B) PD-L1 cell surface expression levels in the resting (white) and proliferating (black) population of CD8<sup>+</sup> lymphocytes after indicated culture conditions. Bar charts present mean values and SEM of median fluorescence intensity ratios examined in three independent experiments. The dashed lines mark an MFI ratio of “1”. (C) Representative western blot of whole-cell lysates from CD8<sup>+</sup> T lymphocytes directly after four days of anti-CD3/CD28 stimulation (activated (d0)) as well as after following 72 h of either mono- or co-culture with M1 MΦ. Molecular weights in kDa are indicated according to the applied standard..... 106

**Figure 36: Cell surface expression levels of PD-L1, CD206 and CD163 in M1-polarized macrophages after co-culture with autologous activated CD8<sup>+</sup> T lymphocytes.** M1-polarized primary human macrophages were mono-cultured or directly co-cultured for 72 h with autologous pre-activated CD8<sup>+</sup> T lymphocytes. (A) Representative histograms from flow cytometric analysis of PD-L1 (left), CD206 (middle) and CD163 (right) cell surface immunofluorescence staining in M1 MΦ after mono- (blue) or co-culture with CD8<sup>+</sup> T lymphocytes (red). Signal specificities were verified by staining with respective isotype control antibodies (white/grey). (B) PD-L1, (C) CD206 and (D) CD163 cell surface levels in M1 MΦ after indicated culture conditions. Bar charts present mean values and SEM of median fluorescence intensity ratios examined in three independent experiments. The dashed lines mark an MFI ratio of “1”..... 107

**Figure 37: Supernatant levels of T lymphocyte- and macrophage-associated cytokines, chemokines, growth factors and effector molecules after direct co-culture of activated CD8<sup>+</sup> T lymphocytes with autologous M1-polarized macrophages.** Pre-activated primary human CD8<sup>+</sup> T lymphocytes and autologous M1-polarized macrophages were either mono-cultured or directly co-cultured for 72 h. Concentrations of (A) IL-8, (B) VEGF, (C) IL-6, (D) TNFα, (E) IFNγ, (F) IL-17A, (G) soluble Fas ligand, (H) Perforin, (I) Granulysin, (J) Granzyme A and (K) Granzyme B were measured by multiplex assay in the culture supernatant of mono-cultured CD8<sup>+</sup> T lymphocytes (white) and M1 MΦ (grey) as well as direct co-cultures (black) after 72 h. Box plots present median values with quartiles (Q<sub>0.75</sub> as upper, Q<sub>0.25</sub> as lower deviation) and bar charts present mean values with SEM of three independent experiments. N.D. = not detectable; \* = p<0.05;..... 109

**Figure 38: Proliferation of activated CD8<sup>+</sup> T lymphocytes after direct co-culture with various PDAC cell lines.** Pre-activated primary human CD8<sup>+</sup> T lymphocytes were either mono- or directly co-cultured for 72 h with Panc1, Panc89 and PancTu-I cells, respectively. (A) Proportion of proliferating cells within CD8<sup>+</sup> T lymphocytes after mono- (white) or indicated co-culture (black) conditions. Dashed line marks the proportion of proliferating cells in mono-cultured T lymphocytes. (B) Median fluorescence intensity (MFI) of CFSE staining in the whole (white) and proliferating (black) population of CD8<sup>+</sup> T lymphocytes after indicated mono- and co-culture settings with PDAC cell lines. Dashed line indicates the CFSE MFI in the whole lymphocyte population and drawn through line indicates the CFSE MFI of the proliferating lymphocyte population of mono-cultured CD8<sup>+</sup> T lymphocytes. (C-E) CFSE profiles of proliferating CD8<sup>+</sup> T lymphocytes after mono-culture (white) and direct co-culture with (C) Panc1, (D) Panc89 and (E) PancTu-I cells. Data present proportions of lymphocytes having divided 1 to 5 times.

The maximum numbers of clearly distinguishable peaks in respective CFSE profiles are indicated by “+”. (A-E) Graphs present data from one experiment..... 111

**Figure 39: PD-1 and PD-L1 cell surface expression levels in CD8<sup>+</sup> T lymphocytes as well as levels of proteins associated with differentiation and proliferation status in various PDAC cell lines after direct co-culture.** Pre-activated primary human CD8<sup>+</sup> T lymphocytes were either mono- or directly co-cultured for 72 h with Panc1, Panc89 and PancTu-I cells, respectively. (A) PD-1 and (B) PD-L1 cell surface levels in the whole (white) and proliferating (black) population of CD8<sup>+</sup> T lymphocytes after indicated culture conditions. Bar charts present median fluorescence intensity ratios examined in one experiment. The dashed lines mark an MFI ratio of “1”. (C) Representative western blot of whole-cell lysates from Panc1, Panc89 and PancTu-I cells after mono- (-) or co-culture with activated CD8<sup>+</sup> T lymphocytes (+). Hsp90 was detected as loading control. Molecular weights in kDa are indicated according to the applied standard. Triangle indicates decreased/increased time of light exposure for vimentin signal detection. .... 112

**Figure 40: Phenotype and proliferation of CD8<sup>+</sup> T lymphocytes after co-culture with PancTu-I cells and autologous M1-polarized macrophages.** Pre-activated primary human CD8<sup>+</sup> T lymphocytes were either mono-cultured (white), indirectly co-cultured with autologous M1 MΦ (banded), directly co-cultured with PancTu-I cells (grey) or co-cultured with both autologous M1 MΦ (indirect) and PancTu-I cells (direct) (black) for 48 h. Comparison of (A) FSC medians, (B) SSC medians, (C) relative vital cell numbers and (D) the proportion of proliferating cells within CD8<sup>+</sup> T lymphocytes from indicated culture settings. Bar charts present mean values with SEM of three independent experiments. (E) CFSE profiles of proliferating CD8<sup>+</sup> T lymphocytes after 48 h of indicated mono- and co-culture conditions. Bar chart presents mean proportions with SEM of T lymphocytes having divided 1 to 5 times in three independent experiments. The maximum numbers of clearly distinguishable peaks in respective CFSE profiles are indicated by “+”..... 115

**Figure 41: PD-1 and PD-L1 cell surface expression levels in CD8<sup>+</sup> T lymphocytes after co-culture with PancTu-I cells and autologous M1-polarized macrophages.** Pre-activated primary human CD8<sup>+</sup> T lymphocytes were either mono-cultured (white), indirectly co-cultured with autologous M1 MΦ (banded), directly co-cultured with PancTu-I cells (grey) or co-cultured with both autologous M1 MΦ (indirect) and PancTu-I cells (direct) (black) for 48 h. (A) PD-1 and (B) PD-L1 cell surface levels in the whole (white) and proliferating (black) population of CD8<sup>+</sup> T lymphocytes after indicated culture conditions. (C) PD-1 cell surface expression levels in populations of CD8<sup>+</sup> T lymphocytes having divided one to six times after indicated mono- and co-culture conditions. (A-C) Bar charts present mean values with SEM of median fluorescence intensity ratios examined in three independent experiments. The dashed lines mark an MFI ratio of “1”. .... 116

**Figure 42: Cell surface expression levels of PD-L1, CD206 and CD163 in M1-polarized macrophages after co-culture with PancTu-I cells and autologous activated CD8<sup>+</sup> T lymphocytes.** Primary human M1-polarized macrophages were either mono-cultured (white), indirectly co-cultured with autologous pre-activated CD8<sup>+</sup> T lymphocytes (banded), PancTu-I cells (grey) or both autologous CD8<sup>+</sup> T lymphocytes and PancTu-I cells (black) for 48 h. (A) PD-L1, (B) CD206 and (C) CD163 cell surface levels in M1 MΦ after indicated culture conditions. Bar charts present mean values with SEM of median fluorescence intensity ratios examined in three independent experiments. The dashed lines mark an MFI ratio of “1”.  
..... 117

**Figure 43: Gene expression profiles of cytokines, chemokines and growth factors in M1-polarized macrophages after co-culture with PancTu-I cells and autologous activated CD8<sup>+</sup> T lymphocytes.** Primary human M1-polarized macrophages were either mono-cultured (white) or indirectly co-cultured with autologous pre-activated CD8<sup>+</sup> T lymphocytes (banded), PancTu-I cells (grey) or both autologous CD8<sup>+</sup> T lymphocytes and PancTu-I cells (black) for 48 h. Relative mRNA levels of (A) IL-1β, (B) IL-6, (C) TNFα, (D) IL-8, (E) IL-10, (F) TGF-β1 and (G) VEGF in M1 MΦ after indicated mono- and indirect co-culture conditions. Messenger RNA levels were normalized to respective GAPDH levels as well as levels detected M1 MΦ from mono-cultures, indicated by dashed lines. Bar charts present mean values with SEM of three independent experiments. \* = p<0.05..... 119

**Figure 44: Cell growth and differentiation of PancTu-I cells after co-culture with activated CD8<sup>+</sup> T lymphocytes and M1-polarized macrophages.** PancTu-I cells were either mono-cultured (white), directly co-cultured with primary human pre-activated CD8<sup>+</sup> T lymphocytes (banded), indirectly co-cultured with M1-polarized macrophages (grey) or co-cultured with both CD8<sup>+</sup> T lymphocytes and M1 MΦ (black) for 48 h. (A) Representative images of confluency analysis on light microscopical phase contrast pictures of PancTu-I cells after indicated culture conditions. (B) Confluency of PancTu-I cell after indicated mono- and co-culture conditions. Bar chart presents mean values with SEM of three independent experiments. (C) Representative western blot of whole-cell lysates from PancTu-I cells after indicated culture conditions. Hsp90 was detected as loading control. Molecular weights in kDa are indicated according to the applied standard. (B) \* = p<0.05; (C) \* = vimentin signal; Scale bar = 500 μm ..... 120

**Figure 45: Supernatant levels of various cytokines, chemokines and growth factors after co-culture of activated CD8<sup>+</sup> T lymphocytes with autologous M1-polarized macrophages and PancTu-I cells.** Pre-activated primary human CD8<sup>+</sup> T lymphocytes (T), M1 MΦ (M) and PancTu-I cells (P) were either mono-cultured (white), co-cultured with a second cell population (grey) or co-cultured all together (black: direct co-culture of PancTu-I cells and CD8<sup>+</sup> T lymphocytes and indirectly co-cultured with M1 MΦ). Concentrations of (A) VEGF, (B) IL-8, (C) IL-6, (D) IFNγ, (E) IL-17A, (F) soluble Fas ligand, (G) Granulysin, (H) Granzyme A, (I) Granzyme B and (J) Perforin were measured by multiplex assay in the culture supernatant of indicated mono- and culture settings. Bar charts present mean values with SEM of three independent experiments. (K) Relative Perforin levels in supernatants of T lymphocyte mono- and co-culture settings normalized to levels detected in supernatants of mono-cultured CD8<sup>+</sup> T lymphocytes indicated by the dashed line. N.D. = not detectable; \* = p<0.05 ..... 122

**Figure 46: Phenotype and proliferation of activated CD8<sup>+</sup> T lymphocytes after treatment with Durvalumab.** Anti-CD3/CD28 pre-activated CD8<sup>+</sup> T lymphocytes were treated with 10 µg/ml Durvalumab (black) or respective IgG<sub>1</sub> isotype control antibody (white) for 72h. Comparison of (A) FSC medians, (B) SSC medians, (C) n-fold vital cell numbers and (D) the proportion of proliferating cells within CD8<sup>+</sup> T lymphocyte populations after indicated treatment. Bar charts present mean values with SEM of three independent experiments. (E) CFSE profiles of proliferating CD8<sup>+</sup> T lymphocytes after 72 h of indicated treatment. Data present mean proportions with SEM of T lymphocytes having divided 1 to 5 times in three independent experiments. The maximum numbers of clearly distinguishable peaks in respective CFSE profiles are indicated by “+” ..... 125

**Figure 47: PD-1 and PD-L1 surface expression in CD8<sup>+</sup> T lymphocytes as well as cytokine levels in culture supernatants after treatment with Durvalumab.** Anti-CD3/CD28 activated CD8<sup>+</sup> T lymphocytes were treated with 10 µg/ml Durvalumab (black) or respective IgG<sub>1</sub> isotype control antibody (white) for 72h. (A) PD-1 and PD-L1 cell surface expression levels in the IgG<sub>1</sub> isotype control antibody (white) and Durvalumab (black) treated CD8<sup>+</sup> lymphocytes. (B) PD-1 cell surface expression levels in CD8<sup>+</sup> T lymphocytes having divided one to six times after indicated treatment. (A+B) Bar charts present mean values and SEM of median fluorescence intensity ratios examined in six independent experiments. The dashed lines mark an MFI ratio of “1”. (C) N-fold supernatant levels of cytokines and effector molecules. Concentrations have been measured by multiplex assay and normalized to levels detected in culture supernatants of CD8<sup>+</sup> T lymphocytes treated with IgG<sub>1</sub> isotype control antibody, indicated by the dashed line. Bar chart presents mean values and SEM of six independent experiments. \* = p<0.05 ..... 126

**Figure 48: Phenotype and proliferation of activated CD8<sup>+</sup> T lymphocytes after direct co-culture with autologous M1-polarized macrophages and treatment with Durvalumab.** Pre-activated primary human CD8<sup>+</sup> T lymphocytes were mono-cultured or directly co-cultured for 72 h with autologous M1-like polarized macrophages and treated with 10µg/ml of either human IgG<sub>1</sub> isotype control antibody (white) or Durvalumab (black). Comparison of (A) FSC medians, (B) SSC medians and (C) the proportion of proliferating cells within CD8<sup>+</sup> T lymphocyte populations after indicated culture settings and treatments. Bar charts present mean values with SEM of three independent experiments. (D) CFSE profiles of proliferating CD8<sup>+</sup> T lymphocytes after 72 h of mono- (m) or co-culture (c) and indicated treatment. Data present mean proportions with SEM of T lymphocytes having divided one to five times in three independent experiments. The maximum numbers of clearly distinguishable peaks in respective CFSE profiles are indicated by “+”. (E) Representative western blot of whole-cell lysates from activated CD8<sup>+</sup> T lymphocytes directly after four days of anti-CD3/CD28 stimulation and activated CD8<sup>+</sup> T lymphocytes after indicated culture settings and treatments. Hsp90 was detected as loading control. Molecular weights in kDa are indicated according to the applied standard. .... 128

**Figure 49: PD-1 and PD-L1 cell surface expression levels in CD8<sup>+</sup> T lymphocytes after direct co-culture with autologous M1-polarized macrophages and treatment with Durvalumab.** Pre-activated primary human CD8<sup>+</sup> T lymphocytes were mono-cultured or directly co-cultured for 72 h with autologous M1-like polarized macrophages and treated with 10µg/ml of either human IgG<sub>1</sub> isotype control antibody (white) or Durvalumab (black). (A) Representative contour plots with attached histograms correlating CFSE with PD-L1 (top panel) and PD-1 (bottom panel) staining in CD8<sup>+</sup> T lymphocytes from mono- (blue) and M1

MΦ co-cultures (red) treated with either human IgG<sub>1</sub> isotype control antibody (left panel) or Durvalumab (right panel). Drawn through (mono-cultured CD8<sup>+</sup> T lymphocytes) and dashed lines (co-cultured CD8<sup>+</sup> T lymphocytes) indicate median fluorescence intensities detected for PD-L1 and PD-1 staining. **(B)** PD-1 and **(D)** PD-L1 cell surface expression levels in CD8<sup>+</sup> T lymphocytes after indicated culture settings and treatments. **(C)** PD-1 cell surface expression levels in populations of CD8<sup>+</sup> T lymphocytes having divided one to six times after indicated culture settings and treatments. **(B-D)** Bar charts present mean values with SEM of median fluorescence intensity ratios examined in three independent experiments. The dashed lines mark an MFI ratio of “1”. \* = p<0.05 ..... 130

**Figure 50: Cell surface expression levels of PD-L1, CD206 and CD163 in M1-polarized macrophages after co-culture with autologous activated CD8<sup>+</sup> T lymphocytes and treatment with Durvalumab.** Primary human M1-polarized macrophages were mono-cultured or directly co-cultured with anti-CD3/CD28 pre-activated autologous CD8<sup>+</sup> T lymphocytes and treated with 10µg/ml of either human IgG<sub>1</sub> isotype control antibody (white, blue) or Durvalumab (black, red) for 72 h. **(A)** Representative histograms from flow cytometric analysis of PD-L1 (left), CD206 (middle) and CD163 (right) cell surface immunofluorescence staining in M1 MΦ after the indicated culture conditions and treatment. Signal specificities were verified by staining with respective isotype control antibodies (dashed). **(B)** PD-L1, **(C)** CD206 and **(D)** CD163 cell surface levels in M1 MΦ after indicated culture settings and treatments. Bar charts present mean values and SEM of median fluorescence intensity ratios examined in three independent experiments. The dashed lines mark an MFI ratio of “1”. \* = p<0.05 ..... 132

**Figure 51: Gene expression profiles of cytokines, chemokines and growth factors in M1-polarized macrophages after co-culture with autologous activated CD8<sup>+</sup> T lymphocytes and treatment with Durvalumab.** Primary human M1-polarized macrophages were mono-cultured or directly co-cultured with anti-CD3/CD28 pre-activated autologous CD8<sup>+</sup> T lymphocytes and treated with 10µg/ml of either human IgG<sub>1</sub> isotype control antibody (white) or Durvalumab (black) for 72 h. Relative mRNA levels of **(A)** IL-1β, **(B)** IL-6, **(C)** IL-8, **(D)** IL-10, **(E)** TGF-β1, **(F)** VEGF and **(G)** TNFα in M1 MΦ after indicated culture settings and treatments. Messenger RNA levels were normalized to respective GAPDH levels as well as levels detected in M1 MΦ from mono-cultures treated with IgG<sub>1</sub> isotype control antibody, indicated by dashed lines. Bar charts present mean values of technical triplicates resulting from one experiment. .... 133

**Figure 52: Levels of T lymphocyte- and macrophage-associated cytokines, chemokines, growth factors and effector molecules in supernatants of directly co-cultured activated CD8<sup>+</sup> T lymphocytes and autologous M1-polarized macrophages treated with Durvalumab.** Pre-activated primary human CD8<sup>+</sup> T lymphocytes (CD8<sup>+</sup> Tc) and M1 MΦ were mono-cultured or directly co-cultured for 72 h and treated with 10µg/ml of either human IgG<sub>1</sub> isotype control antibody (white) or Durvalumab (black). Concentrations of **(A)** VEGF, **(B)** IL-8, **(C)** IL-6, **(D)** soluble Fas ligand, **(E)** Granulysin, **(F)** Granzyme B, **(G)** Perforin, **(H)** IL-17A and **(I)** Granzyme A were measured by multiplex assay in the culture supernatant of indicated culture settings and treatments. Box plots present median values with quartiles (Q<sub>0.75</sub> as upper, Q<sub>0.25</sub> as lower deviation) and bar charts present mean values with SEM of three independent experiments. N.D. = not detectable; \* = p<0.05 ..... 135

**Figure 53: Phenotype and proliferation of activated CD8<sup>+</sup> T lymphocytes after direct co-culture with PancTu-I cells and treatment with Durvalumab.** Pre-activated primary human CD8<sup>+</sup> T lymphocytes were mono-cultured or directly co-cultured for 72 h with PancTu-I cells and treated with 10µg/ml of either human IgG<sub>1</sub> isotype control antibody (white) or Durvalumab (black). Comparison of (A) FSC medians, (B) SSC medians, (C) n-fold vital cell numbers and (D) the proportion of proliferating cells within CD8<sup>+</sup> T lymphocyte populations after indicated culture settings and treatments. Bar charts present mean values with SEM of three independent experiments. (E) Representative western blot of whole-cell lysates from CD8<sup>+</sup> T lymphocytes after indicated culture settings and treatments. Hsp90 was detected as loading control. Molecular weights in kDa are indicated according to the applied standard. (F) CFSE profiles of proliferating CD8<sup>+</sup> T lymphocytes after 72 h of mono- (m) or co-culture (c) and indicated treatment. Data present mean proportions with SEM of T lymphocytes having divided one to six times in three independent experiments. \* = p<0.05 ..... 137

**Figure 54: PD-1 and PD-L1 cell surface expression levels in activated CD8<sup>+</sup> T lymphocytes after direct co-culture with PancTu-I cells and treatment with Durvalumab.** Pre-activated primary human CD8<sup>+</sup> T lymphocytes were mono-cultured (m) or directly co-cultured (c) for 72 h with PancTu-I cells and treated with 10µg/ml of either human IgG<sub>1</sub> isotype control antibody (white) or Durvalumab (black). (A) PD-1 and (C) PD-L1 cell surface expression levels in CD8<sup>+</sup> T lymphocytes after indicated culture settings and treatments. (B) PD-1 cell surface expression levels in populations of CD8<sup>+</sup> T lymphocytes having divided one to six times after indicated culture settings and treatments. (A-C) Bar charts present mean values with SEM of median fluorescence intensity ratios examined in three independent experiments. The dashed lines mark an MFI ratio of “1”. \* = p<0.05..... 138

**Figure 55: Cell growth, phenotype and PD-L1 expression levels of PancTu-I cells after direct co-culture with activated CD8<sup>+</sup> T lymphocytes and Durvalumab treatment.** PancTu-I cells were mono-cultured or directly co-cultured for 72 h with anti-CD3/CD28 pre-activated CD8<sup>+</sup> T lymphocytes and treated with 10µg/ml of either human IgG<sub>1</sub> isotype control antibody (white) or Durvalumab (black). (A) Representative fluorescence microscopical images of PancTu-I cells stained with CellTracker Red CMTPX dye (orange) and Hoechst (blue) after indicated culture settings and treatments. Scale bar = 500 µm (B) Confluency and (C) n-fold vital cell numbers of PancTu-I cell after indicated culture settings and treatments. Bar charts presents mean values with SEM of three independent experiments. (D) Representative fluorescence microscopical images of PancTu-I cells stained for PD-L1 (green) after indicated culture settings and treatments. Nuclei were stained with Hoechst. Scale bar = 200 µm. (E) Representative western blot of whole-cell lysates from PancTu-I cells after indicated culture settings and treatments. Hsp90 was detected as loading control. Molecular weights in kDa are indicated according to the applied standard. (F) Relative PD-L1 mRNA levels in PancTu-I cells after indicated culture settings and treatments. Messenger RNA levels were normalized to respective GAPDH levels as well as levels detected in PancTu-I cells from mono-cultures treated with IgG<sub>1</sub> isotype control antibody. Box plots present median values with quartiles (Q<sub>0.75</sub> as upper, Q<sub>0.25</sub> as lower deviation) of three independent experiments. (G) PD-L1 cell surface expression levels in PancTu-I cells after indicated culture settings and treatments. Bar chart presents mean values with SEM of median fluorescence intensity ratios examined in three independent experiments. \* = p<0.05 ..... 139

**Figure 56: Gene expression profiles of EMT-associated proteins in PancTu-I cells after co-culture with activated CD8<sup>+</sup> T lymphocytes and treatment with Durvalumab.** PancTu-I cells were mono-cultured or directly co-cultured for 72 h with anti-CD3/CD28 pre-activated CD8<sup>+</sup> T lymphocytes and treated with 10µg/ml of either human IgG<sub>1</sub> isotype control antibody (white) or Durvalumab (black). Relative mRNA levels of (A) Vimentin, (B) L1CAM, (C) Zeb-1 and (D) E-cadherin in PancTu-I cells after indicated culture settings and treatments. Messenger RNA levels were normalized to respective GAPDH levels as well as levels detected in PancTu-I cells from mono-cultures treated with IgG<sub>1</sub> isotype control antibody, indicated by dashed lines. Box plots present median values with quartiles (Q<sub>0.75</sub> as upper, Q<sub>0.25</sub> as lower deviation) and bar charts present mean values with SEM of three independent experiments. \* = p<0.05 ..... 142

**Figure 57: Levels of cytokines, chemokines, growth factors and effector molecules in supernatants of directly co-cultured activated CD8<sup>+</sup> T lymphocytes and PancTu-I cells treated with Durvalumab.** Pre-activated primary human CD8<sup>+</sup> T lymphocytes (CD8<sup>+</sup> Tc) and PancTu-I cells were mono-cultured or directly co-cultured for 72 h and treated with 10µg/ml of either human IgG<sub>1</sub> isotype control antibody (white) or Durvalumab (black). Levels of (A) VEGF, (B) IL-6, (C) IL-8, (D) IL-17A, (E) soluble Fas ligand, (F) Perforin, (G) Granzyme A and (H) Granzyme B were measured by multiplex assay in the culture supernatant of indicated culture settings and treatments. Bar charts present mean values with SEM of three independent experiments. N.D. = not detectable; \* = p<0.05 ..... 144

**Supplementary Figure 58: Levels of cytokines, chemokines, growth factors and effector molecules in the supernatant of directly co-cultured activated CD8<sup>+</sup> T lymphocytes and various PDAC cell lines.** Pre-activated primary human CD8<sup>+</sup> T lymphocytes as well as PDAC cell lines Panc1, Panc89 and PancTu-I were either mono-cultured (white) or directly co-cultured (black) for 72 h. Concentrations of (A) VEGF, (B) IL-6, (C) IL-8, (D) IFN $\gamma$ , (E) IL-17A, (F) soluble Fas ligand, (G) Perforin, (H) Granulysin, (I) Granzyme A and (J) Granzyme B were measured by multiplex assay in the culture supernatant of indicated culture settings. Bar charts present data from one experiment. N.D. = not detectable ..... iv

**Supplementary Figure 59: Direct cell-cell interaction of activated CD8<sup>+</sup> T lymphocytes in co-culture with PancTu-I cells.** Pre-activated primary human CD8<sup>+</sup> T lymphocytes were directly co-cultured for with PancTu-I cells. Co-cultures were performed in a humidified incubation chamber of a Lionheart Fx Automated microscope at 37°C and 5 % CO<sub>2</sub>. Representative light microscopical phase contrast images from time-lapse analysis in a total time frame of 80 min at intervals of 20 min. Black arrow heads mark a PancTu-I cell that is encounter by CD8<sup>+</sup> T lymphocytes (highly refractive smaller cells). Pictures were taken at 200-fold magnification. Scale bar = 50 µm..... v



**Supplementary Figure 60: PD-L1 expression levels in M1-polarized macrophages after mono-culture or direct co-cultures with autologous activated CD8<sup>+</sup> T lymphocytes and Durvalumab treatment.** Primary human M1-polarized macrophages were mono-cultured or directly co-cultured with anti-CD3/CD28 pre-activated autologous CD8<sup>+</sup> T lymphocytes and treated with 10µg/ml of either human IgG<sub>1</sub> isotype control antibody (white) or Durvalumab (black) for 72 h. **(A)** Representative western blot of whole-cell lysates from mono-cultured M1 MΦ after indicated treatments. Hsp90 was detected as loading control. Molecular weights in kDa are indicated according to the applied standard. **(B)** Relative mRNA levels of PD-L1 in M1 MΦ after indicated culture settings and treatments. Messenger RNA levels were normalized to respective GAPDH levels as well as levels detected M1 MΦ from mono-cultures treated with IgG<sub>1</sub> isotype control antibody, indicated by dashed line. Bar chart presents mean values of technical triplicates from one experiment. .... v

**Supplementary Figure 61: Normalized levels of cytokines, chemokines, growth factors and effector molecules in the supernatant of directly co-cultured activated CD8<sup>+</sup> T lymphocytes and autologous M1-polarized macrophages treated with Durvalumab.** Pre-activated primary human CD8<sup>+</sup> T lymphocytes (CD8<sup>+</sup> Tc) and M1 MΦ were directly co-cultured for 72 h and treated with 10µg/ml of either human IgG<sub>1</sub> isotype control antibody or Durvalumab. **(A+B)** Concentrations measured in the supernatant of Durvalumab treated co-cultures were normalized to levels detected in supernatants of human IgG<sub>1</sub> isotype control antibody treated co-cultures, indicated by dashed lines. Bar charts present mean values with SEM examined in three independent experiments. .... vi

## List of Tables

|  |           |
|--|-----------|
| <b>Table 1: Selection of T lymphocyte expressed receptors and their respective ligands involved in T lymphocyte co-stimulation.</b> In the column termed “Effect” co-stimulatory interactions are denoted with a “+” and molecules involved in the mediation of co-inhibitory signals are marked with a “-“ .....  | <b>15</b> |
| <b>Table 2: Approved PD-1 or PD-L1 targeting monoclonal agonistic antibodies for cancer immunotherapy.</b> .....   | <b>22</b> |
| <b>Table 3: Approved IHC-based companion and complementary diagnostic assay for evaluation of PD-L1 expression status in tumor tissues.</b> NSCLC = non-small cellular lung carcinoma; UC = Urothelial cancer; SCCHN = Squamous cell carcinoma of head and neck; mAb = monoclonal antibody .....   | <b>23</b> |
| <b>Table 4: BOND-MAX Automated IHC/ISH Stainer program for immunohistochemical detection of PD-L1 in deparaffinized, rehydrated formalin-fixed tissue sections.</b> .....  | <b>55</b> |
| <b>Table 5: Master Mix composition per sample for complementary DNA synthesis from mRNA templates.</b> .....   | <b>58</b> |
| <b>Table 6: Master Mix composition per sample for quantitative real-time polymerase chain reaction from cDNA templates.</b> .....  | <b>58</b> |
| <b>Table 7: Light Cycler program for cDNA amplification and analysis in quantitative real-time polymerase chain reaction.</b> .....  | <b>59</b> |
| <b>Table 8: Parameters for cellular confluency analysis with Gen5 software “cell analysis” application.</b> .....  | <b>63</b> |
| <b>Table 9: Clinic-pathological characteristics of PDAC patients included in the study cohort</b> .....  | <b>65</b> |
| <b>Supplementary Table 10: Summary of immunohistochemical staining evaluation of PD-L1 staining in tumor and stromal cells within PDAC tumor and peritumoral tissue sections.</b> PD-L1 staining is characterized with respect to the proportion of PD-L1 <sup>+</sup> cells (Quantity Score), staining intensity (Intensity Score), local distribution of PD-L1 <sup>+</sup> cells (Cluster Score) as well as expression in lymph follicles (Lymph Score). Immunoreactivity/Tissue Score combines results from Quantity and Intensity Score. PDAC tissue sections were categorized by the proportion of fields of view (FoV) comprising at least one PD-L1 <sup>+</sup> cell (%FoV <sup>+</sup> ). Quantity, Intensity as well as Lymph Scores are presented as median and Tissue, %FoV <sup>+</sup> as well as Cluster Scores as mean values of rated FoV within each tissue. Tissues comprising no neoplastic cells within the respective section but lymph follicles were excluded from Quantity, Intensity, Tissue as well as Cluster scoring and, therefore, denoted as „Missing“.(data published in [264])..... | <b>i</b>  |

---

**Supplementary Table 11: POLE Score criteria.** (data published in [264])..... **ii**

**Supplementary Table 12: Statistical correlation of intra-tumoral PD-L1 staining classified by POLE scoring and stromal as well as epithelial/cancer cell-related parameters in pancreatic tissues of PDAC patients.** For statistical analyses POLE Scores were dichotomized (+P, +O, +L, E) into: +P1 (=P0+P1) vs. +P2 (=P2); +O1 (=O1) vs. +O2 (=O2+O3); +L1 (=L0) vs. +L2 (=L1+L2). Results are shown as p-values from Chi-square/Fisher exact test. Statistically significant correlations ( $p < 0.05$ ) are marked in bold. n.p. (correlation **not possible** because one parameter is constant); n.d. (**not enough data** for statistical analysis); int. = intensity. (data published in [264]) ..... **iii**

## Supplementary Data

### Supplementary Tables

**Supplementary Table 10: Summary of immunohistochemical staining evaluation of PD-L1 staining in tumor and stromal cells within PDAC tumor and peritumoral tissue sections.** PD-L1 staining is characterized with respect to the proportion of PD-L1<sup>+</sup> cells (Quantity Score), staining intensity (Intensity Score), local distribution of PD-L1<sup>+</sup> cells (Cluster Score) as well as expression in lymph follicles (Lymph Score). Immunoreactivity/Tissue Score combines results from Quantity and Intensity Score. PDAC tissue sections were categorized by the proportion of fields of view (FoV) comprising at least one PD-L1<sup>+</sup> cell (%FoV<sup>+</sup>). Quantity, Intensity as well as Lymph Scores are presented as median and Tissue, %FoV<sup>+</sup> as well as Cluster Scores as mean values of rated FoV within each tissue. Tissues comprising no neoplastic cells within the respective section but lymph follicles were excluded from Quantity, Intensity, Tissue as well as Cluster scoring and, therefore, denoted as „Missing“. (data published in [264])

|                      | Quantity Score | n (%)           | Intensity Score | n (%)           | Tissue Score    | n (%)           | %FoV <sup>+</sup> | n (%)           | Lymph Score     | n (%)           | Cluster Score | n (%)     |
|----------------------|----------------|-----------------|-----------------|-----------------|-----------------|-----------------|-------------------|-----------------|-----------------|-----------------|---------------|-----------|
| <b>Tumor</b>         | 0 (0%)         | 44 (78.6)       | 0 (negative)    | 44 (78.6)       | 0               | 1 (1.8)         | ≤ 5%              | 6 (10.7)        | 0 (negative)    | 7 (17.9)        | 0             | 16 (28.6) |
|                      | 1 (≤ 1%)       | 12 (21.4)       | 1 (weak)        | 12 (21.4)       | < 0.1           | 4 (7.1)         | 5% – 10%          | 6 (10.7)        | 1 (weak)        | 17 (43.6)       | < 0.1         | 8 (14.3)  |
|                      | 2 (> 1%)       | 0 (0)           | 2 (moderate)    | 0 (0)           | 0.1 – < 0.2     | 4 (7.1)         | 10% - 20%         | 13 (23.2)       | 2 (strong)      | 15 (38.5)       | 0.1 – < 0.2   | 13 (23.2) |
|                      |                |                 | 3 (strong)      | 0 (0)           | 0.2 - < 0.4     | 9 (16.1)        | 20% - < 50%       | 19 (33.9)       |                 |                 | 0.2 - < 0.3   | 9 (16.1)  |
|                      |                |                 |                 |                 | 0.4 - < 0.7     | 21 (37.5)       | ≥ 50%             | 12 (21.4)       |                 |                 | 0.3 - < 0.4   | 7 (12.5)  |
|                      |                |                 |                 |                 | ≥ 0.8           | 17 (30.4)       |                   |                 |                 |                 | ≥ 0.4         | 3 (5.3)   |
|                      | <b>Total</b>   | <b>56 (100)</b> | <b>56 (100)</b> | <b>56 (100)</b> | <b>56 (100)</b> | <b>56 (100)</b> | <b>56 (100)</b>   | <b>56 (100)</b> | <b>39 (100)</b> | <b>56 (100)</b> |               |           |
| <b>Total/Missing</b> | <b>59 / 3</b>  | <b>59 / 3</b>   | <b>59 / 3</b>   | <b>59 / 3</b>   | <b>59 / 3</b>   | <b>59 / 3</b>   | <b>59 / 3</b>     | <b>59 / 20</b>  | <b>59 / 3</b>   |                 |               |           |
| <b>Peritumoral</b>   | 0 (0%)         | 15 (83.3)       | 0 (negative)    | 15 (83.3)       | 0               | 2 (11.1)        | ≤ 5%              | 6 (33.3)        | 0 (negative)    | 0 (0)           | 0             | 6 (33.3)  |
|                      | 1 (≤ 1%)       | 2 (11.1)        | 1 (weak)        | 3 (16.7)        | < 0.1           | 4 (22.2)        | 5% – 10%          | 1 (5.6)         | 1 (weak)        | 5 (55.6)        | < 0.1         | 2 (11.1)  |
|                      | 2 (> 1%)       | 1 (5.6)         | 2 (moderate)    | 0 (0)           | 0.1 – < 0.2     | 0 (0)           | 10% - 20%         | 4 (22.2)        | 2 (strong)      | 4 (44.4)        | 0.1 – < 0.2   | 4 (22.2)  |
|                      |                |                 | 3 (strong)      | 0 (0)           | 0.2 - < 0.4     | 4 (22.2)        | 20% - < 50%       | 4 (22.2)        |                 |                 | 0.2 - < 0.3   | 4 (22.2)  |
|                      |                |                 |                 |                 | 0.4 - < 0.8     | 4 (22.2)        | ≥ 50%             | 3 (16.7)        |                 |                 | 0.3 - < 0.4   | 2 (11.1)  |
|                      |                |                 |                 |                 | ≥ 0.8           | 4 (22.2)        |                   |                 |                 |                 | ≥ 0.4         | 0         |
|                      | <b>Total</b>   | <b>18 (100)</b> | <b>18 (100)</b> | <b>18 (100)</b> | <b>18 (100)</b> | <b>18 (100)</b> | <b>18 (100)</b>   | <b>18 (100)</b> | <b>9 (100)</b>  | <b>18 (100)</b> |               |           |
| <b>Total/Missing</b> | <b>18 / 0</b>  | <b>18 / 0</b>   | <b>18 / 0</b>   | <b>18 / 0</b>   | <b>18 / 0</b>   | <b>18 / 0</b>   | <b>18 / 0</b>     | <b>18 / 9</b>   | <b>18 / 0</b>   |                 |               |           |

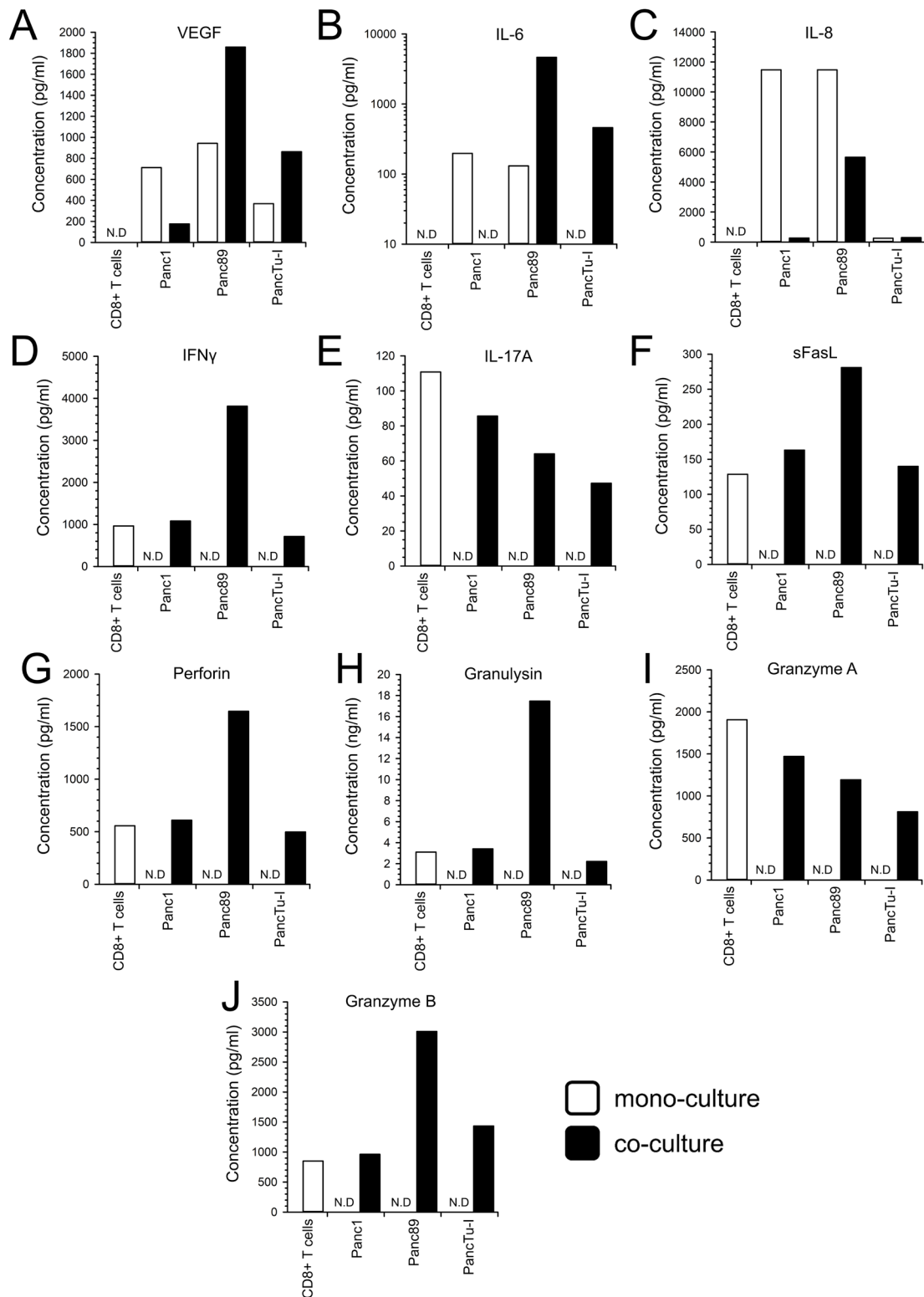
Supplementary Table 11: POLE Score criteria. (data published in [264])

| Parameter | Description  | Values and Criteria                                  |   |                       |                       |
|-----------|--|--|---|-----------------------|-----------------------|
|           |  | 0  | 1   | 2                     | X                     |
| P         | PD-L1 intratumoral overall expression              | Tissue Score = 0<br>or %FoV PD-L1 <sup>+</sup> ≤ 20% | Tissue Score < 0.8<br>and %FoV PD-L1 <sup>+</sup> > 20% | Tissue Score > 0.8    | no ratable structures |
| O         | Cellular Origin of PD-L1                           | 1  | 2   | 3                     | X                     |
|           |  | Cell Score = 1                                       | Cell Score = 2  | Cell Score = 3        | not rated (P0 or P1)  |
| L         | PD-L1 Expression in intratumoral Lymph follicles   | 0  | 1   | 2                     | X                     |
|           |  | Lymph Score = 0                                      | 0 < Lymph Score < 2                                     | Lymph Score = 2       | no ratable structures |
| E         | Enumerated PD-L1 expression (spatial distribution) | 0  | 1   | X                     |                       |
|           |  | Cluster Score < 0.4                                  | Cluster Score ≥ 0.4                                     | no ratable structures |                       |

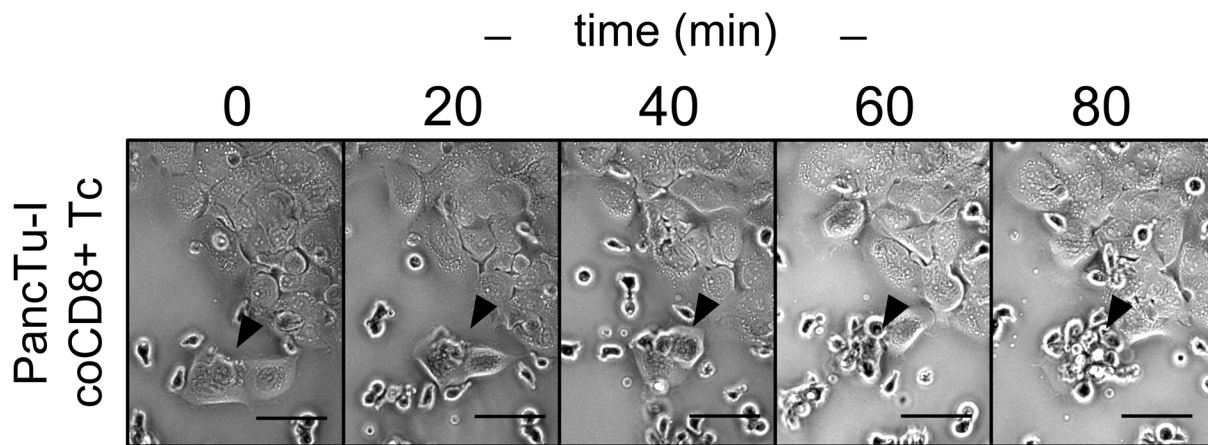
**Supplementary Table 12: Statistical correlation of intra-tumoral PD-L1 staining classified by POLE scoring and stromal as well as epithelial/cancer cell-related parameters in pancreatic tissues of PDAC patients.** For statistical analyses POLE Scores were dichotomized (+P, +O, +L, E) into: +P1 (=P0+P1) vs. +P2 (=P2); +O1 (=O1) vs. +O2 (=O2+O3); +L1 (=L0) vs. +L2 (=L1+L2). Results are shown as p-values from Chi-square/Fisher exact test. Statistically significant correlations (p <0.05) are marked in bold. n.p. (correlation not possible because one parameter is constant); n.d. (not enough data for statistical analysis); int. = intensity. (data published in [264])

|                    | Marker  | PD-L1 Staining |              |              |              |
|--------------------|---|----------------|--------------|--------------|--------------|
|                    |   | +P-Score       | +O-Score     | +L-Score     | E-Score      |
| <b>T cells</b>     | CD3+ (% stroma)                                 | 0.428          | <b>0.018</b> | n.p.         | 0.755        |
|                    | CD4+ (% stroma)                                 | 0.426          | 0.107        | <b>0.045</b> | 0.193        |
|                    | CD8+ (% stroma)                                 | 1.000          | 0.107        | 0.632        | 0.538        |
|                    | CD25+ (% CD3)                                   | 1.000          | n.p.         | 1.000        | 1.000        |
|                    | CD25+ (% CD4)                                   | 1.000          | 0.464        | 0.646        | 0.495        |
|                    | FoxP3+ (% CD3)                                  | 0.631          | 0.464        | 1.000        | 1.000        |
|                    | FoxP3+ (% CD4)                                  | 1.000          | 0.464        | 1.000        | 1.000        |
|                    | $\gamma\delta$ TCR+ (% stroma)                  | 1.000          | 1.000        | 0.640        | 0.492        |
|                    | $\gamma\delta$ TCR+ (duct-associated)           | 1.000          | 1.000        | 1.000        | 0.218        |
| <b>macrophages</b> | CD68+ (% stroma)                                | 0.434          | 1.000        | 1.000        | 0.216        |
|                    | CD68+ (duct-associated)                         | 0.368          | n.p.         | <b>0.048</b> | 0.407        |
|                    | CD163+ (% stroma)                               | 0.447          | 1.000        | 1.000        | 0.230        |
|                    | CD163+ (duct-associated)                        | 0.368          | n.p.         | <b>0.048</b> | 0.407        |
|                    | HLA-DR+ (% stroma)                              | 0.683          | 0.429        | 1.000        | 1.000        |
|                    | HLA-DR+ (duct-associated)                       | 0.797          | 0.446        | 0.417        | 0.653        |
| <b>fibroblasts</b> | $\alpha$ -SMA+ (% stroma)                       | 1.000          | 0.429        | 1.000        | 1.000        |
|                    | $\alpha$ -SMA <sup>high</sup> ( $\alpha$ -SMA+) | 1.000          | <b>0.036</b> | 0.279        | 1.000        |
| <b>EMT</b>         | L1CAM+ (% epithelium)                           | 0.701          | 0.464        | 1.000        | 1.000        |
|                    | L1CAM+ (int. epithelium)                        | 0.447          | 0.464        | 0.646        | 1.000        |
|                    | Vimentin+ (% epithelium)                        | 0.690          | 1.000        | 0.621        | 1.000        |
| <b>Other</b>       | PanCK+ (% section)                              | 0.338          | 1.000        | 0.069        | 0.524        |
|                    | Ki67+ (% epithelium)                            | 0.153          | n.p.         | 0.053        | 1.000        |
| <b>PD-L1</b>       | +P-Score  | ///////        | n.p.         | 0.133        | <b>0.040</b> |
|                    | +O-Score  | n.p.           | ///////      | n.d.         | 1.000        |
|                    | +L-Score  | 0.133          | n.d.         | ///////      | 1.000        |
|                    | E-Score   | <b>0.040</b>   | 1.000        | 1.000        | ///////      |

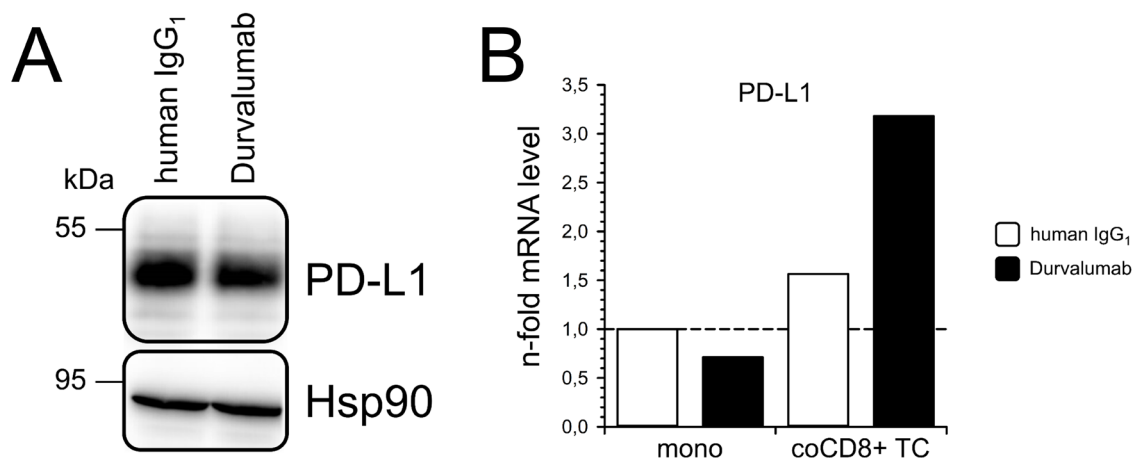
## Supplementary Figures



**Supplementary Figure 58: Levels of cytokines, chemokines, growth factors and effector molecules in the supernatant of directly co-cultured activated CD8<sup>+</sup> T lymphocytes and various PDAC cell lines.** Pre-activated primary human CD8<sup>+</sup> T lymphocytes as well as PDAC cell lines Panc1, Panc89 and PancTu-I were either mono-cultured (white) or directly co-cultured (black) for 72 h. Concentrations of (A) VEGF, (B) IL-6, (C) IL-8, (D) IFN $\gamma$ , (E) IL-17A, (F) soluble Fas ligand, (G) Perforin, (H) Granulysin, (I) Granzyme A and (J) Granzyme B were measured by multiplex assay in the culture supernatant of indicated culture settings. Bar charts present data from one experiment. N.D. = not detectable

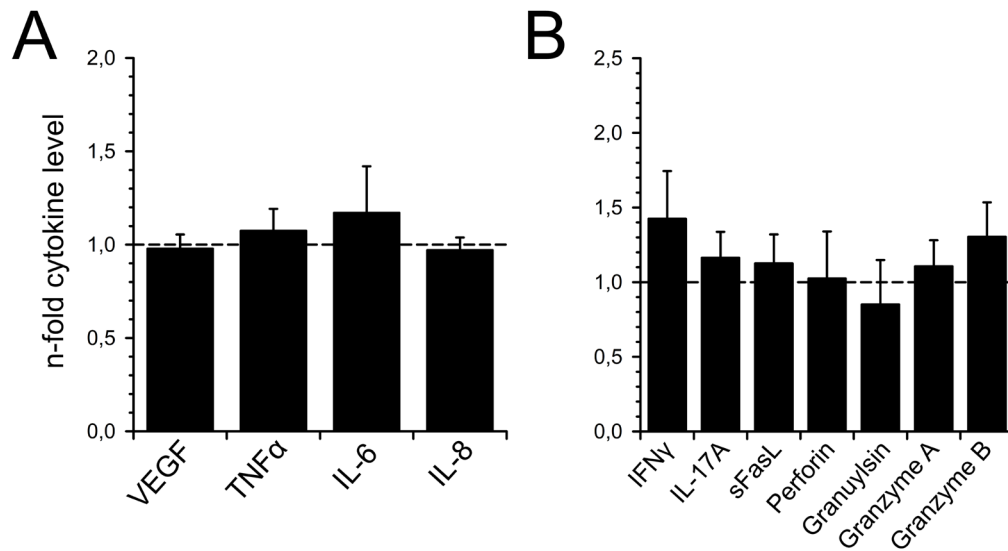


**Supplementary Figure 59: Direct cell-cell interaction of activated CD8<sup>+</sup> T lymphocytes in co-culture with PancTu-I cells.** Pre-activated primary human CD8<sup>+</sup> T lymphocytes were directly co-cultured for with PancTu-I cells. Co-cultures were performed in a humidified incubation chamber of a Lionheart Fx Automated microscope at 37°C and 5 % CO<sub>2</sub>. Representative light microscopical phase contrast images from time-lapse analysis in a total time frame of 80 min at intervals of 20 min. Black arrow heads mark a PancTu-I cell that is encounter by CD8<sup>+</sup> T lymphocytes (highly refractive smaller cells). Pictures were taken at 200-fold magnification. Scale bar = 50 μm



**Supplementary Figure 60: PD-L1 expression levels in M1-polarized macrophages after mono-culture or direct co-cultures with autologous activated CD8<sup>+</sup> T lymphocytes and Durvalumab treatment.** Primary human M1-polarized macrophages were mono-cultured or directly co-cultured with anti-CD3/CD28 pre-activated autologous CD8<sup>+</sup> T lymphocytes and treated with 10 μg/ml of either human IgG<sub>1</sub> isotype control antibody (white) or Durvalumab (black) for 72 h. (A) Representative western blot of whole-cell lysates from mono-cultured M1 MΦ after indicated treatments. Hsp90 was detected as loading control. Molecular weights in kDa are indicated according to the applied standard. (B) Relative mRNA levels of PD-L1 in M1 MΦ after indicated culture settings and treatments. Messenger RNA levels were normalized to respective GAPDH levels as well as levels detected M1 MΦ from mono-cultures treated with IgG<sub>1</sub> isotype control antibody, indicated by dashed line. Bar chart presents mean values of technical triplicates from one experiment.





**Supplementary Figure 61: Normalized levels of cytokines, chemokines, growth factors and effector molecules in the supernatant of directly co-cultured activated CD8<sup>+</sup> T lymphocytes and autologous M1-polarized macrophages treated with Durvalumab.** Pre-activated primary human CD8<sup>+</sup> T lymphocytes (CD8<sup>+</sup> Tc) and M1 M $\Phi$  were directly co-cultured for 72 h and treated with 10 $\mu$ g/ml of either human IgG<sub>1</sub> isotype control antibody or Durvalumab. (A+B) Concentrations measured in the supernatant of Durvalumab treated co-cultures were normalized to levels detected in supernatants of human IgG<sub>1</sub> isotype control antibody treated co-cultures, indicated by dashed lines. Bar charts present mean values with SEM examined in three independent experiments.

## Declaration on oath

Hiermit versichere ich, Sascha Rahn (geboren am 28.10.1988 in Preetz), an Eides statt, dass ich die vorliegende wissenschaftliche Abhandlung mit dem Titel:

**„Characterization of programmed death ligand 1 expression and analyses of its immune-regulatory role in pancreatic ductal adenocarcinoma ”**

nach den Regeln guter wissenschaftlicher Praxis eigenständig verfasst und keine anderen als die angegebenen Hilfsmittel und Quellen benutzt habe. Dabei habe ich keine Hilfe, außer der wissenschaftlichen Beratung durch meine Doktormutter Prof. Dr. rer. nat. Susanne Sebens und durch die namentlich erwähnten Kooperationspartner in Anspruch genommen.

Weder wurde diese Arbeit bisher im Rahmen eines Prüfungsverfahrens vorgelegt, noch wurde ein akademischer Grad entzogen. Teile dieser Arbeit sind zur bereits veröffentlicht und dementsprechend in dieser Arbeit als solche gekennzeichnet.

Kiel, September 2019

---

Sascha Rahn

## Acknowledgements

Zuallererst möchte ich mich bei meiner Doktormutter Prof. Dr. Susanne Sebens bedanken. Ich danke dir, dass du mir die Möglichkeit gegeben hast meine Doktorarbeit in deiner Arbeitsgruppe anzufertigen. Darüber hinaus kann ich dir nicht genug danken für dein unglaubliches Vertrauen, welches du mir entgegengebracht hast, sowie deine zahlreichen Ratschläge auf fachlicher und freundschaftlicher Ebene. Alles in Allem wirst du mir sowohl fachlich als auch menschlich ein Vorbild bleiben und ich freue mich auf weitere gemeinsame berufliche, sportliche und sonstige Projekte in der Zukunft.

Des Weiteren möchte ich Prof. Dr. Regina Scherließ herzlich dafür danken, dass Sie sich dazu bereiterklärt hat das Zweitgutachten für diese Arbeit anzufertigen.

Herrn Prof. Dr. Christoph Röcken möchte ich für die fachliche Unterstützung bei der Analyse und Auswertung der immunohistologischen Färbungen danken. Diesbezüglich gilt mein besonderer Dank auch Sandra Krüger für die Anfertigung der histologischen Färbungen im Rahmen dieser und vieler anderer Arbeiten in meiner Zeit am Institut für Experimentelle Tumorforschung.

Im Institut für Immunologie möchte ich mich ganz herzlich bei Prof. Dr. Daniela Wesch, Dr. Hans Heinrich Oberg, Dr. Christian Peters, Dr. Marcus Lettau und Sandra Ussat bedanken für Ihre stetige Hilfsbereitschaft, das Einlernen in die Durchflusszytometrie, die Organisation der Blutspendeproben, die zahlreichen fachlichen Diskussionen und Ratschläge sowie die schönen gemeinsamen Stunden beim Feierabendbier im Phollkomplex.

Ein ganz besonderer Dank geht an die vielen lieben Kollegen der AG Sebens und des Instituts für Experimentelle Tumorforschung, die ich kennenlernen durfte sowie die Freunde, die ich dort gefunden habe. Ich werde die gemeinsamen Mittagsstunden mit den verrückten Einfällen sowie Diskussionen, aber vor allem euch alle sehr vermissen. Besonders hervorheben möchte ich Dagmar Leisner, Ole Helm, Lennart Lenk, Hendrike Knaack, Kirsten Meinhardt, Lauritz Miarka, Alexander Fabian, Fabrice Viol, Vivien Zimmermann, Philippe Dänzer Barbosa, Jann Buttlar, Lisa Philipp, Silje Beckinger und Tina Daunke. Ich danke euch von Herzen für eure Unterstützung auf und neben der Arbeit in den vergangenen Jahren.

Neben den bereits genannten Personen habe ich das große Glück wundervolle Freunde kennengelernt zu haben. Wir haben zusammen gelacht, gefeiert, uns die Sorgen von der Seele geredet und vor allem ward ihr in guten und schlechten Zeiten immer für mich da! Ihr habt mein Leben ungemein bereichert und dafür danke euch von ganzem Herzen: Philipp Zingler, Florian Peters, Michael Pleß, Tabea Löblein, Dennis Witt, Johanna Ehlers, Vivian Adamski und Fred Armbrust.

Mein allergrößter Dank geht an Anna Willms. Danke, dass du trotz der schwierigen Zeit immer für mich da warst und an mich geglaubt hast. Ich bin froh dich in meinem Leben zu haben. Zu guter Letzt möchte ich meiner Familie danken, die mir stets die nötige Rückendeckung gegeben hat um meinen Weg zu gehen. Ohne euch wäre das alles hier nicht möglich gewesen!

## Curriculum Vitae

### PERSÖNLICHE DATEN

|                       |                            |
|-----------------------|----------------------------|
| Name                  | Sascha Rahn                |
| Geburtsdatum und -ort | 28.10.1988 in Preetz       |
| Adresse               | Waitzstraße 72, 24118 Kiel |
| Staatsangehörigkeit   | deutsch                    |
| Familienstand         | ledig                      |

### SCHULISCHE AUSBILDUNG

|             |                                      |
|-------------|--------------------------------------|
| 1995 – 1999 | Hermann Ehlers Grundschule, Preetz   |
| 1999 – 2008 | Friedrich Schiller Gymnasium, Preetz |
| 2008        | Schulabschluss: Abitur               |

### AKADEMISCHE AUSBILDUNG

|             |   |
|-------------|---|
| 2010 – 2013 | Bachelorstudium im Fachbereich Biologie<br>an der Christian-Albrechts Universität zu Kiel   |
| 2013        | Bachelorarbeit am Institut für Zoophysiologie<br>AG Vergleichende Immunbiologie, Prof. Dr. Leippe<br>an der Christian-Albrechts Universität zu Kiel<br>Titel: „Rekombinante Expression und funktionale Analyse von<br>NK-Lysin aus dem Zebrafisch <i>Danio rerio</i> “  |
| 2013 – 2015 | Masterstudium im Fachbereich Biochemie & Molekularbiologie<br>an der Christian-Albrechts Universität zu Kiel  |
| 2015        | Masterarbeit am Institut für Experimentelle Tumorforschung<br>AG Inflammatorische Karzinogenese, Prof. Dr. Sebens<br>an der Christian-Albrechts Universität zu Kiel<br>Titel: „Inflammation-associated metabolic rewiring in initiation<br>of pancreatic cancer – Impact of macrophage-mediated<br>metabolic alterations on phenotype and tumor-promoting<br>properties in benign and premalignant pancreatic ductal<br>epithelial cells“ |

2016 – 2019

Wissenschaftlicher Mitarbeiter am Institut für Experimentelle  
Tumorforschung an der Christian-Albrechts Universität zu Kiel  
AG Inflammatorische Karzinogenese, Prof. Dr. Sebens  
Dissertationsthema: „Characterization of programmed death  
ligand 1 expression and analyses of its immune-regulatory role  
in pancreatic ductal adenocarcinoma“

---

## Original Publications

**Rahn, S.**, Zimmermann, V., Viol, F., Knaack, H., Stemmer, K., Peters, L., ... & Helm, O. (2018). Diabetes as risk factor for pancreatic cancer: Hyperglycemia promotes epithelial-mesenchymal-transition and stem cell properties in pancreatic ductal epithelial cells. *Cancer letters*, 415, 129-150.

Knaack, H., Lenk, L., Philipp, L. M., Miarka, L., **Rahn, S.**, Viol, F., ... & Tiwari, S. (2018). Liver metastasis of pancreatic cancer: the hepatic microenvironment impacts differentiation and self-renewal capacity of pancreatic ductal epithelial cells. *Oncotarget*, 9(60), 31771.

**Rahn, S.**, Krüger, S., Röcken, C., Helm, O., & Sebens, S. (2019). Response to: 'Patterns of PD-L1 expression and CD8 T cell infiltration in gastric adenocarcinomas and associated immune stroma'. *Gut*, 68(1), 179-180.

**Rahn, S.**, Krüger, S., Mennrich, R., Goebel, L., Wesch, D., Oberg, H. H., ... & Sebens, S. (2019). POLE Score: a comprehensive profiling of programmed death 1 ligand 1 expression in pancreatic ductal adenocarcinoma. *Oncotarget*, 10(16), 1572.

Fabian, A., Stegner, S., Miarka, L., Zimmermann, J., Lenk, L., **Rahn, S.**, ... & Schäuble, S. (2019). Metastasis of pancreatic cancer: An uninfamed liver micromilieu controls cell growth and cancer stem cell properties by oxidative phosphorylation in pancreatic ductal epithelial cells. *Cancer Letters*.

Willms, A., Schitteck, H., **Rahn, S.**, Sosna, J., Mert, U., Adam, D., & Trauzold, A. (2019). Impact of p53 status on TRAIL-mediated apoptotic and non-apoptotic signaling in cancer cells. *PloS one*, 14(4), e0214847.

Miarka, L., Hauser, C., Helm, O., Holdhof, D., Beckinger, S., Egberts, J. H., Gundlach, J.-P., Lenk, L., **Rahn, S.**, Mikulits, W., Trauzold, A., & Sebens, S. (2019). The Hepatic Microenvironment and TRAIL-R2 Impact Outgrowth of Liver Metastases in Pancreatic Cancer after Surgical Resection. *Cancers*, 11(6), 745.

## Conference Paper

**Rahn, S.,** Piller, M., Helm, O., Zimmermann, V., Lenk, L., Knaack, H., Sipos, B., Röcken, C., Schäfer, H., Wesch, D., Sebens, S. (2015) Impact of macrophage-mediated metabolic alterations on phenotype and tumor promoting properties of benign and premalignant pancreatic ductal epithelial cells. Studierendentagung zu den Life Sciences, Kiel

**Rahn, S.,** Piller, M., Helm, O., Zimmermann, V., Lenk, L., Knaack, H., Sipos, B., Röcken, C., Schäfer, H., Wesch, D., Sebens, S. (2016) Inflammation-associated metabolic rewiring in initiation of pancreatic cancer. 36. Jahrestagung Deutscher Pankreas Club, Freising

Zimmermann, V., **Rahn, S.,** Viol, F., Lenk, L., Knaack, H., Helm, O., Sebens, S. (2016) Metabolic disorders and pancreatic cancer: High glucose promotes cancer stemness and epithelial-mesenchymal-transition via TGF- $\beta$  signalling in premalignant pancreatic ductal epithelial cells. 32. Deutscher Krebs Kongress

**Rahn, S.,** Röcken, C., Wesch, D., Sebens, S. (2016) Immune escape in pancreatic ductal adenocarcinoma. Studierendentagung zu den Life Sciences, Kiel

**Rahn, S.,** Helm, O., Sipos, B., Röcken, C., Sebens, S. (2017) Immune escape in pancreatic ductal adenocarcinoma: Challenges and prognostic value of programmed death 1 ligand 1 status. 37. Jahrestagung Deutscher Pankreas Club, Greifswald

Stegner, S., Buttlar, J., Viol, F., Lenk, L., Knaack, H., **Rahn, S.,** Fabian, A., Mikulits, W., Schäfer, H., Helm, O., Sebens, S. (2017) Liver metastases of pancreatic cancer: The interplay of metabolic enzymes and cancer stem cell properties in the context of the hepatic microenvironment. 123. Kongress der Deutschen Gesellschaft für Innere Medizin, Mannheim

**Rahn, S.,** Dänzer Barbosa, P., Plundrich, D., Schäfer, H., Wesch, D., Sipos, B., Helm, O., Sebens, S. (2017) Metabolic alterations precede inflammation-associated pancreatic carcinogenesis: Macrophages promote a protective metabolic shift in pancreatic ductal epithelial cells. 22<sup>nd</sup> Joint Meeting Signal Transduction Society, Weimar

**Rahn, S.,** Krüger, S., Mennrich, R., Goebel, L., Wesch, D., Röcken, C., Helm, O., Sebens, S. (2018) POLE Score: Ein neues Verfahren zur prädiktiven und prognostischen Beurteilung des programmed death 1 ligand 1 Status im duktalem Pankreasadenokarzinom. 38. Jahrestagung Deutscher Pankreas Club, Ulm

**Rahn, S.,** Zimmermann, V., Viol, F., Knaack, H., Stemmer, K., Peters, L., Lenk, L., Ungefroren, H., Saur, D., Schäfer, H., Helm, O., Sebens, S. (2018) Diabetes mellitus als Risikofaktor für die Entstehung des duktalem Pankreasadenokarzinoms – Chronische Hyperglykämie fördert die Epithelial-Mesenchymale Transition und Krebsstammzeleigenschaften prämaligener Gangepithelzellen. 38. Jahrestagung Deutscher Pankreas Club, Ulm

Winter, E., Walter, F., Lettau, M., Heidland, J., **Rahn, S.,** Scherließ, R., Helm, O., Sebens, S. (2018) Tumor vaccination: Chitosan nanoparticles to improve the antigen uptake by dendritic cells for an enhanced tumor-directed immune response. 5<sup>th</sup> European Congress of Immunology, Amsterdam



Walter, F., Winter, E., Heidland, J., Lettau, M., Meier, S., Faltinek, L., Otto, L., Wesch, D., **Rahn, S.**, Scherließ, R., Sebens, S. (2019) Tumor vaccination: Chitosan nanoparticles as antigen vehicles to promote a tumor-directed T cell response. 20<sup>th</sup> International AEK Cancer Congress, Heidelberg

Otto, L., **Rahn, S.**, Winter, E., Walter, F., Faltinek, L. J., Wesch, D., Helm, O., Sebens, S. (2019) Diabetes as a risk factor for pancreatic cancer: Hyperglycaemia and macrophages impact Epithelial-Mesenchymal Transition and stemness features in pancreatic ductal epithelial cells. 20<sup>th</sup> International AEK Cancer Congress, Heidelberg